

Evolution of Novel Antibiotic Scaffolds
Targeting the Nucleic Acid Machineries RNA Polymerase,
DNA Gyrase, and Topoisomerase IV

Dissertation

zur Erlangung des Grades
des Doktors der Naturwissenschaften
der Naturwissenschaftlich-Technischen Fakultät III
Chemie, Pharmazie, Bio- und Werkstoffwissenschaften
der Universität des Saarlandes

von

MSc. Walid Ali Mahmoud Elgaher

Saarbrücken

2016

„Gedruckt mit Unterstützung des Deutschen Akademischen Austauschdienstes“

Tag des Kolloquiums: 08. November 2016

Dekan: Prof. Dr. Dirk Bähre

Vorsitz: Prof. Dr. Rolf Müller

Berichterstatter: Prof. Dr. Rolf W. Hartmann

Prof. Dr. Andreas Speicher

Akad. Mitarbeiter: Dr. Silke Wenzel

Die vorliegende Arbeit wurde von April 2012 bis März 2016 unter Anleitung von Herrn Prof. Dr. Rolf W. Hartmann in der Fachrichtung 8.2 Pharmazeutische und Medizinische Chemie der Naturwissenschaftlich-Technischen Fakultät III der Universität des Saarlandes sowie am Helmholtz Institut für Pharmazeutische Forschung Saarland (HIPS) angefertigt.

*„Wer folgte einem Pfad Wissen darin zu suchen,
erleichtert Allah für ihn einen Weg zum Paradies.“*

Prophet Mohammad

Acknowledgment

To Allah almighty who supported, blessed, and granted me everything I have.

All my sincere appreciations and everlasting thanks to my PhD supervisor Prof. Dr. Rolf W. Hartmann for giving me the honor to work under his supervision and assigning attractive projects to me. Thanks for the golden advices, valuable instructions, experienced decisions, continuous encouragement, efficient assistance, and a lot of things I learned from him that changed my professional and life perspectives as well.

I am greatly indebted to Prof. Dr. Andreas Speicher for his scientific support, constructive comments, and fruitful discussions during my doctorate study.

I express my thanks and gratitude to Dr. Matthias Groh for his sincere training and transfer of knowledge in synthetic chemistry as well as for orchestrating numerous scientific and further tasks in a friendly atmosphere.

I would like to thank Dr. Jörg Haupenthal for the good management and performance of some biological experiments of the RNAP project.

My special thanks to Dr. Mostafa Hamed for the smart management and sincere help in the cystobactamids project.

I am grateful to Prof. Dr. Rolf Müller, Prof. Dr. Andreas Kirschning, Dr. Sascha Baumman, Dr. Jennifer Herrmann, Dr. María Moreno, and Lorenz Siebenbürger for their precious efforts in the cystobactamids project.

Great thanks are presented to Prof. Dr. Yves Mély and his team in particular Dr. Kamal Sharma and Dr. Francesco Saladini for the successful collaboration in the dual RNAP/RT inhibitors project.

I also appreciate Dr. Martina Fruth, Dr. Kristina Hüsecken, Jeaninne Jung, and Jannine Ludwig for their assistance in the biological evaluations of the RNAP project.

Deep thanks are expressed to Dr. Josef Zapp for running and optimizing hundreds of NMR experiments, and Dr. Volker Huch for determination of several X-ray crystal structures as well as Dr. Stefan Boettcher for his help in LC/MS analysis.

I am very thankful to Prof. Dr. Uli Kazmaier for the admission in the Interdisciplinary Graduate School of Natural Product Research and financing participation in conferences.

My endless thanks to the German academic exchange service (DAAD) for the full scholarship and support to get my PhD degree in Germany.

Sincere thanks are to Dr. Matthias Engel, Dr. Martin Frotscher, Dr. Ahmed S. Abdelsamie, Katrin Schmitt, May Concepcion, and Lothar Jager who helped me before the journey to and during the stay in Germany.

Many thanks to all current and former colleagues and employees at the working group of Prof. Hartmann and Helmholtz Institute for Pharmaceutical Research Saarland (HIPS) who are not mentioned by name here for the cooperative atmosphere.

Finally, I would like to present all my thanks to my beloved family: my parents Ali and Samia, my sisters Samar and Norhan, my brother Mohammad, my wife Weam and my children Nermin and Mohammad, who stand beside me in every moment to relief my pains and share my joy feelings. When I see you or hear your voices, I feel like being in heaven and without you, I am lost. To you I dedicate this thesis.

Walid Ali M. Elgaher

August 2016

Abstract

The magic bullets for treating bacterial infection are getting less potent in face of the growing resistance. This warning situation urges for rapid development of new antibacterial weapons effective against resistant pathogens. In this thesis, novel antibiotic scaffolds with low resistance frequency were developed by two strategies.

First, targeting a vital binding site (the switch region) of bacterial RNA polymerase: Following analog design approaches, six ureido-heterocycle-carboxylic acid classes were synthesized based on a previous class. The new compounds show potent activity against Gram-positive pathogens as well as the Gram-negative *E. coli* TolC strain. They are characterized by no cross-resistance with the clinically used RNAP inhibitor rifampicin, lower rate of resistance development, and marginal cytotoxicity to human cells.

These features were employed to target the closely related NNRTI binding site of HIV-1 reverse transcriptase. By structure-based optimization, the first small molecule dual anti-infectives were discovered exhibiting antibacterial and antiretroviral activities on HIV-1 wild type and resistant strains.

Second, optimization of novel natural antibiotics (the cystobactamids) that target DNA gyrase and topoisomerase IV: Pursuing an interactive *de novo* design, both target and antibacterial activities of cystobactamid 507 were enhanced. The new congeners display an outstanding metabolic stability. Moreover, the synthetic route was markedly improved.

Zusammenfassung

Angesichts einer ständig wachsenden Resistenzentwicklung werden die therapeutischen Optionen zur Behandlung bakterieller Infektionen ständig schlechter. Deshalb sind neue Antibiotika gegen resistente Bakterien dringend notwendig. In dieser Doktorarbeit werden neue antibiotisch wirksame Scaffolds durch zwei Strategien entwickelt.

Erstens Hemmstoffe der bakteriellen RNA Polymerase, die an die Switch Region binden: mittels Analog Design wurden Substanzen in sechs Klassen von Ureido-Heterocyclus-Carbonsäuren erhalten. Die Verbindungen zeigten eine starke antibakterielle Aktivität, keine Kreuzresistenz zu dem klinisch verwendeten Rifampicin, eine niedrigere Resistenz-Entwicklungsrate und eine nur geringfügige Toxizität gegenüber humanen Zellen.

In einem weiteren Projekt wurde die Tatsache ausgenutzt, dass die NNRTI Bindestelle der HIV-1 Reversen Transkriptase strukturelle Ähnlichkeiten zur Switch Region hat. Geeignete, oben entwickelte Wirkstoffe wurden nun weiter strukturell optimiert und duale Hemmstoffe mit antibakterieller und antiretroviraler Aktivität an Wildtyp und resistenten Stämmen erhalten.

Zweitens wurde eine Optimierung des natürlich vorkommenden Cystobactamids 507 hinsichtlich DNA Gyrase und Topoisomerase IV unternommen. Diese Ziele und eine Erhöhung der antibakteriellen Aktivität wurde durch interaktives *de novo* Design erreicht. Die neuen Derivate zeigten auch eine verbesserte metabolische Stabilität. Außerdem wurde der synthetische Zugang verbessert.

Papers and Manuscripts Included in This Thesis

This thesis is divided into three publications and one manuscript, which are referred to in the text by their numbers I–IV, respectively.

I Expanding the Scaffold for Bacterial RNA Polymerase Inhibitors: Design, Synthesis and Structure–Activity Relationships of Ureido-Heterocyclic-Carboxylic Acids

Walid A. M. Elgaher, Martina Fruth, Matthias Groh, Jörg Haupenthal and Rolf W. Hartmann

RSC Adv., 2014, 4, 2177–2194.

II Discovery and Structure-Based Optimization of 2-Ureidothiophene-3-Carboxylic Acids as Dual Bacterial RNA Polymerase and Viral Reverse Transcriptase Inhibitors

Walid A. M. Elgaher, Kamal K. Sharma, Jörg Haupenthal, Francesco Saladini, Manuel Pires, Eleonore Real, Yves Mély, and Rolf W. Hartmann

J. Med. Chem., 2016, 59, 7212–7222.

III Synthesis and Biological Evaluation of Cystobactamid 507: A Bacterial Topoisomerase Inhibitor from *Cystobacter* sp.

María Moreno, Walid A. M. Elgaher, Jennifer Herrmann, Nadin Schläger, Mostafa M. Hamed, Sascha Baumann, Rolf Müller, Rolf W. Hartmann, and Andreas Kirschning

Synlett, 2015, 26, 1175–1178.

IV Cystobactamid 507: Concise Synthesis and Design of Non-Covalently Bonded Rigid Analogs Boost Bacterial Topoisomerases IIA Inhibition, Antibacterial Activity and Disclose the Bioactive Conformation

(Manuscript in Submission).

Contribution Report

The author would like to declare his contributions to the papers/manuscript I–IV included in this thesis.

- I** The author designed, synthesized and characterized most of the compounds. He performed all the molecular modelling studies (similarity analysis, flexible alignment and molecular docking). Furthermore, he performed the minimum inhibitory concentration (MIC) assays of selected compounds, and studied the role of cell wall and efflux pumps for the uptake of the compounds into the Gram-negative *E. coli*. In addition, he interpreted the results of the biological experiments, and he conceived and wrote the manuscript.
- II** The author designed, synthesized and characterized most of the compounds. He performed all the molecular modelling studies (molecular docking, similarity analysis, and quantitative structure–activity relationship (QSAR) model). Furthermore, he interpreted the results of the biological experiments, and he conceived and wrote the manuscript.
- III** The author designed, synthesized and characterized the methyl homolog of Cys507. He wrote the corresponding parts of the manuscript.
- IV** The author designed, synthesized and characterized most of the compounds. He performed all the molecular modelling studies (conformational analysis, calculations of molecular dynamics, electrostatic molecular surfaces and backbone curvatures). Furthermore, he performed all conformational studies in solution phase using 2D NOESY and ^1H NMR experiments as well as in solid phase through determination of the crystal structures. In addition, he interpreted the results of the biological experiments, and he conceived and wrote the manuscript.

Further Paper of the Author that is Not Part of This Dissertation

V Surface Plasmon Resonance – More than a Screening Technology: Insights in the Binding Mode of σ 70:core RNAP Inhibitors

Kristina Hüsecken, Stefan Hinsberger, Walid A. M. Elgaher, Jörg Hauptenthal, and Rolf W. Hartmann

Future Med. Chem., 2014, 6, 1551–1565.

Abbreviations

2D	Two dimensional
3D	Three dimensional
ABC	ATP binding cassette
ADMET	Absorption, distribution, metabolism, excretion, and toxicity
AIDS	Acquired immune deficiency syndrome
AMP	Adenosine monophosphate
AMR	Antimicrobial resistance
ART	Antiretroviral therapy
ATP	Adenosine triphosphate
AZT-TP	Azidothymidine triphosphate
BTC	Bis(trichloromethyl) carbonate
CDAD	<i>Clostridium difficile</i> -associated diarrhea
Cys507	Cystobactamid 507
DCM	Dichloromethane
DHF	Dihydrofolic acid
DMEM	Dulbecco's modified Eagle medium
DNA	Deoxyribonucleic acid
dNTP	Deoxyribonucleotide
EFV	Efavirenz
eq	Equation
EtBr	Ethidium bromide
ETR	Etravirine
EU	European Union
FBS	Fetal bovine serum
FDA	Food and Drug Administration
FRET	Förster resonance energy transfer
HAART	Highly active antiretroviral therapy
HIV	Human immunodeficiency virus
HPLC	High-performance liquid chromatography
IC ₅₀	Half-maximum inhibitory concentration
IMHB	Intramolecular hydrogen bond
INPHARMA	Interligand NOE for pharmacophore mapping

ITC	Isothermal titration calorimetry
K_d	Dissociation constant
LE	Ligand efficiency
LLE	Ligand-lipophilicity efficiency
LPS	Lipopolysaccharide
MATE	Multidrug and toxic compound extrusion
MD	Molecular dynamics
MDR	Multidrug resistance
MFS	Major facilitator superfamily
MIC	Minimal inhibitory concentration
MLS	Macrolides, lincosamide, and streptogramin B
MoA	Mode of action
MRSA	Methicillin resistant <i>Staphylococcus aureus</i>
MS	Mass spectrometry
MST	Microscale thermophoresis
Mtb	<i>Mycobacterium tuberculosis</i>
MTT	3-(4,5-dimethylthiazol-2-yl)-2,5-diphenyltetrazolium bromide
Myx	Myxopyronin
NMR	Nuclear magnetic resonance
NNRTI	Non-nucleoside reverse transcriptase inhibitor
NOE	Nuclear Overhauser effect
NPs	Natural products
NRPSs	Nonribosomal peptide synthetases
NRTI	Nucleoside reverse transcriptase inhibitor
NVP	Nevirapine
OD ₆₀₀	Optical density at 600 nm
ODN	Oligonucleotide
OM	Outer membrane
PABA	<i>para</i> -aminobenzoic acid
PA β N	Phenyl-arginine- β -naphthylamide
PBP	Penicillin binding protein
piDAPH4	π -donor-acceptor-polar-hydrophobe four-point pharmacophore
PK	Pharmacokinetic

PKSs	Polyketide synthases
PMBN	Polymyxin B nonapeptide
PMF	Proton motive force
PRPs	Pentapeptide repeat proteins
p/t	primer/template
QRDR	Quinolone resistance-determining region
QS	Quorum sensing
QSAR	Quantitative structure–activity relationships
Rif	Rifampicin; Rifampin
RLU	Relative luminescence unit
RNA	Ribonucleic acid
RNAP	RNA polymerase
RND	Resistance-nodulation-cell division
RPV	Rilpivirine
RT	Reverse transcriptase
SAR	Structure–activity relationship
SMR	Small multidrug resistance
SPR	Surface plasmon resonance
STD	Saturation transfer difference
TAMRA	Carboxytetramethylrhodamine
TB	Tuberculosis
T _c	Tanimoto coefficient
TEA	Triethylamine
US	United States
VRE	Vancomycin-Resistant Enterococci
WHO	World Health Organization
WT	Wild type

Table of Contents

1	Introduction	1
1.1	Antibiotics and their Main Targets	2
1.2	Mechanisms of Bacterial Resistance	6
1.3	Resistance Cost	9
1.4	Strategies to Overcome Bacterial Resistance	11
1.5	Bacterial RNA Polymerase	14
1.6	Bacterial Topoisomerases Type IIA	17
1.7	Molecular Similarity and Drug Design	20
2	Aim of the Thesis	22
3	Results	24
3.1	Expanding the Scaffold for Bacterial RNA Polymerase Inhibitors: Design, Synthesis and Structure Activity Relationships of Ureido-Heterocyclic-Carboxylic Acids	24
3.2	Discovery and Structure-Based Optimization of 2-Ureidothiophene-3-carboxylic Acids as Dual Bacterial RNA Polymerase and Viral Reverse Transcriptase Inhibitors	63
3.3	Synthesis and Biological Evaluation of Cystobactamid 507: A Bacterial Topoisomerase Inhibitor from <i>Cystobacter</i> sp.	89
3.4	Cystobactamid 507: Concise Synthesis and Design of Non-Covalently Bonded Rigid Analogs Boost Bacterial Topoisomerases IIA Inhibition, Antibacterial Activity and Disclose the Bioactive Conformation	97
4	Final Discussion	118
4.1	Structure–Activity Relationships	118
4.2	Mode of Action Studies	123
4.3	Anti-infective Activities and Cytotoxicity to Human Cells	125
4.4	Ureidothiophenes' Uptake and Resistance Mechanisms in <i>E. coli</i>	126
4.5	Frequency of Resistance Development	126
4.6	Scaffold Hopping and Identification of Cys507 Bioactive Conformation via IMHBs	127
4.7	Summary and Outlook	129
5	References	131

6	Supporting Information	140
6.1	Supporting Information for Publication II	140
6.2	Supporting Information for Publication III	149
6.3	Supporting Information for Manuscript IV	166
7	Appendix	234
7.1	Curriculum Vitae	234
7.2	Publications	235
7.3	Conference Contributions	236

1 Introduction

Bacteria are unicellular microorganisms constituting one of the three known life systems (Bacteria, Archaea, and Eukaryotes) (Woese et al. 1990). They live free in soil and water or in symbiosis with other organisms, e.g., plants, animals, and even human. The human body harbors a large number of bacteria living on the skin, in the oral cavity, the respiratory-, gastrointestinal- and urogenital tracts. Our bodies were estimated to contain more than 50% of their cells as bacteria (Sender et al. 2016). This human microbiota has an important role in keeping our bodies healthy. Besides digestion and stimulation of the immune system, the body flora produces numerous active compounds necessary for various functions, e.g., vitamin K, tryptamine (neurotransmitter), polysaccharide A (immunomodulatory), deoxycholic acid (metabomodulatory), and many antibiotics (Donia and Fischbach 2015). However, there are also pathogenic bacteria that cause serious diseases, e.g., TB, pneumonia, and cholera upon infecting the human body or when the immune system is impaired as in case of chemotherapy, leukemia, and HIV infection. Such bacterial infectious diseases are responsible for millions of death cases worldwide each year.

Although it was mysterious at that time, ancient people used antibacterial preparations from molds, plants or insects that were described in traditional medicine for the treatment of bacterial infections. For example, tetracycline was found in the bones from a tomb in the Dakhleh Oasis, Egypt back to the late Roman period (Cook et al. 1989). The relationship between bacteria and disease was proved by Louis Pasteur and the Nobel-laureate Robert Koch in the middle of the nineteenth century. In the early twentieth century, Paul Ehrlich thought of finding a magic bullet that can only kill the pathogen and do not harm the host. Through series of chemical modifications and pharmacological screenings, Ehrlich and his team developed arsphenamine, the first synthetic antibiotic, for the treatment of syphilis. Few years later, sulfa drugs were discovered and in 1940, penicillin could be isolated. Ehrlich's work and Alexander Fleming's discovery dated the beginning of the modern antibiotic era (Aminov 2010).

The discovery of antibiotics witnessed a golden age in the period 1940–1960, when many classes (natural and synthetic) were introduced (Figure 1). Since 1960 hitherto, medicinal chemistry took over the reins in the development of antibiotics (Walsh and Wencewicz 2014). Rising hurdles such as low potency, narrow spectrum, instability, toxicity, etc. could be conquered using the versatile MedChem approaches. Nevertheless, a common drawback of the antibiotics showed up at this period was the lack of innovation, i.e., no new chemical entities were introduced, but peripherally modified derivatives of known antibiotic scaffolds

instead. These generations of antibacterial drugs with minor changes at invariable core structures could be easily prone to bacterial defense mechanisms likewise the parent antibiotics (cross-resistance).

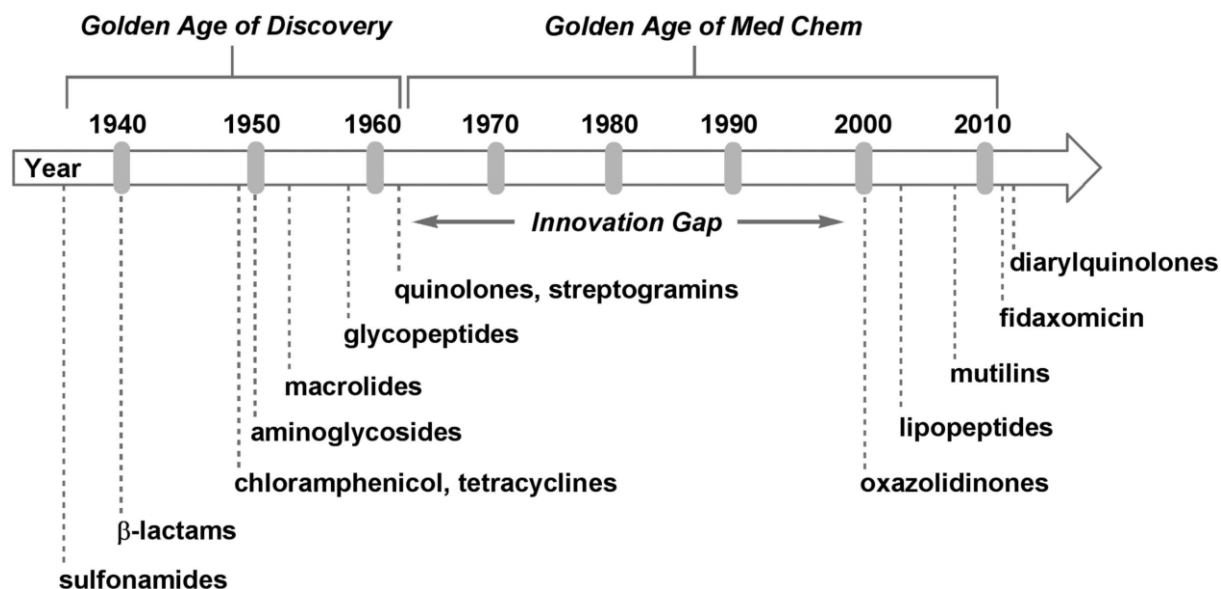


Figure 1. The antibiotics discovery timeline; adapted from (Walsh and Wencewicz 2014).

On the other side, bacteria have evolved resistance against the clinically used antibiotics that rendered them ineffective. This antimicrobial resistance (AMR) has consequences not only on the public health but also it menaces the economic growth. For instance, the additional health care costs for MDR bacterial infections in EU were estimated to be € 1.5 billion per year (Aminov 2010). In US, MRSA infections extra cost \$ 3–4 billion each year (Fischbach and Walsh 2009). Even worse, the current estimation of global death due to AMR is warning that we could find ourselves back in a new preantibiotic era (Arias and Murray 2009).

1.1 Antibiotics and their Main Targets

Antibiotics are chemical compounds that kill or inhibit the growth of bacteria. Besides their use for treatment of acute bacterial infections, they have several necessary applications in surgical operations, transplantations, care of the critical cases or HIV-infected patients and cancer chemotherapy. As a valid antibacterial agent viable for clinical use, the term “magic bullet” was expanded to include other criteria such as selective toxicity against pathogenic bacteria, innocuous to human cells and normal flora, broad spectrum, low tendency toward resistance development, reasonable PK properties relevant to the site of application, e.g., solubility, lipophilicity, chemical and metabolic stability.

The antibiotic mode of action usually is assigned to the intrusion into the function of one or more vital machineries in bacteria: cell wall, cell membrane, nucleic acids (DNA and RNA), protein and metabolites synthesis. The major bacterial targets of antibiotics are described in figure 2.

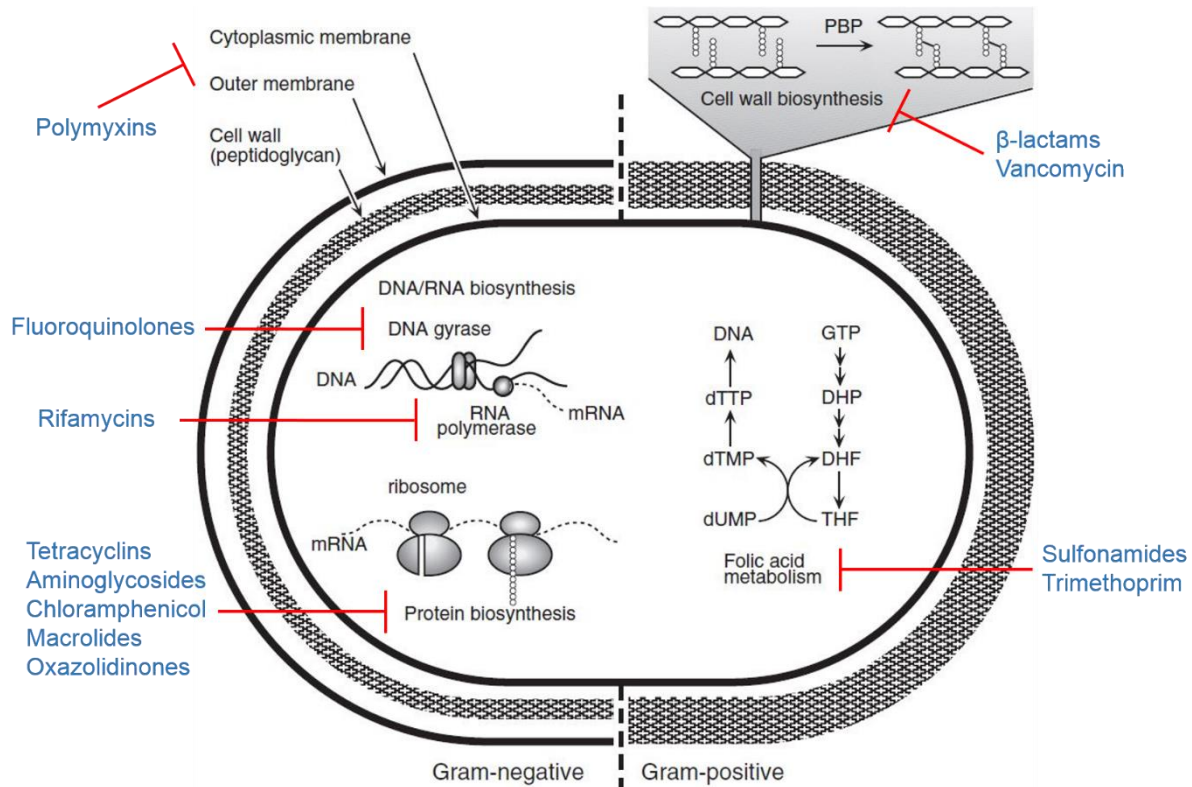


Figure 2. Antibiotic targets in bacteria; adapted from (Yoneyama and Katsumata 2006).

1.1.1 Inhibition of Cell Wall Synthesis

Components of the bacterial cell are enveloped by a phospholipid bilayer (the inner membrane), and a mesh of peptidoglycan (murein) forming the cell wall. In Gram-negative bacteria, an extra layer containing lipopolysaccharide (LPS) surrounds the cell wall (the outer membrane). These barriers are essential for protecting the bacterial cell from osmolysis. Crosslinking of the peptidoglycan network is carried out by transglycosylase and transpeptidase (also known as penicillin binding protein, PBP).

β -Lactam antibiotics, e.g., penicillins, cephalosporins, carbapenems, and monobactams inhibit the peptidoglycan synthesis competitively through mimicking the D-Ala-D-Ala substrate (Figure 3) (Tipper and Strominger 1965). They bind to the PBP irreversibly via opening of the β -lactam ring and acylation of the active site. Another peptidoglycan synthesis inhibitors are the glycopeptides, e.g., vancomycin. They bind to the D-Ala-D-Ala substrates, and hinder their access to PBP (Kohanski et al. 2010).

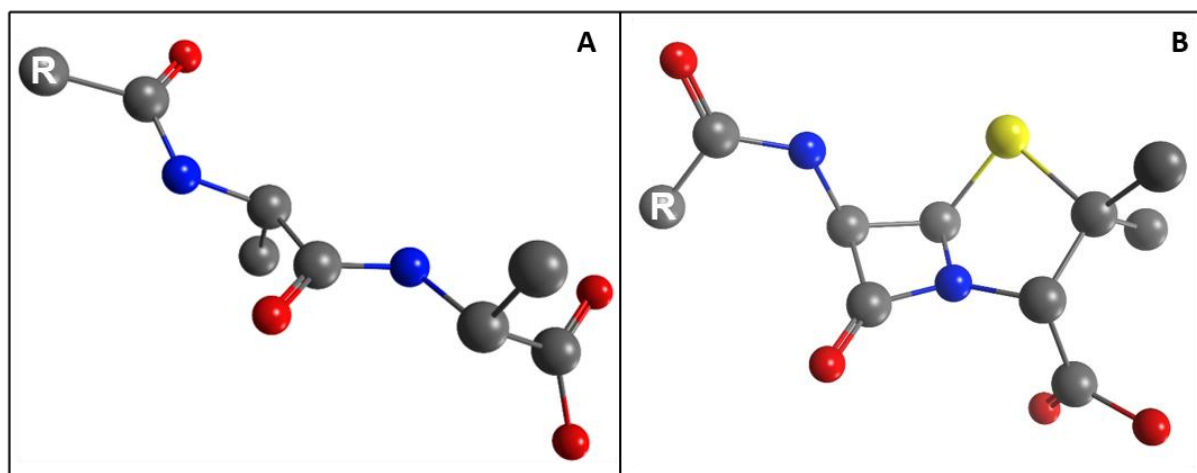


Figure 3. Structural mimicking to the substrate sequence D-Ala-D-Ala (A) by various penicillins (B).

1.1.2 Inhibition of Protein Synthesis

For protein biosynthesis, the genetic data loaded on mRNA are decoded by the action of the ribosome (translation) in a three-step process (initiation, elongation, and termination). Besides the ribosome, tRNAs carrying the amino acids, initiation and release factors are necessary for translation.

Bacterial ribosome is a nucleoprotein consisted of two subunits (30S and 50S). Tetracyclins bind to the 30S subunit and impede the interaction between tRNAs and the ribosome. Aminoglycosides, e.g., streptomycin and gentamicin bind irreversibly to the 16S rRNA component of the 30S subunit. This leads to conformational changes that in turn increase the mRNA codon–tRNA mismatching and subsequent protein mistranslation (Kohanski et al. 2010).

Chloramphenicol and macrolides, e.g., erythromycin interact with the 23S rRNA of 50S subunit and block the peptidyl transferase activity. Oxazolidinones bind to the 50S subunit and inhibit the formation of initiation complex (Kohanski et al. 2010).

1.1.3 Disruption of Cell Membrane

Cell membrane integrity is essential for preventing leakage of cell contents. The cationic peptides polymyxins target the cytoplasmic membrane as well as the outer membrane of Gram-negative bacteria causing an increased permeability and subsequent cell death (Yoneyama and Katsumata 2006).

1.1.4 Inhibition of Nucleic Acid Synthesis

DNA replication and transcription are pivotal processes for bacteria. During DNA replication, two types of topoisomerases are required to modulate and maintain the topology of the

supercoiled DNA strands. Type I topoisomerases temporarily cleave one DNA strand at a time, whereas topoisomerases type II transiently cleave the two DNA strands at the same time in an ATP dependent process. Aminocoumarins and fluoroquinolones target the type II topoisomerases, namely DNA gyrase and Topoisomerase IV. Fluoroquinolones, e.g., norfloxacin, ciprofloxacin, and levofloxacin bind to the DNA-bound gyrase forming a ternary complex. They stabilize the complex in the DNA double-strand cleaved state preventing DNA religation (topoisomerase poisoning) (Kohanski et al. 2010).

The process of RNA synthesis (transcription) is carried out by the DNA-dependent RNA polymerase in three stages (initiation, elongation, and termination). RNAP is a multi-subunit enzyme composed of α_2 , β , β' and ω subunits constituting the core enzyme of a molecular weight ~ 400 kDa. The latter binds to the initiation factor σ forming the holoenzyme. Although the core RNAP is the catalytic active motif, binding to σ factor is a key step for promoter DNA recognition and binding (Murakami and Darst 2003). Rifamycins inhibit transcription through binding to the β subunit of the DNA-bound RNAP adjacent to the active center, leading to a steric interference with the growing RNA transcript (Feklistov et al. 2008).

1.1.5 Inhibition of Metabolite Pathways

Bacterial cells need folic acid as a cofactor for synthesizing nucleotides. Folate biosynthesis starts from *p*-aminobenzoic acid and pteridine in the presence of dihydropteroate synthase to produce dihydropteroic acid. The latter is converted to dihydrofolic acid by dihydrofolate synthase. Subsequent reduction by dihydrofolate reductase yields tetrahydrofolic acid.

Sulfonamides silence dihydropteroate synthase, and trimethoprim inhibits dihydrofolate reductase by competitive binding to the active site through structural mimicking to the corresponding substrates PABA and dihydrofolic acid, respectively (Figure 4) (Yoneyama and Katsumata 2006).

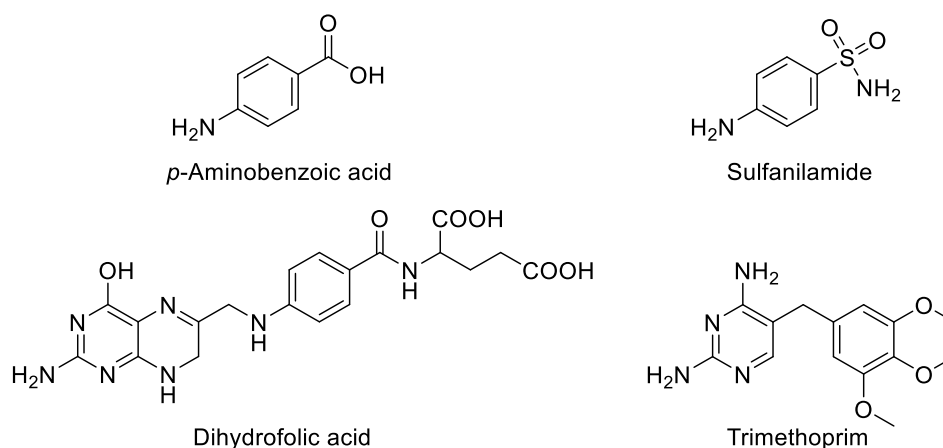


Figure 4. Structural analogy between PABA and sulfanilamide as well as DHF and trimethoprim.

1.2 Mechanisms of Bacterial Resistance

Bacterial resistance is a natural phenomenon, where bacteria protect themselves from antibiotics produced by the same or other species (bacteria, fungi, and plants) during the competition for nutrients or habitat. This is also true for antibiotics developed by human, i.e., as soon as an antibiotic was discovered or approved for clinical use, bacteria evolve special defense mechanisms to withstand the antibiotic damage. Based on its origin, resistance can be classified into two types: intrinsic and acquired. Intrinsic resistance is the inherent ability of bacteria to resist the antibiotic due to presence of a resistance gene in their chromosomes. Acquired resistance occurs due to mutation of the bacterial genome or transfer of the resistance gene through a plasmid or transposon from other resistant bacteria (Yoneyama and Katsumata 2006). The mechanisms of antibiotic resistance are summarized in figure 5.

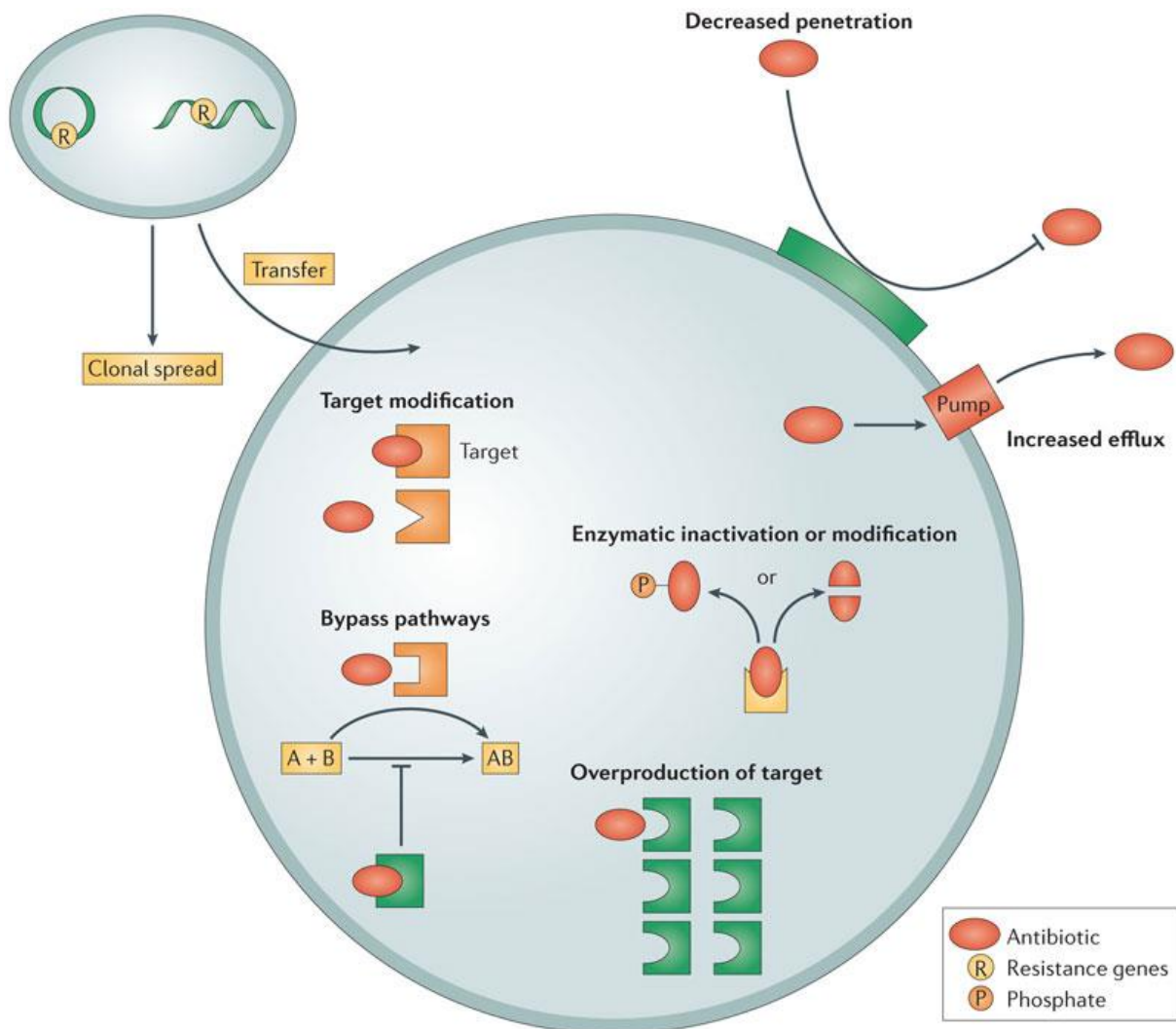


Figure 5. Mechanisms of antibiotic resistance; adapted from (Lewis 2013).

1.2.1 Reduced Permeability

The outer membrane of Gram-negative bacteria, e.g., Enterobacteriaceae and *Pseudomonas* species represents an intrinsic barrier against many of antibiotics. It is a bilayer composed of an interior phospholipid layer and an exterior LPS layer. In addition, protein channels (porins) traversing across the outer membrane are present for transport of small hydrophilic nutrients. Antibiotic uptake into Gram-negative bacteria is limited by the ability to diffuse either through the LPS layer or through the porins. On one hand, the LPS-containing outer membrane shows 2-fold lower permeability than the cytoplasmic membrane for lipophilic compounds (Nikaido 2003). On the other hand, besides their selectivity for size and charge of the molecules, decreasing the number or size of porins is detrimental for the entry of hydrophilic antibiotics into the bacterial cell (Blair et al. 2015).

1.2.2 Increased Efflux

Active transport of antibiotics outside the cell through efflux pumps is a frequent innate resistance mechanism of bacteria. There are five efflux families: the major facilitator superfamily (MFS), the small multidrug resistance (SMR), the resistance-nodulation-cell division (RND), the multidrug and toxic compound extrusion (MATE), and the ATP binding cassette (ABC) superfamily (Putman et al. 2000). Energy required for drug export is either supplied by ATP in case of the ABC superfamily (primary transporters), or through a proton motive force (PMF), or sodium in case of MATE family, for the other families (secondary transporters) (Yoneyama and Katsumata 2006).

Examples for the multidrug efflux pumps are AcrB in *E. coli* and MexB in *P. aeruginosa* that belong to the RND family. They are homotrimers that are located in the inner membrane. They form a tripartite complex with a periplasmic protein AcrA and MexA, respectively, and an outer membrane channel TolC and OprM, respectively. Studies of the AcrB exporter indicated that there are two distinct multisite binding pockets (proximal and distal). These pockets are large and can interact with broad structurally variant substrates mainly through hydrophobic and electrostatic interactions (Nakashima et al. 2011).

Overexpression of efflux pumps plays a key role in resistance. Regulation of efflux pump gene transcription is mediated by local and global regulators such as the transcription factors (MarA, SoxS, and RamA), which activate *acrAB* expression in Enterobacteriaceae (Aleksun and Levy 1997; Pomposiello et al. 2001; Nikaido et al. 2008; Blair et al. 2015).

1.2.3 Inactivation

Bacteria utilize their supplies of enzymes to disable antibiotics, especially those of natural origin, through chemical modifications. One method is the hydrolysis of the antibiotic active moiety, e.g., β -lactams by β -lactamases. Similar to transpeptidases (PBPs), β -lactamases bind to β -lactams through a serine residue at the active site forming penicilloyl-O-Ser β -lactamase intermediates. In contrast to PBPs, these intermediates dissociate rapidly resulting in inactive penicilloic acids with cleaved β -lactam rings (Walsh 2000).

Another method of inactivation is to cap the interacting functional groups, e.g., OH and NH₂ of an antibiotic with masking groups, e.g., acetyl, phosphoryl, and nucleotidyl. This leads to inhibition of crucial contacts with the target protein, and thereby decreasing the binding affinity. Aminoglycosides are inactivated by three classes of modifying enzymes: acetyltransferases that cause N-acetylation using acetyl-CoA, phosphotransferases that induce O-phosphorylation using ATP, and adenylyltransferases that result in O-adenylation via adding AMP moiety from ATP. Chloramphenicol acetyltransferases are responsible for O-acetylation of chloramphenicol using acetyl-CoA (Yoneyama and Katsumata 2006). These capped aminoglycosides and chloramphenicol show low affinity to RNA constituents of the ribosome and are incompetent to hinder protein synthesis.

1.2.4 Alteration of Target

Bacteria can evade the antibiotics' damages by modifications of their targets. Since antibiotic targets are pivotal for bacteria, these modifications should not affect the target fidelity and simultaneously make the target unrecognizable to antibiotics. A modified target can result from mutation in genes encoding this target, or posttranscriptional modification by an enzyme (Spratt 1994).

Vancomycin resistance in VRE is an example for genetic mutation of the target. The *vanHAX* genes encode new pathways for converting the peptidoglycan terminals D-Ala-D-Ala into D-Ala-D-lactate. The new target misses an important hydrogen bond contact with vancomycin. Consequently, the mutant peptidoglycan shows 1000-fold reduced affinity to the antibiotic, but is still valid for cross-linking by PBPs and cell wall biosynthesis (Walsh 2000).

An example for enzyme induced target alteration is the erythromycin resistance due to N6-methylation of the adenine residue A2058 of 23S rRNA by the erythromycin ribosome methylase (Erm). The methylated target has lower affinity to erythromycin and confers cross-resistance to other macrolides, lincosamide, and streptogramin B (MLS resistance phenotype) (Weisblum 1995).

Another example is the quinolone resistance transferred by the *qnr* gene families. These genes encode for pentapeptide repeat proteins (PRPs) that bind to DNA gyrase and topoisomerase IV and rescue them from the fluoroquinolones poisoning effect (Blair et al. 2015). A study of QnrB1 structure, member of PRPs, suggests that these proteins bind to and destabilize the DNA–topoisomerase–quinolone ternary complex. This binding triggers the release of quinolone and resumption of topoisomerase activity (Vetting et al. 2011).

1.2.5 Overproduction

Tolerance to an antibiotic can be attained through an overexpression of the corresponding target genes. In response to target defect by an antibiotic, bacteria overproduce this target in an excess to resume the blocked function. Consequently, a higher concentration of the antibiotic is required to switch off the surplus target entirely. Resistance in clinical isolates of *M. tuberculosis* and other *Mycobacterium* species to isoniazid and ethambutol are supposed to be in part due to the overexpression of *inhA* and *emb* genes, respectively (Chopra 1998).

1.2.6 Bypass

This type of bacterial resistance is typical for antibiotics targeting metabolic pathways, e.g., sulfonamides and trimethoprim. In this case, bacteria evolve a novel protein to take over the function of the inhibited native protein, however structurally different. Such a property makes the new target less vulnerable to the detrimental interactions of the antibiotic and sometimes even more efficient in its function. For instance, two new dihydrofolate reductases were identified in trimethoprim non-susceptible *E. coli* borne by the resistance plasmids R388 and R483. The plasmid enzymes have molecular weight different from that of the chromosomal enzyme, and they are less sensitive to trimethoprim ($IC_{50} 22 \times 10^3$ times higher). Interestingly, the dihydrofolate reductase activity of the R483 carrying *E. coli* is 10-fold higher than that of the wild type (Smith and Amyes 1984).

1.3 Resistance Cost

Bacteria benefit from resistance in presence of an antibiotic selective pressure, however resistant bacteria usually show a reduced fitness, i.e., lower growth rate and decreased virulence compared to non-resistant strains in absence of antibiotics (cost of resistance) (Spratt 1996). This is not surprising, since resistance mutations affect essential targets in bacteria (the antibiotic targets). Even in case of a plasmid-acquired resistance, synthesizing new nucleic acids and proteins imposes an energetic burden, and these macromolecules may perturb the physiological processes in the bacterial cell (Lenski and Nguyen 1988).

Fitness costs can be assessed through comparing the exponential growth rates of the wild type and resistant strains in vitro (Figure 6a). Alternatively, running an in vitro competition assay

for a mixture of the wild type and resistant strains in a certain ratio. By culturing the mixture for several days and calculating the change of the wild type/resistant strains ratio, fitness variation can be evaluated (Figure 6b). This competition assay can also be performed *in vivo* using a suitable animal model for a condition more relevant to that of the clinical infection (Figure 6c) (Di Andersson and Hughes 2010).

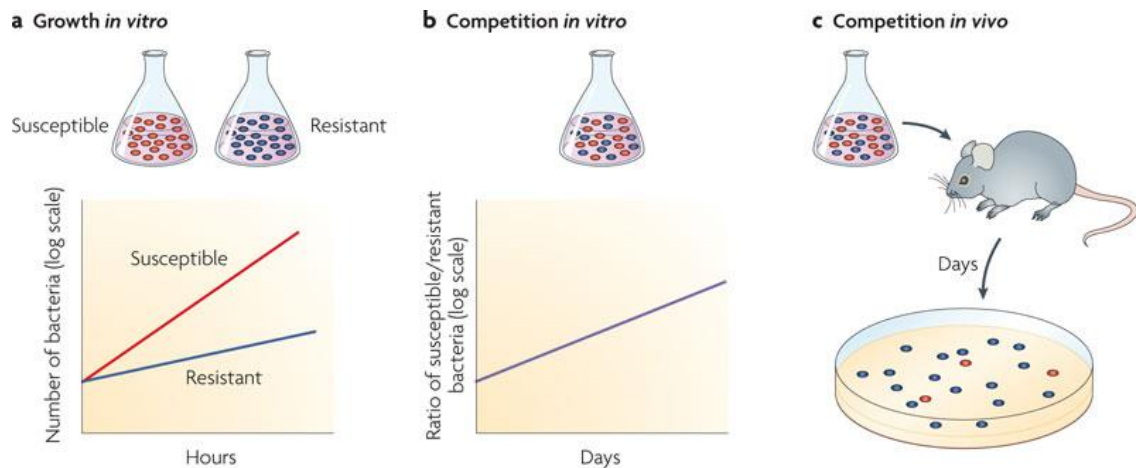


Figure 6. Determination of bacterial fitness; adapted from (Di Andersson and Hughes 2010).

The costs of resistance are variable between high fitness costs to low or no-costs depending on the antibiotic class, mutation site, bacterial species and growth conditions (Di Andersson and Hughes 2010; Melnyk et al. 2015).

Although fitness costs hint at a glimmer of hope regarding the rise of antibiotic resistance, adaptation to resistance costs is another nail in the coffin of currently used antibiotics. Evolution in low fitness resistant bacteria occurs through emergence of a compensatory or suppressor mutation that ameliorates the deleterious effect of the resistance mutation in order to reduce the fitness costs without affecting the resistance. This leads to stabilization of the resistant strains in the bacterial population (Di Andersson and Hughes 2010). For instance, the rifampicin (Rif)-resistant *E. coli* K12 mutants in *rpoB* gene encoding the β subunit of RNAP showed fitness costs that directly correlate with the impaired transcription efficiency. After 200 generations of these mutants by serial passage of cultures in absence of Rif, the isolated clones showed increased fitness without change in the resistance level owing to the compensatory mutations (Reynolds 2000).

Understanding the resistance costs may be the key to the ideal antibiotic. A careful choice of the antibiotic target or targets, which severely affects fitness of bacteria upon resistance mutations, and the compensation mutations are useless or difficult to be attained, should be reflected in an antibiotic with a minimum rate of resistance development (Andersson 2006).

1.4 Strategies to Overcome Bacterial Resistance

Efforts to cope with the antibiotic resistance problem revolve around two main axes, which will be mentioned briefly in the following paragraphs.

1.4.1 Saving our Legacy of the Current Antibiotics

Antibiotic abuse contributes significantly to the resistance problem. Therefore, several antibiotic stewardship policies were launched for using the antibiotics in an optimum way in order to reduce the prevalence of resistance (Dellit et al. 2007; Bartlett et al. 2013). An effective use of antibiotics can be summarized in four rights: right drug, right time, right dose, and right duration (Dryden et al. 2011). Inappropriate use of antibiotics for viral infections can be averted by using a precise diagnostic marker for bacterial infection, e.g., procalcitonin level (Simon et al. 2004). Alternatively, the delayed prescription would be an acceptable compromise, i.e., prescribing the antibiotic few days later only if symptoms do not improve, as viral infections are usually relieved in such period (Bartlett et al. 2013).

Combination therapy (using multiple antibiotics acting on different targets concurrently) is believed to combat resistance effectively likewise the trend followed in HIV and cancer therapy and indeed, it showed success in TB infections (Dellit et al. 2007). However, there are insufficient clinical evidences supporting this strategy for routine use, in addition to other disadvantages such as the increased side effects, cost of medications and potential of multidrug resistance development (Tamma et al. 2012).

Another approach is the combination between an antibiotic and a compound that counteracts the resistance mechanism toward this antibiotic. For instance, enzymatic deactivation of β -lactams was successfully escaped by the β -lactamase inhibitors clavulanic acid and sulbactam. Both agents are β -lactam analogs, and they sacrifice themselves as a substrate to β -lactamases for the β -lactams (Walsh 2000; Drawz and Bonomo 2010). For antibiotics that suffer from reduced permeability through the outer membrane of Gram-negative bacteria, combination with permeability enhancers, e.g., polymyxins seems beneficial (Vaara 1992). Similarly, co-administration of efflux pump inhibitors could retrieve the activity of antibiotics subjected to extrusion outside the cell by the efflux mechanism (Lomovskaya et al. 2001; Lomovskaya and Bostian 2006).

1.4.2 Rapid Development of New Antibiotics for the Next Generations

Besides the above-mentioned guidelines, the discovery and development of novel antibiotics with new scaffolds attacking known/new essential targets in bacteria have become an urgent need to deal with the imminent disaster of AMR.

Natural products remain, as they were previously, a profuse spring for antibiotics. It was estimated that all discovered compounds yet represent only 1% of NPs available from microbial sources (Fischbach and Walsh 2009). The advances in culturing and screening techniques for bacterial secondary metabolites should be directed to underexplored bacterial taxa, e.g., myxobacteria. This would accelerate the discovery of novel chemical classes of antibiotics that can evade the current resistance mechanisms (Fischbach and Walsh 2009).

In addition, mining bacterial genome to identify the gene clusters involved in an antibiotic biosynthesis is helpful for filling the antibiotic pipelines with libraries of derivatives with increased molecular diversity. These “unnatural” natural products can be generated through genetic manipulations such as mutasynthesis and combinatorial biosynthesis using modular polyketide synthases (PKSs), nonribosomal peptide synthetases (NRPSs), and PKS–NRPS hybrids. The multidomain PKSs and NRPSs showed great utilities for assembling large varieties of building blocks, e.g., Acyl CoAs and amino acids (proteinogenic and nonproteinogenic), respectively, as well as further transformation of the functional groups into novel metabolites (Kirschning et al. 2007; Fischbach and Walsh 2006). Nonetheless, the drawbacks of unpredictable products and poor yields besides the laborious work limit the wide application of these techniques (Li and Vederas 2009).

Medicinal chemistry approaches represent a wide platform for innovative antibiotic design and optimization. No matter whether target structural information is available or not, an appropriate paradigm can be tailored to fit with the available data. Starting from correlating the activity of a homologous series with their physicochemical properties and formulating a quantitative structure–activity relationship (QSAR) equation, design and optimization methods have grown to include the ligand-, fragment-, structure- and *in silico*-based approaches (Abraham and Burger 2003).

Moreover, biophysical methods play a prominent role in drug discovery. Among the applied tools are NMR techniques, e.g., chemical-shift perturbation, STD, NOE, and INPHARMA (Sanchez-Pedregal et al. 2005; Pellecchia et al. 2008), fluorescence-based methods, e.g., fluorescence polarization and FRET (Truong and Ikura 2001; Milligan 2004), MS, SPR (Cooper 2002), ITC (Chaires 2008), and MST (Wienken et al. 2010). Using these techniques in combinations provides detailed information about the mode of ligand binding and improves the process of drug design (Renaud and Delsuc 2009).

Now the question is which design perspective to be adopted? As mentioned above, fitness costs should be carefully considered. Design of an antibiotic that interacts with partially or completely conserved binding site having an essential function in the bacterium is favorable, as mutations in these conserved amino acids highly attenuate the fitness, and thus the propensity of resistance development is reduced. Another attitude is the design of a multiple target antibiotic. Antimicrobial agent that can inhibit two or more different targets in bacteria is less vulnerable to resistance emergence, as the simultaneous multiple mutations required to confer resistance, if occurred, would raise the fitness cost and they are less likely to be compensated (Andersson 2006; Silver 2007; Brotz-Oesterhelt and Brunner 2008). Good examples are fluoroquinolones and the recently discovered natural antibiotic teixobactin. The latter binds to multiple targets in Gram-positive bacteria showing no signs of resistance (Ling et al. 2015).

A completely different strategy is to prevent the pathogenicity of bacteria without inhibiting their growth or survival by antivirulence agents. These substances attenuate the bacterial virulence factors such as motility, adhesion, toxins production, etc. through the interference with the quorum sensing (QS) systems. The QS is a cell-to-cell communication in a population of bacteria via signaling molecules (autoinducers) for gene regulation. Autoinducers are released into the environment proportionally to the cell density. They accumulate until reaching a critical concentration, then they bind to their receptors, at cell surface or intracellular, to form transcriptional factors that regulate gene expression (Defoirdt et al. 2010; O'Connell et al. 2013). The rationale behind this strategy is that in contrast to antibiotics, antivirulence agents should not impose high selective pressure on bacteria, as they do not affect bacterial growth and thus the evolution of resistance is unlikely. Nevertheless, this interesting approach faced some criticism such as the narrow spectrum activity and uselessness in case of immunocompromised population, since it depends on the immune system for clearance of bacteria (Alksne and Projan 2000; Lewis 2013). Furthermore, investigations of the effect on fitness suggested that the emergence of resistance could also occur toward the QS inhibitors (Defoirdt et al. 2010). Indeed, antivirulence-resistant strains were isolated in *P. aeruginosa* (Maeda et al. 2012). Summing up, the interference with QS strategy is in its childhood and many questionable points have to be clarified before reaching the clinical trials as antibiotic surrogates (Lewis 2013; O'Connell et al. 2013).

1.5 Bacterial RNA Polymerase

One of the two bacterial targets I focus on in this thesis is the DNA-dependent RNA polymerase. It is an invaluable antibiotic target for many reasons: RNAP provides bacterial cell with mRNA that is essential for protein synthesis and viability assuring efficacy. In addition, RNAP structure is conserved among bacterial species allowing broad spectrum activity. However, its sequence is distinct from mammalian counterparts warranting therapeutic selectivity (Ho et al. 2009). One more advantage is that the atomic structure of RNAP was identified by X-ray crystallography giving a detailed information about the molecular mechanism of transcription process and more insight into the potential binding sites for designing novel inhibitors. These attractive features motivated many researchers and indeed, several chemical classes from NPs or synthetic were discovered as transcription blockers. The binding pockets for these inhibitors were confirmed by X-ray crystal structures. Interestingly, most of them are in close vicinity to each other (Figure 7) (Ho et al. 2009; Murakami 2015; Bae et al. 2015; Ma et al. 2016).

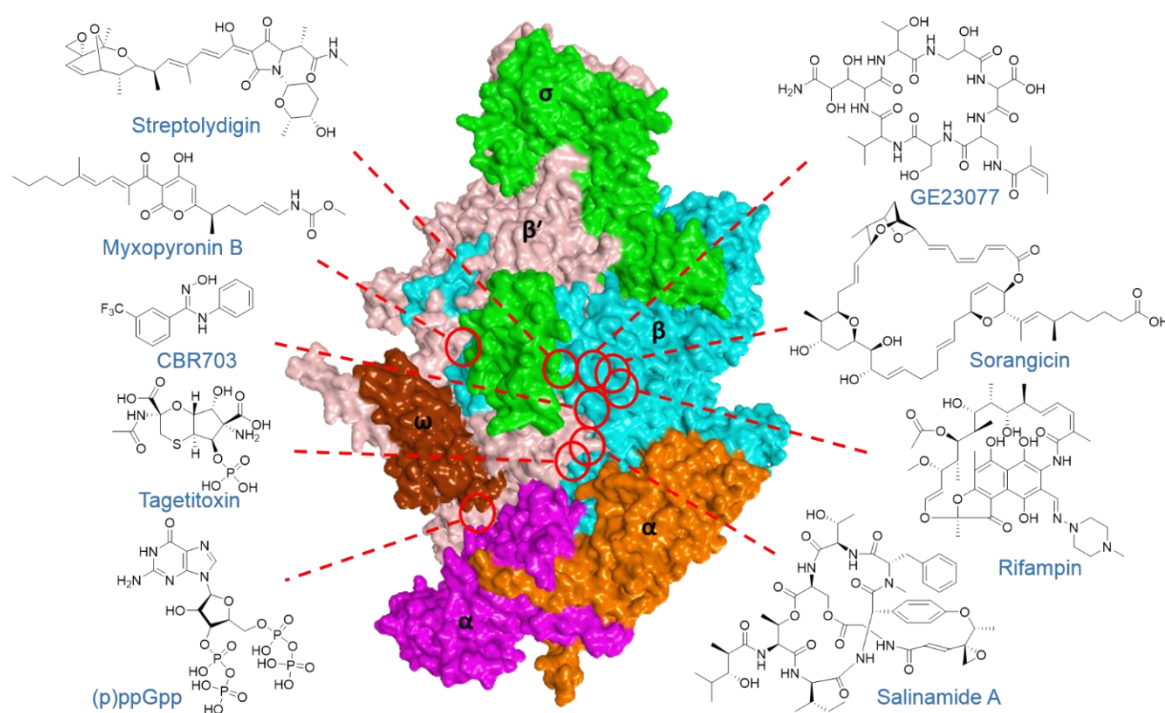


Figure 7. Bacterial RNAP holoenzyme (PDB: 3EQL), and the binding sites for natural and synthetic inhibitors.

Despite these efforts, only two classes were approved for clinical use and serve as proof of principle, namely the rifamycin family for TB infections and the narrow spectrum fidaxomicin for the treatment of *Clostridium difficile*-associated diarrhea (CDAD). This controversy does not humiliate the precious role of RNAP as a bacterial target since this limited number of

successful compounds is mainly attributed to the poor pharmacokinetic and physicochemical properties of the corresponding inhibitors, which are consequently reflected on the *in vivo* efficacy. For example, low membrane permeability (tagetitoxin, salinamide A, and GE23077), tight serum protein binding (myxopyronin, coralloyronin, and ripostatin), cytotoxicity (CBR703), insufficient solubility (myxopyronin and coralloyronin), and chemical instability (myxopyronin, coralloyronin, and ripostatin) (Haebich and Nussbaum 2009; Ma et al. 2016). The critical problem with rifamycins is the development of resistance triggered by mutations in the binding site. Moreover, a cross-resistance occurs against other RNAP inhibitors sharing or overlapping the rifamycins' binding pocket, e.g., sorangicin (Ma et al. 2016). Even worse, these rifamycin-resistant strains show high fitness, due to compensatory mutations, facilitating the rapid prevalence of resistance as mentioned previously in section 1.3 (Comas et al. 2012). As shown above, the structural knowledge about RNAP and its binding sites have not been optimally exploited so far for developing new RNAP inhibitors appropriate for clinical application.

1.5.1 The RNAP “Switch Region”

The overall architecture of core RNAP can be illustrated as a “crab claw” shape. The largest subunits β and β' represent the arms of the claw making a channel or a cleft of 27 Å wide. They are assembled on α subunit dimer at the base of the cleft, where they convene forming the active center. This catalytic site is delineated by Mg^{2+} chelated to three Asp residues from the highly conserved NADFDGD region in β' subunit. At the lower backside of β' subunit, the ω subunit is situated (Figure 7) (Zhang et al. 1999).

Opening of β and β' pincers is a prerequisite for the entrance of DNA strand to the active center cleft and transcription initiation, whereas closure of the claw is important for holding and right positioning of the DNA–RNA hybrid during the elongation phase (Murakami and Darst 2003). A 30° sway of the RNAP clamp (β' pincer) is mediated by a hinge called the “switch region”. This region is composed of five sub-regions (switch 1–5) located at the β – β' interface, distal to the catalytic center and the rifamycins' binding site (Mukhopadhyay et al. 2008).

Recently, the cocrystal structure of the natural antibiotic myxopyronin (Myx) with bacterial RNAP was isolated, and the “switch region” was discovered as its binding site (Mukhopadhyay et al. 2008). Mutagenesis studies in *E. coli* indicated that the “switch region” is also the target of the structurally similar α -pyrone antibiotic coralloyronin as well as the dissimilar macrocyclic lactone antibiotic ripostatin (Mukhopadhyay et al. 2008). The mechanism of action of these antibiotics was proposed to be through “hinge jamming”, i.e.,

locking the RNAP clamp in a closed conformation that prevents entry of double-stranded promoter DNA to the active site cleft and transcription initiation (Mukhopadhyay et al. 2008). Besides being conserved in Gram-positive and Gram-negative bacteria and not conserved in eukaryotic RNAP I, II, and III (allowing a broad spectrum activity and selectivity), the “switch region” would guarantee no cross-resistance with rifamycins or any other RNAP inhibitors owing to the binding sites’ non-proximity (Figure 7) (Mukhopadhyay et al. 2008; Srivastava et al. 2011).

Moreover, studies of the spontaneous resistance frequency to Myx in *S. aureus* showed that although the resistance rate is similar to that of Rif ($4-7 \times 10^{-8}$ per generation), all Myx-resistant strains showed significant fitness costs (4–15% per generation). This was attributed to the vital functions of Myx binding site (the switch region segments SW1 and SW2) in mediating the conformational switches of the RNAP clamp and in binding of DNA. Therefore, mutations in these segments of the “switch region” would reduce the RNAP fidelity and harm the cell viability (Srivastava et al. 2012). Based on the inverse correlation between the fitness costs and prevalence of resistance, these results suggested that Myx resistance would be of low clinical incidence. Furthermore, as the nonzero fitness cost is an authentic feature of the “switch region”, it is not limited to Myx but also would be observed with other RNAP inhibitors targeting the “switch region” (Srivastava et al. 2012). These facts reveal why the “switch region” is a promising binding pocket for molecular intervention.

Accordingly, several attempts to develop synthetic “switch region” inhibitors were performed. Derivatization of Myx delivered an orphan compound (desmethyl myxopyronin B) with better activity against *S. aureus*. Non-surprisingly, no activity against *E. coli* plus inadequate physicochemical properties were encountered like the parent compound (Doundoulakis et al. 2004; Lira et al. 2007).

Following a structure-based *de novo* design, compounds belonging to pyridyl-benzamide scaffold were synthesized and exhibited good RNAP inhibitory activities in the functional assay. However, they displayed no antibacterial effect (McPhillie et al. 2011).

Another group applied a high throughput screening of AstraZeneca corporate compound collection resulting in the squaramides as “switch region” binders. Nonetheless, no activity (>200 μ M) against *S. aureus* and weak antibacterial activity only in the efflux deficient *E. coli tolC* and *H. influenzae acrB* could be attained (Buurman et al. 2012; Molodtsov et al. 2015). Hybridization of Myx α -pyrone core with holothin motif from the RNAP inhibitor holomycin led to enhancement of the hybrid molecules’ hydrophilicity but did not achieve activity against Gram-negative bacteria (Yakushiji et al. 2013).

Using a structure-based pharmacophore model based on Myx-*E. coli* RNAP homology model, a virtual screening of a chemical library (~42,000 compound) was performed. Biological hit validation revealed a compound of 3-ureidothiophene-2-carboxylic acid scaffold with modest activity. Hit optimization improved the activity against RNAP, Gram-positive and the Gram-negative *E. coli tolC* bacteria (Sahner et al. 2013). The binding site of this class was suggested to be the “switch region” as indicated by STD NMR experiments (Fruth et al. 2014).

As indicated above, few chemical scaffolds targeting the “switch region” were discovered with a partial success referring to combined RNAP inhibition and broad antibacterial activities. Thus, the need to discover and further develop novel classes that enrich the chemical diversity of RNAP inhibitors has not been met yet.

1.6 Bacterial Topoisomerases Type IIA

The other validated bacterial targets of main interest in this thesis are DNA gyrase (topoisomerase II) and topoisomerase IV belonging to topoisomerases type IIA subfamily. They are precious antibacterial targets for the following reasons: they are essential for DNA replication and cell division permitting efficacy. They are fundamental elements in all bacterial species allowing a broad spectrum effect. Structurally, they are distinct from their mammalian analogs (DNA gyrase has not even a known counterpart in human) assuring specificity. They possess multiple druggable binding sites for targeting. More importantly, the high sequence homology between DNA gyrase and topoisomerase IV gives the opportunity to inhibit both enzymes simultaneously by a single molecule. Such a dual targeting feature is advantageous regarding lowering the mutation frequency and closing the mutant selection window in order to restrict resistance (Drlica 2003; Bradbury and Pucci 2008).

1.6.1 DNA Gyrase

DNA gyrase is a heterotetramer composed of two GyrA and two GyrB subunits, which are assembled forming the GyrA₂GyrB₂ active holoenzyme (Figure 8). The GyrA subunits harbor the tyrosine containing active site responsible for DNA binding and processing, whereas the GyrB subunits involve the ATP binding sites possessing ATPase activity (Collin et al. 2011). Understanding the process of DNA replication highlights the crucial role of DNA gyrase for bacteria. In order to read the genetic code of the bacterial circular DNA by DNA polymerase, the hydrogen bonded DNA strands are separated by helicase forming the replication fork. As the DNA polymerization progresses, positive supercoiling of the DNA double helix accumulates that should be relaxed in order to proceed. This task is performed by DNA gyrase through cleavage, ATP catalyzed unwinding, and religation of DNA strands (Vos et al. 2011). DNA Gyrase binds covalently, however reversibly, to DNA through a phosphotyrosine bond

between the active site tyrosine in each GyrA protein and a scissile phosphate group at the 5' end of each DNA strand resulting in four base pair staggered nick in DNA. The cleaved strands undergo conformational movement (gate or G-segment DNA), which allow the passage of the other strand (transport or T-segment DNA). Further resealing of the G-segment DNA creates two negative supercoils in the DNA helix (Bax et al. 2010). Noteworthy, DNA gyrase is the unique topoisomerase that can introduce negative supercoils in DNA. Moreover, DNA gyrase is necessary for the transcription process as well. It untangles the positive supercoils generated a head of the translocating RNAP during the elongation stage (Champoux 2001).

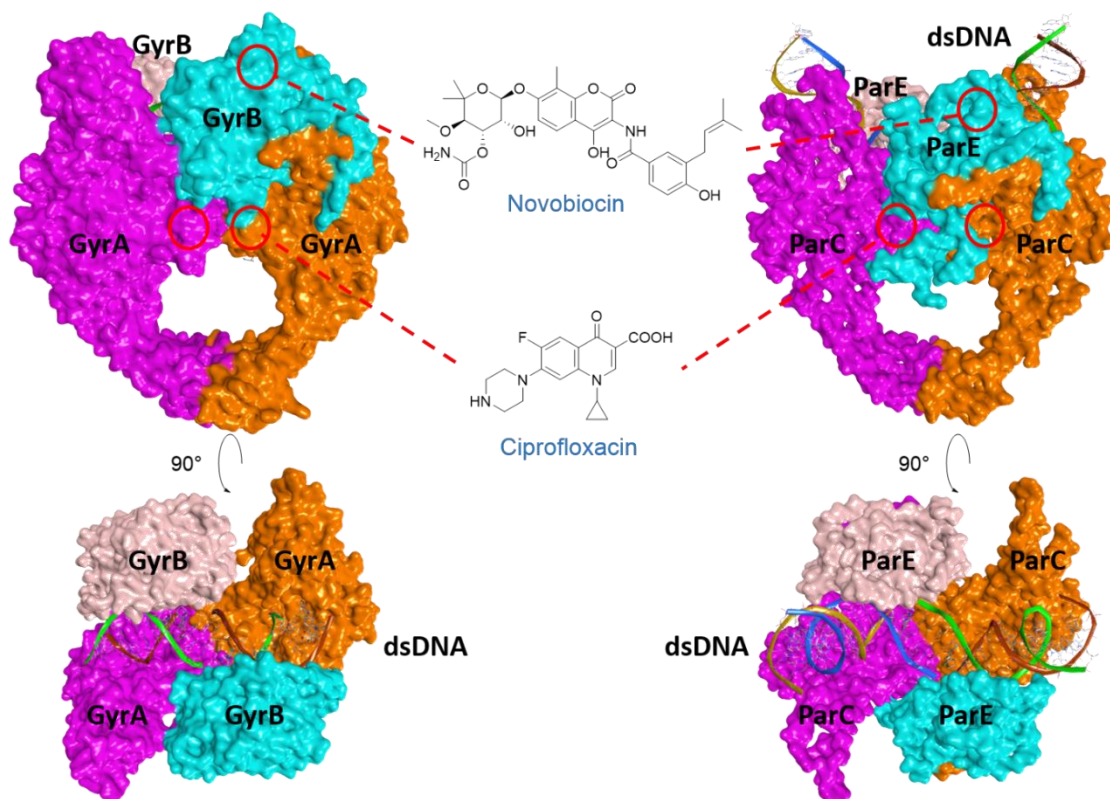


Figure 8. DNA gyrase (left, PDB: 5CDQ), topoisomerase IV (right, PDB: 3FOF), and the binding sites for natural and synthetic inhibitors.

1.6.2 Topoisomerase IV

The general architecture of topoisomerase IV is homologous to DNA gyrase. The heterotetramer is consisted of two ParC and two ParE subunits making the ParC₂ParE₂ active complex (Figure 8). The active site tyrosine is located in the ParC subunit, whereas the ATP binding site is situated in the ParE subunit (Laponogov et al. 2009).

At the end of DNA replication, two interlinked circular DNA molecules are produced (catenanes). Each molecule has one original DNA strand and one new complementary DNA strand. Topoisomerase IV allows the interlinked DNA molecules to come apart (decatenation).

Such a separation of the daughter chromosomes is an essential step for cell division (Laponogov et al. 2009; Veselkov et al. 2016).

1.6.3. Targeting Bacterial Topoisomerases IIA

Inhibitors of bacterial topoisomerases IIA mostly target two major binding sites namely, the ATP binding domain in GyrB and ParE subunits of DNA gyrase and topoisomerase IV, respectively, or the DNA binding domain adjacent to the active site tyrosine in GyrA and ParC subunits of DNA gyrase and topoisomerase IV, respectively (Figure 8).

The natural aminocoumarin antibiotics, e.g., novobiocin and clorobiocin inhibit topoisomerases IIA competitively through binding to the ATPase domain. Consequently, a deprivation of ATP occurs hindering the negative supercoiling and decatenation tasks carried out by DNA gyrase and topoisomerase IV, respectively. Owing to weak activity in Gram-negative bacteria, toxicity, and solubility issues, currently there are no inhibitors of the ATPase domain in clinical use (Collin et al. 2011).

The gold standard for topoisomerases IIA inhibition is the fluoroquinolones, e.g., norfloxacin, ciprofloxacin, and levofloxacin. They bind at the interface between DNA and topoisomerases IIA contiguous with the active site tyrosines, a region also known as the quinolone resistance-determining region (QRDR). Fluoroquinolones trap the DNA–topoisomerases IIA cleaved complexes through blocking the access of the 3'-hydroxyl of the cleaved DNA to the scissile phosphate and thus preventing DNA religation (Bax et al. 2010; Wohlkonig et al. 2010; Chan et al. 2015). Interestingly, the fluoroquinolones' primary target in Gram-negative bacteria is DNA gyrase whereas in Gram-positive species topoisomerase IV is the principal target.

Unfortunately, resistance to fluoroquinolones has emerged via two main mechanisms. First, low accumulation either by reduced gene expression of porins (the fluoroquinolones' gate into bacterial cells), or by overexpression of efflux pumps. Second, target mutation especially in the QRDR. Such mutations usually have an impact on fitness as indicated by a significant increase in doubling time of the fluoroquinolone-resistant *E. coli* mutants in *gyrA* and *parC* genes (Bagel et al. 1999). Similar finding using *Streptococcus pneumoniae* showed that the fitness burdens associated with gene mutations responsible for fluoroquinolone resistance are considerably high. This could account for the steady low frequency of fluoroquinolone-resistant pneumococci in US. However, resistant mutants displaying no detectable fitness costs are found too in the same study (Rozen et al. 2007).

Recently, new natural antibiotics were discovered exhibiting broad spectrum activity, e.g., cystobactamids (Baumann et al. 2014) and albicidin (Kretz et al. 2015). Their target is probably the DNA gyrase with a similar mode of action to that of fluoroquinolones. Such

compounds could be promising new chemical scaffolds to contend with the rebellious resistance problem.

1.7 Molecular Similarity and Drug Design

Finding relationships among biologically active molecules is a property of medicinal chemistry. Recognition of the similarities among these molecules could provide new clues for drug design and help better understanding of the antibiotic mode of action and mechanism of resistance. The following examples illustrate the utility of molecular similarity in the field of antibacterial drug discovery.

1.7.1 Protein Similarity

Generally, proteins having similar sequences are considered to possess similar structures. On this basis, the three dimensional structures for many sequence identified proteins were constructed by the homology or comparative modeling using a known crystal structure of protein with >30% sequence identity as a template. Such models enabled the structure based design approach for inhibitors of difficult crystallizable targets, e.g., membrane bound proteins (Schwede 2003; Cavasotto and Phatak 2009).

On the level of AMR, the high structural homology between DNA gyrase and topoisomerase IV, for example, is beneficial allowing the fluoroquinolones to inhibit both enzymes effectively and thereby having less frequent potential toward resistance development.

1.7.2 Binding Site Similarity

When binding sites in different bacterial enzymes are closely related structurally and/or functionally, it is an attractive opportunity to medicinal chemists for developing a multiple target inhibitor with a minimized risk of target-mediated resistance. A good representative is the topoisomerase IIA inhibitor novobiocin that binds to the ATP binding sites in DNA gyrase GyrB subunit and topoisomerase IV ParE subunit in a similar fashion (Skedelj et al. 2011).

Another interesting instance is the mechanistic function likeness and the common hydrophobic molecular surface, albeit the non-conserved sequence, between the bacterial RNAP “switch region” and the HIV-1 NNRTI binding pocket (Mukhopadhyay et al. 2008). Rational exploitation of these worthy facts could establish for a novel design concept of dual acting anti-infectives for the treatment of HIV-1 and the concomitant bacterial infections.

1.7.3 Substrate–Inhibitor Similarity

Structural analogy between a certain enzyme substrate and the corresponding inhibitor resulting in a disruption of the enzymatic function is a well-established mechanism of antibiotic action. Two previously mentioned examples: The first is the structural closeness of β -lactams to the substrate sequence D-Ala-D-Ala enabling to inhibit PBP and peptidoglycan

synthesis (Figure 3). The second example is the folate biosynthesis inhibition through PABA substrate mimicry by sulfonamides (Figure 4).

1.7.4 Small Molecule Similarity

The premise of molecular similarity, i.e., similar compounds should have similar properties, has been widely employed in drug discovery for ligand-based virtual screening, prediction of pharmacokinetic (ADMET) profile, and estimation of physicochemical properties (Bender and Glen 2004).

Nonetheless, similarity is subjective. Therefore, assigning compound A to be similar to compound B should denote from which aspect and to which extent. For similarity assessment, three components are required. First, the reference compound of known activity or physicochemical property. Second, molecular representation (descriptor) to characterize the analyzed molecules for example by topology (2D), shape (3D), or pharmacophoric features (polar/nonpolar, positively/negatively charged, H-bond donor/acceptor, aromatic/nonaromatic hydrophobic, etc.). A very popular means for molecular expression is the fingerprint. Molecular fingerprint is a binary- or bit string of values 1 or 0 standing for the presence or absence of a certain fragment or feature in the molecule. Third, a similarity coefficient to quantify the degree of likeness between the reference structure and the compared compounds. The most widespread similarity metric is Tanimoto or Jaccard coefficient, which is calculated from the equation $Tc = \frac{c}{a + b - c}$ where a and b are the number of bits in compounds A and B fingerprints, respectively, c is the number of common bits. Tanimoto coefficient values range from zero (no common bits, i.e., non-similar compounds) to one (all bits are the same, i.e., similar molecules) (Willett 2006).

The other way around, dissimilarity can be derived by Soergel distance: $Sg = 1 - Tc$. Identification of dissimilar molecules is desired for chemical diversity enrichment (Nikolova and Jaworska 2003; Maggiora et al. 2014).

Noteworthy, similarity analysis should be handled carefully, i.e., similar molecules should not necessarily have similar bioactivities. As calculated similarities depend on the type of fingerprint used and its relevance to the biological activity (Nikolova and Jaworska 2003). Another point, this similarity ranking is defined for the molecules solely regardless of the interacting milieu. In fact, molecular similarity depends on extrinsic factors above all the target protein (Bender and Glen 2004).

To sum up, utilization of molecular similarity/diversity in an intelligent manner can provide new solutions for the stubborn AMR problem.

2 Aim of the Thesis

Antimicrobial resistance is rapidly mounting in Europe and all over the world. On the other side, the antibiotic pipelines are almost vacant and pharmaceutical companies steadily withdraw from the antibiotic development arena. This gloomy situation necessitates a prompt reaction from all public health sectors to preclude an imminent nightmare of resistance prevalence.

Development of novel antibiotics less prone to AMR is a fundamental solution to the current crisis. In this context, I resume the words of the Infectious Diseases Society of America in its 10 × '20 initiative for a global commitment to develop 10 new antibacterial drugs by 2020: *“As a global society, we have a moral obligation to ensure, in perpetuity, that the treasure of antibiotics is never lost and that no infant, child, or adult dies unnecessarily of a bacterial infection caused by the lack of effective and safe antibiotic therapies.”* (Infectious Diseases Society of America 2010).

Accordingly, the aim of my thesis is to discover and develop novel chemical classes of antibiotics capable of slowing down the resistance rate of pathogenic bacteria. To achieve this goal, I followed two strategies targeting the vital DNA replication and transcription machineries in bacteria.

The first approach is the development of RNAP inhibitors targeting the “switch region” binding site. Inspired by the 3-ureidothiophene-2-carboxylic acid class of transcription inhibitors (Sahner et al. 2013), new classes with various chemical scaffolds are prepared by regioisomers design as well as bioisosteric replacement of the thiophene core by different heterocyclic nuclei in order to enlarge the chemical space of RNAP inhibitors. A comprehensive evaluation of the frontrunners is performed including the antibacterial activity, cross-resistance with rifampicin, rate of resistance, effect of permeability enhancers and efflux pump inhibitors, and cytotoxicity to human cells.

In an advanced step, I would make use of the known mechanistic similarity between the bacterial target (RNAP “switch region”) and the viral target (NNRTI binding pocket) to develop dual acting anti-infectives against bacteria and the AIDS pathogen HIV-1 as well. Precisely, the newly synthesized classes of RNAP “switch region” inhibitors together with the parent thiophene class are screened for the viral reverse transcriptase inhibition. Afterwards, a structure-based optimization for the best class with dual inhibitory activity is pursued. A concurrent study of structure–activity relationships would illuminate the key structural features for further activity enhancement. In addition, the dual inhibitors’ mechanism of action

against RT is investigated. Worth mentioning, HIV cases in Europe increased by 80% in 2013 compared to 2004 (WHO 2014). This alarming situation necessitates innovative strategies for developing a future antiretroviral therapy. Realization of such dual acting antimicrobial agents could be a new hope for HIV patients that are always susceptible to bacterial co-infection.

The second approach is the development of DNA gyrase and topoisomerase IV inhibitors based on the recently discovered natural antibiotics “cystobactamids” isolated from *Cystobacter* sp. (Baumann et al. 2014). The low yield fermentation and the laborious total synthesis impede the improvement of this promising family of antibiotics. Wherefore, I am concerned with not only improving the topoisomerases IIA inhibition, antibacterial activity, and relevant pharmacokinetic properties, but also establishment of a short and efficient synthetic strategy facilitating the rapid access to diverse cystobactamids/analogs. For optimization of DNA gyrase inhibitory activity, an interactive ligand-based design is applied. Besides, conclusion of the structure–activity relationships for upgrading structure and activity as well. Furthermore, a study of the cystobactamids’/analogs’ mode of action is accomplished. My rationale has the following merits: development of broad spectrum antibiotics with high selectivity toward bacteria by choosing conserved targets in bacteria (RNAP and DNA topoisomerases) but are different from (RNAP) or with no counterpart in human (DNA gyrase). Notably, the designed objective compounds have brand new chemical scaffolds that are different from those of other known antibiotics, thus the risk of cross-resistance should be unlikely. Finally, a low rate of resistance development can be achieved by hitting either an indispensable binding site with pivotal function (the “switch region”, where mutations highly affect bacterial fitness and compensatory mutations are helpless), or similar binding sites in multiple targets (DNA gyrase and topoisomerase IV). Together these approaches can give human the upper hand to win the restless race against resistant bacteria.

3 Results

3.1 Expanding the Scaffold for Bacterial RNA Polymerase Inhibitors: Design, Synthesis and Structure Activity Relationships of Ureido-Heterocyclic-Carboxylic Acids

Reprinted with permission from Elgaher, W. A. M.; Fruth, M.; Groh, M.; Haupenthal, J.; Hartmann, R. W. *RSC Adv.* 2014, 4, 2177–2194.

Copyright 2014 Royal Society of Chemistry.

<http://pubs.rsc.org/en/Content/ArticleLanding/2014/RA/C3RA45820B#!divAbstract>

(Publication I)

Abstract

The emergence of bacterial resistance requires the development of new antibiotics with alternative mode of action. Based on class I, developed in our previous study, a new series of RNA polymerase (RNAP) inhibitors targeting the switch region was designed. Feasible synthetic procedures of the aryl-ureido-heterocyclic-carboxylic acids were developed including three regioisomeric thiophene classes (II–IV), as well as three isosteric furan (V, VI) and thiazole (VII) classes. Biological evaluation using a RNAP transcription inhibition assay revealed that class II compounds possess the same activity as the parent class I, whereas classes III, V–VII were active, however with lower potency. Structure activity relationship (SAR) studies, supported by molecular modeling, elucidated the structural requirements necessary for interaction with the binding site. Beside the RNAP inhibitory effects, the new compounds displayed good antibacterial activities against Gram positive bacteria and the Gram negative *E. coli* TolC strain. Moreover, they showed no cross resistance with the clinically used RNAP inhibitor rifampicin (Rif) and a lower rate of resistance compared to Rif.

Introduction

The eternal battle against pathogenic bacteria demands the discovery and development of new weapons aiming vital targets, since the prevalence of antibiotic resistance poses a real threat to human health.^{1,2} Bacterial RNAP is a multisubunit enzyme responsible for transcription.³ It is necessary for cell survival allowing efficacy, and structurally distinguished from eukaryotic counterparts affording therapeutic selectivity.⁴ However, the only clinically used drugs targeting RNAP are the rifamycins which are applied to treat *Mycobacterium tuberculosis* infections, and the recently FDA approved Fidaxomicin for *Clostridium difficile* infections.⁵ Hence, while proven as a drug target, RNAP is still underexploited. Our mission is to discover and optimize RNAP inhibitors with an alternative binding site compared to rifamycins, and consequently, with low probability of cross resistance. Recently the “switch region”, a binding pocket distinct from the rifamycins binding site, was discovered and proved to be a promising target site for antibacterial drug discovery.^{6–8} The RNAP inhibitors myxopyronin B (Myx B), a natural α -pyrone antibiotic isolated from the myxobacterium *Myxococcus fulvus*,⁹ and its synthetic derivative desmethyl myxopyronin B (dMyx B),¹⁰ have been identified to bind to the “switch region”.^{6,7} Although the myxopyronins are highly active in vitro and show no cross resistance to rifamycins,^{6,11,12} their clinical application is hampered by inadequate physicochemical properties.¹³

These facts motivated us and other research groups to develop novel “switch region” inhibitors. McPhillie *et al.* used a structure based *de novo* design based on the crystal structure of the dMyx B binding site. Although the compounds inhibited RNAP, they displayed no antibacterial activity.¹⁴ Buurman *et al.* applied a high throughput screening, identified RNAP inhibitors and confirmed the switch region as their target site. However, they showed only weak antibacterial activity.¹⁵ Yakushiji *et al.* pursued a hybrid strategy, combining the core α -pyrone of Myx with holothin. The resulting RNAP inhibitor was active against Gram positive bacteria.¹⁶

In a previous work of our group, based on a hit candidate discovered by virtual screening, a series of 5-aryl-3-ureidothiophene-2-carboxylic acids (class I) was synthesized and optimized based on SAR studies. Moreover, the binding mode was experimentally validated. The compounds showed good antibacterial activities accompanied by a low resistance frequency (Fig. 1).¹⁷

In this work, we focused on finding new chemical scaffolds inspired from class I with better or at least retained biological activities. To achieve this goal, we followed an analog design

strategy accompanied by SAR exploration (Fig. 1). The study was supported by molecular modeling to gain deeper insights into the structural features necessary for activity.

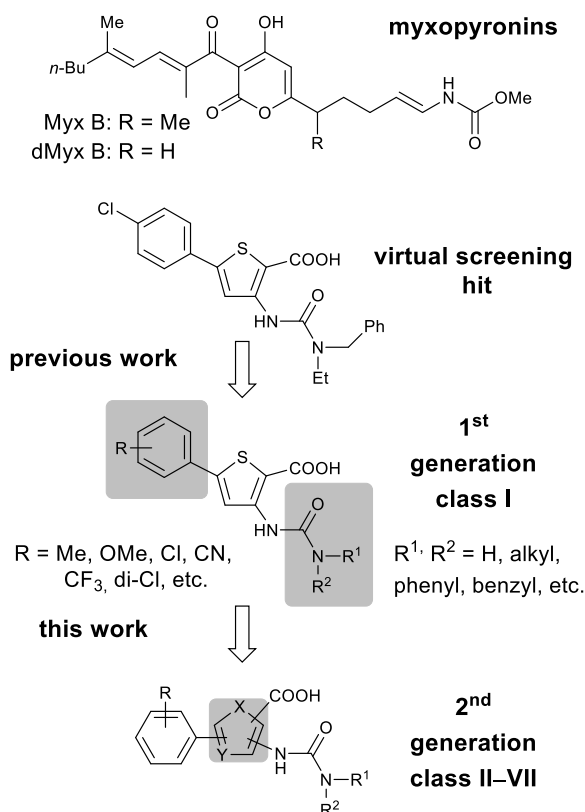


Fig. 1 Development of second generation bacterial RNAP inhibitors of the ureido-heterocyclic-carboxylic acid type.

Results and discussion

Design strategy

Analog design was accomplished through two approaches: *via* design of regioisomers of the parent class I, and *via* bioisosteric exchange of the heterocyclic core. By reversing the positions of ureido and carboxyl substituents of class I (class II), shifting the aryl position in class I (class IV), or shifting the aryl position in class II (class III), three classes of regioisomers were initially investigated to identify the optimum configuration of the aryl-ureido-thiophene-carboxylic acids for interaction with the target enzyme (Fig. 2). Based on our previous results,¹⁷ as aryl motif phenyl rings bearing substituents with high π and σ values, namely 4-chlorophenyl and 3,4-dichlorophenyl, were chosen. It was also shown that at the ureido motif hydrophobic and bulky substituents are preferred, therefore *n*-hexyl, benzyl and *N*-ethylbenzyl amine were employed. In the next step, the biological results of classes I–IV were taken into consideration. Based on classes I and II, displaying the highest RNAP inhibitory activity, the classical isosteric ring equivalents –O– for –S– (classes V and VI) or –N= for –CH= (class VII) were investigated (Fig. 2).

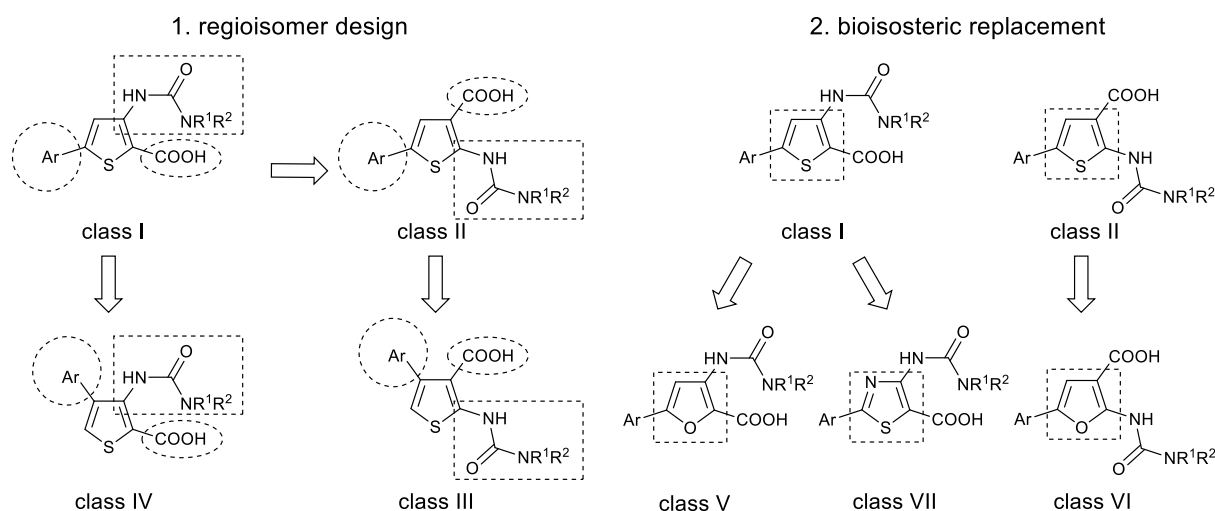
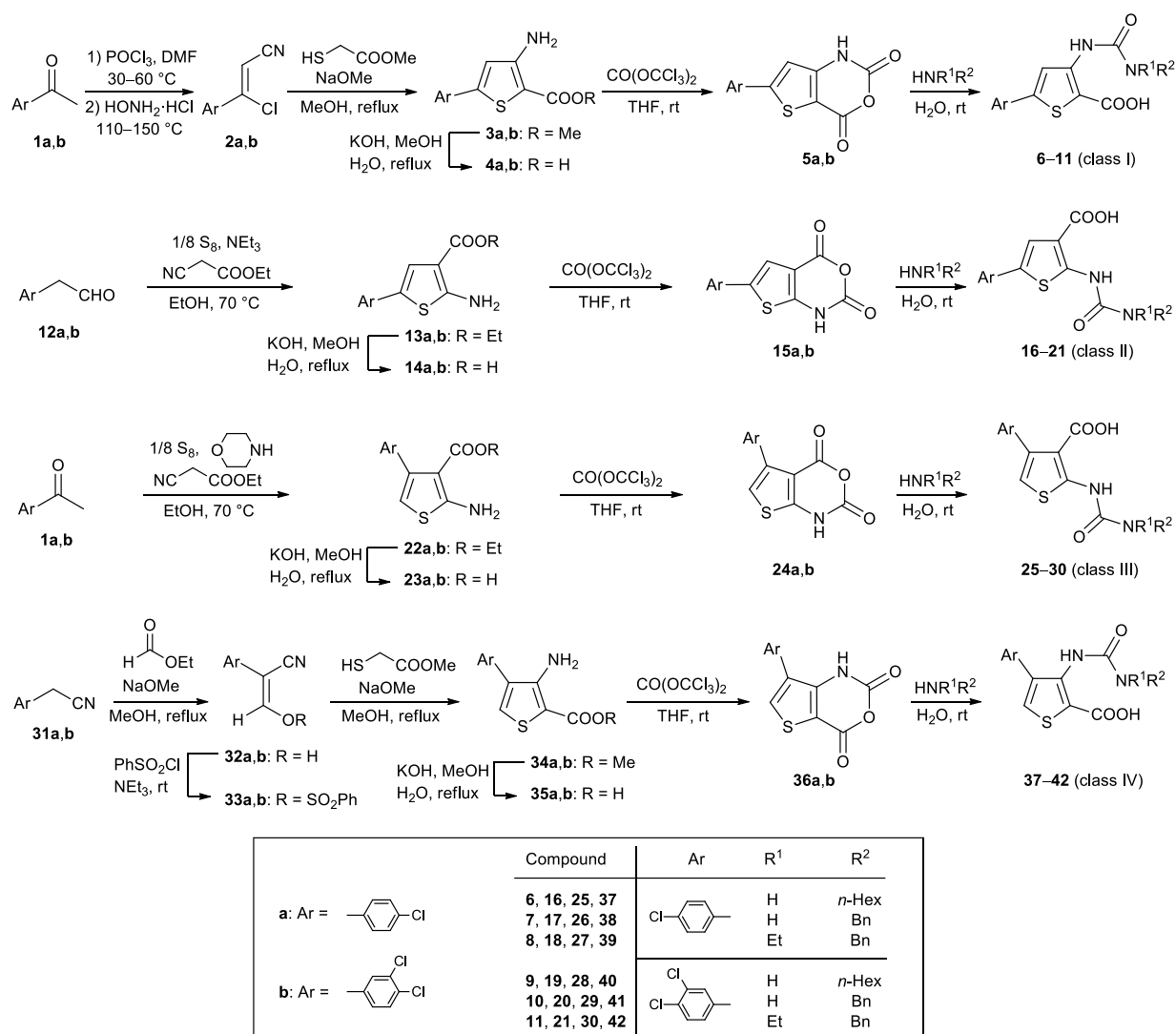


Fig. 2 Analog design strategies based on the parent class I.

Chemistry

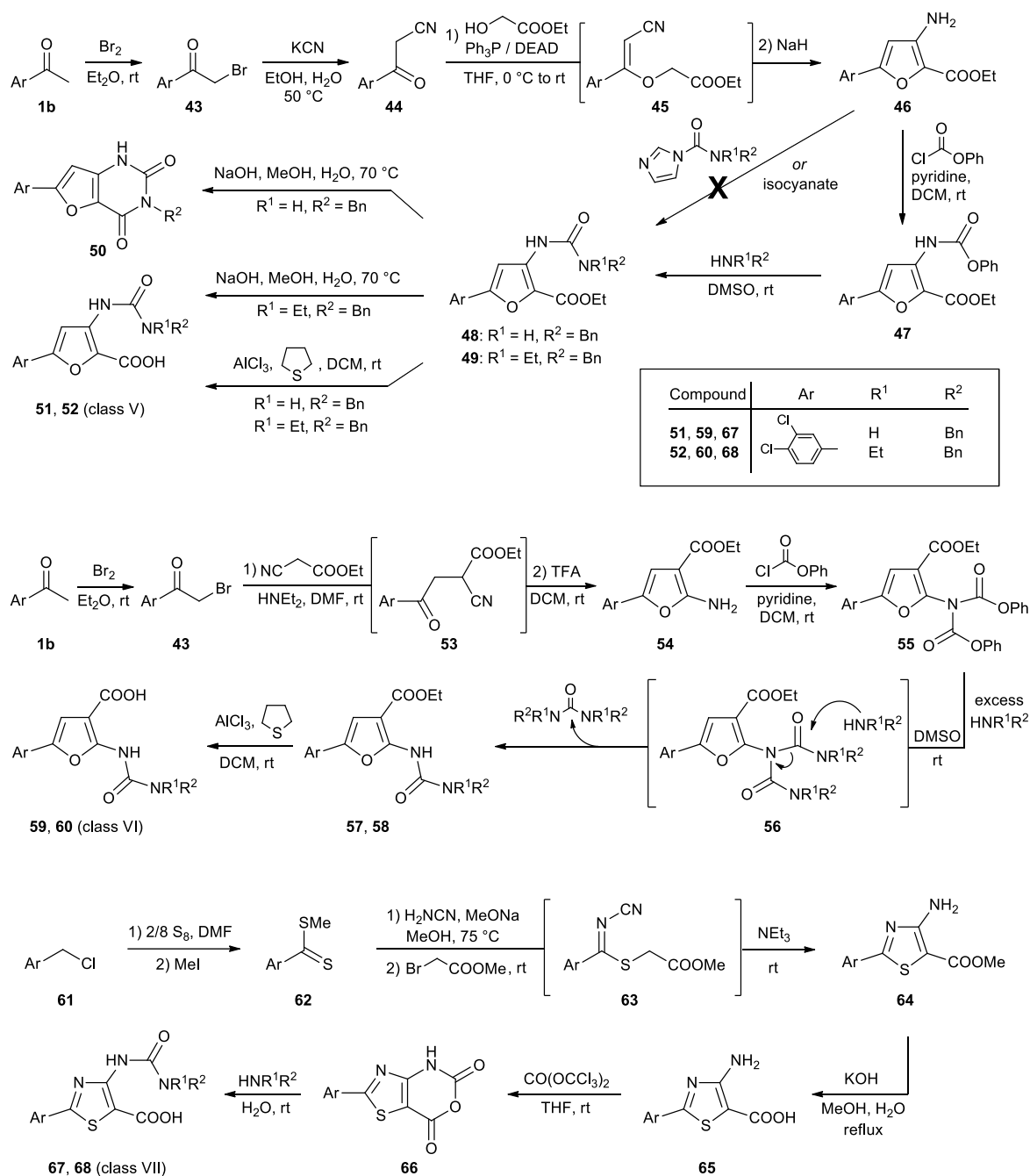
The synthesis of compounds **6–11** (class I) started by reacting the acetophenones **1a,b** (Scheme 1) with POCl₃ in DMF followed by NH₂OH·HCl according to a modified Vilsmeier-Haack-Arnold reaction¹⁸ to give the β-chlorocinnamionitriles **2a,b** which were cyclized using methyl thioglycolate under basic condition (NaOMe) to afford the methyl 5-aryl-3-aminothiophene-2-carboxylates **3a,b**.^{17,19} Esters were saponified to the corresponding acids **4a,b** which were treated with triphosgene to form the thiaisatoic anhydrides **5a,b**. The latter reacted with the appropriate amines in water followed by acidic workup to yield the desired 5-aryl-3-ureidothiophene-2-carboxylic acids **6–11**.^{17,20,21} The compounds of classes II and III were synthesized by a straightforward procedures *via* Gewald reaction of the arylacetaldehydes **12a,b** or the acetophenones **1a,b** (Scheme 1) with ethyl cyanoacetate and elemental sulfur under basic conditions in a one-pot reaction to afford the ethyl esters **13a,b** and **22a,b**.^{22,23} respectively. After saponification, synthesis of both the 5- and 4-aryl-2-ureidothiophene-3-carboxylic acids **16–21** and **25–30** *via* the thiaisatoic anhydrides **15a,b** and **24a,b** was also successfully employed as described for the class I derivatives. The synthesis of compounds of class IV was achieved by treating the arylacetonitriles **31a,b** (Scheme 1) with ethyl formate in presence of NaOMe, followed by acidic workup to furnish the 2-aryl-3-hydroxyacrylonitriles **32a,b**.^{24–26} Ring closure was accomplished by activation of **32a,b** using benzenesulfonyl chloride to yield the sulfonates **33a,b** which reacted with methyl thioglycolate under basic condition to produce the methyl 3-amino-4-arylthiophene-2-carboxylates **34a,b**.²⁶ Further synthetic steps *via* the thiaisatoic anhydrides **36a,b** proceeded smoothly to deliver the desired 4-aryl-3-ureidothiophene-2-carboxylic acids **37–42**.



Scheme 1 Synthesis of compound classes I–IV.

For the synthesis of compounds **51** and **52** (class V), acetophenone **1b** (Scheme 2) was converted to the β -ketonitrile **44** *via* bromination²⁷ and subsequent nucleophilic substitution using KCN.^{28,29} Compound **44** was further reacted under Mitsunobu conditions³⁰ with ethyl glycolate to the intermediate vinyl ether **45** that was cyclized under basic condition (NaH) to yield the ethyl 3-aminofuran-2-carboxylate **46**. We initially attempted to adopt the “isatoic anhydride strategy” for the furan class as described for synthesis of the ureidothiophene analogs. Unfortunately, the required 3-aminofuran-2-carboxylic acid could not be obtained. Various conditions for alkaline hydrolysis of the ester **46** led to decomposition of the furan ring, and a ring opening product was isolated. This observation is attributed to the unusual instability and weak aromatic properties characterizing the aminofurans.^{31–33} Therefore, we decided to postpone the hydrolysis to the end of the synthesis as the ureido-furan derivatives

are less electron rich and should be less prone to decomposition.³⁴ To prepare the urea derivatives, compound **46** was treated directly with the carbamoylimidazoles³⁵ or isocyanate³⁶ but no conversion was observed. Finally, an alternative route *via* the phenyl carbamate **47** followed by nucleophilic substitution with the appropriate amines³⁷ gave the desired ureido-furan-carboxylic esters **48** and **49**. The hydrolysis to the free acids proceeded smoothly under basic condition for the *N*-benzyl-*N*-ethylurea derivative **49** to afford **52**, but for the *N*-benzyl derivative **48** cyclization yielding the uracil derivative **50** occurred. Therefore, non-saponificative, mild dealkylation was conducted using AlCl₃ in tetrahydrothiophene (THT)³⁸ affording the desired carboxylic acid **51**. The synthesis of the regioisomeric furan system class VI proceeded *via* coupling of the phenacyl bromide **43** (Scheme 2) with ethyl cyanoacetate to give the intermediate **53** that was cyclized under acidic condition (TFA) to deliver the 2-aminofuran-carboxylic ester **54**. Interestingly, reaction of **54** with phenyl chloroformate afforded only the diacylated product **55** even when a stoichiometric amount of reagent was used. This is consistent with previous findings regarding the reactivity of 2-aminofurans.³⁹ The subsequent transformation into the urea derivatives **57** and **58** required an excess of the amine to eliminate the second carbamoyl group from the intermediate **56**. Finally, the acids **59** and **60** were obtained by dealkylation using AlCl₃ in THT. The thiazole class VII was prepared starting from the benzyl chloride **61** (Scheme 2) that was reacted with elemental sulfur and alkylated with methyl iodide to give the carbodithioate **62**. For the ring closure, **62** was first reacted with cyanamide in basic medium (NaOMe) and further *S*-alkylated with methyl bromoacetate to give the intermediate **63** that was cyclized under basic conditions affording the 4-aminothiazole ester **64**. After alkaline hydrolysis, the acid **65** was converted to the thiazoloisatoic anhydride **66**. This intermediate reacted in the same manner as described for the thiophene derivatives to the ureidothiazole carboxylic acids **67** and **68**.



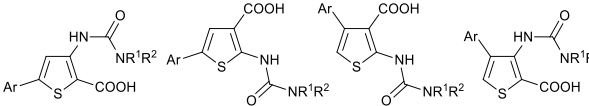
Scheme 2 Synthesis of compound classes V–VII.

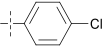
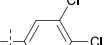
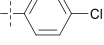
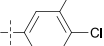
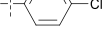
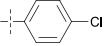
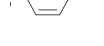
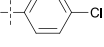
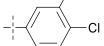
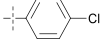
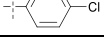
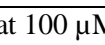


In vitro RNA polymerase inhibitory activity

Compounds of classes I–VII were tested for their inhibitory activity against *E. coli* RNAP and the results are shown in table 1. Generally compounds with 3,4-dichloro substituents exhibited higher activity than 4-chlorophenyl derivatives in the same class. This finding is in accordance with our previous study of the parent class I.¹⁷ An increase of activity was also observed with substituents having larger hydrophobic volume at the ureido motif with the general trend benzylethyl ~ *n*-hexyl > benzyl. Compounds of class II showed RNAP inhibitory activities as good as the parent class I. Interestingly, the 3,4-dichloro derivatives **19–21** (IC₅₀: 18, 43, and

21 μM respectively) showed identical activities to their analogous compounds **9–11** of class I (IC_{50} : 18, 46, and 22 μM respectively). The class III analogs **28–30** displayed moderate activities (IC_{50} : 75, 84, and 57 μM respectively, about 2–4 fold decrease), while class IV derivatives **40–42** possessed weaker activities (IC_{50} : 74 to >100 μM , >4 fold decrease).

Table 1 In vitro inhibitory activity against *E. coli* RNA polymerase.



Compd	Ar	R ¹ R ²	Inhibition of <i>E. coli</i> RNAP ^a
6		H, <i>n</i> -Hex	68 μM
7		H, Bn	31%
8^b		Et, Bn	75 μM
9^b		H, <i>n</i> -Hex	18 μM
10^b		H, Bn	46 μM
11^b		Et, Bn	22 μM
16		H, <i>n</i> -Hex	14%
17		H, Bn	84 μM
18		Et, Bn	54 μM
19		H, <i>n</i> -Hex	18 μM
20		H, Bn	43 μM
21		Et, Bn	21 μM
25		H, <i>n</i> -Hex	11%
26		H, Bn	n.i.
27		Et, Bn	14%
28		H, <i>n</i> -Hex	75 μM
29		H, Bn	84 μM
30		Et, Bn	57 μM
37		H, <i>n</i> -Hex	n.i.
38		H, Bn	n.i.
39		Et, Bn	n.i.
40		H, <i>n</i> -Hex	74 μM
41		H, Bn	8%
42		Et, Bn	100 μM
51		H, Bn	116 μM
52		Et, Bn	61 μM
59		H, Bn	26%
60		Et, Bn	60 μM
67		H, Bn	48 μM
68		Et, Bn	51 μM
Myx B			0.35 μM
Rif			0.03 μM

^a IC_{50} values (μM) or % inhibition at 100 μM of *E. coli* RNAP; n.i. = inhibition $\leq 5\%$ at 100 μM .

^b previously reported¹⁷

The outstanding role of classes I and II regarding RNAP inhibition can be explained on the basis of molecular similarity, i.e., similar molecules exhibit similar activities.^{40–42} The similarity of classes I–IV was analyzed *in silico* by using molecular fingerprint method, where a graph 3-point pharmacophore (GpiDAPH3) was applied as 2D fingerprint system. As similarity metric the Tanimoto coefficient (T_C) was used.⁴³ Class II showed maximum similarity to I ($T_C = 1.00$), followed by III ($T_C = 0.93$), while IV exhibited low similarity ($T_C = 0.65$). Another similarity assessment *via* flexible alignment of classes I–IV revealed that the aryl, ureido, and carboxyl substituents as well as the thiophene core of I and II are coincided (Figure 3A). Class III also matches except that the carboxyl group is located in the opposite position to that of I and II, whereas neither the ureido nor the carboxyl substituents of IV fit to the configuration of I and II (Figure 3A). Hence class I and II are similar with respect to their configuration in space. Consequently they can assume the same orientation and binding mode, which results in the same inhibitory activities. These results were confirmed by docking of compounds **11**, **21**, and **30** representing classes I–III respectively, in the dMyx B binding site of *T. Thermophilus* RNA polymerase (PDB code 3EQL).⁷ Both **11** and **21** bind to the crescent shape pocket in the same manner (Figure 3B, C). The thiophene core is located at the top of the cavity opening, anchored by hydrogen bond or ion pair interaction of the carboxyl group with the β Lys610 residue. The 3,4-dichlorophenyl moiety occupies the lower part of the enecarbamate binding pocket of dMyx B. The ureido group carrying the lipophilic benzyl and ethyl substituents is located deeply in the hydrophobic pocket occupied by the dMyx B dienone side chain, and stabilized by CH- π interaction with β Leu1088 as well as an intramolecular hydrogen bond with the carboxyl group. On the other hand compound **30** (class III) binds mainly through CH- π interaction between the lipophilic substituted ureido moiety and β Leu1088, but lacks the interaction with β Lys610, as the carboxyl group is oriented in the opposite direction (Figure 3D). Accordingly, a lower inhibitory activity of **30** (IC_{50} : 57 μ M) in comparison with compounds **11** or **21** (IC_{50} : 22 μ M, 21 μ M) was observed.

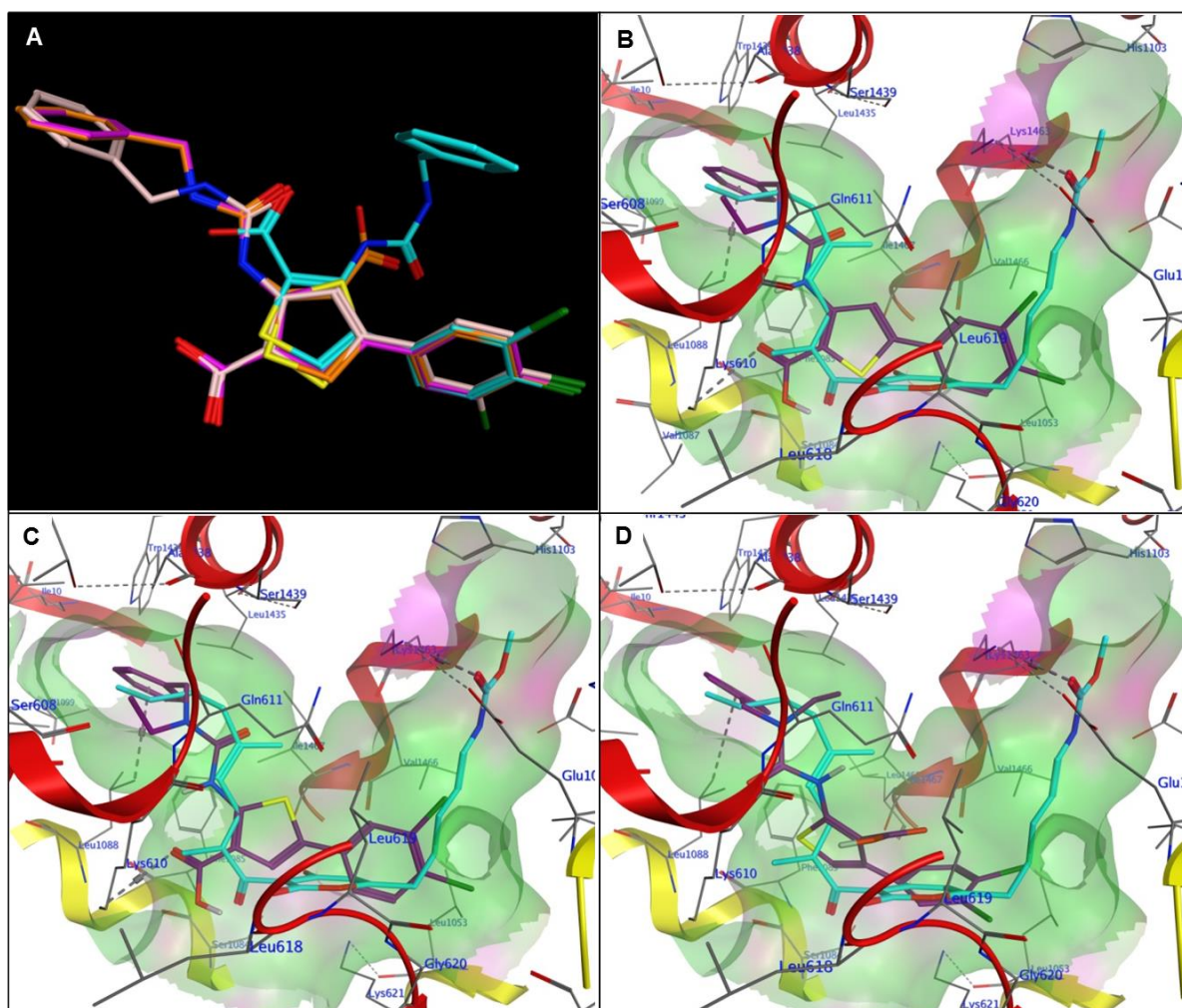


Fig. 3 (A) Flexible alignment of compounds **10** (white), **20** (magenta), **29** (orange), and **41** (turquoise). (B) Docking pose of compound **11** (violet) in the dMyx B (turquoise) binding site: hydrophobic surface (green), polar surface (pink), β chain (yellow), β' chain (red). (C) Docking pose of **21** (violet). (D) Docking pose of **30** (violet).

The effect of exchanging the heterocyclic core on the RNAP inhibitory activity was studied for compounds of classes V–VII. The results revealed that both of the furan classes V and VI displayed about a threefold decrease in activity compared to the corresponding thiophene analogs (class I and II), whereas the thiazole class VII exhibited only a slightly lowered potency (Table 1). By replacement or introduction of hetero atoms the electronic properties as well as the size of the ring is influenced and both effects can have an impact on the affinity to target. The latter is more likely to be responsible for the observed differences in activity. The ring size influences interatomic distances, bond angles, and determines the overall shape of the ligand.⁴⁴ According to the observed activities, thiophene is obviously most appropriate to keep the aryl, ureido, and carboxyl functionalities in the optimal geometry necessary for binding to the target enzyme. This is reflected by the relationship of the angle (α) between the

aryl and ureido substituents and RNAP activity (pIC_{50}) for classes I–VII (Figure 4). A parabolic curve was obtained, with the optimum range for α between 150 and 159° (classes I, II, and VII located at the maximum). The observed exception for class III ($\alpha = 156^\circ$) can be explained by the different localization of the carboxyl group leading to a reduced binding affinity as discussed above.

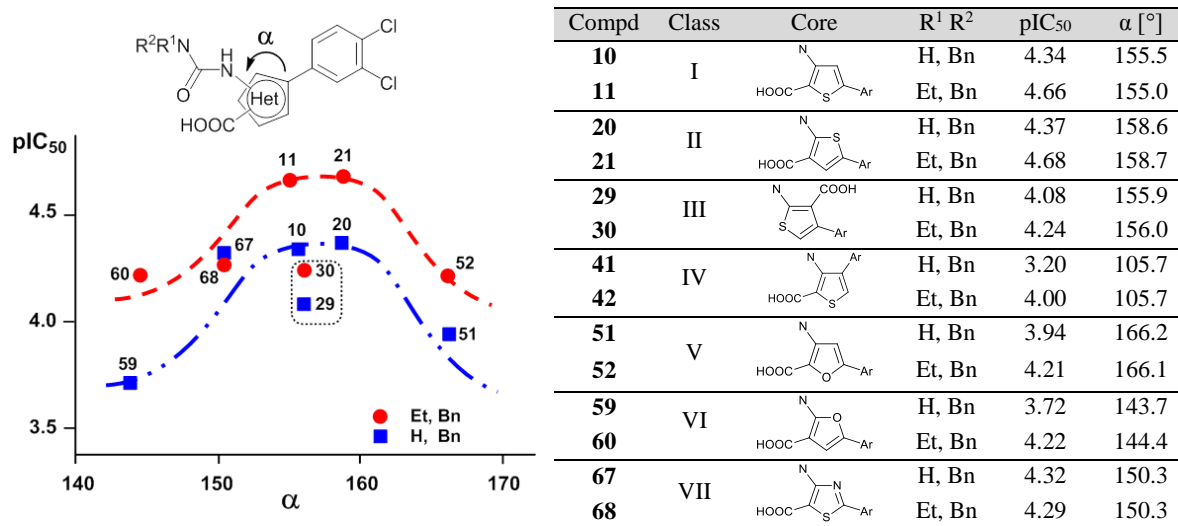


Fig. 4 Relationship between RNAP inhibitory activity (pIC_{50}) and angle α .

Antibacterial activity

To explore the antibacterial spectrum of our RNAP inhibitors, eight compounds representing the most active classes were selected. Compounds with *n*-hexyl substituents were excluded due to solubility problems. The antibacterial activities were evaluated in the Gram positive *B. subtilis* and *S. aureus*, as well as in the Gram negative strains *E. coli* K12, *P. aeruginosa*, *E. coli* TolC, a mutant deficient in the AcrAB-TolC efflux system, and two Rif-resistant *E. coli* TolC mutants and are expressed as minimal inhibitory concentrations (MIC) values. As reference compounds Myx B and Rif were used (Table 2). It was found that the compounds possess antibacterial activities against the Gram positive strains. Regarding the Gram negative bacteria with the exception of *E. coli* TolC, compounds were not active similarly to Myx B. It is noteworthy that the antibacterial activity against *S. aureus* is well correlating with the RNAP inhibitory activity, whereas in case of *B. subtilis* and *E. coli* TolC the correlation was less pronounced. Similar discrepancies between RNAP inhibition and MIC values are also observed for Myx B and Rif (Table 2), and have been frequently reported.^{17,45,46} In the experiments with the Rif-resistant strains all of the five tested compounds representing different classes showed no reduction of antibacterial activity compared to the normal *E. coli*

TolC strain. This demonstrates that there is no cross resistance with Rif as it has been expected due to the different binding sites.

Table 2 Antibacterial activities of selected aryl-ureido-heterocyclic-carboxylic acids.

Compd	IC ₅₀ RNAP (μ M)	MIC ₉₅ (μ g/mL) ^a						
		<i>S. aureus</i>	<i>B. subtilis</i>	<i>E. coli</i> TolC	<i>E. coli</i> TolC β Q513L ^b	<i>E. coli</i> TolC β H526Y ^b	<i>E. coli</i> K12	<i>P. aeruginosa</i>
11	22	8	11	14	14	16	>25	>25
18	54	20	5	11	-	-	>25	>25
21	21	10	2	10	7	9	>25	>25
29	84	80	15	10	-	-	>100	>100
30	57	23	6	7	7	7	>100	>100
52	61	33	12	30	25	25	>50	>50
60	60	28	14	>50	-	-	>50	>50
68	51	36	45	47	50	50	>50	>50
Myx B	0.35	0.5	1	1	1	1	>25	>25
Rif	0.03	0.02	5	6	>100	>100	7	13

^a > MIC determination was limited due to insufficient solubility of the test compound.

^b Rif-resistant *E. coli* TolC strains with mutations in the *rpoB* gene encoding for the RNAP β subunit.

Role of cell wall penetration and drug efflux for antibacterial activity in *E. coli* strains

Considering the facts that RNAP is highly conserved in bacteria,³ and our compounds were active against Gram positive strains as well as *E. coli* TolC, but not against Gram negative bacteria, the most likely conclusion to be drawn is that they are unable to accumulate in the cytoplasm to inhibit RNAP. This could be due to cell wall impermeability, i.e., slow diffusion through porins or the outer membrane (OM) lipid bilayer, efflux mechanisms or both. The observed activity in the TolC mutant lacking the OM part of the tripartite efflux machinery gives a strong hint that efflux plays a prominent role for our compounds. To verify this hypothesis and to get a better understanding of their uptake pathway, the antibacterial effect for selected compounds was determined in presence of the OM permeability enhancer polymyxin B nonapeptide (PMBN)⁴⁷ or the efflux pumps inhibitor PA β N.^{48,49} MIC values were determined against *E. coli* TolC, *E. coli* D22 (LPS mutant with increased OM permeability) and *E. coli* K12 (intact cell wall system) and are shown in table 3.

Table 3 Effect of PMBN and PA β N on antibacterial activities of selected aryl-ureido-heterocyclic-carboxylic acids.

Compd	<i>E. coli</i> TolC			<i>E. coli</i> K12		<i>E. coli</i> D22		
	MIC ₉₅ ^a	MIC ₉₅	MIC ₉₅	MIC ₅₀	MIC ₅₀	MIC ₅₀	MIC ₅₀	
		+ PMBN (1 μ g/mL)	+ PA β N (10 μ g/mL)		+ PMBN (1 μ g/mL)		+ PA β N (20 μ g/mL)	+ PA β N (20 μ g/mL)
11	14	7	1	>25	>25	>25	>50	>25
21	10	4	1	>25	>25	4	>25	12
30	7	5	1	>100	>100	18	40	15
52	30	11	6	>50	>50	>50	>100	49
68	47	22	4	>50	>50	>50	>50	>50

^a MIC values in μ g/mL.

PMBN produced only a slight decrease in *E. coli* TolC MIC values (factors 1.4–2.7) and no effect was observed in the K12 strain. Moreover, the compounds showed no enhanced activity against the *E. coli* D22 strain. It cannot be excluded that an increased membrane permeability may be counteracted by efflux.⁵⁰ It is known that PMBN enhances penetration of antibiotics which diffuse across the OM (10–300 fold decrease in MIC values against *E. coli*), but it has only a slight effect when antibiotics traverse through porins.⁴⁷ Hence, the uptake pathway of our compounds into Gram negative bacteria appears to be mainly permeation through the porins. On the other hand, PAβN increased the susceptibility to the compounds in *E. coli* TolC by factors of 5–14 and by factors ≥ 3 in the K12 and D22 strains. These results indicate that both the OM barrier and efflux pumps contribute to the inactivity of our compounds in Gram negative bacteria, however, efflux mechanisms play the major role. Obviously, beside AcrAB-TolC other efflux systems are involved in *E. coli* drug efflux.

Spontaneous resistance rate

Low propensity of resistance development is a criterion for an effective antibacterial agent. Spontaneous resistance rate towards Myx B in *S. aureus* was found to be 4 to 7×10^{-8} , similar to that of Rif.¹² However, Myx B-resistant mutants possessed higher fitness costs compared to Rif-resistant mutants, giving an advantage to Myx B, and other RNAP “switch region” inhibitors, of having a lower clinical prevalence of resistance than Rif.¹² Determination of in vitro resistance rate for **30** in *E. coli* TolC at $2 \times \text{MIC}$ revealed a significant lower rate ($< 4.2 \times 10^{-11}$) compared to Rif (8.3×10^{-8}) and Myx B (7.1×10^{-8}) as previously observed for the class I derivatives.¹⁷ This observation indicates that the probability of resistance development is reduced with the ureido-thiophene-carboxylic acids compared to MyxB and Rif. An explanation for this finding could be that our compounds occupy only a part of the “switch region” whereas Myx B fills a larger space including the encarbamate binding pocket. Mutations in this part, responsible for Myx resistance,^{6,12} should not prevent our compounds from binding and inhibiting the enzyme.¹⁷ Another explanation for a reduced resistance rate could be an additional effect on another target.

Cytotoxicity

The in vitro toxicity of selected compounds was evaluated by monitoring the cytotoxicity in HEK 293 cells at different time points using doxorubicin (LD_{50} : 0.3 μM) and Rif (LD_{50} : 80 μM) as positive and negative controls respectively. After 72 h, the compounds displayed LD_{50} values in the range of 25 to $>100 \mu\text{M}$ comparable to Rif (Table 4).

Table 4 Cytotoxicity of selected aryl-ureido-heterocyclic-carboxylic acids.

Compd	LD ₅₀ (μM)		
	24 h	48 h	72 h
8	95	78	91
10	>100	>100	>100
11	67	50	46
18	84	82	75
21	61	57	62
30	40	17	25
52	61	61	57
Doxorubicin	5	0.7	0.3
Rif	24% ^a	38% ^a	80

^a at 100 μM

Conclusion

Following an analog design strategy novel chemical scaffolds as bacterial RNAP inhibitors were developed. Derived from the parent class I, a series of regioisomeric ureido-thiophene-carboxylic acid derivatives and bioisosteric heterocyclic classes were designed and studied. The synthetic route *via* the “isatoic anhydrides” for the thiophene and thiazole derivatives was robust and feasible. For the synthesis of the furan derivatives the established strategy had to be modified due to the instability of the furan system. Thereby, class II possessing the same RNAP inhibitory activity as the parent class I, as well as classes III, and V–VII with only slightly lowered potency were discovered. The detailed investigation of the SAR, including molecular alignment, docking studies and angle analysis contributed to a deeper understanding of the structural requirements for interaction with the protein target. The compounds were active against Gram positive bacteria including the pathogen *S. aureus* but ineffective against Gram negative bacteria. The non-susceptibility can be attributed to drug efflux. Nevertheless, the observed low mammalian cytotoxicity, the reduced resistance frequency and the activity against Rif-resistant strains make these novel scaffolds promising for further optimization as antibacterial agents against Gram positive pathogens.

Experimental

Materials and methods

Starting materials and solvents were purchased from commercial suppliers, and used without further purification. All chemical yields refer to purified compounds, and were not optimized. Reaction progress was monitored using TLC Silica gel 60 F₂₅₄ aluminium sheets, and visualization was accomplished by UV at 254 nm. Flash chromatography was performed using silica gel 60 Å (40–63 μm). Preparative RP-HPLC was carried out on a Waters Corporation setup contains a 2767 sample manager, a 2545 binary gradient module, a 2998 PDA detector and a 3100 electron spray mass spectrometer. Purification was performed using a Waters

XBridge column (C18, 150 × 19 mm, 5 μm), a binary solvent system A and B (A = water with 0.1% formic acid; B = MeCN with 0.1% formic acid) as eluent, a flow rate of 20 mL/min and a gradient of 60% to 95% B in 8 min were applied. Melting points were determined on a Stuart Scientific melting point apparatus SMP3 (Bibby Sterilin, UK), and are uncorrected. NMR spectra were recorded either on Bruker DRX-500 (¹H, 500 MHz; ¹³C, 126 MHz), or Bruker Fourier 300 (¹H, 300 MHz; ¹³C, 75 MHz) spectrometer at 300 K. Chemical shifts are recorded as δ values in ppm units by reference to the hydrogenated residues of deuterated solvent as internal standard (CDCl₃: δ = 7.26, 77.02; DMSO-d₆: δ = 2.50, 39.99). Splitting patterns describe apparent multiplicities and are designated as s (singlet), br s (broad singlet), d (doublet), dd (doublet of doublet), t (triplet), q (quartet), m (multiplet). Coupling constants (*J*) are given in Hertz (Hz). Purity of all compounds used in biological assays was ≥95% as measured by LC/MS Finnigan Surveyor MSQ Plus (Thermo Fisher Scientific, Dreieich, Germany). The system consists of LC pump, autosampler, PDA detector, and single-quadrupole MS detector, as well as the standard software Xcalibur for operation. RP C18 Nucleodur 100-5 (125 × 3 mm) column (Macherey-Nagel GmbH, Dühren, Germany) was used as stationary phase, and a binary solvent system A and B (A = water with 0.1% TFA; B = MeCN with 0.1% TFA) was used as mobile phase. In a gradient run the percentage of B was increased from an initial concentration of 0% at 0 min to 100% at 15 min and kept at 100% for 5 min. The injection volume was 10 μL and flow rate was set to 800 μL/min. MS (ESI) analysis was carried out at a spray voltage of 3800 V, a capillary temperature of 350 °C and a source CID of 10 V. Spectra were acquired in positive mode from 100 to 1000 *m/z* and at 254 nm for UV tracing.

Chemistry

Synthesis of 5-(aryl)-3-[3-(substituted)ureido]thiophene-2-carboxylic acids **6–11** was previously described,¹⁷ as well as the experimental data of compounds **8–11**.¹⁷

5-(4'-Chlorophenyl)-3-(3-hexylureido)thiophene-2-carboxylic acid **6**;²¹ beige crystals; mp 198–199 °C; δ_H (300 MHz, DMSO-d₆) 0.86 (3 H, t, *J* = 4.8 Hz, Me), 1.19–1.49 (8 H, m, Me(CH₂)₄CH₂NH), 3.08 (2 H, m, CH₂CH₂NH), 7.50 (2 H, d, *J* = 7.8 Hz, 3',5'Ar-H), 7.63 (1 H, t, *J* = 4.8 Hz, NHCH₂), 7.68 (2 H, d, *J* = 7.8 Hz, 2',6'Ar-H), 8.28 (1 H, s, C4-H), 9.33 (1 H, br s, NHCO), 13.13 (1 H, br s, COOH); δ_C (75 MHz, DMSO-d₆) 14.39 (C6''), 22.54 (C5''), 26.56 (C3''), 29.85 (C2''), 31.47 (C4''), 39.78 (C1''), 107.40 (C2), 118.89 (C4), 127.81 (C2', C6'), 129.77 (C3', C5'), 132.23 (C1'), 134.07 (C4'), 145.64 (C5), 146.74 (C3), 154.25 (NHCO), 165.23 (COOH); *m/z* (ESI+) 381 (17%, (M + H)⁺), 761 (33, 2M + H), 295 (40, M – C₆H₁₃), 236 (100, M – C₆H₁₃, NH, CO₂); t_R = 14.86 min.

3-(3-Benzylureido)-5-(4'-chlorophenyl)thiophene-2-carboxylic acid 7;²¹ white crystals; mp 216–217 °C; δ_{H} (300 MHz, DMSO- d_6) 4.31 (2 H, d, $J = 5.7$ Hz, CH₂), 7.21–7.38 (5 H, m, Ph), 7.51 (2 H, d, $J = 8.6$ Hz, 3',5'Ar-H), 7.70 (2 H, d, $J = 8.6$ Hz, 2',6'Ar-H), 8.22 (1 H, t, $J = 5.7$ Hz, NHCH₂), 8.30 (1 H, s, C4-H), 9.43 (1 H, br s, NHCO), 13.15 (1 H, br s, COOH); δ_{C} (75 MHz, DMSO- d_6) 43.46 (CH₂), 107.42 (C2), 118.91 (C4), 127.30 (C4''), 127.76 (C2'', C6''), 127.87 (C2', C6'), 128.79 (C3'', C5''), 129.79 (C3', C5'), 132.15 (C1'), 134.15 (C4'), 140.26 (C1''), 145.90 (C5), 146.65 (C3), 154.36 (NHCO), 165.16 (COOH); m/z (ESI+) 387 (19%, (M + H)⁺), 772 (10, 2M), 295 (10, M – C₇H₇), 236 (100, M – C₇H₇, NH, CO₂); $t_{\text{R}} = 13.38$ min.

General procedures for synthesis of 2-(aryl)acetaldehydes 12a and 12b

To a stirred ice-cooled suspension of pyridinium chlorochromate (12.9 g, 60.0 mmol) in anhydrous DCM (80 mL), the appropriate 2-(aryl)ethanol^{51,52} (40.0 mmol) in DCM (10 mL) was added in one portion. The reaction mixture was allowed to warm to rt, and stirred for 2 h, then anhydrous Et₂O (100 mL) was added, and the supernatant was decanted from the black gum. The insoluble residue was washed thoroughly with anhydrous Et₂O (2 × 50 mL), the combined organic solution was passed through a short pad of silica, and the solvent was removed by vacuum distillation. The crude product was used directly in the next step without further purification. Purity was determined to be 70–80% as indicated from ¹H-NMR spectra.

2-(4'-Chlorophenyl)acetaldehyde 12a;⁵³ yellow oil; δ_{H} (300 MHz, CDCl₃) 3.67 (2 H, d, $J = 1.0$ Hz, CH₂), 7.15 (2 H, d, $J = 8.1$ Hz, 3',5'Ar-H), 7.33 (2 H, d, $J = 8.1$ Hz, 2',6'Ar-H), 9.74 (1 H, t, $J = 1.0$ Hz, CHO).

2-(3',4'-Dichlorophenyl)acetaldehyde 12b;⁵⁴ yellow oil; δ_{H} (300 MHz, CDCl₃) 3.68 (2 H, d, $J = 1.9$ Hz, CH₂), 7.05 (1 H, dd, $J = 8.0, 2.0$ Hz, 6'Ar-H), 7.32 (1 H, d, $J = 2.0$ Hz, 2'Ar-H), 7.37 (1 H, d, $J = 8.0$ Hz, 5'Ar-H), 9.75 (1 H, t, $J = 1.9$ Hz, CHO).

General procedures for synthesis of ethyl 2-amino-5-(aryl)thiophene-3-carboxylates 13a and 13b

To a stirred suspension of the appropriate aldehyde **12a** or **12b** (30.0 mmol), ethyl cyanoacetate (3.39 g, 30.0 mmol), and sulfur (0.96 g, 30.0 mmol) in EtOH (30 mL), a solution of NEt₃ (4.04 g, 30.0 mmol) in EtOH (5 mL) was added slowly. The reaction mixture was stirred at 70 °C for 12 h, then solvent was removed by vacuum distillation. The obtained residue was dissolved in DCM (50 mL) and washed with water (2 × 50 mL). The organic layer was dried (MgSO₄) and concentrated. The crude material was purified by flash chromatography (SiO₂, *n*-hexane/EtOAc = 6:1).

Ethyl 2-amino-5-(4'-chlorophenyl)thiophene-3-carboxylate 13a (5.49 g, 65%); pale yellow solid; mp 100–101 °C; δ_{H} (300 MHz, CDCl_3) 1.36 (3 H, t, $J = 7.1$ Hz, Me), 4.30 (2 H, q, $J = 7.1$ Hz, CH_2O), 6.03 (2 H, br s, NH_2), 7.21 (1 H, s, C4-H), 7.27 (2 H, d, $J = 8.9$ Hz, 3',5'-Ar-H), 7.35 (2 H, d, $J = 8.9$ Hz, 2',6'-Ar-H); δ_{C} (75 MHz, CDCl_3) 14.54 (Me), 59.94 (CH_2), 108.04 (C3), 121.79 (C4), 123.48 (C5), 125.81 (C2', C6'), 128.91 (C3', C5'), 132.16 (C4'), 132.56 (C1'), 162.17 (C2), 165.29 (C=O); m/z (ESI+) 281 (8%, M^+), 236 (100, $\text{M} - \text{EtO}$); $t_{\text{R}} = 14.05$ min.

Ethyl 2-amino-5-(3',4'-dichlorophenyl)thiophene-3-carboxylate 13b (6.05 g, 64%); pale yellow solid; mp 130–131 °C; δ_{H} (300 MHz, CDCl_3) 1.37 (3 H, t, $J = 7$ Hz, Me), 4.30 (2 H, q, $J = 7.0$ Hz, CH_2O), 6.08 (2 H, br s, NH_2), 7.22 (1 H, dd, $J = 8.0, 2.0$ Hz, 6'-Ar-H), 7.23 (1 H, s, C4-H), 7.36 (1 H, d, $J = 8.0$ Hz, 5'-Ar-H), 7.48 (1 H, d, $J = 2.0$ Hz, 2'-Ar-H); δ_{C} (75 MHz, CDCl_3) 14.53 (Me), 60.03 (CH_2), 108.11 (C3), 121.90 (C4), 122.78 (C6'), 123.74 (C5), 126.11 (C2'), 130.04 (C4'), 130.62 (C5'), 132.91 (C3'), 134.12 (C1'), 162.48 (C2), 165.20 (C=O); m/z (ESI+) 315 (18%, M^+), 270 (100, $\text{M} - \text{EtO}$); $t_{\text{R}} = 15.14$ min.

General procedures for synthesis of 2-amino-5-(aryl)thiophene-3-carboxylic acids 14a and 14b

To a stirred solution of the appropriate ester **13a** or **13b** (25.0 mmol) in MeOH (100 mL), KOH (6.17 g, 110 mmol) in water (100 mL) was added. The reaction mixture was stirred at reflux for 3–5 h (TLC monitoring), then MeOH was evaporated by vacuum distillation. The residue was diluted with water (50 mL) and washed with EtOAc (2×50 mL). The aqueous layer was cooled in an ice bath and acidified by KHSO_4 (saturated aqueous solution) to pH 3–4. The precipitated solid was collected by filtration, washed with cold water (2×30 mL), *n*-hexane (2×30 mL), and dried over CaCl_2 in amber glass vacuum desiccator.

2-Amino-5-(4'-chlorophenyl)thiophene-3-carboxylic acid 14a (4.11 g, 65%); beige solid; mp 195–197 °C; δ_{H} (300 MHz, DMSO-d_6) 7.26 (1 H, s, C4-H), 7.36 (2 H, d, $J = 8.6$ Hz, 3',5'-Ar-H), 7.45 (2 H, d, $J = 8.6$ Hz, 2',6'-Ar-H), 7.47 (2 H, br s, NH_2), 12.10 (1 H, br s, COOH); δ_{C} (75 MHz, DMSO-d_6) 106.36 (C3), 120.76 (C4), 123.19 (C5), 125.94 (C2', C6'), 129.30 (C3', C5'), 130.69 (C4'), 133.31 (C1'), 163.93 (C2), 166.48 (C=O); m/z (ESI+) 253 (72%, M^+), 255 (28, $[\text{M}+2]^+$), 236 (100, $\text{M} - \text{OH}$), 209 (14, $\text{M} - \text{CO}_2$); $t_{\text{R}} = 10.83$ min.

2-Amino-5-(3',4'-dichlorophenyl)thiophene-3-carboxylic acid 14b (5.88 g, 82%); beige solid; mp 229–231 °C; δ_{H} (300 MHz, DMSO-d_6) 7.38 (1 H, dd, $J = 8.0, 2.0$ Hz, 6'-Ar-H), 7.39 (1 H, s, C4-H), 7.52 (1 H, d, $J = 8.0$ Hz, 5'-Ar-H), 7.55 (2 H, br s, NH_2), 7.69 (1 H, d, $J = 2.0$ Hz, 2'-Ar-H), 12.15 (1 H, br s, COOH); δ_{C} (75 MHz, DMSO-d_6) 106.57 (C3), 119.11 (C4),

124.37 (C6'), 124.77 (C5), 125.60 (C2'), 128.26 (C4'), 131.33 (C5'), 132.16 (C3'), 135.18 (C1'), 164.37 (C2), 166.43 (C=O); *m/z* (ESI+) 287 (88%, M⁺), 289 (56, [M+2]⁺), 270 (100, M – OH), 243 (8, M – CO₂), 227 (25, M – CO₂, NH₂); *t_R* = 11.87 min.

General procedures for synthesis of 6-(aryl)-1*H*-thieno[2,3-*d*][1,3]oxazine-2,4-diones 15a and 15b

To a stirred solution of the appropriate acid **14a** or **14b** (6.00 mmol) in THF (60 mL), triphosgene (1.29 g, 4.36 mmol) was added portionwise over 30 min. The reaction mixture was stirred at rt for 2 h, then NaHCO₃ (saturated aqueous solution, 30 mL) was added cautiously, and the resulting mixture was extracted with EtOAc/THF (1:1, 2 × 50 mL). The combined organic layer was washed with brine (50 mL), dried (MgSO₄), and the solvent was removed by vacuum distillation. The obtained crude material was suspended in *n*-hexane/EtOAc (4:1, 50 mL), stirred in a water bath at 40 °C for 10 min, cooled, and collected by filtration.

6-(4'-Chlorophenyl)-1*H*-thieno[2,3-*d*][1,3]oxazine-2,4-dione 15a (1.2 g, 74%); beige solid; mp 254–256 °C; δ_{H} (300 MHz, DMSO-*d*₆) 7.40 (2 H, d, *J* = 8.7 Hz, 3',5'Ar-H), 7.48 (1 H, s, C5-H), 7.60 (2 H, d, *J* = 8.7 Hz, 2',6'Ar-H), 11.73 (1 H, br s, NH); δ_{C} (75 MHz, DMSO-*d*₆) 109.70 (C4a), 119.10 (C5), 126.74 (C2', C6'), 128.28 (C6), 129.39 (C3', C5'), 131.75 (C4'), 133.00 (C1'), 150.22 (C7a), 152.83 (C2), 159.67 (C4); *m/z* (ESI+) 279 (20%, M⁺), 235 (100, M – CO₂); *t_R* = 10.40 min.

6-(3',4'-Dichlorophenyl)-1*H*-thieno[2,3-*d*][1,3]oxazine-2,4-dione 15b (1.5 g, 81%); beige solid; mp >300 °C; δ_{H} (300 MHz, DMSO-*d*₆) 7.61 (2 H, m, 5',6'Ar-H), 7.79 (1 H, s, C5-H), 7.96 (1 H, s, 2'Ar-H), 12.76 (1 H, br s, NH); δ_{C} (75 MHz, DMSO-*d*₆) 111.46 (C4a), 120.60 (C5), 125.72 (C6'), 127.17 (C2'), 130.87 (C4'), 131.57 (C5'), 131.83 (C6), 132.50 (C3'), 133.21 (C1'), 147.81 (C7a), 155.32 (C2), 155.82 (C4); *m/z* (ESI+) 313 (14%, M⁺), 355 (100, M + H, MeCN), 627 (28, 2M + H), 296 (35, M – OH); *t_R* = 11.44 min.

General procedures for synthesis of 5-(aryl)-2-[3-(substituted)ureido]thiophene-3-carboxylic acids 16–21

To a stirred suspension of thiaisatoic anhydride **15a** or **15b** (0.64 mmol) in water (8 mL), the appropriate amine (1.40 mmol) was added. The reaction mixture was stirred at rt for 2 h, then poured on ice-cooled 2M HCl (40 mL), and extracted with EtOAc/THF (1:1, 40 mL). The organic layer was washed with 2M HCl (40 mL), brine (40 mL), dried (MgSO₄), and concentrated in vacuo. The obtained crude material was suspended in *n*-hexane/EtOAc (4:1, 50 mL), stirred in a water bath at 40 °C for 10 min, cooled, and collected by filtration.

5-(4'-Chlorophenyl)-2-(3-hexylureido)thiophene-3-carboxylic acid 16 (132 mg, 54%); pale brown crystals; mp 230–232 °C; δ_{H} (300 MHz, DMSO- d_6) 0.87 (3 H, t, $J = 6.8$ Hz, Me), 1.03–1.57 (8 H, m, Me(CH $_2$) $_4$ CH $_2$ NH), 3.11 (2 H, m, CH $_2$ CH $_2$ NH), 7.40 (2 H, d, $J = 8.6$ Hz, 3',5'-Ar-H), 7.43 (1 H, s, C4-H), 7.59 (2 H, d, $J = 8.6$ Hz, 2',6'-Ar-H), 7.94 (1 H, t, $J = 4.2$ Hz, NHCH $_2$), 10.24 (1 H, br s, NHCO), 12.82 (1 H, br s, COOH); δ_{C} (75 MHz, DMSO- d_6) 14.39 (C6''), 22.54 (C5''), 26.50 (C3''), 29.71 (C2''), 31.43 (C4''), 39.86 (C1''), 111.55 (C3), 121.27 (C4), 126.63 (C2', C6'), 128.77 (C5), 129.45 (C3', C5'), 131.62 (C4'), 133.17 (C1'), 151.41 (C2), 153.88 (NHCO), 166.35 (COOH); m/z (ESI+) 380 (33%, M $^+$), 761 (100, 2M + H), 295 (18, M – C $_6$ H $_{13}$); $t_{\text{R}} = 14.38$ min.

2-(3-Benzylureido)-5-(4'-chlorophenyl)thiophene-3-carboxylic acid 17 (136 mg, 55%); pale brown crystals; mp 250–252 °C; δ_{H} (300 MHz, DMSO- d_6) 4.34 (2 H, d, $J = 5.6$ Hz, CH $_2$), 7.15–7.39 (5 H, m, Ph), 7.41 (2 H, d, $J = 8.6$ Hz, 3',5'-Ar-H), 7.45 (1 H, s, C4-H), 7.59 (2 H, d, $J = 8.6$ Hz, 2',6'-Ar-H), 8.49 (1 H, t, $J = 5.3$ Hz, NHCH $_2$), 10.35 (1 H, br s, NHCO), 12.87 (1 H, br s, COOH); δ_{C} (75 MHz, DMSO- d_6) 43.67 (CH $_2$), 111.79 (C3), 121.29 (C4), 126.68 (C2', C6'), 127.45 (C4''), 127.81 (C2'', C6''), 128.86 (C3'', C5''), 129.02 (C5), 129.46 (C3', C5'), 131.70 (C4'), 133.09 (C1'), 139.75 (C1''), 151.20 (C2), 154.01 (NHCO), 166.29 (COOH); m/z (ESI+) 387 (30%, (M + H) $^+$), 773 (22, 2M + H), 295 (26, M – C $_7$ H $_7$), 170 (100); $t_{\text{R}} = 13.18$ min.

2-(3-Benzyl-3-ethylureido)-5-(4'-chlorophenyl)thiophene-3-carboxylic acid 18 (136 mg, 51%); pale brown crystals; mp 215–216 °C; δ_{H} (300 MHz, DMSO- d_6) 1.16 (3 H, t, $J = 7.1$ Hz, Me), 3.42 (2 H, q, $J = 7.1$ Hz, MeCH $_2$ N), 4.60 (2 H, s, PhCH $_2$ N), 7.24–7.39 (5 H, m, Ph), 7.41 (2 H, d, $J = 8.6$ Hz, 3',5'-Ar-H), 7.48 (1 H, s, C4-H), 7.62 (2 H, d, $J = 8.6$ Hz, 2',6'-Ar-H), 10.96 (1 H, br s, NHCO), 13.15 (1 H, br s, COOH); δ_{C} (75 MHz, DMSO- d_6) 13.52 (Me), 42.42 (MeCH $_2$ N), 49.96 (PhCH $_2$ N), 112.30 (C3), 120.98 (C4), 126.79 (C2', C6'), 127.64 (C4''), 127.75 (C2'', C6''), 129.04 (C3'', C5''), 129.48 (C3', C5'), 129.68 (C5), 131.87 (C4'), 132.97 (C1'), 138.06 (C1''), 151.67 (C2), 153.10 (NHCO), 167.43 (COOH); m/z (ESI+) 415 (100%, (M + H) $^+$), 829 (90, 2M + H); $t_{\text{R}} = 14.08$ min.

5-(3',4'-Dichlorophenyl)-2-(3-hexylureido)thiophene-3-carboxylic acid 19 (165 mg, 62%); beige crystals; mp 245–247 °C; δ_{H} (300 MHz, DMSO- d_6) 0.86 (3 H, t, $J = 6.8$ Hz, Me), 1.16–1.56 (8 H, m, Me(CH $_2$) $_4$ CH $_2$ NH), 3.11 (2 H, m, CH $_2$ CH $_2$ NH), 7.53 (1 H, dd, $J = 8.0, 2.0$ Hz, 6'-Ar-H), 7.56 (1 H, s, C4-H), 7.59 (1 H, d, $J = 8.0$ Hz, 5'-Ar-H), 7.83 (1 H, d, $J = 2.0$ Hz, 2'-Ar-H), 7.97 (1 H, t, $J = 4.7$ Hz, NHCH $_2$), 10.26 (1 H, br s, NHCO), 12.89 (1 H, br s, COOH); δ_{C} (75 MHz, DMSO- d_6) 14.39 (C6''), 22.53 (C5''), 26.49 (C3''), 29.69 (C2''), 31.43 (C4''), 39.85 (C1''), 111.65 (C3), 122.63 (C4), 125.03 (C6'), 126.41 (C2'), 127.27 (C5), 129.29 (C4'), 131.51

(C5'), 132.28 (C3'), 135.00 (C1'), 151.88 (C2), 153.85 (NHCO), 166.27 (COOH); m/z (ESI+) 414 (100%, M⁺), 416 (69, [M+2]⁺), 829 (67, 2M + H), 329 (42, M - C₆H₁₃); t_R = 15.40 min.

2-(3-Benzylureido)-5-(3',4'-dichlorophenyl)thiophene-3-carboxylic acid 20 (194 mg, 72%); white crystals; mp 256–258 °C; δ_H (300 MHz, DMSO-d₆) 4.34 (2 H, d, *J* = 5.6 Hz, CH₂), 7.22–7.39 (5 H, m, Ph), 7.53 (1 H, dd, *J* = 8.0, 2.0 Hz, 6'Ar-H), 7.58 (1 H, s, C4-H), 7.60 (1 H, d, *J* = 8.0 Hz, 5'Ar-H), 7.84 (1 H, d, *J* = 2.0 Hz, 2'Ar-H), 8.51 (1 H, t, *J* = 5.6 Hz, NHCH₂), 10.38 (1 H, br s, NHCO), 12.93 (1 H, br s, COOH); δ_C (75 MHz, DMSO-d₆) 43.68 (CH₂), 111.97 (C3), 122.68 (C4), 125.08 (C6'), 126.47 (C2'), 127.46 (C4''), 127.49 (C5), 127.82 (C2'', C6''), 128.86 (C3'', C5''), 129.37 (C4'), 131.52 (C5'), 132.30 (C3'), 134.94 (C1'), 139.71 (C1''), 151.63 (C2), 153.99 (NHCO), 166.24 (COOH); m/z (ESI+) 421 (47%, (M + H)⁺), 843 (100, 2M + 3H), 329 (11, M - C₇H₇); t_R = 13.94 min.

2-(3-Benzyl-3-ethylureido)-5-(3',4'-dichlorophenyl)thiophene-3-carboxylic acid 21 (210 mg, 73%); beige crystals; mp 228–230 °C; δ_H (300 MHz, DMSO-d₆) 1.16 (3 H, t, *J* = 7.1 Hz, Me), 3.42 (2 H, q, *J* = 7.1 Hz, MeCH₂N), 4.60 (2 H, s, PhCH₂N), 7.24–7.40 (5 H, m, Ph), 7.55 (1 H, dd, *J* = 8.0, 2.0 Hz, 6'Ar-H), 7.59 (1 H, d, *J* = 8.0 Hz, 5'Ar-H), 7.60 (1 H, s, C4-H), 7.86 (1 H, d, *J* = 2.0 Hz, 2'Ar-H), 10.98 (1 H, br s, NHCO), 13.22 (1 H, br s, COOH); δ_C (75 MHz, DMSO-d₆) 13.52 (Me), 42.47 (MeCH₂N), 49.99 (PhCH₂N), 112.45 (C3), 122.35 (C4), 125.17 (C6'), 126.58 (C2'), 127.66 (C4''), 127.76 (C5), 128.15 (C2'', C6''), 129.04 (C3'', C5''), 129.54 (C4'), 131.53 (C5'), 132.33 (C3'), 134.80 (C1'), 138.03 (C1''), 152.11 (C2), 153.07 (NHCO), 167.38 (COOH); m/z (ESI+) 448 (100%, M⁺); t_R = 14.99 min.

Synthesis and characterization of ethyl 2-amino-4-(aryl)thiophene-3-carboxylates **22a**²² and **22b**²³ were previously described.

Synthesis of 2-amino-4-(aryl)thiophene-3-carboxylic acids **23a** and **23b** were performed as described for **14a** and **14b**.

2-Amino-4-(4'-chlorophenyl)thiophene-3-carboxylic acid 23a (3.48 g, 55%); pale brown solid; mp 137–139 °C; δ_H (300 MHz, DMSO-d₆) 6.17 (1 H, s, C5-H), 7.26 (2 H, d, *J* = 8.6 Hz, 3',5'Ar-H), 7.34 (2 H, d, *J* = 8.6 Hz, 2',6'Ar-H), 7.40 (2 H, br s, NH₂), 11.76 (1 H, br s, COOH); δ_C (75 MHz, DMSO-d₆) 103.60 (C3), 105.90 (C5), 127.63 (C2', C6'), 130.87 (C3', C5'), 131.61 (C4'), 137.69 (C4), 139.95 (C1'), 165.71 (C2), 166.66 (C=O); m/z (ESI+) 254 (48%, (M + H)⁺), 507 (4, 2M + H), 236 (100, M - OH); t_R = 10.16 min.

2-Amino-4-(3',4'-dichlorophenyl)thiophene-3-carboxylic acid 23b (3.59 g, 50%); pale brown solid; mp 142–144 °C; δ_H (300 MHz, DMSO-d₆) 6.27 (1 H, s, C5-H), 7.24 (1 H, dd, *J* = 8.0, 2.0 Hz, 6'Ar-H), 7.41 (2 H, br s, NH₂), 7.47 (1 H, d, *J* = 2.0 Hz, 2'Ar-H), 7.53 (1 H, d,

$J = 8.0$ Hz, 5'Ar-H), 11.96 (1 H, br s, COOH); δ_{C} (75 MHz, DMSO- d_6) 103.37 (C3), 106.79 (C5), 129.53 (C6'), 129.75 (C5'), 130.25 (C4'), 130.32 (C2'), 130.86 (C3'), 138.52 (C4), 139.41 (C1'), 165.78 (C2), 166.44 (C=O); m/z (ESI+) 288 (100%, (M + H)⁺), 575 (19, 2M + H), 270 (77, M – OH); $t_{\text{R}} = 11.04$ min.

Synthesis of 5-(aryl)-1*H*-thieno[2,3-*d*][1,3]oxazine-2,4-diones **24a** and **24b** were performed as described for preparation of **15a** and **15b**.

5-(4'-Chlorophenyl)-1*H*-thieno[2,3-*d*][1,3]oxazine-2,4-dione 24a (1.2 g, 71%); pale grey solid; mp 235–237 °C; δ_{H} (300 MHz, DMSO- d_6) 7.16 (1 H, s, C6-H), 7.46 (2 H, d, $J = 8.9$ Hz, 3',5'Ar-H), 7.51 (2 H, d, $J = 8.9$ Hz, 2',6'Ar-H), 12.68 (1 H, br s, NH); δ_{C} (75 MHz, DMSO- d_6) 107.59 (C4a), 116.09 (C6), 128.36 (C2', C6'), 131.12 (C3', C5'), 131.35 (C4'), 133.21 (C5), 137.56 (C1'), 147.93 (C7a), 154.98 (C2), 157.82 (C4); m/z (ESI+) 279 (100%, M⁺), 559 (6, 2M + H); $t_{\text{R}} = 10.23$ min.

5-(3',4'-Dichlorophenyl)-1*H*-thieno[2,3-*d*][1,3]oxazine-2,4-dione 24b (1.5 g, 80%); beige solid; mp 236–238 °C; δ_{H} (300 MHz, DMSO- d_6) 7.27 (1 H, s, C6-H), 7.48 (1 H, dd, $J = 8.0$, 2.0 Hz, 6'Ar-H), 7.68 (1 H, d, $J = 8.0$ Hz, 5'Ar-H), 7.75 (1 H, d, $J = 2.0$ Hz, 2'Ar-H), 12.70 (1 H, br s, NH); δ_{C} (75 MHz, DMSO- d_6) 107.58 (C4a), 117.07 (C6), 129.59 (C6'), 130.51 (C5'), 131.01 (C4'), 131.13 (C2'), 131.15 (C3'), 134.83 (C5), 136.08 (C1'), 147.87 (C7a), 155.07 (C2), 157.85 (C4); m/z (ESI+) 313 (8%, M⁺), 355 (100, M + H, MeCN), 626 (12, 2M), 296 (20, M – OH); $t_{\text{R}} = 10.77$ min.

Synthesis of 4-(aryl)-2-[3-(substituted)ureido]thiophene-3-carboxylic acids **25–30** were performed as described for preparation of **16–21**.

4-(4'-Chlorophenyl)-2-(3-hexylureido)thiophene-3-carboxylic acid 25 (180 mg, 74%); pale grey crystals; mp 191–193 °C; δ_{H} (300 MHz, DMSO- d_6) 0.87 (3 H, t, $J = 6.7$ Hz, Me), 1.21–1.51 (8 H, m, Me(CH₂)₄CH₂NH), 3.10 (2 H, m, CH₂CH₂NH), 6.63 (1 H, s, C5-H), 7.29 (2 H, d, $J = 8.6$ Hz, 3',5'Ar-H), 7.36 (2 H, d, $J = 8.6$ Hz, 2',6'Ar-H), 7.87 (1 H, t, $J = 5.1$ Hz, NHCH₂), 10.39 (1 H, br s, NHCO), 12.50 (1 H, br s, COOH); δ_{C} (75 MHz, DMSO- d_6) 14.39 (C6''), 22.55 (C5''), 26.52 (C3''), 29.78 (C2''), 31.45 (C4''), 39.84 (C1''), 108.92 (C3), 114.32 (C5), 127.73 (C2', C6'), 131.06 (C3', C5'), 131.79 (C4'), 137.31 (C4), 138.31 (C1'), 153.29 (C2), 154.16 (NHCO), 166.76 (COOH); m/z (ESI+) 381 (100%, (M + H)⁺), 761 (51, 2M + H), 295 (77, M – C₆H₁₃), 236 (58, M – C₆H₁₃, NH, CO₂); $t_{\text{R}} = 13.37$ min.

2-(3-Benzylureido)-4-(4'-chlorophenyl)thiophene-3-carboxylic acid 26 (200 mg, 81%); pale brown crystals; mp 197–199 °C; δ_{H} (300 MHz, DMSO- d_6) 4.33 (2 H, d, $J = 5.7$ Hz, CH₂),

6.66 (1 H, s, C5-H), 7.24–7.37 (9 H, m, 4'-ClC₆H₄, Ph), 8.40 (1 H, t, $J = 4.8$ Hz, NHCH₂), 10.60 (1 H, br s, NHCO), 12.56 (1 H, br s, COOH); δ_C (75 MHz, DMSO-d₆) 43.57 (CH₂), 109.64 (C3), 114.39 (C5), 127.39 (C4''), 127.74 (C2'', C6''), 127.75 (C2', C6'), 128.84 (C3'', C5''), 131.08 (C3', C5'), 131.78 (C4'), 137.30 (C4), 138.44 (C1'), 139.96 (C1''), 152.79 (C2), 154.30 (NHCO), 166.85 (COOH); m/z (ESI⁺) 387 (100%, (M + H)⁺), 773 (37, 2M + H), 295 (44, M – C₇H₇), 236 (50, M – C₇H₇, NH, CO₂); $t_R = 12.21$ min.

2-(3-Benzyl-3-ethylureido)-4-(4'-chlorophenyl)thiophene-3-carboxylic acid 27 (240 mg, 90%); pale grey crystals; mp 175–177 °C; δ_H (300 MHz, DMSO-d₆) 1.15 (3 H, t, $J = 6.2$ Hz, Me), 3.41 (2 H, q, $J = 6.2$ Hz, MeCH₂N), 4.60 (2 H, s, PhCH₂N), 6.71 (1 H, s, C5-H), 7.22–7.50 (9 H, m, 4'-ClC₆H₄, Ph), 11.38 (1 H, br s, NHCO), 12.84 (1 H, br s, COOH); δ_C (75 MHz, DMSO-d₆) 13.54 (Me), 42.28 (MeCH₂N), 49.84 (PhCH₂N), 109.67 (C3), 114.80 (C5), 127.58 (C4''), 127.69 (C2'', C6''), 127.74 (C2', C6'), 129.03 (C3'', C5''), 131.22 (C3', C5'), 131.97 (C4'), 137.03 (C4), 138.22 (C1'), 138.46 (C1''), 153.45 (C2), 153.80 (NHCO), 167.93 (COOH); m/z (ESI⁺) 415 (100%, (M + H)⁺), 829 (6, 2M + H), 236 (12, M – C₇H₇, EtN, CO₂); $t_R = 13.18$ min.

4-(3',4'-Dichlorophenyl)-2-(3-hexylureido)thiophene-3-carboxylic acid 28 (172 mg, 65%); pale brown crystals; mp 178–180 °C; δ_H (300 MHz, DMSO-d₆) 0.87 (3 H, t, $J = 6.8$ Hz, Me), 1.21–1.50 (8 H, m, Me(CH₂)₄CH₂NH), 3.10 (2 H, m, CH₂CH₂NH), 6.72 (1 H, s, C5-H), 7.27 (1 H, dd, $J = 8.0, 2.0$ Hz, 6'Ar-H), 7.53 (1 H, d, $J = 2.0$ Hz, 2'Ar-H), 7.56 (1 H, d, $J = 8.0$ Hz, 5'Ar-H), 7.86 (1 H, t, $J = 5.0$ Hz, NHCH₂), 10.49 (1 H, br s, NHCO), 12.62 (1 H, br s, COOH); δ_C (75 MHz, DMSO-d₆) 14.40 (C6''), 22.54 (C5''), 26.51 (C3''), 29.77 (C2''), 31.44 (C4''), 39.82 (C1''), 109.21 (C3), 115.00 (C5), 129.67 (C6'), 129.74 (C5'), 129.82 (C4'), 130.33 (C2'), 131.10 (C3'), 136.99 (C4), 139.16 (C1'), 153.12 (C2), 154.16 (NHCO), 166.70 (COOH); m/z (ESI⁺) 415 (100%, (M + H)⁺), 829 (30, 2M + H), 329 (92, M – C₆H₁₃); $t_R = 14.26$ min.

2-(3-Benzylureido)-4-(3',4'-dichlorophenyl)thiophene-3-carboxylic acid 29 (210 mg, 78%); beige crystals; mp 188–190 °C; δ_H (300 MHz, DMSO-d₆) 4.34 (2 H, d, $J = 5.6$ Hz, CH₂), 6.77 (1 H, s, C5-H), 7.24–7.39 (6 H, m, 6'Ar-H, Ph), 7.53 (1 H, d, $J = 2.0$ Hz, 2'Ar-H), 7.56 (1 H, d, $J = 8.0$ Hz, 5'Ar-H), 8.45 (1 H, t, $J = 5.0$ Hz, NHCH₂), 10.51 (1 H, br s, NHCO), 12.69 (1 H, br s, COOH); δ_C (75 MHz, DMSO-d₆) 43.59 (CH₂), 109.06 (C3), 115.30 (C5), 127.42 (C4''), 127.76 (C2'', C6''), 128.85 (C3'', C5''), 129.75 (C6'), 129.78 (C5'), 129.86 (C4'), 130.38 (C2'), 131.11 (C3'), 136.97 (C4), 139.01 (C1'), 139.88 (C1''), 153.19 (C2), 154.28 (NHCO), 166.48 (COOH); m/z (ESI⁺) 421 (100%, (M + H)⁺), 841 (23, 2M + H), 329 (25, M – C₇H₇); $t_R = 12.98$ min.

2-(3-Benzyl-3-ethylureido)-4-(3',4'-dichlorophenyl)thiophene-3-carboxylic acid 30 (172 mg, 60%); beige crystals; mp 193–195 °C; δ_{H} (300 MHz, DMSO- d_6) 1.15 (3 H, t, $J = 7.0$ Hz, Me), 3.41 (2 H, q, $J = 7.0$ Hz, MeCH $_2$ N), 4.60 (2 H, s, PhCH $_2$ N), 6.80 (1 H, s, C5-H), 7.24–7.39 (6 H, m, 6'Ar-H, Ph), 7.55 (1 H, d, $J = 2.0$ Hz, 2'Ar-H), 7.56 (1 H, d, $J = 8.0$ Hz, 5'Ar-H), 11.43 (1 H, br s, NHCO), 12.92 (1 H, br s, COOH); δ_{C} (75 MHz, DMSO- d_6) 13.54 (Me), 42.27 (MeCH $_2$ N), 49.82 (PhCH $_2$ N), 109.72 (C3), 115.50 (C5), 127.59 (C4''), 127.70 (C2'', C6''), 129.03 (C3'', C5''), 129.84 (C6'), 129.88 (C4', C5'), 130.35 (C2'), 131.26 (C3'), 137.08 (C4), 138.23 (C1'), 138.83 (C1''), 153.46 (C2), 153.78 (NHCO), 167.77 (COOH); m/z (ESI+) 449 (100%, (M + H) $^+$), 897 (7, 2M + H), 270 (13, M – C $_7$ H $_7$, EtN, CO $_2$); $t_{\text{R}} = 14.00$ min.

Synthesis of methyl 3-amino-4-(aryl)thiophene-2-carboxylates **34a**²⁶ and **34b** were performed according to reported procedures.²⁶

Methyl 3-amino-4-(4'-chlorophenyl)thiophene-2-carboxylate 34a²⁶ beige solid; mp 104–105 °C (lit.,²⁶ 106 °C); δ_{H} (300 MHz, CDCl $_3$) 3.86 (3 H, s, OMe), 5.57 (2 H, br s, NH $_2$), 7.23 (1 H, s, C5-H), 7.37 (2 H, d, $J = 8.7$ Hz, 3',5'Ar-H), 7.43 (2 H, d, $J = 8.7$ Hz, 2',6'Ar-H); δ_{C} (75 MHz, CDCl $_3$) 51.39 (Me), 101.69 (C2), 128.88 (C5), 129.39 (C2', C6'), 129.44 (C3', C5'), 132.08 (C4), 132.82 (C1'), 134.00 (C4'), 151.27 (C3), 165.03 (C=O); m/z (ESI+) 268 (16%, (M + H) $^+$), 236 (100, M – MeO); $t_{\text{R}} = 13.20$ min.

Methyl 3-amino-4-(3',4'-dichlorophenyl)thiophene-2-carboxylate 34b white solid; mp 135–137 °C; δ_{H} (300 MHz, DMSO- d_6) 3.76 (3 H, s, OMe), 6.38 (2 H, br s, NH $_2$), 7.45 (1 H, dd, $J = 8.0, 2.0$ Hz, 6'Ar-H), 7.69 (1 H, d, $J = 2.0$ Hz, 2'Ar-H), 7.71 (1 H, d, $J = 8.0$ Hz, 5'Ar-H), 7.78 (1 H, s, C5-H); δ_{C} (75 MHz, DMSO- d_6) 51.65 (Me), 99.91 (C2), 128.75 (C6'), 130.31 (C2'), 130.73 (C4'), 130.77 (C5), 131.39 (C4), 131.60 (C5'), 131.99 (C3'), 135.08 (C1'), 152.58 (C3), 164.64 (C=O); m/z (ESI+) 302 (12%, (M + H) $^+$), 270 (100, M – MeO); $t_{\text{R}} = 12.79$ min.

Synthesis of 3-amino-4-(aryl)thiophene-2-carboxylic acids **35a** and **35b** were performed as described for preparation of **14a** and **14b**.

3-Amino-4-(4'-chlorophenyl)thiophene-2-carboxylic acid 35a (reported as reaction intermediate and not isolated)^{20,55} (5.38 g, 85%); white solid; mp 160–162 °C; δ_{H} (300 MHz, DMSO- d_6) 6.45 (2 H, br s, NH $_2$), 7.49–7.56 (4 H, m, 4'-ClC $_6$ H $_4$), 7.64 (1 H, s, C5-H), 11.86 (1 H, br s, COOH); δ_{C} (75 MHz, DMSO- d_6) 101.28 (C2), 129.32 (C2', C6'), 130.00 (C5), 130.15 (C3', C5'), 132.08 (C4), 132.68 (C1'), 133.62 (C4'), 152.19 (C3), 166.00 (C=O); m/z (ESI+) 254 (18%, (M + H) $^+$), 236 (100, M – OH); $t_{\text{R}} = 10.69$ min.

3-Amino-4-(3',4'-dichlorophenyl)thiophene-2-carboxylic acid 35b (5.52 g, 77%); beige solid; mp 127–129 °C; δ_{H} (300 MHz, DMSO- d_6) 7.46 (1 H, dd, $J = 8.0, 2.0$ Hz, 6'Ar-H), 7.70 (1 H, d, $J = 8.0$ Hz, 5'Ar-H), 7.70 (1 H, d, $J = 2.0$ Hz, 2'Ar-H), 7.73 (1 H, s, C5-H), 7.74 (2 H, br s, NH₂), 12.49 (1 H, br s, COOH); δ_{C} (75 MHz, DMSO- d_6) 101.46 (C2), 128.67 (C6'), 130.21 (C2'), 130.59 (C4'), 130.79 (C5), 130.81 (C5'), 131.36 (C4), 131.96 (C3'), 135.35 (C1'), 152.16 (C3), 165.94 (C=O); m/z (ESI⁺) 287 (12%, M⁺), 270 (100, M – OH); $t_{\text{R}} = 11.53$ min.

Synthesis of 7-(aryl)-1*H*-thieno[3,2-*d*][1,3]oxazine-2,4-diones **36a** and **36b** were performed as described for preparation of **15a** and **15b**.

7-(4'-Chlorophenyl)-1*H*-thieno[3,2-*d*][1,3]oxazine-2,4-dione 36a^{20,55} (1.23 g, 73%); white solid; mp 214–216 °C (lit.,²⁰ 245 °C, lit.,⁵⁵ >260 °C); δ_{H} (300 MHz, DMSO- d_6) 7.49 (2 H, d, $J = 8.8$ Hz, 3',5'Ar-H), 7.54 (2 H, d, $J = 8.8$ Hz, 2',6'Ar-H), 8.25 (1 H, s, C6-H), 11.86 (1 H, br s, NH); δ_{C} (75 MHz, DMSO- d_6) 107.66 (C4a), 129.20 (C2', C6'), 129.35 (C7), 130.97 (C3', C5'), 131.03 (C1'), 133.66 (C4'), 136.87 (C6), 147.24 (C7a), 149.41 (C2), 156.06 (C4); m/z (ESI⁺) 279 (24%, M⁺), 251 (100, M – CO); $t_{\text{R}} = 10.18$ min.

7-(3',4'-Dichlorophenyl)-1*H*-thieno[3,2-*d*][1,3]oxazine-2,4-dione 36b (1.36 g, 72%); beige solid; mp 249–251 °C; δ_{H} (300 MHz, DMSO- d_6) 7.43 (1 H, dd, $J = 8.0, 2.0$ Hz, 6'Ar-H), 7.70 (1 H, d, $J = 2.0$ Hz, 2'Ar-H), 7.73 (1 H, d, $J = 8.0$ Hz, 5'Ar-H), 8.32 (1 H, s, C6-H), 11.96 (1 H, br s, NH); δ_{C} (75 MHz, DMSO- d_6) 107.73 (C4a), 129.58 (C6'), 129.64 (C7), 131.25 (C2'), 131.27 (C5'), 131.71 (C4'), 131.82 (C3'), 132.50 (C1'), 137.70 (C6), 146.70 (C7a), 149.24 (C2), 155.77 (C4); m/z (ESI⁺) 313 (13%, M⁺), 627 (13, 2M + H), 285 (100, M – CO); $t_{\text{R}} = 11.14$ min.

Synthesis of 4-(aryl)-3-[3-(substituted)ureido]thiophene-2-carboxylic acids **37–42** were performed as described for preparation of **16–21**

4-(4'-Chlorophenyl)-3-(3-hexylureido)thiophene-2-carboxylic acid 37²¹ (195 mg, 80%); white crystals; mp 176–178 °C; δ_{H} (300 MHz, DMSO- d_6) 0.86 (3 H, t, $J = 6.4$ Hz, Me), 1.12–1.30 (8 H, m, Me(CH₂)₄CH₂NH), 2.84 (2 H, m, CH₂CH₂NH), 6.88 (1 H, t, $J = 5.9$ Hz, NHCH₂), 7.37 (2 H, d, $J = 7.8$ Hz, 3',5'Ar-H), 7.42 (2 H, d, $J = 7.8$ Hz, 2',6'Ar-H), 7.79 (1 H, s, C5-H), 8.34 (1 H, br s, NHCO), 13.15 (1 H, br s, COOH); δ_{C} (75 MHz, DMSO- d_6) 14.42 (C6''), 22.51 (C5''), 26.31 (C3''), 30.08 (C2''), 31.49 (C4''), 39.47 (C1''), 118.68 (C2), 128.59 (C2', C6'), 128.70 (C3', C5'), 129.01 (C5), 131.83 (C4'), 135.76 (C1'), 138.35 (C4), 142.42 (C3), 154.72 (NHCO), 164.24 (COOH); m/z (ESI⁺) 381 (25%, (M + H)⁺), 761 (17, 2M + H), 295 (53, M – C₆H₁₃), 236 (100, M – C₆H₁₃, NH, CO₂); $t_{\text{R}} = 12.71$ min.

3-(3-Benzylureido)-4-(4'-chlorophenyl)thiophene-2-carboxylic acid 38²¹ (225 mg, 91%); white crystals; mp 196–198 °C (lit.,²¹ 216 °C); δ_{H} (300 MHz, DMSO-*d*₆) 4.10 (2 H, d, $J = 5.9$ Hz, CH₂), 7.06–7.32 (5 H, m, Ph), 7.38–7.46 (5H, m, 4'-ClC₆H₄, NHCH₂), 7.82 (1 H, s, C5-H), 8.49 (1 H, br s, NHCO), 13.23 (1 H, br s, COOH); δ_{C} (75 MHz, DMSO-*d*₆) 43.06 (CH₂), 119.38 (C2), 127.05 (C4''), 127.32 (C2'', C6''), 128.54 (C3'', C5''), 128.75 (C2', C6'), 128.88 (C3', C5'), 129.09 (C5), 131.92 (C4'), 135.68 (C1'), 138.63 (C4), 140.70 (C1''), 142.13 (C3), 155.03 (NHCO), 164.17 (COOH); m/z (ESI+) 387 (40%, (M + H)⁺), 773 (36, 2M + H), 295 (51, M – C₇H₇), 236 (100, M – C₇H₇, NH, CO₂); $t_{\text{R}} = 10.41$ min.

3-(3-Benzyl-3-ethylureido)-4-(4'-chlorophenyl)thiophene-2-carboxylic acid 39²¹ (212 mg, 80%); white crystals; mp 157–159 °C; δ_{H} (500 MHz, DMSO-*d*₆) 1.09 (3 H, t, $J = 6.3$ Hz, Me), 3.24 (2 H, q, $J = 6.6$ Hz, MeCH₂N), 4.37 (2 H, s, PhCH₂N), 7.02–7.32 (5 H, m, Ph), 7.43 (2 H, d, $J = 8.8$ Hz, 3',5'-Ar-H), 7.46 (2 H, d, $J = 8.8$ Hz, 2',6'-Ar-H), 7.83 (1 H, s, C5-H), 8.52 (1 H, br s, NHCO), 13.23 (1 H, br s, COOH); δ_{C} (126 MHz, DMSO-*d*₆) 13.04 (Me), 40.77 (MeCH₂N), 48.40 (PhCH₂N), 119.87 (C2), 126.85 (C4''), 127.18 (C2'', C6''), 128.14 (C3'', C5''), 128.27 (C2', C6'), 128.28 (C5), 128.66 (C3', C5'), 131.56 (C4'), 134.97 (C1'), 138.44 (C4), 138.48 (C1''), 142.51 (C3), 154.37 (NHCO), 163.87 (COOH); m/z (ESI+) 415 (100%, (M + H)⁺), 829 (21, 2M + H), 236 (37, M – C₇H₇, EtN, CO₂); $t_{\text{R}} = 12.74$ min.

4-(3',4'-Dichlorophenyl)-3-(3-hexylureido)thiophene-2-carboxylic acid 40 (220 mg, 83%); white crystals; mp 189–191 °C; δ_{H} (300 MHz, DMSO-*d*₆) 0.85 (3 H, t, $J = 7$ Hz, Me), 1.02–1.39 (8 H, m, Me(CH₂)₄CH₂NH), 2.85 (2 H, m, CH₂CH₂NH), 7.01 (1 H, t, $J = 5.5$ Hz, NHCH₂), 7.38 (1 H, dd, $J = 8.0, 2.0$ Hz, 6'-Ar-H), 7.57 (1 H, d, $J = 8.0$ Hz, 5'-Ar-H), 7.62 (1 H, d, $J = 2.0$ Hz, 2'-Ar-H), 7.89 (1 H, s, C5-H), 8.42 (1 H, br s, NHCO), 13.19 (1 H, br s, COOH); δ_{C} (75 MHz, DMSO-*d*₆) 14.42 (C6''), 22.48 (C5''), 26.29 (C3''), 30.14 (C2''), 31.47 (C4''), 39.53 (C1''), 118.34 (C2), 127.16 (C6'), 128.59 (C2'), 129.67 (C5), 129.82 (C4'), 130.72 (C5'), 131.31 (C3'), 136.81 (C4), 137.56 (C1'), 142.41 (C3), 154.63 (NHCO), 164.21 (COOH); m/z (ESI+) 415 (76%, (M + H)⁺), 829 (37, 2M + H), 329 (100, M – C₆H₁₃), 270 (96, M – C₆H₁₃, NH, CO₂); $t_{\text{R}} = 12.65$ min.

3-(3-Benzylureido)-4-(3',4'-dichlorophenyl)thiophene-2-carboxylic acid 41 (221 mg, 82%); off white crystals; mp 182–184 °C; δ_{H} (300 MHz, DMSO-*d*₆) 4.12 (2 H, d, $J = 5.9$ Hz, CH₂), 7.03–7.35 (5 H, m, Ph), 7.40 (1 H, dd, $J = 8.0, 2.0$ Hz, 6'-Ar-H), 7.51 (1 H, t, $J = 5.9$ Hz, NHCH₂), 7.59 (1 H, d, $J = 8.0$ Hz, 5'-Ar-H), 7.67 (1 H, d, $J = 2.0$ Hz, 2'-Ar-H), 7.91 (1 H, s, C5-H), 8.54 (1 H, br s, NHCO), 12.69 (1 H, br s, COOH); δ_{C} (75 MHz, DMSO-*d*₆) 43.09 (CH₂), 119.18 (C2), 127.04 (C4''), 127.19 (C2'', C6''), 127.36 (C6'), 128.58 (C3'', C5''), 128.80 (C2'), 129.80 (C5), 129.83 (C4'), 130.90 (C5'), 131.42 (C3'), 137.15 (C4), 137.52 (C1'), 140.57

(C1''), 142.09 (C3), 154.98 (NHCO), 164.12 (COOH); m/z (ESI+) 421 (58%, (M + H)⁺), 841 (24, 2M + H), 329 (83, M - C₇H₇), 270 (100, M - C₇H₇, NH, CO₂); t_R = 9.60 min.

3-(3-Benzyl-3-ethylureido)-4-(3',4'-dichlorophenyl)thiophene-2-carboxylic acid 42 (236 mg, 82%); off white crystals; mp 171–173 °C; δ_H (300 MHz, DMSO-d₆) 1.09 (3 H, t, J = 6.8 Hz, Me), 3.25 (2 H, q, J = 6.8 Hz, MeCH₂N), 4.40 (2 H, s, PhCH₂N), 6.91–7.37 (5 H, m, Ph), 7.43 (1 H, dd, J = 8.0, 2.0 Hz, 6'Ar-H), 7.63 (1 H, d, J = 8.0 Hz, 5'Ar-H), 7.70 (1 H, d, J = 2.0 Hz, 2'Ar-H), 7.94 (1 H, s, C5-H), 8.55 (1 H, br s, NHCO), 13.36 (1 H, br s, COOH); δ_C (75 MHz, DMSO-d₆) 13.48 (Me), 41.32 (MeCH₂N), 49.00 (PhCH₂N), 120.31 (C2), 127.35 (C4''), 127.51 (C2'', C6''), 127.70 (C6'), 128.70 (C3'', C5''), 129.01 (C2'), 129.54 (C5), 129.97 (C4'), 130.98 (C5'), 131.50 (C3'), 137.17 (C4), 137.44 (C1'), 138.86 (C1''), 142.85 (C3), 154.80 (NHCO), 164.28 (COOH); m/z (ESI+) 449 (100%, (M + H)⁺), 897 (9, 2M + H), 270 (10, M - C₇H₇, EtN, CO₂); t_R = 13.02 min.

Ethyl 3-amino-5-(3',4'-dichlorophenyl)furan-2-carboxylate 46

To a stirred ice-cooled solution of triphenylphosphine (5.12 g, 19.5 mmol) in anhydrous THF (70 mL), diethyl azodicarboxylate (3.40 g, 19.5 mmol) was added dropwise. After 10 min, ethyl glycolate (2.03 g, 19.5 mmol) was added dropwise, then **44**²⁸ (3.21 g, 15.0 mmol) was added portionwise. The reaction mixture was allowed to warm to rt, and stirred for 15 h. Sodium hydride (55–65% in mineral oil, 1.80 g, 42.0 mmol) was added, and the reaction was further stirred for 6 h. The reaction mixture was treated with water (10 mL), and the solvent was removed by vacuum distillation. The obtained residue was dissolved in EtOAc (70 mL), washed with water (50 mL), dried (MgSO₄), and concentrated. The crude material was purified by flash chromatography (SiO₂, *n*-hexane/EtOAc = 3:1). (3.90 g, 87%); white solid; mp 153–155 °C; δ_H (300 MHz, CDCl₃) 1.42 (3 H, t, J = 7.1 Hz, Me), 4.40 (2 H, q, J = 7.1 Hz, CH₂O), 4.64 (2 H, br s, NH₂), 6.39 (1 H, s, C4-H), 7.47 (1 H, d, J = 8.0 Hz, 5'Ar-H), 7.55 (1 H, dd, J = 8.0, 2.0 Hz, 6'Ar-H), 7.81 (1 H, d, J = 2.0 Hz, 2'Ar-H); δ_C (75 MHz, CDCl₃) 14.65 (Me), 60.13 (CH₂), 100.98 (C4), 124.03 (C6'), 126.16 (C3), 126.62 (C2'), 129.38 (C1'), 130.76 (C5'), 132.98 (C4'), 133.16 (C3'), 144.74 (C2), 153.45 (C5), 160.37 (C=O); m/z (ESI+) 300 (83%, (M + H)⁺), 599 (6, 2M + H), 254 (100, M - EtO); t_R = 13.72 min.

Ethyl 5-(3',4'-dichlorophenyl)-3-(phenoxy-carbonylamino)furan-2-carboxylate 47

To a stirred ice-cooled solution of **46** (1.00 g, 3.33 mmol), and pyridine (264 mg, 3.33 mmol) in anhydrous DCM (20 mL), phenyl chloroformate (525 mg, 3.33 mmol) was added dropwise. The reaction mixture was stirred at rt for 12 h. The solvent was evaporated under vacuum, and

the residue was dissolved in EtOAc (50 mL), washed with 1M HCl (2 × 25 mL), brine (25 mL), dried (MgSO₄), and the solvent was removed by vacuum distillation. The obtained material was triturated with *n*-hexane (20 mL), collected by filtration and dried. (1.20 g, 86%); pale yellow solid; mp 120–121 °C; δ_{H} (300 MHz, CDCl₃) 1.46 (3 H, t, $J = 7.1$ Hz, Me), 4.46 (2 H, q, $J = 7.1$ Hz, CH₂O), 7.18–7.45 (5 H, m, Ph), 7.48 (1 H, d, $J = 8.0$ Hz, 5'Ar-H), 7.51 (1 H, s, C4-H), 7.57 (1 H, dd, $J = 8.0, 2.0$ Hz, 6'Ar-H), 7.85 (1 H, d, $J = 2.0$ Hz, 2'Ar-H), 8.76 (1 H, br s, NHCO); δ_{C} (75 MHz, CDCl₃) 14.51 (Me), 61.19 (CH₂), 102.14 (C4), 121.43 (C2'', C6''), 124.09 (C6'), 126.04 (C4''), 126.68 (C2'), 128.48 (C3), 129.01 (C1'), 129.50 (C3'', C5''), 130.93 (C5'), 133.36 (C4'), 133.42 (C3'), 136.53 (C2), 150.40 (C1''), 151.38 (NHCO), 153.68 (C5), 160.12 (C=O); m/z (ESI+) 420 (100%, (M + H)⁺), 374 (7, M – EtO); $t_{\text{R}} = 17.56$ min.

General procedures for synthesis of ethyl 3-[3-(substituted)ureido]-5-(3',4'-dichlorophenyl)furan-2-carboxylate 48 and 49

To a stirred solution of **47** (300 mg, 0.71 mmol) in anhydrous DMSO (10 mL) under a nitrogen atmosphere, the appropriate amine (0.75 mmol) was added dropwise. The reaction mixture was stirred at rt for 2 h, then EtOAc (50 mL) was added. The organic layer was washed with 2M HCl (2 × 30 mL), 1M NaOH (2 × 30 mL), brine (30 mL), dried (MgSO₄), and the solvent was removed by vacuum distillation. The obtained residues were purified by flash chromatography (SiO₂, *n*-hexane/EtOAc = 1:1).

Ethyl 3-(3-benzylureido)-5-(3',4'-dichlorophenyl)furan-2-carboxylate 48 (283 mg, 92%); white solid; mp 211–213 °C; δ_{H} (300 MHz, DMSO-*d*₆) 1.33 (3 H, t, $J = 7.1$ Hz, Me), 4.33 (2 H, d, $J = 4.7$ Hz, PhCH₂NH), 4.35 (2 H, q, $J = 7.1$ Hz, CH₂O), 7.23–7.38 (5 H, m, Ph), 7.71 (1 H, d, $J = 8.0$ Hz, 5'Ar-H), 7.76 (1 H, dd, $J = 8.0, 2.0$ Hz, 6'Ar-H), 7.87 (1 H, s, C4-H), 8.02 (1 H, d, $J = 2.0$ Hz, 2'Ar-H), 8.06 (1 H, t, $J = 5.8$ Hz, NHCH₂), 8.66 (1 H, br s, NHCO); δ_{C} (75 MHz, DMSO-*d*₆) 14.88 (Me), 43.43 (PhCH₂NH), 60.70 (CH₂O), 104.25 (C4), 125.12 (C6'), 126.71 (C2'), 127.36 (C4''), 127.75 (C2'', C6''), 128.58 (C3), 128.83 (C3'', C5''), 129.77 (C1'), 131.81 (C5'), 132.17 (C4'), 132.51 (C3'), 138.53 (C2), 140.12 (C1''), 152.57 (C5), 154.45 (NHCO), 159.57 (C=O); m/z (ESI+) 433 (100%, (M + H)⁺), 865 (27, 2M + H), 341 (8, M – C₇H₇), 254 (59, M – C₇H₇, NCO, EtO); $t_{\text{R}} = 15.99$ min.

Ethyl 3-(3-benzyl-3-ethylureido)-5-(3',4'-dichlorophenyl)furan-2-carboxylate 49 (278 mg, 85%); reddish liquid; δ_{H} (500 MHz, CDCl₃) 1.25 (3 H, t, $J = 7.3$ Hz, MeCH₂N), 1.36 (3 H, t, $J = 7.3$ Hz, MeCH₂O), 3.42 (2 H, q, $J = 7.3$ Hz, MeCH₂N), 4.36 (2 H, q, $J = 7.3$ Hz, CH₂O), 4.62 (2 H, s, PhCH₂N), 7.25–7.36 (5 H, m, Ph), 7.48 (1 H, d, $J = 8.0$ Hz, 5'Ar-H), 7.60 (1 H, dd, $J = 8.0, 2.0$ Hz, 6'Ar-H), 7.71 (1 H, s, C4-H), 7.89 (1 H, d, $J = 2.0$ Hz, 2'Ar-H), 8.84

(1 H, br s, NHCO); δ_C (126 MHz, CDCl₃) 13.16 (MeCH₂N), 14.51 (MeCH₂O), 42.03 (MeCH₂N), 50.02 (PhCH₂N), 60.80 (CH₂O), 102.98 (C4), 124.12 (C6'), 126.73 (C2'), 127.49 (C4''), 127.58 (C2'', C6''), 127.76 (C3), 128.76 (C3'', C5''), 129.44 (C1'), 130.87 (C5'), 133.11 (C4'), 133.28 (C3'), 137.42 (C2), 137.70 (C1''), 152.94 (C5), 154.11 (NHCO), 159.64 (C=O); m/z (ESI+) 461 (100%, (M + H)⁺), 921 (8, 2M + H); t_R = 17.00 min.

3-Benzyl-6-(3',4'-dichlorophenyl)furo[3,2-d]pyrimidine-2,4(1H,3H)-dione 50

To a stirred solution of **48** (130 mg, 0.3 mmol) in MeOH (10 mL), NaOH (20 mg, 0.5 mmol) in water (10 mL) was added. The reaction mixture was stirred at 70 °C for 3 h. The mixture was concentrated in vacuo. The residue was diluted with water (10 mL), and washed with EtOAc (20 mL). The aqueous layer was cooled in ice bath and acidified with KHSO₄ (saturated aqueous solution) to pH 3–4. The precipitated solid was collected by filtration, washed with cold water (20 mL), and *n*-hexane (20 mL).

(93 mg, 80%); white solid; mp 281–283 °C dec; δ_H (500 MHz, DMSO-d₆) 5.04 (2 H, s, CH₂), 7.23–7.32 (6 H, m, C7-H, Ph), 7.76 (1 H, d, *J* = 8.0 Hz, 5'Ar-H), 7.88 (1 H, dd, *J* = 8.0, 2.0 Hz, 6'Ar-H), 8.20 (1 H, d, *J* = 2.0 Hz, 2'Ar-H), 11.87 (1 H, br s, NH); δ_C (126 MHz, DMSO-d₆) 43.13 (CH₂), 98.87 (C7), 125.03 (C6'), 126.89 (C2'), 127.04 (C4''), 127.37 (C2'', C6''), 128.27 (C3'', C5''), 128.81 (C7a), 129.83 (C1'), 131.39 (C5'), 132.12 (C4'), 132.45 (C3'), 137.35 (C1''), 137.79 (C4a), 150.88 (C4), 153.00 (C2), 156.43 (C6); m/z (ESI+) 387 (68%, (M + H)⁺), 773 (29, 2M + H), 186 (100); t_R = 13.16 min.

General procedures for synthesis of 3-[3-(substituted)ureido]-5-(3',4'-dichlorophenyl)furan-2-carboxylic acid 51 and 52

To a stirred ice-cooled solution of the appropriate ester **48** or **49** (1.00 mmol), and THT (5 mL) in anhydrous DCM (5 mL), AlCl₃ (1.33 g, 10.0 mmol) was added portionwise. The reaction mixture was stirred at rt for 72 h (TLC monitoring, TLC samples were diluted with MeOH). The reaction mixture was concentrated under vacuum, then cold water (10 mL) was added followed by 1M HCl to pH 4–5. The mixture was extracted with EtOAc (3 × 25 mL). The combined organic layers were dried (MgSO₄), and the solvent was removed by vacuum distillation. The crude material was purified using preparative RP-HPLC.

3-(3-Benzylureido)-5-(3',4'-dichlorophenyl)furan-2-carboxylic acid 51 (100 mg, 25%); white crystals; mp 195–197 °C dec; δ_H (500 MHz, DMSO-d₆) 4.31 (2 H, d, *J* = 5.7 Hz, CH₂), 7.23–7.37 (5 H, m, Ph), 7.71 (1 H, d, *J* = 8.0 Hz, 5'Ar-H), 7.77 (1 H, dd, *J* = 8.0, 2.0 Hz, 6'Ar-H), 7.84 (1 H, s, C4-H), 8.03 (1 H, d, *J* = 2.0 Hz, 2'Ar-H), 8.06 (1 H, t, *J* = 5.7 Hz, NHCH₂),

8.65 (1 H, br s, NHCO), 13.23 (1 H, br s, COOH); δ_{C} (125 MHz, DMSO- d_6) 42.92 (CH₂), 103.73 (C4), 124.55 (C6'), 126.11 (C2'), 126.83 (C4''), 127.24 (C2'', C6''), 127.51 (C3), 128.32 (C3'', C5''), 129.51 (C1'), 131.30 (C5'), 131.44 (C4'), 131.99 (C3'), 137.28 (C2), 139.72 (C1''), 151.55 (C5), 154.05 (NHCO), 160.57 (COOH); m/z (ESI+) 405 (90%, (M + H)⁺), 809 (14, 2M + H), 313 (93, M – C₇H₇), 254 (100, M – C₇H₇, NH, CO₂); t_{R} = 13.60 min.

3-(3-Benzyl-3-ethylureido)-5-(3',4'-dichlorophenyl)furan-2-carboxylic acid 52 (120 mg, 28%); pale yellow crystals; mp 160–162 °C dec; δ_{H} (500 MHz, DMSO- d_6) 1.15 (3 H, t, J = 7.2 Hz, Me), 3.38 (2 H, q, J = 6.9 Hz, MeCH₂N), 4.56 (2 H, s, PhCH₂N), 7.25–7.37 (5 H, m, Ph), 7.72 (1 H, d, J = 8.0 Hz, 5'Ar-H), 7.79 (1 H, dd, J = 8.0, 2.0 Hz, 6'Ar-H), 7.82 (1 H, s, C4-H), 8.06 (1 H, d, J = 2.0 Hz, 2'Ar-H), 8.79 (1 H, br s, NHCO), 13.46 (1 H, br s, COOH); δ_{C} (125 MHz, DMSO- d_6) 13.11 (Me), 41.82 (MeCH₂N), 49.39 (PhCH₂N), 103.45 (C4), 124.62 (C6'), 126.23 (C2'), 126.92 (C4''), 127.16 (C2'', C6''), 127.94 (C3), 128.50 (C3'', C5''), 129.39 (C1'), 131.31 (C5'), 131.60 (C4'), 132.02 (C3'), 137.95 (C2), 137.99 (C1''), 151.99 (C5), 153.06 (NHCO), 161.20 (COOH); m/z (ESI+) 433 (66%, (M + H)⁺), 865 (8, 2M + H), 389 (100, [M+H] – CO₂); t_{R} = 13.64 min.

Ethyl 2-amino-5-(3',4'-dichlorophenyl)furan-3-carboxylate 54

To a stirred ice-cooled solution of **43**²⁷ (4.83 g, 18.0 mmol) in anhydrous DMF (13 mL) under a nitrogen atmosphere, ethyl cyanoacetate (2.05 g, 18.0 mmol), and diethylamine (3.95 g, 54.0 mmol) were added slowly. The reaction mixture was allowed to warm to rt, and stirred for 2 h. The mixture was diluted with DCM (100 mL), washed with 2M HCl (2 × 50 mL), dried (MgSO₄), and concentrated under vacuum till half of the volume. Trifluoroacetic acid (50 mL) was added in one portion to the solution. The reaction was stirred at rt for 40 h. The solvent was removed by vacuum distillation. The residue was dissolved in DCM (50 mL), cautiously washed with NaHCO₃ (saturated aqueous solution, 50 mL), the organic layer was dried (MgSO₄), and concentrated. The crude material was purified by flash chromatography (SiO₂, *n*-hexane/EtOAc = 6:1). (2.15 g, 40%); white solid; mp 110–111 °C; δ_{H} (300 MHz, CDCl₃) 1.36 (3 H, t, J = 7.1 Hz, Me), 4.29 (2 H, q, J = 7.1 Hz, CH₂O), 5.62 (2 H, br s, NH₂), 6.78 (1 H, s, C4-H), 7.29 (1 H, dd, J = 8.0, 2.0 Hz, 6'Ar-H), 7.38 (1 H, d, J = 8.0 Hz, 5'Ar-H), 7.57 (1 H, d, J = 2.0 Hz, 2'Ar-H); δ_{C} (75 MHz, CDCl₃) 14.54 (Me), 59.84 (CH₂), 91.80 (C3), 106.46 (C4), 121.60 (C6'), 124.09 (C2'), 129.87 (C4'), 130.10 (C1'), 130.61 (C5'), 132.90 (C3'), 141.30 (C5), 161.55 (C2), 164.83 (C=O); m/z (ESI+) 300 (100%, (M + H)⁺), 599 (79, 2M + H), 254 (91, M – EtO); t_{R} = 15.98 min.

Ethyl 2-[bis(phenoxy-carbonyl)amino]-5-(3',4'-dichlorophenyl)furan-3-carboxylate 55

To a stirred ice-cooled solution of **54** (1.00 g, 3.33 mmol), and pyridine (528 mg, 6.66 mmol) in anhydrous DCM (30 mL), phenyl chloroformate (1.05 g, 6.66 mmol) was added dropwise, and the reaction mixture was stirred at rt for 12 h. The solvent was evaporated under vacuum. The residue was dissolved in EtOAc (60 mL), washed with 1M HCl (2 × 30 mL), brine (30 mL), dried (MgSO₄), and the solvent was removed by vacuum distillation. The crude material was triturated with *n*-hexane (30 mL), collected by filtration and dried. (1.48 g, 82%); white solid; mp 166–168 °C; δ_{H} (300 MHz, CDCl₃) 1.29 (3 H, t, $J = 7.1$ Hz, Me), 4.32 (2 H, q, $J = 7.1$ Hz, CH₂O), 7.02 (1 H, s, C4-H), 7.08–7.34 (10 H, m, 2 Ph), 7.42 (1 H, d, $J = 8.0$ Hz, 5'Ar-H), 7.46 (1 H, dd, $J = 8.0, 2.0$ Hz, 6'Ar-H), 7.72 (1 H, d, $J = 2.0$ Hz, 2'Ar-H); δ_{C} (75 MHz, CDCl₃) 14.31 (Me), 61.37 (CH₂), 107.34 (C4), 114.59 (C3), 121.10 (C2'', C6'', C2''', C6'''), 123.24 (C6'), 125.91 (C2'), 126.59 (C4'', C4'''), 128.97 (C4'), 129.57 (C3'', C5'', C3''', C5'''), 130.98 (C5'), 132.67 (C1'), 133.40 (C3'), 145.63 (C5), 149.04 (N(C=O)₂), 149.64 (C2), 150.24 (C1'', C1'''), 161.41 (C=O); m/z (ESI+) 540 (100%, (M + H)⁺), 494 (13, M – EtO); $t_{\text{R}} = 16.97$ min.

General procedures for synthesis of ethyl 2-[3-(substituted)ureido]-5-(3',4'-dichlorophenyl)furan-3-carboxylate 57 and 58

To a stirred solution of **55** (300 mg, 0.55 mmol) in anhydrous DMSO (10 mL) under a nitrogen atmosphere, the appropriate amine (2.20 mmol) was added dropwise. The reaction mixture was stirred at rt for 2 h, then EtOAc (50 mL) was added. The organic layer was washed with 2M HCl (2 × 30 mL), 1M NaOH (2 × 30 mL), brine (30 mL), dried (MgSO₄), and the solvent was removed by vacuum distillation. The product was purified from the *sym*-urea side product using flash chromatography (SiO₂, EtOAc/THF = 4:1).

Ethyl 2-(3-benzylureido)-5-(3',4'-dichlorophenyl)furan-3-carboxylate 57 (203 mg, 85%); white solid; mp 223–225 °C dec; δ_{H} (500 MHz, DMSO-d₆) 1.28 (3 H, t, $J = 7.0$ Hz, Me), 4.25 (2 H, q, $J = 7.0$ Hz, CH₂O), 4.33 (2 H, d, $J = 5.8$ Hz, PhCH₂NH), 7.26–7.38 (6 H, m, C4-H, Ph), 7.63 (1 H, dd, $J = 8.0, 2.0$ Hz, 6'Ar-H), 7.66 (1 H, d, $J = 8.0$ Hz, 5'Ar-H), 7.89 (2 H, m, 2'Ar-H, NHCH₂), 9.27 (1 H, br s, NHCO); δ_{C} (125 MHz, DMSO-d₆) 14.28 (Me), 43.00 (PhCH₂NH), 59.95 (CH₂O), 99.11 (C3), 107.18 (C4), 122.86 (C6'), 124.32 (C2'), 126.93 (C4''), 127.27 (C2'', C6''), 128.37 (C3'', C5''), 129.29 (C4'), 129.96 (C1'), 131.04 (C5'), 131.78 (C3'), 139.39 (C1''), 143.37 (C5), 152.04 (NHCO), 153.33 (C2), 162.92 (C=O); m/z (ESI+) 433 (100%, (M + H)⁺), 865 (60, 2M + H), 341 (15, M – C₇H₇), 254 (30, M – C₇H₇, NCO, EtO); $t_{\text{R}} = 15.31$ min.

Ethyl 2-(3-benzyl-3-ethylureido)-5-(3',4'-dichlorophenyl)furan-3-carboxylate 58 (208 mg, 82%); reddish liquid; δ_{H} (500 MHz, CDCl_3) 1.26 (3 H, t, $J = 7.0$ Hz, MeCH_2N), 1.33 (3 H, t, $J = 7.0$ Hz, MeCH_2O), 3.41 (2 H, q, $J = 7.0$ Hz, MeCH_2N), 4.27 (2 H, q, $J = 7.0$ Hz, CH_2O), 4.64 (2 H, s, PhCH_2N), 6.82 (1 H, s, C4-H), 7.28–7.37 (5 H, m, Ph), 7.40 (1 H, d, $J = 8.0$ Hz, 5'Ar-H), 7.49 (1 H, dd, $J = 8.0, 2.0$ Hz, 6'Ar-H), 7.72 (1 H, d, $J = 2.0$ Hz, 2'Ar-H), 9.34 (1 H, br s, NHCO); δ_{C} (126 MHz, CDCl_3) 13.15 (MeCH_2N), 14.39 (MeCH_2O), 42.24 (MeCH_2N), 50.11 (PhCH_2N), 60.56 (CH_2O), 97.53 (C3), 104.74 (C4), 122.60 (C6'), 124.92 (C2'), 127.29 (C4''), 127.56 (C2'', C6''), 128.65 (C3'', C5''), 129.71 (C4'), 130.68 (C5'), 130.89 (C1'), 133.01 (C3'), 136.96 (C1''), 144.79 (C5), 151.77 (NHCO), 155.08 (C2), 165.16 (C=O); m/z (ESI+) 461 (100%, (M + H)⁺), 921 (25, 2M + H); $t_{\text{R}} = 16.94$ min.

Synthesis of 2-[3-(substituted)ureido]-5-(3',4'-dichlorophenyl)furan-3-carboxylic acid **59** and **60** were performed as described for preparation of **51** and **52**

2-(3-Benzylureido)-5-(3',4'-dichlorophenyl)furan-3-carboxylic acid 59 (73 mg, 18%); white crystals; mp 200–202 °C dec; δ_{H} (500 MHz, DMSO-d_6) 4.32 (2 H, d, $J = 6.0$ Hz, CH_2), 7.25–7.38 (6 H, m, C4-H, Ph), 7.61 (1 H, dd, $J = 8.0, 2.0$ Hz, 6'Ar-H), 7.66 (1 H, d, $J = 8.0$ Hz, 5'Ar-H), 7.86 (1 H, d, $J = 2.0$ Hz, 2'Ar-H), 7.95 (1 H, t, $J = 5.7$ Hz, NHCH_2), 9.29 (1 H, br s, NHCO), 12.68 (1 H, br s, COOH); δ_{C} (125 MHz, DMSO-d_6) 42.95 (CH_2), 99.52 (C3), 107.73 (C4), 122.74 (C6'), 124.10 (C2'), 126.91 (C4''), 127.25 (C2'', C6''), 128.36 (C3'', C5''), 128.97 (C4'), 130.15 (C1'), 131.10 (C5'), 131.72 (C3'), 139.42 (C1''), 142.85 (C5), 151.98 (NHCO), 153.27 (C2), 164.63 (COOH); m/z (ESI+) 405 (100%, (M + H)⁺), 809 (54, 2M + H), 313 (71, M – C₇H₇), 295 (24, M – C₇H₇, H₂O), 254 (16, M – C₇H₇, NH, CO₂); $t_{\text{R}} = 12.54$ min.

2-(3-Benzyl-3-ethylureido)-5-(3',4'-dichlorophenyl)furan-3-carboxylic acid 60 (95 mg, 22%); white crystals; mp 175–177 °C dec; δ_{H} (500 MHz, DMSO-d_6) 1.11 (3 H, t, $J = 7.2$ Hz, Me), 3.34 (2 H, q, $J = 7.2$ Hz, MeCH_2N), 4.56 (2 H, s, PhCH_2N), 7.26–7.38 (6 H, m, C4-H, Ph), 7.65 (1 H, dd, $J = 8.0, 2.0$ Hz, 6'Ar-H), 7.67 (1 H, d, $J = 8.0$ Hz, 5'Ar-H), 7.91 (1 H, d, $J = 2.0$ Hz, 2'Ar-H), 9.25 (1 H, br s, NHCO), 12.77 (1 H, br s, COOH); δ_{C} (125 MHz, DMSO-d_6) 13.10 (Me), 41.35 (MeCH_2N), 49.11 (PhCH_2N), 104.55 (C3), 107.98 (C4), 123.00 (C6'), 124.45 (C2'), 127.09 (C4''), 127.29 (C2'', C6''), 128.44 (C3'', C5''), 129.47 (C4'), 130.00 (C1'), 131.16 (C5'), 131.81 (C3'), 138.04 (C1''), 144.24 (C5), 152.81 (NHCO), 152.87 (C2), 164.54 (COOH); m/z (ESI+) 433 (100%, (M + H)⁺), 865 (16, 2M + H), 254 (5, M – C₇H₇, EtN, CO₂); $t_{\text{R}} = 13.71$ min.

Methyl 3,4-dichlorobenzenecarbodithioate 62

To a stirred mixture of sulfur (3.52 g, 110 mmol), and NEt_3 (15.2 g, 150 mmol) in DMF (25 mL), 3,4-dichlorobenzyl chloride **61** (9.77 g, 50.0 mmol) was added dropwise. The reaction mixture was stirred at 60 °C for 6 h then cooled in an ice bath. Iodomethane (7.81 g, 55.0 mmol) was added slowly maintaining the temperature below 10 °C. The reaction was further stirred for 1 h then filtered. The filtrate was poured into stirred ice-cooled water (100 mL). The precipitated bright red crystals were collected by filtration, washed with water, and dried. (10.4 g, 88%); red solid; mp 60–62 °C; δ_{H} (500 MHz, CDCl_3) 2.78 (3 H, s, SMe), 7.46 (1 H, d, $J = 8.0$ Hz, C5-H), 7.83 (1 H, dd, $J = 8.0, 2.0$ Hz, C6-H), 8.10 (1 H, d, $J = 2.0$ Hz, C2-H); δ_{C} (126 MHz, CDCl_3) 20.77 (Me), 125.68 (C6), 128.58 (C2), 130.22 (C5), 132.83 (C4), 136.62 (C3), 144.03 (C1), 225.21 (C=S); m/z (ESI+) 236 (22%, M^+), 187 (100, $\text{M} - \text{CH}_2, \text{Cl}$); $t_{\text{R}} = 16.53$ min.

Methyl 4-amino-2-(3',4'-dichlorophenyl)-1,3-thiazole-5-carboxylate 64

To a stirred ice-cooled solution of sodium (0.81 g, 35.0 mmol), and cyanamide (1.27 g, 30.0 mmol) in anhydrous MeOH (50 mL) under a nitrogen atmosphere, compound **62** (7.11 g, 30 mmol) was added portionwise, and the reaction mixture was stirred at 75 °C for 3 h. The solvent was removed under vacuum, and the residue was triturated with ether, and filtered. The intermediate **63** was dissolved in MeOH (50 mL) and methyl bromoacetate (6.88 g, 45.0 mmol) was added dropwise. The reaction mixture was stirred at rt for 2 h then NEt_3 (12.5 mL, 90.0 mmol) was added, and the reaction was further stirred for 12 h. The solvent was removed by vacuum distillation, and the crude material was purified by flash chromatography (SiO_2 , *n*-hexane/EtOAc = 3:1). (3.18 g, 35%); yellow solid; mp 156–158 °C; δ_{H} (500 MHz, CDCl_3) 3.83 (3 H, s, OMe), 5.88 (2 H, br s, NH_2), 7.48 (1 H, d, $J = 8.0$ Hz, 5'Ar-H), 7.69 (1 H, dd, $J = 8.0, 2.0$ Hz, 6'Ar-H), 8.00 (1 H, d, $J = 2.0$ Hz, 2'Ar-H); δ_{C} (126 MHz, CDCl_3) 51.70 (Me), 94.46 (C5), 125.56 (C6'), 128.22 (C2'), 130.98 (C5'), 132.68 (C4'), 133.50 (C3'), 135.32 (C1'), 163.12 (C4), 164.33 (C=O), 167.46 (C2); m/z (ESI+) 303 (17%, $(\text{M} + \text{H})^+$), 344 (100, $\text{M} + \text{H}$, MeCN), 271 (6, $\text{M} - \text{MeO}$); $t_{\text{R}} = 14.39$ min.

4-Amino-2-(3',4'-dichlorophenyl)-1,3-thiazole-5-carboxylic acid 65

To a stirred solution of **64** (3.03 g, 10.0 mmol) in MeOH (30 mL), KOH (2.24 g, 40.0 mmol) in water (30 mL) was added. The reaction mixture was stirred at reflux for 2 h then the MeOH was evaporated by vacuum distillation. The residue was diluted with water (10 mL), and washed with EtOAc (20 mL). The aqueous layer was cooled in an ice bath and acidified by KHSO_4 (saturated aqueous solution) to pH 3–4. The precipitate was collected by filtration, washed with cold water (20 mL), *n*-hexane (20 mL), and dried over CaCl_2 in amber glass

vacuum desiccator. (1.91 g, 66%); yellow solid; mp 131–133 °C dec; δ_{H} (500 MHz, DMSO- d_6) 6.98 (2 H, br s, NH₂), 7.77 (1 H, d, $J = 8.0$ Hz, 5'Ar-H), 7.87 (1 H, dd, $J = 8.0, 2.0$ Hz, 6'Ar-H), 8.09 (1 H, d, $J = 2.0$ Hz, 2'Ar-H), 12.92 (1 H, br s, COOH); δ_{C} (126 MHz, DMSO- d_6) 93.37 (C5), 126.27 (C6'), 127.48 (C2'), 131.53 (C5'), 132.09 (C4'), 132.76 (C3'), 133.65 (C1'), 163.25 (C4), 164.65 (C=O), 165.42 (C2); m/z (ESI+) 289 (20%, (M + H)⁺), 330 (100, M + H, MeCN), 271 (11, M – OH); $t_{\text{R}} = 12.12$ min.

2-(3',4'-Dichlorophenyl)-4H-[1,3]thiazolo[4,5-*d*][1,3]oxazine-5,7-dione **66**

The compound was prepared as described for preparation of **15a** and **15b**. (1.32 g, 70%); yellow solid; mp 219–221 °C dec; δ_{H} (500 MHz, DMSO- d_6) 7.77 (1 H, d, $J = 8.0$ Hz, 5'Ar-H), 8.15 (1 H, dd, $J = 8.0, 2.0$ Hz, 6'Ar-H), 8.37 (1 H, d, $J = 2.0$ Hz, 2'Ar-H), 11.11 (1 H, br s, NH); δ_{C} (126 MHz, DMSO- d_6) 95.81 (C7a), 128.16 (C6'), 129.87 (C2'), 130.72 (C5'), 131.21 (C4'), 131.99 (C3'), 133.07 (C1'), 153.29 (C5), 153.56 (C3a), 164.45 (C7), 165.28 (C2); m/z (ESI+) 314 (100%, M⁺), 355 (94, M + MeCN), 629 (18, 2M + H); $t_{\text{R}} = 11.75$ min.

Synthesis of 2-(3',4'-dichlorophenyl)-4-[3-(substituted)ureido]-1,3-thiazole-5-carboxylic acids **67** and **68** were performed as described for preparation of **16–21**.

4-(3-Benzylureido)-2-(3',4'-dichlorophenyl)-1,3-thiazole-5-carboxylic acid 67 (65 mg, 24%); yellow crystals; mp 213–215 °C; δ_{H} (500 MHz, DMSO- d_6) 4.48 (2 H, d, $J = 5.4$ Hz, CH₂), 7.27–7.40 (5 H, m, Ph), 7.75 (1 H, d, $J = 8.0$ Hz, 5'Ar-H), 7.92 (1 H, dd, $J = 8.0, 2.0$ Hz, 6'Ar-H), 8.18 (1 H, d, $J = 2.0$ Hz, 2'Ar-H), 8.53 (1 H, t, $J = 5.7$ Hz, NHCH₂), 9.04 (1 H, br s, NHCO), 13.80 (1 H, br s, COOH); δ_{C} (125 MHz, DMSO- d_6) 43.38 (CH₂), 102.27 (C5), 126.64 (C6'), 126.99 (C4''), 127.13 (C2'', C6''), 127.93 (C2'), 128.48 (C3'', C5''), 131.45 (C5'), 131.79 (C4'), 132.30 (C3'), 134.40 (C1'), 139.30 (C1''), 152.25 (NHCO), 154.44 (C4), 164.02 (COOH), 165.77 (C2); m/z (ESI+) 422 (100%, (M + H)⁺), 843 (11, 2M + H), 330 (23, M – C₇H₇), 271 (24, M – C₇H₇, NH, CO₂); $t_{\text{R}} = 14.98$ min.

4-(3-Benzyl-3-ethylureido)-2-(3',4'-dichlorophenyl)-1,3-thiazole-5-carboxylic acid 68 (63 mg, 22%); yellow crystals; mp 191–193 °C; δ_{H} (500 MHz, DMSO- d_6) 1.14 (3 H, t, $J = 6.9$ Hz, Me), 3.37 (2 H, q, $J = 6.9$ Hz, MeCH₂N), 4.58 (2 H, s, PhCH₂N), 7.26–7.38 (5 H, m, Ph), 7.81 (1 H, d, $J = 8.0$ Hz, 5'Ar-H), 7.95 (1 H, dd, $J = 8.0, 2.0$ Hz, 6'Ar-H), 8.18 (1 H, d, $J = 2.0$ Hz, 2'Ar-H), 9.64 (1 H, br s, NHCO), 13.57 (1 H, br s, COOH); δ_{C} (125 MHz, DMSO- d_6) 13.16 (Me), 41.44 (MeCH₂N), 49.12 (PhCH₂N), 102.30 (C5), 126.41 (C6'), 127.05 (C4''), 127.27 (C2'', C6''), 127.61 (C2'), 128.43 (C3'', C5''), 131.59 (C5'), 132.15 (C4'), 132.74 (C3'), 133.76 (C1'), 138.24 (C1''), 152.83 (NHCO), 154.86 (C4), 163.98 (COOH), 164.25 (C2); m/z (ESI+) 450 (100%, (M + H)⁺), 899 (4, 2M + H), 271 (4, M – C₇H₇, EtN, CO₂); $t_{\text{R}} = 13.14$ min.

Biology

Transcription assay The assay was performed as described previously⁵⁶ with slight modifications. *E. coli* RNA polymerase holoenzyme was purchased from Epicentre Biotechnologies (Madison, WI). Final concentrations in a total volume of 30 μ L were one unit of RNA polymerase (0.5 μ g) which was used along with 60 nCi of [5,6-³H]-UTP, 400 μ M of ATP, CTP and GTP as well as 100 μ M of UTP, 20 units of RNase inhibitor (RiboLock, Fermentas), 10 mM DTT, 40 mM Tris-HCl (pH 7.5), 150 mM KCl, 10 mM MgCl₂ and 0.1% CHAPS. As a DNA template 3500 ng of religated pcDNA3.1/V5-His-TOPO were used per reaction. Prior to starting the experiment, the compounds were dissolved in DMSO (final concentration during experiment: 2%). Dilution series of the compounds were prepared using a liquid handling system (Janus, PerkinElmer, Waltham, MA). The components described above (including the compounds) were preincubated in absence of NTPs and DNA for 10 min at 25 °C. Transcription reaction was started by the addition of a mixture containing DNA template and NTPs and incubated for 10 min at 37 °C. The reaction was stopped by the addition of 10% TCA, followed by a transfer of this mixture to a 96-well Multiscreen GFB plate (Millipore, Billerica, MA) and incubation for 45 min at 4 °C. The plate underwent several centrifugation and washing steps with 10% TCA and 95% EtOH to remove residual unincorporated ³H-UTP. After that the plate was dried for 30 min at 50 °C and 30 μ L of scintillation fluid (Optiphase Supermix, PerkinElmer) was added to each well. After 10 min the wells were assayed for presence of ³H-RNA by counting using Wallac MicroBeta TriLux system (Perkin Elmer). To obtain inhibition values for each sample, their counts were related to DMSO control.

Determination of IC₅₀ values Three different concentrations of the compound were chosen (two samples for each concentration) in the linear range of the log dose response curve (20–80% inhibition) including concentrations above and below the IC₅₀ value. Values of percent inhibition were plotted versus the inhibitor molar concentrations on a semi-log plot. IC₅₀ values were calculated as the molar concentration causing 50% inhibition of RNAP activity. At least three independent determinations were performed for each compound (standard deviation <20%).

Minimal inhibitory concentration determinations MIC values were determined in 96-well plates (Sarstedt, Nümbrecht, Germany) against *Staphylococcus aureus subsp. aureus* (Newman strain), *Bacillus subtilis subsp. subtilis*, *Pseudomonas aeruginosa* PAO1, *E. coli*

K12, *E. coli* TolC, and the Rif-resistant *E. coli* TolC mutants: *E. coli* TolC β Q513L and *E. coli* TolC β H526Y. As bacteria start OD₆₀₀ 0.03 was used in a total volume of 200 μ L in lysogeny broth (LB) medium containing the compounds dissolved in DMSO (maximal DMSO concentration in the experiment: 1%). Final compound concentrations (in duplicates) were prepared by serial dilution ranging from 0.02–100 μ g/mL depending on their antibacterial activity and solubility in growth medium. The ODs were measured using a POLARstar Omega (BMG labtech, Offenburg, Germany) after inoculation and after incubation for 18 h at 37 °C with 50 rpm (200 rpm for *P. aeruginosa* PAO1). Given MIC values are means of two independent determinations (three if MIC <10 μ g/mL) and defined as the lowest concentration of compound that reduced OD₆₀₀ by \geq 95%.

Selection of Rif-resistant *E. coli* TolC spontaneous mutants An *E. coli* TolC culture with an OD₆₀₀ 0.70 in LB was subcultured to fresh medium containing 3-fold the MIC of Rif every 24h with a dilution factor of 1:5. The cultures were incubated at 37 °C for 24 h with shaking. After 4 cycles the bacteria were transferred on LB agar plates containing 3-fold the MIC of Rif. The plates were incubated at 37 °C for 24 h. Single colonies were picked and transferred to liquid culture in the presence of 3-fold the MIC of Rif. Rif-resistant mutants were characterized by sequencing of RNAP rpoB.

MIC determinations in presence of polymyxin B nonapeptide (PMBN) or phenyl-arginine- β -naphthylamide (PA β N) The same procedures followed as mentioned above with minor modifications: Before inoculation, bacteria were cultured in LB medium containing PMBN (1 μ g/mL) or PA β N (20 μ g/mL) (10 μ g/mL in case of *E. coli* TolC) for 2 h and subsequently diluted with the same medium to OD₆₀₀ 0.06. Inocula of 100 μ L were added to the wells containing 100 μ L of the specific concentrations of the compounds in PMBN/PA β N containing medium. MIC₅₀ values were determined for *E. coli* K12, and *E. coli* D22.

Determination of resistance rate Procedures were performed according to a described method¹² with modifications. Defined numbers of *E. coli* TolC cells (10^4 – 10^{12}) were incubated in LB in presence of the 2 \times MIC of Rif, Myx B or compound **30** in parallel (16 h, 37 °C, 50 rpm, 0.5% DMSO). On each of the three following days, a fraction of each sample was supplemented with fresh compound containing LB followed by recultivation (conditions as before). The final cultures were plated on LB agar to determine the bacterial start concentration

which was needed to yield at least one colony on the plates. This threshold was determined to be the resistance rate.

Cytotoxicity HEK 293 cells, a Human Embryonic Kidney 293 cell line, (2×10^5 cells per well) were seeded in 24-well, flat-bottomed plates. Culturing of cells, incubations and OD measurements were performed as described previously⁵⁷ with slight modifications. 24 h after seeding the cells, the incubation was started by the addition of compounds in a final DMSO concentration of 1%. The living cell mass was determined after 24, 48 and 72 h followed by the calculation of LD₅₀ values.

Computational chemistry

All computational work was performed using Molecular Operating Environment (MOE) version 2010.10, Chemical Computing Group Inc., 1010 Sherbrooke St. West, Suite 910, Montreal, Quebec, H3A 2R7, Canada.

Similarity analysis A database containing the compounds **11**, **21**, **30**, and **42** was created and 2D fingerprint GpiDAPH3 (graph pi-donor-acceptor-polar-hydrophobe-3 point pharmacophore) was calculated for all entries. Compound **11** was selected as reference structure and sent to MOE window. In the database viewer window, similarity search was performed by setting the fingerprint system to GpiDAPH3, and using the similarity metric Tanimoto coefficient (T_C) to measure similarity between molecules. T_C values range from 0 (no similarity) to 1 (complete similarity).

Flexible alignment Four ligands (**10**, **20**, **29**, and **41** representing classes I–IV respectively) were sketched using molecular builder of MOE, and each structure was subjected to energy minimization up to a gradient 0.05 Kcal/mol Å using the MMFF94x force field. The compounds were aligned using the flexible alignment mode of MOE with stochastic conformational search option was turned on, and configuration limit was set to 200 and iteration limit was set to 1000. Alignment had the best similarity score was retained and refined by MOE.

Preparation of protein structure for docking X-ray crystal structure of the *T. Thermophilus* RNA polymerase holoenzyme in complex with dMyx B (Protein Data Bank (PDB) code 3EQL)⁷ was used to perform the molecular docking study. In the sequence editor panel of MOE, chains C and D (corresponding to β and β' subunits respectively) were selected, and all other chains were deleted. Hydrogen atoms were added to the receptor atoms, and the potential of protein was fixed.

Ligand-receptor docking The binding site was set to dummy atoms which were identified by the site finder mode, and the amino acid residues were chosen where dMyx B binds in the switch region. Docking placement was triangle matcher with rotate bonds option was turned on, the 1st rescoring was ASE with force field refinement, and the 2nd rescoring was alpha HB.

Calculation of angle Each structure was loaded from a previously prepared database of the target compounds into the MOE window, then it was subjected to energy minimization up to gradient 0.05 Kcal/mol Å using the MMFF94x force field. Angle between the aryl group and the ureido side chain was determined by activating the measure button and choosing angles option, then selecting carbon atom no. 1 of the aryl group, the corresponding carbon atom on the heterocyclic ring, and nitrogen atom no. 1 of the ureido group respectively.

Acknowledgment

The authors thank Jeannine Jung and Jannine Ludwig for technical assistance, and Dr. Dagmar Kail and Dr. Carsten Börger for performing the RP-HPLC purification. Furthermore we are grateful to Prof. Rolf Müller, Department of Microbial Natural Products at HIPS for kindly providing Myx B. Walid A. M. Elgaher gratefully acknowledges a scholarship from the German Academic Exchange Service (DAAD).

References

- 1 A. R. M. Coates, G. Halls and Y. Hu, *Br. J. Pharmacol.*, 2011, **163**, 184.
- 2 K. Bush, P. Courvalin, G. Dantas, J. Davies, B. Eisenstein, P. Huovinen, G. A. Jacoby, R. Kishony, B. N. Kreiswirth, E. Kutter, S. A. Lerner, S. Levy, K. Lewis, O. Lomovskaya, J. H. Miller, S. Mobashery, L. J. V. Piddock, S. Projan, C. M. Thomas, A. Tomasz, P. M. Tulkens, T. R. Walsh, J. D. Watson, J. Witkowski, W. Witte, G. Wright, P. Yeh and H. I. Zgurskaya, *Nat. Rev. Microbiol.*, 2011, **9**, 894.
- 3 I. Chopra, *Curr. Opin. Investig. Drugs*, 2007, **8**, 600.
- 4 M. X. Ho, B. P. Hudson, K. Das, E. Arnold and R. H. Ebright, *Curr. Opin. Struct. Biol.*, 2009, **19**, 715.
- 5 K. Traynor, *Am. J. Health Syst. Pharm.*, 2011, **68**, 1276.
- 6 J. Mukhopadhyay, K. Das, S. Ismail, D. Koppstein, M. Jang, B. Hudson, S. Sarafianos, S. Tuske, J. Patel, R. Jansen, H. Irschik, E. Arnold and R. H. Ebright, *Cell*, 2008, **135**, 295.
- 7 G. A. Belogurov, M. N. Vassilyeva, A. Sevostyanova, J. R. Appleman, A. X. Xiang, R. Lira, S. E. Webber, S. Klyuyev, E. Nudler, I. Artsimovitch and D. G. Vassilyev, *Nature*, 2009, **457**, 332.
- 8 A. Srivastava, M. Talaue, S. Liu, D. Degen, R. Y. Ebright, E. Sineva, A. Chakraborty, S. Y. Druzhinin, S. Chatterjee, J. Mukhopadhyay, Y. W. Ebright, A. Zozula, J. Shen, S. Sengupta, R. R.

- Niedfeldt, C. Xin, T. Kaneko, H. Irschik, R. Jansen, S. Donadio, N. Connell and R. H. Ebright, *Curr. Opin. Microbiol.*, 2011, **14**, 532.
- 9 H. Irschik, K. Gerth, G. Höfle, W. Kohl and H. Reichenbach, *J. Antibiotics*, 1983, **36**, 1651.
 - 10 T. Doundoulakis, A. X. Xiang, R. Lira, K. A. Agrios, S. E. Webber, W. Sisson, R. M. Aust, A. M. Shah, R. E. Showalter, J. R. Appleman and K. B. Simonsen, *Bioorg. Med. Chem. Lett.*, 2004, **14**, 5667.
 - 11 T. I. Moy, A. Daniel, C. Hardy, A. Jackson, O. Rehrauer, Y. S. Hwang, D. Zou, K. Nguyen, J. A. Silverman, Q. Li and C. Murphy, *FEMS Microbiol. Lett.*, 2011, **319**, 176.
 - 12 A. Srivastava, D. Degen, Y. W. Ebright and R. H. Ebright, *Antimicrob. Agents Chemother.*, 2012, **56**, 6250.
 - 13 D. Haebich and F. von Nussbaum, *Angew. Chem. Int. Ed.*, 2009, **48**, 3397.
 - 14 M. J. McPhillie, R. Trowbridge, K. R. Mariner, A. J. O'Neill, A. P. Johnson, I. Chopra and C. W. G. Fishwick, *ACS Med. Chem. Lett.*, 2011, **2**, 729.
 - 15 E. T. Buurman, M. A. Foulk, N. Gao, V. A. Laganas, D. C. McKinney, D. T. Moustakas, J. A. Rose, A. B. Shapiro and P. R. Fleming, *J. Bacteriol.*, 2012, **194**, 5504.
 - 16 F. Yakushiji, Y. Miyamoto, Y. Kunoh, R. Okamoto, H. Nakaminami, Y. Yamazaki, N. Noguchi and Y. Hayashi, *ACS Med. Chem. Lett.*, 2013, **4**, 220.
 - 17 J. H. Sahner, M. Groh, M. Negri, J. Hauptenthal and R. W. Hartmann, *Eur. J. Med. Chem.*, 2013, **65**, 223.
 - 18 J. Liebscher, B. Neumann and H. Hartmann, *J. Prakt. Chem.*, 1983, **325**, 915.
 - 19 H. Hartmann and J. Liebscher, *Synthesis*, 1984, **3**, 275.
 - 20 F.-X. L. Foulon, E. Braud, F. Fabis, J.-C. Lancelot and S. Rault, *Tetrahedron*, 2003, **59**, 10051.
 - 21 F.-X. L. Foulon, E. Braud, F. Fabis, J.-C. Lancelot and S. Rault, *J. Comb. Chem.*, 2005, **7**, 253.
 - 22 V. M. Tormyshev, D. V. Trukhin, O. Yu. Rogozhnikova, T. V. Mikhalina, T. I. Troitskaya and A. Flinn, *Synlett*, 2006, 2559.
 - 23 A. R. Moorman, R. Romagnoli and P. G. Baraldi, *PCT Int. Appl.*, WO 2002083083 A2, 2002.
 - 24 E. L. Anderson, J. E. Jr. Casey, L. C. Greene, J. J. Lafferty and H. E. Reiff, *J. Med. Chem.*, 1964, **7**, 259.
 - 25 G. Kirsch, M. D. Cagniant and P. Cagniant, *J. Heterocyclic Chem.*, 1982, **19**, 443.
 - 26 F. Jourdan, D. Ladurée and M. Robba, *J. Heterocyclic Chem.*, 1994, **31**, 305.
 - 27 H. Dolman, J. Kuipers, L. C. Niemann and B. Heijne, *Eur. Pat. Appl.*, EP 508527 A1, 1992.
 - 28 R. S. Long, *J. Am. Chem. Soc.*, 1947, **69**, 990.
 - 29 H. K. Gakhar, G. S. Gill and J. S. Multani, *J. Ind. Chem. Soc.*, 1971, **48**, 953.
 - 30 A. M. Redman, J. Dumas and W. J. Scott, *Org. Lett.*, 2000, **2**, 2061.
 - 31 H. B. Stevenson and J. R. Johnson, *J. Am. Chem. Soc.*, 1937, **59**, 2525.
 - 32 G. M. Klein, J. P. Heotis and J. A. Buzard, *J. Biol. Chem.*, 1963, **238**, 1625.
 - 33 J. F. Blount, D. L. Coffen and D. A. Katonak, *J. Org. Chem.*, 1978, **43**, 3821.

- 34 C. Hansch, A. Leo and R. W. Taft, *Chem. Rev.*, 1991, **91**, 165.
- 35 T. Rawling, A. M. McDonagh, B. Tattam and M. Murray, *Tetrahedron*, 2012, **68**, 6065.
- 36 J. Valgeirsson, E. Ø. Nielsen, D. Peters, T. Varming, C. Mathiesen, A. S. Kristensen and U. Madsen, *J. Med. Chem.*, 2003, **46**, 5834.
- 37 B. Thavonekham, *Synthesis*, 1997, **1997**, 1189.
- 38 M. Node, K. Nishide, M. Sai, K. Fuji and E. Fujita, *J. Org. Chem.*, 1981, **46**, 1991.
- 39 M. E. Sitzmann, *J. Heterocyclic Chem.*, 1979, **16**, 477.
- 40 M. A. Johnson and G. M. Maggiora, in *Concepts and Applications of Molecular Similarity*, John Wiley & Sons, New York, 1990.
- 41 Y. C. Martin, J. L. Kofron and L. M. Traphagen, *J. Med. Chem.*, 2002, **45**, 4350.
- 42 A. Bender and R. C. Glen, *Org. Biomol. Chem.*, 2004, **2**, 3204.
- 43 P. Willett, *Drug Discovery Today*, 2006, **11**, 1046.
- 44 C. W. Thornber, *Chem. Soc. Rev.*, 1979, **8**, 563.
- 45 P. Villain-Guillot, M. Gualtieri, L. Bastide, F. Roquet, J. Martinez, M. Amblard, M. Pugniere and J.-P. Leonetti, *J. Med. Chem.*, 2007, **50**, 4195.
- 46 F. Arhin, O. Bélanger, S. Ciblat, M. Dehbi, D. Delorme, E. Dietrich, D. Dixit, Y. Lafontaine, D. Lehoux, J. Liu, G. A. McKay, G. Moeck, R. Reddy, Y. Rose, R. Srikumar, K. S. E. Tanaka, D. M. Williams, P. Gros, J. Pelletier, T. R. Parr and A. R. Far, *Bioorg. Med. Chem.*, 2006, **14**, 5812.
- 47 M. Vaara, *Microbiol. Rev.*, 1992, **56**, 395.
- 48 O. Lomovskaya, M. S. Warren, A. Lee, J. Galazzo, R. Fronko, M. Lee, J. Blais, D. Cho, S. Chamberland, T. Renau, R. Leger, S. Hecker, W. Watkins, K. Hoshino, H. Ishida and V. J. Lee, *Antimicrob. Agents Chemother.*, 2001, **45**, 105.
- 49 R. Chollet, J. Chevalier, A. Bryskier and J.-M. Pagès, *Antimicrob. Agents Chemother.*, 2004, **48**, 3621.
- 50 H. Nikaido, *Microbiol. Mol. Biol. Rev.*, 2003, **67**, 593.
- 51 G. Dong, P. Teo, Z. K. Wickens and R. H. Grubbs, *Science*, 2011, **333**, 1609.
- 52 C. A. Mosley, S. J. Myers, E. E. Murray, R. Santangelo, Y. A. Tahirovic, N. Kurtkaya, P. Mullasseril, H. Yuan, P. Lyuboslavsky, P. Le, L. J. Wilson, M. Yepes, R. Dingleline, S. F. Traynelis and D. C. Liotta, *Bioorg. Med. Chem.*, 2009, **17**, 6463.
- 53 N. Chernyak and S. L. Buchwald, *J. Am. Chem. Soc.*, 2012, **134**, 12466.
- 54 A. Rosowsky, H. Chen, H. Fu and S. F. Queener, *Bioorg. Med. Chem.*, 2003, **11**, 59.
- 55 V. Lisowski, F. Fabis, A. Pierré, D.-H. Caignard, P. Renard and S. Rault, *J. Enzyme Inhib. Med. Chem.*, 2002, **17**, 403.
- 56 J. Haupenthal, K. Hüsecken, M. Negri, C. K. Maurer and R. W. Hartmann, *Antimicrob. Agents Chemother.*, 2012, **56**, 4536.
- 57 J. Haupenthal, C. Baehr, S. Zeuzem and A. Piiper, *Int. J. Cancer*, 2007, **121**, 206.

3.2 Discovery and Structure-Based Optimization of 2-Ureidothiophene-3-carboxylic Acids as Dual Bacterial RNA Polymerase and Viral Reverse Transcriptase Inhibitors

Reprinted with permission from [Elgaher, W. A. M.; Sharma, K. K.; Haupenthal, J.; Saladini, F.; Pires, M.; Real, E.; Mély, Y.; Hartmann, R. W. *J. Med. Chem.* 2016, 59, 7212–7222.](#)

Copyright 2016 American Chemical Society.

<http://pubs.acs.org/doi/abs/10.1021/acs.jmedchem.6b00730>

(Publication II)

ABSTRACT

We are concerned with the development of novel anti-infectives with dual antibacterial and antiretroviral activities for MRSA/HIV-1 co-infection. To achieve this goal, we exploited for the first time the mechanistic function similarity between the bacterial RNA polymerase (RNAP) “switch region” and the viral non-nucleoside reverse transcriptase inhibitor (NNRTI) binding site. Starting from our previously discovered RNAP inhibitors, we managed to develop potent RT inhibitors effective against several resistant HIV-1 strains with maintained or enhanced RNAP inhibitory properties following a structure-based design approach. A quantitative structure–activity relationship (QSAR) analysis revealed distinct molecular features necessary for RT inhibition. Furthermore, mode of action (MoA) studies revealed that these compounds inhibit RT noncompetitively, through a new mechanism via closing of the RT clamp. In addition, the novel RNAP/RT inhibitors are characterized by a potent antibacterial activity against *S. aureus* and *in cellulo* antiretroviral activity against NNRTI-resistant strains. In HeLa and HEK 293 cells, the compounds showed only marginal cytotoxicity.

INTRODUCTION

Human immunodeficiency virus type 1 (HIV-1) is the causative agent of the acquired immune deficiency syndrome (AIDS), which is one of the major lethal infectious diseases endangering humanity. In 2014, more than 37 million people worldwide were HIV-infected with a mortality of approximately 1.2 million.¹ The HIV-1 retrovirus targets the CD4 cells resulting in an impairment of the immune system. In consequence, HIV patients are a defenseless prey for bacterial infections, e.g., tuberculosis (TB) and methicillin-resistant *Staphylococcus aureus* (MRSA).²⁻⁴ MRSA co-infection is characterized by a high incidence rate.⁵ In addition, the emergence of multidrug resistant MRSA markedly increased among HIV patients.^{6,7} Current treatment of HIV infection requires a combination of at least three antiretroviral drugs. This highly active antiretroviral therapy (HAART) permits efficient suppression of virus replication and inhibits disease progression. However, the evolution of antiretroviral drug resistance is still presenting an intractable problem due to the high viral mutation rate and noncompliance to antiretroviral therapy (ART).⁸⁻¹⁰ Although the FDA recently approved a combined ART as one pill daily that could improve patient adherence,¹¹ the resistance issue is not yet solved. Treatment of MRSA/HIV-1 co-infection is even more challenging. In addition to the above-mentioned issues, administration of antibiotics should take into consideration the ongoing prevalence of resistant bacteria in HIV-1 populations,^{6,7} as well as potential drug interactions between antiretroviral and antibacterial agents.¹² Hence, there is an urgent need for a one compound therapy of MRSA/HIV-1 co-infections. Combining antibacterial and antiretroviral properties in a single molecule should be beneficial in different aspects: it will improve patient adherence to ART by reduction of medications' regimen¹¹ and consequently decrease the probability of treatment failure. Moreover, prescribing such anti-infective medication will avoid drug interactions,¹² and lower the costs of care as well.¹³

HIV-1 RT is a key target for ART. It reverse-transcribes the single-stranded viral RNA to double-stranded DNA, which is essential for virus replication.¹⁴ There are two main classes inhibiting RT: nucleoside RT inhibitors (NRTIs) and NNRTIs. NRTIs are nucleotide analogues that are incorporated into viral DNA leading to chain termination. Through binding to an allosteric binding site, NNRTIs inhibit RT noncompetitively.^{15,16} In bacteria, RNAP is an essential enzyme for bacterial viability¹⁷ and has consequently become a pivotal drug target. It is responsible for transcription by converting double-stranded DNA to single-stranded RNA, which is a prerequisite for protein synthesis. Consequently, there is a functional relationship between bacterial RNAP and viral RT. In this context, the clinically used RNAP inhibitor rifampicin does also inhibit viral RT.¹⁸ On the other side, HIV-1 RT monoclonal antibodies

were found to inhibit *E. coli* RNAP, indicating structural and functional similarities between both enzymes.¹⁹ Recently, a new RNAP binding site, the “switch region”, was discovered with a mechanistic function close to that of the NNRTI binding site.²⁰ However, these important insights have not yet been exploited for drug discovery.

In previous works, we developed new classes of RNAP “switch region” inhibitors using different drug design approaches.^{21,22} Their mode of action was confirmed by biophysical methods and mutation studies.²³ Beside their activity against MRSA, the compounds showed no cross-resistance with rifampicin and a low rate of resistance development in *E. coli* TolC.^{22,23} Thus, our RNAP inhibitors should be a good starting point for designing such dual acting anti-infectives. For testing our compounds for RT inhibition, we applied our recently developed Förster resonance energy transfer (FRET) based polymerization assay.²⁴ Nevirapine (NVP) as an NNRTI and zidovudine (AZT-TP) as an NRTI were used as references. For hit optimization, we employed a structure-based design approach. Indeed, we succeeded in developing the first anti-infectives with dual antibacterial and antiretroviral activities.

RESULTS AND DISCUSSION

Design of Compounds and SAR

In order to identify the privileged scaffold for HIV-1 RT inhibition among various classes of switch region binding RNAP inhibitors, we selected eight compounds representing four regioisomeric ureidothiophenes (Chart 1).

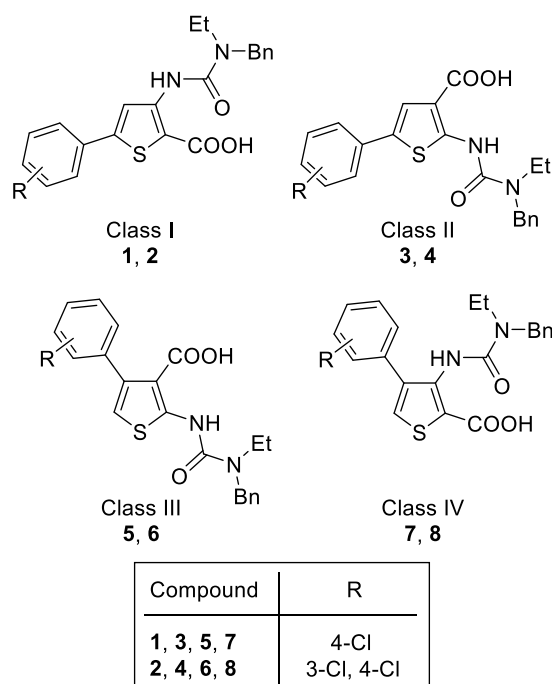


Chart 1. Structures of the Ureidothiophene Regioisomers Used for Finding the Privileged Scaffold for RT Inhibition.

Results revealed that only compound **4** (class II) showed a high RT inhibitory activity ($IC_{50} = 0.9 \mu\text{M}$, Table 1). This indicates that the introduction of an additional chlorine substituent in the 3-position of the phenyl ring leads to a dramatic increase in potency (**4** vs **3**), which is more pronounced than observed for RNAP inhibition.^{21,22} Comparing class II compounds which are highly similar to compounds of class I (the only difference is the position of the S in the thiophene ring) and had shown similar RNAP inhibition,²² strong differences regarding the inhibition of RT were observed, too. This finding can be attributed to the different binding sites and the slight differences in the molecular properties of the ligands. Comparing the RNAP “switch region” and the RT allosteric binding site, it becomes apparent that both pockets are mainly hydrophobic. The RNAP “switch region” is U-shaped with a cavity volume of $\sim 500 \text{ \AA}^3$.²⁵ The RT allosteric binding site is highly flexible regarding size; i.e., it is nonexistent in the absence of NNRTIs,^{26,27} whereas it possesses a cavity volume of $620\text{--}720 \text{ \AA}^3$ in presence of NNRTIs.¹⁴ From analysis of the molecular similarity between class I and II *in silico* by a four-point pharmacophore fingerprint method²⁸ and the Tanimoto coefficient (T_C) as a similarity metric, class I showed partial similarity to II ($T_C = 0.75$). This is in contrast to the results obtained recently using a three-point pharmacophore as a fingerprint.²² As **4** was the only compound showing a strong inhibition against both enzymes, we focused on class II as the most appropriate scaffold for the development of dual RNAP and RT inhibitors.

Table 1. In Vitro Inhibitory Activities of Compounds **1–8** against HIV-1 RT and *E. coli* RNAP

compd	% inhibition of HIV-1 RT at 1 μM	IC_{50} (μM) against <i>E. coli</i> RNAP
1	12 ^a	75
2	24 ^a	22
3	12	54
4	0.9 ^b	21
5	12	>100
6	12	57
7	13 ^c	>200
8	4 ^c	100

^a% inhibition at 25 μM . ^b IC_{50} value (μM). ^c% inhibition at 10 μM .

In the next step, we varied the substituents at the ureido motif of **4** (compounds **9–11**, Table 2). While increasing bulkiness and lipophilicity at the ureido motif led to a potent RNAP inhibitory activity (**10**),^{21,22} the RT inhibitory activities observed for compounds **9–11** were surprising. Exchange of the ethyl substituent by a hydrogen (**9**) as well as by a sterically demanding benzyl substituent (**10**) reduced activity drastically. Activity was restored by omitting the methylene spacer of the R^1 substituent in **9**, i.e., exchanging the benzyl group by

a phenyl (**11**). As compound **11** shows a better ligand efficiency²⁹ and ligand-lipophilicity efficiency²⁹ compared to **4** (LE, 0.32 vs 0.29; LLE, 2.51 vs 2.33), the subsequent structure modifications were performed based on this compound.

Table 2. In Vitro Inhibitory Activities of Compounds **9–20** against HIV-1 RT and *E. coli* RNAP

compd	R ¹	R ²	IC ₅₀ (μM) against HIV-1 RT	IC ₅₀ (μM) against <i>E. coli</i> RNAP
4			0.9	21
9		H	64 ^a	43
10			63 ^a	7
11		H	1.2	20
12		H	0.7	14
13		H	0.8	22
14		H	64 ^a	53
15		H	0.6	27
16		H	0.8	40
17		H	0.3	19
18		H	0.1	26
19		H	0.9	8
20		H	0.6	23
NVP	-	-	0.1	>200
AZT-TP	-	-	7.0	n.d. ^b

^a% inhibition at 25 μM. ^bnot determined.

In order to reduce the number of compounds to be synthesized, we followed a structure-based design strategy. Using a high resolution cocrystal of the RT–NVP complex (PDB code 1VRT),¹⁴ we performed an induced fit molecular docking of **11** into the RT allosteric binding site. The compound adopted a U-shape stabilized by an intramolecular hydrogen bond between the ureido NH and the carboxylate group forming a six membered ring (Figure 1). The thiophene core is located lowermost near the cavity entrance, while the 3,4-dichlorophenyl and the N-phenyl moieties are positioned uppermost overlapping the two pyridine rings of NVP. Four hydrophobic interactions characterize the binding of **11** to the NNRTI binding pocket. Two arene–H interactions can be observed between Leu100 and the thiophene core as well as Leu100 and the 3,4-dichlorophenyl moiety. The latter also binds to Val106 through an arene–H interaction from the other side. The fourth interaction is an edge-to-face (T-shaped) arene interaction between Trp229 and the *m*-position of the N-phenyl group. Binding is further strengthened through a hydrogen bond interaction between Lys101 and the carboxylate C=O group.

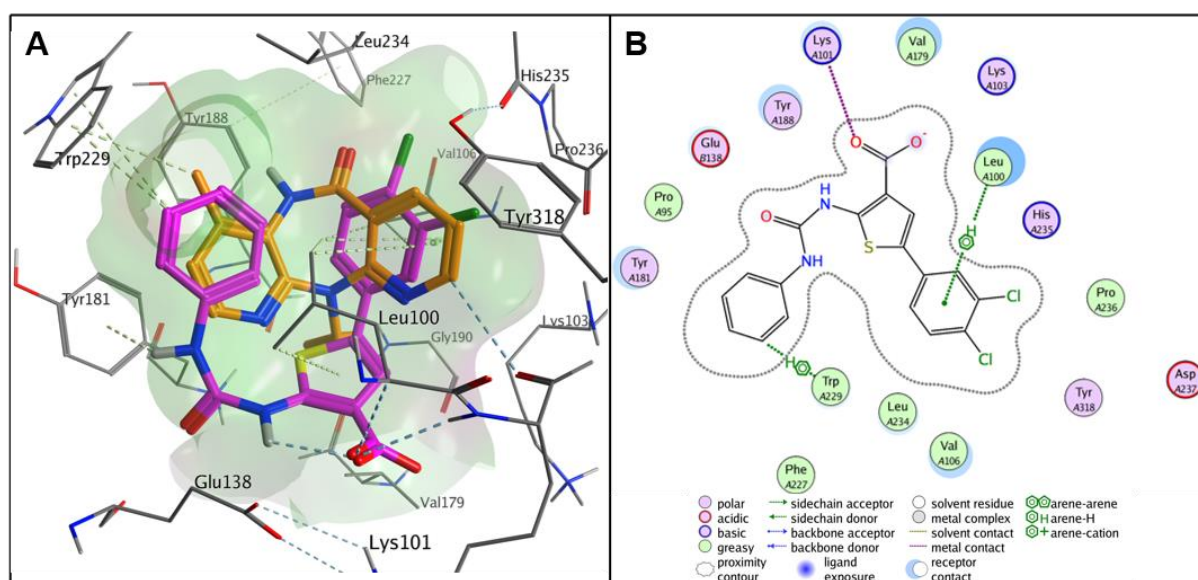


Figure 1. (A) Docking pose of **11** (magenta) compared to NVP (orange) in the RT allosteric binding site: hydrophobic surface (green), polar surface (pink); (B) 2D ligand interactions of **11**.

According to the docking results, all three aromatic motifs of **11** are essential for binding. Moreover, no π – π contacts between **11** and the frequently mutated amino acids Tyr181 and Tyr188¹⁰ were observed. Interestingly, mutations of the amino acids in contact with **11** are known to result in high (Trp229, Val106, Leu100) and low fitness costs (Lys101).^{10,30–32}

Since Trp229, Phe227, and Leu234 belong to the polymerization-essential “primer grip” and are known to show low mutation frequency,^{14,32,33} we further optimized our compounds for interaction with these highly conserved residues. To achieve this goal, we exploited the space between the *p*-position of the N-phenyl moiety and this conserved region by introduction of diverse substituents with varying bulkiness, electronic and lipophilic properties (**12–20**, Table 2). Results indicate that except for compound **14**, the new modifications improve the activity up to 12-fold (**18**). The RT inhibitory activity of compound **18** is comparable to that of NVP and significantly higher than that of AZT-TP. Inspection of the substituent constants and molecular properties of the new compounds (Table S1 in Supporting Information) reveals that hydrophilic and hydrogen bond donor/acceptor substituents at the N-phenyl group are important for activity. Obviously, activity can be enhanced to a certain extent by increasing the conformational flexibility of the compounds. Interestingly, introduction of aromatic moieties (phenyl or 1,2,4-triazolyl) at the sulfonamide or the acetamide group negatively affects RT inhibitory activity (**19** vs **18**, and **16** vs **15**) leading to the hypothesis that too bulky substituents at the ureido motif are not favorable for RT inhibition. These findings are in agreement with our docking model (Figure 1), as these aryl motifs elicit a steric clash with the amino acid residues (Tyr188, Phe227, Trp229, and Leu234) lining the deep side of the NNRTI binding pocket. As a consequence of this, they either are shifted in the binding cavity outward or adopt another conformation leading to lower binding interaction.

For further SAR elucidation, we calculated a QSAR model for compounds **11–20** using a multiple regression analysis

$$pIC_{50} = 4.83 + 1.15 PC^+ - 0.12 vsa_don - 0.27 SMR \quad (1)$$

($n = 10$, $R^2 = 0.94$, $RMSE = 0.13$)

where pIC_{50} is $-\log IC_{50}$, PC^+ is the total positive partial charge, vsa_don is the sum of van der Waals surface areas of pure hydrogen bond donors, and SMR is molecular refractivity.

Equation 1 reveals a role of electrostatic and steric interactions for activity. Increasing the positive partial charge seems beneficial, whereas the number of hydrogen bond donor atoms at the N-phenyl moiety should be kept to a minimum (0–1 atoms). The inverse correlation with molecular refractivity underlines the importance of less polarizable and nonbulky substituents at the ureido motif for RT inhibition.

Regarding RNAP inhibition, the modifications were tolerated or even enhanced the activity (**12** and **19**). This could be attributed to the flexibility of this class of compounds and their ability to adopt more than one binding mode within the RNAP “switch region”.²³

Notably, as NVP shows no RNAP inhibitory activity, this stresses that the 2-ureidothiophen-3-carboxylic acids present a privileged structure for dual RNAP/RT inhibition. The fact that the new inhibitors show different activity profiles against the two target enzymes, resulting in compound **10** as the most potent RNAP inhibitor and **18** as the most active RT inhibitor, indicates specificity of the compounds and excludes promiscuity.

Mode of Action on RT Polymerization

To characterize the mode of action through which our compounds inhibit RT, we monitored first their effects on the binding parameters and orientation of RT on a model primer/template (p/t) duplex. To this end, we used a FRET assay with RT labeled by Alexa488 and a p/t duplex labeled by carboxytetramethylrhodamine (TAMRA).³⁴ The labeled RT mutant was found to bind to the p/t duplex with an affinity of ~3 nM (Figure S1 and Table S2), in good agreement with values reported for DNA p/t sequences in the literature (Table S2).³⁵ Interestingly, similar affinities as well as no change in RT orientation on the duplex were observed in the presence of compounds **4**, **11–13**, and **15–20**, indicating that these compounds marginally affected the binding of RT to the p/t duplexes, as anticipated for NNRTIs (Table S2).

In a next step, we investigated whether these compounds had the same mode of action as NNRTIs. As shown above, the latter bind usually to the hydrophobic pocket in the palm subdomain of p66 and inhibit RT via an allosteric mechanism,^{26,27,36} forcing the p66 thumb into an open extended position with respect to the finger domain, which prevents deoxyribonucleotides (dNTPs) incorporation³⁷ (Figure S2C). In order to monitor the effect of our compounds on the relative motions of the thumb and finger domains, we developed a fluorescence-based assay with a RT double mutant where both Lys287 and Trp24 residues were replaced by cysteine residues.

When the two Cys residues are labeled with Bodipy dyes, the intramolecular distance changes associated with the motion of RT's thumb and finger could be monitored by fluorescence spectroscopy. This distance is a key parameter, as the relative separation between the thumb and finger subdomains defines the opening and closing of the clamp that holds and positions p/t duplexes at the polymerase active site (Figure S2B). A precise positioning of the primer 3'-end with respect to the polymerase active site (Asp110, Asp185, and Asp186) is required for the catalytic addition of a nucleotide. Due to the close proximity of the finger and thumb in the absence of p/t (Figure S2A), the two Bodipy probes were observed to quench each other, providing a low emission (Figure 2A).

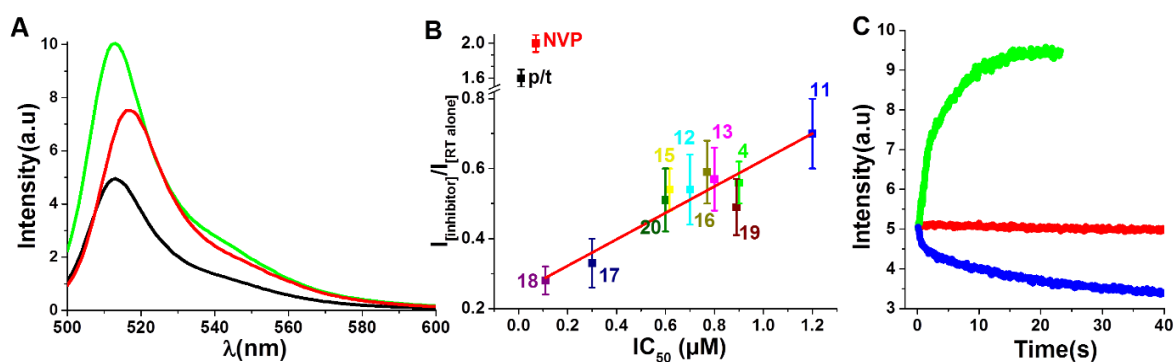


Figure 2. Conformational changes of bodipy-labeled RT p66 W24C+K287C mutant. (A) Emission spectra of 60 nM bodipy-labeled RT in the absence (black line) or in the presence of 160 nM p/t duplex (red line) or 10 μ M NVP (green line). (B) Graph representing the ratio between the fluorescence intensities of the 100 nM doubly-labeled RT in the presence of either the p/t duplex (160 nM) or NVP (10 μ M) or the tested compounds (3 μ M) to the fluorescence intensity of the free form. Red line corresponds to the best fit with linear regression ($y = m \cdot x + b$), with values of slope $m = 0.38 (\pm 0.04) \mu\text{M}$ and intercept $b = 0.25 (\pm 0.03)$. Excitation wavelength was 490 nm and ratios were calculated at emission wavelength of 510 nm. (C) Stopped-flow kinetic traces of 60 nM doubly labeled RT in the absence (red trace) and the presence of 10 μ M NVP (green trace) or compound **11** (blue trace). All traces were fitted by eq 2 and the rate constant values given in Table S2. Excitation wavelength was 490 nm and emission was collected by using a 525/50 nm band pass emission filter.

In contrast, a 1.6-fold increase in Bodipy fluorescence was observed on binding to p/t (Figure 2A and 2B), in line with the expected increase in the distance between the thumb and finger (Figure S2B). An even higher fluorescence increase (2-fold) was observed in the presence of NVP (Figure 2A and Figure 2B), as anticipated from NVP's ability to further separate the two RT subdomains and block them in this open position (Figure S2C). Altogether, the data obtained with the Bodipy-labeled RT were fully consistent with the molecular structures of RT, validating this assay as a convenient means to investigate the inhibitory mechanisms of the synthesized RT inhibitors. In contrast to NVP and p/t duplex, a decrease in Bodipy fluorescence was observed with all tested compounds (Figure 2B). Since no fluorescence quenching was observed when free Bodipy was titrated to the compounds (data not shown), these compounds probably exerted an effect opposite to NVP, decreasing the distance between thumb and finger subdomains. Therefore, the compounds likely exert their inhibitory activity by blocking the RT clamp in a closed conformation.

To get further information on the inhibition mechanism of our compounds, we monitored the changes in fluorescence in real time by stopped-flow (Figure 2C and Table S2). Using NVP as a control, a monoexponential increase of Bodipy emission was observed (Figure 2C and Table S2), suggesting that the NVP-induced opening of RT clamp occurs in a single step. The kinetic traces were fitted by using

$$I(t) = I_F - (I_F - I_0)e^{(-k_{obs}(t-t_0))} \quad (2)$$

where t_0 is the dead time, k_{obs} is the observed kinetic rate constant, and I_0 and I_F are the fluorescence intensities before and after addition of inhibitors, respectively. The I_0 value was obtained from the steady-state fluorescence spectrum of the doubly labeled mutant and was thus fixed.

Similarly, a monoexponential decrease in Bodipy emission was observed with all compounds (Figure 2C and Table S2), suggesting that they induce the closing of RT clamp, also in a single step. The kinetic rate constant values of all compounds were found to fluctuate in a narrow range, indicating that they exhibit similar mechanisms of RT inhibition. Interestingly, a clear correlation could be observed between the closing of the clamp and the IC_{50} values (Figure 2B). This indicates that the inhibitory activity of the compounds is related to their ability to efficiently close the RT clamp and thus hinder the incorporation of dNTPs.

Antibacterial and Antiretroviral Activities

We complemented our *in vitro* results by first evaluating the activity of the new RNAP/RT inhibitors against *S. aureus*. Results revealed a high antibacterial effect for the majority of the compounds with minimum inhibitory concentrations (MICs) between 3 and 13 $\mu\text{g/mL}$ (Table 3). Markedly, these values correlate with the corresponding RNAP inhibitory activities. Second, we applied a cellular infectivity assay to assess the antiretroviral activity of our compounds. This assay is based on the infection of HeLa cells by a third generation of pseudoviral particles,³⁸ mimicking the early steps of the HIV-1 life cycle. Most of the tested compounds exhibited good antiretroviral activities in the low micromolar range (Table 3). Noticeably, a marked difference was observed in the activity profiles when comparing the *in vitro* and *in cellulo* results: The compounds turned out to be less active in the cellular system. This might be due to the lipophilic nature of the compounds leading to an inefficient permeation into the cells, or an interaction with other proteins in the antiviral assay leading to a lowered concentration at the target enzyme.

Next, we examined the effect of our compounds on cell viability in two different cell lines (HeLa and HEK 293) and found them to display only marginal or no cytotoxicity (Table 3).

Table 3. Antibacterial, Antiretroviral, and Cytotoxic Activities of the Dual RNAP/RT Inhibitors

compd	MIC <i>S. aureus</i> ($\mu\text{g/mL}$)	IC ₅₀ Viral infectivity (μM)	% Inhibition of HeLa cell viability at 25 μM	LD ₅₀ HEK 293 cells (μM)
4	10	27	23	58
11	6	20	0	61
12	4	n.i. ^a	0	68
13	8	35	12	80
17	25	30	6	86
18	39	30	0	>100
19	3	n.d. ^b	n.d. ^b	94
20	13	n.d. ^b	n.d. ^b	>100

^aNo inhibition. ^bNot determined.

Antiretroviral Activity in NNRTI-Resistant HIV-1 Strains

On the basis of the docking study, the binding mode of our new NNRTIs could be advantageous regarding the resistance issue. The numerous interactions between our ligands and the NNRTI binding pocket, especially those with the highly conserved amino acids, should only be moderately affected by the single site mutations that result from using other NNRTIs and are responsible for resistance.^{9,10,30} To verify this point and to get more insight into the binding mode of our compounds, we tested the antiviral activity of compounds **11**, **18**, and **19** against the HIV-1 wild-type (WT) NL4-3 and a panel of strains with multiple resistance mutations to clinically used NNRTIs in a TZM-bl cell line based phenotypic assay (Table 4).

Table 4. Antiretroviral Activity of **11**, **18**, **19**, and Reference NNRTIs against HIV-1 WT (114) and NNRTIs-Resistant Strains (12237, 12235, 12231, 12229)

compd ^a	IC ₅₀ (μM)	fold change in susceptibility ^b (biological ^c or clinical ^d cutoff)			
	114 ^e NL4-3 (WT)	12237 ^e (V106I, Y181C, G190A, H221Y) ^f	12235 ^e (A98G, K101E, Y181C, G190A) ^f	12231 ^e (K103N, V179F, Y181C) ^f	12229 ^e (L100I, K103N, H221Y) ^f
11	5	1	3	>4	>4
18	5	1.5	3.5	>4	>4
19	15	>1.5	1	>1.5	>1.5
NVP	0.1 ^g	>200 (4.5) ^c	>200 (4.5) ^c	>200 (4.5) ^c	>200 (4.5) ^c
EFV	0.002 ^g	26 (3) ^c	>200 (3) ^c	90 (3) ^c	>200 (3) ^c
ETR	0.005 ^g	6.0 (2.9) ^d	15 (2.9) ^d	8.8 (2.9) ^d	6.8 (2.9) ^d
RPV	0.0009 ^g	3.5 (2) ^c	22 (2) ^c	2.3 (2) ^c	6.3 (2) ^c

^aEFV = efavirenz, ETR = etravirine, RPV = rilpivirine. ^bResistant virus IC₅₀/WT virus IC₅₀ ratio calculated with the Phenosense assay. ^cThe biological cutoff was determined by in vitro analysis of multiple viral variants not exposed to the drug and defined as the mean fold-change plus 2 standard deviations with respect to the reference viral strain. It is used when a clinical cutoff has not been established. ^dThe clinical cutoff was determined by statistical analysis of clinical data and is defined as the fold-change value corresponding to loss of drug activity in vivo. ^eID of viruses refer to the NIH AIDS Reagent Program catalogue number. ^fThe NNRTIs resistance mutations. ^gIC₅₀ values against WT were previously determined.³⁹

Our results reveal that the tested compounds show good activity against the WT (IC_{50} values of 5–15 μ M) as well as against the mutants 12237 and 12235. In contrast, they are unable to halt the replication of 12231 and 12229 strains. At the same time, the reference drugs NVP, EFV, and ETR show a dramatic loss of potency against all resistant mutants.

These data indicate that our compounds are still able to bind to and to inhibit the RTs with mutations K101E, V106I, Y181C, and G190A, which confer high-level resistance against NNRTIs.^{10,30} This can on the one side be attributed to the presence of essential contacts between our ligands and the amino acid residues of high fitness costs such as Leu100, Phe227, and Trp229. On the other side, due to the conformational flexibility of our compounds they can easily adopt to the steric changes in the binding site of the mutated proteins. Interestingly, the K103N mutation seems to have a negative effect on our compounds' RT inhibition and antiretroviral activity. This result does not contradict our predicted binding mode, since this mutation affects the pocket entrance.⁴⁰ In addition, the L100I mutation may impair the binding to RT.

These findings are consistent with the predicted binding mode of our new NNRTIs and thus further confirm their binding site. Moreover, the fact that no cross-resistance was observed in some NNRTIs-resistant strains is an important advantage over the first (NVP and EFV) and second generation (ETR and RPV) NNRTIs.

Finally, we performed a docking study for the most active compound **18** (Figure 3). Compared to the binding of **11**, the eastern part of the molecules binds identically to the protein. Unexpectedly, in the western part a slight change was observed as the newly introduced methanesulfonamido group leads to CH– π interaction with the highly conserved Trp229. As a consequence of this, the N-phenyl ring is slightly shifted downward away from Trp229. Moreover, an atypical hydrogen bond was identified between the conserved Phe227 (as donor) and the 3,4-dichlorophenyl motif (as acceptor). Furthermore, no π – π interaction was observed between Tyr181 and the N-phenyl moiety (centroid–centroid distance of >4 Å).

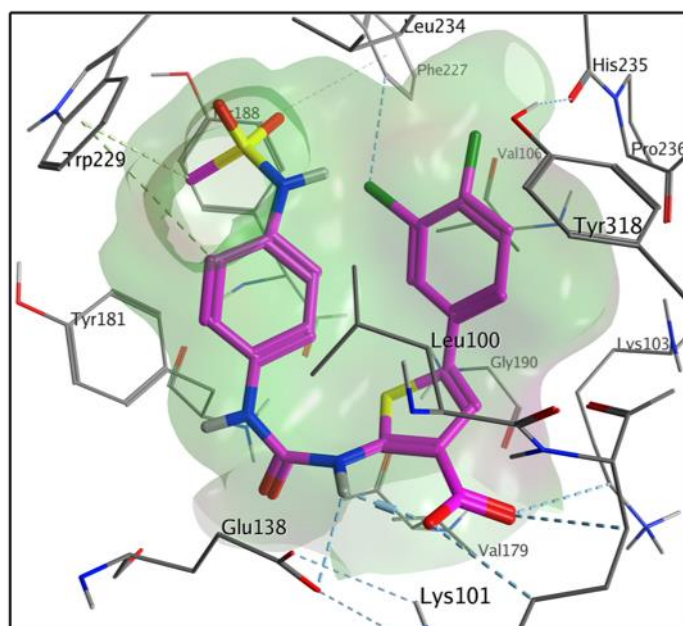
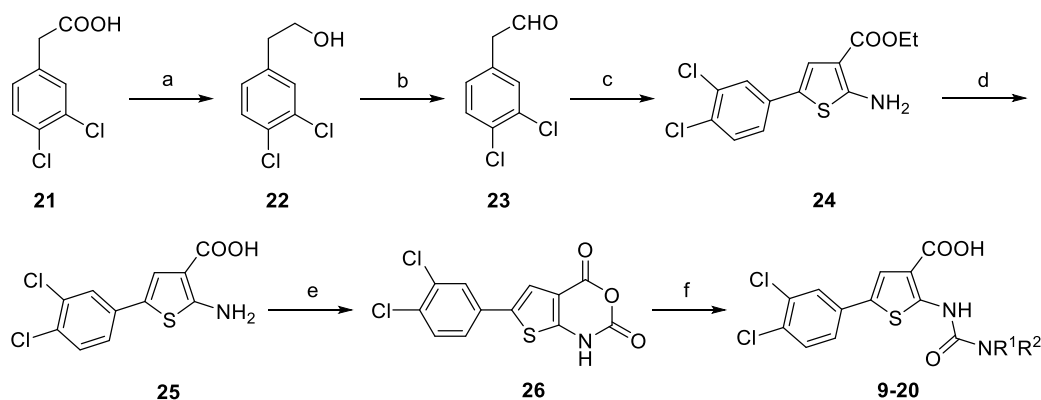


Figure 3. Docking pose of **18** in the NNRTI binding site.

Chemistry

Synthesis of the 5-aryl-2-ureidothiophene-3-carboxylic acids was accomplished through a straightforward procedure starting with 3,4-dichlorophenylacetic acid **21** (Scheme 1). Reduction with LiAlH_4 followed by mild oxidation of the produced alcohol **22** using PCC delivered the arylacetaldehyde **23** in a good yield. Gewald reaction of **23** with ethyl cyanoacetate and elemental sulfur under basic conditions in a one-pot reaction afforded the 2-aminothiophene-3-carboxylate **24**.²² The ester was saponified to the corresponding acid **25**, which was treated with BTC to produce the 6-arylthiaisatoic anhydride **26**. Synthesis was finalized via coupling of **26** and the appropriate amine in water/TEA (2:1) mixture at room temperature followed by acidic workup to yield the 5-aryl-2-ureidothiophene-3-carboxylic acids **9–20**.

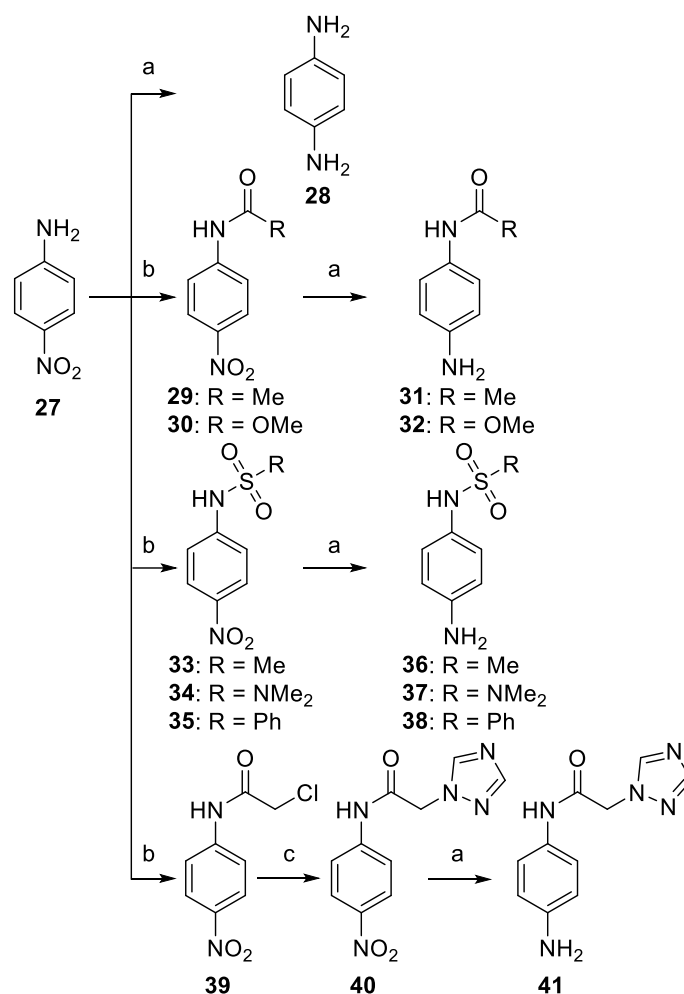
Scheme 1. Synthesis of the 2-Ureidothiophene-3-carboxylic Acids **9–20**^a



^aReagents and conditions: (a) LiAlH_4 , THF, reflux, 2 h; (b) PCC, DCM, rt, 2 h; (c) $1/8 \text{ S}_8$, $\text{NCCH}_2\text{COOEt}$, TEA, EtOH, reflux, 12 h; (d) KOH, MeOH/ H_2O , reflux, 4 h; (e) BTC, THF, rt, 2 h; (f) $\text{R}^1\text{R}^2\text{NH}$, $\text{H}_2\text{O}/\text{TEA}$, rt, 2 h.

The *N*-monosubstituted-*p*-phenylenediamines were prepared from *p*-nitroaniline **27** keeping the nitro moiety as a hidden protected amino group (Scheme 2). Reaction of **27** with acyl chlorides or sulfonyl chlorides in the presence of pyridine yielded the corresponding amides or sulfonamides, respectively. The nitro derivatives were reduced by iron/ammonium chloride mixture to afford the corresponding amines in excellent yields.

Scheme 2. Synthesis of the Intermediate Aromatic Amines^a

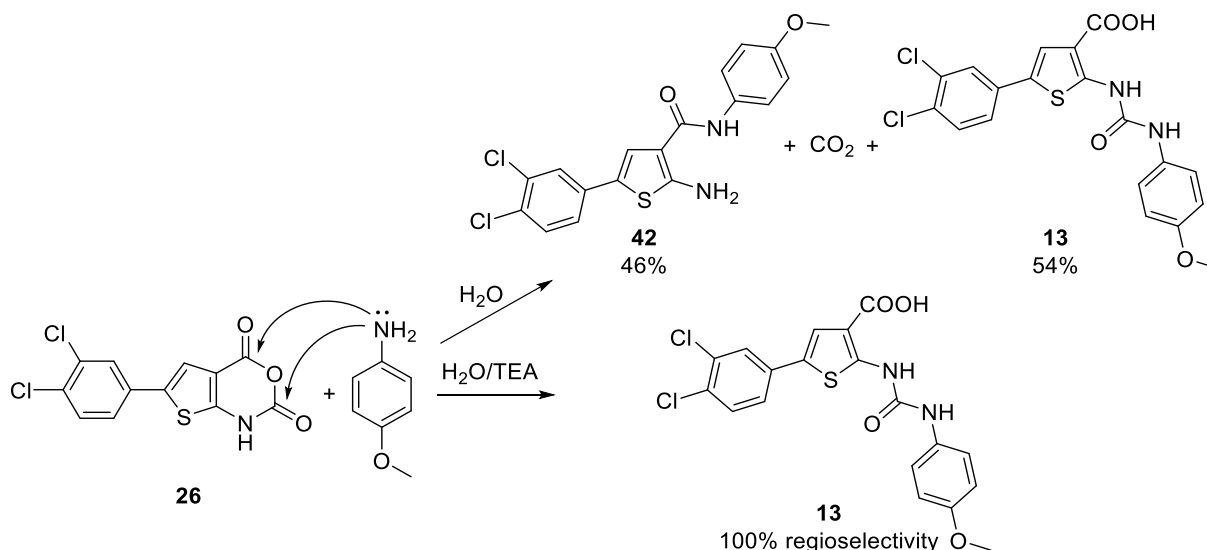


^aReagents and conditions: (a) Fe/ NH_4Cl , EtOH, reflux, 1 h; (b) RCOCl or RSO_2Cl , pyridine/DCM, rt, 12 h; (c) 1,2,4-triazole, $\text{K}_2\text{CO}_3/\text{DMF}$, 70 °C, 1 h.

It is noteworthy that TEA is crucial for formation of the desired ureidothiophene carboxylic acids. Modification of the previous procedures that did not employ TEA in the coupling step^{21,22} was necessary to enhance the reaction regioselectivity. Since the utilized anilines in this work are weak nucleophiles, the coupling reaction using *p*-anisidine for example in absence of TEA afforded a mixture of the amide **42** and the ureidocarboxylic acid **13** in nearly 1:1 ratio as indicated from the ^1H NMR spectrum (Figure S3). In contrast, running the same reaction in the presence of TEA produced exclusively the ureidothiophene carboxylic acid **13**

in 100% regioselectivity (Scheme 3). Moreover, we found that the loss of amine regioselectivity and reactivity is directly proportional to the electron deficiency of the substituted aniline, i.e., no ureidothiophene product could be obtained from the reaction of **26** with *p*-nitroaniline **27** even when TEA was applied.

Scheme 3. Reaction of **26** with *p*-Anisidine in Presence and Absence of TEA



CONCLUSION

In this work we discovered and developed 2-ureidothiophene-3-carboxylic acids as dual bacterial RNAP and HIV-1 RT inhibitors for the treatment of MRSA/HIV-1 co-infections. This development was based on an unprecedented exploitation of the functional and structural similarities between the RNAP “switch region” and the NNRTI allosteric binding site. First, we identified the privileged structure for RT inhibition by screening four regioisomeric classes of “switch region” binding RNAP inhibitors. Next, we explored the steric volume allowed in the NNRTI binding pocket through enlarging the bulkiness of the ureido moiety. Finally, we applied a structure-based design strategy for hit optimization. We were able to improve the RT inhibitory activity in parallel with enhancing, or at least maintaining, the activity against RNAP. SAR studies revealed the importance of hydrophilic nonbulky substituents at the ureido side chain for RT inhibition. A MoA investigation revealed a noncompetitive inhibition mechanism of our compounds, which is typical for NNRTIs. Interestingly, the compounds seem to act through a new mechanism via closing of the RT clamp. The new RNAP/RT inhibitors displayed high potency against *S. aureus* as well as *in cellulo* antiretroviral activity accompanied by marginal or no cytotoxicity. Furthermore, these compounds were active against NNRTI-resistant strains. Thus, our work establishes the basis for the development of a single compound therapy not only against MRSA/HIV but also against other challenging co-infections of major public health concern especially Mtb/HIV co-infection.

EXPERIMENTAL SECTION

Materials and Methods

Starting materials and solvents were purchased from commercial suppliers, and used without further purification. All chemical yields refer to purified compounds and were not optimized. Reaction progress was monitored using TLC Silica gel 60 F₂₅₄ aluminum sheets, and visualization was accomplished by UV at 254 nm. Flash chromatography was performed using silica gel 60 Å (40–63 µm). Preparative RP-HPLC was carried out on a Waters Corporation setup containing a 2767 sample manager, a 2545 binary gradient module, a 2998 PDA detector and a 3100 electron spray mass spectrometer. Purification was performed using a Waters XBridge column (C18, 150 mm × 19 mm, 5 µm), a binary solvent system A and B (A = water with 0.1% formic acid; B = MeCN with 0.1% formic acid) as eluent, a flow rate of 20 mL/min, and a gradient of 60% to 95% B in 8 min were applied. NMR spectra were recorded on either a Bruker DRX-500 (¹H, 500 MHz; ¹³C, 126 MHz) or Bruker Fourier 300 (¹H, 300 MHz; ¹³C, 75 MHz) spectrometer at 300 K. Chemical shifts were recorded as δ values in ppm units by reference to the hydrogenated residues of deuterated solvent as internal standard (CDCl₃, δ = 7.27, 77.00; DMSO-d₆, δ = 2.50, 39.51). Splitting patterns describe apparent multiplicities and are designated as s (singlet), br s (broad singlet), d (doublet), dd (doublet of doublet), t (triplet), q (quartet), m (multiplet). Coupling constants (*J*) are given in Hertz (Hz). Weak or coalesced signals were elucidated by heteronuclear multiple quantum coherence (HMQC) and heteronuclear multiple bond coherence (HMBC) 2D-NMR techniques. Purity of all compounds used in biological assays was ≥ 95% as measured by LC/MS Finnigan Surveyor MSQ Plus (Thermo Fisher Scientific, Dreieich, Germany). The system consists of LC pump, autosampler, PDA detector, and single-quadrupole MS detector, as well as the standard software Xcalibur for operation. RP C18 Nucleodur 100-5 (125 mm × 3 mm) column (Macherey-Nagel GmbH, Dühren, Germany) was used as stationary phase, and a binary solvent system A and B (A = water with 0.1% TFA; B = MeCN with 0.1% TFA) was used as mobile phase. In a gradient run the percentage of B was increased from an initial concentration of 0% at 0 min to 100% at 15 min and kept at 100% for 5 min. The injection volume was 10 µL and the flow rate was set to 800 µL/min. MS (ESI) analysis was carried out at a spray voltage of 3800 V, a capillary temperature of 350 °C and a source CID of 10 V. Spectra were acquired in positive mode from 100 to 1000 m/z and at 254 nm for UV tracing.

General Procedure for Synthesis of 5-(3,4-Dichlorophenyl)-2-[3-(4-(un)substituted-phenyl)ureido]thiophene-3-carboxylic Acids 11–20

To a stirred suspension of the thiaisatoic anhydride **26** (150 mg, 0.48 mmol) in a mixture of water (6 mL) and TEA (1 mL), the appropriate amine (1.0 mmol) in TEA (2 mL) was added. The reaction mixture was stirred at rt overnight, then poured on ice-cooled 2 N HCl (40 mL), and extracted with EtOAc/THF (1:1, 40 mL). The organic layer was washed with cold 2 N HCl/brine (1:1, 2 × 40 mL), dried over anhydrous MgSO₄, and concentrated *in vacuo*. The obtained crude material was suspended in *n*-hexane/EtOAc (4:1, 50 mL), stirred in a water bath at 40 °C for 10 min, cooled, and collected by filtration.

5-(3,4-Dichlorophenyl)-2-(3-phenylureido)thiophene-3-carboxylic Acid (11)

Yield 90%; beige solid; ¹H NMR (500 MHz, DMSO-d₆) δ 13.02 (br s, 1H), 10.61 (br s, 1H), 10.36 (br s, 1H), 7.88 (d, *J* = 2.0 Hz, 1H), 7.63 (s, 1H), 7.60 (d, *J* = 8.0 Hz, 1H), 7.58 (dd, *J* = 8.0, 2.0 Hz, 1H), 7.52 (m, 2H), 7.33 (m, 2H), 7.04 (m, 1H); ¹³C NMR (126 MHz, DMSO-d₆) δ 165.80, 150.98, 150.15, 138.86, 134.31, 131.87, 131.07, 129.07, 128.94 (2C), 127.72, 126.10, 124.70, 122.77, 122.27, 118.49 (2C), 112.36; *m/z* (ESI⁺) 407 [M + H]⁺; *t_R* = 14.49 min.

5-(3,4-Dichlorophenyl)-2-(3-(4-fluorophenyl)ureido)thiophene-3-carboxylic Acid (12)

Yield 82%; gray solid; ¹H NMR (300 MHz, DMSO-d₆) δ 13.04 (br s, 1H), 10.60 (br s, 1H), 10.39 (br s, 1H), 7.88 (d, *J* = 1.5 Hz, 1H), 7.63 (s, 1H), 7.59 (m, 2H), 7.51 (m, 2H), 7.17 (m, 2H); ¹³C NMR (75 MHz, DMSO-d₆) δ 165.81, 157.84 (d, *J* = 239.2 Hz, 1C), 151.00, 150.12, 135.17 (d, *J* = 2.2 Hz, 1C), 134.28, 131.86, 131.07, 129.08, 127.75, 126.10, 124.70, 122.25, 120.27 (d, *J* = 7.5 Hz, 2C), 115.50 (d, *J* = 22.4 Hz, 2C), 112.37; *m/z* (ESI⁺) 424 [M]⁺; *t_R* = 14.96 min.

5-(3,4-Dichlorophenyl)-2-(3-(4-methoxyphenyl)ureido)thiophene-3-carboxylic Acid (13)

Yield 86%; beige solid; ¹H NMR (300 MHz, DMSO-d₆) δ 12.66 (br s, 1H), 10.56 (br s, 1H), 10.16 (br s, 1H), 7.88 (d, *J* = 1.0 Hz, 1H), 7.62 (s, 1H), 7.57 (m, 2H), 7.41 (d, *J* = 8.8 Hz, 2H), 6.91 (d, *J* = 8.8 Hz, 2H), 3.73 (s, 3H); ¹³C NMR (75 MHz, DMSO-d₆) δ 165.86, 155.11, 151.04, 150.40, 134.37, 131.86, 131.78, 131.08, 129.01, 127.52, 126.07, 124.69, 122.27, 120.31 (2C), 114.15 (2C), 112.16, 55.20; *m/z* (ESI⁺) 437 [M + H]⁺; *t_R* = 14.36 min.

2-(3-(4-Aminophenyl)ureido)-5-(3,4-dichlorophenyl)thiophene-3-carboxylic Acid (14)

Yield 80%; pink solid; ¹H NMR (300 MHz, DMSO-d₆) δ 11.88 (br s, 1H), 10.72 (br s, 1H), 9.83 (br s, 1H), 7.84 (d, *J* = 1.0 Hz, 1H), 7.57 (m, 3H), 7.14 (d, *J* = 8.6 Hz, 2H), 6.54 (d, *J* = 8.6 Hz, 2H), 3.43 (br s, 2H); ¹³C NMR (75 MHz, DMSO-d₆) δ 166.19, 151.23, 150.33, 144.86,

134.61, 131.81, 131.06, 128.75, 127.51, 126.94, 125.90, 124.55, 122.55, 120.92 (2C), 114.12 (2C), 112.83; m/z (ESI+) 421 $[M]^+$; t_R = 9.78 min.

2-(3-(4-Acetamidophenyl)ureido)-5-(3,4-dichlorophenyl)thiophene-3-carboxylic Acid (15)

Yield 90%; beige solid; 1H NMR (500 MHz, DMSO- d_6) δ 13.04 (br s, 1H), 10.58 (br s, 1H), 10.27 (br s, 1H), 9.87 (br s, 1H), 7.89 (d, J = 1.9 Hz, 1H), 7.63 (s, 1H), 7.61 (d, J = 8.5 Hz, 1H), 7.58 (dd, J = 8.5, 1.9 Hz, 1H), 7.53 (d, J = 9.1 Hz, 2H), 7.42 (d, J = 9.1 Hz, 2H), 2.02 (s, 3H); ^{13}C NMR (126 MHz, DMSO- d_6) δ 167.91, 165.79, 150.94, 150.27, 134.60, 134.34, 133.93, 131.85, 131.07, 129.02, 127.60, 126.09, 124.70, 122.26, 119.62 (2C), 118.95 (2C), 112.20, 23.87; m/z (ESI+) 464 $[M + H]^+$; t_R = 17.40 min.

2-(3-(4-(2-(1H-1,2,4-Triazol-1-yl)acetamido)phenyl)ureido)-5-(3,4-dichlorophenyl)thiophene-3-carboxylic Acid (16)

Yield 65%; pale gray solid; 1H NMR (500 MHz, DMSO- d_6) δ 13.02 (br s, 1H), 10.94 (br s, 1H), 10.61 (br s, 1H), 10.52 (br s, 1H), 8.65 (s, 1H), 8.04 (s, 1H), 7.89 (d, J = 1.9 Hz, 1H), 7.63 (s, 1H), 7.61 (d, J = 8.5 Hz, 1H), 7.60 (d, J = 9.1 Hz, 2H), 7.58 (dd, J = 8.5, 1.9 Hz, 1H), 7.47 (d, J = 9.1 Hz, 2H), 5.21 (s, 2H); ^{13}C NMR (126 MHz, DMSO- d_6) δ 165.66, 164.11, 150.99, 150.91, 150.13, 145.44, 134.60, 134.35, 133.78, 131.84, 131.09, 129.00, 127.60, 126.08, 124.72, 122.30, 119.83 (2C), 118.94 (2C), 112.35, 51.82; m/z (ESI+) 531 $[M + H]^+$; t_R = 17.10 min.

5-(3,4-Dichlorophenyl)-2-(3-(4-((methoxycarbonyl)amino)phenyl)ureido)thiophene-3-carboxylic Acid (17)

Yield 65%; white solid; 1H NMR (500 MHz, DMSO- d_6) δ 13.01 (br s, 1H), 10.60 (br s, 1H), 10.25 (br s, 1H), 9.55 (br s, 1H), 7.87 (d, J = 1.9 Hz, 1H), 7.62 (s, 1H), 7.60 (d, J = 8.2 Hz, 1H), 7.57 (dd, J = 8.2, 1.9 Hz, 1H), 7.42 (d, J = 8.5 Hz, 2H), 7.40 (d, J = 8.5 Hz, 2H), 3.65 (s, 3H); ^{13}C NMR (126 MHz, DMSO- d_6) δ 165.87, 154.09, 151.01, 150.28, 134.39, 134.36, 133.59, 131.89, 131.11, 129.05, 127.60, 126.10, 124.72, 122.31, 119.23 (2C), 118.91 (2C), 112.34, 51.57; m/z (ESI+) 480 $[M + H]^+$; t_R = 13.46 min.

5-(3,4-Dichlorophenyl)-2-(3-(4-(methylsulfonamido)phenyl)ureido)thiophene-3-carboxylic Acid (18)

Yield 70%; white crystals; 1H NMR (300 MHz, DMSO- d_6) δ 13.01 (br s, 1H), 10.60 (br s, 1H), 10.35 (br s, 1H), 9.54 (br s, 1H), 7.88 (d, J = 1.0 Hz, 1H), 7.62 (s, 1H), 7.58 (d, J = 8.0 Hz, 1H), 7.56 (dd, J = 8.0, 1.0 Hz, 1H), 7.48 (d, J = 8.6 Hz, 2H), 7.19 (d, J = 8.6 Hz, 2H), 2.94 (s, 3H); ^{13}C NMR (75 MHz, DMSO- d_6) δ 165.82, 150.97, 150.16, 135.49, 134.31, 133.08,

131.88, 131.08, 129.07, 127.71, 126.10, 124.72, 122.27, 121.73 (2C), 119.45 (2C), 112.36, 38.95; m/z (ESI+) 499 [M]⁺; t_R = 12.86 min.

5-(3,4-Dichlorophenyl)-2-(3-(4-(phenylsulfonamido)phenyl)ureido)thiophene-3-carboxylic Acid (19)

Yield 88%; reddish solid; ¹H NMR (500 MHz, DMSO-d₆) δ 13.04 (br s, 1H), 10.56 (br s, 1H), 10.29 (br s, 1H), 10.09 (br s, 1H), 7.88 (d, J = 2.2 Hz, 1H), 7.72 (m, 2H), 7.62 (s, 1H), 7.60 (m, 2H), 7.55 (m, 3H), 7.36 (d, J = 9.1 Hz, 2H), 7.03 (d, J = 9.1 Hz, 2H); ¹³C NMR (126 MHz, DMSO-d₆) δ 165.76, 150.87, 150.08, 139.46, 135.56, 134.28, 132.77, 132.27, 131.85, 131.07, 129.16 (2C), 129.06, 127.69, 126.63 (2C), 126.10, 124.70, 122.26, 121.88 (2C), 119.20 (2C), 112.33; m/z (ESI+) 561 [M]⁺; t_R = 17.26 min.

5-(3,4-Dichlorophenyl)-2-(3-(4-((*N,N*-dimethylsulfamoyl)amino)phenyl)ureido)thiophene-3-carboxylic Acid (20)

Yield 79%; beige solid; ¹H NMR (500 MHz, DMSO-d₆) δ 13.06 (br s, 1H), 10.59 (br s, 1H), 10.31 (br s, 1H), 9.72 (br s, 1H), 7.89 (d, J = 2.2 Hz, 1H), 7.63 (s, 1H), 7.61 (d, J = 8.2 Hz, 1H), 7.58 (dd, J = 8.2, 2.2 Hz, 1H), 7.44 (d, J = 9.1 Hz, 2H), 7.18 (d, J = 9.1 Hz, 2H), 2.69 (s, 6H); ¹³C NMR (126 MHz, DMSO-d₆) δ 165.78, 150.95, 150.18, 134.78, 134.31, 133.45, 131.85, 131.07, 129.05, 127.66, 126.10, 124.70, 122.24, 120.95 (2C), 119.32 (2C), 112.27, 37.75 (2C); m/z (ESI+) 529 [M + H]⁺; t_R = 17.20 min.

Experimental procedures for the synthesis of all other target compounds and necessary precursors together with their characterization and NMR spectra are described in detail in the Supporting Information.

Computational Chemistry All computational work was performed using Molecular Operating Environment (MOE) version 2015.10, Chemical Computing Group Inc., 1010 Sherbrooke St. West, Suite 910, Montreal, Quebec, H3A 2R7, Canada.

Similarity Analysis A database containing compounds **2** and **4** was created, and the fingerprint piDAPH4 (π -donor-acceptor-polar-hydrophobe four-point pharmacophore) was calculated for both entries. Compound **4** was selected as a reference structure and sent to MOE window. In the database viewer window, similarity search was performed by setting the fingerprint system to piDAPH4 and using the similarity metric Tanimoto coefficient (T_C) to measure similarity between molecules. T_C values range from 0 (no similarity) to 1 (complete similarity).

Preparation of Ligands and Protein Structure for Docking In the database viewer window, compounds **11** and **18** were selected and washed via compute | molecule | wash command.

Deprotonation of strong acids and protonation of strong bases options were checked in the wash panel. X-ray crystal structure of the HIV-1 RT in complex with NVP (PDB code 1VRT)¹⁴ was used to perform the molecular docking study. Potential was set up to Amber10:EHT for force field and R-field for solvation. Addition of hydrogen atoms and removal of water molecules were performed via LigX module.

Ligand–Receptor Docking By use of the induced fit docking protocol, the binding site was set to dummy atoms which were identified by the site finder mode, and the amino acid residues were chosen where nevirapine binds in the RT allosteric binding site. Docking placement was triangle matcher with rotate bonds option. The first rescoring was ASE with force field refinement, and the second rescoring was alpha HB.

QSAR Analysis A database containing compounds **11–20** was created, and each structure was subjected to energy minimization up to a gradient $0.01 \text{ kcal mol}^{-1} \text{ \AA}^{-2}$ using the MMFF94x force field and distance solvation model. In the database viewer window, molecular descriptors were calculated for all entries via activating the compute panel, choosing descriptors calculate option (Table S1). The QSAR model was computed using partial least-squares (PLS) method.

Binding Measurements were performed at $20 \text{ }^\circ\text{C}$ using a Fluoromax 4 spectrofluorometer (Jobin-Yvon Horiba) by monitoring the increase of FRET efficiency, E_{FRET} , associated with the formation of the complex between Alexa488-labeled RT and TAMRA-labeled p/t duplexes. The FRET efficiency, calculated by $E_{\text{FRET}} = 1 - I_{\text{DA}}/I_{\text{D}}$ (where I_{D} and I_{DA} are the intensities of the Alexa 488 donor in the absence and in the presence of the TAMRA acceptor, respectively), was then plotted as a function of the total concentration of the labeled oligonucleotide (ODN) and fitted with a rewritten Scatchard equation considering a model with a single binding site

$$E_{\text{FRET}} = E_{\text{F}} \left\{ \frac{K_{\text{d}} + M_{\text{tot}} + L_{\text{tot}} - \sqrt{[K_{\text{d}} + M_{\text{tot}} + L_{\text{tot}}]^2 - 4M_{\text{tot}}L_{\text{tot}}}}{2K_{\text{d}}L_{\text{tot}}} \right\} \quad (3)$$

where E_{F} corresponds to the FRET efficiency at saturation, L_{tot} and M_{tot} are respectively the concentration of RT and p/t duplex, and K_{d} is the dissociation constant. Fit parameters were recovered from nonlinear fits of eq 3 to the experimental data sets using a nonlinear least-squares method and the Levenberg–Marquardt algorithm in the Origin 8 software.

RT Inhibitory Activity of Compounds The RT inhibitory activity of compounds was determined as described previously.²⁴ All measurements were carried out using a 23-mer (5'-CAG CAG TAC AAA TGG CAG TAT TC) DNA-primer labeled at the T19 position with cyanine 5 (Cy5), annealed to a 63-mer (3'-TGT CGT CAT GTT TAC CGT CAT AAG TAG

GTG TTA CTA GTC CGA TTT CCC CTA GTC CGA CCC ATG) template labeled at the T2 position with TAMRA. Both TAMRA and Cy5 were covalently attached via a C6 amino link to their respective T residues in the primer and the template. Primer and template ODN were annealed by heating equimolar amounts in buffer at 90 °C for 2 min, followed by cooling to room temperature over several hours. All measurements were performed at 20 °C using a Fluoromax 4 spectrofluorometer (Jobin-Yvon Horiba) or a stopped-flow apparatus (SF3, Biologics). The FRET donor, TAMRA, was excited at 540 nm, and its emission was recorded at 580 nm. Nucleotide incorporation kinetics was triggered by addition of dNTPs in excess to a preincubated mixture of HIV-RT and p/t duplexes at equimolar concentrations. The annealing kinetic traces were adequately fitted using

$$I(t) = I_F - (I_F - I_0)(ae^{(-k_{obs1}(t-t_0))} - (1-a)e^{(-k_{obs2}(t-t_0))}) \quad (4)$$

where t_0 is the dead time, k_{obs1} and k_{obs2} are the observed kinetic rate constants, a is the amplitude of the fast component, and I_0 and I_F are the fluorescence intensities before dNTPs addition and at completion of the reaction, respectively. The I_0 value was obtained from the steady-state fluorescence spectrum of the doubly labeled p/t duplex in the presence of RT and was thus fixed. All fitting procedures were carried out with Origin™ 8.6 software using nonlinear, least-squares methods and the Levenberg-Marquardt algorithm.

HeLa Infectivity and Cytotoxicity Assay The infectivity assay was based on infection of HeLa cells by a third-generation of pseudoparticles³⁸ mimicking the early steps of the HIV-1 virus cycle. The pseudoparticles contain Gag, Gag-pol, RRE, and vesicular stomatitis virus (VSV)-G proteins and a RNA encoding reporter gene for luciferase. The luciferase sequence is incorporated in the host genome during infection by pseudoparticles which allows the possibility to quantify infection. A total of 5×10^3 HeLa cells/well were seeded in 96-wells plate 24 h prior to infection in Dulbecco's modified Eagle medium (Life Technologies) (DMEM) complemented with 10% fetal bovine serum, penicillin (100 UI/mL), and streptomycin (100 µg/mL) and incubated in a 5% CO₂ incubator. After medium removal, an amount of 50 µL of 2 times concentrated solutions of compounds was added 30 min before adding 50 µL of pseudoparticles, which can infect 50% of cells in the presence of polybrene (8 µg/mL). Cells were washed, 24 h after infection, one time by PBS and lysed with passive lysis buffer (Promega) supplemented with 0.5% Triton X-100 for 30 min under constant shaking. Luciferase activity was measured for 10 s in a luminometer (Tristar 2 multimode reader LB 942, Berthold) after injection of 50 µL of luciferine reagent (25 mM tricine buffer

pH = 7.8, 0.5 mM EDTA, pH 7.9, 5 mM MgSO₄, 5 mM DTT, 0.5 mM ATP, 1.65 mM D-luciferin sodium salt, and 0.325 mM coenzyme A sodium salt hydrate).

For each compound, we used, as a control, cells incubated with DMEM containing the same percentage of DMSO (maximum 0.5% v/v) as the solutions with the tested molecules. For each tested molecule and concentration, we calculated the percentage of inhibition (%*inh*) with the following equation

$$\%inh \text{ or } \%cyt = \frac{(Control \ value) - (Sample \ value)}{(Control \ value)} \times 100 \quad (5)$$

Each concentration of tested compound was tested in sextuplicate. To determine the IC₅₀ values, we plotted the percentage of inhibition against the inhibitor concentration (*I*) and fitted it with a modified version of the dose-response effect equation

$$y = \frac{A_1 + (A_2 - A_1)}{1 + 10^{(\log(I_{50}) - \log(I)) * p}} \quad (6)$$

where *A*₁ and *A*₂ represent the percentage of inhibition in the absence (0%) and in saturating concentrations (100%) of inhibitor, respectively. *I*₅₀ represents the half maximal inhibitory concentration and *p* denotes the Hill coefficient.

Cytotoxicity of compounds was quantified by the MTT assay (3-(4,5-dimethylthiazol-2-yl)-2,5-diphenyltetrazolium bromide).⁴¹ Another plate was prepared in the same conditions as for the infectivity assay. 24 h after infection, medium was replaced by 110 μL of a mix containing 100 μL of DMEM and 10 μL of 12 mM MTT solution in PBS and cells were incubated during 4 h. In order to dissolve the insoluble purple formazan reduced by living cells, 85 μL of the mix was replaced by 50 μL of DMSO and gently shaken for 10 min. The absorbance was then measured at 540 nm in a spectrophotometer (Safas Monaco) and converted to percentage of cytotoxicity (% *cyt*), in reference to the control (DMEM + DMSO).

Antiretroviral Assay against HIV-1 WT and NNRTIs-Resistant Strains The WT virus and the NNRTIs-resistant strains were obtained through the NIH AIDS Reagent Program (ARP, www.aidsreagent.org) and have been already characterized by the Phenosense assay (Monogram Biosciences), considered as the reference assay for phenotypic investigation of HIV drug resistance due to its large application in clinical trials. The infectious clones were first transfected in 293LX cells and then expanded in MT-2 cells. The antiretroviral assay was determined in a TZM-bl cell line based phenotypic assay. TZM-bl cells are characterized by the presence of the luciferase and β-galactosidase reporter genes integrated in the cell genome

under control of the HIV-1 LTR promoter. Expression of the reporter genes is regulated by the viral Tat protein, which is produced following transcription of the integrated provirus. TZM-bl cells were seeded at a concentration of 30000 cells/well in a 96-well plate using DMEM medium without fetal bovine serum (FBS) and infected with the viruses in the presence of 20, 10, 5, and 1 μM of each compound. After 48 h, cells were lysed by adding 40 μL of Glo lysis buffer (Promega) to each well for 5 min, and then an amount of 40 μL of Bright-Glo luciferase reagent (Promega) was added to each well for counting relative luminescence units (RLUs) using the Glo-Max multidetection system (Promega). RLU values from each well were elaborated using the GraphPad, version 5.0, software to calculate the IC_{50} of each compound.

RNAP Inhibition, Antibacterial Activity and Cytotoxicity Transcription inhibition assay, determination of IC_{50} values, minimal inhibitory concentrations (MICs), and cytotoxicity in HEK 293 cells were performed as described previously.²²

Supporting Information

The Supporting Information is available free of charge on the ACS Publications website at DOI: 10.1021/acs.jmedchem.6b00730.

Experimental procedures and analytical data for all other compounds; Substituent constants and molecular descriptors of compounds **11–20**; Binding and mechanistic studies of the compounds; ^1H and ^{13}C NMR spectra (PDF)

Molecular formula strings (CSV)

ACKNOWLEDGMENTS

The authors thank Jeannine Jung for technical assistance. Walid A. M. Elgaher gratefully acknowledges a scholarship from the German Academic Exchange Service (DAAD). Kamal K. Sharma, Francesco Saladini, Manuel Pires and part of this work were supported by the European Project THINPAD “Targeting the HIV-1 Nucleocapsid Protein To Fight Antiretroviral Drug Resistance” [FP7-Grant Agreement 601969 to Y.M.].

REFERENCES

- (1) WHO. HIV/AIDS, Fact Sheet No. 360, 2015. <http://www.who.int/mediacentre/factsheets/fs360/en/>.
- (2) Bonnet, M. M. B.; Pinoges, L. L. P.; Varaine, F. F. V.; Oberhauser, B. B. O.; O'Brien, D. D. O.; Kebede, Y. Y. K.; Hewison, C. C. H.; Zachariah, R. R. Z.; Ferradini, L. L. F. Tuberculosis after HAART Initiation in HIV-Positive Patients from Five Countries with a High Tuberculosis Burden. *AIDS (London, U. K.)* **2006**, *20*, 1275–1279.
- (3) Mathews, W. C.; Caperna, J. C.; Barber, R. E.; Torriani, F. J.; Miller, L. G.; May, S.; McCutchan, J. A. Incidence of and Risk Factors for Clinically Significant Methicillin-Resistant Staphylococcus

aureus Infection in a Cohort of HIV-Infected Adults. *J. Acquired Immune Defic. Syndr.* **2005**, *40*, 155–160.

(4) Hidron, A. I.; Kempker, R.; Moanna, A.; Rimland, D. Methicillin-Resistant *Staphylococcus aureus* in HIV-Infected Patients. *Infect. Drug Resist.* **2010**, *3*, 73–86.

(5) Crum-Cianflone, N. F.; Burgi, A. A.; Hale, B. R. Increasing Rates of Community-Acquired Methicillin-Resistant *Staphylococcus aureus* Infections among HIV-Infected Persons. *Int. J. STD AIDS* **2007**, *18*, 521–526.

(6) Martin, J. N.; Rose, D. A.; Hadley, W. K.; Perdreau-Remington, F.; Lam, P. K.; Gerberding, J. L. Emergence of Trimethoprim-Sulfamethoxazole Resistance in the AIDS Era. *J. Infect. Dis.* **1999**, *180*, 1809–1818.

(7) Diep, B. A.; Chambers, H. F.; Graber, C. J.; Szumowski, J. D.; Miller, L. G.; Han, L. L.; Chen, J. H.; Lin, F.; Lin, J.; Phan, T. H.; Carleton, H. A.; McDougal, L. K.; Tenover, F. C.; Cohen, D. E.; Mayer, K. H.; Sensabaugh, G. F.; Perdreau-Remington, F. Emergence of Multidrug-Resistant, Community-Associated, Methicillin-Resistant *Staphylococcus aureus* Clone USA300 in Men Who Have Sex with Men. *Ann. Intern. Med.* **2008**, *148*, 249–257.

(8) Mansky, L. M. HIV Mutagenesis and the Evolution of Antiretroviral Drug Resistance. *Drug Resist. Updates* **2002**, *5*, 219–223.

(9) Asahchop, E. L.; Wainberg, M. A.; Sloan, R. D.; Tremblay, C. L. Antiviral Drug Resistance and the Need for Development of New HIV-1 Reverse Transcriptase Inhibitors. *Antimicrob. Agents Chemother.* **2012**, *56*, 5000–5008.

(10) Tang, M. W.; Shafer, R. W. HIV-1 Antiretroviral Resistance: Scientific Principles and Clinical Applications. *Drugs* **2012**, *72*, e1–e25.

(11) Dejesus, E.; Young, B.; Morales-Ramirez, J. O.; Sloan, L.; Ward, D. J.; Flaherty, J. F.; Ebrahimi, R.; Maa, J.-F.; Reilly, K.; Ecker, J.; McColl, D.; Seekins, D.; Farajallah, A. Simplification of Antiretroviral Therapy to a Single-Tablet Regimen Consisting of Efavirenz, Emtricitabine, and Tenofovir Disoproxil Fumarate versus Unmodified Antiretroviral Therapy in Virologically Suppressed HIV-1-Infected Patients. *J. Acquired Immune Defic. Syndr.* **2009**, *51*, 163–174.

(12) Piscitelli, S. C.; Gallicano, K. D. Interactions among Drugs for HIV and Opportunistic Infections. *N. Engl. J. Med.* **2001**, *344*, 984–996.

(13) Krentz, H. B.; Gill, M. J. Increased Costs of HIV Care Associated with Aging in an HIV-Infected Population. *HIV Med.* **2015**, *16*, 38–47.

(14) Ren, J.; Esnouf, R.; Garman, E.; Somers, D.; Ross, C.; Kirby, I.; Keeling, J.; Darby, G.; Jones, Y.; Stuart, D.; Stammers, D. High Resolution Structures of HIV-1 RT from Four RT-Inhibitor Complexes. *Nat. Struct. Biol.* **1995**, *2*, 293–302.

(15) Ding, J.; Das, K.; Moereels, H.; Koymans, L.; Andries, K.; Janssen, P. A.; Hughes, S. H.; Arnold, E. Structure of HIV-1 RT/TIBO R 86183 Complex Reveals Similarity in the Binding of Diverse Nucleoside Inhibitors. *Nat. Struct. Biol.* **1995**, *2*, 407–415.

- (16) Engelman, A.; Cherepanov, P. The Structural Biology of HIV-1: Mechanistic and Therapeutic Insights. *Nat. Rev. Microbiol.* **2012**, *10*, 279–290.
- (17) Vassylyev, D. G.; Sekine, S.-i.; Laptenko, O.; Lee, J.; Vassylyeva, M. N.; Borukhov, S.; Yokoyama, S. Crystal Structure of a Bacterial RNA Polymerase Holoenzyme at 2.6 Å Resolution. *Nature* **2002**, *417*, 712–719.
- (18) Kotler, M.; Becker, Y. Rifampicin and Distamycin A as Inhibitors of Rous Sarcoma Virus Reverse Transcriptase. *Nat. New Biol.* **1971**, *234*, 212–214.
- (19) Szilvay, A. M.; Stern, B.; Blichenberg, A.; Helland, D. E. Structural and Functional Similarities between HIV-1 Reverse Transcriptase and the Escherichia coli RNA Polymerase β' Subunit. *FEBS Lett.* **2000**, *484*, 43–47.
- (20) Mukhopadhyay, J.; Das, K.; Ismail, S.; Koppstein, D.; Jang, M.; Hudson, B.; Sarafianos, S.; Tuske, S.; Patel, J.; Jansen, R.; Irschik, H.; Arnold, E.; Ebright, R. H. The RNA Polymerase "Switch Region" is a Target for Inhibitors. *Cell* **2008**, *135*, 295–307.
- (21) Sahner, J. H.; Groh, M.; Negri, M.; Hauptenthal, J.; Hartmann, R. W. Novel Small Molecule Inhibitors Targeting the "Switch Region" of Bacterial RNAP: Structure-Based Optimization of a Virtual Screening Hit. *Eur. J. Med. Chem.* **2013**, *65*, 223–231.
- (22) Elgaher, W. A. M.; Fruth, M.; Groh, M.; Hauptenthal, J.; Hartmann, R. W. Expanding the Scaffold for Bacterial RNA Polymerase Inhibitors: Design, Synthesis and Structure–Activity Relationships of Ureido-Heterocyclic-Carboxylic Acids. *RSC Adv.* **2014**, *4*, 2177–2194.
- (23) Fruth, M.; Plaza, A.; Hinsberger, S.; Sahner, J. H.; Hauptenthal, J.; Bischoff, M.; Jansen, R.; Müller, R.; Hartmann, R. W. Binding Mode Characterization of Novel RNA Polymerase Inhibitors Using a Combined Biochemical and NMR Approach. *ACS Chem. Biol.* **2014**, *9*, 2656–2663.
- (24) Sharma, K. K.; Przybilla, F.; Restle, T.; Godet, J.; Mély, Y. FRET-Based Assay to Screen Inhibitors of HIV-1 Reverse Transcriptase and Nucleocapsid Protein. *Nucleic Acids Res.* **2016**, *44*, e74.
- (25) Srivastava, A.; Talaue, M.; Liu, S.; Degen, D.; Ebright, R. Y.; Sineva, E.; Chakraborty, A.; Druzhinin, S. Y.; Chatterjee, S.; Mukhopadhyay, J.; Ebright, Y. W.; Zozula, A.; Shen, J.; Sengupta, S.; Niedfeldt, R. R.; Xin, C.; Kaneko, T.; Irschik, H.; Jansen, R.; Donadio, S.; Connell, N.; Ebright, R. H. New Target for Inhibition of Bacterial RNA Polymerase: 'Switch Region'. *Curr. Opin. Microbiol.* **2011**, *14*, 532–543.
- (26) Rodgers, D. W.; Gamblin, S. J.; Harris, B. A.; Ray, S.; Culp, J. S.; Hellmig, B.; Woolf, D. J.; Debouck, C.; Harrison, S. C. The Structure of Unliganded Reverse Transcriptase from the Human Immunodeficiency Virus Type 1. *Proc. Natl. Acad. Sci. U. S. A.* **1995**, *92*, 1222–1226.
- (27) Esnouf, R.; Ren, J.; Ross, C.; Jones, Y.; Stammers, D.; Stuart, D. Mechanism of Inhibition of HIV-1 Reverse Transcriptase by Non-Nucleoside Inhibitors. *Nat. Struct. Biol.* **1995**, *2*, 303–308.
- (28) Mason, J. S.; Morize, I.; Menard, P. R.; Cheney, D. L.; Hulme, C.; Labaudiniere, R. F. New 4-Point Pharmacophore Method for Molecular Similarity and Diversity Applications: Overview of the

Method and Applications, Including a Novel Approach to the Design of Combinatorial Libraries Containing Privileged Substructures. *J. Med. Chem.* **1999**, *42*, 3251–3264.

(29) Leeson, P. D.; Springthorpe, B. The Influence of Drug-Like Concepts on Decision-Making in Medicinal Chemistry. *Nat. Rev. Drug Discovery* **2007**, *6*, 881–890.

(30) Domaal, R. A.; Demeter, L. M. Structural and Biochemical Effects of Human Immunodeficiency Virus Mutants Resistant to Non-Nucleoside Reverse Transcriptase Inhibitors. *Int. J. Biochem. Cell Biol.* **2004**, *36*, 1735–1751.

(31) Pelemans, H.; Esnouf, R.; de Clercq, E.; Balzarini, J. Mutational Analysis of Trp-229 of Human Immunodeficiency Virus Type 1 Reverse Transcriptase (RT) Identifies This Amino Acid Residue as a Prime Target for the Rational Design of New Non-Nucleoside RT Inhibitors. *Mol. Pharmacol.* **2000**, *57*, 954–960.

(32) Wohrl, B. M.; Krebs, R.; Thrall, S. H.; Le Grice, S. F. J.; Scheidig, A. J.; Goody, R. S. Kinetic Analysis of Four HIV-1 Reverse Transcriptase Enzymes Mutated in the Primer Grip Region of p66. Implications for DNA Synthesis and Dimerization. *J. Biol. Chem.* **1997**, *272*, 17581–17587.

(33) Smerdon, S. J.; Jäger, J.; Wang, J.; Kohlstaedt, L. A.; Chirino, A. J.; Friedman, J. M.; Rice, P. A.; Steitz, T. A. Structure of the Binding Site for Nonnucleoside Inhibitors of the Reverse Transcriptase of Human Immunodeficiency Virus Type 1. *Proc. Natl. Acad. Sci. U. S. A.* **1994**, *91*, 3911–3915.

(34) Sharma, K. K.; Przybilla, F.; Restle, T.; Boudier, C.; Godet, J.; Mély, Y. Reverse Transcriptase in Action: FRET-Based Assay for Monitoring Flipping and Polymerase Activity in Real Time. *Anal. Chem.* **2015**, *87*, 7690–7697.

(35) Grohmann, D.; Godet, J.; Mély, Y.; Darlix, J.-L.; Restle, T. HIV-1 Nucleocapsid Traps Reverse Transcriptase on Nucleic Acid Substrates. *Biochemistry* **2008**, *47*, 12230–12240.

(36) Spence, R.; Kati, W.; Anderson, K.; Johnson, K. Mechanism of Inhibition of HIV-1 Reverse Transcriptase by Nonnucleoside Inhibitors. *Science* **1995**, *267*, 988–993.

(37) Kohlstaedt, L. A.; Wang, J.; Friedman, J. M.; Rice, P. A.; Steitz, T. A. Crystal Structure at 3.5 Å Resolution of HIV-1 Reverse Transcriptase Complexed with an Inhibitor. *Science* **1992**, *256*, 1783–1790.

(38) Dull, T.; Zufferey, R.; Kelly, M.; Mandel, R. J.; Nguyen, M.; Trono, D.; Naldini, L. A Third-Generation Lentivirus Vector with a Conditional Packaging System. *J. Virol.* **1998**, *72*, 8463–8471.

(39) Balamane, M.; Varghese, V.; Melikian, G. L.; Fessel, W. J.; Katzenstein, D. A.; Shafer, R. W. Panel of Prototypical Recombinant Infectious Molecular Clones Resistant to Nevirapine, Efavirenz, Etravirine, and Rilpivirine. *Antimicrob. Agents Chemother.* **2012**, *56*, 4522–4524.

(40) Hsiou, Y.; Ding, J.; Das, K.; Clark, A. D.; Boyer, P. L.; Lewi, P.; Janssen, P. A.; Kleim, J. P.; Rösner, M.; Hughes, S. H.; Arnold, E. The Lys103Asn Mutation of HIV-1 RT: a Novel Mechanism of Drug Resistance. *J. Mol. Biol.* **2001**, *309*, 437–445.

(41) Mosmann, T. Rapid Colorimetric Assay for Cellular Growth and Survival: Application to Proliferation and Cytotoxicity Assays. *J. Immunol. Methods* **1983**, *65*, 55–63.

3.3 Synthesis and Biological Evaluation of Cystobactamid 507: A Bacterial Topoisomerase Inhibitor from *Cystobacter* sp.

Reprinted with permission from Moreno, M.; Elgaher, W. A. M.; Herrmann, J.; Schläger, N.; Hamed, M. M.; Baumann, S.; Müller, R.; Hartmann, R. W.; Kirschning, A. *Synlett* 2015, 26, 1175–1178.

Copyright 2015 Georg Thieme Verlag Stuttgart • New York.

<https://www.thieme-connect.com/products/ejournals/abstract/10.1055/s-0034-1380509>

(Publication III)

Abstract

The first total synthesis of cystobactamid 507, a member of a class of new natural products with strong inhibitory activity towards bacterial topoisomerases, is reported. Synthetic key challenges are the central tetrasubstituted arene and the low chemical reactivity of anilines and *ortho*-phenolic and isopropoxy-substituted benzoic acids. Biological evaluations demonstrate that cystobactamid 507 inhibits several Gram-positive pathogens but at significantly lower concentrations than described for the larger members of this natural product family

Recently, Müller and co-workers reported on an unusual group of nonribosomal peptides called the cystobactamids 919-1, 919-2, and 507 (**1–3**, Figure 1), which were isolated in rather small amounts (<100 µg/L) from *Cystobacter* sp. besides several more structurally similar derivatives that could not be fully characterized yet.¹ They are potent antibacterial agents that inhibit several clinically relevant Gram-negative and Gram-positive bacteria such as *Acinetobacter baumannii* (minimum inhibitory concentration, MIC = 7.4 to >59 µg/mL), *Enterococcus faecalis* (MIC = 0.1–7.4 µg/mL), *Staphylococcus aureus* (MIC = 0.1–32.5 µg/mL), *Streptococcus pneumoniae* (MIC = 0.1–14.7 µg/mL) as well as *E. coli* (MIC = 0.9–29.4 µg/mL).

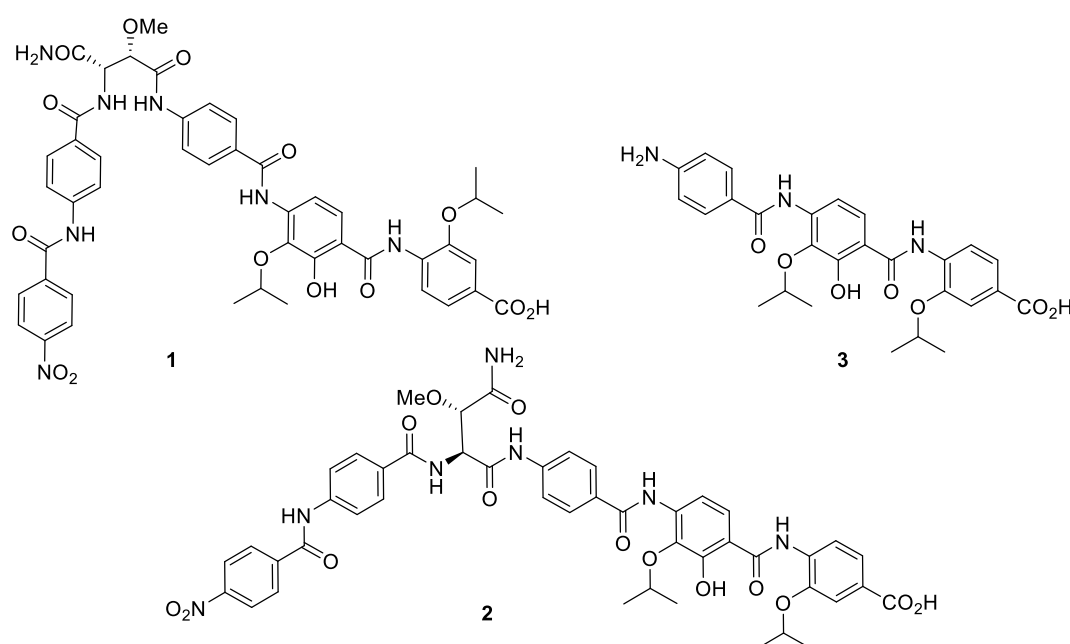


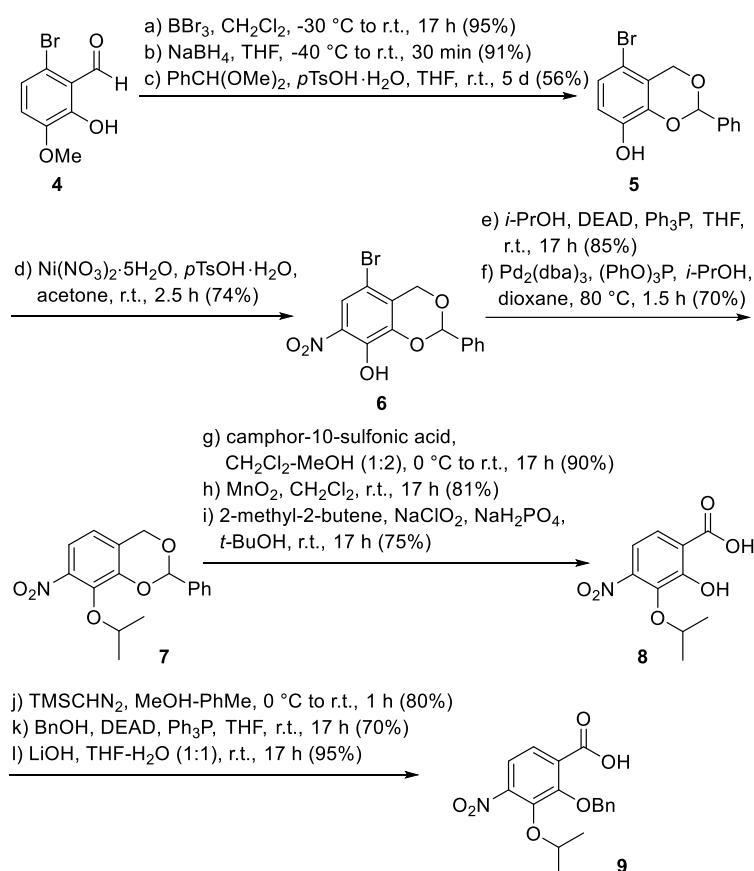
Figure 1 Structures of cystobactamids 919-1, 919-2, 507 (**1–3**)

Most of these strains are made responsible for nosocomial infections.² Preliminary studies showed¹ that the cystobactamids target bacterial type IIa topoisomerases which are validated antibacterial targets. However, as quinolones are not suited anymore to serve as template for new inhibitors the cystobactamids offer new opportunities in search for new anti-infectives,³ especially as this novel structural scaffold and the limited cross-resistance found make the cystobactamids promising lead structures. Structurally, cystobactamid 507 (**3**) is the simplest member. It was reported to exert similar but lower inhibitory activity than cystobactamids **1** and **2**.

En route to **1** and **2** we synthesized cystobactamid 507 (**3**) which additionally would allow us to further test its biological properties. These tests would show whether the trisaryl unit is an essential element for all cystobactamids and furthermore would clarify if minor impurities present in the natural sample did alter the assay read-outs.

Although cystobactamids only contain *p*-aminobenzoic acids we experienced two major synthetic challenges: a) accessing the tetrasubstituted arene unit and b) the lack of reactivity of anilines and the lack for reactivity of *ortho*-substituted phenolic and isopropoxy benzoic acids in amide formations. This amide formation can only proceed under conditions that are different from those established in peptide synthesis.

The synthesis of the tetrasubstituted arene **9** commenced with *o*-bromobenzaldehyde **4**. The bromo substituent served as ‘dummy’ group which can be removed after the selective introduction of the nitrogen functionality at C4. In addition, this starting material allows for differentiating between the two phenolic groups and thus enables selective introduction of the isopropyl group at C3 (Scheme 1).



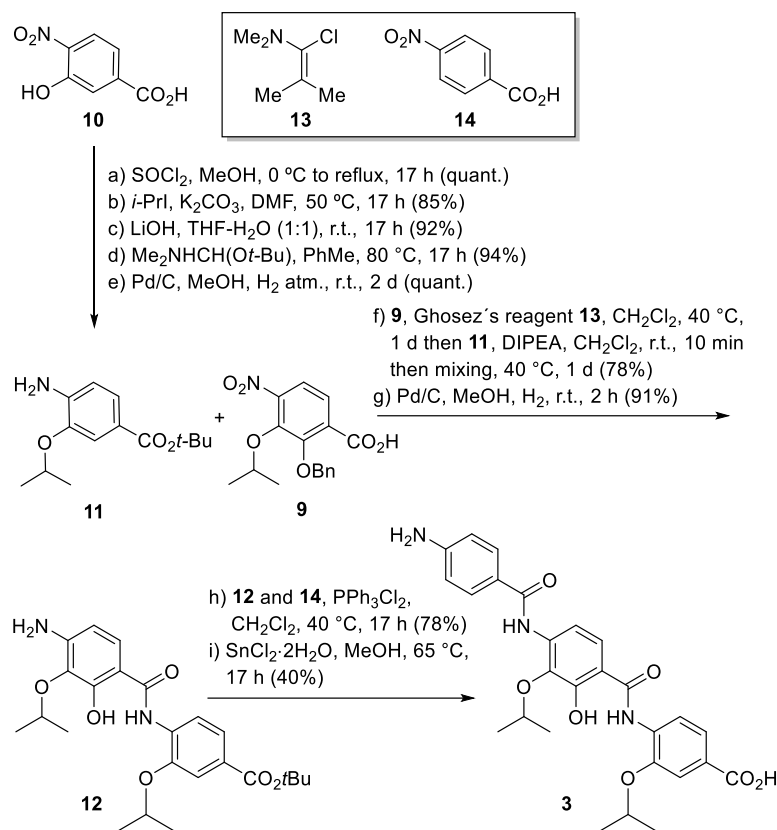
Scheme 1 Synthesis of tetrasubstituted benzoic acid **9**

O-Demethylation of **4**, aldehyde reduction and protection of the benzylic alcohol and one phenolic group as benzylidene acetal yielded phenol **5**. This protection paved the way for introducing a) the nitro group to yield nitroarene **6**⁴ and b) the isopropyl group. Palladium-catalyzed debromination⁵ yielded nitroarene **7**. After removal of the benzylidene protection, the benzylic alcohol was transformed into the carboxylate under standard conditions. The resulting benzoic acid **8** was temporarily methylated in order to protect the *o*-phenolic group, which finally furnished the desired *p*-nitrobenzoic acid **9**. These final steps were crucial as successful amide formation could only be achieved if the *o*-phenolic group is protected.

With this key building block in hand, we could finalize the synthesis of cystobactamid 507 (**3**) by coupling three *p*-aminobenzoic acid units. However, we had to search for conditions that allow for creating an amide bond between two arene moieties. Common reagent systems such as HOAt, EDC, or a mixture of HOBt and EDC that are well established in peptide chemistry gave poor coupling yields. We made the bulky isopropoxy substituents with *ortho* orientation to the amino groups as well as the reduced reactivity of the aromatic amino groups responsible for the difficulties to achieve amide formation.

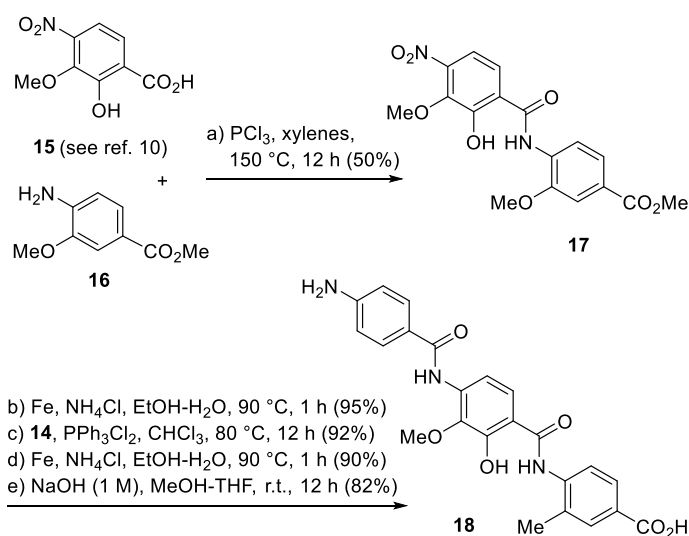
We found that Ghosez's reagent **13**⁶ is best suited to couple benzoates with anilines (Scheme 2). First, aniline **11**, which straightforwardly is accessible from benzoic acid **10**, was coupled⁷ with tetrasubstituted benzoic acid **9** to yield amide **12** after hydrogenation of the nitro group and with concomitant removal of the benzyl protecting group. Next, the second amide coupling⁸ between **12** and *p*-nitrobenzoic acid **14** yielded cystobactamid 507 (**3**) after simultaneous reduction of the nitro group⁹ and removal of the *tert*-butyl ester. It has to be noted that it became necessary to switch from a methyl to a *tert*-butyl ester (**10** → **11**) because the final ester hydrolysis with the corresponding methyl ester (step under basic conditions) led to simultaneous amide hydrolysis of the *p*-aminobenzoic acid moiety.

The NMR spectra and chromatographic parameter (HPLC) for the synthetic material were identical to those collected for natural cystobactamid 507 (**3**).



Scheme 2 Finalization of the synthesis of cystobactamid 507 (**3**)

The synthetic hurdles that we encountered in this synthesis stemmed us to prepare a structurally simplified derivate **18** in which both isopropoxy groups of cystobactamid 507 are replaced by the smaller methoxy groups. Starting from *o*-vanillin the tetrasubstituted central arene unit **15** (Scheme 3 and Supporting Information) was straightforwardly prepared in three steps and coupled with arenes **14** and **16**.¹⁰



Scheme 3 Synthesis of cystobactamid derivative **18**¹⁰

The antibacterial profile and the gyrase inhibitory properties of synthetic cystobactamid 507 (**3**) and derivative **18** were assessed. We found that both compounds showed some inhibitory activity against certain Gram-positive bacteria and an efflux-deficient *E. coli* strain with MIC values between 16 and 128 $\mu\text{g/mL}$ (Table 1). Likewise, the IC_{50} values (half-inhibitory concentration) for *E. coli* gyrase were in the high μM range (ca. 300–500 μM).

Table 1 Biological Activity of **3** and **18**^a

	3	18	CP ^b
<i>E. coli</i> ATCC-25922	>128	>128	0.005
<i>E. coli</i> DSM-1116	>128	>128	0.01
<i>E. coli</i> DSM-26863 ^c	>128	>128	0.003
<i>E. coli</i> DSM-26863/PMBN ^d	32–64	64	0.003
<i>B. subtilis</i> DSM-10	32	128	0.1
<i>E. faecalis</i> ATCC-29212	64–128	>128	0.8
<i>M. luteus</i> DSM-1790	128	64	0.8
<i>S. aureus</i> ATCC-29213	128	64	0.1
<i>S. pneumoniae</i> DSM-20566	64	16	0.8

^a MIC values in $\mu\text{g/mL}$. ^b Ciprofloxacin. ^c *tolC3* genotype. ^d Cotreatment with 3 $\mu\text{g/ml}$ polymyxin B nonapeptide.

It has to be stressed that *Cystobacter* sp. generates only very small amounts (<100 $\mu\text{g/L}$) of cystobactamids and their isolation is further hampered by the fact that the fermentation broth contains at least a dozen structurally closely related cystobactamids.¹ It has already been pointed out that the natural product **3** might be contaminated with trace amounts of cystobactamid hexapeptides, which are responsible for the sample's moderate antibacterial activity.

Here we could demonstrate that synthetic **3** still shows some antibacterial activity mainly against Gram-positive bacteria, which is, however, by 1 to 2 orders of magnitudes less pronounced than initially described for natural cystobactamid 507. Interestingly, also the simpler methyl derivative **18** exhibits a comparable activity spectrum to that of synthetic **3**.

We conclude that the western part of larger cystobactamids including the β -methoxyasparagine linker is mandatory for full biological activity in cell-based studies as well as in vitro topoisomerase inhibition experiments. One reason for the lack of antibacterial activity against Gram-negative pathogens might be explained by insufficient penetration of **3**

and **18** through the outer bacterial membrane as demonstrated by the finding that the trisaryl compounds are only active against *E. coli* with increased permeability (Table 1). However, since both tested synthetic compounds **3** and **18** exhibit some residual antibacterial and gyrase inhibitory activity modification of the trisaryl unit might be a promising starting point for the optimization of the larger cystobactamid scaffold.

In summary, we reported on the first synthesis of the new antibiotic cystobactamid **3**. We were able to access the synthetically challenging tetrasubstituted benzoic acid **9** and establish coupling conditions for anilines with bulky isopropoxy groups positioned in the *ortho* position. This work paves the way for preparing libraries of cystobactamid derivatives. Additionally, this work provided a first insight into structure–activity relationships. Clearly, all structural elements present in the larger cystobactamids are essential for their potent antibacterial properties. This work is important for initiating a medicinal chemistry program for further improving the biological profile of the cystobactamids.

Final Synthetic Step and Analytical Data for Cystobactamid C (**3**)

tert-Butyl-4-[2-hydroxy-3-isopropoxy-4-(4-nitrobenzamido)benzamido]-3-

isopropoxybenzoate (**S13**, 8.1 mg, 0.014 mmol) was dissolved in MeOH (1 mL). SnCl₂·2H₂O (9.2 mg, 0.041 mmol) was added, and the reaction mixture was stirred under refluxing conditions for 17 h. The solvent was evaporated under reduced pressure and the residue diluted with EtOAc. After addition of a saturated solution of NaHCO₃ and separation of the phases, the aqueous layer was extracted with EtOAc (1×). The aqueous layer was acidified with 1 M HCl until pH = ca. 1 and extracted with EtOAc (3×). The combined organic layers were washed with brine (1×), dried over anhydrous MgSO₄, and filtered. The crude product was purified by preparative HPLC (RP-18; run time 100 min; H₂O–MeCN = 100: 0 to 0: 100; *t*_R = 47 min) providing the title compound **3** (2.8 mg, 5.5 μmol, 40%) as a semisolid material.

¹H NMR (400 MHz, MeOD): δ = 8.46 (d, *J* = 8.6 Hz, 1 H), 7.80 (d, *J* = 8.6 Hz, 1 H), 7.75 (d, *J* = 8.6 Hz, 1 H), 7.72 (d, *J* = 8.6 Hz, 2 H), 7.71–7.64 (m, 2 H), 6.74 (d, *J* = 8.6 Hz, 2 H), 4.78 (hept, *J* = 6.1 Hz, 1 H), 4.55 (hept, *J* = 6.1 Hz, 1 H), 1.46 (d, *J* = 6.1 Hz, 6 H), 1.35 (d, *J* = 6.1 Hz, 6 H) ppm.

¹³C NMR (125 MHz, MeOD): δ = 167.80 (Cq), 167.02 (Cq), 154.27 (Cq), 152.92 (Cq), 148.39 (Cq), 138.21 (Cq), 138.16 (Cq), 134.11 (Cq), 130.23 (CH), 125.50 (CH), 124.02 (CH), 122.35 (Cq), 121.26 (CH), 116.22 (CH, Cq), 115.22 (Cq), 114.79 (CH), 114.32 (CH), 77.13 (CH), 73.26 (CH), 22.71 (CH₃), 22.32 (CH₃) ppm.

ESI-HRMS: *m/z* calcd for C₂₇H₃₀N₃O₇ [M + H]⁺: 508.2084; found: 508.2085.

Acknowledgement

This work was supported by the German Center for Infection Research (DZIF) and the Fonds der Chemischen Industrie.

Supporting Information

Supporting information for this article is available online at <http://dx.doi.org/10.1055/s-0034-1380509>. Included are experimental procedures, spectral data and copies of ^1H and ^{13}C NMR spectra of all new compounds and intermediates.

References

- (1) Baumann, S.; Herrmann, J.; Raju, R.; Steinmetz, H.; Mohr, K. I.; Hüttel, S.; Harmrolfs, K.; Stadler, M.; Müller, R. *Angew. Chem. Int. Ed.* **2014**, *53*, 14605; a range of new cystobactamid derivatives will be reported elsewhere.
- (2) Weinstein, R. A.; Gaynes, R.; Edwards, J. R. *Clin. Infect. Dis.* **2005**, *41*, 848.
- (3) Hooper, D. C. *Emerg. Infect. Dis.* **2001**, *7*, 337.
- (4) Anuradha, V.; Srinivas, P. V.; Aparna, P.; Rao, J. M. *Tetrahedron Lett.* **2006**, *47*, 4933.
- (5) Moon, J.; Lee, S. *J. Organomet. Chem.* **2009**, *694*, 473.
- (6) Devos, A.; Remion, J.; Frisque-Hesbain, A.-M.; Colens, A.; Ghosez, L. *J. Chem. Soc., Chem. Commun.* **1979**, 1180.
- (7) Prabhakaran, P.; Barnard, A.; Murphy, N. S.; Kilner, C. A.; Edwards, T. A.; Wilson, A. J. *Eur. J. Org. Chem.* **2013**, 3504.
- (8) Yap, J. L.; Cao, X.; Vanommeslaeghe, K.; Jung, K.-Y.; Peddaboina, C.; Wilder, P. T.; Nan, A.; MacKerell, A. D. Jr.; Smytheb, W. R. Jr.; Fletcher, S. *Org. Biomol. Chem.* **2012**, *10*, 2928.
- (9) Satoh, T.; Suzuki, S.; Suzuki, Y.; Miyaji, Y.; Imai, Z. *Tetrahedron Lett.* **1969**, 4555.
- (10) The synthesis of albicidin, a natural product closely related to the cystobactamids, was recently reported: Kretz, J.; Kerwat, D.; Schubert, V.; Grätz, S.; Pesic, A.; Semsary, S.; Cociancich, S.; Royer, M.; Süssmuth, R. *Angew. Chem.* **2015**, *126*, 1992.

3.4 Cystobactamid 507: Concise Synthesis and Design of Non-Covalently Bonded Rigid Analogs Boost Bacterial Topoisomerases IIA Inhibition, Antibacterial Activity and Disclose the Bioactive Conformation

To the work accomplished in this section, the following names are appreciated for their contribution:

Mostafa M. Hamed: designed and synthesized some cystobactamid 507 analogs.

Sascha Baumann: performed the gyrase and topoisomerase IV inhibition assays. In addition, he performed the mode of binding studies.

Jennifer Herrmann: determined the antibacterial activity of the compounds.

Lorenz Siebenbürger: performed the metabolic stability study.

(Manuscript in Submission IV)

ABSTRACT

Lack of new antibiotics and the increasing antimicrobial resistance are the main concern of healthcare community nowadays, which necessitates the search for new antibacterial agents to combat resistant bacteria. Recently, we discovered a novel natural class of antibiotics called the cystobactamids with potent antibacterial activity. In this work, we describe a brief total synthesis of the natural product cystobactamid 507 (Cys507) and a successful modification and optimization of its structure into new analogs with superior topoisomerases IIA inhibition and antibacterial activity. This was accomplished through: (i) Interactive *de novo* design of conformationally restricted analogs via intramolecular hydrogen bonds (IMHBs). (ii) Establishment of straightforward synthetic strategies valid for versatile peptidomimetics. (iii) Careful study of structure–activity relationship (SAR) and identification of the bioactive conformation. Our findings enabled us to further develop more potent compounds with structure simplification of Cys507. Deeper insight into the mode of action revealed that this class of antibiotics uses DNA minor groove binding as part of the drug–target interaction without showing significant intercalation. The natural compound and the optimized analogs possess exceptionally high metabolic stability.

INTRODUCTION

The ongoing prevalence of antibiotic resistant bacteria poses an imminent threat to humanity.¹ At the same time, big pharma companies steadily retreat from the antibiotic drug discovery field.² Such a paradox exaggerates the crisis, and urgently requires more efforts to discover novel antibiotics with new chemical entities or alternative modes of action. Nature represents a rich repository of antibiotics. In the last decades, about 75% of the clinically approved antibacterial agents were natural products (NPs) or modified NPs.³ Markedly, only one-eighth of these antibiotics are unmodified NPs,³ while the major part had to be modified in order to optimize activity, stability and drug-like physicochemical properties. Modifications of NPs are pursued through two main routes. One route is the utilization of synthetic biology techniques where the NPs producing organisms or other hosts are exploited as experienced NPs factories. This necessitates the identification of the gene clusters responsible for the NPs biosynthesis. Genetic manipulation thereof can be used to generate a library of “unnatural” NPs.⁴ However, this combinatorial biosynthesis can have drawbacks such as low yields or unpredictable products besides being laborious.⁴ The other route is the application of medicinal chemistry approaches. A structure-based approach depends on the co-crystal structure of the antibiotic-bound molecular target. Very often, this structural information is not available as numerous natural antibiotics act on either unknown or multiple targets.⁵⁻⁸ The ligand-based approach is more convenient. Based on the antibiotics’ structures, hundreds of derivatives can be produced semi-synthetically or *de novo*.⁹ However, a general characteristic of the aforementioned strategies is that they are committed to the antibiotics’ scaffolds. Accordingly, the possibility of resistance development against the new derivatives is as likely as the parent molecules. Hence, intelligent strategies should be introduced to develop new scaffolds from natural antibiotics, and avoid occurrence of a second innovation gap.¹⁰

“Nature is the best”,¹¹⁻¹³ this common belief is accounted by the selective natural evolution of antibiotics over millions of years, yet one should also consider that nature produced antibiotics for own purpose not for clinical use. Can human have the upper hand over Mother Nature? Herein we provide a proof for a previous postulation that a medicinal chemist is able to improve the antibacterial properties of NPs.⁹

Recently, we reported the discovery of a new family of antibiotics called the cystobactamids isolated from *Cystobacter* sp. (Chart 1, compounds **1–3**).¹⁴ Cystobactamid 919-1 (**1**) and 919-2 (**2**) have hexapeptidic structures comprised of three *p*-aminobenzoic acid motifs (eastern part) and two *p*-nitro/aminobenzoic acids (western part) linked via β -methoxy- α -asparagine and β -methoxyasparagine, respectively. Cystobactamid 507 (**3**) is a tripeptide, representing

the eastern part of the full-length molecules **1** and **2**. The cystobactamids display broad spectrum antibacterial activity through inhibition of topoisomerases type IIA in bacteria, namely DNA gyrase and topoisomerase IV.¹⁴ In this work, we focused on the optimization and SAR elaboration of the potential “drug-like” molecule and the common pharmacophoric feature among the cystobactamids (compound **3**, Chart 1). We were able to develop synthetic analogs from the same/new scaffold of **3** with improved target and antibacterial activity, together with a high metabolic stability. This was achieved through a rational *de novo* design, understanding of the ligand–target interaction, and developing practical synthetic procedures following the economic synthesis guidelines.¹⁵

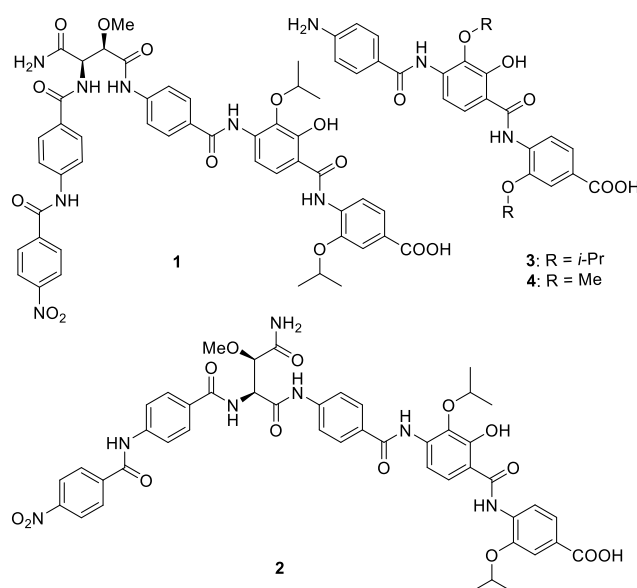


Chart 1. Cystobactamid antibiotics **1–3** and Cys507-methyl homolog **4**

RESULTS AND DISCUSSION

Compounds Design and DNA Gyrase Inhibitory Activity (SAR)

We focused on DNA gyrase for drawing SAR, as it is the primary target of cystobactamids in *Escherichia coli*.¹⁴ Previously we described the total synthesis of **3** and the methyl homolog **4** (Chart 1).¹⁶ Compound **4** showed a slight decrease in activity suggesting that the natural antibiotic **3** can be amenable to modification. Before starting an extensive synthetic program, we aimed at identifying the key structural features of **3** responsible for activity. Inspection of Cys507 structure revealed that it is reminiscent of the α -helix mimetics 3-O-alkylated benzamides.¹⁷ However, **3** has a unique hydroxyl group at position 2 of the middle ring and unsubstituted N-terminal moiety (Chart 1). Since type of side chains and conformation are major factors controlling the activity of α -helix mimetics, it was rational to start with evaluating the importance of isopropoxy side chains for the gyrase inhibitory activity of **3**.

Accordingly, we designed the analog **5** with a smaller alkoxy group (methoxy), and **6** with a halogen (chlorine) instead of the isopropoxy group at the middle ring, while keeping the other isopropoxy at the C-terminal ring (Chart 2).

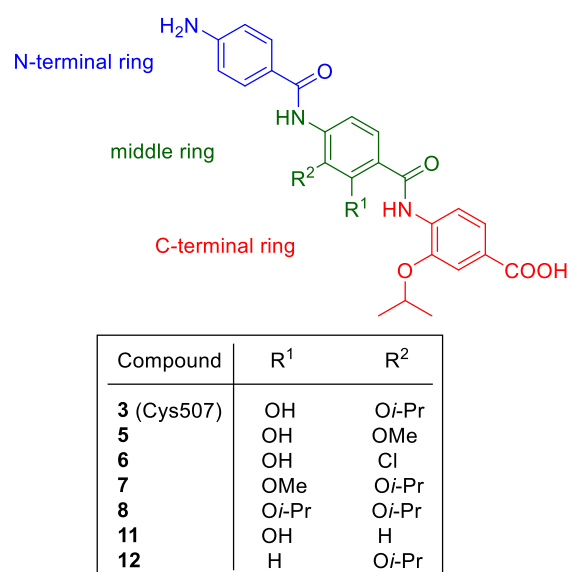


Chart 2. Structures of Cys507 analogs.

Replacement of the isopropoxy side chain with methoxy did not show a remarkable change in the gyrase inhibitory activity, while replacing it with chlorine resulted in a significant loss of activity (Table 1). This result indicates that varied alkoxy side chains can be tolerated, and they are more favorable than halogens at the middle ring. This could be due to involvement of the alkoxy groups in the ligand–target interaction and restricting the conformation, via IMHB and steric effect, in an optimum orientation necessary for binding. Comparing the activity of **4** with **5** revealed that modification of the isopropoxy group into methoxy at the C-terminal ring lessens the activity, suggesting that the isopropoxy side chain is preferred at the C-terminal ring owing to its steric and hydrophobic properties. Consequently, we maintained it in the next steps of optimization.

Table 1. In Vitro Inhibitory Activities of **3–16** in the Gyrase Supercoiling Assay and Topoisomerase IV Relaxation Assay

Compd	<i>E. coli</i> gyrase	<i>E. coli</i> topoisomerase IV	Compd	<i>E. coli</i> gyrase	<i>E. coli</i> topoisomerase IV
	IC ₅₀ (μM)	IC ₅₀ (μM)		IC ₅₀ (μM)	IC ₅₀ (μM)
3 (Cys507)	355 ± 25	>500	10	50 ± 10	147 ± 10
4	463 ± 28	n.d. ^a	11	>1000	n.d.
5	360 ± 26	n.d.	12	165 ± 18	n.d.
6	>1000	n.d.	13	85 ± 12	255 ± 14
7	115 ± 18	n.d.	14	101 ± 15	n.d.
8	60 ± 10	175 ± 10	15	110 ± 20	n.d.
9	195 ± 20	n.d.	16	106 ± 18	n.d.

^aNot determined.

As a next step, we performed *in silico* conformational analysis of **3–5** to identify possible conformations of the molecules and their relative energies. Generally, the compounds adopt linear conformations with a backbone curvature¹⁷ about 158° (see SI). They can assume two constrained conformations (*anti* and *syn*) with respect to the alkoxy side chains. These two conformations are controlled by the hydroxyl group at the middle ring. The lowest energy conformation is the *anti* form where the isopropoxy groups projected from two opposing sides of the molecule (Figure 1A). The *anti* conformer is stabilized by three IMHBs. First, five membered IMHB between C4–NH and C3–alkoxy group (restricting rotation of the C-terminal ring around Ar–NH axis). Second, six membered IMHB between C1'–CO and C2'–OH (restricting rotation of the middle ring around Ar–CO axis). Third, five membered IMHB between C4'–NH and C3'–alkoxy group (restricting rotation of the middle ring around Ar–NH axis). In *syn* conformation, the isopropoxy groups projected from the same side of the molecule (Figure 1B). The *syn* conformer is stabilized also by three IMHBs similar to the *anti* form except that C2'–OH switched from HB donor to HB acceptor and formed six membered IMHB with C4–NH (restricting rotation of the middle ring around Ar–CO axis). Interestingly, the energy difference between *anti* and *syn* forms is 0.4–0.7 kcal/mol. This dE value is a minor energy difference, which could allow the molecules to switch between both conformations at ambient temperature.

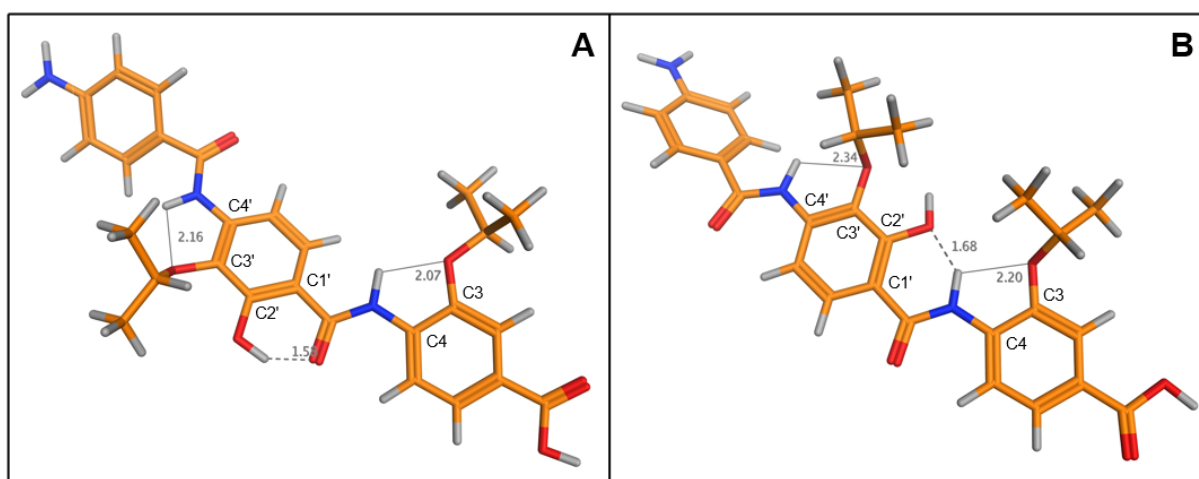


Figure 1. Conformational analysis of Cys507 (**3**): A) *anti* form (lowest energy conformation); B) *syn* form (dE 0.4 kcal/mol).

Results of *in silico* analysis prompted us to investigate the privileged conformation of this type of compounds, containing the hydroxyl motif, experimentally in solution. Therefore, we performed NOESY study of compounds **3–5**, their ester derivatives, and nitro esters in

standard NMR solvents and in a biomimetic environment.¹⁸ Results of the NOESY study were in agreement with molecular dynamics (MD) calculations. All compounds showed a strong cross peak between C4–NH and C6'–H, and weak or no cross peak with C2'–OH, indicating that these compounds exist predominantly in the *anti* conformation in solution (Figure 2 and SI). Moreover, variations at the C- and N-terminals have a little impact, if any, on conformational preference. Noteworthy, the same results were obtained when running the experiments in the usual NMR solvents (DMSO-*d*₆, acetone-*d*₆, and CDCl₃, see SI).

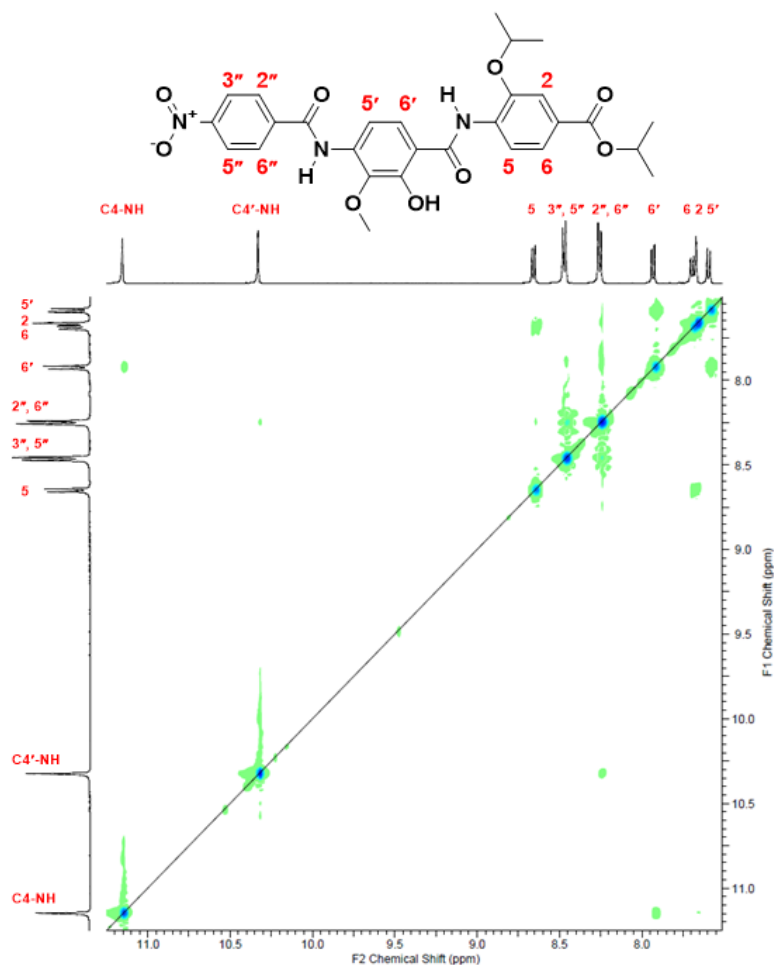


Figure 2. 2D-NOESY spectrum of compound **58** in a cryoprotective mixture (20% H₂O/DMSO-*d*₆).

The fact that the *anti* conformer was prevalent in solution raised the question if the *syn* conformer can actually exist under physiological conditions. We assumed that both conformations could be available owing to the small energy difference. To verify this, ¹H NMR experiment was performed where the chemical shift of **58** was measured at different temperatures (20 and 37 °C). This slight increment in temperature should enhance the interconversion between both conformations, which would reflect on the chemical shift of the

hydroxyl group. Indeed, we found that the chemical shift of C2'-OH moved up field from 12.50 ppm at 20 °C (mostly HB donor form, *anti*) to 12.45 ppm at 37 °C (pushing the conformational equilibrium to HB acceptor form, *syn*) (Figure 3). This indicates that these compounds can easily interconvert from *anti* to *syn* at physiological temperature.

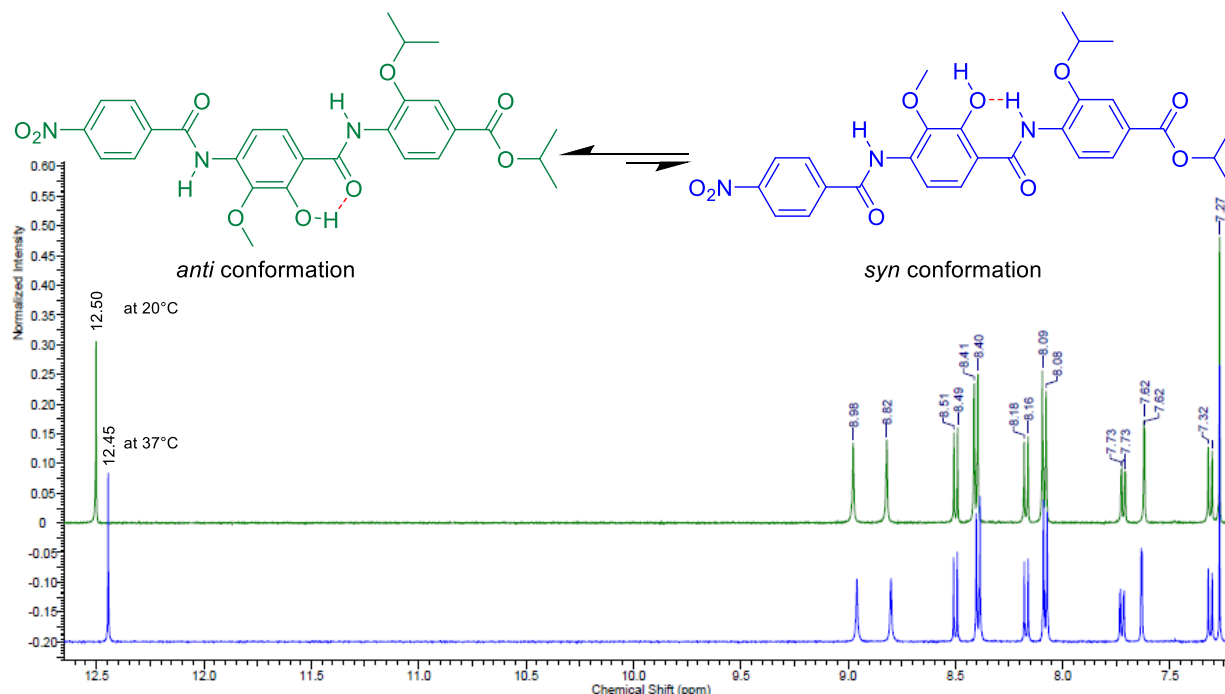


Figure 3. ^1H NMR chemical shift of compound **58** at 20 °C (green) and 37 °C (blue) in CDCl_3 .

Another evidence, by inspecting the crystal structure of the dipeptide precursor of **4** (compound **86**), we found that it adopted *syn* conformation (Figure 4), in spite of showing a prevalence of the *anti* conformation in solution similarly to the previous tripeptide compounds (see SI). This finding demonstrates that the *syn* conformation can even exist in the solid state. Thus, we could conclude that the hydroxyl group at position 2 of the middle ring plays a principal role in controlling the conformation of Cys507 and its congeners. It would give preference to the most stable *anti* conformation. Nevertheless, as the energy barrier between both conformations is low, the molecules can exist in the *syn* conformation as well.

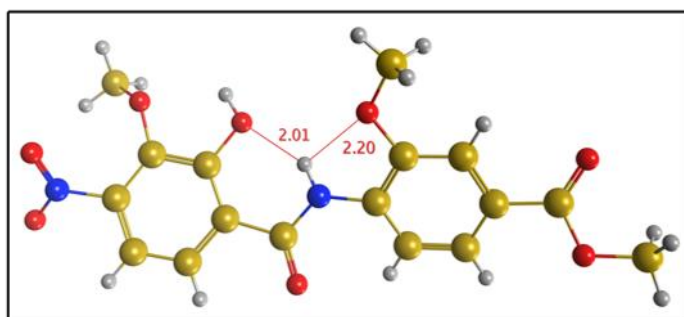


Figure 4. X-ray crystal structure of compound **86** adopting *syn* conformation via IMHB.

Moving forward to understand more about the conformation–activity relationship, since Cys507 and all compounds prepared so far took on the *anti* form mainly, we designed compounds that preferably exist in the *syn* form. This was carried out via masking the switchable hydroxyl motif and converting it into HB acceptor group only, which could stabilize the *syn* conformation. Accordingly, we synthesized compound **7** bearing a methoxy group instead of hydroxyl (Chart 2). MD calculations indicated that **7** adopted typically the most stable *syn* conformation with a large dE between the *anti* conformation (3.8 kcal/mol). NOESY study showed cross peak between C4–NH and C2'–OMe, and no cross peak with C6'–H proving that *syn* conformation is predominant (Figure 5 and SI).

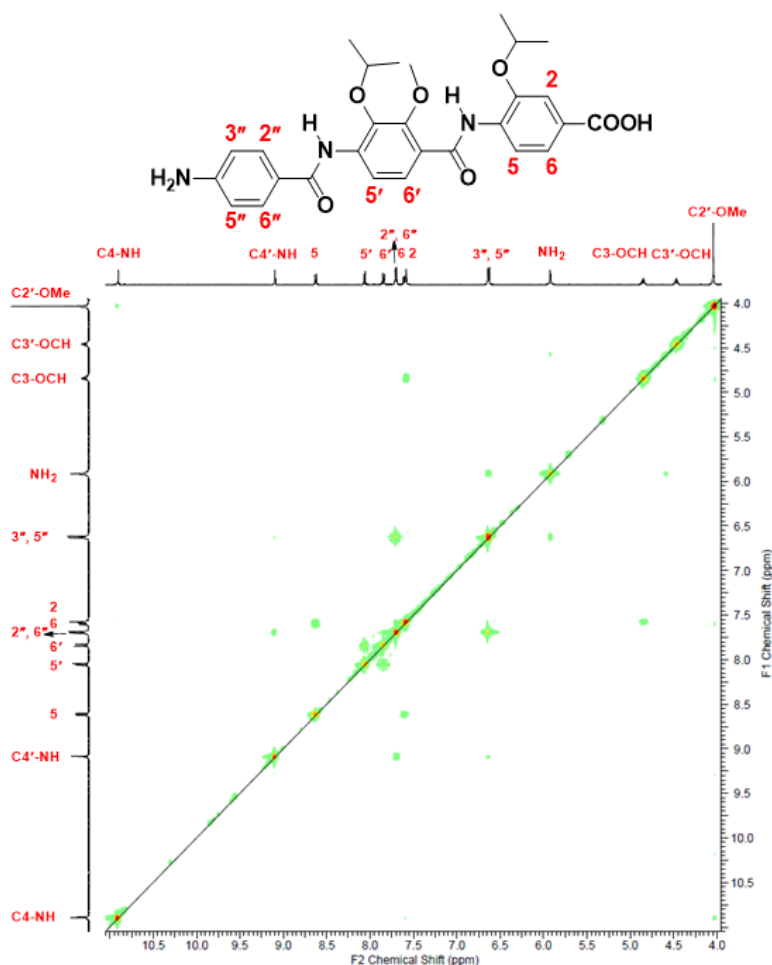


Figure 5. 2D-NOESY spectrum of compound **7** in DMSO- d_6 .

Compound **7** showed a 3-fold more potent gyrase inhibitory activity than **3** (Table 1). This result revealed that the hydroxyl group is not necessary for the interaction with the target. At the same time, this raised a new question whether this enhancement was due to inducing the *syn* conformation, hinting at the bioactive conformation, or it was due to an additional hydrophobic interaction caused by the newly introduced alkoxy group at position 2 of the middle ring. To clarify these issues, we tested each factor separately.

First, we designed compound **8** (Chart 2) bearing an isopropoxy group in place of methoxy in **7**. This modification resulted in further improvement in activity (6-fold compared to **3**). These results indicated that besides their effect on restricting the conformation to *syn* form, alkoxy groups at position 2 of the middle ring could also contribute to binding interactions with the target. In this aspect, the isopropoxy group is more beneficial than the methoxy.

Second, for proving the bioactive conformation without any other influencing factors, we utilized IMHB in an unprecedented manner. We designed two intramolecular hydrogen bonded rigid Cys507 analogs with a new scaffold, namely the pyridine derivatives **9** and **10** (Chart 3). Compound **9** can adopt solely *anti* conformation via replacing the exocyclic HB donor/acceptor hydroxyl group of **3** with an endocyclic nitrogen atom of 4-isopropoxy-5-aminopicolinic acid, whereas **10** can adopt just *syn* conformation via the 6-isopropoxy regioisomer. Conformations are stabilized by a bifurcated IMHB between C4–NH and both oxygen atom of C3–isopropoxy and nitrogen atom of the pyridine ring. X-ray crystal structures of the compounds were in conformity with our design concept (Figure 6 and SI). We proved rigidity of **9** and **10** by MD calculations (no other conformation appeared up to dE 7.0 kcal/mol), and NOESY experiments where no cross peaks were observed between C4–NH and pyridine C3–H. Moreover, they displayed no change in conformation at high temperature up to 340 K (SI). Results of gyrase inhibition assay revealed that **10** was 4–7-fold more potent than **9** and **3** (Table 1). This indicates that the *syn* conformer is indeed the bioactive conformation of **3** that is responsible for binding to DNA–gyrase complex and producing the inhibitory effect.

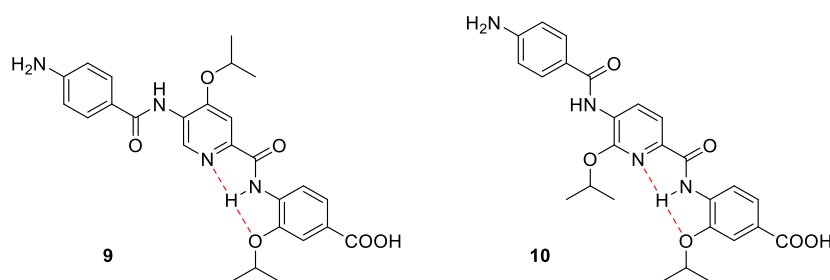


Chart 3. Structures of the IMHB rigid Cys507 analogs **9** and **10**.

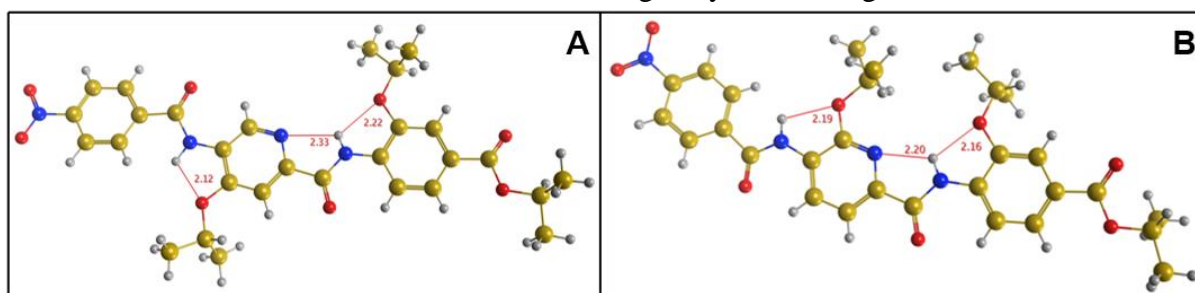


Figure 6. X-ray crystal structures of the nitro ester precursors of **9** (**82**, A) and **10** (**83**, B) adopting *anti* and *syn* conformation, respectively via IMHB.

Our design strategy has the advantages of improving the solubility and the ligand-lipophilicity efficiency¹⁹ (LLE: 3.54 for **10** vs 1.75 for **3**) by introducing a polar pyridine ring in lieu of a benzene. In addition, removal of the hydroxyl group, while keeping the right conformation, lowered the molecular weight (better drug-likeness) and enhanced the ligand efficiency¹⁹ (LE: 0.17 for **10** vs 0.13 for **3**). More importantly, hopping of Cys507 scaffold, to the novel pyridine based core, can circumvent the probable cross-resistance against the cystobactamids.²⁰ Furthermore, to the best of our knowledge this is the first time proving the bioactive conformation via non-covalently bonded rigid structures without using the classical methods of cyclization and introduction of additional covalent bonds.²¹

From another perspective of optimization, since structure complexity of NPs hinders the rapid development of drug-like molecules,⁹ we aimed at simplification of Cys507 structure based on our findings. We started with omitting either the isopropoxy or the hydroxyl group from the middle ring as in compounds **11** and **12**, respectively (Chart 2). Removal of the isopropoxy group resulted in a dramatic loss of activity, which emphasized the importance of alkoxy side chains for binding (Table 1). Interestingly, removing the hydroxyl group increased the activity 2-fold compared to **3** (Table 1). This confirms that the hydroxyl group is not essential for activity, and goes together with our findings. Since presence of the hydroxyl shifted the conformational equilibrium in favor of the less potent *anti* form, removal of it permitted free rotation of the middle ring around Ar–CO axis, and consequently shifted the equilibrium more toward the bioactive *syn* conformation. This was evidenced in the NOESY of **12** where two cross peaks of equal intensities were observed between C4–NH and C2'–H (*syn*) and C6'–H (*anti*) (SI).

Stepping forward from this point, we focused on improving the molecular recognition and affinity of our synthetic analogs through mimicking the steric and electrostatic properties of the natural ligand **3**.²² Therefore, we designed compounds **13** and **14** where a hydroxyl or isopropoxy group was introduced at the N-terminal ring of **12** and **11**, respectively (Chart 4). We chose this position to maintain the beneficial free rotation of the middle ring (Chart 4). Introducing the hydroxyl moiety at position 2 of the N-terminal ring in **13** was intended to mimic the overall shape of **3** by conserving the backbone curvature via IMHB (Figure 7). In addition, calculation of total hydrophobic-, polar-, positive-, and negative- VDW surface area of **3**, **13**, and **14** indicated that the compounds have the same values (SI). Indeed, the new modifications resulted in further enhancement in activity (Table 1). These results clearly demonstrate that the isopropoxy side chains play an essential role in binding interactions (**3** and **14** vs **11**). Moreover, changing the distance between them could be tolerated to some extent

owing to flexibility of the new analog. Furthermore, besides hydrophobic interactions and conformational preferences, simulation of the molecular features of Cys507 seems to be advantageous for improving the affinity.

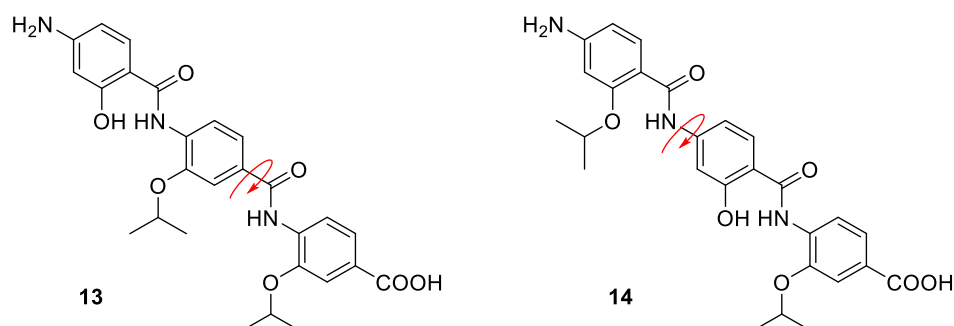


Chart 4. Structures of the freely rotating Cys507 analogs **13** and **14**

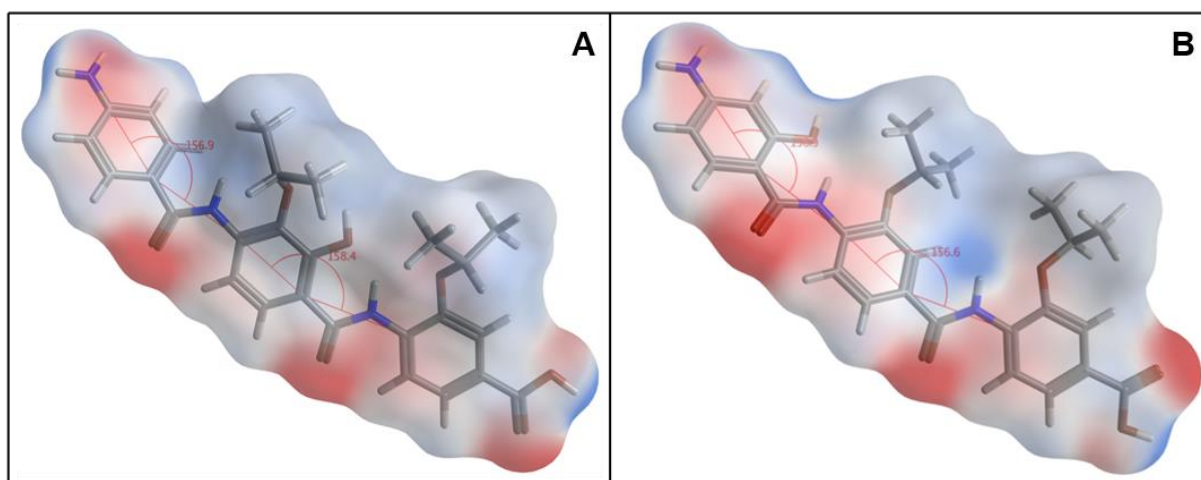


Figure 7. Electrostatic molecular surface and backbone curvature of Cys507 (A) and **13** (B): (red) negatively charged surface; (blue) positively charged surface; (white) neutral surface.

Finally, we evaluated the relevance of the terminal carboxyl group for activity through testing the isopropyl esters of **5** and the most potent compounds **7**, **8**, **10** and **12–14**. Ester derivatives showed 2 to >10-fold decrease in activity suggesting that the free carboxyl motif is necessary for activity (SI). For evaluating the role of the terminal amino group, we modified the amino terminals of **13** and **14** into nitro (compounds **15** and **16**, respectively) bearing in mind that cystobactamids **1** and **2** have terminal nitro moieties. Results indicated that the amino motif can be replaced by nitro without affecting the gyrase inhibitory activity (Table 1).

Topoisomerase IV Inhibitory Activity

We tested the effect of Cys507 and the best three gyrase inhibitors **8**, **10**, and **13** on topoisomerase IV, the second bacterial target of the cystobactamids family.¹⁴ Cys507 did not show detectable inhibition up to 500 μ M, whereas the new analogs showed moderate inhibitory activity with \sim 3-fold lower potency compared to that against gyrase (Table 1). These results indicate that modifications applied to improve the DNA gyrase inhibitory activity are also valid for topoisomerase IV, possibly due to the high homology between both enzymes.²³ Furthermore, despite different sensitivities of the enzymes, the compounds followed the same trend of activity order. This points that the new Cys507 analogs act with a similar mode of action on both targets.

Mode of Action Study

We reported that the cystobactamids are type IIA topoisomerase poisons and their primary binding site is located at the gyrase–DNA interface as described for the clinically used quinolone antibiotics.¹⁴ To gain deeper insight into the binding site of the cystobactamids, we were interested if and how cystobactamids and their analogs bind to the DNA part of the target site. There are predominantly two binding modes of small molecule ligands to DNA: minor groove binding or intercalation.²⁴ Intercalation is of particular interest, as compounds utilizing this binding mode may trigger genotoxic effects in eukaryotes.²⁵ DNA minor groove binding and intercalation can be addressed using displacement titration experiments utilizing fluorescent dyes whose fluorescence is increased upon DNA binding. Suitable probes for DNA minor groove binders in this context are the well-established Hoechst dyes.²⁶ DNA intercalation based binding mode can be tracked via the DNA intercalating dye ethidium bromide (EtBr).²⁷ Titration of calf thymus DNA bound Hoechst 33342 with Cys507, its analogs as well as **1** and **2** induced a concentration dependent loss of Hoechst 33342 fluorescence (Figure 8A and SI). No compound-induced quenching of the Hoechst 33342 fluorescence in absence of DNA was observed. This indicated that all the compounds were able to displace the Hoechst 33342 from DNA suggesting that the DNA binding site of the cystobactamids is the minor groove. When we performed the same experiments in presence of EtBr, we were pleased to find that the majority of the tested compounds (including the cystobactamids **1** and **2**) did not show any significant intercalation activity up to concentrations of 500 μ M (Figure 8B and SI). An exception was compound **15**, which reduced EtBr fluorescence \sim 50% at the highest tested concentration. This finding underlines the importance of a parallel monitoring of the activity of the modified compounds on gyrase as well as their

DNA intercalative behavior as subtle changes may have an impact on the binding mode (**13** vs **15**). Taken together the results indicate that Cys507 and analogs are indeed able to bind to DNA utilizing a minor groove binding mode. Intercalation only seems to play an insignificant role for this small molecule–DNA interaction.

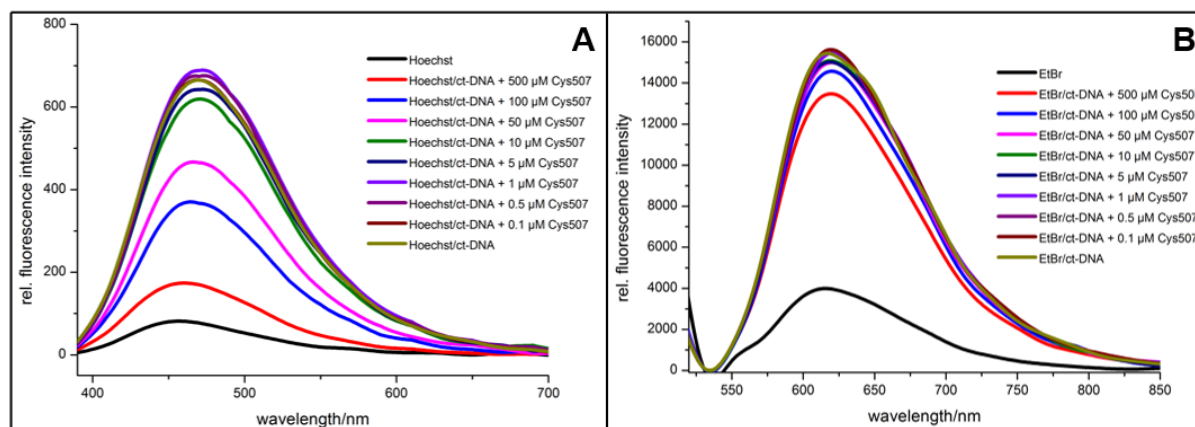


Figure 8. DNA interaction of Cys507: A) Concentration dependent decrease in fluorescence of the DNA minor groove binding dye Hoechst 33342 bound to calf thymus DNA (ct-DNA, 15 μM each) upon titration with Cys507; B) No change in fluorescence of the ct-DNA bound intercalating dye EtBr upon titration with Cys507.

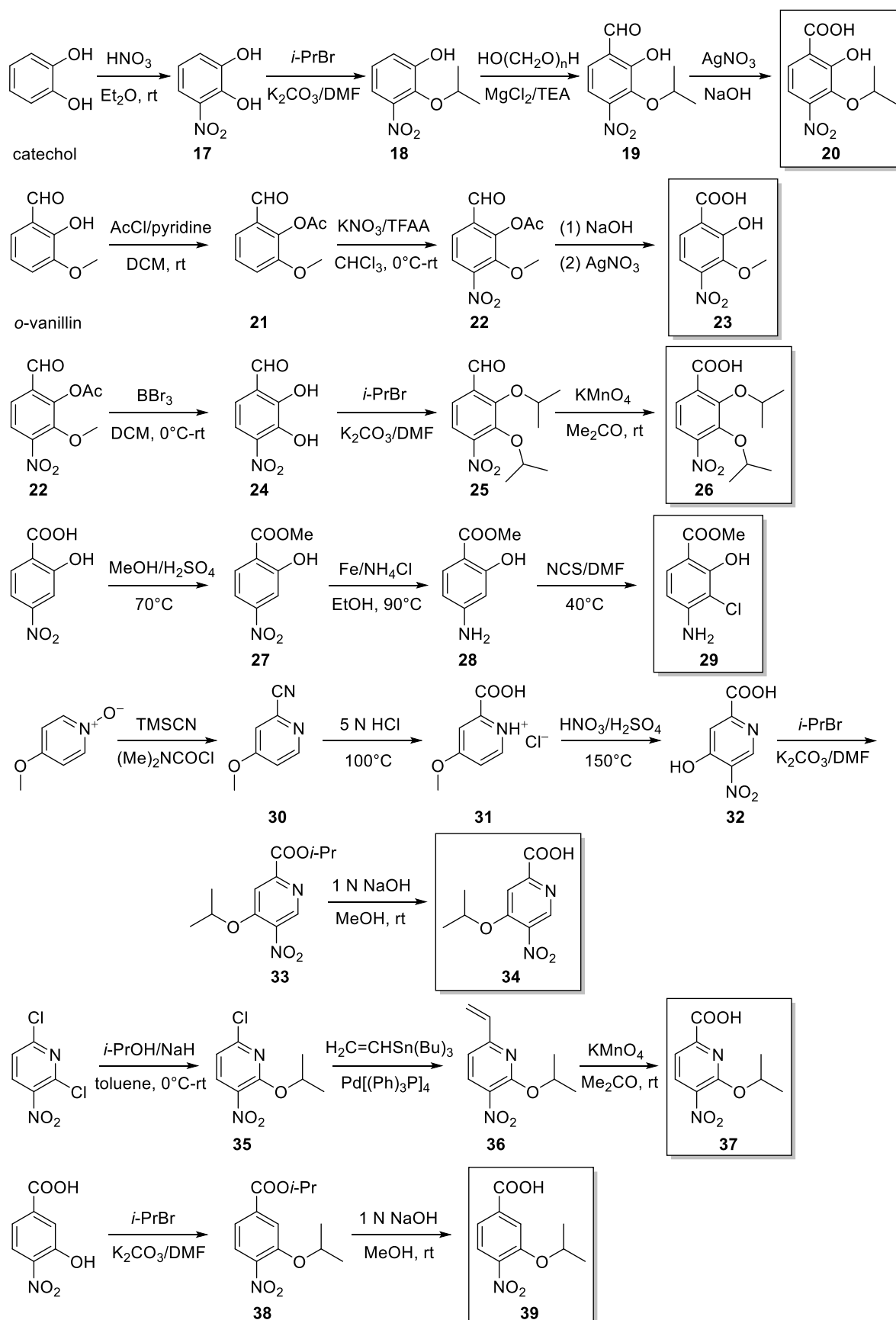
Plotting of the Hoechst 33342 spectra maxima vs compounds' concentrations delivered sigmoidal shaped curves, which could be fitted using Hill's equation (see SI). This allowed the determination of a value for "50% displacement of Hoechst 33342". Although this value does not contain absolute information about DNA affinity and the number of binding sites, it allows a "face-to-face" comparison of the apparent "minor groove affinity" of the different compounds (SI). Remarkably, these values do not significantly correlate with the gyrase activity of the respective compounds (SI). This indicates that DNA interaction by minor groove binding alone is only of secondary importance for the specificity of the cystobactamids/analogs–target interaction. The main fraction of activity-conferring interactions (the ligand–target specificity) could thus be interactions of the inhibitor with a specific conformation or state of DNA, the single or complexed proteins (GyrA and GyrB) or the whole DNA–protein complex. This is also underlined by the fact that all tested cystobactamids have a preference for gyrase over topoisomerase IV (Table 1) and up to 145-fold for **2**.¹⁴

Chemistry

We applied a retrosynthetic approach for synthesizing Cys507 and its analogs. All compounds are constituted of three units of either *p*-aminobenzoic acid or 5-aminopicolinic acid

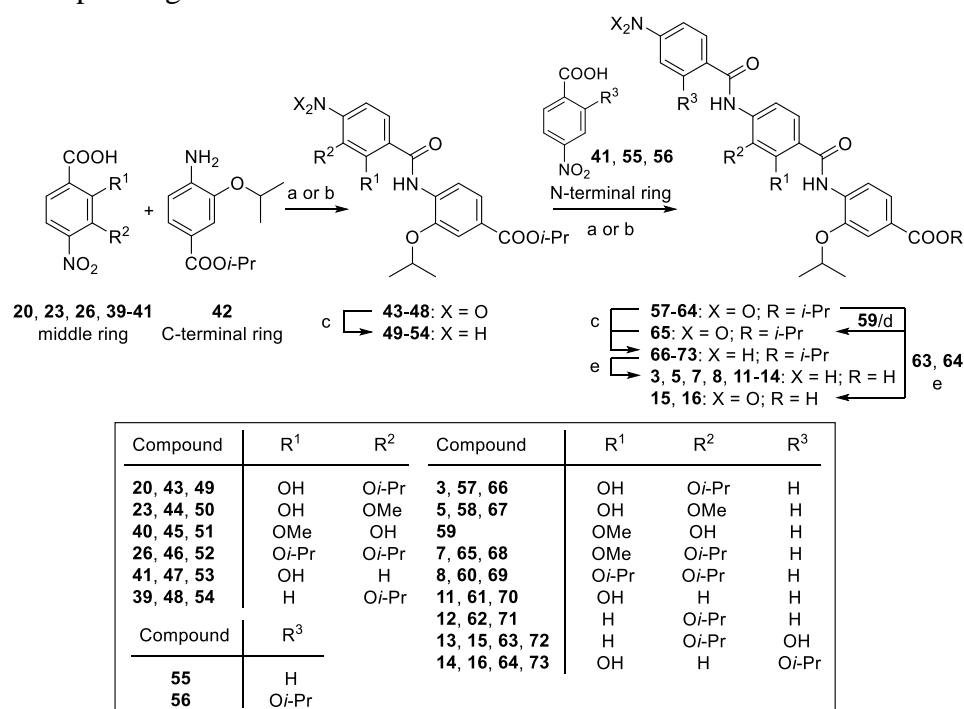
derivatives linked by amide bonds. Preparation of the individual middle, C- and N-terminal rings was firstly performed followed by the coupling process. Synthesis of the middle rings was the bottleneck step, as it required long tedious steps for preparation and separation of the desired regioisomer in a poor yield.^{16, 28-30} Some substitution patterns were even unknown in literature, e.g., compound **26** and **34** (Scheme 1). Herein we established brief efficient synthetic pathways for new and reported amino acids that are precursors of other NPs.^{31,32} Compounds **20**, **23**, **26**, **34**, **37**, and **39** were prepared as N-protected amino acids using the nitro moiety as a hidden protected amino group, whereas compound **29** was prepared as C-protected amino acid. We created a shortcut to the natural middle ring of Cys507 (compound **20**) in only four steps, instead of twelve,¹⁶ starting from a low-cost reactant (catechol). Nitration of catechol to the 3-nitro derivative **17** and then regioselective isopropylation of **17** at the 2-hydroxy position using a stoichiometric amount of 2-bromopropane provided compound **18**. Ortho formylation of **18** with paraformaldehyde in MgCl₂/TEA/MeCN mixture under strictly dry conditions produced the *p*-nitrobenzaldehyde **19**. Finally, compound **19** was oxidized using AgNO₃ under basic condition to yield the corresponding acid **20**. Synthesis of **23** started via acetylation of *o*-vanillin followed by nitration of **21** using KNO₃/trifluoroacetic anhydride mixture to afford the *p*-nitrobenzaldehyde **22**. Oxidation of **22** with AgNO₃ delivered the acid **23**. Universal O-demethylation and deacetylation of **22** using BBr₃ produced the dihydroxy derivative **24**. Isopropylation of **24** to the aldehyde **25** followed by oxidation with KMNO₄ afforded the carboxylic acid **26**. Structure of **26** was confirmed by X-ray (SI). Compound **29** was prepared through esterification of 4-nitrosalicylic acid to the methyl ester **27**. Chemical reduction of **27** via heating with iron in ethanol resulted in the corresponding amine **28**. Chlorination of the activated **28** using *N*-chlorosuccinimide yielded **29**. Synthesis of 4-isopropoxypicolinic acid **34** was accomplished via Fife reaction of 4-methoxypyridine-*N*-oxide to furnish the nitrile derivative **30**. Acidic hydrolysis of **30** then nitration of the hydrochloride salt **31** produced exclusively the O-demethylated 5-nitro derivative **32**. Isopropylation of **32** followed by saponification of the isopropyl ester **33** gave the picolinic acid **34**. Structure of **34** was evidenced by X-ray (SI). The 6-isopropoxypicolinic acid **37** was obtained from 2,6-dichloro-3-nitropyridine via the reaction with isopropyl alcohol under basic condition to yield **35**. Stille coupling of **35** produced the vinyl derivative **36**, which was oxidized to afford the picolinic acid **37**. Compound **39** was prepared by first alkylation of 3-hydroxy-4-nitrobenzoic acid then hydrolysis of the produced ester **38**. Synthesis of the C- and N-terminal rings was performed similarly (SI).

Scheme 1. Synthetic Pathways of the C- or N-Protected Middle Rings **20**, **23**, **26**, **29**, **34**, **37**, and **39**



In the amide coupling process three obstacles were encountered: presence of other interfering groups (free hydroxyl), inactivated carboxylic acids, and weakly reactive aromatic amines. We developed two straightforward strategies for amide coupling that could overcome these difficulties. Moreover, activation of carboxylic acids and OH protection³¹ were unnecessary, therefore these methods spared time, effort and money required for additional steps. For instance, synthesis of Cys507 was accomplished in overall 11 steps instead of 21 reported before.¹⁶ The first strategy (Scheme 2) started with coupling of the N-protected middle rings **20**, **23**, **26**, and **39–41** to the C-protected C-terminal ring **42** using either dichlorotriphenylphosphorane or phosphorus trichloride as coupling reagent to afford the dipeptides **43–48**. The nitro derivatives **43–48** were chemically reduced to the corresponding amines **49–54**. A second coupling cycle of the dipeptides **49–54** to the N-terminal rings **41**, **55**, and **56** was performed to furnish the tripeptides **57–64**. Compound **65** was obtained via alkylation of **59** with isopropyl bromide in K₂CO₃/DMF mixture. Further reduction of the nitro derivatives **57**, **58**, and **60–65** produced the amino esters **66–73**. Finally, C-deprotection via ester hydrolysis yielded the amino acids **3** (Cys507), **5**, **7**, **8**, and **11–14**. The nitro acids **15** and **16** were prepared also using the same strategy where the tripeptide nitro esters **63** and **64**, respectively were saponified.

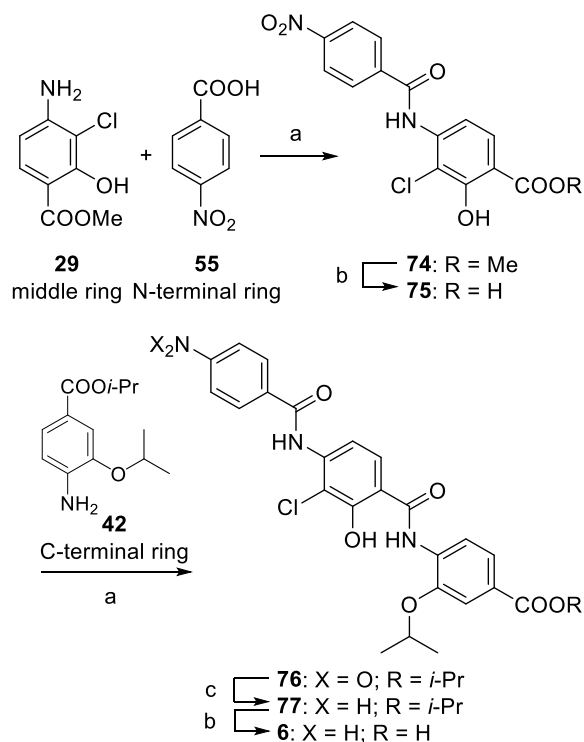
Scheme 2. First Coupling Strategy for Synthesizing Compounds **3** (Cys507), **5**, **7**, **8**, **11–16**, and the Corresponding Esters^a



^aReagents and conditions: (a) Cl₂PPh₃, CHCl₃, 80 °C, 12 h; (b) PCl₃, xylenes, 150 °C, 12 h; (c) Fe, NH₄Cl, EtOH/H₂O, 90 °C, 1 h; (d) 2-bromopropane, K₂CO₃, DMF, 80 °C, 12 h; (e) 1 N NaOH, MeOH/THF, rt, 12 h.

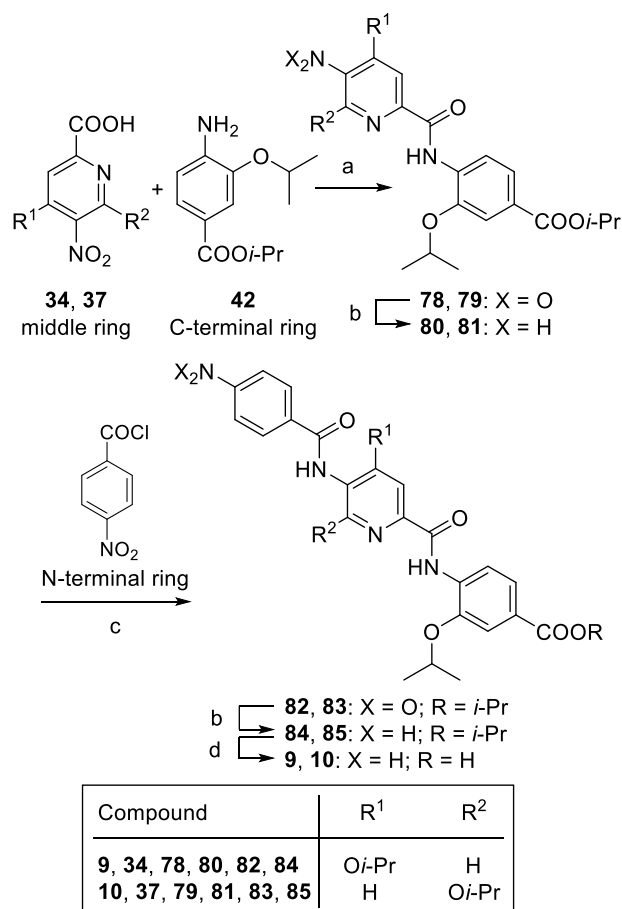
The second strategy (Scheme 3) started with coupling of the C-protected middle ring **29** to the N-protected N-terminal ring **55** via dichlorotriphenylphosphorane to yield the dipeptide **74**. Ester hydrolysis of **74** afforded the corresponding acid **75**, which was coupled to the C-terminal ring **42** using the same coupling reagent to produce the tripeptide **76**. Reduction of **76** to the corresponding amine **77** and final ester saponification afforded the amino acid **6**.

Scheme 3. Second Coupling Strategy for Synthesizing Compound **6**^a



^aReagents and conditions: (a) Cl_2PPh_3 , CHCl_3 , 80 °C, 12 h; (b) 1 N NaOH, MeOH/THF, rt, 12 h; (c) Fe, NH_4Cl , EtOH/ H_2O , 90 °C, 1 h.

Synthesis of the pyridine containing derivatives **9** and **10** was similar to the first strategy (Scheme 4). However, as the picolinic acids **34** and **37** did not contain hydroxyl group, we used less selective coupling reagents. The first coupling was achieved using EDC/HOBt, whereas the second coupling was carried out via acylation of the amino dipeptides **80** and **81** with *p*-nitrobenzoyl chloride to give the tripeptides **82** and **83**, respectively. Noteworthy, the coupling reagent dichlorotriphenylphosphorane was also tried, and efficiently produced the target amides in good to excellent yields.

Scheme 4. Synthesis of the Pyridine Containing Tripeptides **9** and **10**^a

^aReagents and conditions: (a) EDC/HOBt, DMF, CHCl₃, 0 °C–rt, 12 h; (b) Fe, NH₄Cl, EtOH/H₂O, 90 °C, 1 h; (c) DCM, pyridine, rt, 24 h; (d) 1 N NaOH, MeOH/THF, rt, 12 h.

Antibacterial Activity

All active compounds were evaluated for their antibacterial activity against a panel of Gram-positive and Gram-negative bacteria (Table 2). The new Cys507 analogs showed up to 8–16-fold improved activities against Gram-positive strains compared to the parent antibiotic Cys507. A good correlation between the antibacterial effects and topoisomerases IIA inhibitory activities was observed. In contrast to **1** and **2**,¹⁴ Cys507 and analogs did not show significant activity against *E. coli* wild-type, but they were active against the efflux-deficient *E. coli* *tolC3* mutant. These results implied that efflux mechanisms of *E. coli* affected most of the compounds. Some compounds, e.g., **8** and **13**, suffered from penetration issues through the Gram-negative outer membrane as indicated by the enhanced MIC values (8-fold) in presence of a permeability enhancer.

Table 2. Antibacterial Activities of Cys507 and its Synthetic Analogs

Compd	MIC ($\mu\text{g/mL}$)						
	<i>S. aureus</i> Newman	<i>S. pneumoniae</i> DSM-20566	<i>M. luteus</i> DSM-1790	<i>E. faecalis</i> ATCC-29212	<i>E. coli</i> DSM-1116	<i>E. coli</i> DSM-26863 ^b	<i>E. coli</i> DSM-26863 + PMBN ^c
3 (Cys507)	n.d. ^a	64	128	64–128	>128	>128	32–64
5	64	16–32	>64	>64	>64	>64	>64
7	32	16	64	32	>64	4	2
8	8	8–16	32	16–32	>64	32	4
10	8	>64	8–16	>64	>64	16	4
13	32	8	>64	64	>64	32	4
14	8	4–8	64	32	>64	16	4

^aNot determined; ^b*tolC3* genotype; ^c3 $\mu\text{g/ml}$ polymyxin B nonapeptide.

Metabolic Stability

Besides effectiveness against bacteria, metabolic stability of antibiotic leads is a crucial feature of optimization.⁹ We investigated Cys507 and the analogs **8**, **10**, and **13** for their phase I and II metabolic biotransformation using human liver S9 fraction. Cys507 and all synthetic compounds displayed an extraordinary high metabolic stability ($t_{1/2} > 240$ min). These results underline the following conclusions: First, although being peptidomimetics, compounds with amide linkages between non-proteinogenic amino acids are highly resistant to phase I proteolytic enzymes. Second, the phase II vulnerable hydroxyl group of Cys507 and **13** was not affected by the conjugating enzymes. This is in line with our gyrase inhibition results confirming that this unique hydroxyl group is almost inaccessible for intermolecular interaction, and in principle plays an intramolecular role. Lastly, conformational modification (*anti* to *syn*), e.g., compounds **8** and **10** maintained the outstanding metabolic stability.

CONCLUSIONS

We improved the synthesis, topoisomerases IIA inhibition and antibacterial activity of the novel antibiotic Cys507 through an interactive rational design of Cys507 analogs and establishment of concise robust synthetic procedures. SAR revealed importance of the alkoxy side chains and irrelevance of the hydroxyl group for gyrase inhibition. The terminal carboxyl and amino/nitro moieties were necessary for activity. Moreover, simulation of Cys507 molecular shape and electrostatic properties could also play a positive role. We exploited IMHB in a pioneer method to prove the bioactive conformation of Cys507 as *syn* form. Studying the privileged molecular conformation in solution as well as solid state enabled us to deduce the conformation–activity relationship. We found that the prevailing *anti* conformation

of Cys507 should be forced in the inverse direction (*syn*) or at least liberated to improve the activity. Modification of the Cys507 scaffold to a pyridine based structure increased chemical diversity, which is an intrinsic criterion to combat antibiotic resistance.¹⁰ Furthermore, we succeeded in simplification of Cys507 structure, bearing a middle ring with challenging tetrasubstitution pattern, into chemically feasible analogs while maintaining the enhanced activity. It could be shown that the cystobactamids' and analogs' mode of action is at least in part mediated by DNA minor groove binding and not intercalation. High activity and specificity seem to be mediated by further interactions with the target protein–DNA complex, e.g., protein contacts or binding to specific conformational states of the biomacromolecules. An important advantage of Cys507 and the novel analogs is the high metabolic stability. This work facilitates the rapid development of cystobactamids and similar antibiotics.³¹ Prediction of compound activity can be approached *in silico* by analyzing the preferred conformation. This saves efforts required for generating large futile libraries and enriches the number of active hits. Finally, we emphasized that medicinal chemist is able to trim and optimize natural antibiotics into more active drug-like compounds suitable for clinical application. Nonetheless, nature inspiration should be indispensable.

EXPERIMENTAL SECTION

Experimental procedures for the synthesis of the final compounds and the intermediates as well as their characterization, NMR spectra, computational work, biological experiments and X-ray crystallographic data are described in details in the Supporting Information.

ACKNOWLEDGMENTS

We thank Prof. Andreas Speicher for supporting the conformational study and Dr. Josef Zapp for performing the NMR experiments. Walid A. M. Elgaher gratefully acknowledges a scholarship from the German Academic Exchange Service (DAAD).

REFERENCES

- (1) Arias, C. A.; Murray, B. E., *N. Engl. J. Med.* **2009**, *360*, 439-443.
- (2) Cooper, M. A.; Shlaes, D., *Nature* **2011**, *472*, 32.
- (3) Newman, D. J.; Cragg, G. M., *J. Nat. Prod.* **2016**, *79*, 629-661.
- (4) Floss, H. G., *J. Biotechnol.* **2006**, *124*, 242-257.
- (5) Tulp, M.; Bohlin, L., *Bioorg. Med. Chem.* **2005**, *13*, 5274-5282.
- (6) Chopra, I., *Antimicrob. Agents Chemother.* **1994**, *38*, 637-640.
- (7) Singh, M. P.; Zaccardi, J.; Greenstein, M., *J. Antibiot. (Tokyo)* **1998**, *51*, 1109-1112.
- (8) Ling, L. L.; Schneider, T.; Peoples, A. J.; Spoering, A. L.; Engels, I.; Conlon, B. P.; Mueller, A.; Schaberle, T. F.; Hughes, D. E.; Epstein, S.; Jones, M.; Lazarides, L.; Steadman, V. A.; Cohen, D.

- R.; Felix, C. R.; Fetterman, K. A.; Millett, W. P.; Nitti, A. G.; Zullo, A. M.; Chen, C.; Lewis, K., *Nature* **2015**, *517*, 455-459.
- (9) von Nussbaum, F.; Brands, M.; Hinzen, B.; Weigand, S.; Habich, D., *Angew. Chem. Int. Ed. Engl.* **2006**, *45*, 5072-5129.
- (10) Fischbach, M. A.; Walsh, C. T., *Science* **2009**, *325*, 1089-1093.
- (11) Wilson, R. M.; Danishefsky, S. J., *Acc. Chem. Res.* **2006**, *39*, 539-549.
- (12) Berdy, J., *J. Antibiot. (Tokyo)* **2012**, *65*, 385-395.
- (13) Cragg, G. M.; Newman, D. J., *Biochim. Biophys. Acta.* **2013**, *1830*, 3670-3695.
- (14) Baumann, S.; Herrmann, J.; Raju, R.; Steinmetz, H.; Mohr, K. I.; Huttel, S.; Harmrolfs, K.; Stadler, M.; Muller, R., *Angew. Chem. Int. Ed. Engl.* **2014**, *53*, 14605-14609.
- (15) Newhouse, T.; Baran, P. S.; Hoffmann, R. W., *Chem. Soc. Rev.* **2009**, *38*, 3010-3021.
- (16) Moreno, M.; Elgaher, W. A. M.; Herrmann, J.; Schläger, N.; Hamed, M. M.; Baumann, S.; Müller, R.; Hartmann, R. W.; Kirschning, A., *Synlett* **2015**, *26*, 1175-1178.
- (17) Saraogi, I.; Incarvito, C. D.; Hamilton, A. D., *Angew. Chem. Int. Ed. Engl.* **2008**, *47*, 9691-9694.
- (18) Spadaccini, R.; Temussi, P. A., *Cell. Mol. Life Sci.: CMLS* **2001**, *58*, 1572-1582.
- (19) Leeson, P. D.; Springthorpe, B., *Nat. Rev. Drug Discov.* **2007**, *6*, 881-890.
- (20) Vieweg, L.; Kretz, J.; Pesic, A.; Kerwat, D.; Gratz, S.; Royer, M.; Cociancich, S.; Mainz, A.; Sussmuth, R. D., *J. Am. Chem. Soc.* **2015**, *137*, 7608-7611.
- (21) Carney, D. W.; Schmitz, K. R.; Truong, J. V.; Sauer, R. T.; Sello, J. K., *J. Am. Chem. Soc.* **2014**, *136*, 1922-1929.
- (22) Böhm, H.-J.; Klebe, G., *Angew. Chem. Int. Ed. Engl.* **1996**, *35*, 2588-2614.
- (23) Kato, J.; Nishimura, Y.; Imamura, R.; Niki, H.; Hiraga, S.; Suzuki, H., *Cell* **1990**, *63*, 393-404.
- (24) Blackburn, G. M.; Gait, M. J.; Loakes, D.; Williams, D. M., *Nucleic Acids in Chemistry and Biology* 3rd ed.; The Royal Society of Chemistry: 2006; p i-470.
- (25) Ferguson, L. R.; Denny, W. A., *Mutat. Res.* **2007**, *623*, 14-23.
- (26) Pjura, P. E.; Grzeskowiak, K.; Dickerson, R. E., *J. Mol. Biol.* **1987**, *197*, 257-271.
- (27) Tse, W. C.; Boger, D. L., *Acc. Chem. Res.* **2004**, *37*, 61-69.
- (28) Kato, S.; Morie, T., *J. Heterocyclic Chem.* **1996**, *33*, 1171-1178.
- (29) Pomel, V.; Rovera, J. C.; Godard, A.; Marsais, F.; Queguiner, G., *J. Heterocyclic Chem.* **1996**, *33*, 1995-2005.
- (30) Bosmans, J.-P. R. M. A.; Berthelot, D. J.-C.; Pieters, S. M. A.; Verbist, B. M. P.; De Cleyn, M. A. J. Equilibrative nucleoside transporter ENT1 inhibitors. WO 2009062990 A2, 2009.
- (31) Kretz, J.; Kerwat, D.; Schubert, V.; Gratz, S.; Pesic, A.; Semsary, S.; Cociancich, S.; Royer, M.; Sussmuth, R. D., *Angew. Chem. Int. Ed. Engl.* **2015**, *54*, 1969-1973.
- (32) Kishimoto, S.; Nishimura, S.; Hatano, M.; Igarashi, M.; Takeya, H., *J. Org. Chem.* **2015**, *80*, 6076-6082.

4 Final Discussion

In the following sections, reference to the compounds mentioned in chapter 3 is modified to the compound's number accompanied by the roman number of the corresponding paper/manuscript, e.g., compound **3** in paper **III** is labeled compound **3/III** for the sake of clarity.

4.1 Structure–Activity Relationships

Building relationships between the chemical structure and the bioactivity for a set of compounds is a fundamental tool in medicinal chemistry. It enables the determination of the structural features necessary for evoking the biological activity. By this knowledge, both structure optimization and activity improvement can be achieved.

4.1.1 Ureido-Heterocyclic-Carboxylic Acids as *E. coli* RNAP Inhibitors

The goal of the development of novel classes of RNAP “switch region” inhibitors is addressed in publications **I** and **II**. The starting point was the previously discovered and optimized class of 5-aryl-3-ureidothiophene-2-carboxylic acids (class I) (Sahner et al. 2013). Three new groups of regioisomers were designed (classes II–IV) by altering the position of the aryl ring or exchanging the positions of the carboxyl and ureido moieties at the thiophene nucleus. Compounds of class II (5-aryl-2-ureidothiophene-3-carboxylic acids) showed decent RNAP inhibitory activities that are equipotent to those of class I. Class III compounds (4-aryl-2-ureidothiophene-3-carboxylic acids) exhibited moderate activities, whereas the candidates of class IV (4-aryl-3-ureidothiophene-2-carboxylic acids) suffered from a dramatic loss of activity. This indicates that the favorable arrangement of the aryl, ureido, and carboxyl motifs at the thiophene ring for optimum RNAP inhibition is afforded by class I and II. The exciting identical activities of class I and II could be clarified on molecular similarity basis. *In silico* similarity analysis, flexible alignment, and docking in the “switch region” binding site demonstrated that compounds of class I and II are capable of adopting the same orientation and binding interactions within the “switch region” leading to equivalent RNAP inhibitory activities.

After establishing the proper configuration of the aryl, ureido, and carboxyl functionalities, the thiophene core was swapped for other five membered heterocycles generating three more classes. Classes V and VI bearing furan rings showed 3-fold reduced activity compared to classes I and II, whereas class VII with a thiazole nucleus displayed only a slight decrease in

activity. This result indicates that the isosteric replacement of $-S-$ by $-O-$ negatively affects the affinity to RNAP, whereas substitution of $=N-$ for $=CH-$ can be tolerated. This could be accounted by alterations in lipophilicity, electronic distribution and particularly the ring size of the thiophene nucleus, which controls interatomic distances, bond angles as well as the overall shape of the molecule. This assumption is supported by the clear relationship obtained from plotting the angle (α) between the aryl and ureido arms of classes I–VII (Figure 9) versus the corresponding RNAP inhibitory activity. The resultant parabolic curve underlines the role of molecular geometry in binding and reveals the optimum α values of 150° – 159° for the activity of these classes against RNAP.

The SARs of the substituents at the aryl and ureido groups are consistent with the former findings (Sahner et al. 2013). Increasing the lipophilicity and electron withdrawing properties at the aryl ring improves the activity, e.g., **19/I** vs **16/I** and **21/I** vs **18/I**. At the ureido group, substituents with large hydrophobic volume are useful, e.g., **19/I**, **21/I**, **10/II** and **19/II**. No wonder that the best RNAP inhibitory activity is associated with lipophilic fragments at both the aryl and ureido motifs of the molecule. This is ascribed to the hydrophobic nature of the respective binding pocket, the “switch region” (Mukhopadhyay et al. 2008).

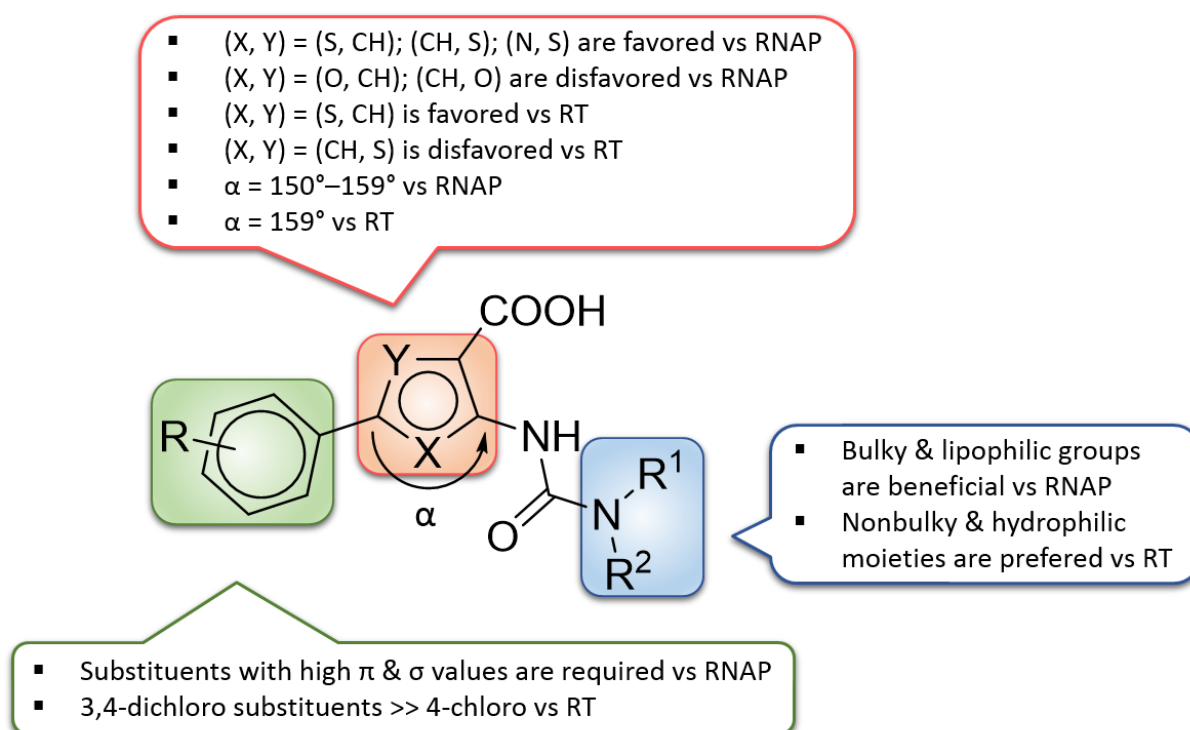


Figure 9. SARs of the 2-ureidothiophene-3-carboxylic acids as *E. coli* RNAP and HIV-1 RT inhibitors.

4.1.2 Ureidothiophene-Carboxylic Acids as RT Inhibitors

Publication II deals with the discovery and development of dual bacterial RNAP and HIV-1 RT inhibitors. Screening of 8 candidates from the previously developed RNAP “switch region” inhibitors, representing the ureidothiophene classes I–IV, for RT inhibitory activity resulted in merely compound **4/II** (class II) with good dual activity against both targets. This result indicates that the additional chloro substituent at 3-position of the aryl group has a positive effect on the RT inhibitory activity (**4/II** vs **3/II**), which is more significant than that against RNAP. Another remark, although the assumption that similar molecules show similar activities holds true for **4/II** (class II) and **2/II** (class I) regarding RNAP inhibitory activity, it turns out to be improper concerning RT inhibition. This can be assigned to differences between the binding sites (the “switch region” and the NNRTI binding pocket) and the slight variances in the structure as well ($T_c = 0.75$ using four-point pharmacophore fingerprint).

Optimization of compound **4/II** began with modification of the ureido moiety. Substituting the N-benzyl-N-ethyl motif with N,N-dibenzyl group (**10/II**) improved RNAP inhibition 3-fold as expected, however the activity against RT decreased dramatically. This finding indicates that in contrast to RNAP inhibition, too bulky and lipophilic substituent at the ureido moiety is disfavored for RT inhibition. Substitution with just N-benzyl group (**9/II**) negatively affected the activity against both RNAP and RT. Interestingly, the dual activity was restored by omitting the methylene linker from **9/II** (**11/II**). As compound **11/II** has higher ligand efficiency than **4/II**, it was utilized for the next step of optimization pursuing a structure-based design approach.

Molecular docking of **11/II** into the RT allosteric binding site suggested that all three aromatic motifs of **11/II** are necessary for binding. They are involved in four hydrophobic interactions with Trp229, Val106 and Leu100, which are responsible for high fitness costs upon mutation. According to this binding mode, diverse substituents at *p*-position of the N-phenyl ring were introduced to make use of the volume between it and the highly conserved region (Trp229, Phe227, and Leu234) in order to improve the affinity and decrease the resistance propensity. Indeed, the new derivatives showed enhanced RT inhibition up to 12-fold (**18/II**) achieving comparable activity to that of NVP and superior potency to that of AZT-TP. Remarkably, addition of a phenyl or 1,2,4-triazolyl ring to the sulfonamide or the acetamide group negatively affects the RT inhibitory activity (**19/II** vs **18/II** and **16/II** vs **15/II**). This result is in agreement with the previous hypothesis that too sterically demanding substituents at the ureido group are not preferred (Figure 9).

To get more insight into SARs, a QSAR model for compounds **11/II**–**20/II** is calculated using a multiple regression analysis. The output equation highlights the role of electrostatic and steric interactions for activity. Increasing the positive partial charge stands advantageous, whereas the number of hydrogen bond donor atoms at the N-phenyl moiety should be kept to a minimum (0–1 atoms). The inverse relationship with molecular refractivity underlines the importance of less polarizable and non-bulky substituents at the ureido motif for RT inhibition.

4.1.3 Cystobactamid 507 analogs as DNA Gyrase Inhibitors

Publication III and manuscript IV focus on the development of novel DNA gyrase and topoisomerase IV inhibitors based on the natural antibiotic Cystobactamid 507 (Cys507). Preliminary modulation of Cys507 structure by synthesizing the methyl homolog **18/III** led to just a slight reduction in activity indicating that the natural compound is open for modification. Reviewing the Cys507 structure revealed some similarity to the α -helix mimetics 3-O-alkylated benzamides. Nonetheless, Cys507 has a unique hydroxyl group at position 2' of the middle ring and unsubstituted N-terminal moiety (Figure 10). As type of side chains and conformation are key factors controlling the activity of α -helix mimetics, a rational design was pursued to evaluate the role of isopropoxy side chains and conformation for the gyrase inhibitory activity of Cys507.

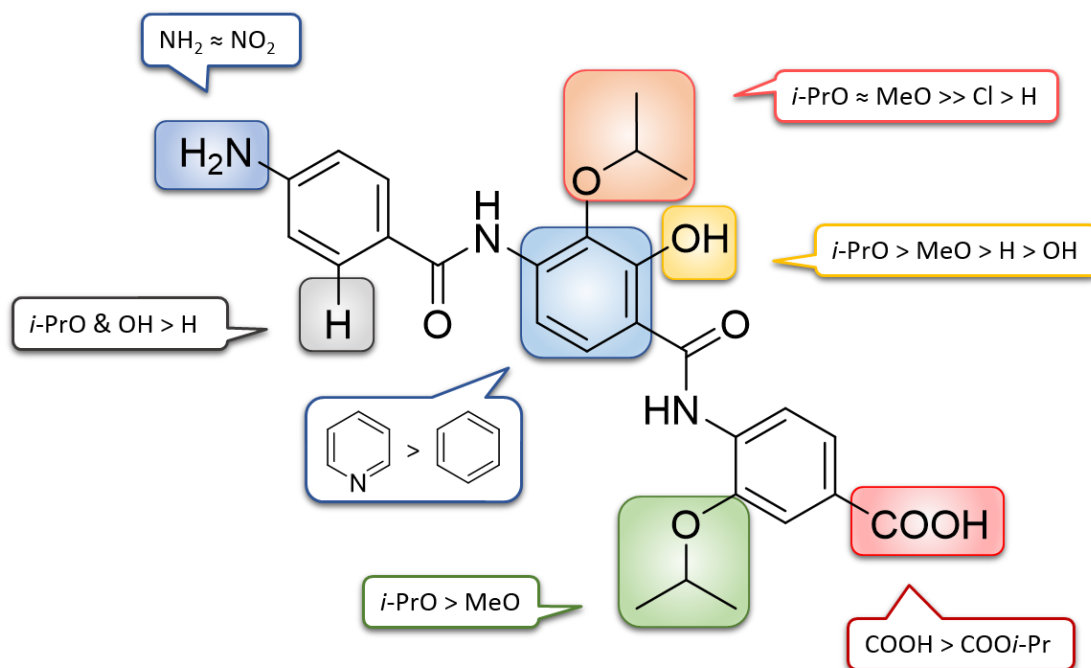


Figure 10. SARs of the cystobactamid 507 analogs as DNA gyrase inhibitors.

Compound **5/IV** with a methoxy group at the middle ring showed an equipotent activity to Cys507, whereas replacement of the isopropoxy with chlorine (**6/IV**) resulted in a dramatic loss in potency. This indicates that the alkoxy groups at the middle ring are essential for activity as they probably contribute in the ligand–target interaction and restrict the conformation, via IMHB and steric effect, in an optimum orientation necessary for binding. On the other side, modification of the isopropoxy group to methoxy at the C-terminal ring seems noxious (**5/IV** vs **18/III**). This result suggests that the isopropoxy side chain at the C-terminal ring is preferred due to its steric and hydrophobic features. Therefore, it was conserved in the next steps of optimization.

Conformational analysis of Cys507, **18/III** and **5/IV** revealed that these ligands can adopt two constrained conformations (*syn* and *anti*) referring to the orientation of the alkoxy groups. Both conformers are stabilized by three IMHBs. The 2'-hydroxyl group at the middle ring controls the conformation via either acting as a HB donor (triggering *anti*) or acceptor (triggering *syn*). The energetically favored conformation is *anti*, however interconversion to *syn* is readily accessible thanks to the low energy difference ($dE = 0.4\text{--}0.7$ kcal/mol). These *in silico* findings are strengthened by 2D NOESY studies in a biomimetic environment demonstrating that *anti* is the privileged conformation. In addition, the incidence of *syn* conformation is evidenced by ^1H NMR experiment and X-ray crystal structure.

Since the synthesized compounds so far adopt mainly *anti* conformation, new compounds were designed to adopt *syn* conformation predominantly through hiding the HB donor property of the 2'-hydroxyl and keeping the HB acceptor function by converting it to an alkoxy group. The design principle is verified experimentally by 2D NOESY. Compounds **7/IV** and **8/IV** displayed 3–6-fold improved activity, respectively compared to Cys507. This result points out that the hydroxyl group is not essential for gyrase inhibition. Moreover, the newly introduced alkoxy groups at 2' position of the middle ring boost the activity not only due to restricting the conformation to *syn* form, but also as they elicit additional hydrophobic interaction with the target. In this context, the isopropoxy group is more beneficial than the methoxy.

To confirm that the *syn* conformer is the bioactive conformation, two rigid pyridine-based Cys507 analogs adopting only *anti* (**9/IV**) or *syn* (**10/IV**) conformation were designed. Results showed that **10/IV** is 4–7-fold more active than **9/IV** and Cys507, respectively.

Based on the previous findings, simplification of Cys507 structure is attempted to accelerate the development process to a drug-like molecule. Removal of the isopropoxy side chain at the middle ring (**11/IV**) is detrimental. In contrast, omitting the hydroxyl group (**12/IV**) improves the activity 2-fold compared to Cys507. The enhanced activity of **12/IV** is probably credited

to the increase in rotational freedom of the middle ring leading to displacing the conformational equilibrium in favor of the *syn* form. Returning the missing moieties to the truncated Cys507 derivatives (**11/IV**, **12/IV**) at position 2" of the N-terminal ring (**13/IV**, **14/IV**) further augmented the activity. These results are in line with the aforementioned findings underlining the importance of the alkoxy group and non-significance of the hydroxyl motif for activity. In addition, allowing a free rotation of the middle ring seems beneficial. Furthermore, simulation of Cys507 steric and electrostatic properties promotes molecular recognition of the synthetic analogs leading to a positive impact on the activity.

Comparing the gyrase inhibitory activities of the active compounds to the corresponding isopropyl esters obviously discloses the significance of the free carboxyl group for activity. On the other side, replacement of the amino moiety with nitro (**15/IV**, **16/IV**) does not affect the activity markedly.

4.2 Mode of Action Studies

4.2.1 Reverse Transcriptase Inhibition by 2-Ureidothiophene-3-Carboxylic Acids

Investigations of the mechanism of action of the 2-ureidothiophene-3-carboxylic acids as RT inhibitors are described in publication II. The HIV-1 RT converts the single-stranded viral RNA to double-stranded DNA necessary for replication (reverse transcription). There are two major classes of RT inhibitors: nucleoside RT inhibitors (NRTIs) are nucleotide analogs that are incorporated into viral DNA hindering further extension of DNA chain (chain termination). The NNRTIs inhibit RT allosterically via binding to a hydrophobic pocket in the palm domain of p66 subunit. They cause the p66 thumb to be stiffened in an open extended conformation to the finger domain. Opening and closing of the thumb and finger domains (RT clamp) is crucial for grasping and positioning primer/template (p/t) duplex at the polymerase active site. The NNRTIs-induced interruption with this motion hinders the catalytic addition of nucleotides.

First, the effect of the dual RNAP/RT inhibitors on the binding parameters of RT to a p/t duplex was monitored by applying a FRET assay. The binding affinity of RT to p/t duplex was determined to be about 3 nM. In presence of the compounds, similar values were obtained. This indicates that likewise the NNRTIs, the ureidothiophenes marginally affect the binding of RT to p/t duplex.

Afterwards, the effect of the compounds on the relative motions of the thumb and finger domains was characterized by utilizing a fluorescence-based assay. The doubly labeled RT showed low fluorescence in absence of p/t duplex referring to the proximity of thumb and finger

domains. In presence of the p/t duplex, a 1.6-fold increase in fluorescence was observed hinting to the increased distance between the two clamp domains. More fluorescence amplification (2-fold) was noted in the presence of the NNRTI nevirapine as anticipated for its mechanism of action. In contrast, a reduction in fluorescence was observed with the ureidothiophenes denoting a decrease in the distance between thumb and finger domains. This result indicates that these compounds probably exert an opposite effect to nevirapine through jamming the RT clamp in a closed conformation. Interestingly, this mechanism is typical for the RNAP “switch region” inhibitors, e.g., myxopyronin pointing out that the dual inhibitors block the bacterial and viral targets almost by the same mechanism.

Noteworthy, further evidence that the dual inhibitors bind to the NNRTI binding pocket is concluded from the results of the antiretroviral assays using HIV-1 resistant strains having mutations in the NNRTI binding site. Compounds **11/II**, **18/II**, and **19/II**, being active against HIV-1 wild type, lose their activity against two out of four NNRTIs-resistant mutants.

In conclusion, the ureidothiophenes inhibit RT non-competitively like NNRTIs. Remarkably, they undertake a new mechanism of action through closing of the RT clamp.

4.2.2 DNA Gyrase Inhibition by Cystobactamids and their Analogs

Cystobactamids are topoisomerases IIA poisons that bind at the gyrase–DNA interface partially overlapping the fluoroquinolones’ binding site (Baumann et al. 2014). Deeper insight into the binding mode of the cystobactamids/analogs is gained in manuscript IV. The investigations focus on the site of binding to the DNA part of the target complex. Accordingly, two parallel titration experiments were performed with the cystobactamids/analogs using calf thymus DNA in the presence of either the DNA minor groove binding dye Hoechst 33342 or the DNA intercalating dye EtBr. The concentration dependent decrease in Hoechst 33342 fluorescence with all cystobactamids/analogs reveals that they are able to displace the dye from DNA suggesting that their DNA binding site is the minor groove. On the other side, fortunately, the non-remarkable change in EtBr fluorescence with cystobactamids and most of the analogs indicates that they lack an intercalation activity.

Taken together, these findings demonstrate that the cystobactamids/analogs are in fact able to bind to DNA targeting the minor groove as a site of interaction. Moreover, they exhibit non-significant intercalation.

4.3 Anti-infective Activities and Cytotoxicity to Human Cells

Back to the “magic bullet” concept, a successful antibiotic should have a broad spectrum antibacterial activity and no cytotoxicity to human cells.

4.3.1 The Dual RNAP/RT Inhibitors “Ureidothiophene Carboxylic Acids”

Evaluation of the antibacterial activity of the developed ureidothiophene classes revealed that the compounds are highly active against Gram-positive bacteria, e.g., *S. aureus* and *B. subtilis* (MIC₉₅ values are down to 2 µg/mL). Notably, the antibacterial effects correlate well with the respective RNAP inhibitory activities of the compounds. Unfortunately, they do not show growth inhibition of the Gram-negative wild type strains, e.g., *E. coli* K12 and *P. aeruginosa* O1. Interestingly, the compounds display significant antibacterial activities on the Gram-negative *E. coli* TolC strain, which is a mutant lacking the outer membrane channel of the tripartite AcrB multidrug efflux pump. This finding implies that the novel RNAP inhibitors can efficiently permeate through the outer membrane of Gram-negative bacteria. However, they are readily recognized by an innate resistance mechanism “the efflux pumps”.

Impressively, the antibacterial potencies of the compounds are fully retained against Rif-resistant *E. coli* TolC strains. This result demonstrates that indeed the compounds possess no cross-resistance with rifamycins as intended for the “switch region” inhibitors.

Assessment of the antiretroviral activities of the dual RNAP/RT inhibitors using cellular infectivity assay indicated that the compounds exhibit good intracellular inhibitory activities of HIV-1 replication in the low micromolar range (IC₅₀ values of 5–15 µM). Moreover, the antiretroviral spectrum of the compounds is extended to include some HIV-1 strains with multiple resistance mutations to clinically used NNRTIs. The finding that these dual acting anti-infectives display no cross-resistance in NNRTIs-resistant HIV-1 strains presents a leading advantage over the first and second generation NNRTIs.

The effect of the novel anti-infective class on human cell viability was investigated in two different cell lines (HeLa and HEK 293). Results indicated that the compounds exhibit only marginal or no cytotoxicity.

4.3.2 The Topoisomerases IIA Inhibitors “Cystobactamids and Analogs”

Determination of the antibacterial properties of the developed Cys507 analogs revealed that the new congeners display up to 8–16-fold improved activities against a panel of Gram-positive strains compared to the parent antibiotic Cys507. In addition, a good correlation between the antibacterial effects and topoisomerases IIA inhibitory activities is observed. Likewise Cys507 and in contrast to Cys919-2, the new analogs lack an antibacterial effect on

E. coli wild type, although they show good activities against the efflux mutant *E. coli tolC3*. This refers again to the efflux issue as a major mechanism of resistance to such compounds in Gram-negative pathogens.

4.4 Ureidothiophenes' Uptake and Resistance Mechanisms in *E. coli*

The fact that the ureidothiophene RNAP inhibitors show decent antibacterial activities toward Gram-positive pathogens but not toward Gram-negative species, although they are active against *E. coli* TolC strain, prompted more investigations for gaining deeper insight into the mechanisms of uptake and non-susceptibility in Gram-negative bacteria represented by *E. coli*. For this objective, the antibacterial effects of the ureidothiophenes were assessed on three different *E. coli* strains: *E. coli* K12 (wild type with intact cell wall and efflux systems), *E. coli* D22 (mutant defective in the outer membrane LPS layer), and *E. coli* TolC (mutant defective in the AcrB efflux pump). Furthermore, the antibacterial assays were performed under three various conditions: normal growth conditions, in the presence of PMBN (an outer membrane permeability enhancer), and in the presence of PA β N (a universal efflux pump inhibitor).

Results revealed that the activities are not improved against neither the more permeable *E. coli* D22 strain nor the wild type *E. coli* K12 in the presence of PMBN. Just a non-significant decrease in MIC values (1.4–2.7-fold) is detected with *E. coli* TolC in the presence of PMBN. On the other hand, activities are markedly enhanced in the presence of PA β N against *E. coli* K12 and *E. coli* D22 strains (≥ 3 -fold) as well as *E. coli* TolC (5–14-fold).

These findings indicate that the outer membrane barrier plays a non-significant role in the resistance to the ureidothiophenes. However, the efflux pumps are most probably the main factor responsible for non-susceptibility in Gram-negative bacteria. Furthermore, they suggest that the uptake route of these compounds is primarily through the porins (Vaara 1992).

4.5 Frequency of Resistance Development

As mentioned in section 1.2, bacterial resistance is a natural incident. It is an underestimation of these smart microorganisms to think about an unbeatable antibacterial agent with no symptoms of resistance. The real thinking is to find an antibiotic that can decelerate the rate of resistance development. Targeting the RNAP “switch region” or the homologous DNA gyrase and topoisomerase IV simultaneously, as followed in this work, could be the appropriate approaches.

Determination of spontaneous resistance frequency of compound **30/I** as example for the new RNAP inhibitors revealed an outstanding (>1690-fold) lower rate than Rif and even the

“switch region” binder Myx. This can be clarified by the fact that the new compounds partially occupy the “switch region” unlike Myx that plugs the binding site entirely. Mutations in the Myx enecarbamate pocket, triggering Myx resistance (Srivastava et al. 2012), should not impair the binding nor the inhibitory activities of the compounds as proposed for their binding mode (Fruth et al. 2014). Molecular flexibility of this class contributes to the low resistance frequency too, as indicated by INPHARMA studies suggesting that the ureidothiophenes can adopt two different binding modes within the “switch region” (Fruth et al. 2014). Another reason could be an additional effect on a further target site.

Summing up, this finding indicates that indeed the propensity of resistance development is significantly decreased by the ureidothiophenes compared to clinically used antibiotics such as rifampin.

4.6 Scaffold Hopping and Identification of Cys507 Bioactive Conformation via IMHBs

The utilities of IMHB for improving the ligand-target binding, physicochemical properties, and scaffold hopping are well established in medicinal chemistry (Kuhn et al. 2010). Scaffold hopping refers to the identification of isofunctional chemical structures with different molecular frameworks (Schneider et al. 1999). Hopping to a new chemical scaffold could be beneficial for overcoming potency, pharmacokinetic and intellectual property issues encountered with the parent backbone (Bohm et al. 2004; Sun et al. 2012).

Conformational analysis of Cys507 revealed that the compound adopts two predominant conformations (*anti* or *syn*) stabilized by IMHBs with more tendency toward the *anti* form in solution (Figure 11). Identification of the bioactive conformation (the target-bound conformation) is a valuable tool in drug design for increasing the binding affinity to the target. This bound conformation can be determined by X-ray structure or NMR spectroscopy (Gonnella et al. 1995; Abraham and Burger 2003; Jimenez-Barbero et al. 2006). Nevertheless, these techniques have some limitations (Abraham and Burger 2003; Hawkins et al. 2008). Alternatively, the bioactive conformation can be designated by monitoring the effect of freezing the compound in its putative conformations on activity. The classical approaches followed for this purpose are restriction of the conformational freedom by cyclization or multiple bond formation and increasing the rotation barriers by steric hinderance.

Manuscript IV describes a pioneer method to recognize the bioactive conformation of Cys507 utilizing IMHB. Through replacement of the phenolic core with a pyridine system, two IMHB rigid Cys507 analogs (**9/IV** and **10/IV**) preorganized in *anti* and *syn* conformation, respectively, are designed (Figure 11). Molecular rigidity of these ligands is confirmed by MD

calculations, in solution (2D NOESY at variable temperature) as well as in solid state (X-ray crystal structure). Results revealed that compound **10/IV** (*syn*) is 4–7-fold more potent than **9/IV** (*anti*) and Cys507 indicating that the *syn* form is most likely the target bound conformation of Cys507.

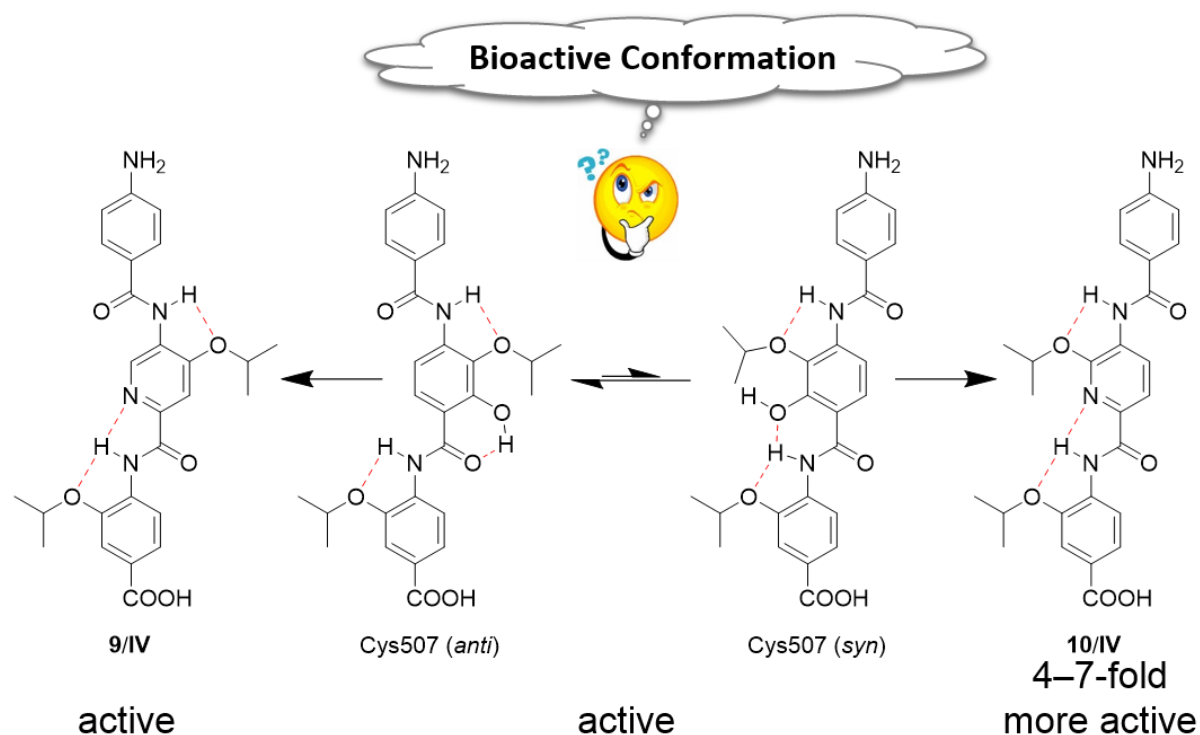


Figure 11. Proving the bioactive conformation of Cys507 via IMHB rigid analogs.

This novel approach for detecting the bioactive conformation via non-covalently bonded rigid structures presents several advantages: First, ligand efficiency is improved by omitting the hydroxyl group and conserving the *syn* conformation merely via IMHB in lieu of additional rings or bulky moieties. Second, solubility and ligand-lipophilicity efficiency are increased by substitution of a polar pyridine ring for benzene. Third, binding affinity of the rigid ligand is enhanced by reducing the unfavorable entropic contribution to the Gibbs free energy of binding $\Delta G = \Delta H - T\Delta S$ (Klebe 2015). Last but not most importantly, leaping of Cys507 scaffold to the novel pyridine-based chemotype with a conformationally-locked property could circumvent the potential resistance to the cystobactamids (Bastida et al. 2006; Fischbach and Walsh 2009).

4.7 Summary and Outlook

4.7.1 Evolution of the First Small Molecule Dual Bacterial RNAP and HIV-1 RT Inhibitors

Novel classes of bacterial RNAP “switch region” inhibitors are discovered through two analog design strategies. The new compounds exhibit potent antibacterial activities on Gram-positive pathogens and only the efflux mutant Gram-negative bacteria. They are characterized by a significant low rate of resistance development, no cross-resistance with other RNAP inhibitors and marginal cytotoxicity to human cells. These promising features were the cornerstone for further improvement by targeting the HIV-1 NNRTI binding site to develop the first small molecule bacterial RNAP and HIV-1 RT inhibitors. The highlight of them is the ability to prevent the replication of some HIV-1 NNRTI-resistant strains.

Altogether, these ureidothiophene-based RNAP/RT inhibitors possessing novel chemical scaffold launch a new hope toward the development of dual acting anti-infectives with low resistance propensity for the treatment of HIV and bacterial co-infection.

High lipophilicity of these classes that might be a drawback can be circumvented by decoration with hydrophilic substituents at the solvent exposed positions of the structure. Alternatively, scaffold hopping could be an appropriate solution, especially after establishing the binding mode of these compounds within the RNAP “switch region” (Fruth et al. 2014).

4.7.2 Improvement of Cystobactamids’ Synthesis, Topoisomerases IIA Inhibition and Antibacterial Activities

The natural antibiotic family of cystobactamids targeting the bacterial topoisomerases IIA looks very attractive as a competent solution for AMR problem. In this thesis, a multifaceted medicinal chemistry optimization of the cystobactamid class has been achieved.

Based on Cys507, numerous tripeptidic analogs are developed with enhanced inhibitory effects up to 7-fold on the bacterial targets (DNA gyrase and topoisomerase IV) and 8–16-fold more potent antibacterial activities against Gram-positive species. In addition, the new Cys507 analogs are characterized by an excellent metabolic stability.

Pruning the Cys507 structure is attained by a careful study of SARs and conformation–activity relationships. Moreover, the bioactive conformation is recognized by an innovative method using IMHBs instead of covalent bonds for conformation restriction. Furthermore, scaffold hopping of Cys507 to pyridine-based surrogates meets the need for increasing molecular diversity and enlargement of the chemical space of antibiotics.

Total synthesis feasibility is improved too through establishment of definitely brief and economic synthetic route for Cys507 and its building blocks common to all other cystobactamids. This new synthetic shortcut would accelerate the optimization process of the more potent members of cystobactamid family, e.g., Cys919-2 and other Cys507 scaffold-bearing hexapeptides.

5 References

- Abraham, Donald J.; Burger, Alfred (2003): Burger's medicinal chemistry and drug discovery. Vol. 1, Drug discovery. 6th ed. / edited by Donald J. Abraham. Hoboken, N. J., Chichester: Wiley.
- Alekshun, M. N.; Levy, S. B. (1997): Regulation of chromosomally mediated multiple antibiotic resistance: the mar regulon. *Antimicrob. Agents Chemother.* 41, 2067–2075.
- Alksne, Lefa E.; Projan, Steven J. (2000): Bacterial virulence as a target for antimicrobial chemotherapy. *Curr. Opin. Biotechnol.* 11, 625–636.
- Aminov, Rustam I. (2010): A brief history of the antibiotic era: lessons learned and challenges for the future. *Front. Microbiol.* 1, article 134.
- Andersson, Dan I. (2006): The biological cost of mutational antibiotic resistance: any practical conclusions? *Curr. Opin. Microbiol.* 9, 461–465.
- Arias, Cesar A.; Murray, Barbara E. (2009): Antibiotic-Resistant Bugs in the 21st Century — A Clinical Super-Challenge. *N. Engl. J. Med.* 360, 439–443.
- Bae, Brian; Nayak, Dhananjaya; Ray, Ananya; Mustaev, Arkady; Landick, Robert; Darst, Seth A. (2015): CBR antimicrobials inhibit RNA polymerase via at least two bridge-helix cap-mediated effects on nucleotide addition. *Proc. Natl. Acad. Sci. U. S. A.* 112, E4178-87.
- Bagel, Simone; Hüllen, Volker; Wiedemann, Bernd; Heisig, Peter (1999): Impact of gyrA and parC Mutations on Quinolone Resistance, Doubling Time, and Supercoiling Degree of *Escherichia coli*. *Antimicrob. Agents Chemother.* 43, 868–875.
- Bartlett, John G.; Gilbert, David N.; Spellberg, Brad (2013): Seven ways to preserve the miracle of antibiotics. *Clin. Infect. Dis.* 56, 1445–1450.
- Bastida, Agatha; Hidalgo, Ana; Chiara, Jose Luis; Torrado, Mario; Corzana, Francisco; Perez-Canadillas, Jose Manuel et al. (2006): Exploring the use of conformationally locked aminoglycosides as a new strategy to overcome bacterial resistance. *J. Am. Chem. Soc.* 128, 100–116.
- Baumann, Sascha; Herrmann, Jennifer; Raju, Ritesh; Steinmetz, Heinrich; Mohr, Kathrin I.; Huttel, Stephan et al. (2014): Cystobactamids: myxobacterial topoisomerase inhibitors exhibiting potent antibacterial activity. *Angew. Chem. Int. Ed.* 53, 14605–14609.
- Bax, Benjamin D.; Chan, Pan F.; Eggleston, Drake S.; Fosberry, Andrew; Gentry, Daniel R.; Gorrec, Fabrice et al. (2010): Type IIA topoisomerase inhibition by a new class of antibacterial agents. *Nature* 466, 935–940.

- Bender, Andreas; Glen, Robert C. (2004): Molecular similarity: a key technique in molecular informatics. *Org. Biomol. Chem.* 2, 3204–3218.
- Blair, Jessica M. A.; Webber, Mark A.; Baylay, Alison J.; Ogbolu, David O.; Piddock, Laura J. V. (2015): Molecular mechanisms of antibiotic resistance. *Nat. Rev. Microbiol.* 13, 42–51.
- Bohm, Hans-Joachim; Flohr, Alexander; Stahl, Martin (2004): Scaffold hopping. *Drug Discov. Today Technol.* 1, 217–224.
- Bradbury, Barton J.; Pucci, Michael J. (2008): Recent advances in bacterial topoisomerase inhibitors. *Curr. Opin. Pharmacol.* 8, 574–581.
- Brotz-Oesterhelt, Heike; Brunner, Nina A. (2008): How many modes of action should an antibiotic have? *Curr. Opin. Pharmacol.* 8, 564–573.
- Buurman, Ed T.; Foulk, Melinda A.; Gao, Ning; Laganas, Valerie A.; McKinney, David C.; Moustakas, Demetri T. et al. (2012): Novel rapidly diversifiable antimicrobial RNA polymerase switch region inhibitors with confirmed mode of action in *Haemophilus influenzae*. *J. Bacteriol.* 194, 5504–5512.
- Cavasotto, Claudio N.; Phatak, Sharangdhar S. (2009): Homology modeling in drug discovery: current trends and applications. *Drug Discov. Today* 14, 676–683.
- Chaires, Jonathan B. (2008): Calorimetry and thermodynamics in drug design. *Annu. Rev. Biophys.* 37, 135–151.
- Champoux, J. J. (2001): DNA topoisomerases: structure, function, and mechanism. *Annu. Rev. Biochem.* 70, 369–413.
- Chan, Pan F.; Srikannathasan, Velupillai; Huang, Jianzhong; Cui, Haifeng; Fosberry, Andrew P.; Gu, Minghua et al. (2015): Structural basis of DNA gyrase inhibition by antibacterial QPT-1, anticancer drug etoposide and moxifloxacin. *Nat. Commun.* 6, article 10048.
- Chopra, I. (1998): Over-expression of target genes as a mechanism of antibiotic resistance in bacteria. *J. Antimicrob. Chemother.* 41, 584–588.
- Collin, Frederic; Karkare, Shantanu; Maxwell, Anthony (2011): Exploiting bacterial DNA gyrase as a drug target: current state and perspectives. *Appl. Microbiol. Biotechnol.* 92, 479–497.
- Comas, Inaki; Borrell, Sonia; Roetzer, Andreas; Rose, Graham; Malla, Bijaya; Kato-Maeda, Midori et al. (2012): Whole-genome sequencing of rifampicin-resistant *Mycobacterium tuberculosis* strains identifies compensatory mutations in RNA polymerase genes. *Nat. Genet.* 44, 106–110.

- Cook, Megan; Molto, El; Anderson, C. (1989): Fluorochrome labelling in roman period skeletons from dakhleh oasis, Egypt. *Am. J. Phys. Anthropol.* 80, 137–143.
- Cooper, Matthew A. (2002): Optical biosensors in drug discovery. *Nat. Rev. Drug Discov.* 1, 515–528.
- Defoirdt, Tom; Boon, Nico; Bossier, Peter (2010): Can bacteria evolve resistance to quorum sensing disruption? *PLoS Pathog.* 6, e1000989.
- Dellit, Timothy H.; Owens, Robert C.; McGowan, John E., JR; Gerding, Dale N.; Weinstein, Robert A.; Burke, John P. et al. (2007): Infectious Diseases Society of America and the Society for Healthcare Epidemiology of America guidelines for developing an institutional program to enhance antimicrobial stewardship. *Clin. Infect. Dis.* 44, 159–177.
- Di Andersson; Hughes, D. (2010): Antibiotic resistance and its cost: is it possible to reverse resistance? *Nat. Rev. Microbiol.* 8, 260–271.
- Donia, M. S.; Fischbach, M. A. (2015): Small molecules from the human microbiota. *Science* 349, 1254766.
- Doundoulakis, Thomas; Xiang, Alan X.; Lira, Ricardo; Agrios, Konstantinos A.; Webber, Stephen E.; Sisson, Wes et al. (2004): Myxopyronin B analogs as inhibitors of RNA polymerase, synthesis and biological evaluation. *Bioorg. Med. Chem. Lett.* 14, 5667–5672.
- Drawz, Sarah M.; Bonomo, Robert A. (2010): Three decades of beta-lactamase inhibitors. *Clin. Microbiol. Rev.* 23, 160–201.
- Drlica, Karl (2003): The mutant selection window and antimicrobial resistance. *J. Antimicrob. Chemother.* 52, 11–17.
- Dryden, Matthew; Johnson, Alan P.; Ashiru-Oredope, Diane; Sharland, Mike (2011): Using antibiotics responsibly: right drug, right time, right dose, right duration. *J. Antimicrob. Chemother.* 66, 2441–2443.
- Feklistov, Andrey; Mekler, Vladimir; Jiang, Qiaorong; Westblade, Lars F.; Irschik, Herbert; Jansen, Rolf et al. (2008): Rifamycins do not function by allosteric modulation of binding of Mg²⁺ to the RNA polymerase active center. *Proc. Natl. Acad. Sci. U. S. A.* 105, 14820–14825.
- Fischbach, M. A.; Walsh, C. T. (2009): Antibiotics for Emerging Pathogens. *Science* 325, 1089–1093.

- Fischbach, Michael A.; Walsh, Christopher T. (2006): Assembly-line enzymology for polyketide and nonribosomal Peptide antibiotics: logic, machinery, and mechanisms. *Chem. Rev.* 106, 3468–3496.
- Fruth, Martina; Plaza, Alberto; Hinsberger, Stefan; Sahner, Jan Henning; Haupenthal, Jorg; Bischoff, Markus et al. (2014): Binding mode characterization of novel RNA polymerase inhibitors using a combined biochemical and NMR approach. *ACS Chem. Biol.* 9, 2656–2663.
- Gonnella, N. C.; Bohacek, R.; Zhang, X.; Kolossvary, I.; Paris, C. G.; Melton, R. et al. (1995): Bioactive conformation of stromelysin inhibitors determined by transferred nuclear Overhauser effects. *Proc. Natl. Acad. Sci.* 92, 462–466.
- Haebich, Dieter; Nussbaum, Franz von (2009): Lost in transcription–inhibition of RNA polymerase. *Angew. Chem. Int. Ed.* 48, 3397–3400.
- Hawkins, Paul C. D.; Warren, Gregory L.; Skillman, A. Geoffrey; Nicholls, Anthony (2008): How to do an evaluation: pitfalls and traps. *J. Comput. Aided Mol. Des.* 22, 179–190.
- Ho, Mary X.; Hudson, Brian P.; Das, Kalyan; Arnold, Eddy; Ebright, Richard H. (2009): Structures of RNA polymerase-antibiotic complexes. *Curr. Opin. Struct. Biol.* 19, 715–723.
- Infectious Diseases Society of America (2010): The 10 x '20 Initiative: pursuing a global commitment to develop 10 new antibacterial drugs by 2020. *Clin. Infect. Dis.* 50, 1081–1083.
- Jimenez-Barbero, Jesus; Canales, Angeles; Northcote, Peter T.; Buey, Ruben M.; Andreu, Jose Manuel; Diaz, J. Fernando (2006): NMR determination of the bioactive conformation of peloruside A bound to microtubules. *J. Am. Chem. Soc.* 128, 8757–8765.
- Kirschning, Andreas; Taft, Florian; Knobloch, Tobias (2007): Total synthesis approaches to natural product derivatives based on the combination of chemical synthesis and metabolic engineering. *Org. Biomol. Chem.* 5, 3245–3259.
- Klebe, Gerhard (2015): Applying thermodynamic profiling in lead finding and optimization. *Nat. Rev. Drug Discov.* 14, 95–110.
- Kohanski, Michael A.; Dwyer, Daniel J.; Collins, James J. (2010): How antibiotics kill bacteria: from targets to networks. *Nat. Rev. Microbiol.* 8, 423–435.
- Kretz, Julian; Kerwat, Dennis; Schubert, Vivien; Gratz, Stefan; Pesic, Alexander; Semsary, Siamak et al. (2015): Total synthesis of albicidin: a lead structure from *Xanthomonas albilineans* for potent antibacterial gyrase inhibitors. *Angew. Chem. Int. Ed.* 54, 1969–1973.

- Kuhn, Bernd; Mohr, Peter; Stahl, Martin (2010): Intramolecular hydrogen bonding in medicinal chemistry. *J. Med. Chem.* 53, 2601–2611.
- Laponogov, Ivan; Sohi, Maninder K.; Veselkov, Dennis A.; Pan, Xiao-Su; Sawhney, Ritica; Thompson, Andrew W. et al. (2009): Structural insight into the quinolone-DNA cleavage complex of type IIA topoisomerases. *Nat. Struct. Mol. Biol.* 16, 667–669.
- Lenski, Richard E.; Nguyen, Toai T. (1988): Stability of recombinant DNA and its effects on fitness. *Trends Ecol. Evol.* 3, S18-S20.
- Lewis, Kim (2013): Platforms for antibiotic discovery. *Nat. Rev. Drug Discov.* 12, 371–387.
- Li, Jesse W-H; Vederas, John C. (2009): Drug discovery and natural products: end of an era or an endless frontier? *Science* 325, 161–165.
- Ling, Losee L.; Schneider, Tanja; Peoples, Aaron J.; Spoering, Amy L.; Engels, Ina; Conlon, Brian P. et al. (2015): A new antibiotic kills pathogens without detectable resistance. *Nature* 517, 455–459.
- Lira, Ricardo; Xiang, Alan X.; Doundoulakis, Thomas; Biller, William T.; Agrios, Konstantinos A.; Simonsen, Klaus B. et al. (2007): Syntheses of novel myxopyronin B analogs as potential inhibitors of bacterial RNA polymerase. *Bioorg. Med. Chem. Lett.* 17, 6797–6800.
- Lomovskaya, O.; Warren, M. S.; Lee, A.; Galazzo, J.; Fronko, R.; Lee, M. et al. (2001): Identification and characterization of inhibitors of multidrug resistance efflux pumps in *Pseudomonas aeruginosa*: novel agents for combination therapy. *Antimicrob. Agents Chemother.* 45, 105–116.
- Lomovskaya, Olga; Bostian, Keith A. (2006): Practical applications and feasibility of efflux pump inhibitors in the clinic--a vision for applied use. *Biochem. Pharmacol.* 71, 910–918.
- Ma, Cong; Yang, Xiao; Lewis, Peter J. (2016): Bacterial Transcription as a Target for Antibacterial Drug Development. *Microbiol. Mol. Biol. Rev.* 80, 139–160.
- Maeda, Toshinari; Garcia-Contreras, Rodolfo; Pu, Mingming; Sheng, Lili; Garcia, Luis Rene; Tomas, Maria; Wood, Thomas K. (2012): Quorum quenching quandary: resistance to antivirulence compounds. *ISME J.* 6, 493–501.
- Maggiore, Gerald; Vogt, Martin; Stumpfe, Dagmar; Bajorath, Jurgen (2014): Molecular similarity in medicinal chemistry. *J. Med. Chem.* 57, 3186–3204.
- McPhillie, Martin J.; Trowbridge, Rachel; Mariner, Katherine R.; O'Neill, Alex J.; Johnson, A. Peter; Chopra, Ian; Fishwick, Colin W. G. (2011): Structure-based ligand design of novel bacterial RNA polymerase inhibitors. *ACS Med. Chem. Lett.* 2, 729–734.

- Melnyk, Anita H.; Wong, Alex; Kassen, Rees (2015): The fitness costs of antibiotic resistance mutations. *Evol. Appl.* 8, 273–283.
- Milligan, Graeme (2004): Applications of bioluminescence- and fluorescence resonance energy transfer to drug discovery at G protein-coupled receptors. *Eur. J. Pharm. Sci.* 21, 397–405.
- Molodtsov, Vadim; Fleming, Paul R.; Eyermann, Charles J.; Ferguson, Andrew D.; Foulk, Melinda A.; McKinney, David C. et al. (2015): X-ray crystal structures of *Escherichia coli* RNA polymerase with switch region binding inhibitors enable rational design of squaramides with an improved fraction unbound to human plasma protein. *J. Med. Chem.* 58, 3156–3171.
- Mukhopadhyay, Jayanta; Das, Kalyan; Ismail, Sajida; Koppstein, David; Jang, Minyoung; Hudson, Brian et al. (2008): The RNA polymerase "switch region" is a target for inhibitors. *Cell* 135, 295–307.
- Murakami, Katsuhiko S. (2015): Structural biology of bacterial RNA polymerase. *Biomolecules* 5, 848–864.
- Murakami, Katsuhiko S.; Darst, Seth A. (2003): Bacterial RNA polymerases. The whole story. *Curr. Opin. Struct. Biol.* 13, 31–39.
- Nakashima, Ryosuke; Sakurai, Keisuke; Yamasaki, Seiji; Nishino, Kunihiko; Yamaguchi, Akihito (2011): Structures of the multidrug exporter AcrB reveal a proximal multisite drug-binding pocket. *Nature* 480, 565–569.
- Nikaido, Eiji; Yamaguchi, Akihito; Nishino, Kunihiko (2008): AcrAB multidrug efflux pump regulation in *Salmonella enterica* serovar Typhimurium by RamA in response to environmental signals. *J. Biol. Chem.* 283, 24245–24253.
- Nikaido, H. (2003): Molecular Basis of Bacterial Outer Membrane Permeability Revisited. *Microbiol. Mol. Biol. Rev.* 67, 593–656.
- Nikolova, Nina; Jaworska, Joanna (2003): Approaches to Measure Chemical Similarity - a Review. *QSAR Comb. Sci.* 22, 1006–1026.
- O'Connell, Kieron M. G.; Hodgkinson, James T.; Sore, Hannah F.; Welch, Martin; Salmond, George P. C.; Spring, David R. (2013): Combating multidrug-resistant bacteria: current strategies for the discovery of novel antibacterials. *Angew. Chem. Int. Ed.* 52, 10706–10733.
- Pellecchia, Maurizio; Bertini, Ivano; Cowburn, David; Dalvit, Claudio; Giralt, Ernest; Jahnke, Wolfgang et al. (2008): Perspectives on NMR in drug discovery: a technique comes of age. *Nat. Rev. Drug Discov.* 7, 738–745.

- Pomposiello, P. J.; Bennik, M. H.; Demple, B. (2001): Genome-wide transcriptional profiling of the *Escherichia coli* responses to superoxide stress and sodium salicylate. *J. Bacteriol.* *183*, 3890–3902.
- Putman, M.; van Veen, H. W.; Konings, W. N. (2000): Molecular Properties of Bacterial Multidrug Transporters. *Microbiol. Mol. Biol. Rev.* *64*, 672–693.
- Renaud, Jean-Paul; Delsuc, Marc-Andre (2009): Biophysical techniques for ligand screening and drug design. *Curr. Opin. Pharmacol.* *9*, 622–628.
- Reynolds, Mary G. (2000): Compensatory Evolution in Rifampin-Resistant *Escherichia coli*. *Genetics* *156*, 1471–1481.
- Rozen, Daniel E.; McGee, Lesley; Levin, Bruce R.; Klugman, Keith P. (2007): Fitness costs of fluoroquinolone resistance in *Streptococcus pneumoniae*. *Antimicrob. Agents Chemother.* *51*, 412–416.
- Sahner, J. Henning; Groh, Matthias; Negri, Matthias; Hauptenthal, Jorg; Hartmann, Rolf W. (2013): Novel small molecule inhibitors targeting the "switch region" of bacterial RNAP: structure-based optimization of a virtual screening hit. *Eur. J. Med. Chem.* *65*, 223–231.
- Sanchez-Pedregal, Victor M.; Reese, Marcel; Meiler, Jens; Blommers, Marcel J. J.; Griesinger, Christian; Carlomagno, Teresa (2005): The INPHARMA method: protein-mediated interligand NOEs for pharmacophore mapping. *Angew. Chem. Int. Ed.* *44*, 4172–4175.
- Schneider, Gisbert; Neidhart, Werner; Giller, Thomas; Schmid, Gerard (1999): "Scaffold-Hopping" by Topological Pharmacophore Search. A Contribution to Virtual Screening. *Angew. Chem. Int. Ed.* *38*, 2894–2896.
- Schwede, T. (2003): SWISS-MODEL. An automated protein homology-modeling server. *Nucleic Acids Res.* *31*, 3381–3385.
- Sender, Ron; Fuchs, Shai; Milo, Ron (2016): Revised estimates for the number of human and bacteria cells in the body. doi: <http://dx.doi.org/10.1101/036103>.
- Silver, Lynn L. (2007): Multi-targeting by monotherapeutic antibacterials. *Nat. Rev. Drug Discov.* *6*, 41–55.
- Simon, Liliana; Gauvin, France; Amre, Devendra K.; Saint-Louis, Patrick; Lacroix, Jacques (2004): Serum procalcitonin and C-reactive protein levels as markers of bacterial infection: a systematic review and meta-analysis. *Clin. Infect. Dis.* *39*, 206–217.
- Skedelj, Veronika; Tomasic, Tihomir; Masic, Lucija Peterlin; Zega, Anamarija (2011): ATP-binding site of bacterial enzymes as a target for antibacterial drug design. *J. Med. Chem.* *54*, 915–929.

- Smith, J. T.; Amyes, S. G. B. (1984): Bacterial resistance to antifolate chemotherapeutic agents mediated by plasmids. *Br. Med. Bull.* 40, 42–46.
- Spratt, B. (1994): Resistance to antibiotics mediated by target alterations. *Science* 264, 388–393.
- Spratt, Brian G. (1996): Antibiotic resistance. Counting the cost. *Curr. Biol.* 6, 1219–1221.
- Srivastava, Aashish; Degen, David; Ebright, Yon W.; Ebright, Richard H. (2012): Frequency, spectrum, and nonzero fitness costs of resistance to myxopyronin in *Staphylococcus aureus*. *Antimicrob. Agents Chemother.* 56, 6250–6255.
- Srivastava, Aashish; Talaue, Meliza; Liu, Shuang; Degen, David; Ebright, Richard Y.; Sineva, Elena et al. (2011): New target for inhibition of bacterial RNA polymerase: 'switch region'. *Curr. Opin. Microbiol.* 14, 532–543.
- Sun, Hongmao; Tawa, Gregory; Wallqvist, Anders (2012): Classification of scaffold-hopping approaches. *Drug Discov. Today* 17, 310–324.
- Tamma, Pranita D.; Cosgrove, Sara E.; Maragakis, Lisa L. (2012): Combination therapy for treatment of infections with gram-negative bacteria. *Clin. Microbiol. Rev.* 25, 450–470.
- Tipper, D. J.; Strominger, J. L. (1965): Mechanism of action of penicillins: a proposal based on their structural similarity to acyl-D-alanyl-D-alanine. *Proc. Natl. Acad. Sci. U. S. A.* 54, 1133–1141.
- Truong, Kevin; Ikura, Mitsuhiro (2001): The use of FRET imaging microscopy to detect protein–protein interactions and protein conformational changes in vivo. *Curr. Opin. Struct. Biol.* 11, 573–578.
- Vaara, M. (1992): Agents that increase the permeability of the outer membrane. *Microbiol. Rev.* 56, 395–411.
- Veselkov, Dennis A.; Laponogov, Ivan; Pan, Xiao Su; Selvarajah, Jogitha; Skamrova, Galyna B.; Branstrom, Arthur et al. (2016): Structure of a quinolone-stabilized cleavage complex of topoisomerase IV from *Klebsiella pneumoniae* and comparison with a related *Streptococcus pneumoniae* complex. *Acta Crystallogr. D Struct. Biol.* 72, 488–496.
- Vetting, M. W.; Hegde, S. S.; Wang, M.; Jacoby, G. A.; Hooper, D. C.; Blanchard, J. S. (2011): Structure of QnrB1, a plasmid-mediated fluoroquinolone resistance factor. *J. Biol. Chem.* 286, 25265–25273.
- Vos, Seychelle M.; Tretter, Elsa M.; Schmidt, Bryan H.; Berger, James M. (2011): All tangled up: how cells direct, manage and exploit topoisomerase function. *Nat. Rev. Mol. Cell Biol.* 12, 827–841.

- Walsh, C. (2000): Molecular mechanisms that confer antibacterial drug resistance. *Nature* 406, 775–781.
- Walsh, Christopher T.; Wencewicz, Timothy A. (2014): Prospects for new antibiotics: a molecule-centered perspective. *J. Antibiot. (Tokyo)* 67, 7–22.
- Weisblum, B. (1995): Erythromycin resistance by ribosome modification. *Antimicrob. Agents Chemother.* 39, 577–585.
- WHO (2014): Europe's HIV response falls short in curbing the epidemic: 80% more new HIV cases compared to 2004. Available online at <http://www.euro.who.int/en/media-centre/sections/press-releases/2014/europes-hiv-response-falls-short-in-curbing-the-epidemic-80-more-new-hiv-cases-compared-to-2004>.
- Wienken, Christoph J.; Baaske, Philipp; Rothbauer, Ulrich; Braun, Dieter; Duhr, Stefan (2010): Protein-binding assays in biological liquids using microscale thermophoresis. *Nat. Commun.* 1, article 100.
- Willett, Peter (2006): Similarity-based virtual screening using 2D fingerprints. *Drug Discov. Today* 11, 1046–1053.
- Woese, C. R.; Kandler, O.; Wheelis, M. L. (1990): Towards a natural system of organisms. Proposal for the domains Archaea, Bacteria, and Eucarya. *Proc. Natl. Acad. Sci. U. S. A.* 87, 4576–4579.
- Wohlkonig, Alexandre; Chan, Pan F.; Fosberry, Andrew P.; Homes, Paul; Huang, Jianzhong; Kranz, Michael et al. (2010): Structural basis of quinolone inhibition of type IIA topoisomerases and target-mediated resistance. *Nat. Struct. Mol. Biol.* 17, 1152–1153.
- Yakushiji, Fumika; Miyamoto, Yuko; Kunoh, Yuki; Okamoto, Reiko; Nakaminami, Hidemasa; Yamazaki, Yuri et al. (2013): Novel hybrid-type antimicrobial agents targeting the switch region of bacterial RNA polymerase. *ACS Med. Chem. Lett.* 4, 220–224.
- Yoneyama, Hiroshi; Katsumata, Ryoichi (2006): Antibiotic resistance in bacteria and its future for novel antibiotic development. *Biosci. Biotechnol. Biochem.* 70, 1060–1075.
- Zhang, Gongyi; Campbell, Elizabeth A.; Minakhin, Leonid; Richter, Catherine; Severinov, Konstantin; Darst, Seth A. (1999): Crystal Structure of *Thermus aquaticus* Core RNA Polymerase at 3.3 Å Resolution. *Cell* 98, 811–824.

6 Supporting Information

This chapter contains the supporting information of the studies presented in chapter 3. It includes further experimental procedures and results, as well as additional figures.

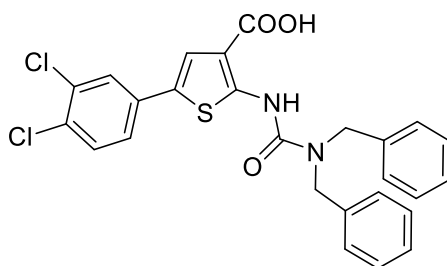
6.1 Supporting Information for Publication II

Full supporting information is available on the ACS Publications website at: <http://pubs.acs.org/doi/suppl/10.1021/acs.jmedchem.6b00730>.

6.1.1 Chemistry

Synthesis and experimental data of compounds **1–9** and **22–26** were described in a previous work¹ and references therein. Compounds **21** and **27** are commercially available.

2-(3,3-Dibenzylureido)-5-(3,4-dichlorophenyl)thiophene-3-carboxylic acid (**10**)



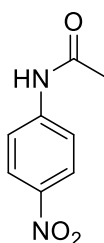
Synthesis of compound **10** was performed as described previously for **9**.¹

Yield 90%; beige solid; ¹H NMR (300 MHz, DMSO-d₆) δ 12.91 (br s, 1H), 10.99 (br s, 1H), 7.87 (d, *J* = 1.0 Hz, 1H), 7.58 (m, 3H), 7.34 (m, 10H), 4.67 (s, 4H); ¹³C NMR (75 MHz, DMSO-d₆) δ 166.70, 153.17, 151.30, 136.89 (2C), 134.26, 131.85, 131.05, 129.11, 128.60 (4C), 127.85, 127.39 (2C), 127.14 (4C), 126.14, 124.72, 121.86, 112.22, 50.34 (2C); *m/z* (ESI⁺) 510 [M]⁺; *t_R* = 16.01 min.

General procedure for synthesis of *N*-(substituted)-4-nitroanilines **29**, **30**, **33–35** and **39**

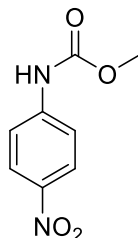
To a stirred solution of 4-nitroaniline **27** (1.38 g, 10 mmol), and pyridine (0.9 mL, 11 mmol) in DCM (50 mL), the appropriate acyl/sulfonyl/sulfamoyl chloride (11 mmol) was added drop wise. The reaction mixture was stirred at room temperature overnight then solvent was removed by vacuum distillation. The obtained material was triturated with cold 1 N HCl (50 mL) and collected by filtration, washed with cold 1 N HCl, water then *n*-hexane.

N-(4-Nitrophenyl)acetamide (**29**)



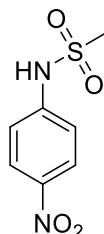
Yield 94%; greenish yellow solid; $^1\text{H NMR}$ (300 MHz, DMSO-d_6) δ 9.73 (br s, 1H), 7.94 (d, $J = 9.1$ Hz, 2H), 7.60 (d, $J = 9.1$ Hz, 2H), 1.99 (s, 3H); $^{13}\text{C NMR}$ (75 MHz, DMSO-d_6) δ 169.03, 144.65, 142.13, 124.14 (2C), 118.33 (2C), 23.87; m/z (ESI+) 181 $[\text{M} + \text{H}]^+$; $t_{\text{R}} = 9.52$ min.

Methyl (4-nitrophenyl)carbamate (30)



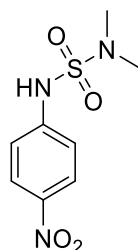
Yield 93%; greenish yellow solid; $^1\text{H NMR}$ (300 MHz, DMSO-d_6) δ 10.37 (br s, 1H), 8.19 (d, $J = 9.2$ Hz, 2H), 7.68 (d, $J = 9.2$ Hz, 2H), 3.72 (s, 3H); $^{13}\text{C NMR}$ (75 MHz, DMSO-d_6) δ 153.82, 145.75, 141.74, 125.14 (2C), 117.71 (2C), 52.28; m/z (ESI+) 197 $[\text{M} + \text{H}]^+$; $t_{\text{R}} = 8.95$ min.

***N*-(4-Nitrophenyl)methanesulfonamide (33)**



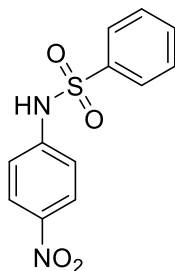
Yield 75%; greenish yellow solid; $^1\text{H NMR}$ (300 MHz, DMSO-d_6) δ 10.73 (br s, 1H), 8.22 (d, $J = 9.2$ Hz, 2H), 7.37 (d, $J = 9.2$ Hz, 2H), 3.18 (s, 3H); $^{13}\text{C NMR}$ (75 MHz, DMSO-d_6) δ 145.38, 143.28, 126.28 (2C), 118.64 (2C), 40.78; m/z (ESI+) 216 $[\text{M}]^+$; $t_{\text{R}} = 7.77$ min.

***N,N*-Dimethyl-*N'*-(4-nitrophenyl)sulfamide (34)**



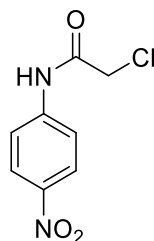
Yield 70%; yellow solid.

***N*-(4-Nitrophenyl)benzenesulfonamide (35)**



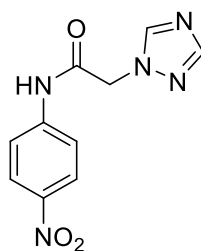
Yield 92%; yellow crystal; ^1H NMR (300 MHz, DMSO- d_6) δ 10.44 (br s, 1H), 8.04 (d, $J = 9.1$ Hz, 2H), 7.87 (dd, $J = 8.3, 1.2$ Hz, 2H), 7.50 (m, 3H), 7.29 (d, $J = 9.1$ Hz, 2H); ^{13}C NMR (75 MHz, DMSO- d_6) δ 143.80, 142.85, 139.02, 132.82, 128.81 (2C), 126.70 (2C), 124.76 (2C), 117.88 (2C); m/z (ESI+) 278 $[\text{M}]^+$; $t_{\text{R}} = 12.32$ min.

2-Chloro-*N*-(4-nitrophenyl)acetamide (**39**)



Yield 98%; greenish yellow solid; ^1H NMR (300 MHz, DMSO- d_6) δ 10.87 (br s, 1H), 8.23 (d, $J = 9.2$ Hz, 2H), 7.83 (d, $J = 9.2$ Hz, 2H), 4.33 (s, 2H); ^{13}C NMR (75 MHz, DMSO- d_6) δ 165.57, 144.56, 142.61, 125.02 (2C), 119.08 (2C), 43.56; m/z (ESI+) 214 $[\text{M}]^+$; $t_{\text{R}} = 10.63$ min.

N-(4-Nitrophenyl)-2-(1*H*-1,2,4-triazol-1-yl)acetamide (**40**)



To a stirred mixture of 1,2,4-triazole (1.04 g, 15 mmol) and K_2CO_3 (2.42 g, 17.5 mmol) in DMF (40 mL), 2-chloro-*N*-(4-nitrophenyl)acetamide **39** (3.22 g, 15 mmol) was added. The reaction was stirred at 70 °C for 1 h and at room temperature for further 1 h, then it was poured onto ice cooled water (50 mL). The precipitate was collected by filtration, washed with cold water then *n*-hexane.

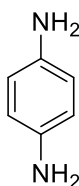
Yield 96%; yellow solid; ^1H NMR (300 MHz, DMSO- d_6) δ 11.00 (br s, 1H), 8.57 (s, 1H), 8.24 (d, $J = 9.2$ Hz, 2H), 8.01 (s, 1H), 7.82 (d, $J = 9.2$ Hz, 2H), 5.22 (s, 2H); ^{13}C NMR (75 MHz, DMSO- d_6) δ 165.64, 151.43, 145.65, 144.49, 142.60, 125.08 (2C), 119.03 (2C), 51.86; m/z (ESI+) 248 $[\text{M} + \text{H}]^+$; $t_{\text{R}} = 8.84$ min.

General procedure for synthesis of *N*-((un)substituted)-1,4-phenylenediamines **28**, **31**, **32**, **36–38** and **41**

To a stirred solution of 4-nitroaniline **27** or derivatives (5 mmol) in EtOH (30 mL), iron powder (1.40 g, 25 mmol) was added at 55 °C followed by NH_4Cl (133 mg, 2.5 mmol) solution in water (15 mL). The reaction was heated at 90 °C for 1 h, then iron was filtered while hot and the filtrate was concentrated *in vacuo*. The residue was diluted with water (15 mL) and basified by NaHCO_3 (saturated aqueous solution) to pH 7–8. The mixture was extracted with EtOAc (3 \times 20 mL). The combined

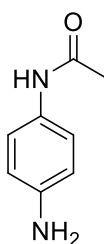
organic extract was washed with brine, dried over anhydrous MgSO_4 , and the solvent was removed by vacuum distillation. The obtained material was triturated with *n*-hexane, and collected by filtration.

1,4-Phenylenediamine (28)



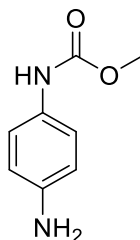
Yield 65%; pink crystals; ^1H NMR (300 MHz, CDCl_3) δ 6.58 (s, 4H), 3.33 (br s, 4H); ^{13}C NMR (75 MHz, CDCl_3) δ 138.54 (2C), 116.69 (4C); m/z (ESI+) 150 $[\text{M} + \text{H} + \text{MeCN}]^+$; $t_{\text{R}} = 0.88$ min.

N-(4-Aminophenyl)acetamide (31)



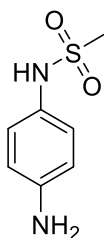
Yield 86%; buff solid; ^1H NMR (300 MHz, DMSO-d_6) δ 8.98 (br s, 1H), 7.20 (d, $J = 8.6$ Hz, 2H), 6.52 (d, $J = 8.6$ Hz, 2H), 3.89 (br s, 2H), 1.99 (s, 3H); ^{13}C NMR (75 MHz, DMSO-d_6) δ 167.83, 142.94, 129.19, 121.18 (2C), 114.36 (2C), 23.41; m/z (ESI+) 151 $[\text{M} + \text{H}]^+$; $t_{\text{R}} = 1.08$ min.

Methyl (4-aminophenyl)carbamate (32)

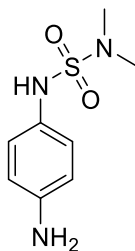


Yield 82%; pink solid; ^1H NMR (500 MHz, CDCl_3) δ 7.14 (br s, 2H), 6.64 (d, $J = 8.8$ Hz, 2H), 6.49 (br s, 1H), 3.75 (s, 3H), 3.58 (br s, 2H); ^{13}C NMR (126 MHz, CDCl_3) δ 154.53, 142.74, 129.15, 121.03 (2C), 115.54 (2C), 52.16; m/z (ESI+) 167 $[\text{M} + \text{H}]^+$; $t_{\text{R}} = 4.58$ min.

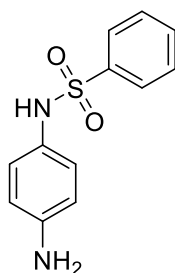
N-(4-Aminophenyl)methanesulfonamide (36)



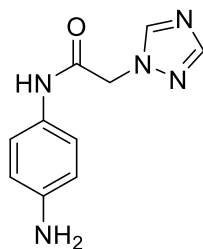
Yield 85%; reddish solid; ^1H NMR (500 MHz, DMSO-d_6) δ 8.90 (br s, 1H), 6.89 (d, $J = 8.8$ Hz, 2H), 6.52 (d, $J = 8.8$ Hz, 2H), 5.01 (br s, 2H), 2.80 (s, 3H); ^{13}C NMR (126 MHz, DMSO-d_6) δ 146.68, 125.99, 124.83 (2C), 114.11 (2C), 38.16; m/z (ESI+) 187 $[\text{M} + \text{H}]^+$; $t_{\text{R}} = 2.50$ min.

***N'*-(4-Aminophenyl)-*N,N*-dimethylsulfamide (37)**

Yield 68%; beige crystals; ^1H NMR (300 MHz, DMSO- d_6) δ 8.90 (br s, 1H), 6.91 (d, $J = 6.5$ Hz, 2H), 6.48 (d, $J = 6.5$ Hz, 2H), 4.41 (br s, 2H), 2.64 (s, 6H); ^{13}C NMR (75 MHz, DMSO- d_6) δ 144.92, 126.99, 123.59 (2C), 114.21 (2C), 37.72 (2C); m/z (ESI+) 216 $[\text{M} + \text{H}]^+$; $t_{\text{R}} = 2.11$ min.

***N*-(4-Aminophenyl)benzenesulfonamide (38)**

Yield 90%; pink solid; ^1H NMR (300 MHz, DMSO- d_6) δ 9.11 (br s, 1H), 7.62 (m, 2H), 7.43 (m, 1H), 7.34 (m, 2H), 6.72 (d, $J = 8.6$ Hz, 2H), 6.40 (d, $J = 8.6$ Hz, 2H), 4.02 (br s, 2H); ^{13}C NMR (75 MHz, DMSO- d_6) δ 145.00, 139.47, 131.77, 128.20 (2C), 126.59 (2C), 126.33, 124.60 (2C), 114.47 (2C); m/z (ESI+) 249 $[\text{M} + \text{H}]^+$; $t_{\text{R}} = 8.27$ min.

***N*-(4-Aminophenyl)-2-(1*H*-1,2,4-triazol-1-yl)acetamide (41)**

Yield 75%; pale grey solid; ^1H NMR (300 MHz, DMSO- d_6) δ 9.82 (br s, 1H), 8.36 (s, 1H), 7.84 (s, 1H), 7.21 (s, 2H), 6.52 (s, 2H), 4.98 (s, 2H), 4.39 (br s, 2H); ^{13}C NMR (75 MHz, DMSO- d_6) δ 162.93, 150.92, 144.72, 144.27, 127.77, 120.90 (2C), 114.01 (2C), 51.71; m/z (ESI+) 218 $[\text{M} + \text{H}]^+$; $t_{\text{R}} = 0.91$ min.

6.1.2 Substituent Constants and Molecular Descriptors

Table S1. Substituent Constants^a and Molecular Descriptors of Compounds **11–20**^a

Compound	R	RT IC ₅₀ (μM)	pIC ₅₀ (-log IC ₅₀)	π	σ	KierFlex	PC ⁺	V _{sa_don}	SMR
11	H	1.2	5.92	0.00	0.00	5.0488	4.7140	11.3652	10.5818
12	F	0.7	6.15	0.14	0.06	5.2057	4.7540	11.3652	10.5776
13	OMe	0.8	6.10	-0.02	-0.27	5.7827	4.9260	11.3652	11.2370
14	NH ₂	20.0	4.70	-1.23	-0.66	5.2823	5.4640	29.1076	11.0230
15		0.6	6.22	-0.97	0.00	6.1130	5.8310	17.0477	12.0121
16		0.8	6.10	-	-	6.6457	5.8310	17.0477	13.4674
17		0.3	6.52	-0.52	-0.17	6.6264	6.1110	17.0477	12.1845
18		0.1	7.00	-1.18	0.03	7.2103	6.6210	19.4404	12.4284
19		0.9	6.05	0.45	0.01	7.4366	6.5160	19.4404	14.3068
20		0.6	6.22	-	-	7.9895	6.5160	19.4404	13.2047

^aπ: Lipophilicity constant; σ: Hammett constant; KierFlex: Kier molecular flexibility index³; PC⁺: total positive partial charge; v_{sa_don}: approximation to the sum of van der Waals surface areas of pure hydrogen bond donors; SMR: molecular refractivity including implicit hydrogens.

6.1.3 Binding and Mechanistic Studies of the Compounds

To perform binding studies, RT labeled with Alexa488 at position 69 in the finger subdomain of p66, was titrated with increasing concentrations of a model p/t duplex, where the template oligonucleotide sequence was labeled by carboxytetramethylrhodamine (TAMRA) at 7 nt away from the 3'-OH end of the primer (Figure S1A). The FRET efficiency is also sensitive to RT orientation on the duplex, with high FRET being obtained when RT is bound in polymerase orientation (polymerization site is towards 3'-OH end of primer). Binding affinities were obtained by fitting the FRET efficiency at different concentrations of p/t duplexes (Figure S1B) to eq 3, by assuming a single binding site for RT on the p/t.

A: Sequence used in study

5' -CAGCAGTACAAATGGCAGTATT-3'

3' -TGTCGTCATGTTTACCGTCATAAGTAGGTTTACTAGTCCGATTTCCCTAGTCCGACCCATG-5'

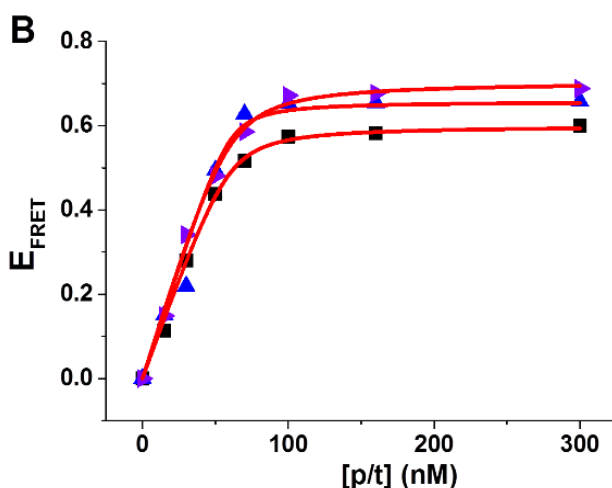


Figure S1. Effect of compounds **4** and **17** on the binding of RT to p/t duplex: (A) Sequence of the p/t duplex used in this study. The FRET acceptor fluorophore, TAMRA, is attached to the Thr residue in red in the template sequence; (B) The FRET efficiencies for 60 nM Alexa488-labelled RT are plotted against increasing concentrations of TAMRA-labeled p/t duplex in the absence (black squares) and in the presence of compound **4** (blue triangle) or compound **17** (violet triangle). FRET efficiencies were calculated as described in the methods section. Red lines represent the best fits of the experimental data to eq 3 and the values given in Table S2.

Table S2. Binding and Kinetic Parameters of the Interaction between RT and p/t Duplex in the Presence of the Inhibitors

Sample	K_d (nM) ^a	Kinetic rate constants, k_{obs} (s ⁻¹), $\times 10^3$ ^b
RT	2.6 (± 0.2)	--
RT + NVP	3.5 (± 0.2)	223 (± 10)
RT + 4	3.0 (± 0.3)	67 (± 5)
RT + 11	2.2 (± 0.2)	41 (± 10)
RT + 12	3.4 (± 0.1)	52 (± 6)
RT + 13	1.9 (± 0.2)	60 (± 7)
RT + 15	3.1 (± 0.3)	76 (± 8)
RT + 16	3.7 (± 0.4)	49 (± 6)
RT + 17	3.5 (± 0.4)	87 (± 5)
RT + 18	2.9 (± 0.3)	97 (± 10)
RT + 19	3.3 (± 0.4)	50 (± 5)
RT + 20	2.8 (± 0.4)	47 (± 9)

^aBinding parameters were obtained as described in the materials and methods section. RT was labeled at position 69 of the p66 domain with alexa488 dye. Experiments were repeated at least 3 times; ^bA RT mutant doubly labeled at positions 24 and 287 with bodipy dyes was used. Rate constants are calculated by using eq 2.

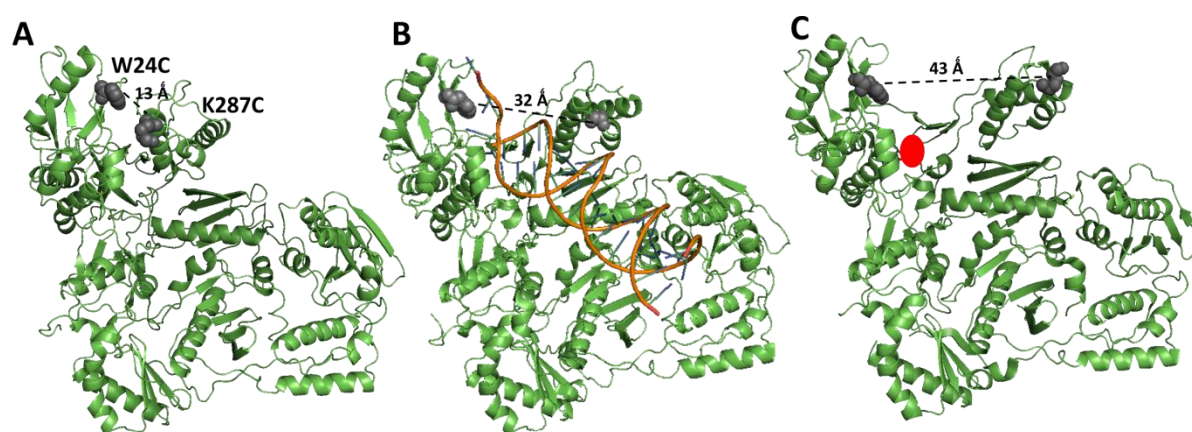


Figure S2. Distance changes between thumb and finger subdomains of RT: 3D structure of HIV-1 RT in the absence (A) and presence of either DNA/DNA p/t (B) or nevirapine (red oval) (C). The recombinantly engineered cysteines in thumb and finger are shown by gray spheres. The average distance between finger and thumb varies from ~ 13 Å (in the absence of duplex) to ~ 43 Å (in the presence of NVP). The figures were prepared by using structures in protein data bank (PDB ID: 1DLO, 1R0A and 1S1U).

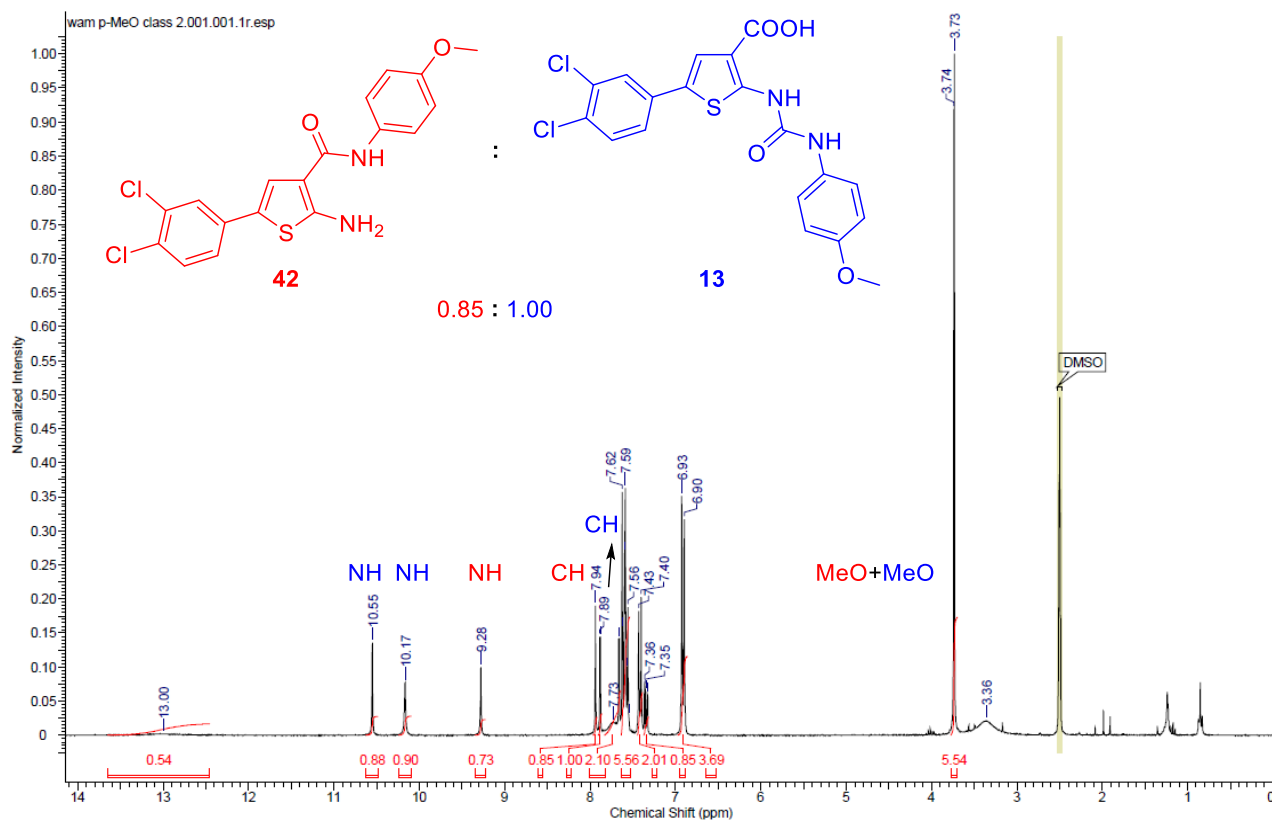


Figure S3. ¹H NMR spectrum (300 MHz, DMSO-d₆) indicating the formation of a mixture of the ureidothiophene **13** (blue) and the thiophenamide **42** (red) in 1.00:0.85 ratio, respectively from the reaction of compound **26** with *p*-anisidine in absence of TEA.

6.1.4 REFERENCES

- (1) Elgaher, W. A. M.; Fruth, M.; Groh, M.; Hauptenthal, J.; Hartmann, R. W. Expanding the Scaffold for Bacterial RNA Polymerase Inhibitors: Design, Synthesis and Structure–Activity Relationships of Ureido-Heterocyclic-Carboxylic Acids. *RSC Adv.* **2014**, *4*, 2177–2194.
- (2) Abraham, D. J.; Burger, A. *Burger's medicinal chemistry and drug discovery. Vol. 1, Drug discovery*; Wiley: Hoboken, N.J., Chichester, 2003.
- (3) Kier, L. B. An Index of Molecular Flexibility from Kappa Shape Attributes. *Quant. Struct.-Act. Relat.* **1989**, *8*, 221–224.

6.2 Supporting Information for Publication III

Full supporting information is available on the Thieme E-Journals website at:

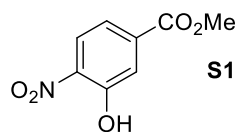
<http://dx.doi.org/10.1055/s-0034-1380509>.

6.2.1 General Information

All reactions were performed in oven dried glassware under an atmosphere of nitrogen gas unless otherwise stated. ^1H -NMR spectra were recorded at 300 MHz with a Bruker Fourier 300 or 400 MHz with a Bruker AVS-400 or at 500 MHz with a Bruker DRX-500. ^{13}C -NMR spectra were recorded at 75 MHz with a Bruker Fourier 300 or 100 MHz with a Bruker AVS-400 or 125 MHz with a Bruker DRX-500. Multiplicities are described using the following abbreviations: s = singlet, d = doublet, t = triplet, q = quartet, m = multiplet, hept = heptuplet, b = broad. Chemical shift values of ^1H and ^{13}C NMR spectra are commonly reported as values in ppm relative to residual solvent signal as internal standard. The multiplicities refer to the resonances in the off-resonance decoupled spectra. These were elucidated using the distortionless enhancement by polarization transfer (DEPT) spectral editing technique, with secondary pulses at 90° and 135° , and/or Heteronuclear Multiple Quantum Coherence (HMQC) and Heteronuclear Multiple Bond Coherence (HMBC) 2D-NMR techniques. Multiplicities are reported using the following abbreviations: s = singlet (due to quaternary carbon), d = doublet (methine), t = triplet (methylene), q = quartet (methyl). Mass spectra (EI) were obtained at 70 eV with a type VG Autospec spectrometer (Micromass), with a type LCT (ESI) (Micromass) or with a type Q-TOF (Micromass) spectrometer in combination with a Waters Aquity Ultrapformance LC system, or by LC/MS Finnigan Surveyor MSQ Plus (Thermo Fisher Scientific, Dreieich, Germany). The system consists of LC pump, autosampler, PDA detector, and single-quadrupole MS detector, as well as the standard software Xcalibur for operation. Analytical thin-layer chromatography was performed using precoated silica gel 60 F₂₅₄ plates (Merck, Darmstadt), and the spots were visualized with UV light at 254 nm or alternatively by staining with potassium permanganate, phosphomolybdic acid, 2,4-dinitrophenol or *p*-anisaldehyde solutions. Tetrahydrofuran (THF) was distilled under nitrogen from sodium/benzophenone. Dichloromethane (CH_2Cl_2) was dried using a Solvent Purification System (SPS). Commercially available reagents were used as supplied. Preparative high performance liquid chromatography using a Merck Hitachi LaChrom system (pump L- 7150, interface D-7000, diode array detector L-7450 ($\lambda = 220\text{-}400$ nm, preferred monitoring at $\lambda = 230$ nm)) with column (abbreviation referred to in the experimental part given in parentheses): Trentec Reprosil-Pur 120 C18 AQ 5 μm , 250 \times 8 mm, with guard column, 40 \times 8 mm (C18-SP). Flash column chromatography was performed on Merck silica gel 60 (230-400 mesh). Eluents used for flash chromatography were distilled prior to use. Melting points were measured using a SRS OptiMelt apparatus or a Stuart Scientific melting point apparatus SMP3 (Bibby Sterilin, UK). Arenes **5**, **11** and *p*-nitrobenzoic acid **15** are commercially available.

6.2.2 Synthesis of Cystobactamid 507

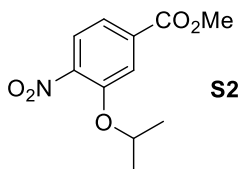
Methyl 3-hydroxy-4-nitrobenzoate (**S1**)



3-Hydroxy-2-nitrobenzoic acid (**10**) (5.10 g, 27.85 mmol) was dissolved in MeOH (43 mL) and cooled to 0 °C. SOCl₂ (3.20 mL, 43.69 mmol) was slowly added and the reaction mixture was stirred under refluxing conditions for 17 hours. The residual oil was redissolved in MeOH and concentrated (4× in order to remove the excess of SOCl₂), to yield the title compound **S1** (5.49 g, 27.85 mmol, quantitative) as a yellow solid.

mp: 91–92 °C; ¹H NMR (400 MHz, CDCl₃) δ 10.49 (s, 1H_{-OH}), 8.17 (d, *J* = 8.8 Hz, 1H), 7.83 (d, *J* = 1.8 Hz, 1H), 7.61 (dd, *J* = 8.8, 1.8 Hz, 1H), 3.96 (s, 3H) ppm; ¹³C NMR (100 MHz, CDCl₃) δ 164.96 (Cq), 154.81 (Cq), 138.14 (Cq), 135.95 (Cq), 125.41 (CH), 121.81 (CH), 120.74 (CH), 53.06 (CH₃) ppm; HRMS (ESI): Calculated for C₈H₆NO₅ (M-H)⁻: 196.0246, found: 196.0249.

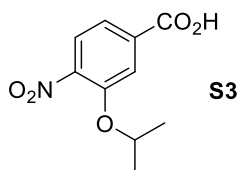
Methyl 3-isopropoxy-4-nitrobenzoate (**S2**)



Methyl 3-hydroxy-4-nitrobenzoate **S1** (5.47 g, 27.75 mmol) was dissolved in DMF (32.4 mL). K₂CO₃ (19.17 g, 138.73 mmol) and *i*PrI (3.90 mL, 38.85 mmol) were added, and the reaction mixture was stirred at 50 °C for 17 hours. The resulting mixture was poured into ethyl acetate (100 mL) and washed with H₂O (2×) and brine (1×). The organic layer was dried over MgSO₄, filtered and the solvent was evaporated *in vacuo* to give an oily residue, which was purified by flash chromatography (petroleum ether/ethyl acetate= 8:2) to yield the title compound **S2** (5.66 g, 23.66 mmol, 85%) as a yellow oil.

¹H NMR (400 MHz, CDCl₃) δ 7.75 (d, *J* = 8.4 Hz, 2H), 7.64 (dd, *J* = 8.4, 1.6 Hz, 1H), 4.77 (hept, *J* = 6.1 Hz, 1H), 3.95 (s, 3H), 1.41 (d, *J* = 6.1 Hz, 6H) ppm; ¹³C NMR (100 MHz, CDCl₃) δ 165.48 (Cq), 150.92 (Cq), 143.90 (Cq), 134.57 (Cq), 125.20 (CH), 121.24 (CH), 117.08 (CH), 73.15 (CH), 52.92 (CH₃), 21.93 (CH₃) ppm; HRMS (Qtof): Calculated for C₁₁H₁₃NO₅Na (M+Na)⁺: 262.0691, found: 262.0700.

3-Isopropoxy-4-nitrobenzoic acid (**S3**)

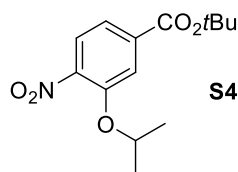


Methyl 3-isopropoxy-4-nitrobenzoate (**S2**) (4.75 g, 19.87 mmol) was dissolved in a mixture of THF/H₂O (105 mL/105 mL). Then, solid LiOH (4.76 g, 198.68 mmol) was added and the reaction

mixture was stirred at room temperature for 17 hours. The aqueous layer was acidified with 1 M HCl until pH~1 was reached and extracted with ethyl acetate (3×). The organic extracts were combined, dried over anhydrous MgSO₄ and filtered. The solvent was concentrated *in vacuo* to yield the title compound **S3** (4.12 g, 18.29 mmol, 92%) as a pale yellow solid.

mp: 178–180 °C; ¹H NMR (400 MHz, CDCl₃) δ 7.80 (d, *J* = 1.5 Hz, 1H), 7.79 (d, *J* = 9.0 Hz, 1H), 7.74 (dd, *J* = 9.0, 1.5 Hz, 1H), 4.79 (hept, *J* = 6.0 Hz, 1H), 1.43 (d, *J* = 6.0 Hz, 6H) ppm; ¹³C NMR (100 MHz, CDCl₃) δ 169.91 (Cq), 150.93 (Cq), 144.52 (Cq), 133.44 (Cq), 125.30 (CH), 121.91 (CH), 117.49 (CH), 73.29 (CH), 21.92 (CH₃) ppm; HRMS (ESI): Calculated for C₁₀H₁₀NO₅ (M-H): 224.0559, found: 224.0557.

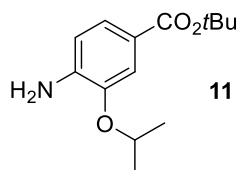
***tert*-Butyl-3-isopropoxy-4-nitrobenzoate (S4)**



3-Isopropoxy-4-nitrobenzoic acid (**S3**) (0.40 g, 1.77 mmol) was dissolved in toluene (8 mL). Dimethylformamide di-*tert*-butyl acetal (5.1 ml, 21.32 mmol) was added at room temperature and the resulting reaction mixture was heated up to 80 °C and stirred for 17 hours. The solvent was removed under reduced pressure and the crude product was purified by flash column chromatography (petroleum ether/ethyl acetate= 95:5) to afford the title compound **S4** (0.47 g, 1.65 mmol, 94% yield) as a pale yellow solid.

mp: 68–70 °C; ¹H NMR (400 MHz, CDCl₃) δ 7.75 (d, *J* = 8.4 Hz, 1H), 7.72 (d, *J* = 1.6 Hz, 1H), 7.59 (dd, *J* = 8.4, 1.6 Hz, 1H), 4.77 (hept, *J* = 6.0 Hz, 1H), 1.63 (s, 9H), 1.43 (d, *J* = 6.0 Hz, 6H) ppm; ¹³C NMR (100 MHz, CDCl₃) δ 164.08 (Cq), 150.92 (Cq), 143.56 (Cq), 136.56 (Cq), 125.06 (CH), 121.06 (CH), 116.99 (CH), 82.59 (Cq), 73.11 (CH), 28.23 (CH₃), 21.97 (CH₃) ppm; HRMS (ESI): Calculated for C₁₀H₁₀NO₅ (M+Na)⁺: 304.1161, found: 304.1161.

***tert*-Butyl 4-amino-3-isopropoxybenzoate (11)**

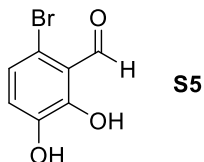


tert-Butyl 3-isopropoxy-4-nitrobenzoate (**S4**) (0.43 g, 1.54 mmol) was dissolved in MeOH (13 mL) and degassed. Pd/C (10% wt., 82.0 mg, 0.077 mmol) was added and vacuum was applied under cooling to remove air. The flask was flushed with H₂ gas and the suspension was stirred for 2 days at room temperature. The catalyst was filtered over Celite[®] and washed with MeOH. The solvent was removed under reduced pressure to yield the title compound **11** (0.39 g, 1.54 mmol, quantitative) as a dark oil.

¹H NMR (400 MHz, CDCl₃) δ 7.46 (dd, *J* = 8.1, 1.8 Hz, 1H), 7.43 (d, *J* = 1.8 Hz, 1H), 6.64 (d, *J* = 8.1 Hz, 1H), 4.61 (hept, *J* = 6.0 Hz, 1H), 4.16 (s, 2H_{NH2}), 1.57 (s, 9H), 1.36 (d, *J* = 6.0 Hz, 6H) ppm; ¹³C

NMR (100 MHz, CDCl₃) δ 166.33 (Cq), 144.35 (Cq), 141.83 (Cq), 123.71 (CH), 121.68 (Cq), 114.19 (CH), 113.45 (CH), 80.19 (Cq), 70.98 (CH), 28.46 (CH₃), 22.37 (CH₃) ppm; HRMS (ESI): Calculated for C₁₄H₂₂NO₃ (M+H)⁺: 252.1600, found: 252.1597.

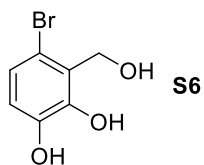
6-Bromo-2,3-dihydroxybenzaldehyde (S5)



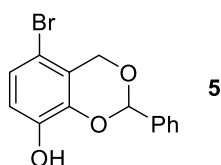
To a solution of 6-bromo-2-hydroxy-3-methoxybenzaldehyde (**4**) (25.0 g, 108.2 mmol) in CH₂Cl₂ (270 mL) at -30 °C was slowly added BBr₃ (1 M in CH₂Cl₂, 200.0 mL, 200.0 mmol) via dropping funnel over a period of 45 minutes. The solution was allowed to warm to room temperature and stirred 17 hours. H₂O was added and the reaction mixture was stirred for additional 30 minutes. The solution was then extracted with ethyl acetate (3 \times) and washed with H₂O (1 \times). The combined, organic layers were dried over anhydrous MgSO₄, filtered and concentrated *in vacuo* to give the title compound **S5** (22.16 g, 102.11 mmol, 95%) as a yellow solid.

mp: 135–136 °C; ¹H NMR (400 MHz, CDCl₃) δ 12.13 (d, *J* = 0.5 Hz, 1H_{OH}), 10.27 (s, 1H_{CHO}), 7.07 (d, *J* = 8.5 Hz, 1H), 7.02 (dd, *J* = 8.5, 0.5 Hz, 1H), 5.67 (b, 1H_{OH}) ppm; ¹³C NMR (100 MHz, CDCl₃) δ 198.42 (Cq), 151.19 (Cq), 144.99 (Cq), 124.40 (CH), 121.96 (CH), 117.45 (Cq), 116.05 (Cq) ppm; HRMS (ESI): Calculated for C₇H₄BrO₃ (M-H)⁻: 214.9344, found: 214.9343.

4-Bromo-3-hydroxymethylbenzene-1,2-diol (S6)

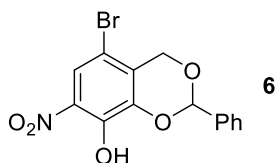


To a solution of 6-bromo-2,3-dihydroxybenzaldehyde (**S5**) (22.16 g, 102.10 mmol) in THF (650 mL) at -40 °C was added NaBH₄ (3.86 g, 102.10 mmol) in three portions. The resulting mixture was stirred for 30 minutes at room temperature. A saturated aqueous solution of NH₄Cl (300 mL) was added and the mixture was stirred for another 10 minutes, before being finally treated with 1 M HCl (300 mL). After 10 minutes of additional stirring, the aqueous phase was extracted with ethyl acetate (3 \times). The combined, organic extracts were dried over anhydrous MgSO₄ and filtered. The solvent was removed under reduced pressure to yield the title compound **S6** (20.27 g, 92.53 mmol, 91%) as a colorless solid. mp: 90–92 °C; ¹H NMR (400 MHz, MeOD) δ 6.88 (d, *J* = 8.5 Hz, 1H), 6.64 (d, *J* = 8.5 Hz, 1H), 4.82 (s, 2H) ppm; ¹³C NMR (100 MHz, MeOD) δ 147.06 (Cq), 146.07 (Cq), 126.88 (Cq), 123.86 (CH), 116.55 (CH), 114.41 (Cq), 61.13 (CH₂) ppm; HRMS (ESI): Calculated for C₇H₆BrO₃ (M-H)⁻: 216.9500, found: 216.9505.

5-Bromo-2-phenyl-4*H*-benzo-[1,3]-dioxin-8-ol (5)

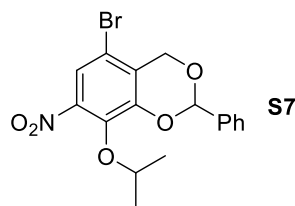
A solution of 4-bromo-3-hydroxymethylbenzene-1,2-diol (**S6**) (20.27 g, 92.53 mmol) in THF (550 mL) was treated with PhCH(OMe)₂ (20.8 mL, 138.8 mmol) and *p*TsOH.H₂O (0.19 g, 1.02 mmol). The mixture was stirred at room temperature for 5 days. CH₂Cl₂ was added and then washed successively with 5% aqueous NaHCO₃ (1×) and brine (1×). The aqueous phase was extracted with ethyl acetate (3×). The combined, organic extracts were dried over anhydrous MgSO₄, filtered and the solvent was removed under reduced pressure. Purification by flash chromatography (petroleum ether/ethyl acetate= 95/5) afforded 5-bromo-2-phenyl-4*H*-benzo-[1,3]-dioxin-8-ol (**5**) (16.02 g, 52.16 mmol, 56%) as a colorless solid.

mp: 89–91 °C; ¹H NMR (400 MHz, CDCl₃) δ 7.62–7.55 (m, 2H), 7.50–7.43 (m, 3H), 7.07 (d, *J* = 8.6 Hz, 1H), 6.78 (d, *J* = 8.6 Hz, 1H), 5.97 (s, 1H), 5.40 (s, 1H_{OH}), 4.99 (s, 2H) ppm; ¹³C NMR (100 MHz, CDCl₃) δ 143.99 (Cq), 141.77 (Cq), 136.14 (Cq), 130.13 (CH), 128.79 (CH), 126.68 (CH), 124.90 (CH), 120.95 (Cq), 115.00 (CH), 109.40 (Cq), 99.98 (CH), 67.8 (CH₂) ppm; HRMS (ESI): Calculated for C₁₄H₁₀BrO₃ (M-H)⁻: 304.9813, found: 304.9813.

5-Bromo-7-nitro-2-phenyl-4*H*-benzo-[1,3]-dioxin-8-ol (6)

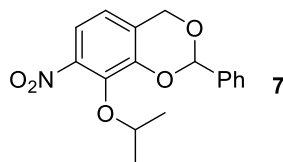
5-Bromo-2-phenyl-4*H*-benzo-[1,3]-dioxin-8-ol (**5**) (6.00 g, 19.54 mmol; max. amount) was dissolved in acetone (250 mL). Then, Ni(NO₃)₂.5H₂O (5.68 g, 19.54 mmol) and *p*TSA.H₂O (3.72 g, 19.54 mmol) were added. The mixture was stirred at room temperature for 2.5 hours. The reaction mixture was filtered through a pad of Celite®, washed with CH₂Cl₂ and concentrated *in vacuo*. Purification by flash chromatography (dry load: SiO₂ + CH₂Cl₂; petroleum ether/ethyl acetate= 9:1) yielded the title compound **6** (5.08 g, 14.43 mmol, 74%) as a bright yellow solid.

mp: 154–156 °C; ¹H NMR (400 MHz, CDCl₃) δ 10.60 (b, 1H_{OH}), 7.96 (s, 1H), 7.65–7.57 (m, 2H), 7.48–7.42 (m, 3H), 6.02 (s, 1H), 4.99 (s, 2H) ppm; ¹³C NMR (100 MHz, CDCl₃) δ 144.88 (Cq), 135.45 (Cq), 133.17 (Cq), 130.16 (CH), 128.95 (Cq), 128.86 (CH), 126.65 (CH), 119.17 (CH), 109.16 (Cq), 99.87 (CH), 67.37 (CH₂) ppm; HRMS (ESI): Calculated for C₁₄H₉BrNO₅ (M-H)⁻: 349.9664, found: 349.9660.

5-Bromo-8-isopropoxy-7-nitro-2-phenyl-4H-benzo-[1,3]-dioxin (S7)

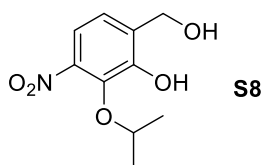
5-Bromo-7-nitro-2-phenyl-4H-benzo-[1,3]-dioxin-8-ol (**6**) (13.79 g, 39.16 mmol) was dissolved in THF (429 mL). *i*PrOH (4.00 mL, 50.91 mmol) and PPh₃ (13.87 g, 52.87 mmol) were added, and the mixture was stirred until all components were dissolved. DEAD (2.2 M in toluene, 23.1 mL, 50.91 mmol) was slowly added via syringe pump and the mixture was stirred at room temperature 17 hours. The solvent was evaporated *in vacuo* to give an oily residue, which was purified by flash chromatography (petroleum ether/ethyl acetate= 96:4) to yield the title compound **S7** (13.08 g, 33.18 mmol, 85%) as a colorless solid.

mp: 87–89 °C; ¹H NMR (400 MHz, CDCl₃) δ 7.59 (s, 1H), 7.59–7.54 (m, 2H), 7.50–7.43 (m, 3H), 5.97 (s, 1H), 5.00 (s, 2H), 4.69 (hept, *J* = 6.2 Hz, 1H), 1.31 (d, *J* = 6.2 Hz, 3H), 1.28 (d, *J* = 6.2 Hz, 3H) ppm; ¹³C NMR (100 MHz, CDCl₃) δ 149.04 (Cq), 144.46 (Cq), 139.87 (Cq), 135.71 (Cq), 130.05 (CH), 128.80 (CH), 126.36 (CH), 126.15 (Cq), 119.80 (CH), 112.67 (Cq), 99.66 (CH), 78.10 (CH), 67.63 (CH₂), 22.63 (CH₃), 22.37 (CH₃) ppm; HRMS (Qtof): Calculated for C₁₇H₁₆BrNO₅Na (M+Na)⁺: 416.0110, found: 416.0101.

8-Isopropoxy-7-nitro-2-phenyl-4H-benzo-[1,3]-dioxin (7)

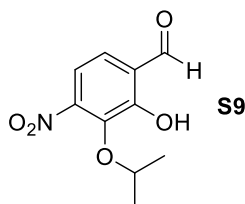
5-Bromo-8-isopropoxy-7-nitro-2-phenyl-4H-benzo-[1,3]-dioxin (**S7**) (4.00 g, 10.15 mmol), Pd₂(dba)₃ (0.93 g, 1.01 mmol), (PhO)₃P (0.53 mL, 2.03 mmol), Cs₂CO₃ (4.30 g, 13.19 mmol) and *i*PrOH (4.7 mL, 60.88 mmol) were dissolved in 1,4-dioxane (28 mL). The oil bath was preheated to 60°C and the mixture was stirred at 80°C for 1.5 hours. The reaction mixture was filtered through a pad of Celite® and washed with ethyl acetate. The combined, organic extracts were dried over anhydrous MgSO₄, filtered and concentrated *in vacuo*. The crude material was purified by flash chromatography (petroleum ether/ethyl acetate= 96:4) to yield the title compound **7** (2.24 g, 7.10 mmol, 70%) as a pale yellow solid.

mp: 80–82 °C; ¹H NMR (400 MHz, CDCl₃) δ 7.65–7.55 (m, 2H), 7.51–7.41 (m, 3H), 7.37 (d, *J* = 8.5 Hz, 1H), 6.81 (d, *J* = 8.5 Hz, 1H), 6.01 (s, 1H), 5.19 (d, *J* = 15.5 Hz, 1H), 5.03 (d, *J* = 15.5 Hz, 1H), 4.71 (hept, *J* = 6.2 Hz, 1H), 1.32 (d, *J* = 6.2 Hz, 3H), 1.28 (d, *J* = 6.2 Hz, 3H) ppm; ¹³C NMR (100 MHz, CDCl₃) δ 147.67 (Cq), 144.27 (Cq), 140.55 (Cq), 136.26 (Cq), 129.85 (CH), 128.72 (CH), 126.54 (Cq), 126.34 (CH), 118.82 (CH), 116.69 (CH), 99.61 (CH), 77.71 (CH), 66.44 (CH₂), 22.65 (CH₃), 22.41 (CH₃) ppm; HRMS (QToF): Calculated for C₁₇H₁₇NO₅Na (M+Na)⁺: 338.1004. Found: 338.1003.

6-Hydroxymethyl-2-isopropoxy-3-nitrophenol (S8)

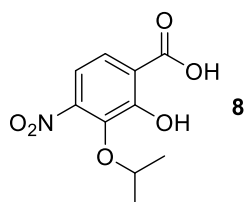
To a mixture of 8-isopropoxy-7-nitro-2-phenyl-4*H*-benzo-[1,3]-dioxin (**7**) (4.24 g, 13.43 mmol) in MeOH (102 mL) and CH₂Cl₂ (42 mL) at 0 °C was added camphor sulfonic acid (3.12 g, 13.43 mmol). The mixture was stirred at room temperature for 17 hours. The reaction mixture was quenched with Et₃N until pH~8, concentrated *in vacuo* and purified by flash chromatography (petroleum ether/ethyl acetate= 7:3) to yield the title compound **S8** (2.75 g, 12.09 mmol, 90%) as a light brown solid.

mp: 39–41 °C; ¹H NMR (400 MHz, CDCl₃) δ 7.46 (d, *J* = 7.4 Hz, 1H), 7.12 (d, *J* = 7.4 Hz, 1H), 6.61 (s, 1H_{OH}), 4.81 (d, *J* = 3.5 Hz, 2H), 4.39 (hept, *J* = 7.4 Hz, 1H), 1.36 (d, *J* = 6.2 Hz, 6H) ppm; ¹³C NMR (100 MHz, CDCl₃) δ 149.07 (Cq), 138.67 (Cq), 132.55 (Cq), 122.28 (CH), 116.63 (CH), 79.38 (CH), 61.47 (CH₂), 22.65 (CH₃) ppm; HRMS (ESI): Calculated for C₁₀H₁₂NO₅ (M-H): 226.0715, found: 226.0717.

2-Hydroxy-3-isopropoxy-4-nitrobenzaldehyde (S9)

6-Hydroxymethyl-2-isopropoxy-3-nitrophenol (**S8**) (2.97 g, 13.05 mmol) was dissolved in CH₂Cl₂ (58 mL). Then MnO₂ (11.35 g, 130.53 mmol) was added and the mixture was stirred at room temperature for 17 hours. The mixture was filtered through a pad of Celite[®] and washed with CH₂Cl₂. The solvent was concentrated to give the title compound **S9** (2.38 g, 10.57 mmol, 81%) as a brown oil.

¹H NMR (400 MHz, CDCl₃) δ 11.44 (s, 1H_{CHO}), 9.97 (s, 1H_{OH}), 7.39 (d, *J* = 8.4 Hz, 1H), 7.23 (d, *J* = 8.4 Hz, 1H), 4.88 (hept, *J* = 6.2 Hz, 1H), 1.33 (d, *J* = 6.2 Hz, 6H) ppm; ¹³C NMR (100 MHz, CDCl₃) δ 196.39 (Cq), 156.53 (Cq), 149.36 (Cq), 139.74 (Cq), 127.28 (CH), 122.57 (Cq), 114.32 (CH), 77.42 (CH), 22.51 (CH₃) ppm; HRMS (ESI): Calculated for C₁₀H₁₀NO₅ (M-H): 224.0559. Found: 224.0535.

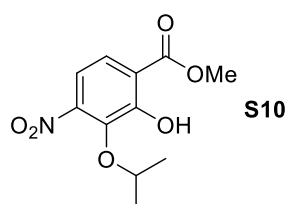
2-Hydroxy-3-isopropoxy-4-nitrobenzoic acid (8)

2-Hydroxy-3-isopropoxy-4-nitrobenzaldehyde (**S9**) (2.36 g, 10.49 mmol) was dissolved in *tert*-butanol (71 mL). 2-Methyl-2-butene (2M in THF, 36.7 mL, 73.45 mmol) and a solution of NaClO₂ (2.85 g, 31.48 mmol) and NaH₂PO₄ (6.32 g, 47.22 mmol) in H₂O (51 mL) were added in sequential order. The

reaction mixture was stirred at room temperature for 17 hours. 6 M NaOH was added until pH~10 and the solvent was concentrated *in vacuo*. H₂O was added and the organic layer was extracted with petroleum ether (2×). The aqueous layer was acidified with 6 M HCl until pH~1 and extracted with ethyl acetate (3×). The organic extracts were combined, dried over MgSO₄ and filtered. The solvent was concentrated *in vacuo* to yield the title compound **8** (1.90 g, 7.87 mmol, 75%) as a yellow semisolid material.

¹H NMR (400 MHz, MeOD) δ 7.72 (d, *J* = 8.7 Hz, 1H), 7.15 (d, *J* = 8.7 Hz, 1H), 4.86–4.82 (m, 1H), 1.27 (d, *J* = 6.2 Hz, 6H) ppm; ¹³C NMR (100 MHz, MeOD) δ 172.74 (Cq), 158.01 (Cq), 149.63 (Cq), 139.97 (Cq), 125.8 (CH), 117.41 (Cq), 113.75 (CH), 77.54 (CH), 22.59 (CH₃) ppm; HRMS (ESI): Calculated for C₁₀H₁₀NO₆ (M-H)⁻: 240.0508, found: 240.0511.

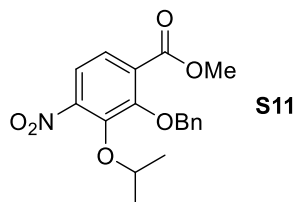
Methyl 2-hydroxy-3-isopropoxy-4-nitrobenzoate (S10)



TMSCHN₂ (2.0 M in Et₂O, 0.87 mL, 1.75 mmol) was added to a solution of 2-hydroxy-3-isopropoxy-4-nitrobenzoic acid (**8**) (0.32 g, 1.35 mmol) in a mixture 5/1 of toluene/MeOH (10.4/2 mL) at 0 °C. After stirring at 0 °C for 1 hour, the reaction was terminated by addition of acetic acid. The solvent was evaporated *in vacuo* to give an oily residue, which was purified by flash chromatography (petroleum ether/ethyl acetate= 95:5) to yield the title compound **S10** (0.72 g, 2.82 mmol, 80%) as a yellow oil.

¹H NMR (400 MHz, CDCl₃) δ 11.29 (s, 1H_{OH}), 7.63 (d, *J* = 8.8 Hz, 1H), 7.12 (d, *J* = 8.8 Hz, 1H), 4.84 (hept, *J* = 6.2 Hz, 1H), 4.00 (s, 3H), 1.32 (d, *J* = 6.2 Hz, 6H) ppm; ¹³C NMR (100 MHz, CDCl₃) δ 169.98 (Cq), 157.03 (Cq), 149.21 (Cq), 139.84 (Cq), 123.92 (CH), 115.68 (Cq), 113.35 (CH), 77.36 (CH), 53.21 (CH₃), 22.47 (CH₃) ppm; HRMS (ESI): Calculated for C₁₁H₁₂NO₆ (M-H)⁻: 254.0665, found: 254.0666.

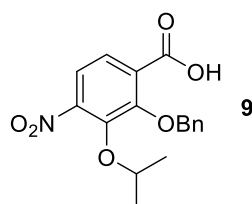
Methyl 2-benzyloxy-3-isopropoxy-4-nitrobenzoate (S11)



Methyl 2-hydroxy-3-isopropoxy-4-nitrobenzoate (**S10**) (0.87 g, 3.47 mmol) was dissolved in THF (38 mL). BnOH (0.47 mL, 4.51 mmol) and PPh₃ (1.23 g, 4.68 mmol) were added, and the mixture was stirred until all components are dissolved. DEAD (2.2 M in toluene, 2.05 mL, 4.51 mmol) was slowly added via syringe pump and the mixture was stirred at room temperature 17 hours. The solvent was

evaporated *in vacuo* to give an oily residue, which was purified by flash chromatography (petroleum ether/ethyl acetate= 95:5) to yield the title compound **S11** (0.84 g, 2.43 mmol, 70%) as a colorless oil. ^1H NMR (400 MHz, CDCl_3) δ 7.53 (d, J = 8.6 Hz, 1H), 7.50 (d, J = 8.6 Hz, 1H), 7.48–7.44 (m, 2H), 7.42–7.35 (m, 3H), 5.14 (s, 2H), 4.74 (hept, J = 6.2 Hz, 1H), 3.86 (s, 3H), 1.28 (d, J = 6.2 Hz, 6H) ppm; ^{13}C NMR (100 MHz, CDCl_3) δ 165.27 (Cq), 153.38 (Cq), 148.37 (Cq), 145.65 (Cq), 136.36 (Cq), 130.85 (Cq), 128.72 (CH), 128.71 (CH), 128.65 (CH), 125.07 (CH), 119.29 (CH), 78.18 (CH), 76.39 (CH₂), 52.81 (CH₃), 22.45 (CH₃) ppm; HRMS (QToF): Calculated for $\text{C}_{18}\text{H}_{19}\text{NO}_6\text{Na}$ ($\text{M}+\text{Na}$)⁺: 368.1110, found: 368.1112.

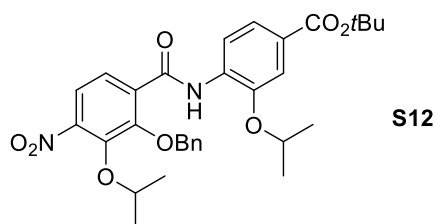
2-Benzoyloxy-3-isopropoxy-4-nitrobenzoic acid (**9**)



Methyl 2-benzyloxy-3-isopropoxy-4-nitrobenzoate (**S11**) (0.82 g, 2.38 mmol) was dissolved in a mixture 1/1 of THF/ H_2O (12.6/12.6 mL). Then, solid LiOH (0.57 g, 23.76 mmol) was added and the reaction mixture was stirred at room temperature for 17 hours. The aqueous layer was acidified with 1 M HCl until pH~1 and extracted with ethyl acetate (3 \times). The organic extracts were combined, dried over anhydrous MgSO_4 and filtered. The solvent was concentrated *in vacuo* to yield the title compound **9** (0.75 g, 2.26 mmol, 95%) as a yellow semisolid material.

^1H NMR (400 MHz, CDCl_3) δ 7.91 (d, J = 8.7 Hz, 1H), 7.58 (d, J = 8.7 Hz, 1H), 7.39–7.41 (m, 5H), 5.35 (s, 2H), 4.67 (hept, J = 6.0 Hz, 1H), 1.35 (d, J = 6.0 Hz, 6H) ppm; ^{13}C NMR (100 MHz, CDCl_3) δ 163.55 (Cq), 152.60 (Cq), 149.55 (Cq), 144.60 (Cq), 133.91 (Cq), 129.91 (CH), 129.45 (CH), 129.28 (CH), 127.15 (Cq), 127.11 (CH), 120.13 (CH), 79.15 (CH), 77.89 (CH₂), 22.52 (CH₃) ppm; HRMS (ESI): Calculated for $\text{C}_{17}\text{H}_{16}\text{NO}_6$ ($\text{M}-\text{H}$)⁻: 330.0978, found: 330.0976.

tert-Butyl 4-[2-(benzyloxy)-3-isopropoxy-4-nitrobenzamido]-3-isopropoxybenzoate (**S12**)

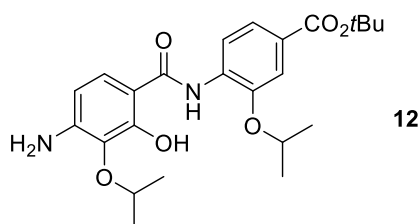


2-Benzoyloxy-3-isopropoxy-4-nitrobenzoic acid (**9**) (23.3 mg, 0.070 mmol) was dissolved in CH_2Cl_2 (3.5 mL) and preactivated with Ghosez's reagent (**13**) (37.2 μL , 0.28 mmol) for 1 day at 40 $^\circ\text{C}$. *tert*-Butyl 4-amino-3-isopropoxybenzoate (**11**) (61.6 mg, 0.25 mmol) was dissolved in CH_2Cl_2 (3.5 mL) and *N,N*-diisopropylethylamine (DIPEA) was added (0.10 mL, 0.57 mmol). The solution containing the acyl chloride was then added and the reaction mixture was stirred for 1 day at 40 $^\circ\text{C}$. The solvent was removed and the crude product was purified by preparative HPLC (RP-18; run time 100 min;

H₂O/MeCN= 100 : 0 → 0 : 100; tr = 62 min) providing the title compound **S12** (0.32 g, 0.056 mmol, 80%) as a light orange oil.

¹H NMR (400 MHz, CDCl₃) δ 10.33 (s, 1H_{NH}), 8.52 (d, *J* = 8.6 Hz, 1H), 7.85 (d, *J* = 8.6 Hz, 1H), 7.63 (dd, *J* = 8.6, 1.7 Hz, 1H), 7.59 (d, *J* = 8.6 Hz, 1H), 7.55 (d, *J* = 1.7 Hz, 1H), 7.24–7.13 (m, 5H), 5.25 (s, 2H), 4.70 (hept, *J* = 6.1 Hz, 1H), 4.63 (hept, *J* = 6.1 Hz, 1H), 1.61 (s, 9H), 1.39 (d, *J* = 6.1 Hz, 6H), 1.27 (d, *J* = 6.1 Hz, 6H) ppm; ¹³C NMR (100 MHz, CDCl₃) δ 165.72 (Cq), 161.32 (Cq), 151.06 (Cq), 147.88 (Cq), 146.06 (Cq), 145.21 (Cq), 134.13 (Cq), 133.02 (CH), 132.42 (Cq), 130.00 (CH), 129.40 (CH), 128.66 (CH), 127.57 (Cq), 125.77 (CH), 123.06 (CH), 120.03 (CH), 119.34 (CH), 113.18 (CH), 81.19 (Cq), 78.88 (CH), 77.37 (CH₂), 71.67 (CH), 28.40 (CH₃), 22.57 (CH₃), 22.11 (CH₃) ppm; HRMS (ESI): Calculated for C₃₁H₃₆N₂O₈Na (M+Na)⁺: 587.2369, found: 587.2368.

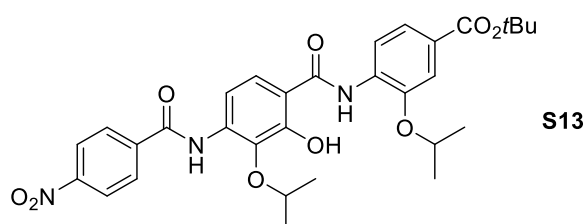
***tert*-Butyl 4-(4-amino-2-hydroxy-3-isopropoxybenzamido)-3-isopropoxybenzoate (12)**



tert-Butyl 4-[2-(benzyloxy)-3-isopropoxy-4-nitrobenzamido]-3-isopropoxybenzoate (**S12**) (59.0 mg, 0.10 mmol) was dissolved in MeOH (1.0 mL) and degassed. Pd/C (10% wt., 10.0 mg, 0.0095 mmol) was added and vacuum was applied under cooling to remove air. The flask was flushed with H₂ gas and the suspension was stirred for 2 hours at room temperature. The catalyst was filtered off over a pad of Celite®, washed with MeOH and the solvent was removed under reduced pressure. The title compound **12** (42.1 mg, 0.095 mmol, 91%) was obtained as a yellow oil.

¹H NMR (400 MHz, CDCl₃) δ 12.27 (s, 1H_{OH}), 8.79 (s, 1H_{NH}), 8.46 (d, *J* = 8.6 Hz, 1H), 7.63 (dd, *J* = 8.6, 1.8 Hz, 1H), 7.55 (d, *J* = 1.8 Hz, 1H), 7.07 (d, *J* = 8.6 Hz, 1H), 6.28 (d, *J* = 8.6 Hz, 1H), 4.74 (hept, *J* = 6.2 Hz, 1H), 4.68 (hept, *J* = 6.2 Hz, 1H), 4.27 (b, 2H_{NH2}), 1.60 (s, 9H), 1.43 (d, *J* = 6.1 Hz, 6H), 1.34 (d, *J* = 6.1 Hz, 6H) ppm; ¹³C NMR (100 MHz, CDCl₃) δ 168.49 (Cq), 165.70 (Cq), 156.38 (Cq), 146.38 (Cq), 145.96 (Cq), 132.29 (Cq), 131.98 (Cq), 127.06 (Cq), 123.16 (CH), 121.43 (CH), 118.92 (CH), 113.32 (CH), 106.56 (Cq), 106.25 (CH), 81.09 (Cq), 74.41 (CH), 72.02 (CH), 28.39 (CH₃), 22.87 (CH₃), 22.40 (CH₃) ppm; HRMS (ESI): Calculated for C₂₄H₃₃N₂O₆ (M+H)⁺: 445.2339, found: 445.2337.

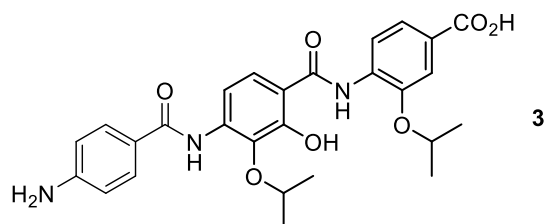
***tert*-Butyl 4-(2-hydroxy-3-isopropoxy-4-(4-nitrobenzamido)benzamido)-3-isopropoxybenzoate (S13)**



tert-Butyl 4-(4-amino-2-hydroxy-3-isopropoxybenzamido)-3-isopropoxybenzoate (**12**) (29.0 mg, 0.065 mmol) and *p*-nitrobenzoic acid (**14**) (21.8 mg, 0.13 mmol) were dissolved in CH₂Cl₂ (0.65 mL). PPh₃Cl₂ (0.13 g, 0.39 mmol) was added and the mixture was stirred under refluxing conditions for 17 hours. The solvent was evaporated *in vacuo* to give an oily residue, which was purified by flash chromatography (petroleum ether/ethyl acetate= 8:2) to yield the title compound **S13** (28.7 mg, 0.048 mmol, 78%) as a yellow semisolid.

¹H NMR (400 MHz, CDCl₃) δ 12.49 (s, 1H_{-OH}), 8.96 (s, 1H_{-NH}), 8.93 (s, 1H_{-NH}), 8.47 (d, *J* = 8.8 Hz, 1H), 8.40 (d, *J* = 8.8 Hz, 2H), 8.17 (d, *J* = 8.8 Hz, 1H), 8.07 (d, *J* = 8.8 Hz, 2H), 7.65 (dd, *J* = 8.8, 1.6 Hz, 1H), 7.58 (d, *J* = 1.6 Hz, 1H), 7.29 (d, *J* = 8.8 Hz, 1H), 4.93 (hept, *J* = 6.1 Hz, 1H), 4.77 (hept, *J* = 6.1 Hz, 1H), 1.61 (s, 9H), 1.46 (d, *J* = 6.1 Hz, 6H), 1.38 (d, *J* = 6.1 Hz, 6H) ppm; ¹³C NMR (100 MHz, CDCl₃) δ 168.03 (Cq), 165.52 (Cq), 163.22 (Cq), 155.07 (Cq), 150.12 (Cq), 146.18 (Cq), 140.19 (Cq), 136.64 (Cq), 135.05 (Cq), 131.48 (Cq), 128.32 (CH), 127.88 (Cq), 124.41 (CH), 123.06 (CH), 120.67 (CH), 119.12 (CH), 113.30 (CH), 112.23 (Cq), 109.93 (CH), 81.29 (Cq), 75.60 (CH), 72.21 (CH), 28.37 (CH₃), 23.09 (CH₃), 22.40 (CH₃) ppm; HRMS (ESI): Calculated for C₃₁H₃₆N₃O₉ (M+H)⁺: 594.2452, found: 594.2454.

Cystobactamid C (**3**)



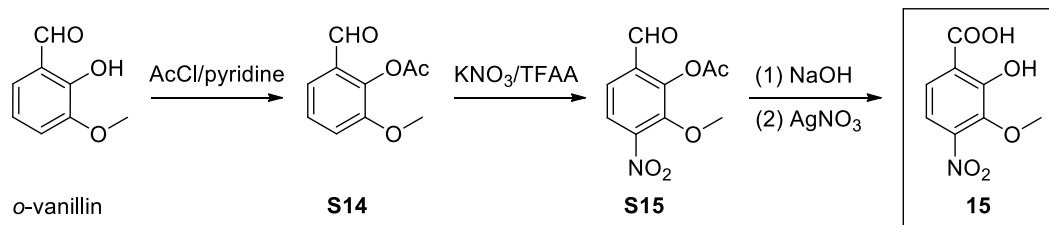
tert-Butyl 4-(2-hydroxy-3-isopropoxy-4-(4-nitrobenzamido)benzamido)-3-isopropoxybenzoate (**S13**) (8.1 mg, 0.014 mmol) was dissolved in MeOH (1 mL). SnCl₂·2H₂O (9.2 mg, 0.041 mmol) was added and the reaction mixture was stirred under refluxing conditions for 17 hours. The solvent was evaporated under reduced pressure and the residue diluted with EtOAc. After addition of a saturated solution of NaHCO₃ and separation of the phases, the aqueous layer was extracted with EtOAc (1×). The aqueous layer was acidified with 1 M HCl until pH~1 and extracted with EtOAc (3×). The combined organic layers were washed with brine (1×), dried over anhydrous MgSO₄ and filtered. The crude product was purified by preparative HPLC (RP-18; run time 100 min; H₂O/MeCN= 100 : 0 → 0 : 100; tr = 47 min) providing the title compound **3** (2.8 mg, 5.5 mmol, 40%) as a semisolid material.

¹H NMR (400 MHz, MeOD) δ 8.46 (d, *J* = 8.6 Hz, 1H), 7.80 (d, *J* = 8.6 Hz, 1H), 7.75 (d, *J* = 8.6 Hz, 1H), 7.72 (d, *J* = 8.6 Hz, 2H), 7.71–7.64 (m, 2H), 6.74 (d, *J* = 8.6 Hz, 2H), 4.78 (hept, *J* = 6.1 Hz, 1H), 4.55 (hept, *J* = 6.1 Hz, 1H), 1.46 (d, *J* = 6.1 Hz, 6H), 1.35 (d, *J* = 6.1 Hz, 6H) ppm; ¹³C NMR (125 MHz, MeOD) δ 167.80 (Cq), 167.02 (Cq), 154.27 (Cq), 152.92 (Cq), 148.39 (Cq), 138.21 (Cq), 138.16 (Cq), 134.11 (Cq), 130.23 (CH), 125.50 (CH), 124.02 (CH), 122.35 (Cq), 121.26 (CH), 116.22 (CH, Cq), 115.22 (Cq), 114.79 (CH), 114.32 (CH), 77.13 (CH), 73.26 (CH), 22.71 (CH₃), 22.32 (CH₃) ppm; HRMS (ESI): Calculated for C₂₇H₃₀N₃O₇ (M+H)⁺: 508.2084, found: 508.2085.

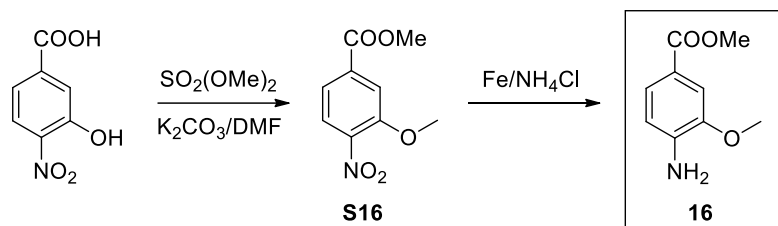
6.2.3 Synthesis of cystobactamid 507 derivative 18

Scheme S1. Overview on the synthesis of compound 18

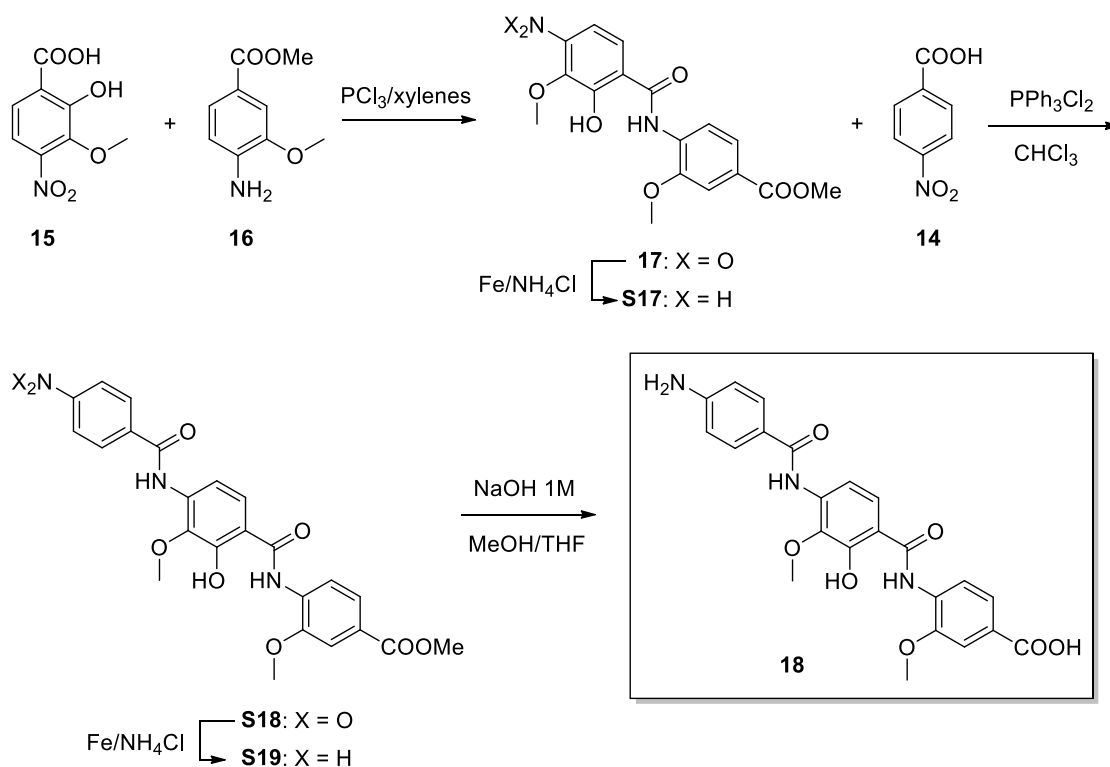
Step 1: Synthesis of the tetrasubstituted arene

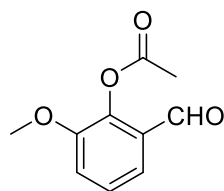


Step 2: Synthesis of the trisubstituted arene

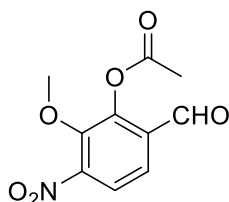


Step 3: Synthesis of compound 18



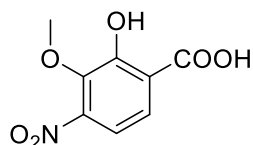
2-Formyl-6-methoxyphenyl acetate (S14)

To a stirred solution of *o*-vanillin (4.56 g, 30 mmol), and pyridine (2.43 mL, 30 mmol) in CH₂Cl₂ (40 mL), acetyl chloride (2.36 g, 30 mmol) was added drop wise. The reaction was stirred at room temperature overnight then the solvent was removed by vacuum distillation. The obtained material was triturated with cold dil. HCl and collected by filtration, washed with cold water and then with *n*-hexane. Yield 94% (off-white solid); mp: 75–76 °C; ¹H NMR^{S1} (300 MHz, CDCl₃) δ 10.14 (s, 1H), 7.47 (dd, *J* = 8.1, 1.6 Hz, 1H), 7.34 (t, *J* = 8.1 Hz, 1H), 7.22 (dd, *J* = 8.1, 1.6 Hz, 1H), 3.89 (s, 3H), 2.41 (s, 3H); ¹³C NMR (75 MHz, CDCl₃) δ 188.68 (CH), 168.68 (Cq), 151.76 (Cq), 141.54 (Cq), 129.22 (Cq), 126.77 (CH), 121.29 (CH), 117.83 (CH), 56.35 (CH₃), 20.39 (CH₃); *m/z* (ESI+) 195 [M + H]⁺.

6-Formyl-2-methoxy-3-nitrophenyl acetate (S15)

To a stirred ice-cold suspension of **S14** (1.94 g, 10 mmol), and KNO₃ (1.01 g, 10 mmol) in CHCl₃ (15 mL), trifluoroacetic anhydride (12 mL) was added. The reaction was stirred in an ice bath for 2 h then at room temperature overnight. The reaction was diluted very carefully with water (50 mL) and extracted with CHCl₃ (3 × 30 mL). The combined organic extracts were dried with anhydrous MgSO₄, and the solvent was removed by vacuum distillation. The residue was dissolved in toluene and purified using flash chromatography (SiO₂, *n*-hexane/EtOAc = 3:1).

Yield 45% (yellow oil); ¹H NMR^{S2} (300 MHz, CDCl₃) δ 10.10 (s, 1H), 7.80 (d, *J* = 8.6 Hz, 1H), 7.72 (d, *J* = 8.6 Hz, 1H), 3.99 (s, 3H), 2.48 (s, 3H); ¹³C NMR (75 MHz, CDCl₃) δ 186.95 (CH), 168.14 (Cq), 147.71 (Cq), 146.92 (Cq), 146.74 (Cq), 132.13 (Cq), 124.98 (CH), 122.22 (CH), 62.91 (CH₃), 20.43 (CH₃); *m/z* (ESI+) 239 [M]⁺.

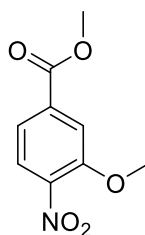
2-Hydroxy-3-methoxy-4-nitrobenzoic acid (15)

To a stirred suspension of **S15** (957 mg, 4 mmol) in water (50 mL), NaOH (0.8 g, 20 mmol) was added. The reaction was heated under refluxing conditions for 2 h then cooled to room temperature. AgNO₃ (3.4 g, 20 mmol) was added portionwise and the reaction mixture was heated under refluxing conditions overnight before it was cooled and filtered through a pad of CeliteTM. The filtrate was cooled in an ice

bath and acidified by HCl 37% to pH 3–4. The precipitated solid was collected by filtration, washed with cold water and then with *n*-hexane.

Yield 65% (beige solid); mp: 203–205 °C; $^1\text{H NMR}^{\text{S2}}$ (300 MHz, DMSO- d_6) δ 13.67 (br s, 1H), 7.69 (d, $J = 8.7$ Hz, 1H), 7.32 (d, $J = 8.7$ Hz, 1H), 5.70 (br s, 1H), 3.93 (s, 3H); $^{13}\text{C NMR}$ (75 MHz, DMSO- d_6) δ 170.81 (Cq), 155.95 (Cq), 147.25 (Cq), 140.53 (Cq), 125.22 (CH), 117.88 (Cq), 112.69 (CH), 61.42 (CH $_3$); m/z (ESI+) 213 [M] $^+$.

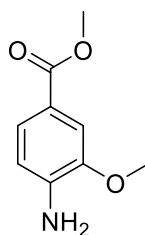
Methyl 3-methoxy-4-nitrobenzoate (S16)



To a stirred mixture of 3-hydroxy-4-nitrobenzoic acid (9.16 g, 50 mmol) and K_2CO_3 (15.2 g, 110 mmol) in DMF (150 mL), dimethyl sulfate (25.2 g, 200 mmol) was added portionwise. The reaction mixture was heated at 90 °C overnight and then cooled to room temperature. The reaction mixture was poured onto ice-cooled water (400 mL), the precipitate was collected by filtration, washed with cold water and then with *n*-hexane.

Yield 95% (pale yellow solid); mp: 90–91 °C; $^1\text{H NMR}^{\text{S3}}$ (300 MHz, CDCl_3) δ 7.84 (d, $J = 8.4$ Hz, 1H), 7.77 (d, $J = 1.6$ Hz, 1H), 7.70 (dd, $J = 8.4, 1.6$ Hz, 1H), 4.02 (s, 3H), 3.97 (s, 3H); $^{13}\text{C NMR}^{\text{S3}}$ (75 MHz, CDCl_3) δ 165.22 (Cq), 152.46 (Cq), 142.41 (Cq), 134.90 (Cq), 125.34 (CH), 121.40 (CH), 114.63 (CH), 56.76 (CH $_3$), 52.84 (CH $_3$); m/z (ESI+) 212 [M + H] $^+$.

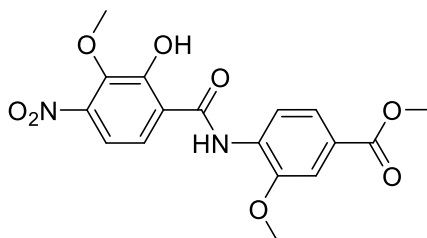
Methyl 4-amino-3-methoxybenzoate (16)



To a stirred solution of **S16** (2.11 g, 10 mmol) in EtOH (60 mL), iron powder (2.80 g, 50 mmol) was added at 55 °C followed by an aqueous solution of NH_4Cl (266 mg, 5 mmol in 30 mL). The reaction mixture was heated at 90 °C for 1 h, then iron was filtered off while the suspension was still hot and the filtrate was concentrated *in vacuo*. The residue was diluted with water (30 mL) and treated with a saturated aqueous solution of NaHCO_3 (to pH 7–8). The reaction mixture was extracted with EtOAc (3 \times 30 mL). The combined organic extracts were washed with brine, dried over anhydrous MgSO_4 , and the solvent was removed by vacuum distillation. The obtained material was triturated with *n*-hexane, and collected by filtration.

Yield 85% (beige crystals); mp: 130–132 °C; $^1\text{H NMR}^{\text{S3}}$ (500 MHz, CDCl_3) δ 7.55 (dd, $J = 8.2, 1.6$ Hz, 1H), 7.46 (d, $J = 1.6$ Hz, 1H), 6.67 (d, $J = 8.2$ Hz, 1H), 4.24 (br s, 2H), 3.90 (s, 3H), 3.87 (s, 3H); $^{13}\text{C NMR}^{\text{S3}}$ (126 MHz, CDCl_3) δ 167.29 (Cq), 146.09 (Cq), 140.99 (Cq), 124.02 (CH), 119.49 (Cq), 113.11 (CH), 111.10 (CH), 55.56 (CH_3), 51.68 (CH_3); m/z (ESI+) 182 $[\text{M} + \text{H}]^+$.

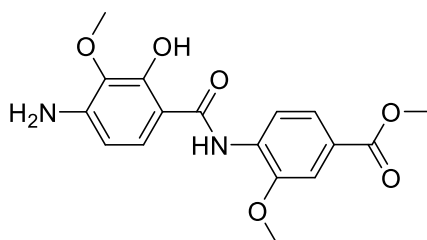
Methyl 4-(2-hydroxy-3-methoxy-4-nitrobenzamido)-3-methoxybenzoate (17)



To a stirred solution of arene **15** (213 mg, 1 mmol) in a mixture of xylenes (30 mL) and CH_2Cl_2 (5 mL), arene **16** (181 mg, 1 mmol) was added. The reaction mixture was heated to 60 °C and then PCl_3 (0.05 mL, 0.5 mmol) was added. The reaction mixture was heated at 150 °C for 12 h. The solvent was removed by vacuum distillation. The residue was dissolved in MeOH and mixed with silica gel and the resulting paste was dried *in vacuo*. The silica adsorbed material was purified using flash chromatography (SiO_2 , *n*-hexane/EtOAc = 1:1).

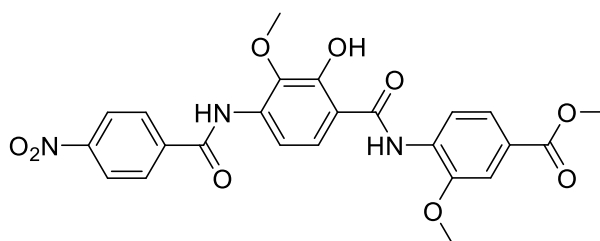
Yield 50% (yellow solid); mp: 189–191 °C; $^1\text{H NMR}$ (500 MHz, CDCl_3) δ 12.07 (br s, 1H), 9.02 (br s, 1H), 8.51 (d, $J = 8.5$ Hz, 1H), 7.77 (dd, $J = 8.5, 1.9$ Hz, 1H), 7.64 (d, $J = 1.9$ Hz, 1H), 7.43 (d, $J = 8.8$ Hz, 1H), 7.30 (d, $J = 8.8$ Hz, 1H), 4.09 (s, 3H), 4.05 (s, 3H), 3.94 (s, 3H); $^{13}\text{C NMR}$ (126 MHz, CDCl_3) δ 166.43 (Cq), 166.32 (Cq), 156.64 (Cq), 147.93 (Cq), 146.76 (Cq), 142.87 (Cq), 130.28 (Cq), 126.55 (Cq), 123.35 (CH), 120.54 (CH), 119.47 (CH), 118.99 (Cq), 113.54 (CH), 110.94 (CH), 62.01 (CH_3), 56.34 (CH_3), 52.28 (CH_3); m/z (ESI+) 377 $[\text{M} + \text{H}]^+$.

Methyl 4-(4-amino-2-hydroxy-3-methoxybenzamido)-3-methoxybenzoate (S17)

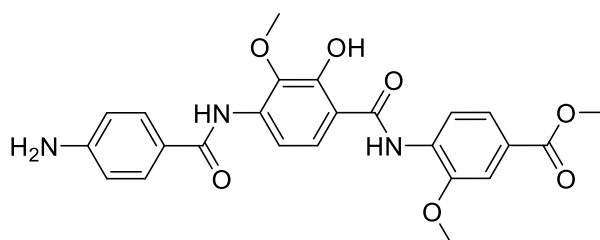


To a stirred solution of **17** (150 mg, 0.4 mmol) in EtOH (20 mL), iron powder (112 mg, 2 mmol) was added at 55 °C followed by NH_4Cl (11 mg, 0.2 mmol) solution in water (2 mL). The reaction was heated at 90 °C for 1 h, then iron was filtered while hot and the filtrate was concentrated *in vacuo*. The residue was diluted with water (20 mL) and treated with a saturated aqueous solution NaHCO_3 (to pH 7–8). The reaction mixture was extracted with EtOAc (3×20 mL). The combined organic extracts were washed with brine, dried over anhydrous MgSO_4 , and the solvent was removed by vacuum distillation. The obtained material was triturated with *n*-hexane, and collected by filtration.

Yield 95% (pale yellow solid); m/z (ESI+) 347 $[\text{M} + \text{H}]^+$.

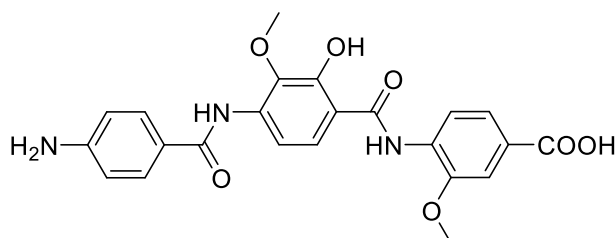
Methyl 4-[2-hydroxy-3-methoxy-4-(4-nitrobenzamido)benzamido]-3-methoxybenzoate (S18)

To a stirred solution of **S17** (115 mg, 0.33 mmol), **14** (56 mg, 0.33 mmol) in anhydrous CHCl_3 (30 mL) under a nitrogen atmosphere, dichlorotriphenylphosphorane (500 mg, 1.5 mmol) was added. The reaction mixture was heated at 80 °C for 12 h. The solvent was removed by vacuum distillation. The residue was dissolved in toluene and purified by flash chromatography (SiO_2 , *n*-hexane/EtOAc = 1:1). Yield 92% (yellow crystals); m/z (ESI+) 496 $[\text{M} + \text{H}]^+$.

Methyl 4-[4-(4-aminobenzamido)-2-hydroxy-3-methoxybenzamido]-3-methoxybenzoate (S19)

To a stirred solution of **S18** (124 mg, 0.25 mmol) in EtOH (20 mL), iron powder (70 mg, 1.25 mmol) was added at 55 °C followed by an aqueous solution of NH_4Cl (7 mg, 0.12 mmol in 2 mL). The reaction mixture was heated at 90 °C for 1 h, then iron was filtered while hot and the filtrate was concentrated *in vacuo*. The residue was diluted with water (15 mL) and treated with a saturated aqueous solution of NaHCO_3 (to pH 7–8). The reaction mixture was extracted with EtOAc/THF (1:1, 3 × 20 mL). The combined organic extracts were washed with brine, dried over anhydrous MgSO_4 , and the solvent was removed by vacuum distillation. The obtained material was triturated with *n*-hexane/EtOAc (6:1, 50 mL), and collected by filtration.

Yield 90% (white crystals); m/z (ESI+) 466 $[\text{M} + \text{H}]^+$.

4-[4-(4-Aminobenzamido)-2-hydroxy-3-methoxybenzamido]-3-methoxybenzoic acid (18)

To a stirred solution of **S19** (46 mg, 0.1 mmol) in a mixture of MeOH (3 mL) and THF (1 mL), NaOH 1 M (0.5 mL) was added. The reaction mixture was stirred at room temperature overnight. The solvent was evaporated *in vacuo*. The remaining residue was dissolved in water (10 mL), cooled in an ice bath and acidified by a saturated aqueous solution KHSO_4 (to pH 6), then extracted with EtOAc/THF (1:1,

3 × 20 mL). The combined organic extracts were washed with brine, dried over anhydrous MgSO₄, and the solvent was removed by vacuum distillation. The obtained material was triturated with *n*-hexane/EtOAc (4:1, 25 mL), and collected by filtration.

Yield 82% (pale yellow crystals); mp: 219–221 °C; ¹H NMR (500 MHz, DMSO-*d*₆) δ 12.71 (br s, 1H), 11.55 (br s, 1H), 10.96 (br s, 1H), 9.16 (br s, 1H), 8.46 (d, *J* = 8.2 Hz, 1H), 7.80 (d, *J* = 8.8 Hz, 1H), 7.71 (d, *J* = 8.8 Hz, 2H), 7.66 (d, *J* = 8.8 Hz, 1H), 7.62 (dd, *J* = 8.2, 1.6 Hz, 1H), 7.57 (d, *J* = 1.6 Hz, 1H), 6.63 (d, *J* = 8.8 Hz, 2H), 5.86 (br s, 2H), 3.97 (s, 3H), 3.78 (s, 3H); ¹³C NMR (126 MHz, DMSO-*d*₆) δ 166.99 (Cq), 165.03 (Cq), 163.83 (Cq), 152.60 (Cq), 149.96 (Cq), 148.43 (Cq), 139.10 (Cq), 136.47 (Cq), 131.95 (Cq), 129.42 (2CH), 125.91 (Cq), 125.23 (CH), 122.68 (CH), 120.25 (Cq), 119.63 (CH), 115.01 (Cq), 113.63 (CH), 112.77 (2CH), 111.15 (CH), 60.44 (CH₃), 56.17 (CH₃); *m/z* (ESI+) 452 [M + H]⁺.

6.2.4 Biological evaluation

Compounds **3** and **18** have been tested in antimicrobial susceptibility and *in vitro* gyrase assays as described previously.^{S4} The IC₅₀ values on *E. coli* gyrase of synthetic **3** and **18** were 328 μM and 463 μM, respectively.

6.2.5 Reference supporting information

- S1. Wriede, U.; Fernandez, M.; West, K. F.; Harcour, D.; Moore, H. W. *J. Org. Chem.* **1987**, *52*, 4485–4489.
- S2. Kato, S.; Morie, T. *J. Heterocyclic Chem.* **1996**, *33*, 1171–1178.
- S3. Mok, N. Y.; Chadwick, J.; Kellett, K. A. B.; Casas-Arce, E.; Hooper, N. M.; Johnson, A. P.; Fishwick, C. W. G. *J. Med. Chem.* **2013**, *56*, 1843–1852.
- S4. Baumann, S.; Herrmann, J.; Raju, R.; Steinmetz, H.; Mohr, K. I.; Hüttel, S.; Harmrolfs, K.; Stadler, M.; Müller, R. *Angew. Chem. Int. Ed.* **2014**, *53*, 14605–14609.

6.3 Supporting Information for Manuscript IV

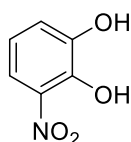
6.3.1 Materials and Methods

Starting materials and solvents were purchased from commercial suppliers, and used without further purification. All chemical yields refer to purified compounds and were not optimized. Reaction progress was monitored using TLC silica gel 60 F₂₅₄ aluminum sheets, and visualization was accomplished by UV at 254 nm. Flash chromatography was performed using silica gel 60 Å (40–63 μm). Preparative RP-HPLC was carried out on a Waters Corporation setup containing a 2767 sample manager, a 2545 binary gradient module, a 2998 PDA detector and a 3100 electron spray mass spectrometer. Purification was performed using a Waters XBridge column (C18, 150 mm × 19 mm, 5 μm), a binary solvent system A and B (A = water with 0.1% formic acid; B = MeCN with 0.1% formic acid) as eluent, a flow rate of 20 mL/min, and a gradient of 60% to 95% B in 8 min were applied. Melting points were determined on a Stuart Scientific melting point apparatus SMP3 (Bibby Sterilin, UK), and are uncorrected. NMR spectra were recorded on either a Bruker DRX-500 (¹H, 500 MHz; ¹³C, 126 MHz) or Bruker Fourier 300 (¹H, 300 MHz; ¹³C, 75 MHz) spectrometer at 300 K. Chemical shifts were recorded as δ values in ppm units by reference to the hydrogenated residues of deuterated solvent as internal standard (CDCl₃, δ = 7.27, 77.00; DMSO-d₆, δ = 2.50, 39.51, acetone-d₆: δ = 2.05, 29.92, 206.68). Splitting patterns describe apparent multiplicities and are designated as s (singlet), br s (broad singlet), d (doublet), dd (doublet of doublet), t (triplet), q (quartet), m (multiplet). Coupling constants (*J*) are given in hertz (Hz). Weak or coalesced signals were elucidated by heteronuclear multiple quantum coherence (HMQC) and heteronuclear multiple bond coherence (HMBC) 2D-NMR techniques. Purity of all compounds used in biological assays was ≥ 95% as measured by LC/MS Finnigan Surveyor MSQ Plus (Thermo Fisher Scientific, Dreieich, Germany). The system consists of LC pump, autosampler, PDA detector, and single-quadrupole MS detector, as well as the standard software Xcalibur for operation. RP C18 Nucleodur 100-5 (125 mm × 3 mm) column (Macherey-Nagel GmbH, Dühren, Germany) was used as stationary phase, and a binary solvent system A and B (A = water with 0.1% TFA; B = MeCN with 0.1% TFA) was used as mobile phase. In a gradient run the percentage of B was increased from an initial concentration of 0% at 0 min to 100% at 15 min and kept at 100% for 5 min. The injection volume was 10 μL and flow rate was set to 800 μL/min. MS (ESI) analysis was carried out at a spray voltage of 3800 V, a capillary temperature of 350 °C, and a source CID of 10 V. Spectra were acquired in positive mode from 100 to 1000 *m/z* and at 254 nm for UV tracing.

6.3.2 Chemistry

Synthesis and experimental data of compounds **21–23** and **86** were described in a previous work.¹ Compounds **40**, **41** and **55** are commercially available.

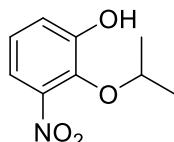
3-Nitrobenzene-1,2-diol **17**



To a stirred solution of catechol (20.0 g, 182 mmol) in diethyl ether (450 mL) cooled at 0 °C in an ice bath, fuming HNO₃ (9 mL) was added dropwise. The reaction mixture was allowed to warm to room temperature and was further stirred for 24 h. Solvent was removed *in vacuo*. The residue was dissolved in EtOAc and purified using flash chromatography (SiO₂, *n*-hexane–EtOAc = 4:1).

Yield 50%; yellow crystals; ¹H NMR (300 MHz, CDCl₃) δ 10.63 (br s, 1H), 7.66 (dd, *J* = 8.7, 1.4 Hz, 1H), 7.25 (dq, *J* = 8.1, 0.7 Hz, 1H), 6.91 (dd, *J* = 8.7, 8.1 Hz, 1H), 5.87 (br s, 1H); ¹³C NMR (75 MHz, CDCl₃) δ 146.50, 142.77, 133.74, 121.67, 119.74, 115.80; *m/z* (ESI+) 155 [M]⁺.

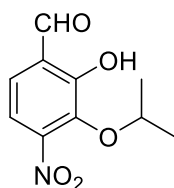
2-Isopropoxy-3-nitrophenol **18**



To a stirred mixture of **17** (12.41 g, 80 mmol) and K₂CO₃ (11.06 g, 80 mmol) in DMF (120 mL), 2-bromopropane (9.84 g, 80 mmol) was added. The reaction mixture was stirred at 90 °C overnight. Solvent was evaporated *in vacuo*. The residue was diluted with water (200 mL) and the medium was acidified cautiously by KHSO₄ (saturated aqueous solution) to pH 4–5. The resulting mixture was extracted with EtOAc (3 × 200 mL). The combined organic extract was washed with brine, dried over anhydrous MgSO₄, and the solvent was removed by vacuum distillation. The residue was purified using flash chromatography (SiO₂, *n*-hexane–EtOAc = 5:1 to 3:1).

Yield 60%; yellow oil; ¹H NMR (300 MHz, CDCl₃) δ 7.47 (dd, *J* = 8.2, 1.7 Hz, 1H), 7.22 (dd, *J* = 8.2, 1.7 Hz, 1H), 7.09 (t, *J* = 8.2 Hz, 1H), 6.05 (br s, 1H), 4.32 (septet, *J* = 6.1 Hz, 1H), 1.37 (d, *J* = 6.1 Hz, 6H); ¹³C NMR (75 MHz, CDCl₃) δ 151.35, 142.97, 138.61, 123.95, 120.07, 116.97, 79.58, 22.46 (2C); *m/z* (ESI+) 198 [M + H]⁺.

2-Hydroxy-3-isopropoxy-4-nitrobenzaldehyde **19**

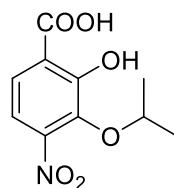


To a stirred mixture of **18** (2.96 g, 15 mmol), anhydrous MgCl₂ (7.14 g, 75 mmol) and dry TEA (Na) (15.18 g, 150 mmol) in dry MeCN (molecular sieve) (75 mL), dry paraformaldehyde (Al₂O₃) (3.15 g, 105 mmol) was added under a nitrogen atmosphere. The reaction mixture was stirred at 90 °C for 24 h. The reaction was quenched with water (100 mL) and the medium was acidified by 37% HCl to pH 4–5. The mixture was extracted with EtOAc (3 × 100 mL). The combined organic extract was washed with brine, dried over anhydrous MgSO₄, and the solvent was removed by vacuum distillation. The residue was purified using flash chromatography (SiO₂, *n*-hexane–EtOAc = 3:1).

Yield 40%; yellow oil; ¹H NMR (500 MHz, CDCl₃) δ 11.44 (br s, 1H), 9.98 (s, 1H), 7.39 (d, *J* = 8.5 Hz, 1H), 7.24 (d, *J* = 8.5 Hz, 1H), 4.89 (septet, *J* = 6.3 Hz, 1H), 1.33 (d, *J* = 6.3 Hz, 6H); ¹³C NMR

(126 MHz, CDCl₃) δ 196.24, 156.36, 149.19, 139.57, 127.12, 122.42, 114.15, 77.25, 22.32 (2C); m/z (ESI+) 225 [M]⁺.

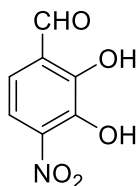
2-Hydroxy-3-isopropoxy-4-nitrobenzoic acid **20**



To a stirred solution of **19** (901 mg, 4 mmol) and NaOH (640 mg, 16 mmol) in water (30 mL), AgNO₃ (2.04 g, 12 mmol) was added. The reaction mixture was stirred at 100 °C overnight. The medium was adjusted to pH 9–10 by NaHCO₃ (saturated aqueous solution), if necessary, and was filtered through a pad of diatomaceous earth. The filtrate was cooled in an ice bath and was carefully acidified by 37% HCl to pH 3–4. The precipitated solid was collected by filtration, washed with cold water then *n*-hexane.

Yield 55%; yellow solid; ¹H NMR (500 MHz, DMSO-*d*₆) δ 7.66 (d, *J* = 8.8 Hz, 1H), 7.28 (d, *J* = 8.8 Hz, 1H), 4.75 (septet, *J* = 6.0 Hz, 1H), 1.20 (d, *J* = 6.0 Hz, 6H); ¹³C NMR (126 MHz, DMSO-*d*₆) δ 171.22, 155.94, 148.28, 138.01, 124.75, 116.98, 112.63, 75.87, 22.08 (2C); m/z (ESI+) 241 [M]⁺.

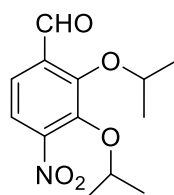
2,3-Dihydroxy-4-nitrobenzaldehyde **24**



To a stirred solution of **22** (1.2 g, 5 mmol) in DCM (10 mL) cooled at 0 °C in an ice bath, BBr₃ (1 M solution in DCM, 20 mL) was added carefully under a nitrogen atmosphere. The reaction mixture was allowed to warm to room temperature and was further stirred overnight. Solvent was removed *in vacuo*. The residue was cautiously diluted with water (50 mL) and the medium was acidified by 2 N HCl to pH 4–5, if necessary. The mixture was extracted with EtOAc (3 × 30 mL). The combined organic extract was washed with brine, dried over anhydrous MgSO₄, and the solvent was removed by vacuum distillation. The residue was dissolved in CHCl₃ and purified using flash chromatography (SiO₂, DCM–MeOH = 98:2).

Yield 68%; red crystals; ¹H NMR (500 MHz, CDCl₃) δ 11.20 (br s, 1H), 10.60 (br s, 1H), 10.04 (s, 1H), 7.75 (d, *J* = 8.8 Hz, 1H), 7.25 (d, *J* = 8.8 Hz, 1H); ¹³C NMR (126 MHz, CDCl₃) δ 195.87, 152.88, 145.63, 136.27, 123.09, 121.42, 114.52; m/z (ESI+) 183 [M]⁺; t_R = 9.54 min.

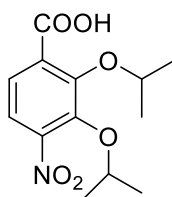
2,3-Diisopropoxy-4-nitrobenzaldehyde **25**



To a stirred mixture of **24** (732 mg, 4 mmol) and K_2CO_3 (1.38 g, 10 mmol) in DMF (20 mL), 2-bromopropane (1.48 g, 12 mmol) was added. The reaction mixture was stirred at 80 °C overnight. Solvent was evaporated *in vacuo*, and the residue was diluted with water (30 mL). The resulting mixture was extracted with EtOAc (3 × 30 mL). The combined organic extract was washed with brine, dried over anhydrous $MgSO_4$, and the solvent was removed by vacuum distillation. The residue was dissolved in toluene and purified using flash chromatography (SiO_2 , *n*-hexane–EtOAc = 6:1).

Yield 76%; yellow oil; 1H NMR (500 MHz, $CDCl_3$) δ 10.42 (s, 1H), 7.65 (d, $J = 8.5$ Hz, 1H), 7.48 (d, $J = 8.5$ Hz, 1H), 4.82 (septet, $J = 6.0$ Hz, 1H), 4.70 (septet, $J = 6.3$ Hz, 1H), 1.35 (d, $J = 6.0$ Hz, 6H), 1.31 (d, $J = 6.3$ Hz, 6H); ^{13}C NMR (126 MHz, $CDCl_3$) δ 189.07, 155.51, 150.01, 145.03, 133.69, 122.21, 118.94, 77.56, 77.21, 22.24 (2C), 22.22 (2C); m/z (ESI+) 267 [M]⁺; $t_R = 16.45$ min.

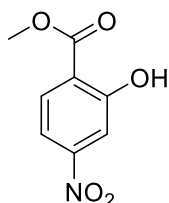
2,3-Diisopropoxy-4-nitrobenzoic acid **26**



To a stirred solution of **25** (1.07 g, 4 mmol) in acetone (12 mL), $KMnO_4$ (1.26 g, 8 mmol) solution in 50% aq. acetone (28 mL) was added. The reaction mixture was stirred at room temperature for 24 h, then 1 N NaOH (5 mL) was added. The resulting mixture was filtered through a pad of diatomaceous earth, and the filtrate was concentrated *in vacuo*. The residue was cooled in an ice bath and carefully acidified by $KHSO_4$ (saturated aqueous solution) to pH 4–5, then extracted with EtOAc (3 × 25 mL). The combined organic extract was washed with brine, dried over anhydrous $MgSO_4$, and the solvent was removed by vacuum distillation. The obtained material was triturated with *n*-hexane (25 mL), and collected by filtration.

Yield 90%; beige crystals; 1H NMR (500 MHz, $DMSO-d_6$) δ 13.43 (br s, 1H), 7.61 (d, $J = 8.5$ Hz, 1H), 7.48 (d, $J = 8.5$ Hz, 1H), 4.68 (septet, $J = 6.0$ Hz, 1H), 4.49 (septet, $J = 6.3$ Hz, 1H), 1.22 (d, $J = 6.3$ Hz, 6H), 1.18 (d, $J = 6.0$ Hz, 6H); ^{13}C NMR (126 MHz, $DMSO-d_6$) δ 166.37, 150.26, 147.38, 143.72, 132.73, 124.38, 118.36, 76.81, 76.40, 22.04 (2C), 21.93 (2C); m/z (ESI+) 283 [M]⁺; $t_R = 14.09$ min.

Methyl 2-hydroxy-4-nitrobenzoate **27**

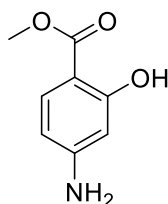


To a stirred solution of 2-hydroxy-4-nitrobenzoic acid **41** (1.10 g, 6 mmol) in MeOH (20 mL), concd H_2SO_4 (2 mL) was added drop wise. The reaction mixture was stirred at 70 °C overnight, then solvent was concentrated *in vacuo*. The residue was diluted with water (25 mL) and neutralized by Na_2CO_3 (saturated aqueous solution) to pH 7–8. The mixture was extracted with EtOAc (3 × 25 mL). The

combined organic extract was washed with brine, dried over anhydrous MgSO_4 , and the solvent was evaporated by vacuum distillation. The obtained material was triturated with *n*-hexane (50 mL), and collected by filtration.

Yield 96%; yellow crystals; ^1H NMR (300 MHz, CDCl_3) δ 10.98 (br s, 1H), 8.03 (d, $J = 8.8$ Hz, 1H), 7.82 (d, $J = 2.2$ Hz, 1H), 7.71 (dd, $J = 8.8, 2.2$ Hz, 1H), 4.03 (s, 3H); ^{13}C NMR (75 MHz, CDCl_3) δ 169.24, 161.99, 152.15, 131.21, 117.14, 113.50, 113.04, 53.09; m/z (ESI+) 198 $[\text{M} + \text{H}]^+$; $t_{\text{R}} = 13.68$ min.

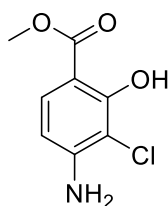
Methyl 4-amino-2-hydroxybenzoate **28**



To a stirred solution of **27** (986 mg, 5 mmol) in EtOH (40 mL), iron powder (1.40 g, 25 mmol) was added at 55 °C followed by NH_4Cl (134 mg, 2.5 mmol) solution in water (15 mL). The reaction mixture was stirred at 90 °C for 1 h, then iron was filtered on hot and the filtrate was concentrated *in vacuo*. The residue was diluted with water (25 mL) and basified by NaHCO_3 (saturated aqueous solution) to pH 8–9. The mixture was extracted with EtOAc (3×25 mL). The combined organic extract was washed with brine, dried over anhydrous MgSO_4 , and the solvent was removed by vacuum distillation. The obtained material was triturated with *n*-hexane (25 mL), and collected by filtration.

Yield 80%; beige crystals; ^1H NMR (300 MHz, CDCl_3) δ 10.93 (br s, 1H), 7.62 (d, $J = 8.9$ Hz, 1H), 6.17 (d, $J = 2.2$ Hz, 1H), 6.15 (dd, $J = 8.9, 2.2$ Hz, 1H), 4.10 (br s, 2H), 3.88 (s, 3H); ^{13}C NMR (75 MHz, CDCl_3) δ 170.45, 163.58, 153.33, 131.63, 106.80, 103.05, 100.76, 51.72; m/z (ESI+) 168 $[\text{M} + \text{H}]^+$; $t_{\text{R}} = 9.83$ min.

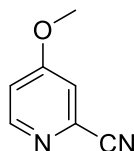
Methyl 4-amino-3-chloro-2-hydroxybenzoate **29**



To a stirred solution of **28** (1 g, 6 mmol) in DMF (20 mL), *N*-chlorosuccinimide (801 mg, 6 mmol) solution in DMF (5 mL) was added drop wise. The reaction mixture was stirred at 40 °C overnight, then solvent was removed *in vacuo*. The residue was diluted with water (50 mL) and basified by Na_2CO_3 (saturated aqueous solution) to pH 8–9. The mixture was extracted with EtOAc (3×30 mL). The combined organic extract was washed with brine, dried over anhydrous MgSO_4 , and the solvent was removed by vacuum distillation. The residue was dissolved in CHCl_3 and purified using flash chromatography (SiO_2 , *n*-hexane–EtOAc = 4:1).

Yield 70%; white crystals; $^1\text{H NMR}$ (300 MHz, CDCl_3) δ 11.61 (br s, 1H), 7.57 (d, $J = 8.8$ Hz, 1H), 6.28 (d, $J = 8.8$ Hz, 1H), 4.59 (br s, 2H), 3.91 (s, 3H); $^{13}\text{C NMR}$ (75 MHz, CDCl_3) δ 170.42, 158.90, 149.26, 128.78, 106.10, 104.93, 103.31, 52.01; m/z (ESI+) 202 $[\text{M} + \text{H}]^+$; $t_{\text{R}} = 13.10$ min.

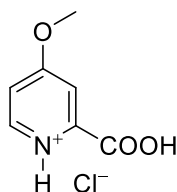
4-Methoxypicolinonitrile **30**



To a stirred solution of 4-methoxypyridine-*N*-oxide hydrate (2.50 g, 20 mmol) in DCM (25 mL), trimethylsilyl cyanide (2.58 g, 26 mmol) was added. The reaction mixture was stirred at room temperature for 10 min, then dimethylcarbamoyl chloride (2.80 g, 26 mmol) was added portion wise, and the reaction was further stirred at room temperature for 24 h. The reaction was quenched carefully with K_2CO_3 10% (25 mL) and allowed to stir for 15 min. The organic layer was separated and aqueous layer was extracted with DCM (2×20 mL) then diethyl ether (1×20 mL). The combined organic extract was dried over anhydrous MgSO_4 , and the solvent was removed by vacuum distillation. The residue was triturated with *n*-hexane (50 mL), and collected by filtration.

Yield 70%; white crystals; $^1\text{H NMR}$ (300 MHz, CDCl_3) δ 8.51 (d, $J = 5.8$ Hz, 1H), 7.22 (d, $J = 2.5$ Hz, 1H), 7.01 (dd, $J = 5.8, 2.5$ Hz, 1H), 3.91 (s, 3H); $^{13}\text{C NMR}$ (75 MHz, CDCl_3) δ 165.92, 152.23, 134.99, 117.12, 115.37, 112.61, 55.80; m/z (ESI+) 135 $[\text{M} + \text{H}]^+$; $t_{\text{R}} = 8.27$ min.

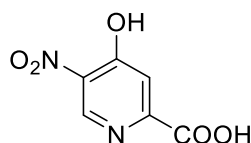
2-Carboxy-4-methoxypyridin-1-ium chloride **31**



To the picolinonitrile **30** (1.61 g, 12 mmol), 5 N HCl (40 mL) was added. The reaction mixture was stirred at 100°C overnight, then solvent was evaporated to dryness. The obtained material was triturated with *n*-hexane (50 mL), and collected by filtration.

Yield 95%; white crystals; $^1\text{H NMR}$ (300 MHz, DMSO-d_6) δ 9.80 (br s, 1H), 8.71 (d, $J = 6.5$ Hz, 1H), 7.81 (d, $J = 2.7$ Hz, 1H), 7.62 (dd, $J = 6.5, 2.7$ Hz, 1H), 7.47 (t, $J = 50.0$ Hz, 3H), 4.10 (s, 3H); $^{13}\text{C NMR}$ (75 MHz, DMSO-d_6) δ 171.09, 161.45, 145.70, 144.30, 114.16, 112.97, 57.77; m/z (ESI+) 154 $[\text{M} - \text{Cl}]^+$; $t_{\text{R}} = 1.48$ min.

4-Hydroxy-5-nitropicolinic acid **32**

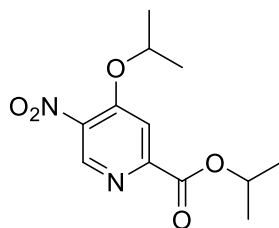


To the picolinic acid hydrochloride salt **31** (3.79 g, 20 mmol), concd H_2SO_4 (8 mL) was carefully added. The mixture was stirred for 5 min then a mixture of concd H_2SO_4 (2 mL) and fuming HNO_3 (10 mL)

was added. The reaction mixture was stirred at 150 °C for 48 h, then it was cooled in an ice bath and carefully neutralized with NH₄OH 25% till pH 6–7. The pale yellow precipitate was collected by filtration, washed with cold water and *n*-hexane. Filtrate was extracted with THF (3 × 30 mL). The combined organic extract was dried over anhydrous MgSO₄, and the solvent was removed by vacuum distillation. The residue was triturated with *n*-hexane (50 mL), and filtered to afford a second crop of the product.

Yield 50%; pale yellow solid; ¹H NMR (500 MHz, DMSO-*d*₆) δ 8.50 (s, 1H), 7.56 (br s, 2H), 6.77 (s, 1H); ¹³C NMR (126 MHz, DMSO-*d*₆) δ 169.66, 161.54, 145.32, 139.14, 137.77, 120.95; *m/z* (ESI+) 185 [M + H]⁺; *t*_R = 1.16 min.

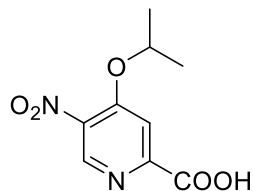
Isopropyl 4-isopropoxy-5-nitropicolinate **33**



To a stirred mixture of **32** (921 mg, 5 mmol) and K₂CO₃ (1.38 g, 10 mmol) in DMF (25 mL), 2-bromopropane (1.84 g, 15 mmol) was added. The reaction mixture was stirred at 90 °C overnight. Solvent was evaporated *in vacuo*, and the residue was diluted with water (30 mL). The resulting mixture was extracted with EtOAc (3 × 30 mL). The combined organic extract was washed with brine, dried over anhydrous MgSO₄, and the solvent was removed by vacuum distillation. The residue was dissolved in toluene and purified using flash chromatography (SiO₂, *n*-hexane–EtOAc = 1:1).

Yield 75%; pale yellow crystals; ¹H NMR (500 MHz, CDCl₃) δ 8.93 (s, 1H), 7.77 (s, 1H), 5.28 (septet, *J* = 6.3 Hz, 1H), 4.88 (septet, *J* = 6.0 Hz, 1H), 1.42 (d, *J* = 6.0 Hz, 6H), 1.38 (d, *J* = 6.3 Hz, 6H); ¹³C NMR (126 MHz, CDCl₃) δ 163.24, 157.82, 152.31, 146.56, 138.47, 111.21, 73.77, 70.58, 21.56 (2C), 21.39 (2C); *m/z* (ESI+) 269 [M + H]⁺; *t*_R = 15.57 min.

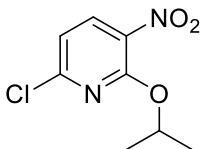
4-Isopropoxy-5-nitropicolinic acid **34**



To a stirred solution of **33** (536 mg, 2 mmol) in MeOH (10 mL), 1 N NaOH (5 mL) was added. The reaction was stirred at room temperature overnight. Solvent was evaporated *in vacuo*. The remaining residue was dissolved in water (15 mL), cooled in an ice bath and acidified by KHSO₄ (saturated aqueous solution) to pH 6, then extracted with EtOAc/THF (1:1, 3 × 30 mL). The combined organic extract was washed with brine, dried over anhydrous MgSO₄, and the solvent was removed by vacuum distillation. The obtained material was triturated with *n*-hexane (30 mL), and collected by filtration.

Yield 85%; beige solid; $^1\text{H NMR}$ (500 MHz, DMSO-d_6) δ 13.76 (br s, 1H), 9.03 (s, 1H), 7.90 (s, 1H), 5.13 (septet, $J = 6.0$ Hz, 1H), 1.35 (d, $J = 6.0$ Hz, 6H); $^{13}\text{C NMR}$ (126 MHz, DMSO-d_6) δ 164.97, 157.17, 152.76, 146.07, 138.42, 111.53, 73.62, 21.28 (2C); m/z (ESI+) 227 $[\text{M} + \text{H}]^+$; $t_{\text{R}} = 12.88$ min.

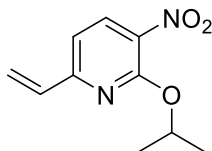
6-Chloro-2-isopropoxy-3-nitropyridine **35**



To a stirred solution of 2,6-dichloro-3-nitropyridine (3.86 g, 20 mmol) in toluene (30 mL) cooled at 0 °C in an ice bath, 2-propanol (1.44 g, 24 mmol) was added. The reaction mixture was stirred at 0 °C for 15 min, then NaH (50–60% in mineral oil, 1.22 g, 28 mmol) was added portion wise under a nitrogen atmosphere, and the reaction was further stirred at room temperature overnight. The reaction was quenched with brine, then diluted with water and extracted with EtOAc (3×30 mL). The combined organic extract was dried over anhydrous MgSO_4 , and the solvent was removed by vacuum distillation. The residue was dissolved in toluene and purified using flash chromatography (SiO_2 , n -hexane–EtOAc = 5:1).

Yield 70%; yellowish white crystals; $^1\text{H NMR}$ (300 MHz, CDCl_3) δ 8.22 (d, $J = 8.2$ Hz, 1H), 6.98 (d, $J = 8.2$ Hz, 1H), 5.51 (septet, $J = 6.2$ Hz, 1H), 1.44 (d, $J = 6.2$ Hz, 6H); $^{13}\text{C NMR}$ (75 MHz, CDCl_3) δ 155.71, 152.72, 137.33, 132.66, 115.88, 72.48, 21.71 (2C); m/z (ESI+) 217 $[\text{M} + \text{H}]^+$; $t_{\text{R}} = 12.82$ min.

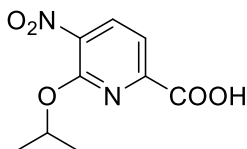
2-Isopropoxy-3-nitro-6-vinylpyridine **36**



To a stirred solution of **35** (650 mg, 3 mmol), and tributyl(vinyl)tin (1.0 g, 3.15 mmol) in toluene (20 mL) under a nitrogen atmosphere, tetrakis(triphenylphosphine) palladium(0) (175 mg, 0.15 mmol) was added. The reaction mixture was stirred at 110 °C overnight. The reaction was quenched with brine, then extracted with EtOAc (3×25 mL). The combined organic extract was dried over anhydrous MgSO_4 , and the solvent was removed by vacuum distillation. The obtained material was purified using flash chromatography (SiO_2 , n -hexane–EtOAc = 6:1).

Yield 90%; yellow oil; $^1\text{H NMR}$ (500 MHz, CDCl_3) δ 8.22 (d, $J = 8.2$ Hz, 1H), 6.90 (d, $J = 8.2$ Hz, 1H), 6.73 (dd, $J = 17.3, 10.7$ Hz, 1H); 6.38 (dd, $J = 17.3, 1.6$ Hz, 1H); 5.63 (dd, $J = 10.7, 1.6$ Hz, 1H); 5.58 (septet, $J = 6.3$ Hz, 1H), 1.44 (d, $J = 6.3$ Hz, 6H); $^{13}\text{C NMR}$ (126 MHz, CDCl_3) δ 157.40, 155.57, 135.88, 134.92, 132.83, 122.37, 113.86, 70.67, 21.79 (2C); m/z (ESI+) 208 $[\text{M}]^+$; $t_{\text{R}} = 13.37$ min.

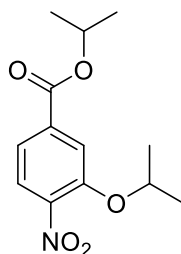
6-isopropoxy-5-nitropicolinic acid **37**



To a stirred solution of **36** (625 mg, 3 mmol) in acetone (10 mL), KMnO_4 (1.90 g, 12 mmol) solution in 50% aq. acetone (50 mL) was added. The reaction mixture was stirred at room temperature for 24 h, then 1 N NaOH (3 mL) was added. The resulting mixture was filtered through a pad of diatomaceous earth, and the filtrate was concentrated *in vacuo*. The residue was cooled in an ice bath and carefully acidified by KHSO_4 (saturated aqueous solution) to pH 4–5, then extracted with EtOAc (3×25 mL). The combined organic extract was washed with brine, dried over anhydrous MgSO_4 , and the solvent was removed by vacuum distillation. The obtained material was triturated with *n*-hexane (25 mL), and collected by filtration.

Yield 75%; beige crystals; ^1H NMR (500 MHz, DMSO-d_6) δ 13.64 (br s, 1H), 8.50 (d, $J = 7.9$ Hz, 1H), 7.75 (d, $J = 7.9$ Hz, 1H), 5.52 (septet, $J = 6.0$ Hz, 1H), 1.35 (d, $J = 6.0$ Hz, 6H); ^{13}C NMR (126 MHz, DMSO-d_6) δ 164.37, 154.12, 149.14, 136.17, 136.09, 117.71, 71.00, 21.51 (2C); m/z (ESI+) 227 $[\text{M} + \text{H}]^+$; $t_{\text{R}} = 9.01$ min.

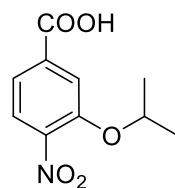
Isopropyl 3-isopropoxy-4-nitrobenzoate **38**



To a stirred mixture of 3-hydroxy-4-nitrobenzoic acid (7.33 g, 40 mmol) and K_2CO_3 (13.8 g, 100 mmol) in DMF (120 mL), 2-bromopropane (14.8 g, 120 mmol) was added. The reaction mixture was stirred at 90 °C overnight. The mixture was poured on to ice cooled water (400 mL) and extracted with EtOAc (3×100 mL). The combined organic extract was washed with brine, dried over anhydrous MgSO_4 , and the solvent was removed by vacuum distillation. The obtained material was used directly in the next step without further purification.

Yield 95%; pale yellow liquid; ^1H NMR (300 MHz, CDCl_3) δ 7.73 (d, $J = 8.0$ Hz, 1H), 7.71 (d, $J = 2.0$ Hz, 1H), 7.61 (dd, $J = 8.0, 2.0$ Hz, 1H), 5.24 (septet, $J = 6.3$ Hz, 1H), 4.75 (septet, $J = 6.0$ Hz, 1H), 1.39 (d, $J = 6.0$ Hz, 6H), 1.37 (d, $J = 6.3$ Hz, 6H); ^{13}C NMR (75 MHz, CDCl_3) δ 164.25, 150.67, 143.56, 135.19, 124.86, 120.92, 116.89, 72.92, 69.54, 21.75 (2C), 21.71 (2C); m/z (ESI+) 268 $[\text{M} + \text{H}]^+$; $t_{\text{R}} = 13.69$ min.

3-Isopropoxy-4-nitrobenzoic acid **39**

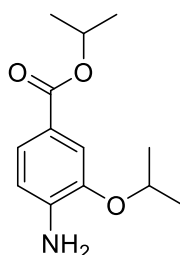


To a stirred solution of **38** (2.67 g, 10 mmol) in MeOH (25 mL), 1 N NaOH (50 mL) was added. The reaction was stirred at 100 °C for 2 h, then solvent was concentrated *in vacuo*. The remaining residue

was diluted with water (25 mL), cooled in an ice bath and acidified by KHSO₄ (saturated aqueous solution) to pH 3–4. The precipitate was collected by filtration, washed with water, then *n*-hexane.

Yield 93%; beige solid; ¹H NMR (500 MHz, DMSO-*d*₆) δ 13.62 (br s, 1H), 7.91 (d, *J* = 8.5 Hz, 1H), 7.76 (d, *J* = 1.6 Hz, 1H), 7.61 (dd, *J* = 8.5, 1.6 Hz, 1H), 4.90 (septet, *J* = 6.0 Hz, 1H), 1.29 (d, *J* = 6.0 Hz, 6H); ¹³C NMR (126 MHz, DMSO-*d*₆) δ 165.86, 149.61, 143.27, 135.43, 124.88, 121.25, 116.53, 72.45, 21.51 (2C); *m/z* (ESI+) 226 [M + H]⁺; *t_R* = 9.69 min.

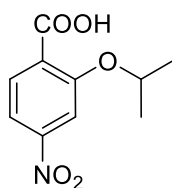
Isopropyl 4-amino-3-isopropoxybenzoate **42**



To a stirred solution of **38** (2.67 g, 10 mmol) in EtOH (60 mL), iron powder (2.80 g, 50 mmol) was added at 55 °C followed by NH₄Cl (266 mg, 5 mmol) solution in water (30 mL). The reaction mixture was stirred at 90 °C for 1 h, then iron was filtered on hot and the filtrate was concentrated *in vacuo*. The residue was diluted with water (30 mL) and basified by NaHCO₃ (saturated aqueous solution) to pH 8–9. The mixture was extracted with EtOAc (3 × 30 mL). The combined organic extract was washed with brine, dried over anhydrous MgSO₄, and the solvent was removed by vacuum distillation. The obtained material was used directly in the next step without further purification.

Yield 90%; pale green liquid; ¹H NMR (300 MHz, CDCl₃) δ 7.54 (dd, *J* = 8.1, 2.0 Hz, 1H), 7.50 (d, *J* = 2.0 Hz, 1H), 6.80 (d, *J* = 8.1 Hz, 1H), 5.21 (septet, *J* = 6.2 Hz, 1H), 4.82 (br s, 2H), 4.65 (septet, *J* = 6.0 Hz, 1H), 1.38 (d, *J* = 6.0 Hz, 6H), 1.35 (d, *J* = 6.2 Hz, 6H); ¹³C NMR (75 MHz, CDCl₃) δ 166.22, 144.94, 139.89, 123.49, 121.73, 114.62, 114.16, 71.00, 67.72, 22.12 (2C), 21.99 (2C); *m/z* (ESI+) 238 [M + H]⁺; *t_R* = 11.62 min.

2-Isopropoxy-4-nitrobenzoic acid **56**



Synthesis of **56** was performed similarly as described for **39** starting with the carboxylic acid **41**.

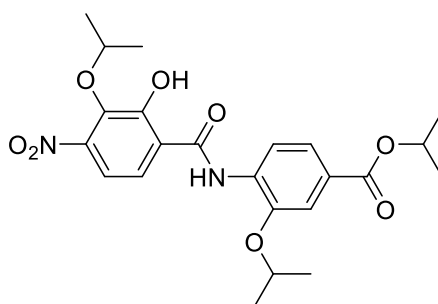
Yield 87%; beige solid; ¹H NMR (500 MHz, DMSO-*d*₆) δ 12.85 (br s, 1H), 7.84 (d, *J* = 2.1 Hz, 1H), 7.80 (dd, *J* = 8.4, 2.1 Hz, 1H), 7.76 (d, *J* = 8.4 Hz, 1H), 4.83 (septet, *J* = 6.0 Hz, 1H), 1.30 (d, *J* = 6.0 Hz, 6H); ¹³C NMR (126 MHz, DMSO-*d*₆) δ 166.60, 155.94, 149.68, 130.70, 129.73, 114.99, 109.38, 71.84, 21.54 (2C); *m/z* (ESI+) 226 [M + H]⁺; *t_R* = 9.48 min.

General procedure for amide coupling using dichlorotriphenylphosphorane

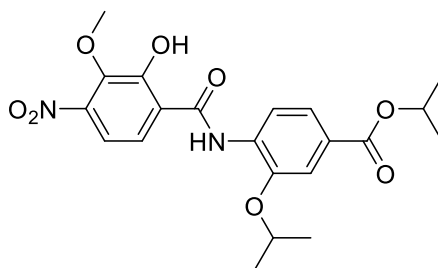
To a stirred solution of the N-protected carboxylic acid (1 mmol) and the C-protected amine (1 mmol) in anhydrous CHCl_3 (50 mL) under a nitrogen atmosphere, dichlorotriphenylphosphorane (1.5 g, 4.5 mmol) was added. The reaction mixture was heated at 80 °C overnight. Solvent was removed by vacuum distillation. The residue was dissolved in toluene and purified using flash chromatography (SiO_2 , *n*-hexane–EtOAc = 4:1 or 2:1 or 1:1).

General procedure for amide coupling using phosphorus trichloride

To a stirred solution of the N-protected carboxylic acid (1 mmol) in a mixture of xylenes (30 mL) and DCM (5 mL), the C-protected amine (1 mmol) was added. The reaction was warmed to 60 °C then phosphorus trichloride (0.05 mL, 0.5 mmol) was added. The reaction mixture was heated at 150 °C overnight. Solvent was removed by vacuum distillation. The residue was dissolved in MeOH and mixed with silica gel and the resulting paste was dried *in vacuo*. The silica adsorbed material was purified using flash chromatography (SiO_2 , *n*-hexane–EtOAc = 1:1).

Isopropyl 4-(2-hydroxy-3-isopropoxy-4-nitrobenzamido)-3-isopropoxybenzoate 43

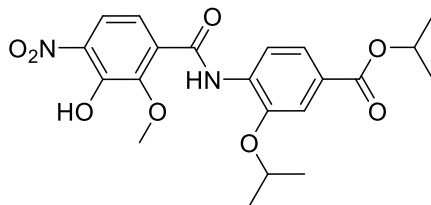
Yield 87%; yellow solid; ^1H NMR (500 MHz, CDCl_3) δ 11.86 (br s, 1H), 9.20 (br s, 1H), 8.51 (d, J = 8.5 Hz, 1H), 7.72 (dd, J = 8.5, 1.9 Hz, 1H), 7.62 (d, J = 1.9 Hz, 1H), 7.37 (d, J = 8.8 Hz, 1H), 7.29 (d, J = 8.8 Hz, 1H), 5.26 (septet, J = 6.3 Hz, 1H), 4.85 (septet, J = 6.0 Hz, 1H), 4.80 (septet, J = 6.0 Hz, 1H), 1.46 (d, J = 6.0 Hz, 6H), 1.39 (d, J = 6.3 Hz, 6H), 1.36 (d, J = 6.0 Hz, 6H); ^{13}C NMR (126 MHz, CDCl_3) δ 166.02, 165.56, 156.26, 147.20, 146.15, 140.59, 131.15, 127.14, 122.95, 120.00, 119.37, 118.88, 113.73, 113.19, 77.59, 72.02, 68.61, 22.37 (2C), 22.17 (2C), 21.94 (2C); m/z (ESI+) 461 [$\text{M} + \text{H}$] $^+$.

Isopropyl 4-(2-hydroxy-3-methoxy-4-nitrobenzamido)-3-isopropoxybenzoate 44

Yield 85%; yellow solid; ^1H NMR (500 MHz, CDCl_3) δ 12.14 (br s, 1H), 9.12 (br s, 1H), 8.50 (d, J = 8.5 Hz, 1H), 7.73 (dd, J = 8.5, 1.6 Hz, 1H), 7.63 (d, J = 1.6 Hz, 1H), 7.37 (d, J = 8.8 Hz, 1H), 7.32 (d, J = 8.8 Hz, 1H), 5.26 (septet, J = 6.3 Hz, 1H), 4.81 (septet, J = 6.0 Hz, 1H), 4.10 (s, 3H), 1.47 (d, J =

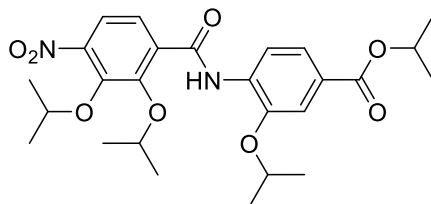
6.0 Hz, 6H), 1.39 (d, $J = 6.3$ Hz, 6H); ^{13}C NMR (126 MHz, CDCl_3) δ 166.14, 165.52, 156.70, 146.68, 146.16, 142.93, 130.94, 127.28, 122.93, 120.19, 119.40, 119.16, 113.64, 113.18, 72.06, 68.64, 62.01, 22.18 (2C), 21.94 (2C); m/z (ESI+) 433 $[\text{M} + \text{H}]^+$; $t_{\text{R}} = 16.84$ min.

Isopropyl 4-(3-hydroxy-2-methoxy-4-nitrobenzamido)-3-isopropoxybenzoate 45



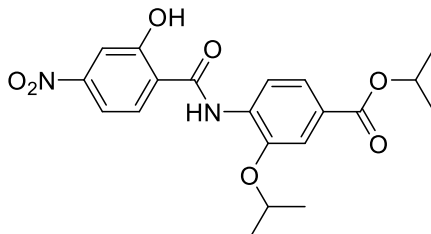
Yield 68%; yellow solid; ^1H NMR (500 MHz, DMSO-d_6) δ 10.99 (br s, 1H), 10.72 (s, 1H), 8.56 (d, $J = 8.4$ Hz, 1H), 7.81 (d, $J = 9.0$ Hz, 1H), 7.60 (dd, $J = 8.4, 1.7$ Hz, 1H), 7.58 (m, 2H), 5.12 (septet, $J = 6.3$ Hz, 1H), 4.85 (septet, $J = 6.0$ Hz, 1H), 3.99 (s, 3H), 1.39 (d, $J = 6.0$ Hz, 6H), 1.32 (d, $J = 6.3$ Hz, 6H); ^{13}C NMR (126 MHz, DMSO-d_6) δ 164.79, 161.19, 148.52, 146.16, 146.07, 139.79, 132.53, 130.59, 125.72, 122.22, 119.87, 119.82, 119.29, 112.95, 71.25, 68.10, 62.21, 21.67 (2C), 21.61 (2C); m/z (ESI+) 433 $[\text{M} + \text{H}]^+$; $t_{\text{R}} = 16.85$ min.

Isopropyl 4-(2,3-diisopropoxy-4-nitrobenzamido)-3-isopropoxybenzoate 46



Yield 70%; yellowish orange solid; ^1H NMR (500 MHz, DMSO-d_6) δ 10.22 (s, 1H), 8.54 (d, $J = 8.5$ Hz, 1H), 7.78 (s, 2H), 7.61 (m, 2H), 5.13 (septet, $J = 6.2$ Hz, 1H), 4.78 (septet, $J = 6.1$ Hz, 1H), 4.68 (septet, $J = 6.3$ Hz, 1H), 4.59 (septet, $J = 6.0$ Hz, 1H), 1.34 (d, $J = 6.0$ Hz, 6H), 1.32 (d, $J = 6.3$ Hz, 6H), 1.27 (d, $J = 6.1$ Hz, 6H), 1.25 (d, $J = 6.2$ Hz, 6H); ^{13}C NMR (126 MHz, DMSO-d_6) δ 164.75, 161.91, 149.68, 147.63, 146.13, 143.89, 133.18, 132.42, 125.84, 125.22, 122.49, 119.44, 119.17, 113.73, 78.32, 77.38, 72.01, 68.12, 22.02 (2C), 21.88 (2C), 21.70 (2C), 21.68 (2C); m/z (ESI+) 503 $[\text{M} + \text{H}]^+$; $t_{\text{R}} = 17.52$ min.

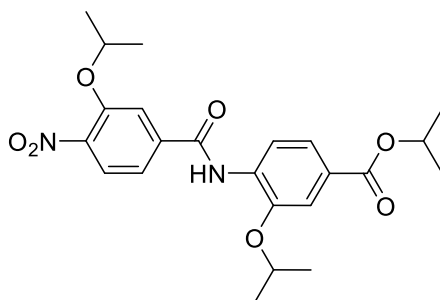
Isopropyl 4-(2-hydroxy-4-nitrobenzamido)-3-isopropoxybenzoate 47



Yield 55%; yellow solid; ^1H NMR (500 MHz, DMSO-d_6) δ 12.73 (br s, 1H), 11.20 (s, 1H), 8.62 (d, $J = 8.5$ Hz, 1H), 8.26 (d, $J = 8.7$ Hz, 1H), 7.86 (d, $J = 2.2$ Hz, 1H), 7.80 (dd, $J = 8.7, 2.3$ Hz, 1H), 7.59 (dd, $J = 8.5, 1.7$ Hz, 1H), 7.56 (d, $J = 1.7$ Hz, 1H), 5.12 (septet, $J = 6.3$ Hz, 1H), 4.80 (septet, $J = 6.0$ Hz, 1H), 1.38 (d, $J = 6.0$ Hz, 6H), 1.32 (d, $J = 6.3$ Hz, 6H); ^{13}C NMR (126 MHz, DMSO-d_6) δ 164.79,

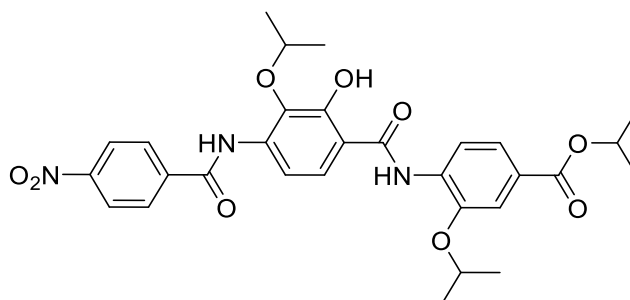
161.32, 156.36, 150.01, 145.89, 133.28, 132.79, 125.36, 124.35, 122.51, 118.86, 114.03, 113.39, 111.69, 71.67, 68.03, 21.74 (2C), 21.67 (2C); m/z (ESI+) 403 [M + H]⁺; t_R = 14.18 min.

Isopropyl 3-isopropoxy-4-(3-isopropoxy-4-nitrobenzamido)benzoate 48



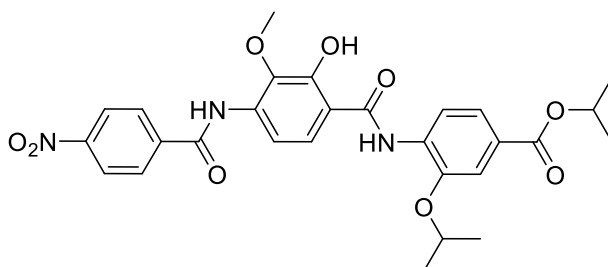
Yield 98%; yellow solid; ¹H NMR (500 MHz, CDCl₃) δ 8.79 (br s, 1H), 8.56 (d, J = 8.5 Hz, 1H), 7.85 (d, J = 8.5 Hz, 1H), 7.71 (d, J = 8.2 Hz, 1H), 7.68 (s, 1H), 7.60 (s, 1H), 7.35 (d, J = 8.2 Hz, 1H), 5.24 (septet, J = 6.3 Hz, 1H), 4.80 (septet, J = 6.0 Hz, 1H), 4.78 (septet, J = 6.0 Hz, 1H), 1.43 (d, J = 6.0 Hz, 12H), 1.38 (d, J = 6.3 Hz, 6H); ¹³C NMR (126 MHz, CDCl₃) δ 165.58, 163.05, 151.46, 145.81, 142.79, 139.47, 131.97, 126.58, 125.67, 122.99, 118.72, 117.19, 115.37, 113.08, 73.05, 71.84, 68.44, 22.13 (2C), 21.90 (2C), 21.76 (2C); m/z (ESI+) 445 [M + H]⁺; t_R = 15.79 min.

Isopropyl 4-(2-hydroxy-3-isopropoxy-4-(4-nitrobenzamido)benzamido)-3-isopropoxybenzoate 57



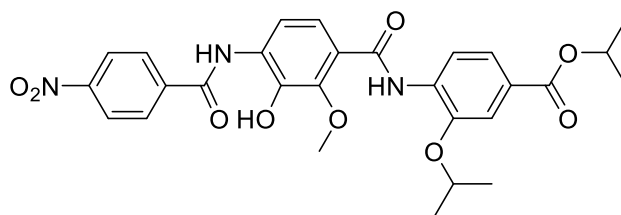
Yield 62%; yellow solid; ¹H NMR (500 MHz, CDCl₃) δ 12.47 (br s, 1H), 8.98 (br s, 1H), 8.94 (br s, 1H), 8.50 (d, J = 8.5 Hz, 1H), 8.41 (d, J = 8.8 Hz, 2H), 8.18 (d, J = 8.8 Hz, 1H), 8.08 (d, J = 8.8 Hz, 2H), 7.72 (dd, J = 8.5, 1.6 Hz, 1H), 7.62 (d, J = 1.6 Hz, 1H), 7.30 (d, J = 8.8 Hz, 1H), 5.26 (septet, J = 6.3 Hz, 1H), 4.94 (septet, J = 6.3 Hz, 1H), 4.80 (septet, J = 6.0 Hz, 1H), 1.48 (d, J = 6.0 Hz, 6H), 1.39 (d, J = 6.3 Hz, 12H); ¹³C NMR (126 MHz, CDCl₃) δ 167.90, 165.65, 163.05, 154.91, 149.97, 146.04, 140.02, 136.51, 134.90, 131.60, 128.16 (2C), 126.58, 124.23 (2C), 123.01, 120.50, 119.04, 113.25, 112.04, 109.80, 75.43, 72.08, 68.49, 22.91 (2C), 22.21 (2C), 21.95 (2C); m/z (ESI+) 580 [M + H]⁺.

Isopropyl 4-(2-hydroxy-3-methoxy-4-(4-nitrobenzamido)benzamido)-3-isopropoxybenzoate 58



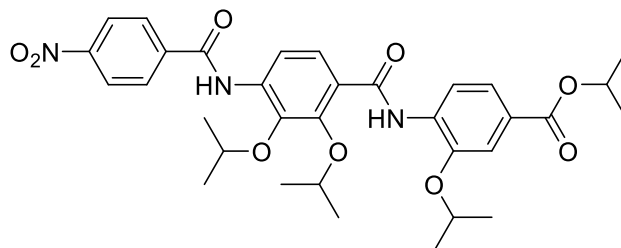
Yield 94%; yellow crystals; $^1\text{H NMR}$ (500 MHz, CDCl_3) δ 12.48 (br s, 1H), 8.97 (br s, 1H), 8.81 (br s, 1H), 8.50 (d, $J = 8.5$ Hz, 1H), 8.40 (d, $J = 9.1$ Hz, 2H), 8.17 (d, $J = 8.8$ Hz, 1H), 8.08 (d, $J = 9.1$ Hz, 2H), 7.72 (dd, $J = 8.5, 1.9$ Hz, 1H), 7.62 (d, $J = 1.9$ Hz, 1H), 7.31 (d, $J = 8.8$ Hz, 1H), 5.26 (septet, $J = 6.3$ Hz, 1H), 4.80 (septet, $J = 6.0$ Hz, 1H), 4.10 (s, 3H), 1.48 (d, $J = 6.0$ Hz, 6H), 1.39 (d, $J = 6.3$ Hz, 6H); $^{13}\text{C NMR}$ (126 MHz, CDCl_3) δ 167.79, 165.65, 163.42, 154.84, 150.01, 146.06, 139.98, 136.99, 135.63, 131.55, 128.37 (2C), 126.65, 124.19 (2C), 123.01, 120.84, 119.07, 113.27, 112.21, 109.94, 72.10, 68.52, 60.91, 22.21 (2C), 21.96 (2C); $^1\text{H NMR}$ (500 MHz, DMSO-d_6) δ 11.48 (br s, 1H), 11.07 (br s, 1H), 10.26 (br s, 1H), 8.61 (d, $J = 8.5$ Hz, 1H), 8.38 (d, $J = 8.8$ Hz, 2H), 8.19 (d, $J = 8.8$ Hz, 2H), 7.85 (d, $J = 8.8$ Hz, 1H), 7.60 (dd, $J = 8.5, 1.6$ Hz, 1H), 7.58 (d, $J = 1.6$ Hz, 1H), 7.52 (d, $J = 8.8$ Hz, 1H), 5.12 (septet, $J = 6.0$ Hz, 1H), 4.78 (septet, $J = 6.0$ Hz, 1H), 3.77 (s, 3H), 1.40 (d, $J = 6.0$ Hz, 6H), 1.32 (d, $J = 6.0$ Hz, 6H); $^{13}\text{C NMR}$ (126 MHz, DMSO-d_6) δ 164.91, 164.43, 162.97, 149.73, 149.30, 146.12, 141.00, 140.13, 135.25, 133.77, 129.45 (2C), 125.64, 125.02, 123.64 (2C), 122.53, 119.18, 117.22, 115.49, 113.62, 71.94, 68.02, 60.59, 21.73 (2C), 21.72 (2C); m/z (ESI+) 552 $[\text{M} + \text{H}]^+$; $t_{\text{R}} = 16.56$ min.

Isopropyl 4-(3-hydroxy-2-methoxy-4-(4-nitrobenzamido)benzamido)-3-isopropoxybenzoate 59



Yield 63%; yellow solid; $^1\text{H NMR}$ (500 MHz, DMSO-d_6) δ 10.87 (s, 1H), 10.21 (br s, 1H), 9.81 (br s, 1H), 8.66 (d, $J = 8.4$ Hz, 1H), 8.39 (m, 2H), 8.23 (m, 2H), 7.61 (m, 3H), 7.58 (d, $J = 1.8$ Hz, 1H), 5.13 (septet, $J = 6.3$ Hz, 1H), 4.87 (septet, $J = 6.0$ Hz, 1H), 3.98 (s, 3H), 1.41 (d, $J = 6.0$ Hz, 6H), 1.33 (d, $J = 6.3$ Hz, 6H); $^{13}\text{C NMR}$ (126 MHz, DMSO-d_6) δ 164.87, 164.24, 162.18, 149.32, 147.44, 145.69, 143.03, 139.80, 133.22, 131.04, 129.40 (2C), 125.01, 123.58 (2C), 122.46, 122.36, 120.83, 120.17, 118.79, 112.86, 71.18, 68.01, 61.75, 21.69 (2C), 21.67 (2C); m/z (ESI+) 552 $[\text{M} + \text{H}]^+$; $t_{\text{R}} = 16.53$ min.

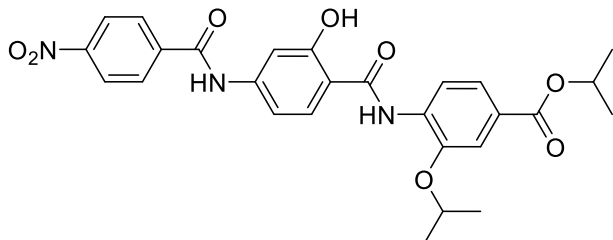
Isopropyl 4-(2,3-diisopropoxy-4-(4-nitrobenzamido)benzamido)-3-isopropoxybenzoate 60



Yield 63%; yellow solid; $^1\text{H NMR}$ (500 MHz, DMSO-d_6) δ 10.39 (br s, 1H), 10.15 (br s, 1H), 8.61 (d, $J = 8.5$ Hz, 1H), 8.39 (d, $J = 8.8$ Hz, 2H), 8.21 (d, $J = 8.8$ Hz, 2H), 7.79 (d, $J = 8.8$ Hz, 1H), 7.78 (d, $J = 8.8$ Hz, 1H), 7.62 (dd, $J = 8.5, 1.9$ Hz, 1H), 7.59 (d, $J = 1.9$ Hz, 1H), 5.13 (septet, $J = 6.3$ Hz, 1H), 4.76 (septet, $J = 6.0$ Hz, 1H), 4.63 (septet, $J = 6.3$ Hz, 1H), 4.47 (septet, $J = 6.3$ Hz, 1H), 1.35 (d, $J = 6.0$ Hz, 6H), 1.33 (d, $J = 6.3$ Hz, 6H), 1.28 (d, $J = 6.3$ Hz, 6H), 1.27 (d, $J = 6.3$ Hz, 6H); $^{13}\text{C NMR}$ (126

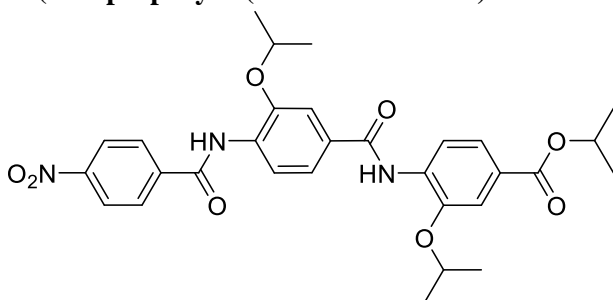
MHz, DMSO- d_6) δ 164.78, 163.81, 162.70, 149.35, 149.09, 145.82, 143.60, 139.69, 136.49, 133.09, 129.14 (2C), 125.53, 125.22, 125.19, 123.74 (2C), 122.65, 120.25, 118.71, 113.87, 77.31, 76.02, 72.23, 68.00, 22.21 (2C), 21.89 (2C), 21.76 (2C), 21.68 (2C); m/z (ESI+) 622 $[M + H]^+$; $t_R = 17.56$ min.

Isopropyl 4-(2-hydroxy-4-(4-nitrobenzamido)benzamido)-3-isopropoxybenzoate 61



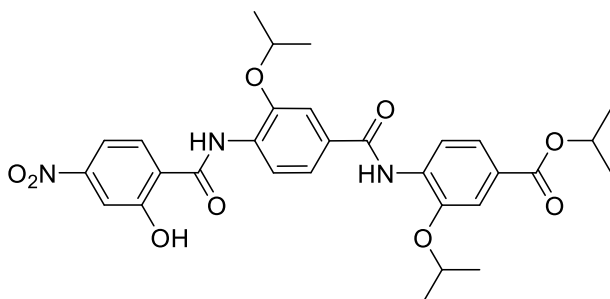
Yield 50%; yellow solid; 1H NMR (500 MHz, DMSO- d_6) δ 11.82 (s, 1H), 11.18 (s, 1H), 10.78 (s, 1H), 8.65 (d, $J = 8.5$ Hz, 1H), 8.38 (m, 2H), 8.19 (m, 2H), 8.03 (d, $J = 8.7$ Hz, 1H), 7.90 (d, $J = 2.0$ Hz, 1H), 7.58 (m, 2H), 7.29 (dd, $J = 8.8, 2.0$ Hz, 1H), 5.12 (septet, $J = 6.2$ Hz, 1H), 4.78 (septet, $J = 6.0$ Hz, 1H), 1.38 (d, $J = 6.0$ Hz, 6H), 1.32 (d, $J = 6.2$ Hz, 6H); ^{13}C NMR (126 MHz, DMSO- d_6) δ 164.91, 164.48, 162.82, 156.51, 149.26, 145.68, 143.30, 140.38, 134.18, 131.68, 129.39 (2C), 124.53, 123.55 (2C), 122.61, 118.49, 114.55, 113.45, 111.81, 107.42, 71.63, 67.90, 21.74 (2C), 21.70 (2C); m/z (ESI+) 522 $[M + H]^+$; $t_R = 13.95$ min.

Isopropyl 3-isopropoxy-4-(3-isopropoxy-4-(4-nitrobenzamido)benzamido)benzoate 62



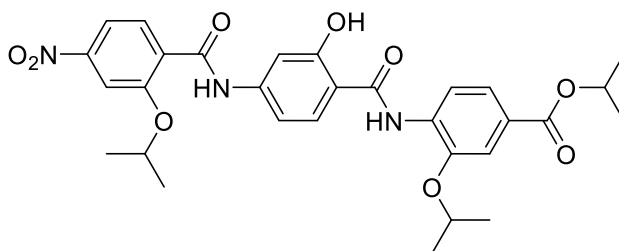
Yield 93%; yellow solid; 1H NMR (500 MHz, $CDCl_3$) δ 8.88 (br s, 1H), 8.81 (br s, 1H), 8.68 (d, $J = 8.5$ Hz, 1H), 8.62 (d, $J = 8.5$ Hz, 1H), 8.41 (d, $J = 8.8$ Hz, 2H), 8.08 (d, $J = 8.8$ Hz, 2H), 7.73 (dd, $J = 8.5, 1.9$ Hz, 1H), 7.66 (d, $J = 1.9$ Hz, 1H), 7.62 (d, $J = 1.9$ Hz, 1H), 7.44 (dd, $J = 8.5, 1.9$ Hz, 1H), 5.26 (septet, $J = 6.3$ Hz, 1H), 4.85 (septet, $J = 6.0$ Hz, 1H), 4.79 (septet, $J = 6.0$ Hz, 1H), 1.48 (d, $J = 6.0$ Hz, 6H), 1.46 (d, $J = 6.0$ Hz, 6H), 1.39 (d, $J = 6.3$ Hz, 6H); ^{13}C NMR (126 MHz, $CDCl_3$) δ 165.82, 164.31, 163.07, 149.85, 146.68, 145.77, 140.28, 132.75, 131.23, 130.76, 128.19 (2C), 125.94, 124.22 (2C), 123.17, 119.28, 118.72, 118.50, 113.19, 111.90, 71.97, 71.89, 68.37, 22.24 (2C), 22.21 (2C), 21.98 (2C); m/z (ESI+) 564 $[M + H]^+$; $t_R = 16.49$ min.

Isopropyl 4-(4-(2-hydroxy-4-nitrobenzamido)-3-isopropoxybenzamido)-3-isopropoxybenzoate 63



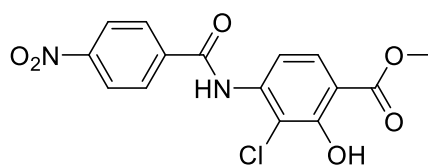
Yield 49%; yellow solid; ^1H NMR (500 MHz, DMSO-d_6) δ 12.73 (br s, 1H), 11.19 (s, 1H), 9.33 (s, 1H), 8.66 (d, $J = 8.2$ Hz, 1H), 8.29 (d, $J = 8.5$ Hz, 1H), 8.21 (d, $J = 8.2$ Hz, 1H), 7.88 (d, $J = 1.5$ Hz, 1H), 7.82 (dd, $J = 8.5, 1.5$ Hz, 1H), 7.64 (d, $J = 1.5$ Hz, 1H), 7.58 (m, 3H), 5.13 (septet, $J = 4.7$ Hz, 1H), 4.88 (septet, $J = 5.0$ Hz, 1H), 4.73 (septet, $J = 5.4$ Hz, 1H), 1.42 (d, $J = 5.0$ Hz, 6H), 1.36 (d, $J = 5.4$ Hz, 6H), 1.33 (d, $J = 4.7$ Hz, 6H); ^{13}C NMR (126 MHz, DMSO-d_6) δ 164.85, 164.17, 161.29, 156.29, 150.01, 147.66, 146.08, 132.79, 132.74, 132.15, 129.40, 126.08, 124.42, 122.01, 121.32, 120.34, 119.08, 114.11, 113.81, 112.01, 111.69, 71.58, 71.50, 68.09, 21.84 (2C), 21.68 (4C); m/z (ESI+) 580 $[\text{M} + \text{H}]^+$; $t_{\text{R}} = 17.67$ min.

Isopropyl 4-(2-hydroxy-4-(2-isopropoxy-4-nitrobenzamido)benzamido)-3-isopropoxybenzoate 64



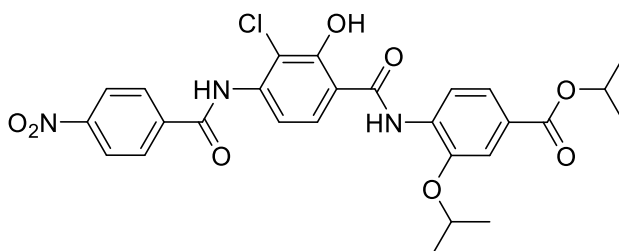
Yield 41%; yellow solid; ^1H NMR (500 MHz, DMSO-d_6) δ 11.80 (s, 1H), 11.17 (s, 1H), 10.54 (s, 1H), 8.65 (d, $J = 8.5$ Hz, 1H), 8.01 (d, $J = 8.7$ Hz, 1H), 7.90 (m, 2H), 7.83 (m, 2H), 7.56 (m, 2H), 7.16 (dd, $J = 8.7, 1.9$ Hz, 1H), 5.12 (septet, $J = 6.2$ Hz, 1H), 4.89 (septet, $J = 6.0$ Hz, 1H), 4.78 (septet, $J = 6.0$ Hz, 1H), 1.38 (d, $J = 6.0$ Hz, 6H), 1.35 (d, $J = 6.0$ Hz, 6H), 1.32 (d, $J = 6.2$ Hz, 6H); ^{13}C NMR (126 MHz, DMSO-d_6) δ 164.91, 163.79, 162.80, 156.66, 155.22, 149.47, 145.66, 143.13, 134.21, 132.33, 131.89, 130.46, 124.50, 122.61, 118.45, 115.31, 114.36, 113.45, 111.06, 108.87, 106.68, 72.36, 71.63, 67.90, 21.73 (2C), 21.70 (2C), 21.58 (2C); m/z (ESI+) 580 $[\text{M} + \text{H}]^+$; $t_{\text{R}} = 15.71$ min.

Methyl 3-chloro-2-hydroxy-4-(4-nitrobenzamido)benzoate 74



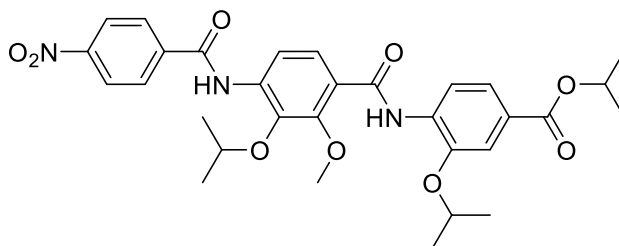
Yield 90%; yellow crystals; ^1H NMR (500 MHz, CDCl_3) δ 11.62 (br s, 1H), 8.39 (d, $J = 9.1$ Hz, 2H), 8.36 (d, $J = 9.1$ Hz, 2H), 7.85 (d, $J = 8.5$ Hz, 1H), 7.27 (br s, 1H), 6.53 (d, $J = 8.5$ Hz, 1H), 4.01 (s, 3H); ^{13}C NMR (126 MHz, CDCl_3) δ 170.08, 158.62, 150.84, 150.27, 145.28, 139.73, 130.59 (2C), 128.50, 123.70 (2C), 112.23, 110.85, 110.21, 52.73; m/z (ESI+) 351 $[\text{M} + \text{H}]^+$; $t_{\text{R}} = 15.02$ min.

Isopropyl 4-(3-chloro-2-hydroxy-4-(4-nitrobenzamido)benzamido)-3-isopropoxybenzoate 76



Yield 92%; beige solid; $^1\text{H NMR}$ (500 MHz, CDCl_3) δ 13.06 (br s, 1H), 8.98 (br s, 1H), 8.71 (br s, 1H), 8.48 (d, $J = 8.5$ Hz, 1H), 8.41 (d, $J = 8.8$ Hz, 2H), 8.28 (d, $J = 9.1$ Hz, 1H), 8.12 (d, $J = 8.8$ Hz, 2H), 7.71 (dd, $J = 8.5, 1.9$ Hz, 1H), 7.63 (d, $J = 1.9$ Hz, 1H), 7.50 (d, $J = 9.1$ Hz, 1H), 5.26 (septet, $J = 6.3$ Hz, 1H), 4.81 (septet, $J = 6.0$ Hz, 1H), 1.49 (d, $J = 6.0$ Hz, 6H), 1.39 (d, $J = 6.3$ Hz, 6H); $^{13}\text{C NMR}$ (126 MHz, CDCl_3) δ 167.06, 165.58, 163.38, 158.33, 150.20, 146.09, 139.47, 139.32, 131.22, 128.44 (2C), 126.94, 124.31, 124.29 (2C), 122.99, 119.20, 113.23, 111.90, 111.46, 110.75, 72.13, 68.58, 22.22 (2C), 21.95 (2C); m/z (ESI+) 556 $[\text{M} + \text{H}]^+$; $t_{\text{R}} = 16.99$ min.

Isopropyl 3-isopropoxy-4-(3-isopropoxy-2-methoxy-4-(4-nitrobenzamido)benzamido)benzoate
65

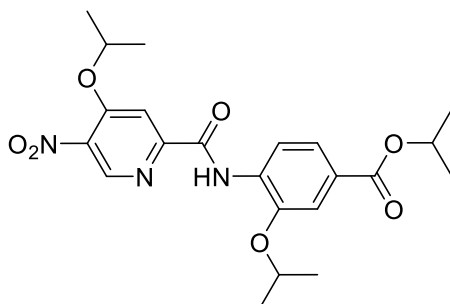


To a stirred mixture of **59** (138 mg, 0.25 mmol) and K_2CO_3 (35 mg, 0.25 mmol) in DMF (10 mL), 2-bromopropane (37 mg, 0.3 mmol) was added. The reaction mixture was stirred at 90 °C overnight. Solvent was evaporated *in vacuo*, and the residue was diluted with water (20 mL). The resulting mixture was extracted with EtOAc (3 \times 20 mL). The combined organic extract was washed with brine, dried over anhydrous MgSO_4 , and the solvent was removed by vacuum distillation. The residue was dissolved in toluene and purified using flash chromatography (SiO_2 , *n*-hexane–EtOAc = 2:1).

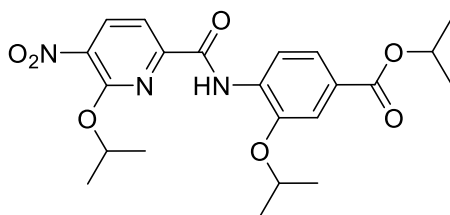
Yield 67%; pale yellow solid; $^1\text{H NMR}$ (500 MHz, DMSO-d_6) δ 10.92 (br s, 1H), 10.18 (br s, 1H), 8.63 (d, $J = 8.5$ Hz, 1H), 8.40 (d, $J = 8.8$ Hz, 2H), 8.21 (d, $J = 8.8$ Hz, 2H), 7.88 (d, $J = 8.8$ Hz, 1H), 7.83 (d, $J = 8.8$ Hz, 1H), 7.61 (dd, $J = 8.5, 1.6$ Hz, 1H), 7.59 (d, $J = 1.6$ Hz, 1H), 5.13 (septet, $J = 6.3$ Hz, 1H), 4.86 (septet, $J = 6.0$ Hz, 1H), 4.43 (septet, $J = 6.3$ Hz, 1H), 4.06 (s, 3H), 1.40 (d, $J = 6.0$ Hz, 6H), 1.33 (d, $J = 6.3$ Hz, 6H), 1.29 (d, $J = 6.3$ Hz, 6H); $^{13}\text{C NMR}$ (126 MHz, DMSO-d_6) δ 164.85, 163.82, 161.78, 152.04, 149.37, 145.70, 143.11, 139.66, 136.83, 133.22, 129.16 (2C), 125.51, 125.07, 123.76 (2C), 122.66, 122.46, 120.03, 118.70, 113.06, 76.67, 71.36, 68.02, 61.89, 22.27 (2C), 21.68 (2C), 21.62 (2C); m/z (ESI+) 594 $[\text{M} + \text{H}]^+$; $t_{\text{R}} = 17.26$ min.

General procedure for synthesis of the dipeptides 78 and 79.

To a stirred solution of the 5-nitropicolinic acid **34** or **37** (226 mg, 1 mmol), and **42** (237 mg, 1 mmol) in a mixture of anhydrous CHCl_3 (50 mL) and DMF (1 mL) cooled at 0 °C in an ice bath, HOBt (676 mg, 5 mmol) was added under a nitrogen atmosphere followed by EDC (958 mg, 5 mmol). The reaction was stirred at 0 °C for 2 h, then at room temperature overnight. Solvent was removed by vacuum distillation. The residue was dissolved in toluene and purified using flash chromatography (SiO_2 , *n*-hexane–EtOAc = 2:1).

Isopropyl 3-isopropoxy-4-(4-isopropoxy-5-nitropicolinamido)benzoate 78

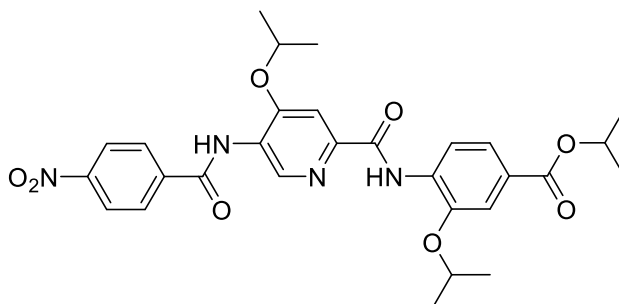
Yield 70%; pale yellow solid; $^1\text{H NMR}$ (500 MHz, CDCl_3) δ 10.80 (br s, 1H), 8.98 (s, 1H), 8.62 (d, $J = 8.5$ Hz, 1H), 8.01 (s, 1H), 7.73 (dd, $J = 8.5, 1.9$ Hz, 1H), 7.63 (d, $J = 1.9$ Hz, 1H), 5.26 (septet, $J = 6.3$ Hz, 1H), 4.99 (septet, $J = 6.0$ Hz, 1H), 4.75 (septet, $J = 6.0$ Hz, 1H), 1.50 (d, $J = 6.0$ Hz, 6H), 1.47 (d, $J = 6.0$ Hz, 6H), 1.39 (d, $J = 6.3$ Hz, 6H); $^{13}\text{C NMR}$ (126 MHz, CDCl_3) δ 165.72, 160.29, 158.81, 154.12, 146.66, 145.93, 138.43, 132.10, 126.68, 123.05, 118.68, 113.92, 108.61, 74.06, 72.21, 68.43, 22.11 (2C), 21.96 (2C), 21.60 (2C); m/z (ESI+) 446 $[\text{M} + \text{H}]^+$; $t_{\text{R}} = 19.75$ min.

Isopropyl 3-isopropoxy-4-(6-isopropoxy-5-nitropicolinamido)benzoate 79

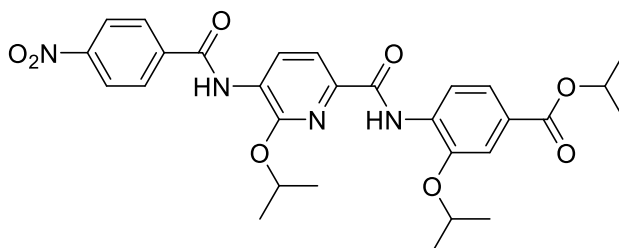
Yield 90%; yellow solid; $^1\text{H NMR}$ (500 MHz, CDCl_3) δ 10.30 (br s, 1H), 8.70 (d, $J = 8.5$ Hz, 1H), 8.38 (d, $J = 8.2$ Hz, 1H), 7.99 (d, $J = 8.2$ Hz, 1H), 7.73 (dd, $J = 8.5, 1.9$ Hz, 1H), 7.63 (d, $J = 1.9$ Hz, 1H), 5.71 (septet, $J = 6.3$ Hz, 1H), 5.26 (septet, $J = 6.0$ Hz, 1H), 4.84 (septet, $J = 6.3$ Hz, 1H), 1.52 (d, $J = 6.3$ Hz, 6H), 1.44 (d, $J = 6.3$ Hz, 6H), 1.39 (d, $J = 6.0$ Hz, 6H); $^{13}\text{C NMR}$ (126 MHz, CDCl_3) δ 165.72, 160.07, 154.66, 150.44, 146.20, 136.53, 136.47, 131.64, 126.65, 122.90, 118.89, 115.18, 112.97, 71.38, 71.22, 68.48, 22.09 (2C), 21.96 (2C), 21.79 (2C); m/z (ESI+) 446 $[\text{M} + \text{H}]^+$; $t_{\text{R}} = 20.00$ min.

General procedure for synthesis of the tripeptides 82 and 83.

To a stirred solution of the amino ester **80** or **81** (207 mg, 0.5 mmol), and pyridine (0.1 mL) in DCM (20 mL), 4-nitrobenzoyl chloride (185 mg, 1 mmol) was added. The reaction mixture was stirred at room temperature for 24 h then water (20 mL) and 1 N HCl (2 mL) were added. The mixture was extracted with DCM (2×20 mL) then EtOAc (1×20 mL). The combined organic extract was dried over anhydrous MgSO_4 , and the solvent was removed by vacuum distillation. The residue was dissolved in toluene and purified using flash chromatography (SiO_2 , n -hexane–EtOAc = 1:1).

Isopropyl 3-isopropoxy-4-(4-isopropoxy-5-(4-nitrobenzamido)picolinamido)benzoate 82

Yield 90%; pale yellow crystals; $^1\text{H NMR}$ (500 MHz, CDCl_3) δ 10.91 (br s, 1H), 9.72 (s, 1H), 8.65 (d, $J = 8.5$ Hz, 1H), 8.51 (br s, 1H), 8.42 (d, $J = 9.1$ Hz, 2H), 8.08 (d, $J = 9.1$ Hz, 2H), 7.89 (s, 1H), 7.73 (dd, $J = 8.5, 1.9$ Hz, 1H), 7.63 (d, $J = 1.9$ Hz, 1H), 5.25 (septet, $J = 6.3$ Hz, 1H), 4.96 (septet, $J = 6.0$ Hz, 1H), 4.74 (septet, $J = 6.0$ Hz, 1H), 1.51 (d, $J = 6.0$ Hz, 6H), 1.49 (d, $J = 6.0$ Hz, 6H), 1.39 (d, $J = 6.3$ Hz, 6H); $^{13}\text{C NMR}$ (126 MHz, CDCl_3) δ 165.87, 162.95, 161.98, 153.17, 150.02, 147.07, 146.57, 139.65, 139.60, 132.89, 128.30 (2C), 127.08, 125.95, 124.26 (2C), 123.15, 118.39, 114.12, 105.44, 72.59, 72.29, 68.27, 22.14 (2C), 21.97 (2C), 21.94 (2C); m/z (ESI+) 565 $[\text{M} + \text{H}]^+$; $t_{\text{R}} = 19.73$ min.

Isopropyl 3-isopropoxy-4-(6-isopropoxy-5-(4-nitrobenzamido)picolinamido)benzoate 83

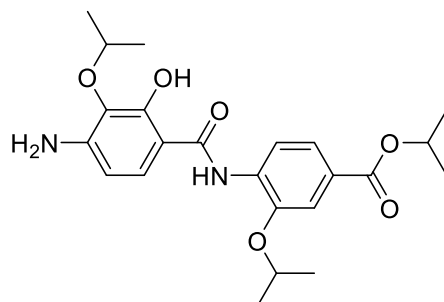
Yield 80%; yellow crystals; $^1\text{H NMR}$ (500 MHz, CDCl_3) δ 10.33 (br s, 1H), 8.95 (d, $J = 8.2$ Hz, 1H), 8.74 (d, $J = 8.5$ Hz, 1H), 8.59 (br s, 1H), 8.41 (d, $J = 8.8$ Hz, 2H), 8.07 (d, $J = 8.8$ Hz, 2H), 8.01 (d, $J = 8.2$ Hz, 1H), 7.72 (dd, $J = 8.5, 1.6$ Hz, 1H), 7.62 (d, $J = 1.6$ Hz, 1H), 5.69 (septet, $J = 6.3$ Hz, 1H), 5.25 (septet, $J = 6.0$ Hz, 1H), 4.83 (septet, $J = 6.3$ Hz, 1H), 1.54 (d, $J = 6.3$ Hz, 6H), 1.45 (d, $J = 6.3$ Hz, 6H), 1.39 (d, $J = 6.0$ Hz, 6H); $^{13}\text{C NMR}$ (126 MHz, CDCl_3) δ 165.90, 163.44, 161.81, 150.71, 150.03, 146.02, 141.18, 139.62, 132.47, 128.25 (2C), 127.14, 125.85, 125.59, 124.26 (2C), 123.01, 118.66, 117.18, 113.00, 71.11, 70.03, 68.34, 22.15 (2C), 22.13 (2C), 21.97 (2C); m/z (ESI+) 565 $[\text{M} + \text{H}]^+$; $t_{\text{R}} = 16.93$ min.

General procedure for reduction of the nitro derivatives.

To a stirred solution of the nitro ester (0.4 mmol) in EtOH (20 mL), iron powder (112 mg, 2 mmol) was added at 55 °C followed by NH_4Cl (11 mg, 0.2 mmol) solution in water (2 mL). The reaction was heated at 90 °C for 1 h, then iron was filtered on hot and the filtrate was concentrated *in vacuo*. The residue was diluted with water (20 mL) and basified by NaHCO_3 (saturated aqueous solution) to pH 7–8. The mixture was extracted with EtOAc/THF (1:1, 3 \times 20 mL). The combined organic extract was washed with brine, dried over anhydrous MgSO_4 , and the solvent was removed by vacuum distillation.

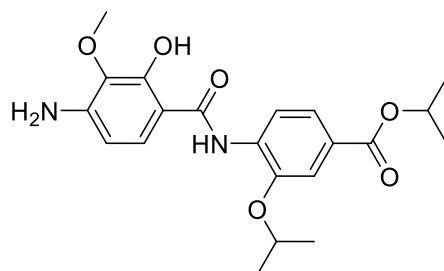
The obtained material was dissolved in toluene and purified using flash chromatography (SiO₂, *n*-hexane–EtOAc = 2:1 or 1:1).

Isopropyl 4-(4-amino-2-hydroxy-3-isopropoxybenzamido)-3-isopropoxybenzoate 49



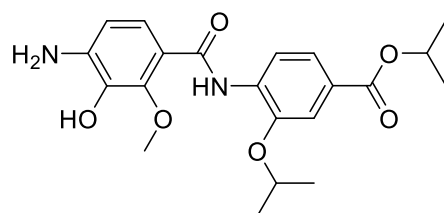
Yield 90%; colorless crystals; ¹H NMR (500 MHz, CDCl₃) δ 12.26 (br s, 1H), 8.82 (br s, 1H), 8.49 (d, *J* = 8.5 Hz, 1H), 7.69 (dd, *J* = 8.5, 1.9 Hz, 1H), 7.59 (d, *J* = 1.9 Hz, 1H), 7.08 (d, *J* = 8.8 Hz, 1H), 6.29 (d, *J* = 8.8 Hz, 1H), 5.25 (septet, *J* = 6.3 Hz, 1H), 4.76 (septet, *J* = 6.0 Hz, 1H), 4.69 (septet, *J* = 6.0 Hz, 1H), 4.29 (br s, 2H), 1.44 (d, *J* = 6.0 Hz, 6H), 1.38 (d, *J* = 6.3 Hz, 6H), 1.34 (d, *J* = 6.0 Hz, 6H); ¹³C NMR (126 MHz, CDCl₃) δ 168.34, 165.83, 156.21, 146.27, 145.80, 132.40, 131.79, 125.73, 123.10, 121.30, 118.83, 113.26, 106.35, 106.11, 74.25, 71.86, 68.34, 22.70 (2C), 22.20 (2C), 21.96 (2C); *m/z* (ESI⁺) 431 [M + H]⁺.

Isopropyl 4-(4-amino-2-hydroxy-3-methoxybenzamido)-3-isopropoxybenzoate 50



Yield 92%; beige crystals; ¹H NMR (500 MHz, CDCl₃) δ 12.31 (br s, 1H), 8.80 (br s, 1H), 8.49 (d, *J* = 8.5 Hz, 1H), 7.69 (dd, *J* = 8.5, 1.6 Hz, 1H), 7.59 (d, *J* = 1.6 Hz, 1H), 7.09 (d, *J* = 8.8 Hz, 1H), 6.30 (d, *J* = 8.8 Hz, 1H), 5.25 (septet, *J* = 6.3 Hz, 1H), 4.76 (septet, *J* = 6.0 Hz, 1H), 4.33 (br s, 2H), 3.92 (s, 3H), 1.44 (d, *J* = 6.0 Hz, 6H), 1.38 (d, *J* = 6.3 Hz, 6H); ¹³C NMR (126 MHz, CDCl₃) δ 168.26, 165.80, 156.15, 145.81, 145.32, 134.04, 132.28, 125.81, 123.08, 121.64, 118.84, 113.26, 106.40, 106.14, 71.87, 68.36, 59.72, 22.20 (2C), 21.96 (2C); *m/z* (ESI⁺) 403 [M + H]⁺; *t_R* = 15.56 min.

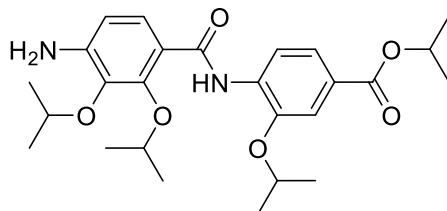
Isopropyl 4-(4-amino-3-hydroxy-2-methoxybenzamido)-3-isopropoxybenzoate 51



Yield 71%; orange solid; ¹H NMR (500 MHz, DMSO-*d*₆) δ 10.74 (s, 1H), 8.74 (s, 1H), 8.66 (d, *J* = 8.5 Hz, 1H), 7.56 (m, 2H), 7.40 (d, *J* = 8.6 Hz, 1H), 6.52 (d, *J* = 8.6 Hz, 1H), 5.50 (s, 2H), 5.12 (septet, *J* = 6.2 Hz, 1H), 4.83 (septet, *J* = 6.3 Hz, 1H), 3.87 (s, 3H), 1.40 (d, *J* = 5.9 Hz, 6H), 1.32 (d, *J* = 6.1 Hz,

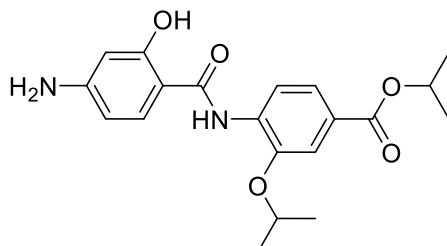
6H); ^{13}C NMR (126 MHz, DMSO- d_6) δ 164.95, 163.07, 147.39, 145.32, 144.09, 134.86, 134.04, 124.07, 123.13, 122.41, 118.31, 112.73, 112.24, 109.60, 71.00, 67.86, 61.37, 21.70 (2C), 21.67 (2C); m/z (ESI+) 403 [M + H] $^+$; t_R = 14.99 min.

Isopropyl 4-(4-amino-2,3-diisopropoxybenzamido)-3-isopropoxybenzoate 52



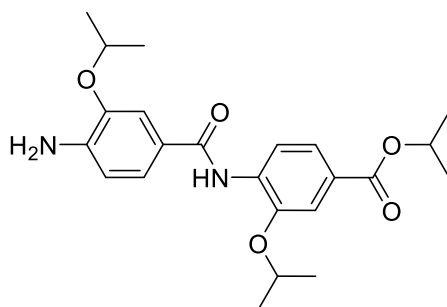
Yield 68%; yellow solid; ^1H NMR (500 MHz, DMSO- d_6) δ 10.37 (s, 1H), 8.59 (d, J = 8.5 Hz, 1H), 7.57 (dd, J = 8.4, 1.8 Hz, 1H), 7.55 (d, J = 1.8 Hz, 1H), 7.50 (d, J = 8.7 Hz, 1H), 6.56 (d, J = 8.7 Hz, 1H), 5.62 (s, 2H), 5.11 (septet, J = 6.3 Hz, 1H), 4.71 (septet, J = 6.1 Hz, 1H), 4.59 (septet, J = 6.2 Hz, 1H), 4.44 (septet, J = 6.1 Hz, 1H), 1.34 (d, J = 6.1 Hz, 6H), 1.32 (d, J = 6.3 Hz, 6H), 1.28 (d, J = 6.1 Hz, 6H), 1.23 (d, J = 6.2 Hz, 6H); ^{13}C NMR (126 MHz, DMSO- d_6) δ 164.87, 163.56, 149.71, 148.04, 145.61, 135.22, 134.00, 126.43, 124.26, 122.72, 118.45, 115.06, 114.01, 110.04, 76.24, 73.55, 72.29, 67.84, 22.11 (2C), 21.92 (2C), 21.79 (2C), 21.69 (2C); m/z (ESI+) 473 [M + H] $^+$; t_R = 16.86 min.

Isopropyl 4-(4-amino-2-hydroxybenzamido)-3-isopropoxybenzoate 53



Yield 87%; beige solid; ^1H NMR (500 MHz, DMSO- d_6) δ 11.05 (s, 1H), 10.90 (s, 1H), 8.62 (d, J = 8.5 Hz, 1H), 7.69 (d, J = 9.2 Hz, 1H), 7.55 (dd, J = 8.5, 1.7 Hz, 1H), 7.52 (d, J = 1.7 Hz, 1H), 6.18 (m, 2H), 5.84 (s, 2H), 5.11 (septet, J = 6.3 Hz, 1H), 4.73 (septet, J = 6.0 Hz, 1H), 1.35 (d, J = 6.0 Hz, 6H), 1.31 (d, J = 6.3 Hz, 6H); ^{13}C NMR (126 MHz, DMSO- d_6) δ 164.99, 163.82, 157.64, 153.98, 145.46, 134.93, 132.41, 123.70, 122.64, 118.22, 113.46, 106.77, 106.69, 99.37, 71.52, 67.77, 21.75 (2C), 21.71 (2C); m/z (ESI+) 373 [M + H] $^+$; t_R = 12.26 min.

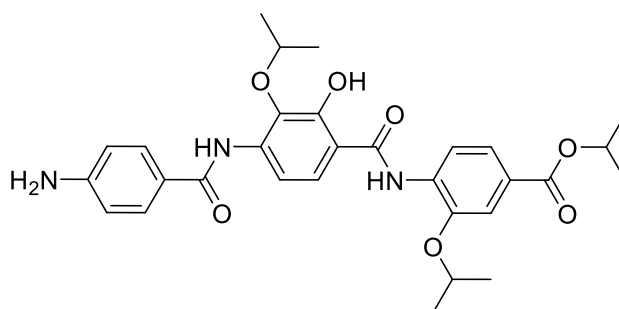
Isopropyl 4-(4-amino-3-isopropoxybenzamido)-3-isopropoxybenzoate 54



Yield 99%; beige solid; ^1H NMR (500 MHz, CDCl_3) δ 8.75 (br s, 1H), 8.62 (d, J = 8.5 Hz, 1H), 7.71 (dd, J = 8.5, 1.9 Hz, 1H), 7.59 (d, J = 1.9 Hz, 1H), 7.46 (d, J = 1.9 Hz, 1H), 7.27 (dd, J = 8.2, 1.9 Hz,

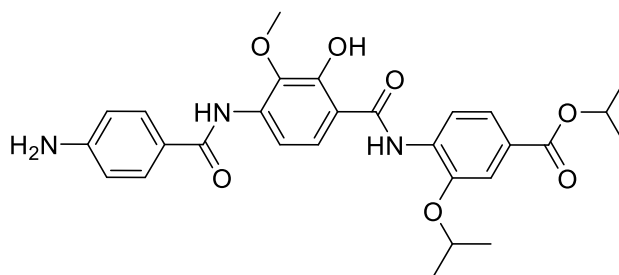
1H), 6.74 (d, $J = 8.2$ Hz, 1H), 5.25 (septet, $J = 6.3$ Hz, 1H), 4.76 (septet, $J = 6.0$ Hz, 1H), 4.69 (septet, $J = 6.0$ Hz, 1H), 4.22 (br s, 2H), 1.44 (d, $J = 6.0$ Hz, 6H), 1.41 (d, $J = 6.0$ Hz, 6H), 1.38 (d, $J = 6.3$ Hz, 6H); ^{13}C NMR (126 MHz, CDCl_3) δ 165.95, 165.06, 145.56, 144.85, 141.33, 133.40, 125.21, 124.17, 123.25, 119.83, 118.30, 113.59, 113.18, 112.36, 71.70, 70.81, 68.23, 22.22 (2C), 22.19 (2C), 21.97 (2C); m/z (ESI+) 415 $[\text{M} + \text{H}]^+$; $t_{\text{R}} = 14.82$ min.

Isopropyl 4-(4-(4-aminobenzamido)-2-hydroxy-3-isopropoxybenzamido)-3-isopropoxybenzoate 66



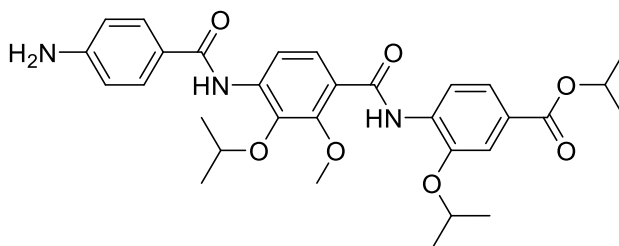
Yield 85%; white solid; ^1H NMR (500 MHz, CDCl_3) δ 12.38 (br s, 1H), 8.96 (br s, 1H), 8.81 (br s, 1H), 8.50 (d, $J = 8.5$ Hz, 1H), 8.21 (d, $J = 9.1$ Hz, 1H), 7.76 (d, $J = 8.8$ Hz, 2H), 7.71 (dd, $J = 8.5, 1.9$ Hz, 1H), 7.61 (d, $J = 1.9$ Hz, 1H), 7.27 (d, $J = 9.1$ Hz, 1H), 6.75 (d, $J = 8.8$ Hz, 2H), 5.26 (septet, $J = 6.3$ Hz, 1H), 4.88 (septet, $J = 6.3$ Hz, 1H), 4.78 (septet, $J = 6.0$ Hz, 1H), 4.10 (br s, 2H), 1.47 (d, $J = 6.0$ Hz, 6H), 1.39 (d, $J = 6.3$ Hz, 6H), 1.38 (d, $J = 6.3$ Hz, 6H); ^{13}C NMR (126 MHz, CDCl_3) δ 168.13, 165.72, 164.91, 154.92, 150.25, 146.01, 137.97, 134.36, 131.87, 128.97 (2C), 126.32, 123.85, 123.02, 120.58, 118.95, 114.33 (2C), 113.26, 110.84, 109.83, 75.12, 72.07, 68.43, 22.83 (2C), 22.19 (2C), 21.95 (2C); m/z (ESI+) 550 $[\text{M} + \text{H}]^+$.

Isopropyl 4-(4-(4-aminobenzamido)-2-hydroxy-3-methoxybenzamido)-3-isopropoxybenzoate 67



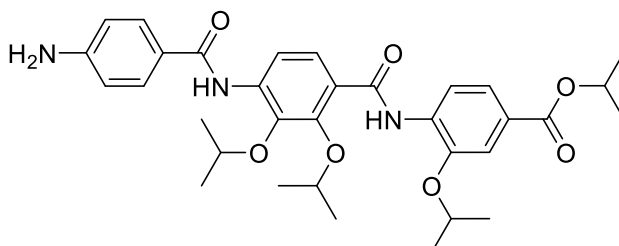
Yield 90%; pale yellow crystals; ^1H NMR (500 MHz, CDCl_3) δ 12.39 (br s, 1H), 8.95 (br s, 1H), 8.69 (br s, 1H), 8.50 (d, $J = 8.5$ Hz, 1H), 8.19 (d, $J = 9.1$ Hz, 1H), 7.75 (d, $J = 8.8$ Hz, 2H), 7.71 (dd, $J = 8.5, 1.9$ Hz, 1H), 7.61 (d, $J = 1.9$ Hz, 1H), 7.28 (d, $J = 9.1$ Hz, 1H), 6.74 (d, $J = 8.8$ Hz, 2H), 5.26 (septet, $J = 6.3$ Hz, 1H), 4.78 (septet, $J = 6.0$ Hz, 1H), 4.11 (br s, 2H), 4.05 (s, 3H), 1.47 (d, $J = 6.0$ Hz, 6H), 1.39 (d, $J = 6.3$ Hz, 6H); ^{13}C NMR (126 MHz, CDCl_3) δ 168.01, 165.71, 165.20, 154.86, 150.36, 146.03, 137.08, 136.57, 131.80, 129.15 (2C), 126.39, 123.77, 123.03, 120.96, 118.98, 114.28 (2C), 113.28, 111.00, 109.96, 72.10, 68.45, 60.68, 22.20 (2C), 21.96 (2C); m/z (ESI+) 522 $[\text{M} + \text{H}]^+$; $t_{\text{R}} = 16.20$ min.

Isopropyl 4-(4-(4-aminobenzamido)-3-isopropoxy-2-methoxybenzamido)-3-isopropoxybenzoate 68



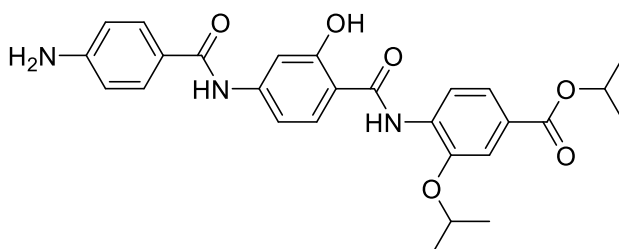
Yield 65%; pale orange solid; $^1\text{H NMR}$ (500 MHz, DMSO-d_6) δ 10.90 (br s, 1H), 9.08 (br s, 1H), 8.63 (d, $J = 8.5$ Hz, 1H), 8.06 (d, $J = 8.8$ Hz, 1H), 7.84 (d, $J = 8.8$ Hz, 1H), 7.70 (d, $J = 8.8$ Hz, 2H), 7.61 (dd, $J = 8.5, 1.6$ Hz, 1H), 7.58 (d, $J = 1.6$ Hz, 1H), 6.64 (d, $J = 8.8$ Hz, 2H), 5.91 (br s, 2H), 5.13 (septet, $J = 6.3$ Hz, 1H), 4.85 (septet, $J = 6.0$ Hz, 1H), 4.47 (septet, $J = 6.3$ Hz, 1H), 4.04 (s, 3H), 1.40 (d, $J = 6.0$ Hz, 6H), 1.33 (d, $J = 6.3$ Hz, 6H), 1.32 (d, $J = 6.3$ Hz, 6H); $^{13}\text{C NMR}$ (126 MHz, DMSO-d_6) δ 164.86, 164.44, 161.90, 152.73, 151.59, 145.62, 140.67, 138.06, 133.35, 129.10 (2C), 125.78, 124.92, 122.47, 120.54, 119.78, 118.61, 117.27, 113.01, 112.87 (2C), 76.48, 71.33, 68.00, 61.77, 22.34 (2C), 21.68 (2C), 21.62 (2C); m/z (ESI+) 564 $[\text{M} + \text{H}]^+$; $t_{\text{R}} = 16.82$ min.

Isopropyl 4-(4-(4-aminobenzamido)-2,3-diisopropoxybenzamido)-3-isopropoxybenzoate 69



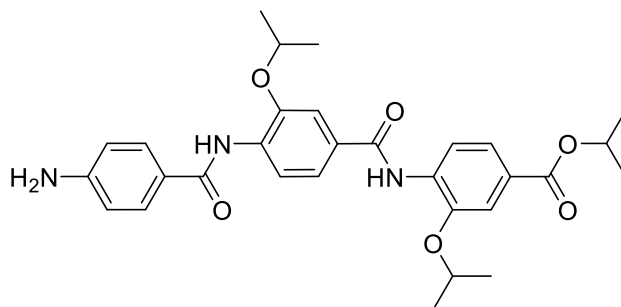
Yield 51%; white solid; $^1\text{H NMR}$ (500 MHz, DMSO-d_6) δ 10.38 (br s, 1H), 9.07 (br s, 1H), 8.62 (d, $J = 8.2$ Hz, 1H), 8.02 (d, $J = 8.5$ Hz, 1H), 7.74 (d, $J = 8.5$ Hz, 1H), 7.70 (d, $J = 8.8$ Hz, 2H), 7.61 (dd, $J = 8.2, 1.6$ Hz, 1H), 7.58 (d, $J = 1.6$ Hz, 1H), 6.63 (d, $J = 8.8$ Hz, 2H), 5.89 (br s, 2H), 5.13 (septet, $J = 6.3$ Hz, 1H), 4.76 (septet, $J = 6.0$ Hz, 1H), 4.62 (septet, $J = 6.0$ Hz, 1H), 4.52 (septet, $J = 6.3$ Hz, 1H), 1.35 (d, $J = 6.0$ Hz, 6H), 1.32 (d, $J = 6.3$ Hz, 6H), 1.31 (d, $J = 6.3$ Hz, 6H), 1.27 (d, $J = 6.0$ Hz, 6H); $^{13}\text{C NMR}$ (126 MHz, DMSO-d_6) δ 164.79, 164.45, 162.81, 152.68, 148.61, 145.77, 141.15, 137.73, 133.22, 129.08 (2C), 125.43, 125.03, 123.45, 122.65, 119.84, 118.65, 117.51, 113.86, 112.85 (2C), 77.15, 75.70, 72.23, 67.97, 22.24 (2C), 21.89 (2C), 21.76 (2C), 21.67 (2C); m/z (ESI+) 592 $[\text{M} + \text{H}]^+$; $t_{\text{R}} = 17.23$ min.

Isopropyl 4-(4-(4-aminobenzamido)-2-hydroxybenzamido)-3-isopropoxybenzoate 70



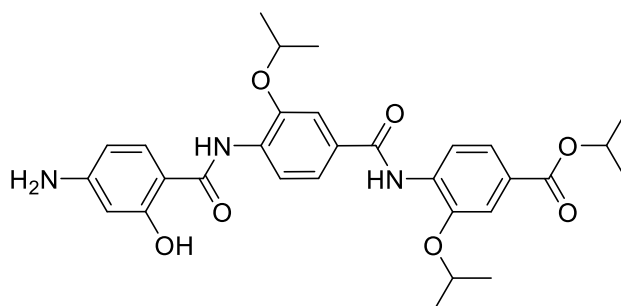
Yield 79%; beige solid; $^1\text{H NMR}$ (500 MHz, DMSO-d_6) δ 11.67 (s, 1H), 11.17 (s, 1H), 9.98 (s, 1H), 8.65 (d, $J = 8.5$ Hz, 1H), 7.95 (d, $J = 8.7$ Hz, 1H), 7.90 (d, $J = 2.0$ Hz, 1H), 7.74 (d, $J = 8.7$ Hz, 2H), 7.57 (m, 2H), 7.24 (dd, $J = 8.8, 2.0$ Hz, 1H), 6.61 (d, $J = 8.7$ Hz, 2H), 5.82 (s, 2H), 5.12 (septet, $J = 6.2$ Hz, 1H), 4.77 (septet, $J = 6.0$ Hz, 1H), 1.37 (d, $J = 6.0$ Hz, 6H), 1.32 (d, $J = 6.2$ Hz, 6H); $^{13}\text{C NMR}$ (126 MHz, DMSO-d_6) δ 165.68, 164.93, 163.05, 156.50, 152.46, 145.65, 144.56, 134.34, 131.35, 129.63 (2C), 124.38, 122.61, 120.67, 118.46, 113.46, 113.31, 112.51 (2C), 111.53, 106.82, 71.63, 67.88, 64.89, 21.73 (2C), 21.70 (2C); m/z (ESI+) 492 $[\text{M} + \text{H}]^+$; $t_{\text{R}} = 12.94$ min.

Isopropyl 4-(4-(4-aminobenzamido)-3-isopropoxybenzamido)-3-isopropoxybenzoate 71



Yield 96%; white solid; $^1\text{H NMR}$ (500 MHz, CDCl_3) δ 8.88 (br s, 1H), 8.70 (br s, 1H), 8.69 (d, $J = 8.5$ Hz, 1H), 8.62 (d, $J = 8.5$ Hz, 1H), 7.74 (d, $J = 8.8$ Hz, 2H), 7.72 (dd, $J = 8.5, 1.6$ Hz, 1H), 7.62 (d, $J = 1.9$ Hz, 1H), 7.61 (d, $J = 1.6$ Hz, 1H), 7.41 (dd, $J = 8.5, 1.9$ Hz, 1H), 6.75 (d, $J = 8.8$ Hz, 2H), 5.25 (septet, $J = 6.3$ Hz, 1H), 4.80 (septet, $J = 6.0$ Hz, 1H), 4.77 (septet, $J = 6.0$ Hz, 1H), 4.09 (br s, 2H), 1.47 (d, $J = 6.0$ Hz, 6H), 1.45 (d, $J = 6.0$ Hz, 6H), 1.39 (d, $J = 6.3$ Hz, 6H); $^{13}\text{C NMR}$ (126 MHz, CDCl_3) δ 165.87, 164.98, 164.63, 150.16, 146.40, 145.74, 132.98, 132.65, 129.23, 128.94 (2C), 125.69, 124.17, 123.17, 118.88, 118.78, 118.42, 114.32 (2C), 113.19, 111.87, 71.88, 71.73, 68.30, 22.21 (4C), 21.97 (2C); m/z (ESI+) 534 $[\text{M} + \text{H}]^+$; $t_{\text{R}} = 15.30$ min.

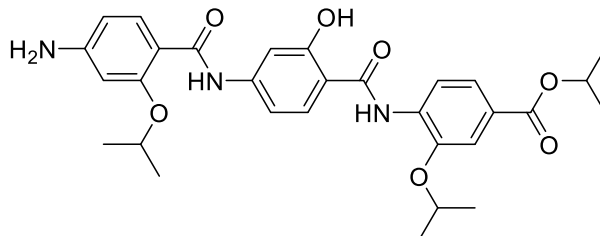
Isopropyl 4-(4-(4-amino-2-hydroxybenzamido)-3-isopropoxybenzamido)-3-isopropoxybenzoate 72



Yield 41%; beige solid; $^1\text{H NMR}$ (500 MHz, DMSO-d_6) δ 11.06 (s, 1H), 10.87 (s, 1H), 9.26 (s, 1H), 8.65 (d, $J = 8.5$ Hz, 1H), 8.23 (d, $J = 8.5$ Hz, 1H), 7.70 (d, $J = 9.1$ Hz, 1H), 7.60 (dd, $J = 8.5, 1.9$ Hz, 1H), 7.58 (d, $J = 1.9$ Hz, 1H), 7.57 (d, $J = 1.9$ Hz, 1H), 7.53 (dd, $J = 8.5, 1.9$ Hz, 1H), 6.18 (m, 2H), 5.83 (s, 2H), 5.13 (septet, $J = 6.3$ Hz, 1H), 4.81 (septet, $J = 6.0$ Hz, 1H), 4.74 (septet, $J = 6.0$ Hz, 1H), 1.39 (d, $J = 6.0$ Hz, 6H), 1.36 (d, $J = 6.0$ Hz, 6H), 1.33 (d, $J = 6.3$ Hz, 6H); $^{13}\text{C NMR}$ (126 MHz, DMSO-d_6) δ 164.85, 164.29, 163.83, 157.64, 153.92, 147.46, 145.67, 133.77, 132.93, 132.36, 127.68,

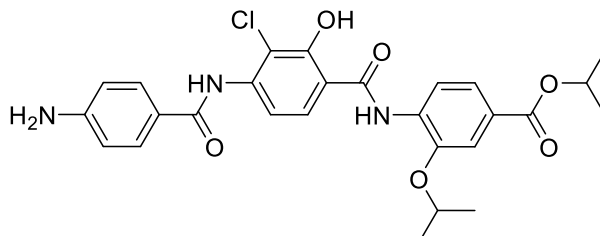
125.86, 122.05, 121.03, 120.33, 118.48, 113.76, 111.98, 106.78, 106.65, 99.37, 71.57, 71.28, 68.05, 21.84 (2C), 21.66 (4C); m/z (ESI+) 550 $[M + H]^+$; $t_R = 16.67$ min.

Isopropyl 4-(4-(4-amino-2-isopropoxybenzamido)-2-hydroxybenzamido)-3-isopropoxybenzoate 73



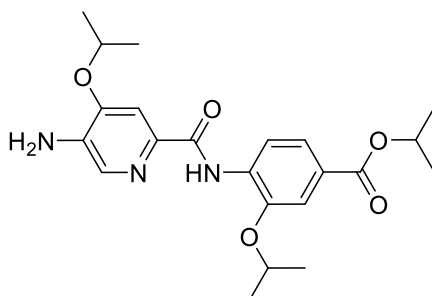
Yield 73%; pale orange solid; 1H NMR (500 MHz, DMSO- d_6) δ 11.72 (s, 1H), 11.15 (s, 1H), 10.18 (s, 1H), 8.65 (d, $J = 8.5$ Hz, 1H), 7.98 (d, $J = 8.5$ Hz, 1H), 7.79 (d, $J = 1.9$ Hz, 1H), 7.71 (d, $J = 8.5$ Hz, 1H), 7.58 (dd, $J = 8.5, 1.6$ Hz, 1H), 7.55 (d, $J = 1.6$ Hz, 1H), 7.04 (dd, $J = 8.5, 1.9$ Hz, 1H), 6.33 (d, $J = 1.9$ Hz, 1H), 6.27 (dd, $J = 8.5, 1.9$ Hz, 1H), 5.92 (br s, 2H), 5.12 (septet, $J = 6.3$ Hz, 1H), 4.78 (septet, $J = 6.0$ Hz, 1H), 4.72 (septet, $J = 6.0$ Hz, 1H), 1.46 (d, $J = 6.0$ Hz, 6H), 1.38 (d, $J = 6.0$ Hz, 6H), 1.32 (d, $J = 6.3$ Hz, 6H); ^{13}C NMR (126 MHz, DMSO- d_6) δ 164.91, 163.64, 162.89, 157.15, 156.79, 154.19, 145.62, 143.70, 134.28, 132.95, 131.92, 124.39, 122.60, 118.41, 113.45, 113.43, 110.69, 108.97, 106.85, 106.11, 97.87, 71.59, 71.49, 67.88, 21.95 (2C), 21.73 (2C), 21.69 (2C); m/z (ESI+) 550 $[M + H]^+$; $t_R = 14.40$ min.

Isopropyl 4-(4-(4-aminobenzamido)-3-chloro-2-hydroxybenzamido)-3-isopropoxybenzoate 77



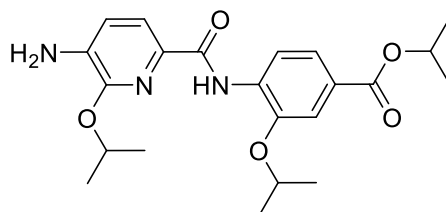
Yield 92%; white solid; 1H NMR (500 MHz, $CDCl_3$) δ 12.98 (br s, 1H), 8.96 (br s, 1H), 8.62 (br s, 1H), 8.48 (d, $J = 8.5$ Hz, 1H), 8.31 (d, $J = 8.8$ Hz, 1H), 7.77 (d, $J = 8.5$ Hz, 2H), 7.70 (dd, $J = 8.5, 1.6$ Hz, 1H), 7.61 (d, $J = 1.6$ Hz, 1H), 7.45 (d, $J = 8.8$ Hz, 1H), 6.74 (d, $J = 8.5$ Hz, 2H), 5.25 (septet, $J = 6.3$ Hz, 1H), 4.78 (septet, $J = 6.0$ Hz, 1H), 4.20 (br s, 2H), 1.47 (d, $J = 6.0$ Hz, 6H), 1.38 (d, $J = 6.3$ Hz, 6H); ^{13}C NMR (126 MHz, $CDCl_3$) δ 167.33, 165.63, 165.07, 158.19, 150.76, 146.04, 140.65, 131.46, 129.22 (2C), 126.65, 124.18, 123.08, 122.97, 119.09, 114.29 (2C), 113.22, 110.74, 110.61, 110.56, 72.10, 68.48, 22.17 (2C), 21.92 (2C); m/z (ESI+) 526 $[M + H]^+$; $t_R = 16.82$ min.

Isopropyl 4-(5-amino-4-isopropoxypicolinamido)-3-isopropoxybenzoate 80



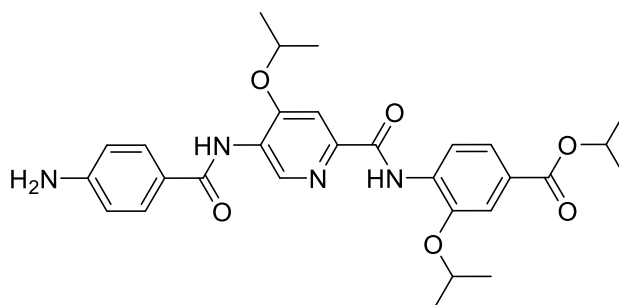
Yield 95%; white crystals; ^1H NMR (500 MHz, CDCl_3) δ 10.73 (br s, 1H), 8.65 (d, $J = 8.5$ Hz, 1H), 7.98 (s, 1H), 7.72 (dd, $J = 8.5, 1.9$ Hz, 1H), 7.71 (s, 1H), 7.61 (d, $J = 1.9$ Hz, 1H), 5.24 (septet, $J = 6.3$ Hz, 1H), 4.82 (septet, $J = 6.0$ Hz, 1H), 4.70 (septet, $J = 6.0$ Hz, 1H), 4.09 (br s, 2H), 1.46 (d, $J = 6.0$ Hz, 6H), 1.42 (d, $J = 6.0$ Hz, 6H), 1.38 (d, $J = 6.3$ Hz, 6H); ^{13}C NMR (126 MHz, CDCl_3) δ 166.00, 163.08, 151.07, 146.39, 141.90, 136.09, 134.22, 133.52, 125.29, 123.28, 118.24, 114.24, 105.70, 72.18, 70.84, 68.15, 22.13 (2C), 21.97 (2C), 21.92 (2C); m/z (ESI+) 416 $[\text{M} + \text{H}]^+$; $t_{\text{R}} = 18.92$ min.

Isopropyl 4-(5-amino-6-isopropoxy-picolinamido)-3-isopropoxybenzoate 81

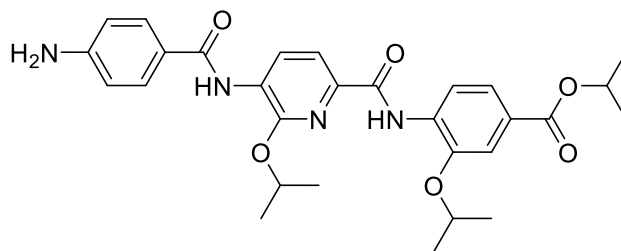


Yield 92%; beige crystals; ^1H NMR (500 MHz, CDCl_3) δ 10.31 (br s, 1H), 8.74 (d, $J = 8.5$ Hz, 1H), 7.77 (d, $J = 7.9$ Hz, 1H), 7.70 (dd, $J = 8.5, 1.9$ Hz, 1H), 7.60 (d, $J = 1.9$ Hz, 1H), 6.97 (d, $J = 7.9$ Hz, 1H), 5.59 (septet, $J = 6.3$ Hz, 1H), 5.25 (septet, $J = 6.3$ Hz, 1H), 4.80 (septet, $J = 6.0$ Hz, 1H), 4.22 (br s, 2H), 1.45 (d, $J = 6.3$ Hz, 6H), 1.44 (d, $J = 6.0$ Hz, 6H), 1.38 (d, $J = 6.3$ Hz, 6H); ^{13}C NMR (126 MHz, CDCl_3) δ 166.04, 163.03, 149.67, 145.96, 135.41, 134.92, 133.22, 125.18, 123.07, 119.16, 118.42, 117.67, 113.08, 71.13, 68.31, 68.17, 22.15 (2C), 22.11 (2C), 21.98 (2C); m/z (ESI+) 416 $[\text{M} + \text{H}]^+$; $t_{\text{R}} = 15.35$ min.

Isopropyl 4-(5-(4-aminobenzamido)-4-isopropoxypicolinamido)-3-isopropoxybenzoate 84



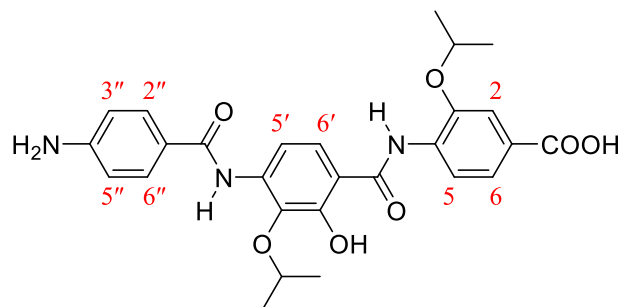
Yield 95%; white crystals; mp 196–198 °C; ^1H NMR (500 MHz, CDCl_3) δ 10.95 (br s, 1H), 9.74 (s, 1H), 8.65 (d, $J = 8.2$ Hz, 1H), 8.40 (br s, 1H), 7.84 (s, 1H), 7.74 (d, $J = 8.8$ Hz, 2H), 7.73 (dd, $J = 8.2, 1.9$ Hz, 1H), 7.62 (d, $J = 1.9$ Hz, 1H), 6.75 (d, $J = 8.8$ Hz, 2H), 5.25 (septet, $J = 6.3$ Hz, 1H), 4.92 (septet, $J = 6.0$ Hz, 1H), 4.72 (septet, $J = 6.0$ Hz, 1H), 4.13 (br s, 2H), 1.50 (d, $J = 6.0$ Hz, 6H), 1.48 (d, $J = 6.0$ Hz, 6H), 1.38 (d, $J = 6.3$ Hz, 6H); ^{13}C NMR (126 MHz, CDCl_3) δ 165.94, 164.74, 162.38, 152.72, 150.36, 146.57, 145.72, 139.25, 133.16, 129.08 (2C), 128.25, 125.71, 123.41, 123.20, 118.30, 114.30 (2C), 114.21, 105.25, 72.33, 72.09, 68.21, 22.12 (2C), 21.97 (2C), 21.94 (2C); m/z (ESI+) 535 $[\text{M} + \text{H}]^+$; $t_{\text{R}} = 19.36$ min.

Isopropyl 4-(5-(4-aminobenzamido)-6-isopropoxy-picolinamido)-3-isopropoxybenzoate 85

Yield 95%; beige crystals; ^1H NMR (500 MHz, CDCl_3) δ 10.34 (br s, 1H), 8.95 (d, $J = 8.2$ Hz, 1H), 8.75 (d, $J = 8.5$ Hz, 1H), 8.49 (br s, 1H), 7.97 (d, $J = 8.2$ Hz, 1H), 7.73 (d, $J = 8.5$ Hz, 2H), 7.72 (dd, $J = 8.5, 1.9$ Hz, 1H), 7.62 (d, $J = 1.9$ Hz, 1H), 6.75 (d, $J = 8.5$ Hz, 2H), 5.67 (septet, $J = 6.3$ Hz, 1H), 5.25 (septet, $J = 6.3$ Hz, 1H), 4.82 (septet, $J = 6.3$ Hz, 1H), 4.12 (br s, 2H), 1.52 (d, $J = 6.3$ Hz, 6H), 1.45 (d, $J = 6.3$ Hz, 6H), 1.39 (d, $J = 6.3$ Hz, 6H); ^{13}C NMR (126 MHz, CDCl_3) δ 165.97, 165.27, 162.22, 150.52, 150.40, 146.03, 139.77, 132.78, 129.02 (2C), 126.87, 126.29, 125.63, 123.55, 123.07, 118.64, 117.35, 114.30 (2C), 113.07, 71.15, 69.52, 68.26, 22.17 (2C), 22.13 (2C), 21.98 (2C); m/z (ESI+) 535 $[\text{M} + \text{H}]^+$; $t_{\text{R}} = 16.12$ min.

General procedure for synthesis of the carboxylic acids 3 (Cys507), 5–16 and 75.

To a stirred solution of the amino/nitro ester (0.2 mmol) in a mixture of MeOH (6 mL) and THF (2 mL), 1 N NaOH (1 mL) was added. The reaction was stirred at room temperature overnight. Solvent was concentrated *in vacuo*. The remaining residue was dissolved in water (10 mL), cooled in an ice bath and acidified by KHSO_4 (saturated aqueous solution) to pH 6, then extracted with EtOAc/THF (1:1, 3×20 mL). The combined organic extract was washed with brine, dried over anhydrous MgSO_4 , and the solvent was removed by vacuum distillation. The obtained material was triturated with *n*-hexane/EtOAc (4:1, 25 mL), and collected by filtration.

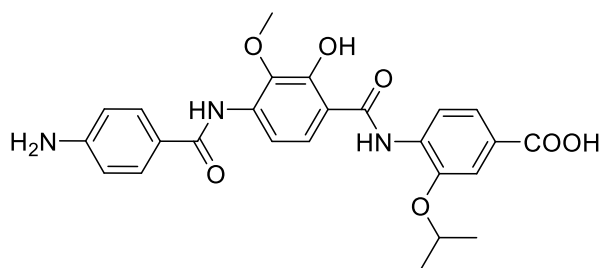
4-(4-(4-Aminobenzamido)-2-hydroxy-3-isopropoxybenzamido)-3-isopropoxybenzoic acid 3

Yield 96%; beige solid; m/z (ESI+) 508 $[\text{M} + \text{H}]^+$.

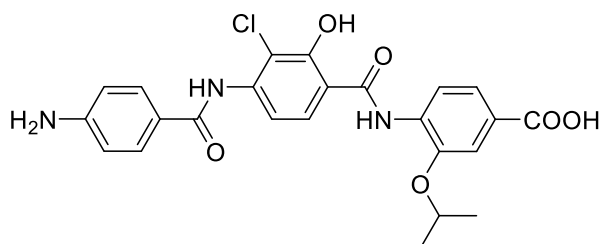
Table S1. ^1H and ^{13}C NMR data of Cys507 in DMSO- d_6 and acetone- d_6 .^a

Position	DMSO- d_6		Acetone- d_6	
	δ_{H} (multi., J in Hz)	δ_{C}	δ_{H} (multi., J in Hz)	δ_{C}
1	-	125.80	-	127.11
2	7.57 (d, 1.9)	113.91	7.69 (d, 1.6)	114.63
3	-	146.47	-	147.84
4	-	133.24	-	133.36
5	8.48 (d, 8.2)	119.76	8.50 (d, 8.5)	120.79
6	7.59 (dd, 8.2, 1.9)	122.61	7.72 (dd, 8.5, 1.6)	123.70
C1-COOH	12.77	166.97	not appeared	167.26
C3-OCH(CH ₃) ₂	4.75 (sept, 6.0)	71.73	4.88 (sept, 6.0)	72.89
C3-OCH(CH ₃) ₂	1.37 (d, 6.0)	21.69	1.47 (d, 6.0)	22.26
C4-NH	10.92 (br s)	-	9.64 (br s)	-
1'	-	115.51	-	112.39
2'	-	115.66	-	154.45
3'	-	150.33	-	137.16
4'	-	137.39	-	135.22
5'	-	136.88	-	139.16
6'	-	136.99	-	111.31
	7.64 (d, 8.8)	114.20	8.18 (d, 8.8)	111.31
	7.67 (d, 8.8)	113.91		
	7.78 (d, 8.8)	124.95	7.65 (d, 8.8)	123.38
C1'-C=O	-	163.86	-	168.26
	-	163.89		
C2'-OH	11.22 (br s)	-	not appeared	-
C3'-OCH(CH ₃) ₂	4.35 (sept, 6.0)	75.38	4.78 (sept, 6.0)	76.02
C3'-OCH(CH ₃) ₂	1.28 (d, 6.0)	22.05	1.38 (d, 6.0)	22.90
	1.29 (d, 6.0)	22.05		
C4'-NH	9.10 (br s)	-	8.82 (br s)	-
	9.20 (br s)	-		
1''	-	120.14	-	122.59
	-	121.02		
2'', 6''	7.70 (d, 8.8)	129.12	7.75 (d, 8.8)	129.85
	7.79 (d, 8.8)	129.00		
3'', 5''	6.63 (d, 8.8)	112.83	6.79 (d, 8.8)	114.39
	6.82 (d, 8.8)	111.72		
4''	-	150.77	-	153.49
	-	152.59		
C1''-C=O	-	164.49	-	165.26
	-	164.53		
C4''-NH ₂	4.63 (t, 5.7)	-	5.43 (br s)	-
	5.87 (br s)	-		
	7.20 (t, 5.7)	-		

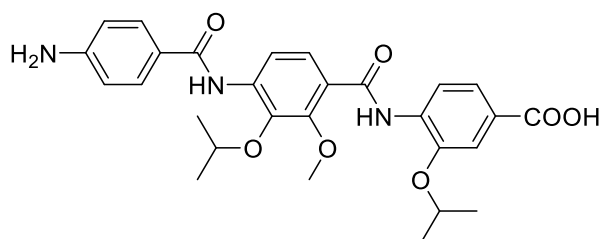
^aTwo rotamers of Cys507 were observed in DMSO- d_6 . By changing the solvent, only single values were observed in acetone- d_6 .

4-(4-(4-Aminobenzamido)-2-hydroxy-3-methoxybenzamido)-3-isopropoxybenzoic acid 5

Yield 85%; pale yellow crystals; $^1\text{H NMR}$ (500 MHz, DMSO-d_6) δ 12.79 (br s, 1H), 11.38 (br s, 1H), 10.98 (br s, 1H), 9.22 (br s, 1H), 8.56 (d, $J = 8.5$ Hz, 1H), 7.80 (d, $J = 8.8$ Hz, 1H), 7.73 (d, $J = 8.5$ Hz, 2H), 7.65 (d, $J = 8.8$ Hz, 1H), 7.59 (dd, $J = 8.5, 1.6$ Hz, 1H), 7.57 (d, $J = 1.6$ Hz, 1H), 6.69 (d, $J = 8.5$ Hz, 2H), 5.39 (br s, 2H), 4.76 (septet, $J = 6.0$ Hz, 1H), 3.78 (s, 3H), 1.39 (d, $J = 6.0$ Hz, 6H); $^{13}\text{C NMR}$ (126 MHz, DMSO-d_6) δ 166.99, 165.03, 163.28, 151.46, 149.53, 146.13, 139.38, 136.34, 133.45, 129.43 (2C), 125.62, 125.55, 122.65, 121.21, 119.28, 115.71, 113.89, 113.75, 113.43 (2C), 71.72, 60.40, 21.73 (2C); m/z (ESI+) 480 $[\text{M} + \text{H}]^+$; $t_{\text{R}} = 14.53$ min.

4-(4-(4-Aminobenzamido)-3-chloro-2-hydroxybenzamido)-3-isopropoxybenzoic acid 6

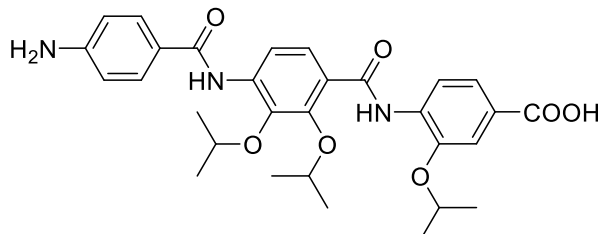
Yield 90%; pale yellow solid; $^1\text{H NMR}$ (500 MHz, DMSO-d_6) δ 12.82 (br s, 1H), 11.96 (br s, 1H), 10.88 (br s, 1H), 9.44 (br s, 1H), 8.39 (d, $J = 8.2$ Hz, 1H), 8.03 (d, $J = 8.8$ Hz, 1H), 7.74 (d, $J = 8.8$ Hz, 2H), 7.60 (dd, $J = 8.2, 1.6$ Hz, 1H), 7.59 (d, $J = 1.6$ Hz, 1H), 7.58 (d, $J = 8.8$ Hz, 1H), 6.63 (d, $J = 8.8$ Hz, 2H), 5.99 (br s, 2H), 4.77 (septet, $J = 6.3$ Hz, 1H), 1.38 (d, $J = 6.3$ Hz, 6H); $^{13}\text{C NMR}$ (126 MHz, DMSO-d_6) δ 166.95, 164.88, 163.82, 153.43, 152.73, 147.09, 140.51, 132.57, 129.56 (2C), 128.25, 126.50, 122.40, 120.72, 119.82, 116.44, 116.30, 116.12, 113.81, 112.70 (2C), 71.54, 21.71 (2C); m/z (ESI+) 484 $[\text{M} + \text{H}]^+$; $t_{\text{R}} = 15.32$ min.

4-(4-(4-Aminobenzamido)-3-isopropoxy-2-methoxybenzamido)-3-isopropoxybenzoic acid 7

Yield 43%; beige solid; $^1\text{H NMR}$ (500 MHz, DMSO-d_6) δ 12.82 (br s, 1H), 10.90 (br s, 1H), 9.09 (br s, 1H), 8.62 (d, $J = 8.2$ Hz, 1H), 8.06 (d, $J = 8.8$ Hz, 1H), 7.84 (d, $J = 8.8$ Hz, 1H), 7.70 (d, $J = 8.5$ Hz, 2H), 7.60 (dd, $J = 8.2, 1.6$ Hz, 1H), 7.58 (d, $J = 1.6$ Hz, 1H), 6.63 (d, $J = 8.5$ Hz, 2H), 5.92 (br s, 2H), 4.85 (septet, $J = 6.0$ Hz, 1H), 4.47 (septet, $J = 6.0$ Hz, 1H), 4.04 (s, 3H), 1.40 (d, $J = 6.0$ Hz, 6H), 1.32

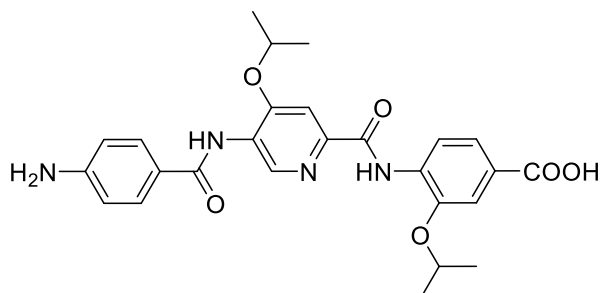
(d, $J = 6.0$ Hz, 6H); ^{13}C NMR (126 MHz, DMSO- d_6) δ 166.96, 164.45, 161.87, 152.74, 151.59, 145.55, 140.72, 138.04, 133.03, 129.11 (2C), 125.79, 125.47, 122.67, 120.61, 119.78, 118.58, 117.31, 113.14, 112.87 (2C), 76.50, 71.14, 61.78, 22.36 (2C), 21.66 (2C); m/z (ESI+) 522 $[\text{M} + \text{H}]^+$; $t_{\text{R}} = 15.58$ min.

4-(4-(4-Aminobenzamido)-2,3-diisopropoxybenzamido)-3-isopropoxybenzoic acid 8



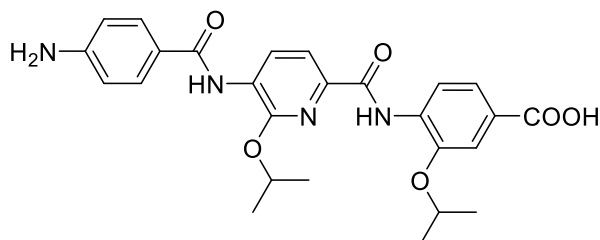
Yield 81%; beige solid; ^1H NMR (500 MHz, DMSO- d_6) δ 12.82 (br s, 1H), 10.36 (br s, 1H), 9.06 (br s, 1H), 8.60 (d, $J = 8.5$ Hz, 1H), 8.01 (d, $J = 8.8$ Hz, 1H), 7.75 (d, $J = 8.8$ Hz, 1H), 7.70 (d, $J = 8.8$ Hz, 2H), 7.61 (dd, $J = 8.5, 1.9$ Hz, 1H), 7.58 (d, $J = 1.9$ Hz, 1H), 6.63 (d, $J = 8.8$ Hz, 2H), 5.90 (br s, 2H), 4.75 (septet, $J = 6.0$ Hz, 1H), 4.63 (septet, $J = 6.3$ Hz, 1H), 4.52 (septet, $J = 6.0$ Hz, 1H), 1.35 (d, $J = 6.0$ Hz, 6H), 1.31 (d, $J = 6.0$ Hz, 6H), 1.27 (d, $J = 6.3$ Hz, 6H); ^{13}C NMR (126 MHz, DMSO- d_6) δ 166.88, 164.45, 162.79, 152.66, 148.60, 145.71, 141.15, 137.69, 132.89, 129.08 (2C), 125.58, 125.44, 123.52, 122.83, 119.87, 118.64, 117.50, 113.94, 112.87 (2C), 77.12, 75.70, 72.02, 22.25 (2C), 21.90 (2C), 21.79 (2C); m/z (ESI+) 550 $[\text{M} + \text{H}]^+$; $t_{\text{R}} = 13.10$ min.

4-(5-(4-Aminobenzamido)-4-isopropoxypicolinamido)-3-isopropoxybenzoic acid 9



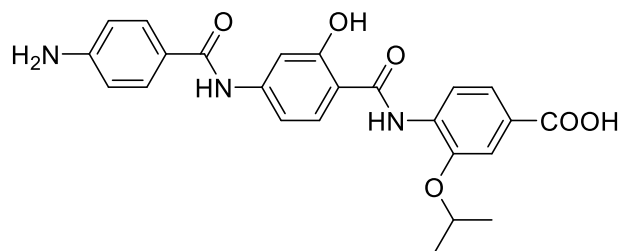
Yield 93%; beige solid; mp 299–301 °C; ^1H NMR (500 MHz, DMSO- d_6) δ 12.87 (br s, 1H), 10.79 (br s, 1H), 9.15 (s, 1H), 9.07 (br s, 1H), 8.56 (d, $J = 8.5$ Hz, 1H), 7.80 (s, 1H), 7.70 (d, $J = 8.5$ Hz, 2H), 7.64 (dd, $J = 8.5, 1.6$ Hz, 1H), 7.60 (d, $J = 1.6$ Hz, 1H), 6.63 (d, $J = 8.5$ Hz, 2H), 5.92 (br s, 2H), 4.99 (septet, $J = 6.0$ Hz, 1H), 4.77 (septet, $J = 6.0$ Hz, 1H), 1.40 (d, $J = 6.0$ Hz, 6H), 1.39 (d, $J = 6.0$ Hz, 6H); ^{13}C NMR (126 MHz, DMSO- d_6) δ 166.92, 164.88, 161.48, 155.39, 152.80, 146.01, 145.67, 142.30, 132.39, 129.52 (2C), 128.30, 125.85, 123.02, 119.68, 117.75, 114.22, 112.74 (2C), 106.03, 72.03, 71.69, 21.86 (2C), 21.42 (2C); m/z (ESI+) 493 $[\text{M} + \text{H}]^+$; $t_{\text{R}} = 18.34$ min.

4-(5-(4-Aminobenzamido)-6-isopropoxypicolinamido)-3-isopropoxybenzoic acid 10



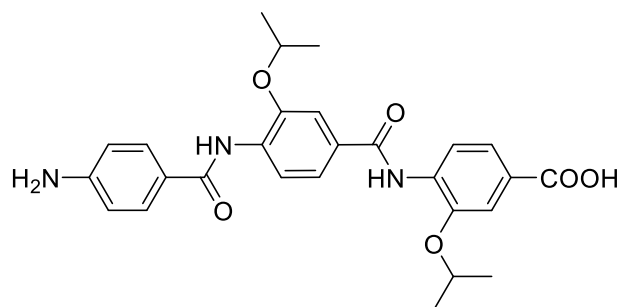
Yield 90%; off-white crystals; ^1H NMR (500 MHz, DMSO- d_6) δ 13.61 (br s, 1H), 10.31 (br s, 1H), 8.99 (br s, 1H), 8.62 (d, $J = 7.9$ Hz, 1H), 8.60 (d, $J = 8.2$ Hz, 1H), 7.82 (d, $J = 7.9$ Hz, 1H), 7.67 (d, $J = 8.5$ Hz, 2H), 7.62 (dd, $J = 8.2, 1.6$ Hz, 1H), 7.61 (d, $J = 1.6$ Hz, 1H), 6.64 (d, $J = 8.5$ Hz, 2H), 5.93 (br s, 2H), 5.54 (septet, $J = 6.3$ Hz, 1H), 4.86 (septet, $J = 6.0$ Hz, 1H), 1.47 (d, $J = 6.3$ Hz, 6H), 1.38 (d, $J = 6.0$ Hz, 6H); ^{13}C NMR (126 MHz, DMSO- d_6) δ 167.12, 165.07, 161.33, 152.91, 151.88, 145.61, 139.36, 131.67, 129.34 (2C), 128.38, 127.07, 126.58, 122.54, 119.69, 117.80, 116.33, 113.16, 112.82 (2C), 71.07, 69.26, 21.70 (2C), 21.64 (2C); m/z (ESI+) 493 $[\text{M} + \text{H}]^+$; $t_{\text{R}} = 12.75$ min.

4-(4-(4-Aminobenzamido)-2-hydroxybenzamido)-3-isopropoxybenzoic acid 11

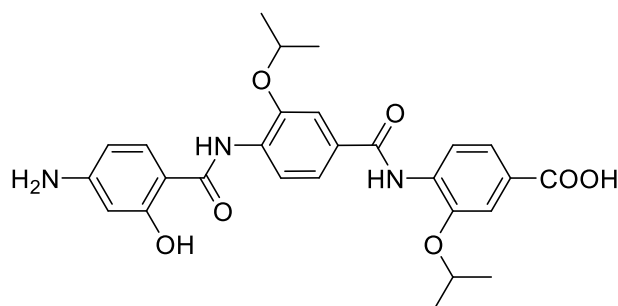


Yield 73%; beige solid; ^1H NMR (500 MHz, DMSO- d_6) δ 12.75 (br s, 1H), 11.67 (s, 1H), 11.15 (s, 1H), 10.00 (s, 1H), 8.63 (d, $J = 8.5$ Hz, 1H), 7.96 (d, $J = 8.5$ Hz, 1H), 7.90 (d, $J = 1.6$ Hz, 1H), 7.75 (d, $J = 8.5$ Hz, 2H), 7.58 (dd, $J = 8.5, 1.6$ Hz, 1H), 7.56 (d, $J = 1.6$ Hz, 1H), 7.25 (dd, $J = 8.5, 1.6$ Hz, 1H), 6.65 (d, $J = 8.5$ Hz, 2H), 5.85 (br s, 2H), 4.77 (septet, $J = 6.0$ Hz, 1H), 1.37 (d, $J = 6.0$ Hz, 6H); ^{13}C NMR (126 MHz, DMSO- d_6) δ 167.03, 165.66, 163.04, 156.50, 151.79, 145.58, 144.49, 133.99, 131.36, 129.63 (2C), 124.93, 122.79, 121.18, 118.44, 113.55, 113.40, 112.91 (2C), 111.54, 106.86, 71.43, 21.77 (2C); m/z (ESI+) 450 $[\text{M} + \text{H}]^+$; $t_{\text{R}} = 9.33$ min.

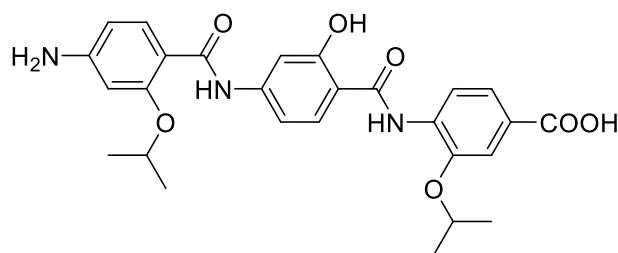
4-(4-(4-Aminobenzamido)-3-isopropoxybenzamido)-3-isopropoxybenzoic acid 12



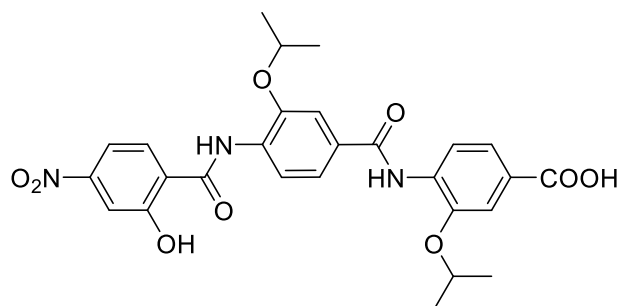
Yield 94%; white solid; ^1H NMR (500 MHz, DMSO- d_6) δ 12.69 (br s, 1H), 9.29 (br s, 1H), 8.89 (br s, 1H), 8.32 (d, $J = 8.2$ Hz, 1H), 8.19 (d, $J = 8.2$ Hz, 1H), 7.65 (d, $J = 8.5$ Hz, 2H), 7.60 (dd, $J = 8.2, 1.6$ Hz, 1H), 7.60 (d, $J = 1.6$ Hz, 1H), 7.58 (d, $J = 1.6$ Hz, 1H), 7.55 (dd, $J = 8.2, 1.6$ Hz, 1H), 6.64 (d, $J = 8.5$ Hz, 2H), 5.89 (br s, 2H), 4.80 (septet, $J = 6.0$ Hz, 1H), 4.72 (septet, $J = 6.0$ Hz, 1H), 1.40 (d, $J = 6.0$ Hz, 6H), 1.36 (d, $J = 6.0$ Hz, 6H); ^{13}C NMR (126 MHz, DMSO- d_6) δ 167.02, 164.48, 164.31, 152.67, 147.58, 146.90, 132.48, 132.34, 129.11, 128.96 (2C), 126.75, 122.23, 121.24, 120.23, 120.19, 120.04, 113.92, 112.95 (2C), 112.14, 71.44, 71.41, 21.81 (2C), 21.73 (2C); m/z (ESI+) 492 $[\text{M} + \text{H}]^+$; $t_{\text{R}} = 12.06$ min.

4-(4-(4-Amino-2-hydroxybenzamido)-3-isopropoxybenzamido)-3-isopropoxybenzoic acid 13

Yield 70%; beige solid; $^1\text{H NMR}$ (500 MHz, DMSO-d_6) δ 11.20 (s, 1H), 10.91 (s, 1H), 9.26 (s, 1H), 8.65 (d, $J = 8.5$ Hz, 1H), 8.19 (d, $J = 8.2$ Hz, 1H), 7.71 (d, $J = 8.5$ Hz, 1H), 7.59 (dd, $J = 8.2, 1.6$ Hz, 1H), 7.58 (d, $J = 1.9$ Hz, 1H), 7.56 (d, $J = 1.6$ Hz, 1H), 7.53 (dd, $J = 8.5, 1.9$ Hz, 1H), 6.24 (d, $J = 1.6$ Hz, 1H), 6.20 (dd, $J = 8.5, 1.6$ Hz, 1H), 5.97 (br s, 3H), 4.81 (septet, $J = 6.0$ Hz, 1H), 4.73 (septet, $J = 6.0$ Hz, 1H), 1.39 (d, $J = 6.0$ Hz, 6H), 1.36 (d, $J = 6.0$ Hz, 6H); $^{13}\text{C NMR}$ (126 MHz, DMSO-d_6) δ 167.00, 164.34, 163.80, 157.68, 153.29, 147.50, 145.69, 133.77, 132.59, 132.43, 127.81, 126.50, 122.25, 121.13, 120.41, 118.49, 113.86, 111.98, 107.18, 106.99, 99.89, 71.37, 71.33, 21.89 (2C), 21.73 (2C); m/z (ESI+) 508 $[\text{M} + \text{H}]^+$; $t_{\text{R}} = 15.23$ min.

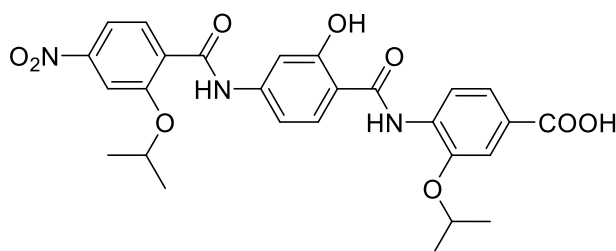
4-(4-(4-Amino-2-isopropoxybenzamido)-2-hydroxybenzamido)-3-isopropoxybenzoic acid 14

Yield 69%; beige solid; $^1\text{H NMR}$ (500 MHz, DMSO-d_6) 12.77 (br s, 1H), 11.72 (s, 1H), 11.13 (s, 1H), 10.18 (s, 1H), 8.63 (d, $J = 8.5$ Hz, 1H), 7.98 (d, $J = 8.8$ Hz, 1H), 7.77 (d, $J = 1.6$ Hz, 1H), 7.71 (d, $J = 8.5$ Hz, 1H), 7.58 (dd, $J = 8.5, 1.6$ Hz, 1H), 7.55 (d, $J = 1.6$ Hz, 1H), 7.05 (dd, $J = 8.8, 1.6$ Hz, 1H), 6.33 (d, $J = 1.6$ Hz, 1H), 6.27 (dd, $J = 8.5, 1.6$ Hz, 1H), 5.91 (br s, 2H), 4.77 (septet, $J = 6.0$ Hz, 1H), 4.72 (septet, $J = 6.0$ Hz, 1H), 1.46 (d, $J = 6.0$ Hz, 6H), 1.37 (d, $J = 6.0$ Hz, 6H); $^{13}\text{C NMR}$ (126 MHz, DMSO-d_6) δ 167.05, 163.67, 162.92, 157.19, 156.82, 154.22, 145.59, 143.70, 133.96, 132.99, 131.96, 124.98, 122.81, 118.45, 113.55, 113.54, 110.72, 109.00, 106.89, 106.15, 97.92, 71.54, 71.43, 21.97 (2C), 21.79 (2C); m/z (ESI+) 508 $[\text{M} + \text{H}]^+$; $t_{\text{R}} = 11.35$ min.

4-(4-(2-Hydroxy-4-nitrobenzamido)-3-isopropoxybenzamido)-3-isopropoxybenzoic acid 15

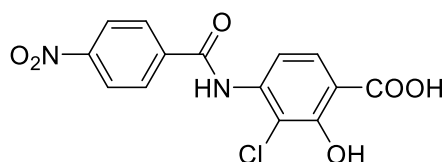
Yield 76%; yellow solid; ^1H NMR (500 MHz, DMSO-d_6) δ 12.36 (br s, 2H), 11.38 (br s, 1H), 9.29 (s, 1H), 8.67 (d, $J = 8.5$ Hz, 1H), 8.28 (d, $J = 8.8$ Hz, 1H), 8.19 (d, $J = 8.5$ Hz, 1H), 7.86 (d, $J = 1.9$ Hz, 1H), 7.77 (dd, $J = 8.8, 1.9$ Hz, 1H), 7.63 (d, $J = 1.6$ Hz, 1H), 7.60 (dd, $J = 8.5, 1.6$ Hz, 1H), 7.58 (dd, $J = 8.5, 1.6$ Hz, 1H), 7.57 (d, $J = 1.6$ Hz, 1H), 4.87 (septet, $J = 6.0$ Hz, 1H), 4.73 (septet, $J = 6.0$ Hz, 1H), 1.41 (d, $J = 6.0$ Hz, 6H), 1.36 (d, $J = 6.0$ Hz, 6H); ^{13}C NMR (126 MHz, DMSO-d_6) δ 167.02, 164.16, 161.51, 157.13, 150.03, 147.56, 146.11, 132.69, 132.42, 132.25, 129.38, 126.75, 124.44, 122.19, 121.21, 120.30, 119.10, 113.91, 113.51, 111.99, 111.85, 71.47, 71.39, 21.80 (2C), 21.69 (2C); m/z (ESI+) 538 $[\text{M} + \text{H}]^+$; $t_{\text{R}} = 14.46$ min.

4-(2-Hydroxy-4-(2-isopropoxy-4-nitrobenzamido)benzamido)-3-isopropoxybenzoic acid 16



Yield 75%; pale yellow solid; ^1H NMR (500 MHz, DMSO-d_6) δ 12.75 (br s, 1H), 11.79 (s, 1H), 11.15 (s, 1H), 10.54 (s, 1H), 8.63 (d, $J = 8.4$ Hz, 1H), 8.01 (d, $J = 8.7$ Hz, 1H), 7.90 (m, 2H), 7.81 (m, 2H), 7.56 (m, 2H), 7.16 (dd, $J = 8.7, 1.8$ Hz, 1H), 4.89 (septet, $J = 6.0$ Hz, 1H), 4.78 (septet, $J = 6.0$ Hz, 1H), 1.38 (d, $J = 6.0$ Hz, 6H), 1.35 (d, $J = 6.0$ Hz, 6H); ^{13}C NMR (126 MHz, DMSO-d_6) δ 167.00, 163.80, 162.78, 156.65, 155.22, 149.47, 145.59, 143.09, 133.86, 132.35, 131.89, 130.46, 125.06, 122.78, 118.45, 115.32, 114.41, 113.54, 111.05, 108.88, 106.69, 72.37, 71.42, 21.77 (2C), 21.59 (2C); m/z (ESI+) 538 $[\text{M} + \text{H}]^+$; $t_{\text{R}} = 16.01$ min.

3-Chloro-2-hydroxy-4-(4-nitrobenzamido)benzoic acid 75



Yield 75%; pale yellow solid; m/z (ESI+) 337 $[\text{M} + \text{H}]^+$; $t_{\text{R}} = 17.50$ min.

6.3.3 2D-NOESY Measurement in a Cryoprotective Mixture

NMR spectrum was recorded on Bruker DRX-500 spectrometer at 300 K. Compound **58** was prepared as 20 mM solution in H₂O/DMSO-d₆ (20% V/V). Sample was degased *via* flushing the tube with nitrogen gas, cooling in liquid nitrogen until freezing, then application of vacuum until attaining the room temperature. The process was repeated three times and then the tube was covered and sealed with parafilm.

Conformational Interconversion at physiological Temperature

¹H NMR spectra were determined for compound **58** (20 mM solution in CDCl₃) at 293 and 310 K. Analysis of spectra was performed using ACD/NMR Processor Academic Edition version 12.01.

Effect of Temperature on Rigidity 2D-NOESY was measured for compound **9** in DMSO-d₆ at different temperatures (300, 320, 340, and 360 K). No change in NOESY spectra up to 340 K. At 360 K, a very weak cross peak between the C4–NH and the pyridine C3–H started to appear (Figure S19 and S20).

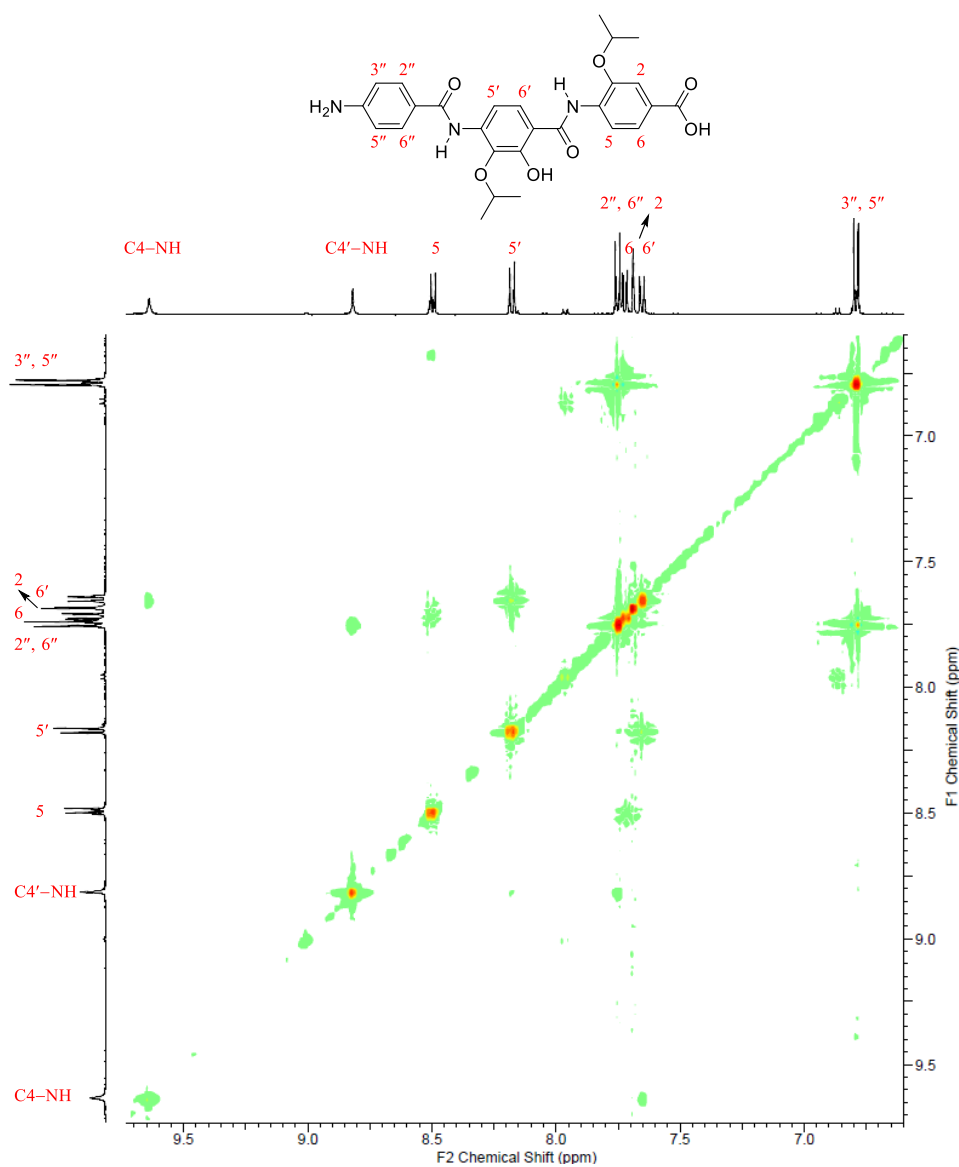
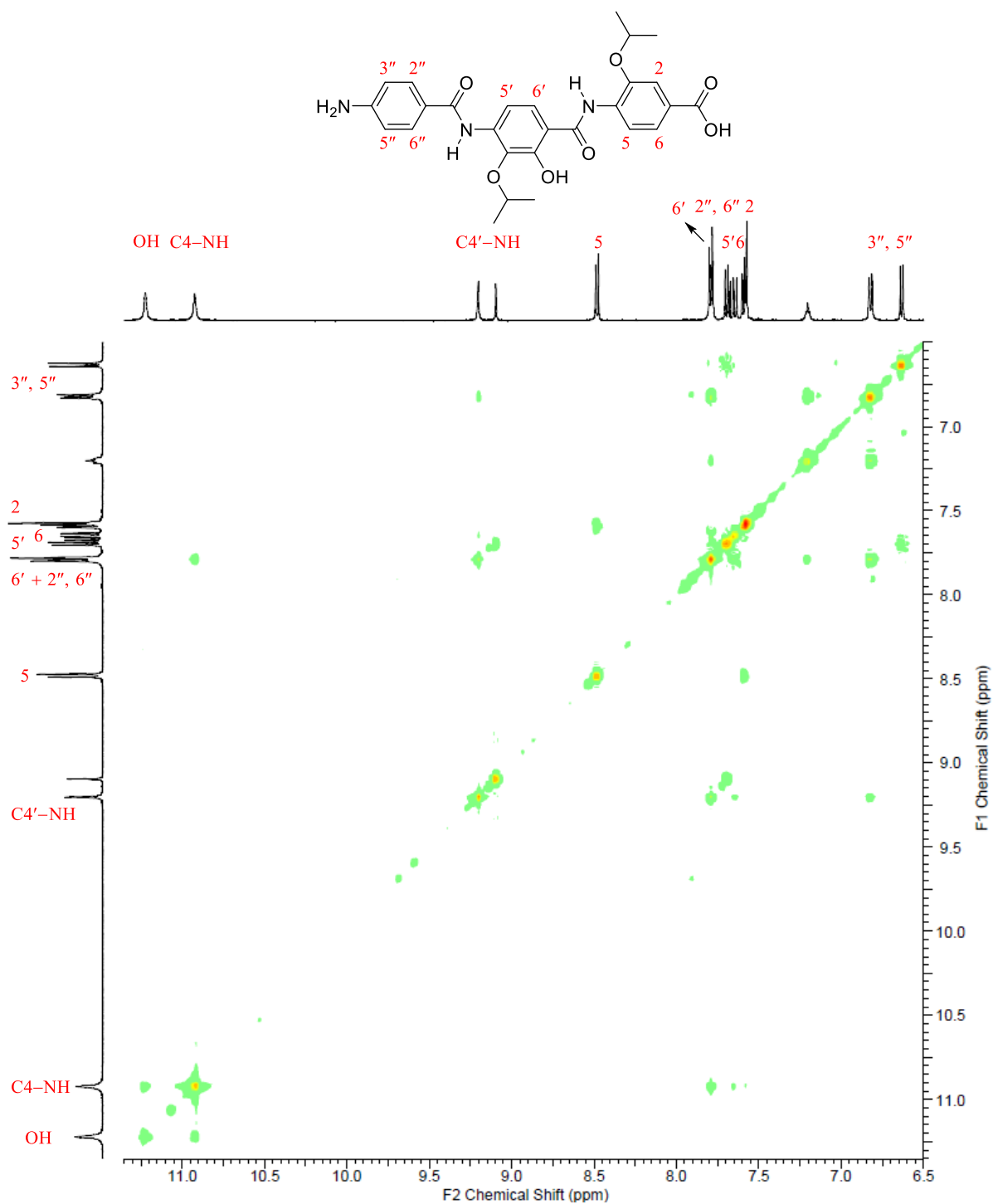
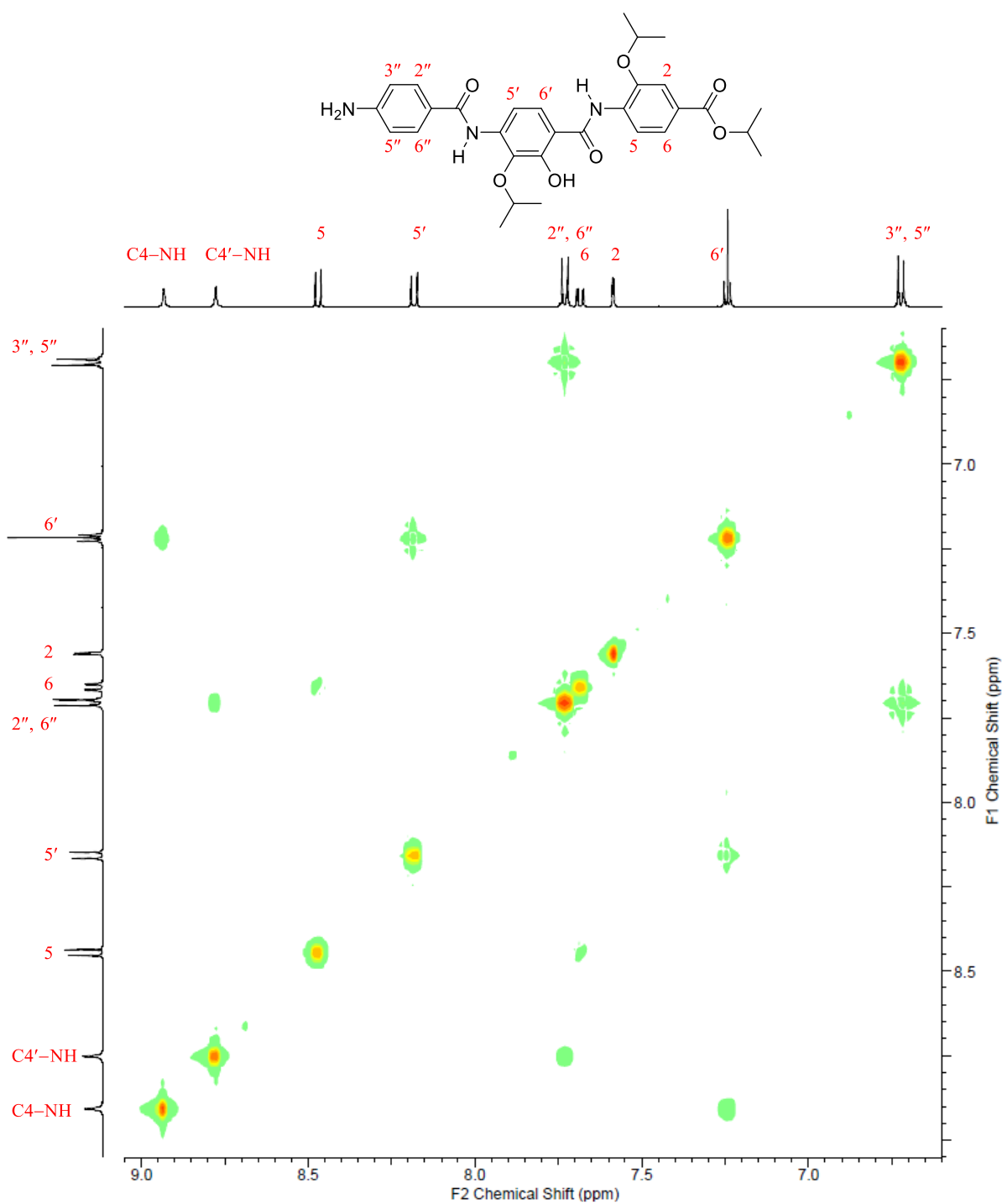
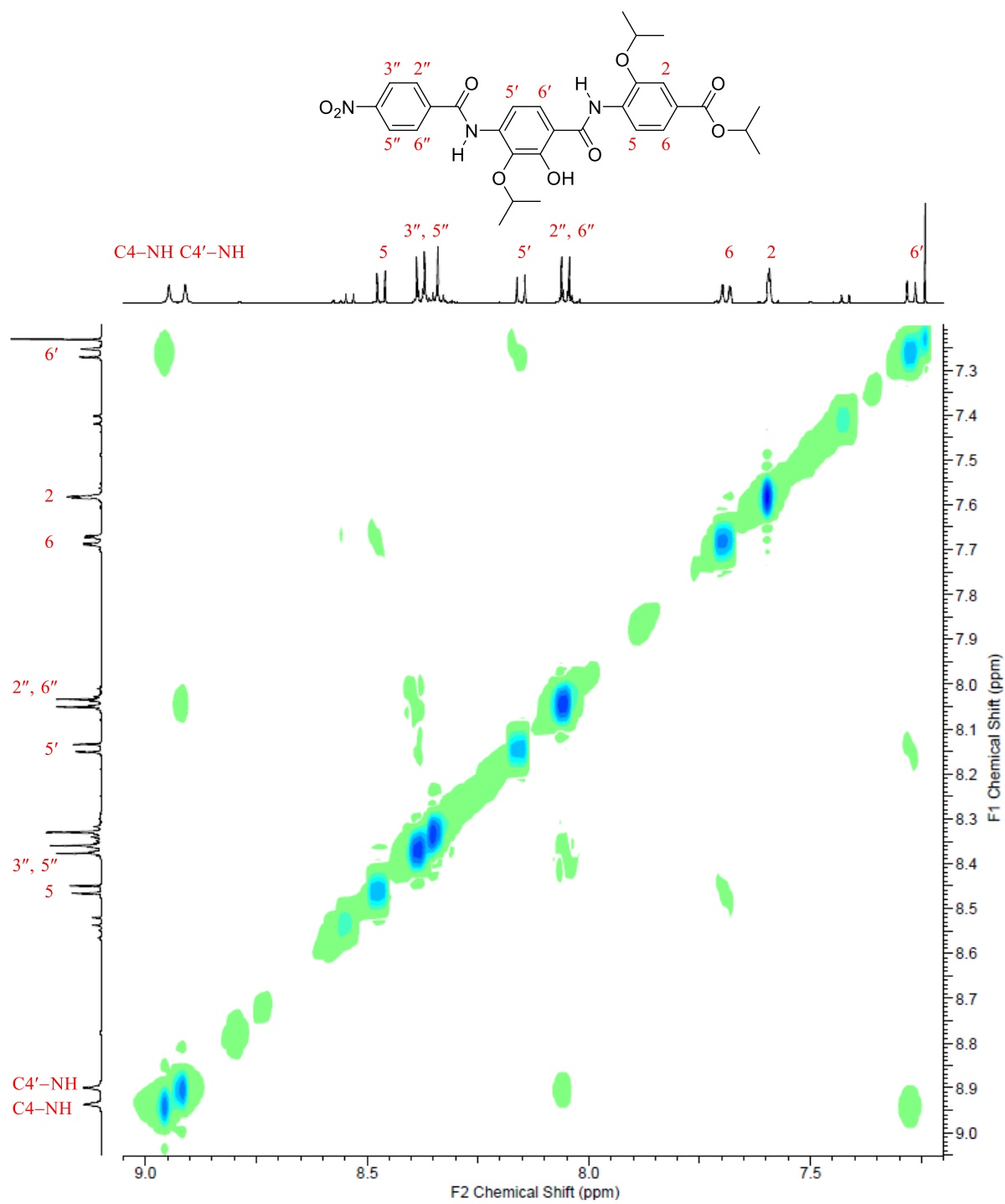
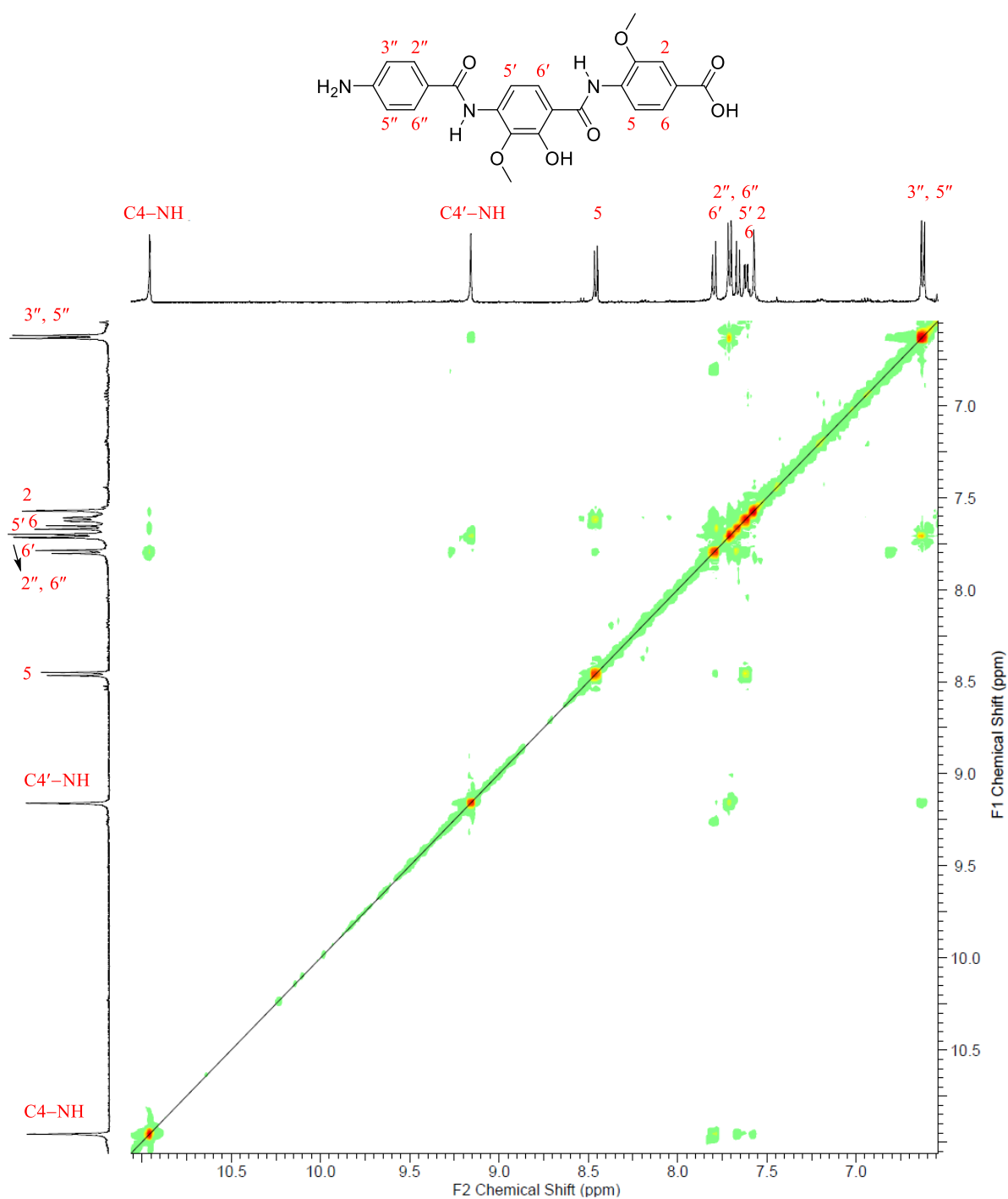


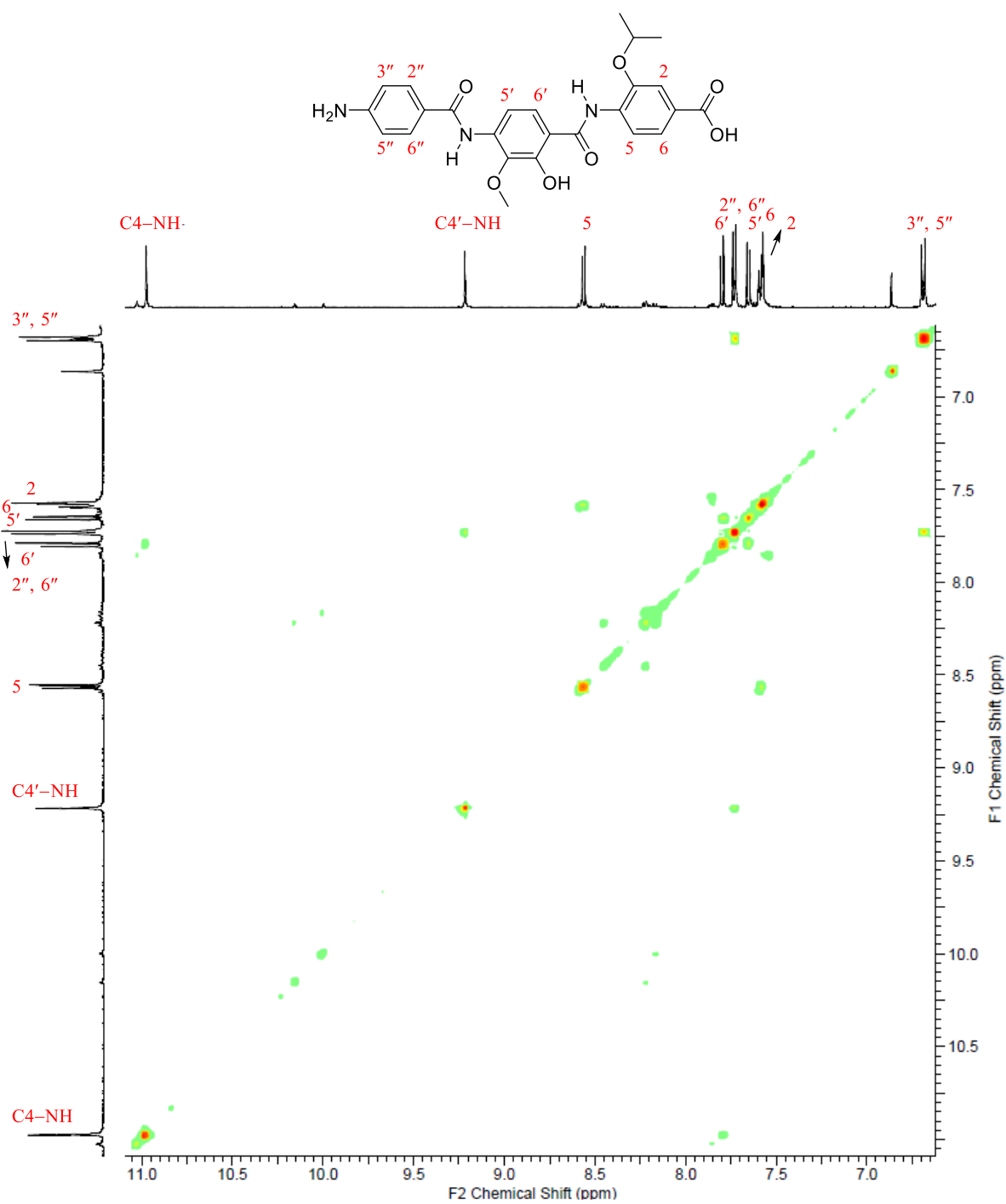
Figure S1. 2D-NOESY spectrum of Cys507 (**3**) in acetone-d₆

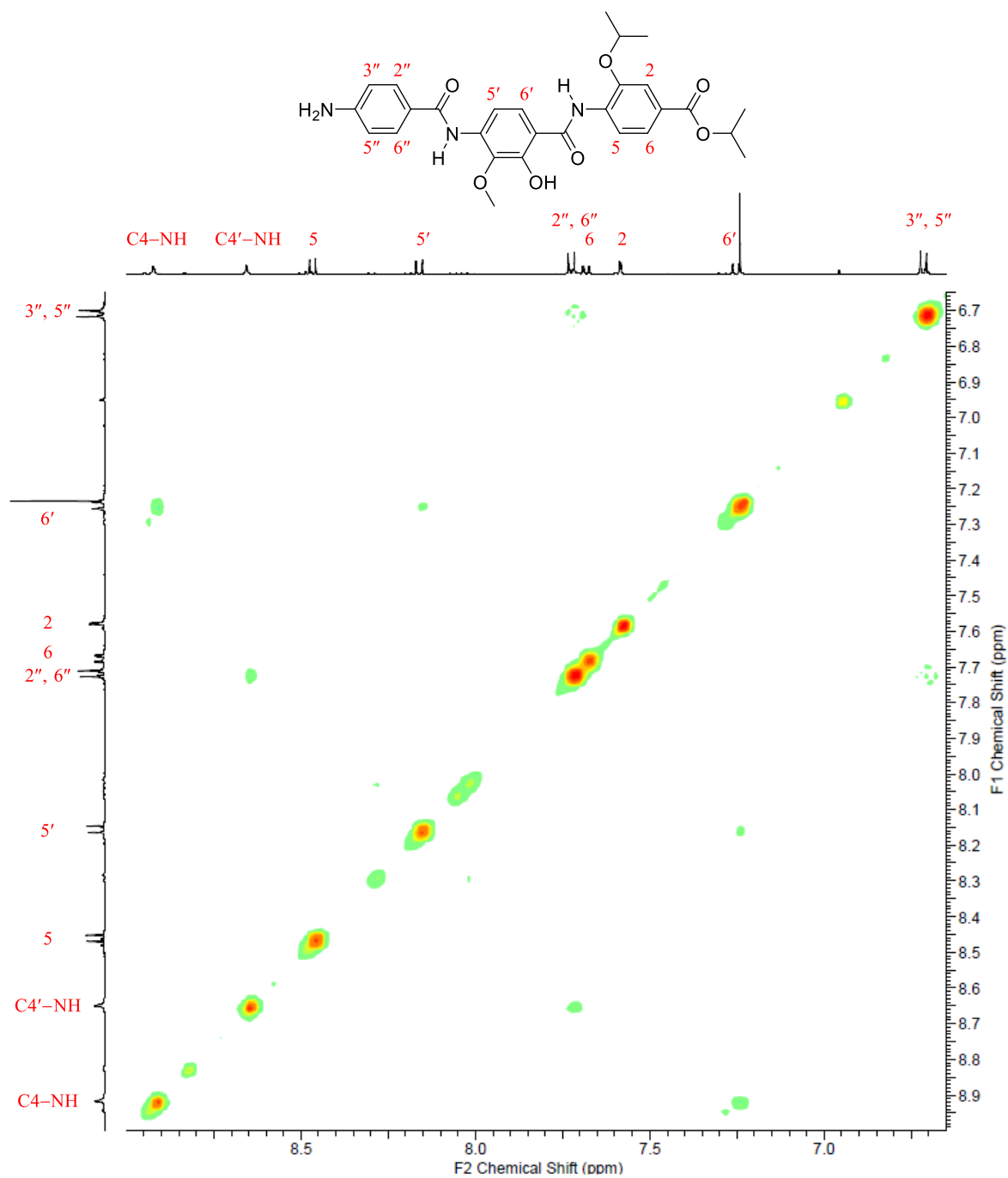
Figure S2. 2D-NOESY spectrum of Cys507 (**3**) in DMSO- d_6

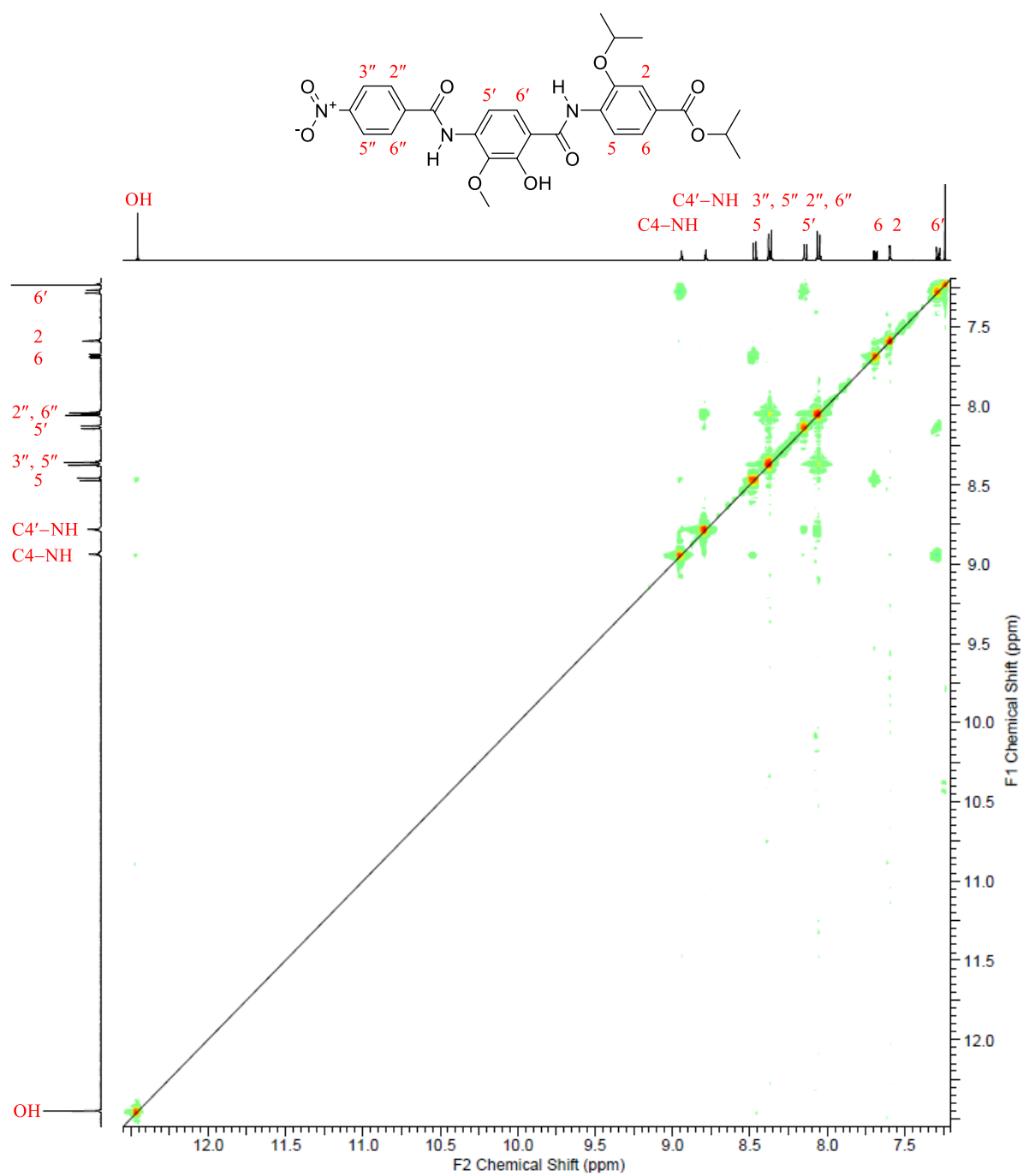
Figure S3. 2D-NOESY spectrum of compound **66** in CDCl₃

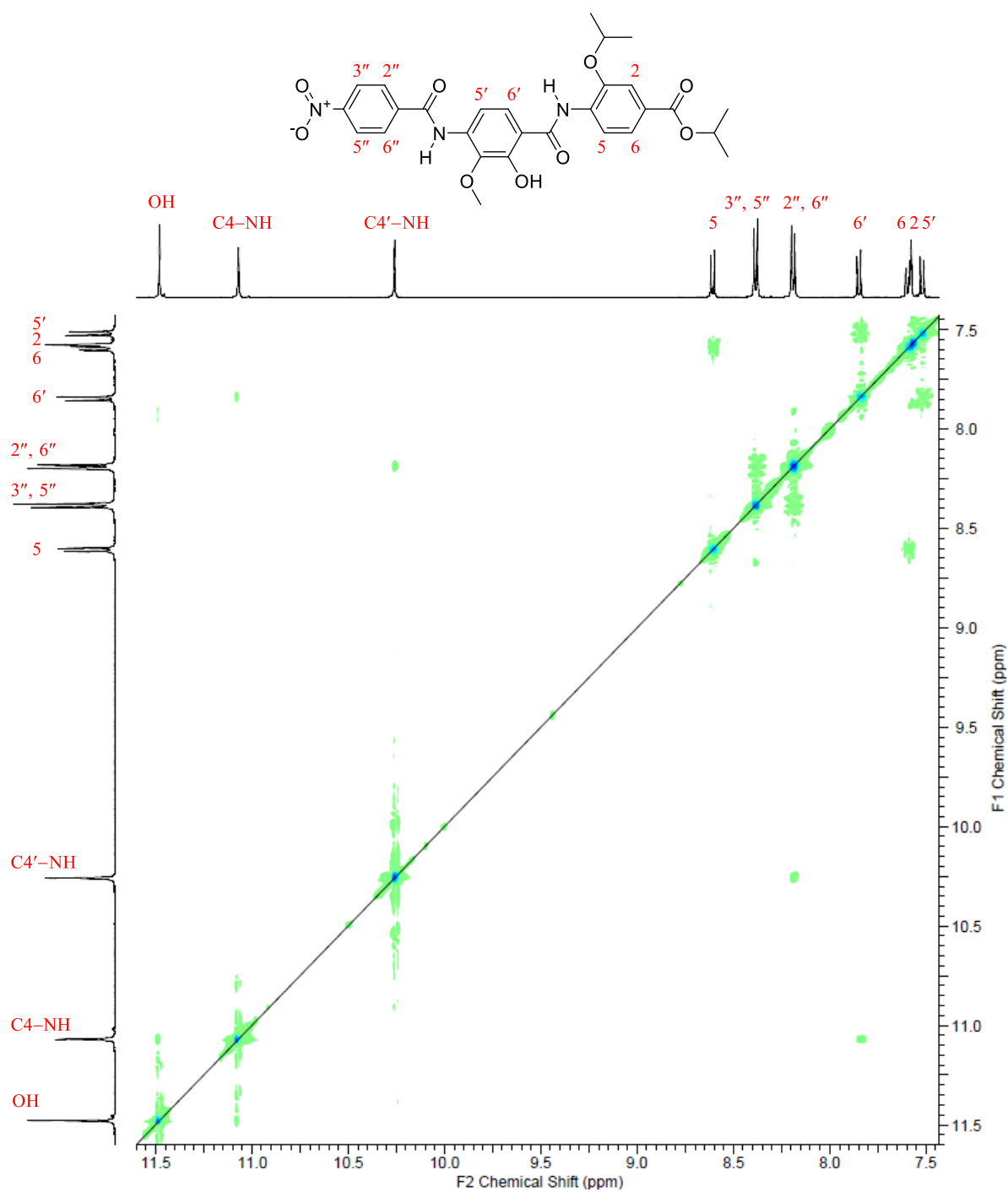
Figure S4. 2D-NOESY spectrum of compound **57** in CDCl₃

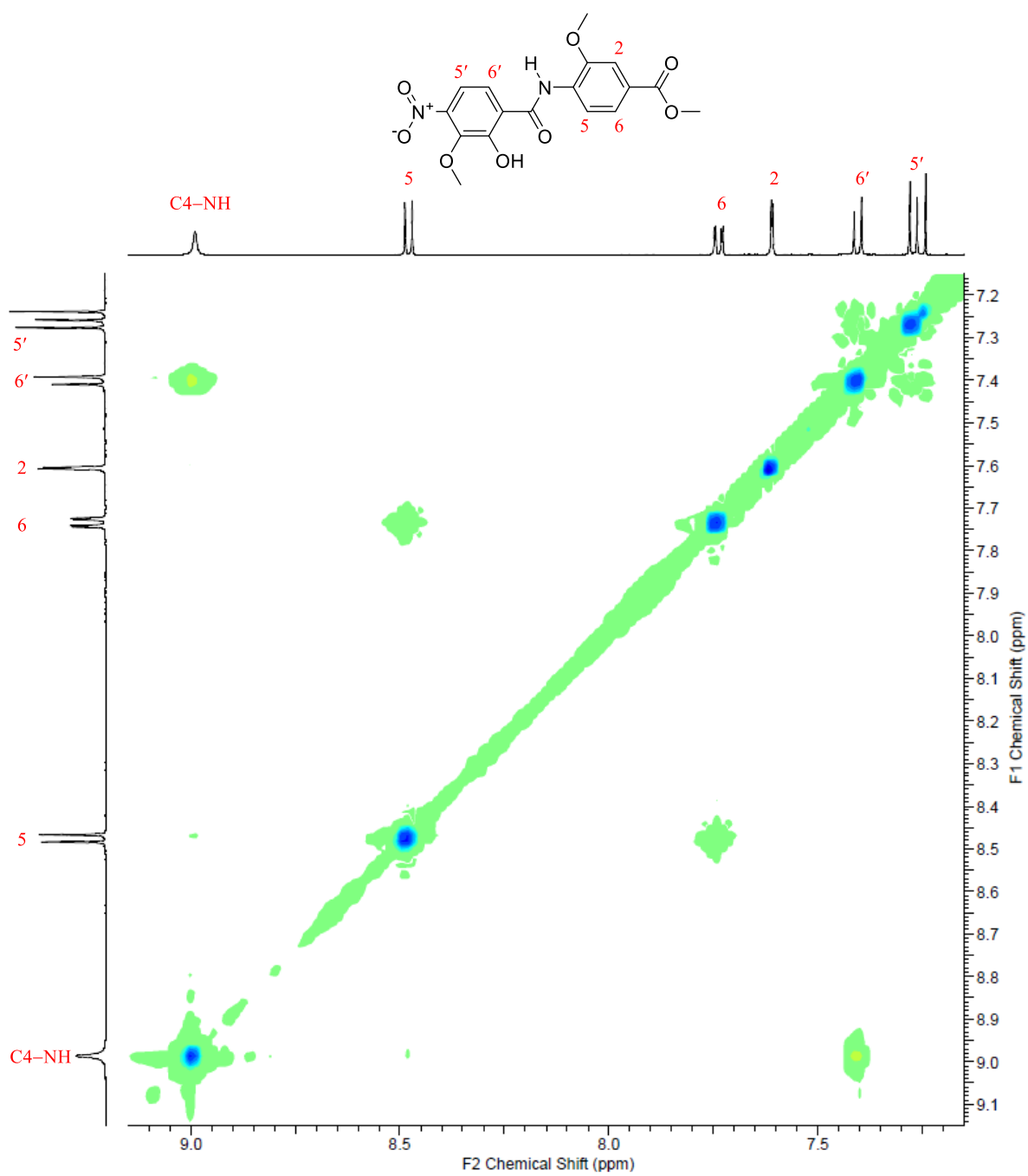
Figure S5. 2D-NOESY spectrum of compound **4** in DMSO- d_6

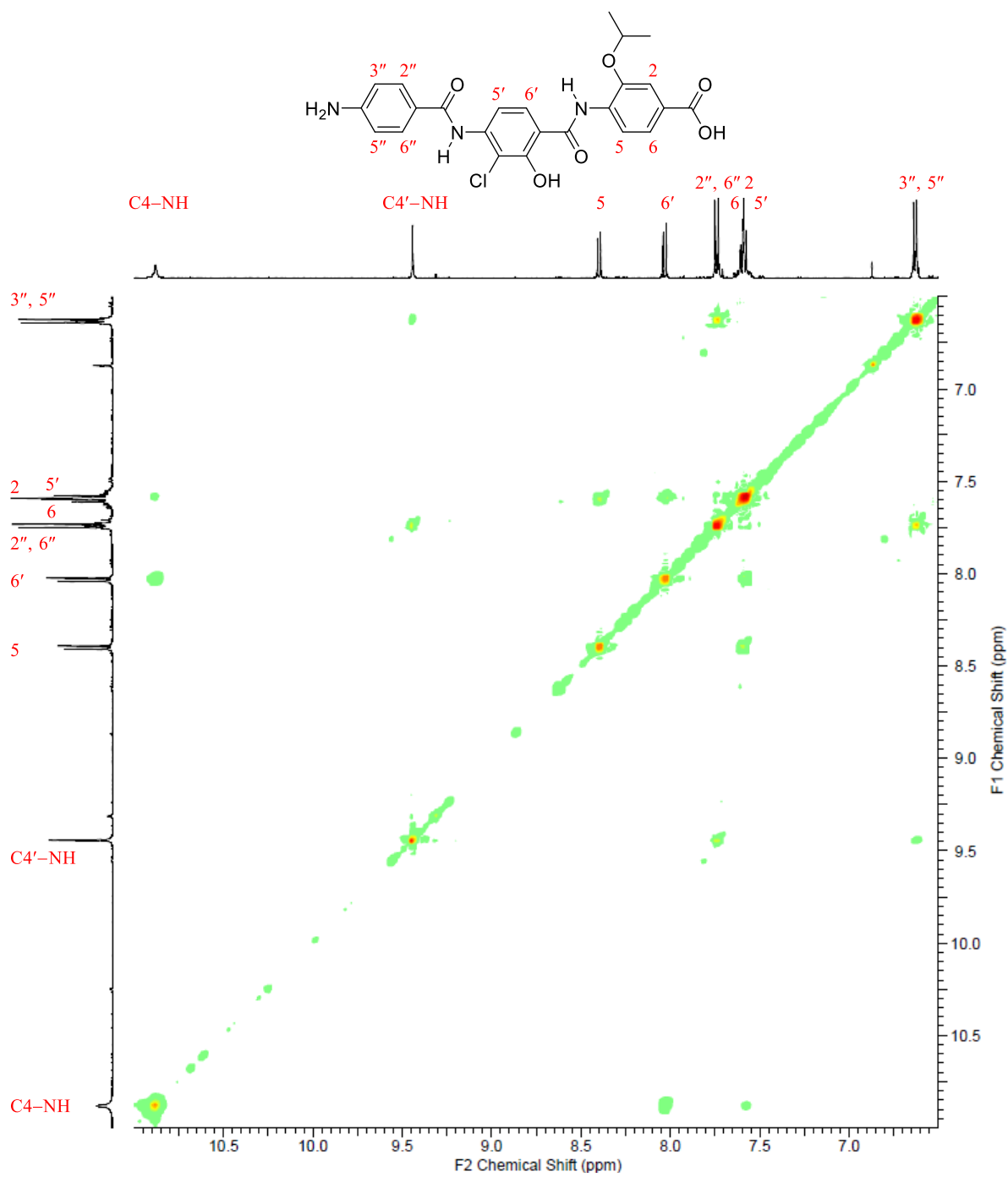
Figure S6. 2D-NOESY spectrum of compound **5** in DMSO-d_6

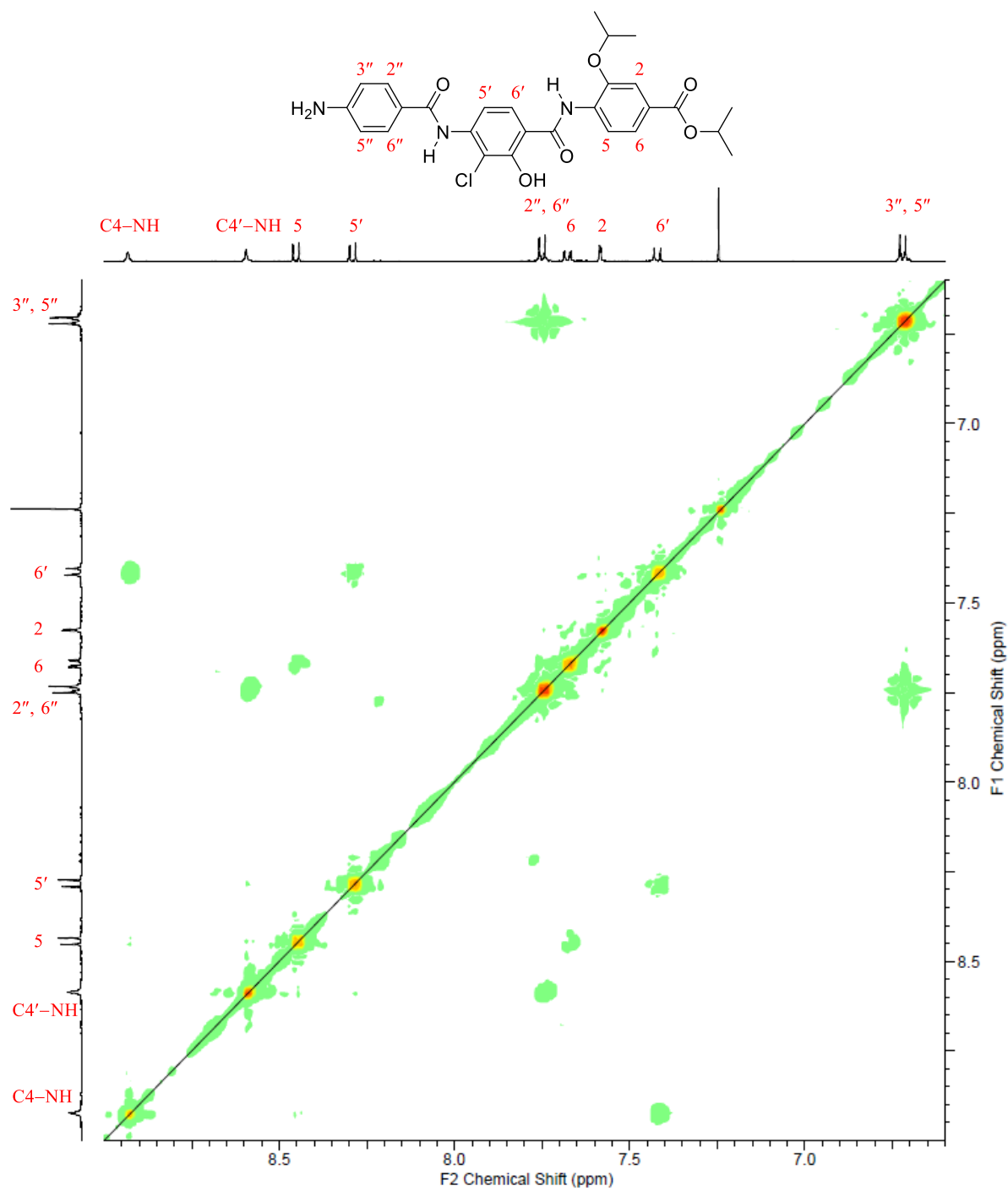
Figure S7. 2D-NOESY spectrum of compound **67** in CDCl₃

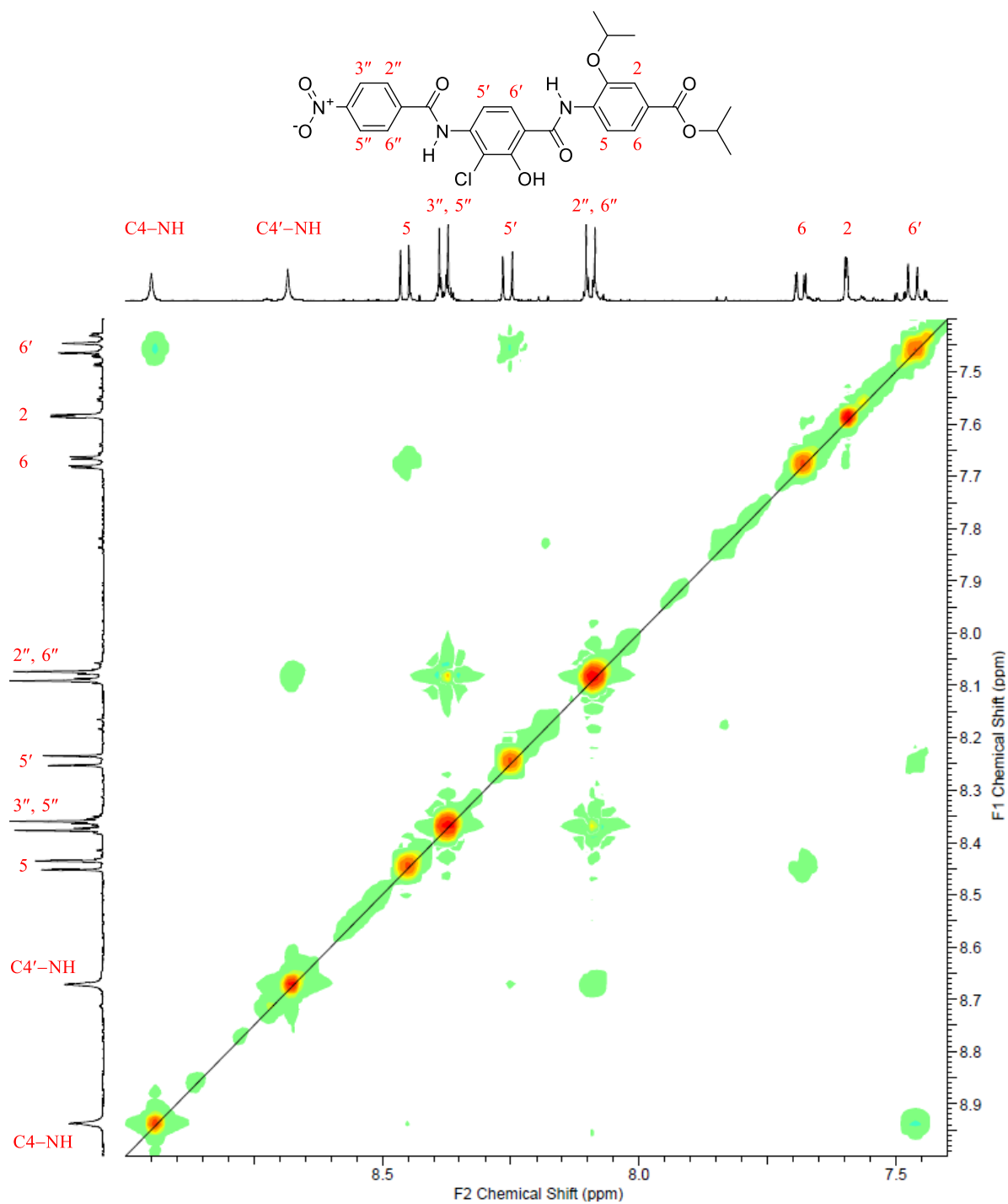
Figure S8. 2D-NOESY spectrum of compound **58** in CDCl_3

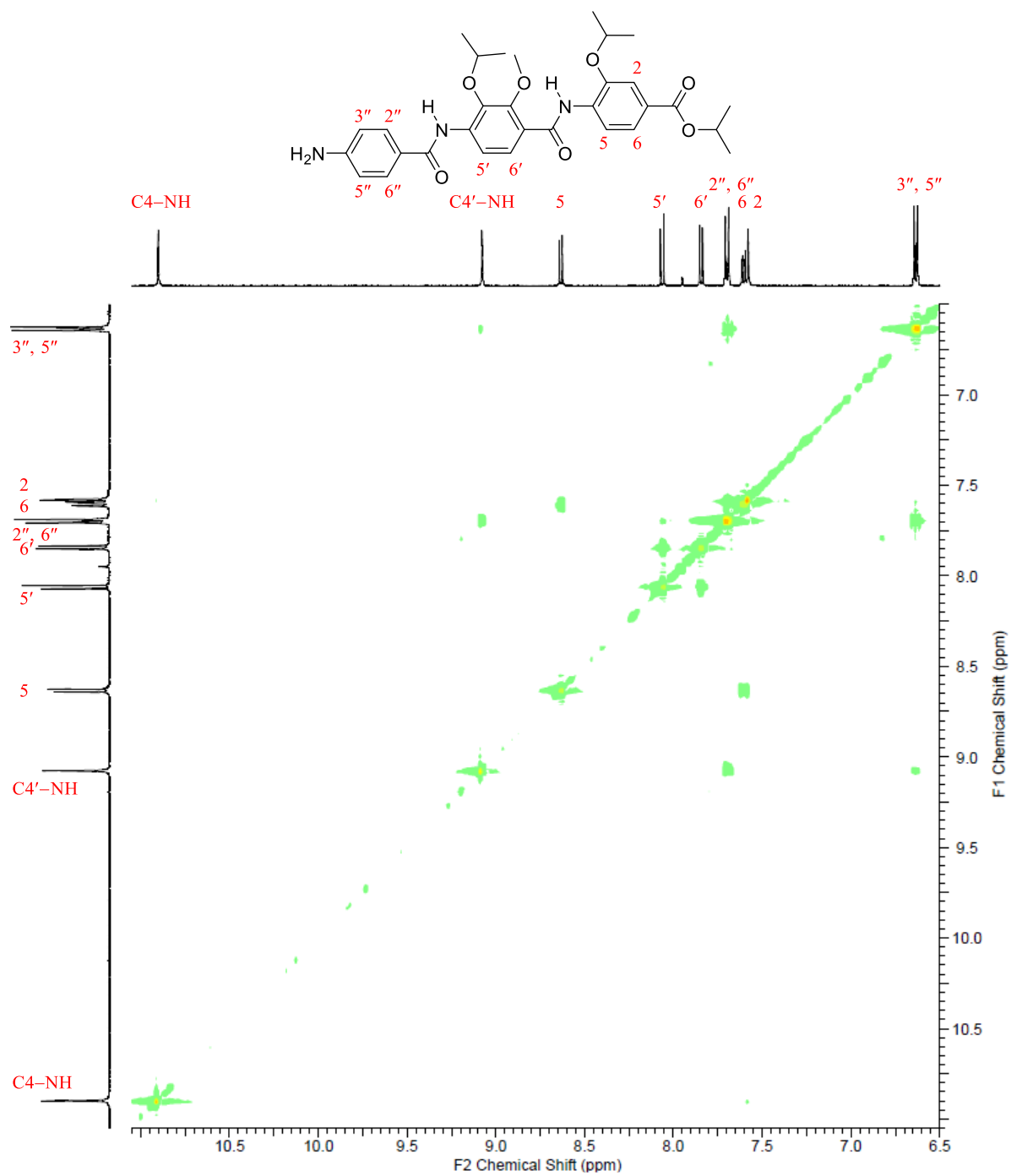
Figure S9. 2D-NOESY spectrum of compound **58** in DMSO-d₆

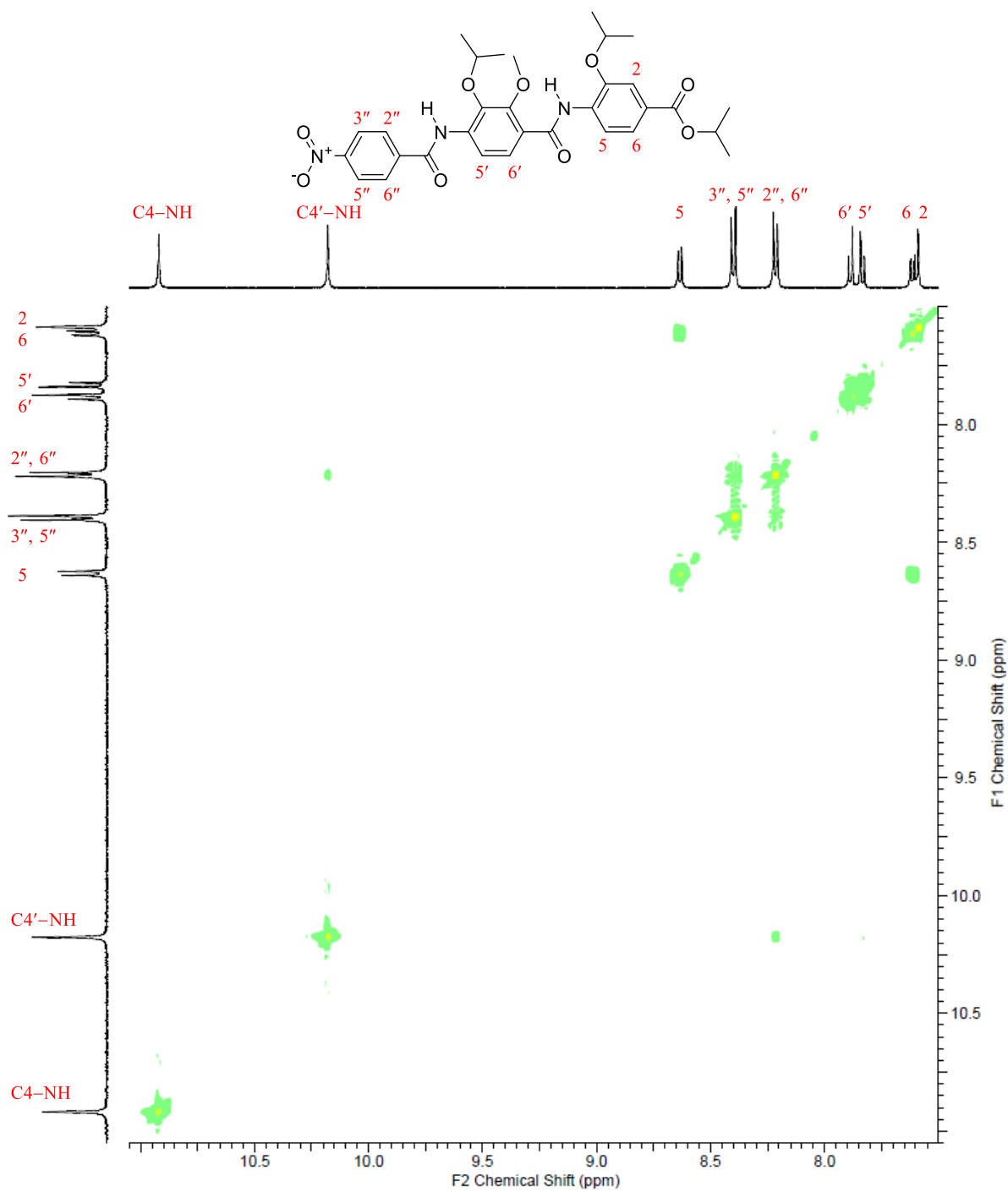
Figure S10. 2D-NOESY spectrum of compound **86** in CDCl₃

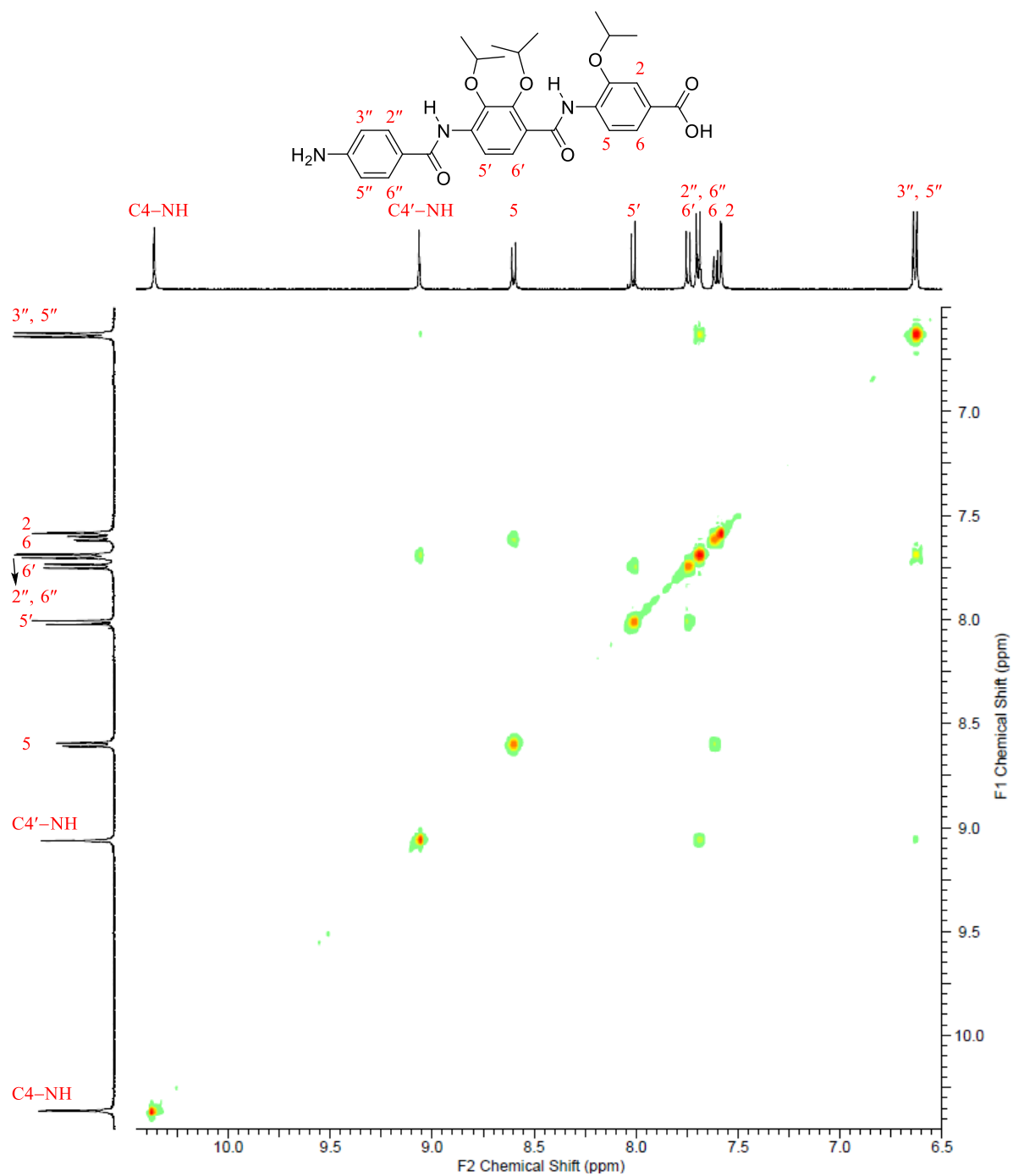
Figure S11. 2D-NOESY spectrum of compound **6** in DMSO-d₆

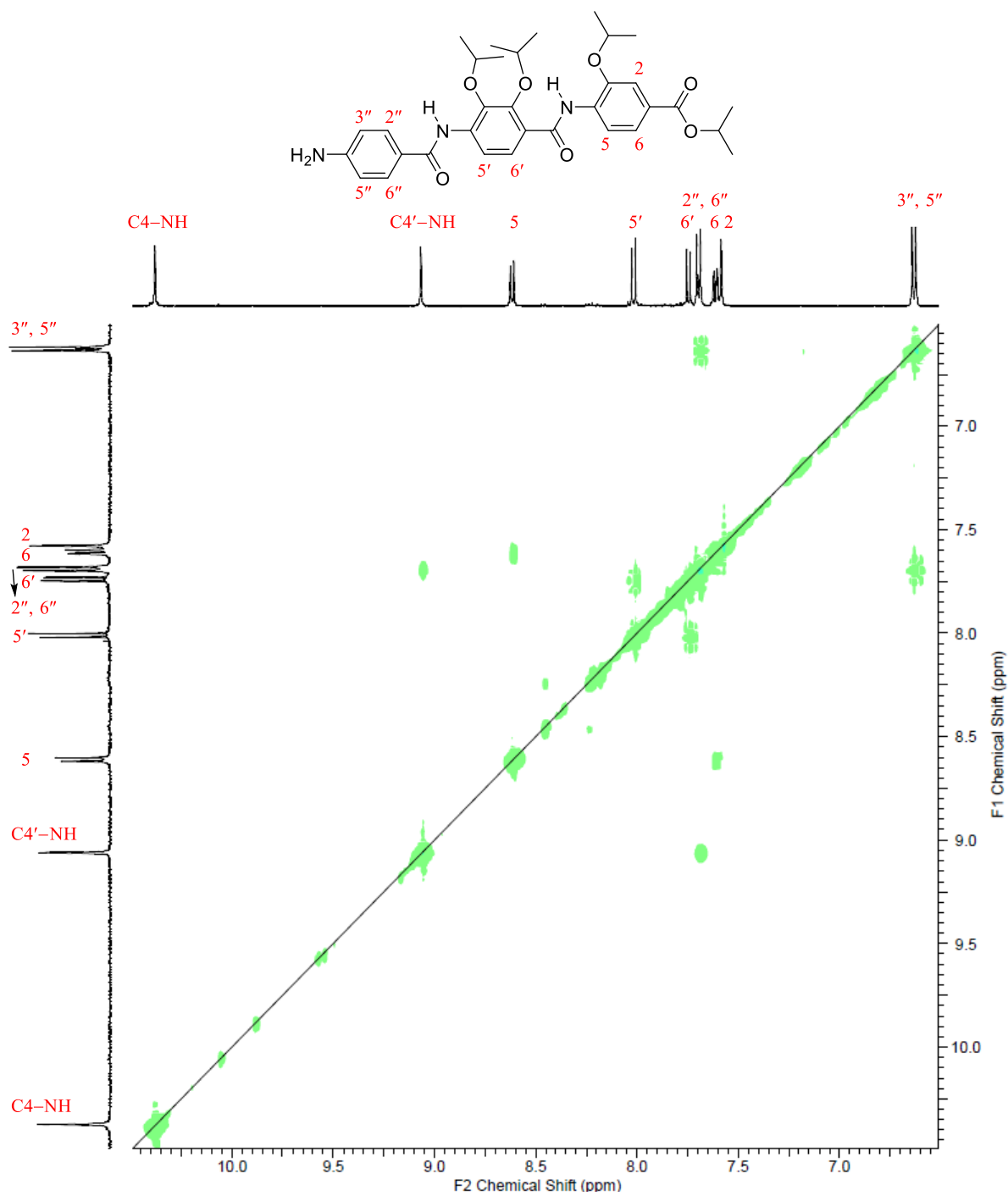
Figure S12. 2D-NOESY spectrum of compound **77** in CDCl₃

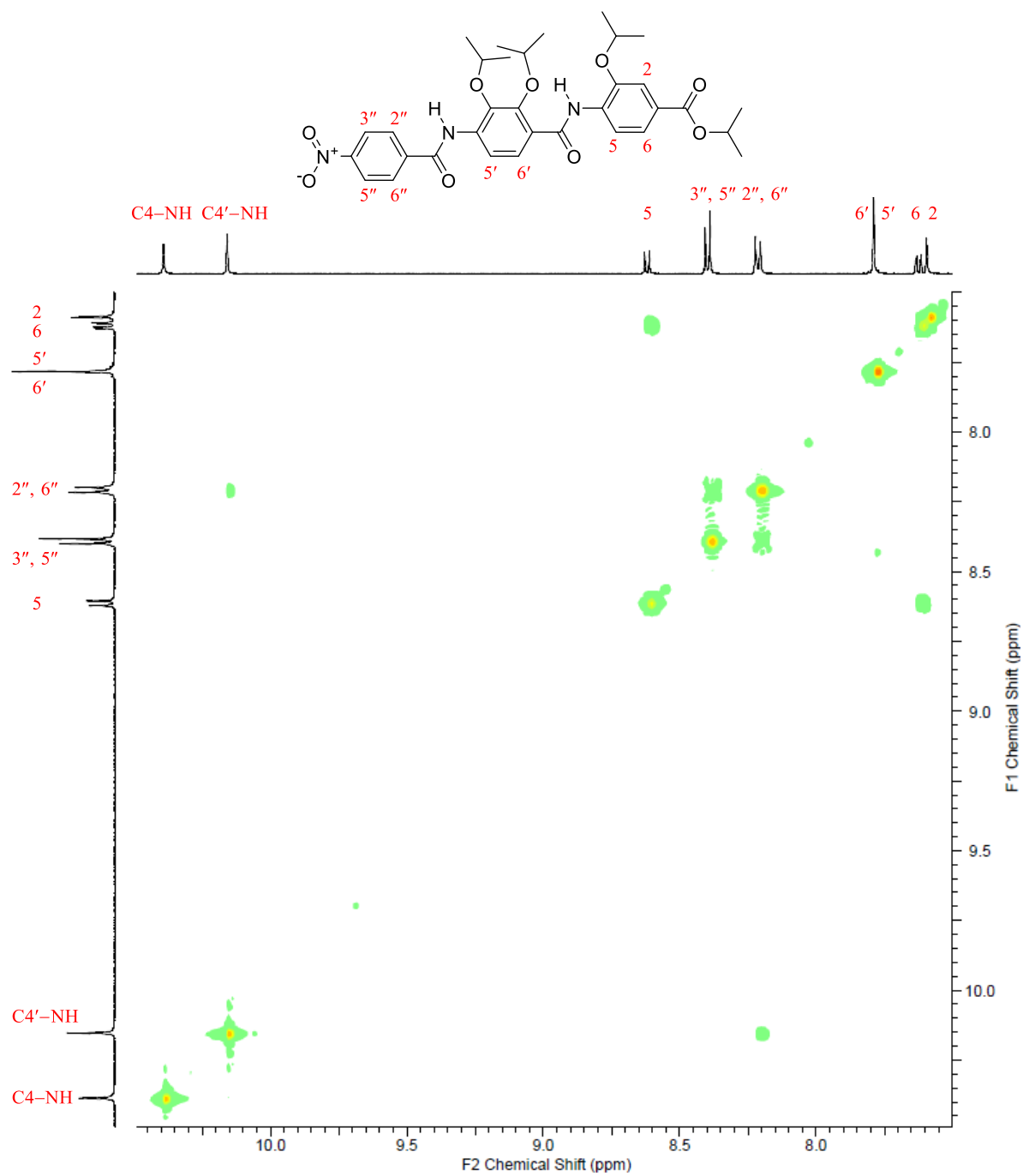
Figure S13. 2D-NOESY spectrum of compound **76** in CDCl₃

Figure S14. 2D-NOESY spectrum of compound **68** in DMSO-d₆

Figure S15. 2D-NOESY spectrum of compound **65** in DMSO- d_6

Figure S16. 2D-NOESY spectrum of compound **8** in DMSO- d_6

Figure S17. 2D-NOESY spectrum of compound **69** in DMSO- d_6

Figure S18. 2D-NOESY spectrum of compound **60** in DMSO-d₆

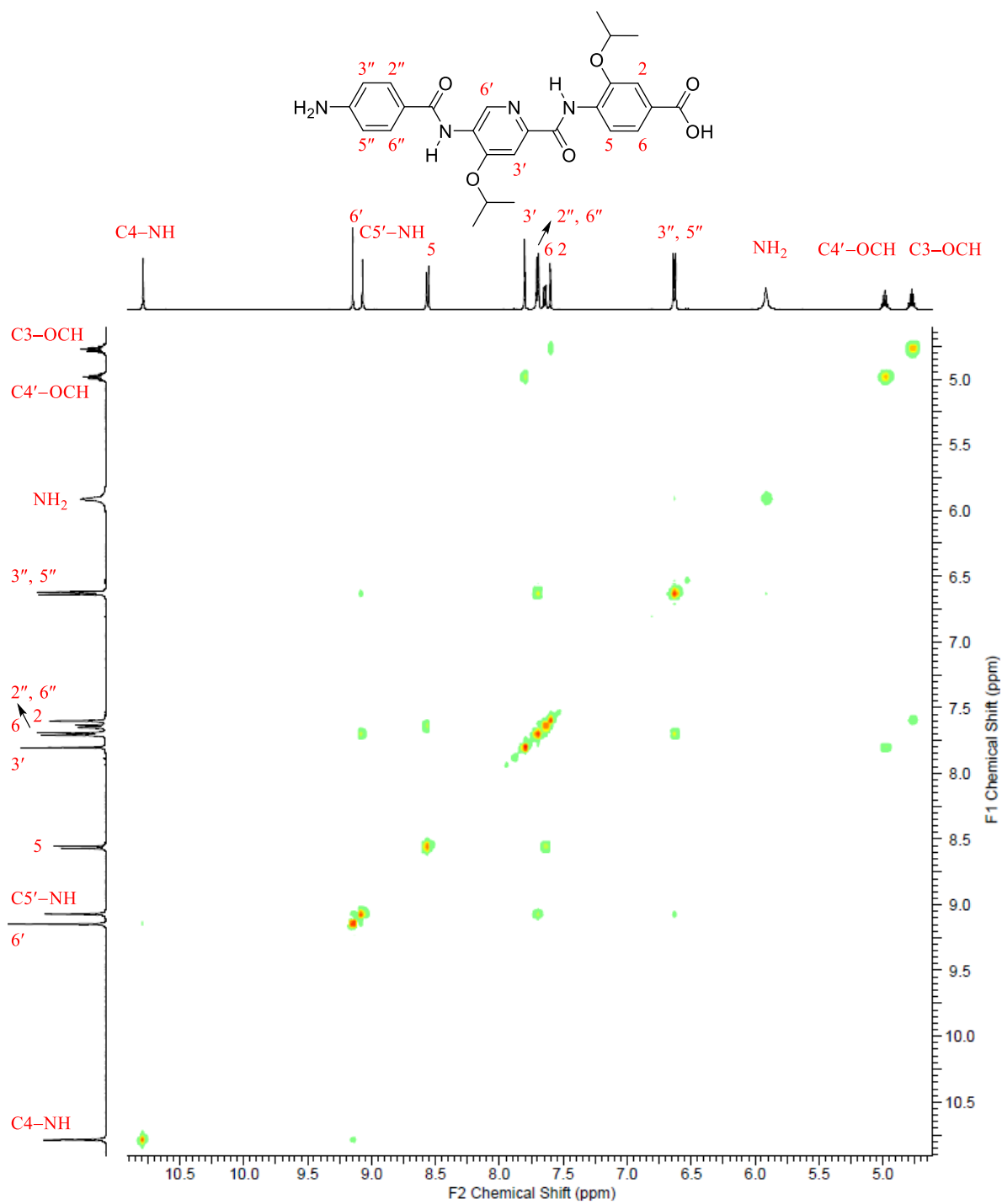
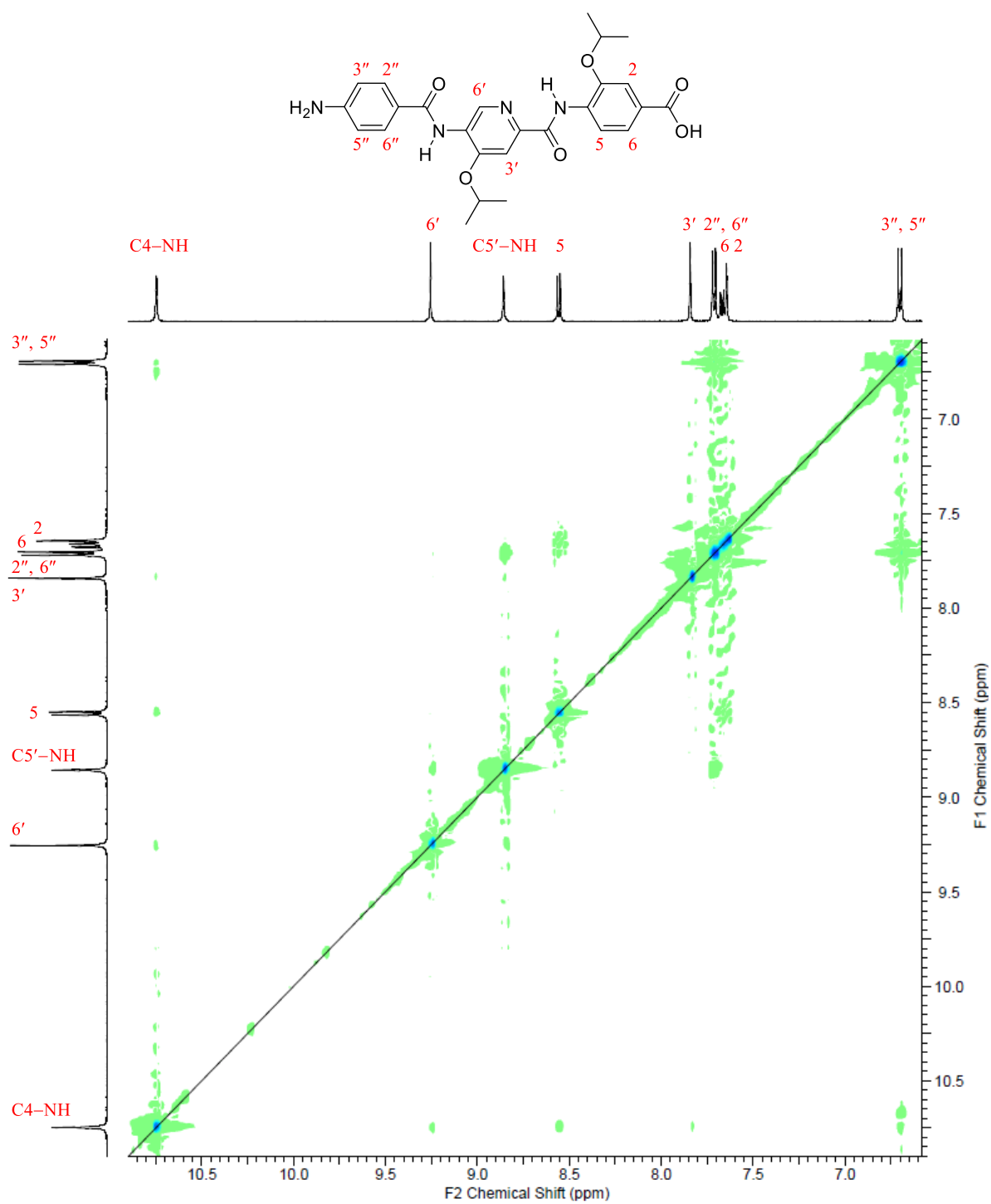
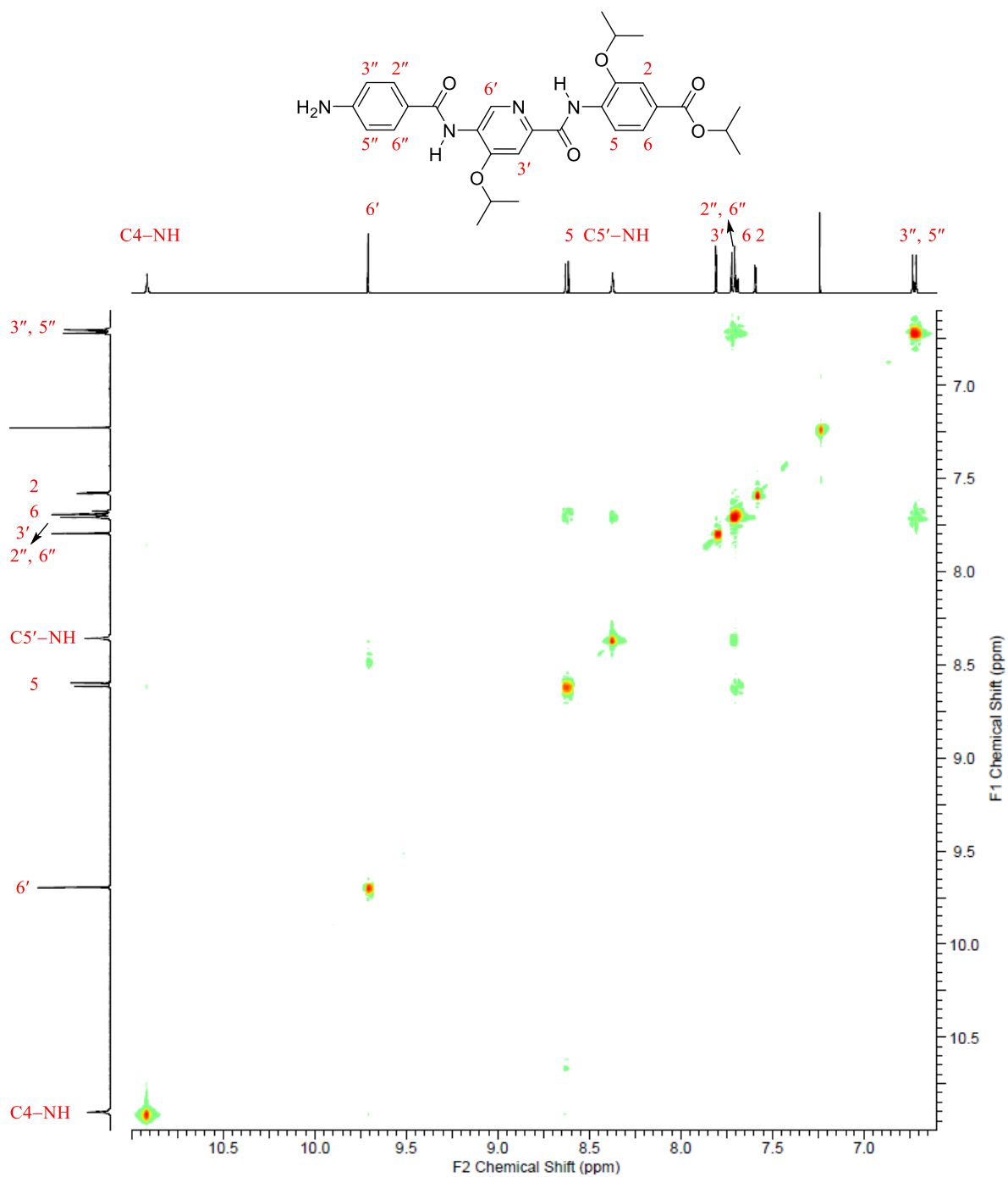
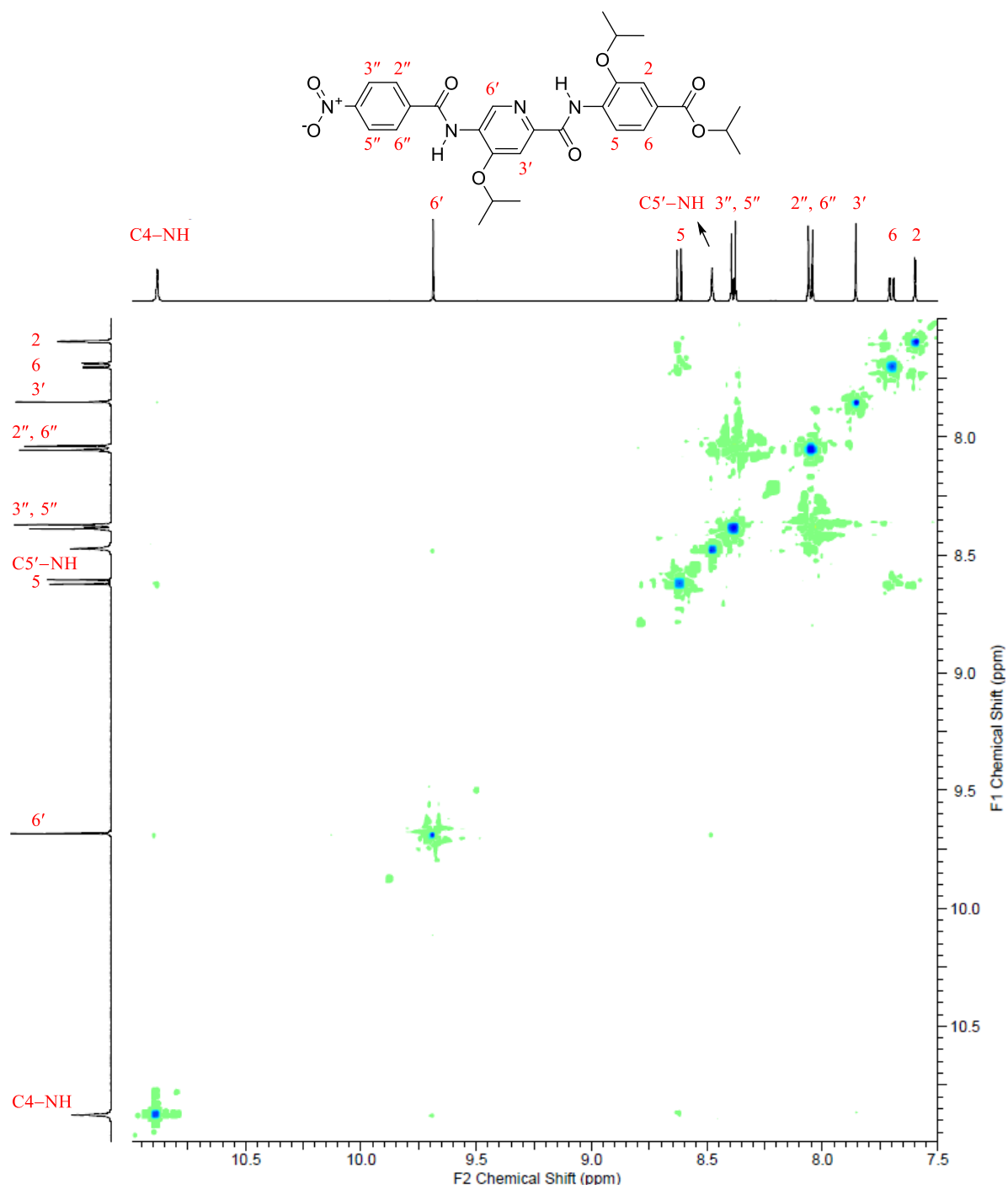
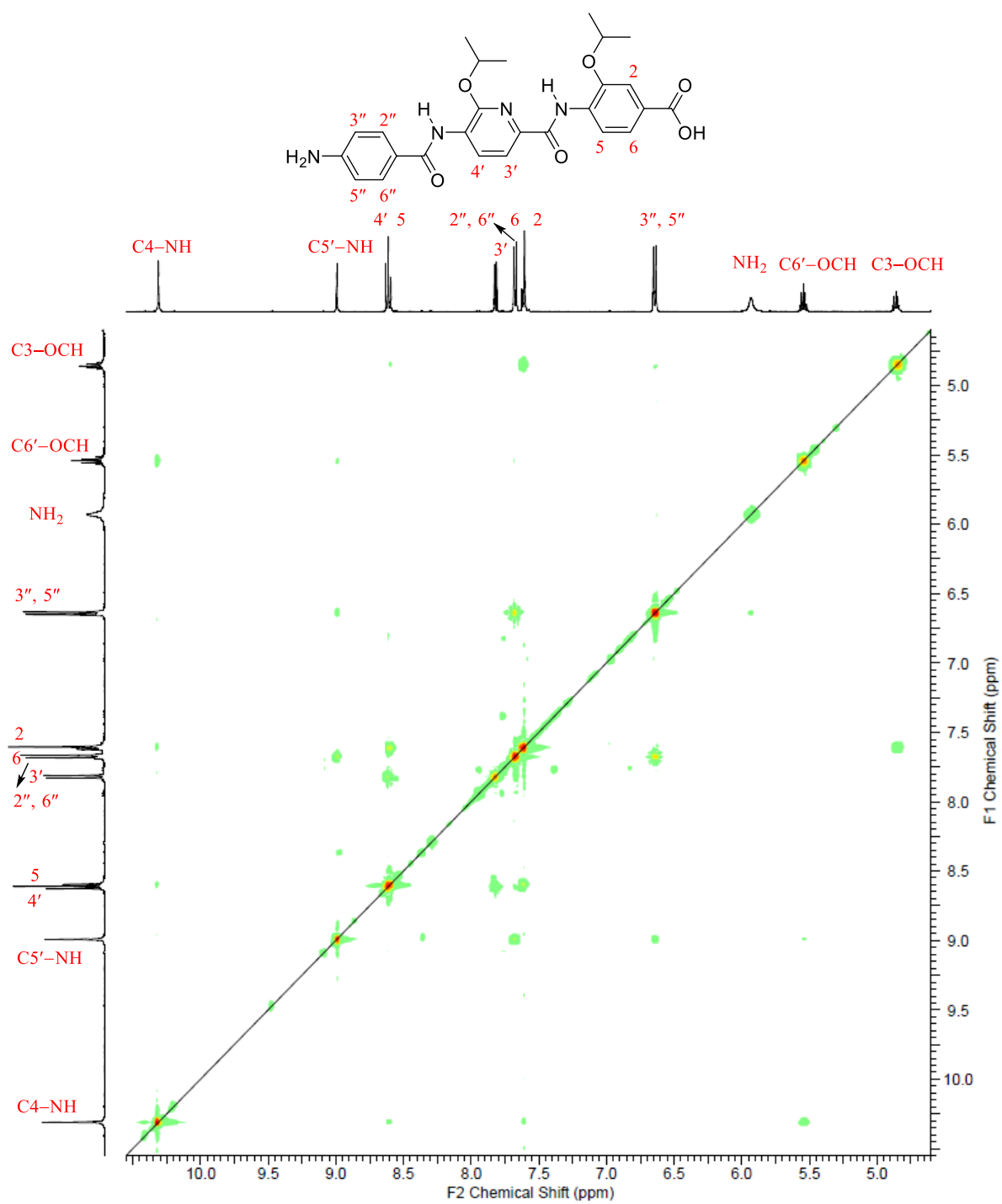


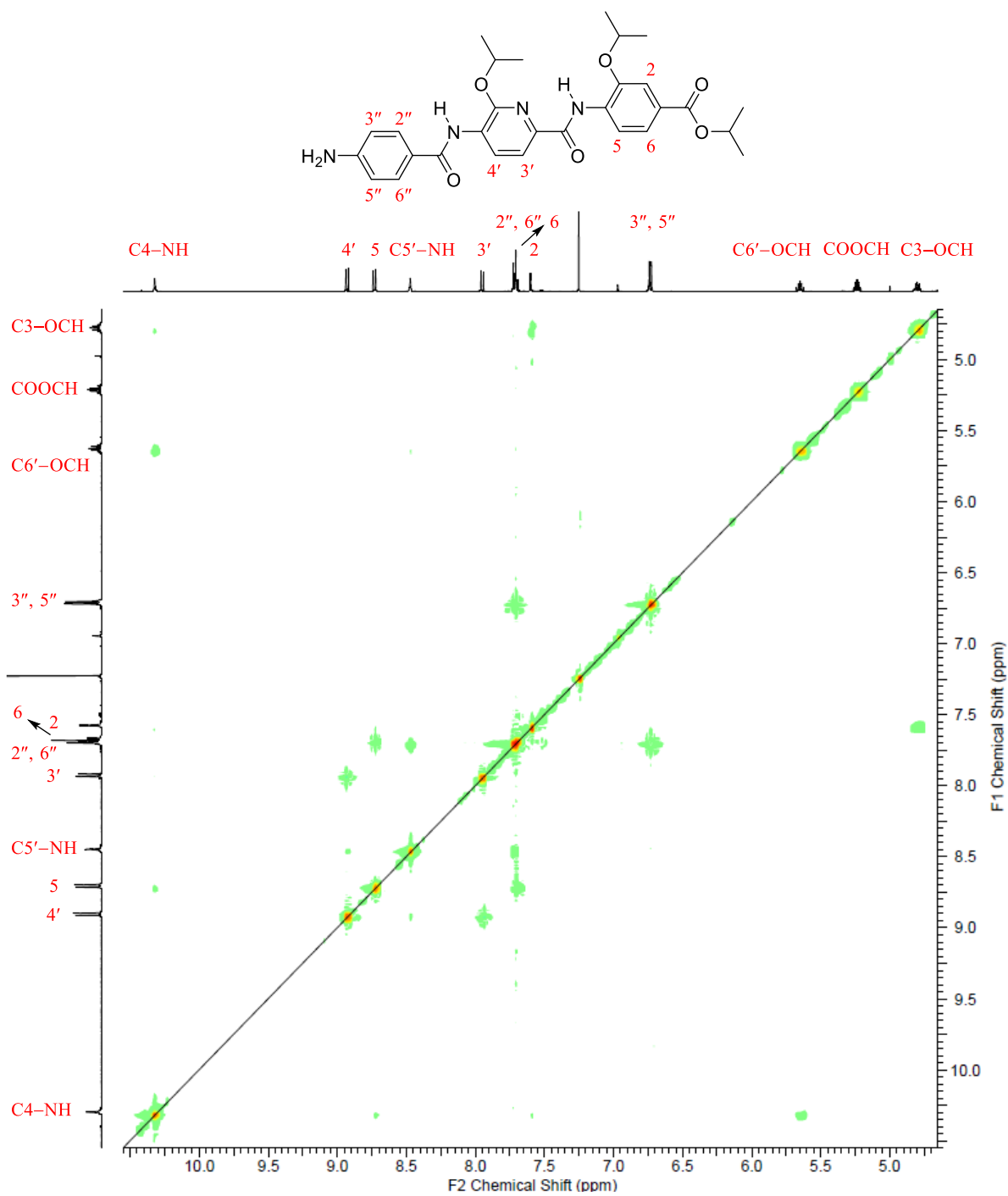
Figure S19. 2D-NOESY spectrum of compound **9** in DMSO-d₆ at 300 K

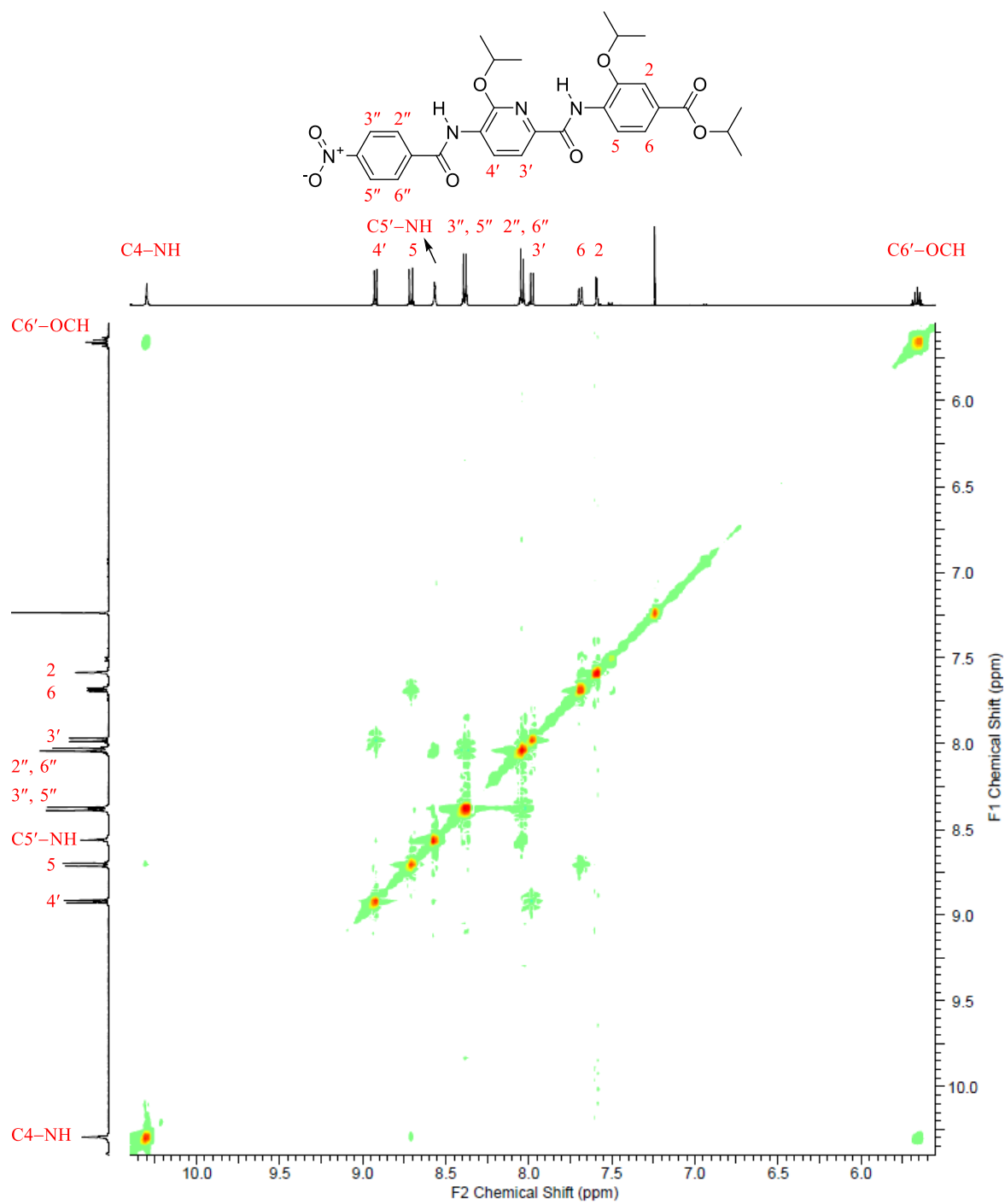
Figure S20. 2D-NOESY spectrum of compound **9** in DMSO-d₆ at 360 K

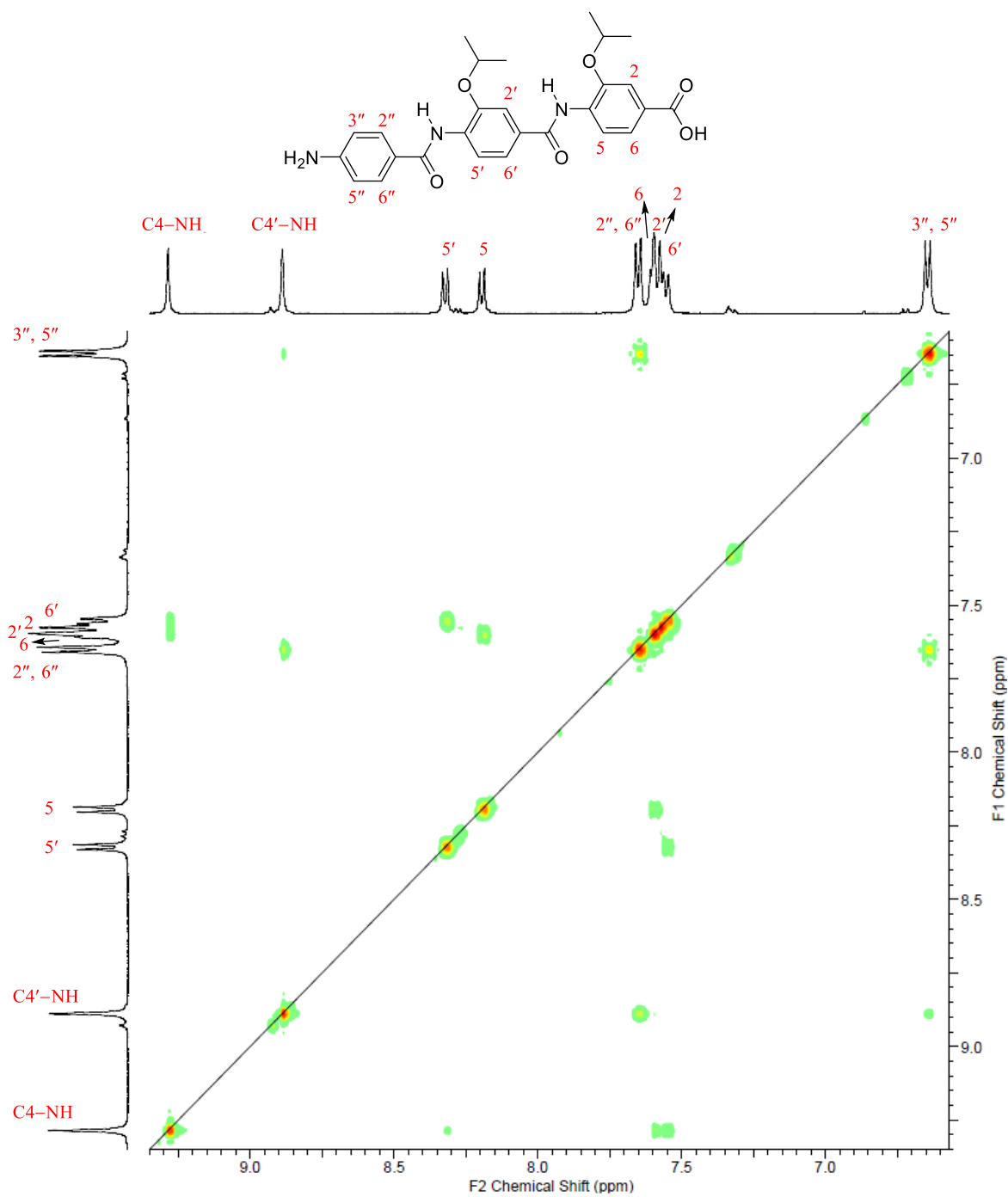
Figure S21. 2D-NOESY spectrum of compound **84** in CDCl₃

Figure S22. 2D-NOESY spectrum of compound **82** in CDCl₃

Figure S23. 2D-NOESY spectrum of compound **10** in DMSO-d₆

Figure S24. 2D-NOESY spectrum of compound **85** in CDCl₃

Figure S25. 2D-NOESY spectrum of compound **83** in CDCl₃

Figure S26. 2D-NOESY spectrum of compound **12** in DMSO-d₆

6.3.4 Computational Chemistry

All computational work was performed using Molecular Operating Environment (MOE) version 2015.10, Chemical Computing Group Inc., 1010 Sherbrooke St. West, Suite 910, Montreal, Quebec, H3A 2R7, Canada.

Conformational Analysis A database containing Cys507 and all analogues was created, and each structure was subjected to energy minimization up to a gradient 0.01 kcal/mol/Å using the MMFF94x force field and distance solvation model. Conformational search was performed using low mode MD method, with energy window of 7.0 kcal/mol and conformation limit of 10000 as conformer filters.

Backbone Curvature Calculation Structures of *anti* or *syn* conformation were loaded separately from the previously prepared conformational database into the MOE window. Angle of inclination of the aryl rings on each other was determined via activating the measure button, choosing angles option, then selecting the carbon atom of the aryl ring bound to the amide nitrogen atom, the carbon atom on the corresponding aryl ring bound to the amide carbonyl group, and the γ carbon atom on the same ring respectively.

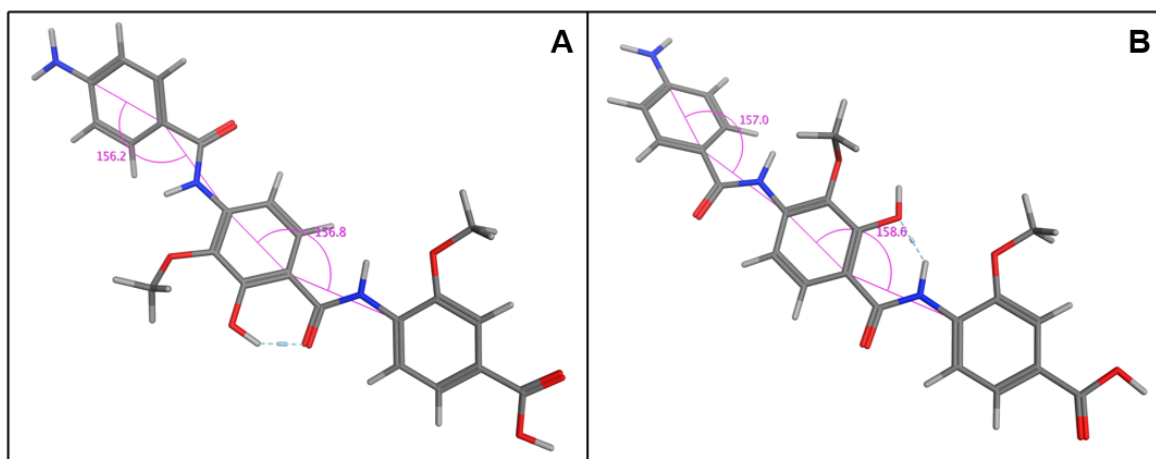


Figure S27. Conformational analysis of **4**: A) *anti*-form (lowest energy conformation); B) *syn*-form (dE 0.7 kcal/mol).

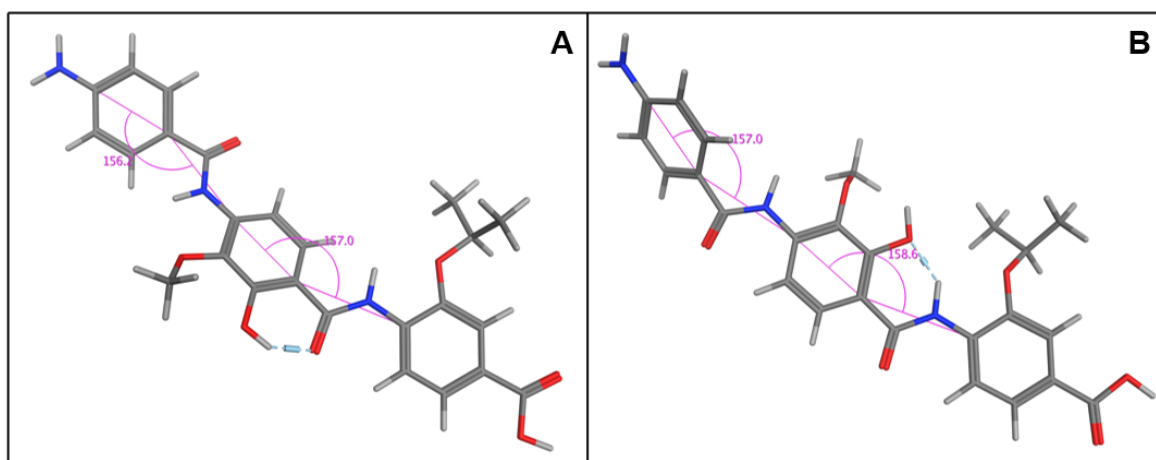


Figure S28. Conformational analysis of **5**: A) *anti*-form (lowest energy conformation); B) *syn*-form (dE 0.5 kcal/mol).

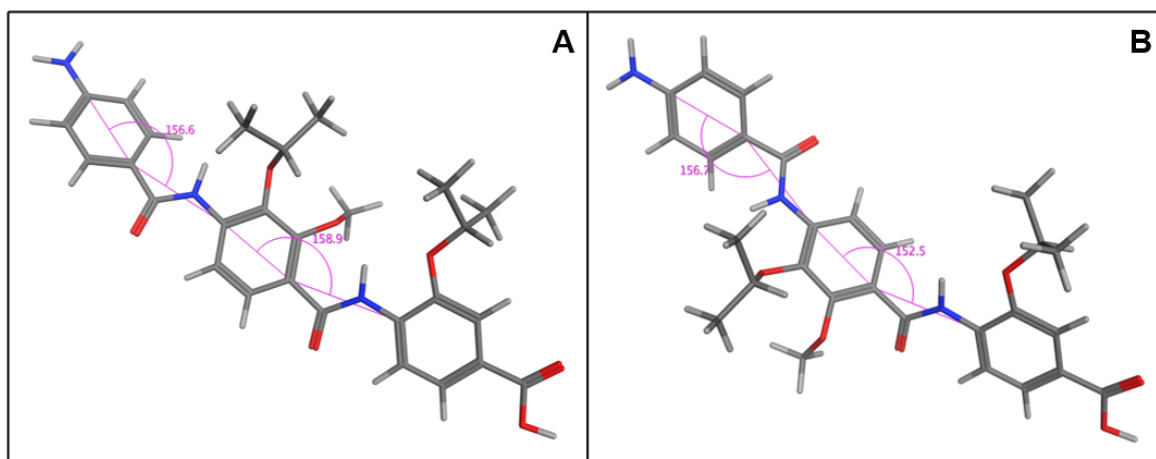


Figure S29. Conformational analysis of **7**: A) *syn*-form (lowest energy conformation); B) *anti*-form (dE 3.8 kcal/mol).

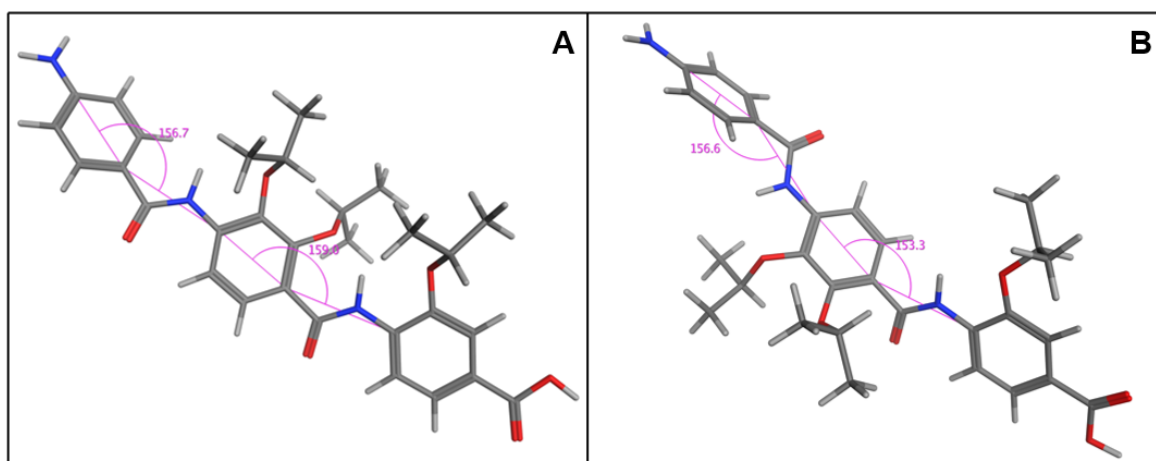


Figure S30. Conformational analysis of **8**: A) *syn*-form (lowest energy conformation); B) *anti*-form (dE 4.6 kcal/mol).

Calculation of Electrostatic Surface Structure of Cys507 or **13** was loaded from the previously prepared conformational database into the MOE window. Electrostatic surface was calculated via activating the compute panel, choosing surfaces and maps, then molecular surface option. Atoms were selected as ligand atoms near ligand atoms and color as electrostatics. Electrostatic field was calculated using Gaussian screened Coulomb potential.

Calculation of Molecular Descriptors In the database viewer window, molecular descriptors were calculated for all entries via activating the compute panel, choosing descriptors calculate option. Cys507, **13**, and **14** have the same values.

Compound	Cys507, 13 , 14
Total hydrophobic vdw surface area (Q_VSA_HYD)	335.4886
Total polar vdw surface area (Q_VSA_POL)	173.7101
Total positive vdw surface area (Q_VSA_POS)	330.7362
Total negative vdw surface area (Q_VSA_NEG)	178.4624

6.3.5 X-ray Structure Determination

Compounds were dissolved either in EtOAc (**26**), THF (**82**), *n*-hexane:EtOAc, 1:1 (**85**) or CDCl₃ (**80**, **83** and **86**) at room temperature. Crystals were obtained by slow evaporation of solvent. Single crystal X-ray diffraction data were collected at 152 K on a Bruker AXS X8APEX CCD diffractometer operating with graphite-monochromatized Mo K α radiation. Frames of 0.5° oscillation were exposed. Deriving reflections were in the θ range of 2–29° with a completeness of ~99%. Structure solution and full least-squares refinement with anisotropic thermal parameters of all non-hydrogen atoms were performed using SHELX.²

Crystallographic data of the compounds:

26: Monoclinic, P2₁/c, *a* = 11.3140(4), *b* = 8.3739(3), *c* = 15.1390(6) Å, β = 107.3082(18)°.

80: Monoclinic, P2₁/n, *a* = 8.5870(5), *b* = 21.3246(11), *c* = 12.3202(5) Å, β = 102.7567(8)°.

82: Triclinic, P-1, *a* = 11.1067(15), *b* = 12.0269(18), *c* = 12.2433(17) Å, α = 71.838(7), β = 69.391(6), γ = 69.464(7)°.

83: Orthorhombic, Pca2₁, *a* = 23.9033(8), *b* = 10.6916(3), *c* = 22.4998(7) Å.

85: Monoclinic, P2₁/c, *a* = 13.4709(10), *b* = 21.9747(16), *c* = 9.5297(6) Å, β = 97.940(2)°.

86: Triclinic, P-1, *a* = 7.5890(3), *b* = 10.7739(5), *c* = 11.6933(6) Å, α = 64.668(2), β = 83.738(2), γ = 71.654(2)°.

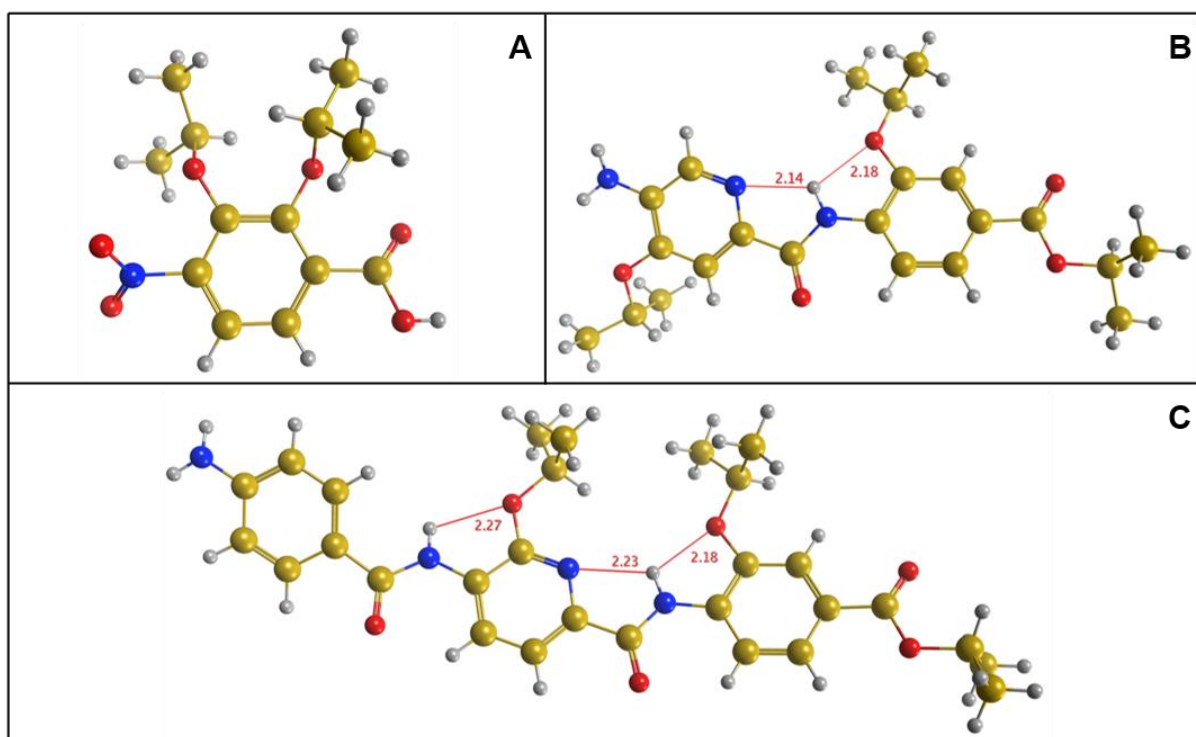


Figure S31. Crystal structures of compounds **26** (A), **80** (B) and **85** (C).

6.3.6 Biology

Cloning, Expression and Purification of *E. coli* GyrA and GyrB

GyrA and GyrB full-length genes were amplified by PCR from *E. coli* genomic DNA (Phusion polymerase, Thermo Scientific) using the following primer pairs (Sigma-Aldrich):

GyrA Forward (NdeI): ATCATATGAGCGACCTTGCGAGAGAAATTAC

GyrA Reverse (XhoI): ATCTCGAGTTCTTCTTCTGGCTCGTCGTCACG

GyrB Forward (NdeI): ATCATATGTCGAATTCTTATGACTCCTCCAG

GyrB Reverse (XhoI): ATCTCGAGAATATCGATATTCGCCGCTTTCAGG

The obtained amplicons were ligated into the pET-28b expression vector system (N-terminal His₆-tag)(Novagen) using an *NdeI/XhoI* strategy and transformed into *E. coli* HS996 cells for selection (kanamycin). Positive clones were picked and verified by Sanger sequencing. For protein expression the constructs pET28-GyrA and pET28-GyrB were transformed into *E. coli* BL21 cells. 1–2 L of LB-medium were inoculated 1:10 with fresh overnight cultures and incubated for 1–2 h at 37 °C, 200 rpm. The cultures were then transferred to 16 °C, 200 rpm and the expression was induced after 30 min by the addition of 0.1 mM IPTG. The cells were harvested after 24 h, washed with ice-cold 50 mM NaH₂PO₄/Na₂HPO₄ pH 8.0, 300 mM NaCl buffer and the cell pellet was stored at -80 °C.

For purification, protein crude extracts were prepared by ultrasonification in ice-cold 50 mM NaH₂PO₄/Na₂HPO₄ pH 8.0, 300 mM NaCl, 40 mM imidazole (2 mL/g cell fresh weight). The N-terminally His₆-tagged GyrA and GyrB fusion constructs were then purified using Ni²⁺-NTA affinity chromatography (ÄKTA FPLC system + 5mL Ni²⁺-NTA columns, GE Healthcare) followed by size-exclusion chromatography (Superdex 200 increase 10/300 GL, GE Healthcare). The purity of the protein constructs was verified by 15% SDS-PAGE. Standard yields for GyrA and GyrB were in the range of 5–10 mg fusion protein per liter culture. Purified GyrA and GyrB were desalted using PD10 columns and stored in GyrA storage buffer (50 mM Tris-HCl pH 7.5, 100 mM KCl, 1 mM EDTA, 2 mM dithiothreitol, 20% (v/v) glycerol)³ and GyrB storage buffer (50 mM Tris-HCl pH 7.5, 150 mM NaCl, 1 mM EDTA, 2 mM dithiothreitol, 20% (v/v) glycerol)³ at -80 °C, respectively. Molar concentrations were determined by UV spectroscopy using the following extinction coefficients: $e_{280}(\text{GyrA})$: 48270 M⁻¹ cm⁻¹; $e_{280}(\text{GyrB})$: 68020 M⁻¹ cm⁻¹.

Reconstitution of *E. coli* Gyrase

E. coli gyrase tetramers were reconstituted by mixing 5 μM of each subunit. Final concentration of the gyrase stock: 1.25 μM.

Cloning, Expression and Purification of *E. coli* Topoisomerase (TopA)

The TopA full-length gene were amplified by PCR from *E. coli* genomic DNA (Phusion polymerase, Thermo Scientific) using the following primer pairs (Sigma-Aldrich):

TopA Forward (Nde): ATCATATGGGTAAAGCTCTTGTCATCG

TopA Reverse (Xho): ATCTCGAGTTATTTTTTTCCTTCAACCCATTTGC

The obtained amplicons were ligated into the pET-28b expression vector system (N-terminal His₆-tag) (Novagen) using an *NdeI/XhoI* strategy and transformed into *E. coli* HS996 cells for selection (kanamycin). Positive clones were picked and verified by Sanger sequencing. For protein expression the constructs pET28-TopA was transformed into *E. coli* BL21 cells. 1–2 L of LB-medium were inoculated 1:10 with fresh overnight cultures and incubated for 1–2 h at 37 °C, 200 rpm. The cultures were then transferred to 16 °C, 200 rpm and the expression was induced after 30 min by the addition of 0.1 mM IPTG. The cells were harvested after 24 h, washed with ice-cold 50 mM NaH₂PO₄/Na₂HPO₄ pH 8.0, 300 mM NaCl buffer and the cell pellet was stored at -80 °C.

For purification, protein crude extracts were prepared by ultrasonification in ice-cold 50 mM NaH₂PO₄/Na₂HPO₄ pH 8.0, 300 mM NaCl, 40 mM imidazole (2 mL/g cell fresh weight). The N-terminally His₆-tagged TopA fusion constructs was then purified using Ni²⁺-NTA affinity chromatography (ÄKTA FPLC system + 5mL Ni²⁺-NTA columns, GE Healthcare) followed by size-exclusion chromatography (Superdex 200 increase 10/300 GL, GE Healthcare). The purity of the protein constructs was verified by 15% SDS-PAGE. Standard yields for TopA were in the range of 5–10 mg fusion protein per liter culture. Purified TopA was desalted using PD10 columns and stored in TopA storage buffer (25 mM Tris-HCl pH 7.5, 150 mM NaCl, 1 mM EDTA, 1 mM dithiothreitol, 20% (v/v) glycerol)³ at -80 °C. Molar concentrations were determined by UV spectroscopy using the following extinction coefficient: $e_{280}(\text{TopA}): 95700 \text{ M}^{-1} \text{ cm}^{-1}$.

Preparation of pBR322 Plasmid Substrate

An original batch of pBR322 plasmid was purchased from Inspiralis (Norwich, UK), transformed into *E. coli* HS996 for amplification (selection using ampicillin) and stored at -80 °C as glycerol stock. For plasmid preparation 5 L of LB medium (ampicillin) were inoculated using this strain and grown overnight at 37 °C, 220 rpm. The plasmids were isolated using the Qiagen GigaPrep Kit (Qiagen, Hilden, Germany) and stored in MilliQ-H₂O at -20 °C. The plasmid isolated by this strategy is 100% supercoiled and could be used for TopA assays directly.

For the preparation of 100% relaxed plasmid as substrate for gyrase assays, 2 mg/mL plasmid were combined with 1 μM *E. coli* TopA in TopA reaction buffer (20 mM Tris-HCl pH 8.0, 50 mM potassium acetate, 10 mM magnesium acetate, 2 mM dithiothreitol and 100 μg/mL (w/v) bovine serum albumin) at 37 °C for 2 h.³ After phenol-chloroform extraction, the DNA was precipitated using EtOH/sodium acetate method, dissolved in MilliQ-H₂O and stored at -20 °C.

Gyrase Supercoiling Assay

N-terminally His-tagged *E. coli* gyrase was used. For standard reactions 0.5 μg relaxed plasmid were mixed with 1 unit (20.5 nM) gyrase in 1× reaction buffer (35 mM Tris-HCl pH 7.6, 24 mM KCl, 2 mM dithiothreitol, 4 mM MgCl₂, 1.8 mM spermidine, 0.1 mg/mL bovine serum albumin, 1 mM ATP, 5% (v/v) glycerol) (30 μL final volume) and incubated for 30 min at 37 °C. The reactions were quenched by the addition of DNA gel loading buffer containing 1% (w/v) SDS. The samples were separated on 0.8% (w/v) agarose gels and DNA was visualized using ethidium bromide. All NPs and compounds

stock solutions and dilutions were prepared in DMSO and added to the supercoiling reactions giving a final DMSO concentration of 5% (v/v). Control reactions were: no enzyme and a standard reaction in presence of 5% (v/v) DMSO. All reaction samples were equilibrated for 15 min at room temperature in the absence of DNA. Then the relaxed plasmid was added to start the reaction. All reactions were performed in triplicates

Topoisomerase IV Relaxation Assay

Commercial *E. coli* topoisomerase IV relaxing kits (Inspiralis, Norwich, UK) were used. For standard reactions 0.5 μ g supercoiled plasmid were mixed with 1 unit (~20.5 nM) topoisomerase IV in 1 \times reaction buffer (see kit manual) and incubated for 30 min at 37 °C. The reactions were quenched by the addition of DNA gel loading buffer containing 1% (w/v) SDS. The samples were separated on 0.8% (w/v) agarose gels and DNA was visualized using ethidium bromide. Control reactions were: no enzyme and a standard reaction in presence of 5% (v/v) DMSO. All reaction samples were equilibrated for 15 min at room temperature in the absence of DNA. Then the relaxed plasmid was added to start the reaction. All reactions were performed in triplicates.

Quantification and Analysis

To determine IC₅₀ values, agarose gels were digitalized using standard gel documentation instruments and supercoiled (gyrase) and relaxed (topoisomerase IV) plasmid was quantified using Adobe Photoshop (Histogram mode). Intensities were normalized (% enzyme activity = SC / (SC + relaxed)). Plotting of these values versus the compound concentration yielded sigmoidal shaped curves, which were fitted using Hill's equation (Origin Pro 8.5).⁴ All determined IC₅₀ values are the averages of three independent experiments.

Table S2. In vitro inhibitory activities of esterified Cys507 analogues and their parent compounds in the gyrase supercoiling assay.

Free acid	IC ₅₀ <i>E. coli</i> gyrase (μ M)	Corresponding ester	IC ₅₀ <i>E. coli</i> gyrase (μ M)
5	360 \pm 26	67	>500
7	115 \pm 18	68	>500
8	60 \pm 10	69	>500
10	50 \pm 10	85	>500
12	165 \pm 18	71	>500
13	85 \pm 12	72	473 \pm 20
14	101 \pm 15	73	180 \pm 38

DNA Competition Assay Using Hoechst 33342 and Ethidium Bromide (EtBr)

EtBr and Hoechst 33342 competitive binding assays were performed⁵ by recording the emission spectra of solutions (30 μL) containing varying concentrations of cystobactamid derivatives (in DMSO; 500–0.1 μM and 5% DMSO final), 15 μM calf thymus DNA (Sigma-Aldrich) and 15 μM of EtBr or Hoechst 33342 in 25 mM sodium phosphate buffer (pH 7.5), 150 mM NaCl.

All measurements (triplicates) were performed in 384 well plates (black, low volume) (Corning, Corning, NY, USA) using a Tecan infinite II reader (Tecan, Switzerland) using the following (standard) parameters: Bandwidth 20 nm, 10 flashes, integration time 20 μs , no delay, no pause, Z: 20000

Hoechst 33342: λ_{ex} : 355 nm, λ_{em} : 370–850 nm in 20 nm steps

Ethidium bromide: λ_{ex} : 480 nm, λ_{em} : 490–850 nm in 20 nm steps

All samples were mixed and incubated at room temperature for 30 min before each measurement.

Quantification and Analysis

To determine apparent values for the compounds' "minor groove affinities" (50% displacement of Hoechst 33342), the values of the Hoechst 33342 fluorescence spectra peak maxima were plotted vs. compound concentration (in μM) and fitted using Hill's equation (Origin Pro 8.5).⁴ All determined values are the averages of three independent experiments.

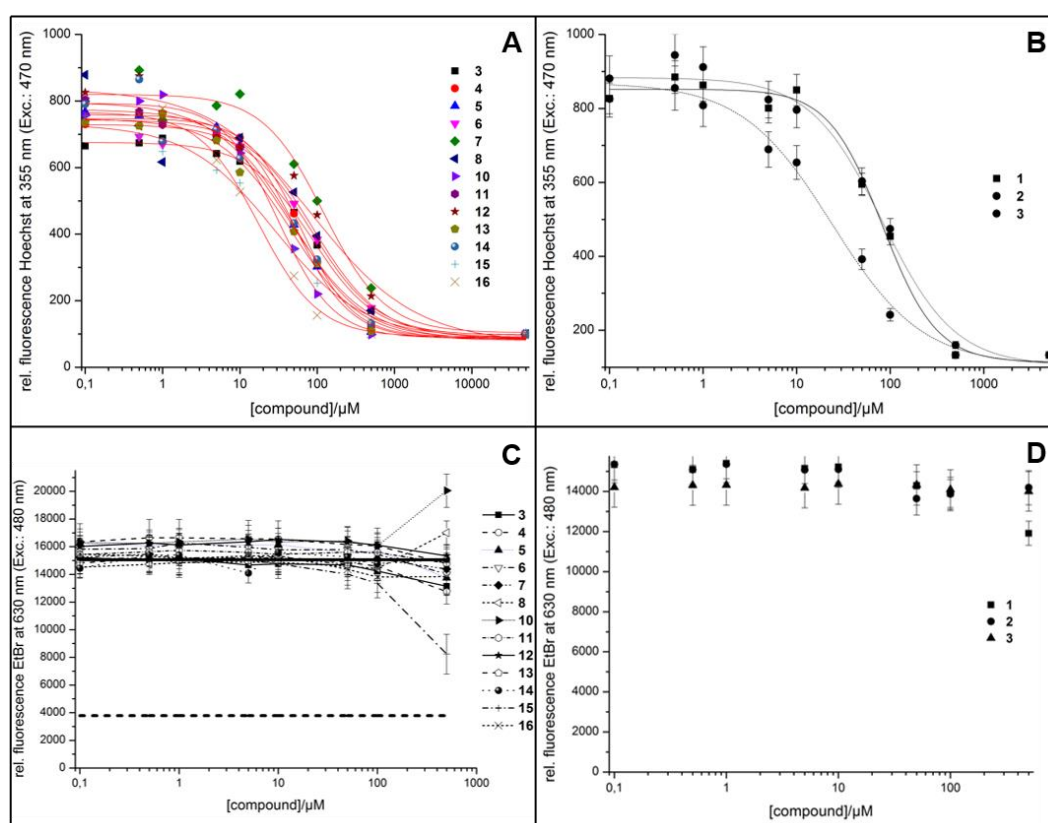
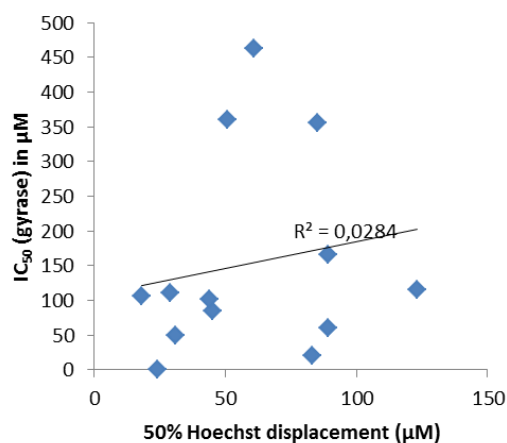


Figure S32. Competition titration of ct-DNA (15 μM) bound Hoechst 33342 (15 μM) (A, B) and EtBr (15 μM) (C, D) with Cys507 analogues (A, C) and natural cystobactamids (B, D). The relative fluorescence intensity at the peak maximum (470 nm for Hoechst 33342 and 630 nm for EtBr, respectively) is plotted vs the respective Cys507 analogue concentration. The solid- and dashed line represent the fluorescence intensity of the ct-DNA bound and DNA-free dyes, respectively.

Table S3. Apparent “minor groove affinities” (50% displacement of Hoechst 33342) and IC₅₀ values (gyrase supercoiling) for **1–16**

Compound	50% Displacement of Hoechst 33342 (μM)	IC ₅₀ <i>E. coli</i> gyrase (μM)
1	83 ± 10	21 ± 6
2	24 ± 4	0.26 ± 0.06
3	85 ± 18	355 ± 25
4	61 ± 5	463 ± 28
5	51 ± 3	360 ± 26
6	83 ± 21	>1000
7	123 ± 33	115 ± 18
8	89 ± 4	60 ± 10
9	n.d.	195 ± 20
10	31 ± 5	50 ± 10
11	49 ± 7	>1000
12	89 ± 34	165 ± 18
13	45 ± 8	85 ± 12
14	44 ± 16	101 ± 15
15	29 ± 6	110 ± 20
16	18 ± 3	106 ± 18

Figure S33. Scatterplot of apparent “minor groove affinities” (50% displacement of Hoechst 33342) vs the IC₅₀ values (gyrase supercoiling) for **1–16**

Minimal Inhibitory Concentration (MIC) Determination

MIC values were determined as described elsewhere.⁴ Bacterial cultures were handled according to standard procedures and were obtained from the German Collection of Microorganisms and Cell Cultures (*Deutsche Sammlung von Mikroorganismen und Zellkulturen*, DSMZ), the American Type Culture Collection (ATCC) or were part of our internal strain collection. In brief, bacteria in mid-log phase were diluted to achieve a final inoculum of ca. 5×10^5 – 5×10^6 cfu/mL in Tryptic Soy broth (1.7% peptone casein, 0.3% peptone soymeal, 0.25% glucose, 0.5% NaCl, 0.25% K₂HPO₄; pH 7.3; *E. faecalis*, *S. pneumoniae*), or Mueller-Hinton broth (1.75% casein hydrolysate, 0.2% beef infusion, 0.15% starch; pH 7.4; used for all other listed bacteria). *E. faecalis* and *S. pneumoniae* cultures were grown under microaerophilic conditions without shaking and all other listed microorganisms were grown on a shaker (200 rpm) at 37 °C. *E. coli* DSM-26863 was grown with or without PMBN (polymyxin B nonapeptide) at sublethal concentration (3 µg/mL) for permeabilization. Serial dilutions of the compounds were prepared from DMSO stocks in sterile 96-well plates. The cell suspension was added and microorganisms were grown for 16–20 h. Growth inhibition was assessed by visual inspection and given MIC values determined in two independent experiments are the lowest concentration of antibiotic at which no visible growth was observed.

Metabolic Stability Assay

Metabolic stability of compounds **3**, **8**, **10**, and **13** was determined by incubation of 1 µM compound with 1 mg/mL pooled mammalian liver S9 fraction (BD Gentest), 2 mM NADPH regenerating system, 1 mM UDPGA, 0.1 mM PAPS and 10 mM magnesium chloride in 200 mM potassium hydrogen phosphate buffer (pH 7.4) at 37 °C for 0, 5, 15 and 60 min. At the given time points, two volumes of acetonitrile containing internal standard were added to stop the incubation. Concentration of the remaining test compound was determined using LC-MS/MS and used to determine the half-life ($t_{1/2}$).

6.3.7 References

1. Moreno, M.; Elgaher, W. A. M.; Herrmann, J.; Schläger, N.; Hamed, M. M.; Baumann, S.; Müller, R.; Hartmann, R. W.; Kirschning, A. *Synlett* **2015**, 26, 1175–1178.
2. Sheldrick, G. M. *Acta Cryst.* **2008**, A64, 112–122.
3. Shapiro, A.; Jahic, H.; Prasad, S.; Ehmann, D.; Thresher, J.; Gao, N.; Hajec, L. *J. Biomol. Screen.* **2010**, 15, 1088–1098.
4. Baumann, S.; Herrmann, J.; Raju, R.; Steinmetz, H.; Mohr, K. I.; Huttel, S.; Harmrolfs, K.; Stadler, M.; Müller, R. *Angew. Chem. Int. Ed.* **2014**, 53, 14605–14609.
5. Kunwar, A.; Simon, E.; Singh, U.; Chittela, R. K.; Sharma, D.; Sandur, S. K.; Priyadarsini, I. K. *Chem. Biol. Drug Des.* **2011**, 77, 281–287.

7 Appendix

7.1 Curriculum Vitae

Personal Data

Name	Walid Ali Mahmoud Mohammad Elgaher
Date of birth	01.10.1982
Nationality	Egyptian
Marital status	Married
E-mail	walid.mohammed@helmholtz-hzi.de; walid.elgaher@yahoo.com

Education

2012–2016	PhD study under supervision of Prof. Dr. Rolf W. Hartmann, Helmholtz Institute for Pharmaceutical Research Saarland, Saarbrücken, Germany Thesis: " <i>Evolution of novel antibiotic scaffolds targeting the nucleic acid machineries RNA polymerase, DNA Gyrase, and Topoisomerase IV</i> "
2005–2010	Master degree in Pharmaceutical Organic Chemistry, Faculty of Pharmacy, Assiut University, Egypt Thesis: " <i>Synthesis of some 1,3-dimethyl-8-substituted xanthine derivatives of antiasthmatic and antibacterial activities</i> "
1999–2004	Bachelor degree in Pharmaceutical Sciences (<i>Excellent with degree of honor</i>), Faculty of Pharmacy, Assiut University, Egypt

Teaching Experience

03.2010–now	Assistant lecturer at Department of Pharmaceutical Organic Chemistry, Faculty of Pharmacy, Assiut University, Assiut, Egypt
12.2004–	Demonstrator at Department of Pharmaceutical Organic Chemistry, Faculty of Pharmacy, Assiut University, Assiut, Egypt
03.2010	Pharmacy, Assiut University, Assiut, Egypt

Membership

05.2013–	Interdisciplinary Graduate School of Natural Product Research, Saarland University
08.2016	

Honors and Awards

05.2011–	German Egyptian Research Long-term Scholarship (GERLS) by the Egyptian Ministry of Higher Education (MHE) and the German Academic Exchange Service (DAAD) for doctorate study in Germany.
03.2016	
03.2016	Poster Award by the German Chemical Society, German Pharmaceutical Society, and Société de Chimie Thérapeutique at Frontiers in Medicinal Chemistry, Bonn, Germany

7.2 Publications

- 1 Elgaher, W. A. M.; Sharma, K. K.; Hauptenthal, J.; Saladini, F.; Pires, M.; Real, E.; Mély, Y.; Hartmann, R. W. Discovery and Structure-Based Optimization of 2-Ureidothiophene-3-Carboxylic Acids as Dual Bacterial RNA Polymerase and Viral Reverse Transcriptase Inhibitors, *J. Med. Chem.* **2016**, *59*, 7212–7222.
- 2 Baumann, S.; Herrmann, J.; Mohr, K.; Steinmetz, H.; Gerth, K.; Raju, R.; Müller, R.; Hartmann, R.; Hamed, M.; Elgaher, W. A. M.; Moreno, M.; Gille, F.; Wang, L. L.; Kirschning, A.; Hüttel, S. Novel Cystobactamides, WO 2016082934 A1 (**2016**).
- 3 Baumann, S.; Herrmann, J.; Mohr, K.; Steinmetz, H.; Gerth, K.; Raju, R.; Müller, R.; Hartmann, R.; Hamed, M.; Elgaher, W. A. M.; Moreno, M.; Gille, F.; Wang, L. L.; Kirschning, A. Cystobactamides, WO 2015003816 A2 (**2015**).
- 4 Moreno, M.; Elgaher, W. A. M.; Herrmann, J.; Schläger, N.; Hamed, M.; Baumann, S.; Müller, R.; Hartmann, R.; Kirschning, A. Synthesis and biological evaluation of cystobactamid 507: A bacterial topoisomerase inhibitor from *Cystobacter* sp., *Synlett* **2015**, *26*, 1175–1178.
- 5 Elgaher, W. A. M.; Fruth, M.; Groh, M.; Hauptenthal, J.; Hartmann, R. W. Expanding the scaffold for bacterial RNA polymerase inhibitors: Design, synthesis and structure activity relationships of ureido-heterocyclic-carboxylic acids, *RSC Adv.* **2014**, *4*, 2177–2194.
- 6 Hüsecken, K.; Hinsberger, S.; Elgaher, W. A. M.; Hauptenthal, J.; Hartmann, R. W. Surface plasmon resonance – more than a screening technology: insights in the binding mode of σ^{70} :core RNAP inhibitors, *Future Med. Chem.* **2014**, *6*, 1551–1565.
- 7 *New theophylline derivatives: Design, synthesis, antiasthmatic, and antibacterial activities*, Elgaher, W. A. M.; Lambert Academic Publishing GmbH & Co. KG, Saarbrücken, Germany, **2011**.
- 8 Hayallah, A. M.; Elgaher, W. A.; Salem, O. I.; Abdel Alim, A. A. M. Design and synthesis of some new theophylline derivatives with bronchodilator and antibacterial Activities, *Arch. Pharm. Res.* **2011**, *34*, 3–21.
- 9 Elgaher, W. A.; Hayallah, A. M.; Salem, O. I. A.; Abdel Alim A. A. M. Synthesis, anti-bronchoconstrictive, and antibacterial activities of some new 8-substituted-1,3-dimethylxanthine derivatives, *Bull. Pharm. Sci., Assiut University*, **2009**, *32*, 153–187.

7.3 Conference Contributions

7.3.1 Poster Presentations

- 1 Elgaher, W.; Sharma, K.; Hauptenthal, J.; Mély, Y.; Hartmann, R. Discovery and structure-based optimization of 2-ureidothiophene-3-carboxylic acids as dual bacterial RNAP and HIV-1 RT inhibitors, 6th HIPS Symposium Recent Developments in Infection Research, June **2016**, Saarbrücken, Germany.
- 2 Elgaher, W. A. M.; Sharma, K.; Hauptenthal, J.; Mély, Y.; Hartmann, R. W. Discovery and structure-based optimization of 2-ureidothiophene-3-carboxylic acids as dual bacterial RNAP and HIV-1 RT inhibitors, *Frontiers in Medicinal Chemistry*, March **2016**, Bonn, Germany.
- 3 Elgaher, W. A. M.; Sharma, K.; Hauptenthal, J.; Mély, Y.; Hartmann, R. W. Design and synthesis of 2-ureidothiophene-3-carboxylic acids as dual bacterial RNAP and HIV-1 RT inhibitors for treatment of patients co-infected with MRSA and HIV-1, Annual Meeting of the German Pharmaceutical Society-DPhG “I3-Interactions, Integrations and Innovations”, September **2015**, Düsseldorf, Germany.
- 4 Elgaher, W.; Sharma, K.; Hauptenthal, J.; Mély, Y.; Hartmann, R. Design and synthesis of 2-ureidothiophene-3-carboxylic acids as dual bacterial RNAP and HIV-1 RT inhibitors for treatment of patients co-infected with MRSA and HIV-1, 5th HIPS Symposium on Pharmaceutical Sciences devoted to Infection Research, July **2015**, Saarbrücken, Germany.
- 5 Elgaher, W. A. M.; Sahner, J. H.; Groh, M.; Hauptenthal, J.; Hartmann, R. W. Design, Synthesis, SAR Exploration and Optimization of Novel Bacterial RNA Polymerase Inhibitors Targeting the Switch Region, Annual Meeting of the German Pharmaceutical Society-DPhG “Trends and Perspectives in Pharmaceutical Sciences”, September **2014**, Frankfurt, Germany.
- 6 Baumann, S.; Herrmann, J.; Raju, R.; Hüttel, S.; Elgaher, W.; Hamed, M.; Mohr, K.; Steinmetz, H.; Bernecker, S.; Stadler, M.; Hartmann, R.; Müller, R. The Cystobactamides: novel antibacterial leads? 4th HIPS Symposium on Pharmaceutical Sciences devoted to Infection Research, June **2014**, Saarbrücken, Germany.
- 7 Elgaher, W. A. M.; Sahner, J. H.; Groh, M.; Hauptenthal, J.; Hartmann, R. W. Design, Synthesis, SAR Exploration and Optimization of Novel Bacterial RNA Polymerase Inhibitors Targeting the Switch Region, *Frontiers in Medicinal Chemistry*, March **2014**, Tübingen, Germany.

- 8 Elgaher, W. A. M.; Sahner, J. H.; Groh, M.; Hauptenthal, J.; Hartmann, R. W. Structure-based design of novel bacterial RNAP inhibitors targeting the switch region, Summer School on Drug Design, September **2013**, University of Vienna, Vienna, Austria.
- 9 Elgaher, W. A. M.; Sahner, J. H.; Groh, M.; Hauptenthal, J.; Hartmann, R. W. Structure-based design of novel bacterial RNAP inhibitors targeting the switch region, 3rd HIPS Symposium on Pharmaceutical Sciences devoted to Infection Research, July **2013**, Saarbrücken, Germany.
- 10 Elgaher, W. A. M.; Sahner, J. H.; Groh, M.; Hauptenthal, J.; Hartmann, R. W. Novel bacterial RNA polymerase inhibitors: Structure–activity exploration and optimization of the aryl-ureidothiophene-carboxylic acids, 2nd International Conference on Antimicrobial Research (ICAR 2012), November **2012**, Lisbon, Portugal.

7.3.2 Oral Presentations

- 1 Discovery and structure-based optimization of 2-ureidothiophene-3-carboxylic acids as dual bacterial RNAP and HIV-1 RT inhibitors, 5th Summer Symposium – Graduate School of Natural Product Research, August **2016**, Saarbrücken, Germany.
- 2 Discovery and structure-based optimization of 2-ureidothiophene-3-carboxylic acids as dual bacterial RNAP and HIV-1 RT inhibitors, German Pharmaceutical Society (DPhG) – Doctoral Meeting, March **2016**, Aachen, Germany.
- 3 Expanding the scaffold for bacterial RNA polymerase inhibitors: Design, synthesis and structure–activity relationships of ureido heterocyclic carboxylic acids, 2nd Summer Symposium – Graduate School of Natural Product Research, July **2013**, Saarbrücken, Germany.